N75.32165
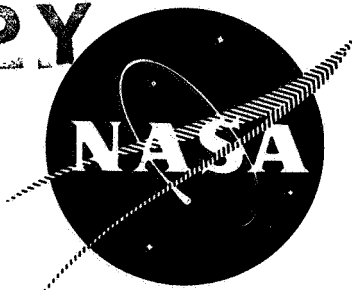
NAS9-12802
NASA-CR-
LINE ITEM NO. 5
MA-129T
R-9686

NASA CR-

144440

SPACE SHUTTLE

ORBIT MANEUVERING ENGINE

REUSABLE THRUST CHAMBER PROGRAM

FINAL REPORT

29 AUGUST 1975

Prepared For

National Aeronautics and Space Adminstration
Lyndon B. Johnson Space Center
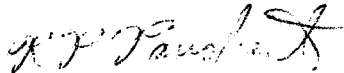Houston, Texas   77058

Rockwell International
Rocketdyne Division
6633 Canoga Avenue
Canoga Park, California   91304

NASA-CR-

SPACE SHUTTLE

ORBIT MANEUVERING ENGINE

REUSABLE THRUST CHAMBER PROGRAM

NAS9-12802

FINAL REPORT

Prepared by

[signature]

R. P. Pauckert
SS/OME Principal Engineer

[signature]

R. D. Tobin

Approved by

[signature]

R. D. Paster
Program Manager
SS/APS Programs

ROCKETDYNE DIVISION OF ROCKWELL INTERNATIONAL CORPORATION
6633 CANOGA AVENUE, CANOGA PARK, CA   91304
R-9686

FOREWORD

This report and the final summary report describe the
analytical and experimental studies conducted by the
Rocketdyne Division of Rockwell International Corporation
from June 1972 through November 1974 under contract
NAS9-12802. The NASA/JSC Technical Monitor was Merlyn
Lausten.

ABSTRACT

An analytical and experimental program was conducted
from June 1972 through January 1975 to provide informa-
tion for thrust chamber and propellant selection and
basic OME operating data. Parametric data was generated
analytically for several propellant combinations and
thrust chamber cooling concepts.

Subscale and full scale injector tests were conducted
to characterize the performance, stability, and heat
flux of various injector patterns. Electrically heated
tube, channel, and panel tests were conducted to define
safety margins under nominal and adverse off-design
operating conditions for regeneratively cooled thrust
chambers. Two full scale regeneratively cooled chambers
were designed, fabricated, and tested at simulated
altitude conditions to provide steady-state and transient
data at nominal and off-design conditions.

CONTENTS

ILLUSTRATIONS

R-9686

TABLES

INTRODUCTION

The Space Shuttle Orbit Maneuvering Engine reusable thrust chamber investigation was initiated prior to the selection of the OMS propellant combination, the thrust chamber cooling technique and the contractors for the Space Shuttle Orbiter, the Orbit Maneuvering System (OMS) and the Orbit Maneuvering Engine (OME). The initial purpose of the contract was to provide engine data, with emphasis on the thrust chamber, to the potential contractors to assist in evaluating various OME configurations and selecting the configuration to be used for the OMS.

Later, when the orbit maneuvering system and engine became more clearly defined, the program continued to provide basic technical data in areas to support the main stream OMS and OME programs. The program provided data on performance, stability, and thermal characteristics of an OME operating with an alternate injector configuration and with alternate propellants. Design, manufacturing, and operating characteristics of an electroformed, regeneratively cooled thrust chamber were derived from the program tasks. The program also provided, through subscale and full scale tests, data relating to off-design and transient operation. The program conducted by Rocketdyne under NASA Contract NAS9-12802, extended from June 1972 through January 1975. Efforts along similar lines were conducted under Contracts NAS9-12803 and NAS9-13133 by other propulsion contractors.

SUMMARY

The program was conducted in thirteen tasks. The report is presented topically to which the tasks were addressed as follows.

Configuration and Propellant Selection

Task I   - Reusable Thrust Chamber Evaluation

Task II - Alternate OME Propellants

Injector Evaluation

Task VI   - Hot Fuel Element Investigation

Task XI   - OME Injector

Regenerative Cooling Investigations

Task VII   - Heat Transfer Testing

Task IX   - Adverse Operating Conditions

Task XIII - Subscale He Ingestion and 2-D Heat Transfer Test

Demonstration Chamber

Task III   - Demonstration Chamber Design

Task IV   - Demonstration Chamber Fabrication

Task V   - Demonstration Chamber Test

Task VIII - Alternate Propellant Demonstration

Integrated Thrust Chamber

Task X   - Integrated Thrust Chamber Fabrication

Task XII   - Integrated Thrust Chamber Test

Comparison of 8- and 10-Inch Diameter Chambers

Task X   - Integrated Thrust Chamber Fabrication

The schedule of these tasks is shown in Fig. 1.

The Configuration and Propellant Selection studies (Tasks I & II) were directed towards supplying engine data to NASA and to potential orbiter and OMS contractors to assist in configuration selection and evaluation.

SCHEDULE

1974   1973   1972

TASK

I   Reusable Thrust Chamber Evaluation
II   Alternate OME Propellants
III   Demonstration Thrust Chamber Design
IV   Demonstration Thrust Chamber Fabrication
V   Demonstration Thrust Chamber Test
VI   Hot Fuel Element Investigation
VII   Heat Transfer Testing
VIII   Alternate Propellant Demonstration
IX   Adverse Operating Conditions Test
X   Integrated T/C Fabrication
XI   OME Injector
XII   Integrated T/C Test
XIII   Subscale He Ingestion and
       2-D Heat Trasnfer Test

Figure 1. NAS9-12802 Program Tasks Schedule

The reusable Thrust Chamber Evaluation (Task I), entailed the design
and analysis of promising reuseable thrust chamber concepts applicable
to the SS/OME with NTO/MMH and NTO/50-50 propellants in regenerative
and film cooled thrust chambers. Parametric data was generated describing
engine weights, performance, inlet pressures, envelope, reliability,
maintainability, and costs. The total engine was considered in these
evaluations and included the thrust chamber assembly, propellant valve
and ducts, gimbaling actuator ring, ring, and bearing, and the electrical
and pneumatic systems. Detailed point designs were generated for each
thrust chamber and the two propellant combinations. The parametric data
was based on perturbing the point designs. The results were published
in NASA-CR-128675 and NASA-CR-141671. Rocketdyne selected a NTO/MMH
Regeneratively cooled engine as the optimum configuration.

The Alternate OME Propellant Combinations Study, entailed design and
analysis of promising reuseable thrust chamber concepts applicable to
the SS/OME with LOX/Amine and LOX/hydrocarbon propellants. Detailed
point designs were generated and then perturbed to provide parametric
data. The propellant combinations considered were LOX/MMH, LOX/50-50,
LOX/N_2H_4, LOX/RP-1 and LOX/C_3H_8. Based on these studies, Rocketdyne
selected a LOX/MMH regenerative cooled engine as the most attractive
alternate configuration relative to the NTO/amine systems. The pro-
pellant and engine selection were approved by NASA/JSC as the baseline
for the remainder of the program.

Hot-fire test of subscale injectors were conducted under the Hot Fuel
Element Investigation (Task VI). Performance, thermal, and stability
evaluation of like-doublet and triplet element configurations were made
for injectors designed to be used with a regeneratively cooled thrust
chamber. The triplet element was rejected because of a performance
sensitivity to fuel temperature. The effects of elementary geometry
and propellant temperature were investigated for like-doublet elements.
The results of these investigations were used to design a full-scale
injector. Details of this task are reported in NASA-CR-141677.

The OME injector investigation (Task XI) comprised three subtasks the
objectives of which were: 1) to experimentally determine the stability
of an existing 8-inch diameter injector (L/D #1); 2) to design, fabricate,
and test a 10-inch diameter injector (L/D #4); 3) to conduct stability
analyses including review of existing stability data and model testing.
The results of the test programs with the 8-inch and 10-inch diameter
injectors are given in NASA-CR-140358 and NASA-CR-141674, respectively.
The 8-inch configuration was completely stable with 15% area acoustic
cavity and radial dams in the primary fuel manifold. Stability was
marginal when the acoustic cavity area was reduced to 12% of the chamber
cross-sectional area. The 10-inch diameter injector was stable with 10%
area cavities and had a flux sufficiently low to permit operation without
supplementary boundary layer coolant. However, the performance of this
injector was low, apparently due to poor mixing efficiency.

Stability data from this contract as well as from contracts NAS9-12803 and NAS9-13133 were reviewed and interpreted. The data implied that it was highly probable that a coupling between the chamber acoustics and the feed system hydraulics, particularly the injector, existed and was responsible for instabilities at the frequency noted on all three contracts. The cavity model tests provided data to correlate the effective cavity depth with physical dimensions of the cavities. The results of the stability analysis and model tests were reported in NASA-CR-141676.

The Heat Transfer Testing (Task VI) comprised a heated tube test program to characterize the cooling capability of OME thrust chamber coolants. MMH and 50-50 fuels were tested in electrically heated steel tubes to establish convective cooling safety factor correlations for steady-state conditions. The results of these correlations were used to design the regeneratively cooled thrust chambers. The results indicated fairly similar cooling correlations for both fuels. The results of the tests were reported in NASA-CR-141672.

Electrically heated tube experiments were extended in the Adverse Operating Conditions Tests (Task IX) to investigate off-design operation of the OME thrust chamber and to determine the effects of a symmetrical heating in the channel type construction of the OME thrust chamber. Restarts with a hot chamber and helium bubble and froth ingestion were investigated. Cooling correlations for an electrically heated channel test section were experimentally determined and compared well with analytical preductions based on data from circular tube experiments. The results of the tests were reported in NASA-CR-134282.

The electrically heated channel tests continued in the Subscale Helium Ingestion and Two-Dimensional Heating Tests (Task XIII). The objectives were to determine transient and steady-state helium ingestion capabilities of the OME thrust chamber using heated single and multiple channels and to verify the application of one-dimensional test data to two-dimensional analysis of thrust chamber walls. The results of this test program indicated that the channel burnout heat flux values analytically derived from one-dimensional (heated tube) were valid. This was verified with both single channels and three-channel test panels. Helium froth degraded the heat flux capability of round tubes significantly but had only a slight affect on burnout capability of channels. Helium bubbles of infinite duration and plugged channels were simulated by operating the three-channel panel with no flow in the center channel. Correlations were generated to permit designing a chamber to operate with a single channel plugged. It was determined that helium bubble could flow through a single channel for several seconds without overheating that channel or the adjacent channels. The results were reported in NASA-CR-141560.

The Demonstrator Thrust Chamber Design effort (Task III) entailed the detailed design of an experimental thrust chamber which would demonstrate critical design, fabrication, and operating areas of a regeneratively cooled OME reuseable thrust chamber. The chamber was designed with heavy weight inlet and outlet manifolds to permit test flexibility and to reduce fabrication cost. The results of the design and analysis conducted under this task were published in NASA-CR-141673. The chamber was a single up-pass regenerative cooled design from expansion area ratio of 7 to the injector-end. The chamber had a contraction ratio of 2 and the distance from the injector to the throat was 14.7 inches. Supplementary boundary layer coolant was introduced by a separate ring between the combustion chamber and injector. Coolant passages were machined into a CRES liner and the outer wall formed by electroforming nickel over the liner. The chamber was designed to operate for more than 1000 cycles at a thrust level of 6000 lbs, a chamber pressure of 125 psia, and a propellant mixture ratio of 1.65 using NTO and MMH propellants with generous safety factors on all of these parameters. A regeneratively cooling safety factor of 1.5 at the most severe off-design conditions was provided.

In addition to fabricating the chamber described above, a radiation cooled coated Columbium nozzle was also fabricated under Task IV. The nozzle extended the area ratio from 7 to 9 to match the altitude test facility and to provide data for the most critical region of the flight radiation cooled nozzle.

The regeneratively cooled demonstrator thrust chamber was tested (Task V) at simulated altitude conditions at Rocketdyne and NASA/White Sands Test Facilities. The chamber was tested with two injectors using different like-doublet element patterns. Tests were conducted with saturated and unsaturated propellants over the complete range of anticipated chamber pressure and propellant mixture ratio. High pressure tests to simulate a potential space tug application and low pressure tests to simulate propellant tank pressurization system failure were also conducted. The test program is described in NASA-CR-140321.

In the Alternate Propellant Demonstration Task (Task VI), the testing continued with NTO/50-50 propellants. Performance, thermal, and stability characteristics of the demonstration chamber were evaluated over the anticipated operating range of chamber pressures and propellant mixture ratios. The results of this program were also reported in NASA-CR-140321.

The primary objective of the Integrated Thrust Chamber Fabrication Task (Task X) was to design and fabricate an 8-inch diameter integrated regeneratively cooled thrust chamber which simulates the performance, thermal, and hydraulic characteristics of the OME flight configuration. The overall dimensions of the chamber were similar to the demonstration chamber. However, the channel geometry was updated and the injector-end was modified to include acoustic cavities and flight type propellant manifolds for integration with the injector. The chamber was extensively instrumented to record outside

wall temperatures and propellant temperatures in the manifolds. The chamber was fabricated by milling channels into the CRES liner and closing them with electroformed nickel.

The integrated thrust chamber was tested in two phases at NASA/WSTF (Task XII). The first series of tests, reported in NASA/CR-134256 was primarily oriented to obtain steady-state performance data in vacuum with a high area ratio nozzle. The second series, reported in NASA-CR-140250, was conducted to obtain OME start, shutdown, and restart data. Operation under throttled conditions and without boundary layer cooling was also demonstrated during the second series.

Thrust chambers with contraction ratios of 2 and 3 were compared analytically (Task X). The results indicated the superiority of the low-contraction ratio when to minimize OMS inert weight. The high-contraction ratio chamber resulted in a slightly lower OMS tanked weight. The results were reported in NASA-CR-141675.

The major hardware fabricated under this contract is described in Table I.

TABLE 1

NAS9-12802 MAJOR HARDWARE SUMMARY

COMPONENT	DESIGN CHARACTERISTICS	MEASURED CHARACTERISTICS	TEST EXPOSURE	
			No. of Starts	Total Duration
Demonstrator Thrust Chamber	Flight type jacket, 180 channels, 0.060 inch constant channel width(stepped to 0.120 inch in nozzle), 0.040 inch minimum land width, 0.078-0.175 inch channel height profile, thermal safety factor > 2 at nominal conditions, predicted life - 4000 cycles. Spun/machined 321 CRES liner with 0.030 inch electroformed nickel closeout. Combuster: 8 inch I.D. X 14.7 inch with ϵ_c=2. Silicide-coated columbium nozzle for $7 < E \le 9$. Separate fuel FLC injector manifold.	13 psi jacket pressure drop and 700 BTU/sec heat load at nominal conditions with L/D #1 injector.	112	1042
Integrated Thrust Chamber	Flight type (except inlet manifold) .120 constant width (0.114 inch) channels. Channel height profile (0.042-0.146 inches) at nominal conditions with 0.038 inch minimum land width. Thermal safety factor nominally > 2. Predicted life 5000 cycles, 304L CRES liner with 0.025 inch electroformed nickel closeout. Acoustic cavities part of chamber.	15 psi jacket pressure drop and 750 BTU/sec chamber heat load L/D #1 injector.	156	1190
L/D #1 Injector	8.2 inch diameter. 186 like doublet elements. Minimum orifice diameters; oxidizer - 0.028 inches, fuel - 0.032 inches. 68 boundary layer coolant orifices (0.020 inch diameter). Flight type .321 CRES material. Electrodischarge machined orifices (EDM).	Pressure drops at nominal conditions: Oxidizer - 56 psi, fuel - 61 psi. Nominal vacuum I_s - 310 sec.	302	1775

TABLE 1 Cont'd.

NAS9-12802 MAJOR HARDWARE SUMMARY

COMPONENTS	DESIGN CHARACTERISTICS	MEASURED CHARACTERISTICS	TEST EXPOSURE	
			No. of Starts	Total Duration
L/D #4 Injector	10 inch diameter. 229 like doublet elements minimum orifice diameters: Oxidizer - 0.029 inches; fuel - 0.031 inches. Flight type 321 CRES. EDM orifices.	Approximate pressure drops at nominal conditions = Oxidizer - 65 psi; fuel - 50 psi	28	108

CONCLUSIONS

The analyses and tests conducted during this program lead to the general conclusion that a regeneratively cooled NTO/MMH engine can provide a lighweight, stable, propulsion system with high performance. Specific conclusions are best described in the order of the particular study areas.

The propellant and cooling method analyses lead to the conclusion that the regeneratively cooled NTO/MMH engine was the optimum of the various candidates studied based on considerations of performance, weight, development risk, cost, safety, maintainability, reliability, and air pollution. NTO/50-50, LOX/MMH, and LOX/50-50 were the alternate preferences in that order.

It was concluded from the subscale injector tests that the like-doublet injector would produce higher and more stable performance at OME operating conditions than injectors using either unlike-doublet or triplet elements. The highest performance could be obtained with a 45 degree cant angle and an impingment distance of approximately 0.4 inches. Mixture ratio, chamber pressure, and oxidizer temperature do not significantly affect C* efficiency which is limited by mixing more than by vaporization.

The thrust chamber cooling tests using electrically heated tubes and channels lead to the conclusion that regenerative cooling at OME design and off-design conditions can be accomplished with reasonable design parameters and factors of safety. Data obtained with simple round-tube data can be used to define steady-state safety factors for chambers using channel wall construction. The OME chamber can be started safely when hot due to a previous firing or heating by plume impingment from other engines. The chamber can tolerate large continuous helium bubbles in the fuel, but the safety factor is degraded by the presence of froth-like helium bubbles. The design of the cooling jacket would probably have to be modified to permit operation with a completely plugged channel.

The full-scale injector test programs demonstrated that a like-doublet injector provides safe, stable operation with moderately high performance. The injector can be stabilized with an acoustic cavity having a gradual contoured entrance. The conclusion from an analytical comparison of chambers using 8- and 10-inch diameter injectors was that, if the injectors provided equal C* performance, the resulting weight, pressure, and nozzle comparison resulted in higher system performance for the 8-inch chamber based on minimizing OMS inert weight. A slightly lower OMS tanked weight would result from the use of a 10-inch injector. The same study lead to the the conclusion that a chamber having lands of constant width was superior to a chamber having coolant channels of constant width.

It was concluded from the stability model tests and analysis that instabilities encountered in the frequency vicinity of 2600 hz are probably due to the interaction of feed system dynamics and chamber acoustics. Chamber oscillating modes can be accurately predicted by model test data. The resonant frequency of the acoustic cavity is independent of the location of the downstream portion of the cavity.

The demonstrator chamber tests verified the analytical conclusions regarding safe engine operation at nominal and anticipated off-design conditions. In fact, it was concluded that the analyses were somewhat conservative regarding regenerative cooling safety factor and radiation nozzle temperatures. The fabrication of this chamber also demonstrated the feasibility of CRES channel-wall chambers using an electroformed nickel closeout. The feasibility of repairing certain types of chamber damage by electroforming was also demonstrated. It was concluded that the chamber could operate safely with NTO/50-50 propellants over the range tested at slightly higher performance than NTO/MMH provided.

Fabrication of a flightweight OME thrust chamber was demonstrated (excepting the inlet manifold) by the integrated chamber. Safe operation was demonstrated at nominal and anticipated off-design conditions with this chamber. The thrust chamber and injector can survive a fuel depletion condition and can operate stably in the blowdown mode to approximately 70 psia. Propellant saturation does not significantly affect either the performance or heat transfer characteristics of the engine. The L/D #1 injector in a 14.7-inch long chamber and a nozzle having an area ratio of 72 with 2.7 percent Boundary Layer Coolant provides 310 seconds specific impulse. Eliminating the BLC would increase performance by 1-1/2 seconds and still permit safe operation over the expected range of operating conditions. Simultaneously lengthening the chamber to 16 inches and eliminating the BLC would result in a specific impulse of 313 seconds and a thermal safety factor of 1.4 at nominal conditions.

Tests conducted with the integrated chamber and OMS simulated ducting lead to the conclusion that oxidizer depletion occurs within 10 seconds after engine shutdown for all anticipated operating conditions. Fuel depletion times range from one second after a long-duration test to 10 minutes after a 1-second test with cold fuel. Posttest accelerations in the order of 300 g's can result from low level combustion. These accelerations are not detrimental to the engine and can be avoided by a brief purge of the oxidizer system after shutdown. The engine does not impose any limitations on OMS restart times.

RECOMMENDATIONS

The stability and safety of injectors utilizing like-doublet elements
in regeneratively cooled chambers was demonstrated in this program.
Efforts should be made to improve the performance of this injector
type while maintaining the present stability and safety characteristics.
Cold flow tests of existing full-scale injectors should be made to
establish mixing characteristics. Design and analysis efforts based on
the cold flow results should be followed by injector subscale and
full-scale tests.

Although the injector was stabilized by the proper acoustic cavity
configuration, a 2600 hz oscillation has occurred with some cavity
configurations on this and other programs. The persistance of this
oscillation in some cases may be the result of a feed system interaction.
This possibility should be further investigated in order to better
understand and control the stability of the OME.

The LOX/MMH propellant combination was determined analytically to be a
strong alternate candidate for the OME but was rejected primarily because
of lack of experience. This propellant combination should be tested using
a like-doublet element injector which is compatible with LOX/MMH to
provide performance, thermal, and stability data for future generation
Orbit Maneuvering Engines.

1.0 PROPELLANT AND CONFIGURATION SELECTION

One of the first objectives of the program was to provide Orbit Maneuvering Engine designs, parametric data and recommendations to NASA and to potential contractors for the Space Shuttle Orbiter Vehicle and Orbit Maneuvering System. These data were used in the selection of propellants, chamber cooling concept, and design parameters. The study (Tasks I and II) was conducted by first generating fairly detailed point designs. The point designs were perturbed to provide parametric weight, envelope, performance, and inlet pressure data. The point designs also served as the basis for comparisons of reliability, maintainability, safety development risk, and program costs. Details of the analyses were presented in NASA-CR-128675, and NASA-CR-141671.

1.1 POINT DESIGNS

Regenerative and film cooled engines were designed for pressure fed orbital maneuvering engines for the Space Shuttle Orbiter Vehicle. General ground rules for the designs and analyses are given in Table 2. Layout drawings of these engine assemblies are shown in Figs. 2 and 3. The engine components include propellant ducting with flex joints for gimbaling, a quad-redundant bipropellant valve, injector, thrust chamber, nozzle extension, and throat gimbal ring. A pneumatic pressure system to actuate the propellant valves was later added and is shown installed on the regeneratively cooled engine in Fig. 4 .

Propellant ducting carries the propellants from the vehicle interface on the gimbal ring to the valves and then to the injector and chamber. The valve mounting orientation which minimized duct weight was selected for each chamber cooling method: perpendicular to the chamber axis for the regeneratively cooled chamber; parallel to the axis for the film cooled chamber.

The method of attaching components was based on tradeoffs between reliability, maintainability, and weight. Components of lower reliability, such as the valve, are bolted onto the assembly to provide easy access for maintenance and repair. The injector and chamber were anticipated to have higher reliabilities and are, therefore, welded together to reduce engine weight. This configuration is also more reliable since it eliminates two injector-to-chamber seals (the fuel-to-hot gas seal and the fuel-to-ambient seal). If either the injector or chamber is damaged, they can be removed by machining to save the undamaged part.

TABLE 2

GENERAL GROUND RULES

• ENGINE ASSEMBLY INCLUDES	THRUST CHAMBER
	INJECTOR (IGNITER FOR LOX)
	THROAT GIMBAL RING (7 DEGREE)
	SERIES/PARALLEL VALVE
	DUCTS
• COOLING CONCEPTS	REGENERATIVE AND DUMP/FILM
• MINIMUM CYCLE LIFE CAPABILITY	1000 CYCLES
• OPERATING DURATION	15 HOURS
• CONTRACTION AREA RATIO	2
• NOZZLE LENGTH	70 PERCENT
• RADIATION SKIRT MATERIAL	COATED COLUMBIUM $1600 < T \leq 2400$ F
	COATED TITANIUM $T \leq 1600$ F
• VALVE AND INJECTOR MATERIAL	CRES
• VALVE ACTUATION	PNEUMATIC

Valve Position Indicator

Valve Actuator Connector

Fuel Inlet

Pneumatic Inlet

Oxidizer Inlet

Injector Face

Engine Mount Plane

Gimbal Plane

19.9

19.9

76.0

50.0 Dia

R-9686/1-3
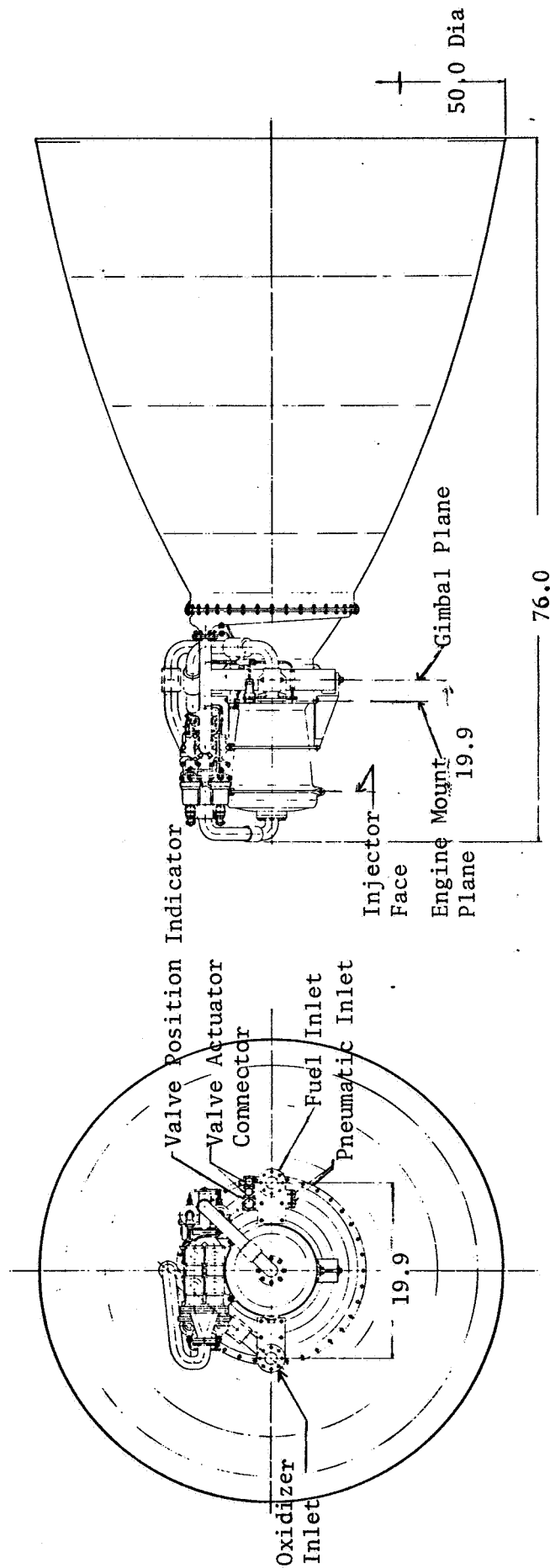
Figure 2   Regeneratively Cooled OME

50.0
$\epsilon = 75$

73.2

Gimbal Plane

Injector Face

Engine Mount
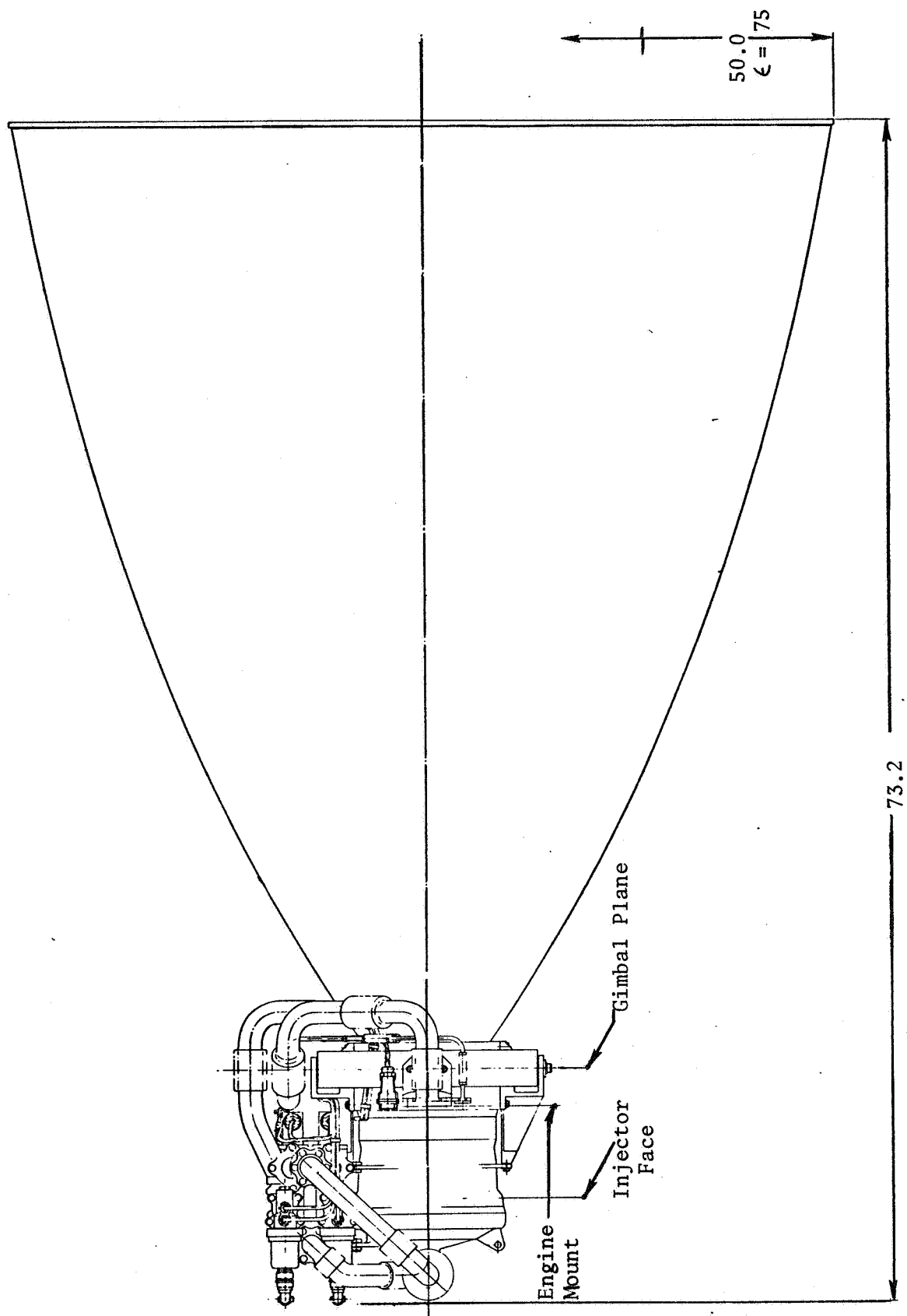
Figure 3 . Dump/Film Cooled OME

Figure 4 . SS/OME Assembly

VALVE POSITION INDICATOR CONNECTOR

VALVE ACTUATOR CONNECTOR

FUEL INLET

VALVE ACTUATION MODULE

R-9686
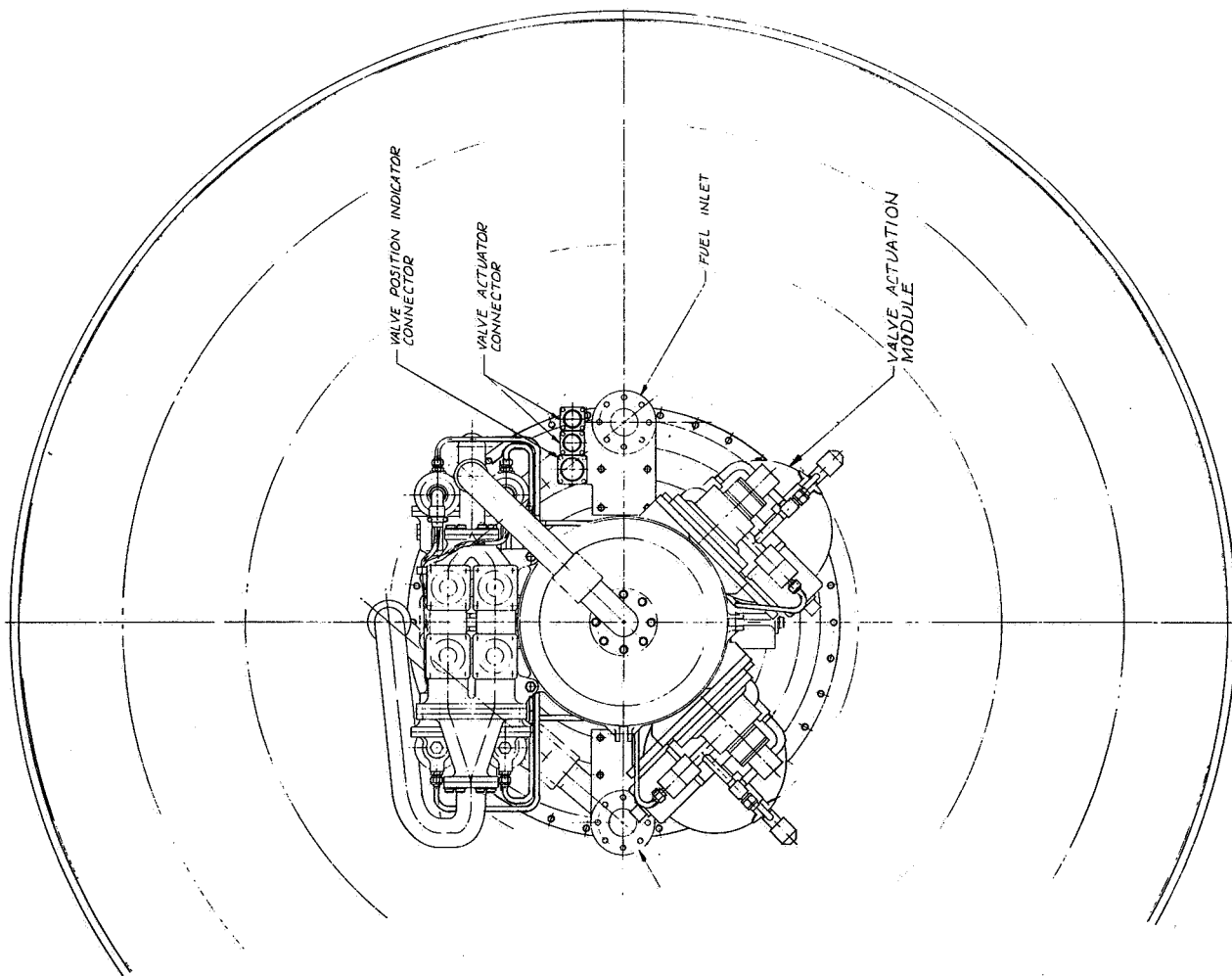
All propellant ducts, the nozzle skirt, the propellant valves, valve actuation system, and the gimbal ring are bolted assemblies in the regeneratively cooled engine. Additional weight savings could be effected by welding these components. The film cooled engine nozzle is welded to form an integral part of the combustor (both columbium).

The OME flightweight valve is a quad-redundant valve (four valves in a series parallel arrangement) to provide redundancy with either a failed open or failed closed valve. Individual oxidizer and fuel valves are mechanically linked to ensure mixture ratio control should a single valve malfunction. Each oxidizer/fuel valve combination is operated pneumatically by its own actuator and pilot valve.

A ball type closure element provides low actuation force requirement and, therefore, low valve assembly weight. A low pressure drop in the valve ensures that the engine will operate within specified limits if a valve malfunction occurs. Loss of electrical signal to any valve results in closing of the valve by pneumatic and spring forces. The valve will, therefore, continue to operate with an increase in ΔP of approximately 5 psi if electrical or pneumatic control of one side is lost.

Injectors with the appropriate type elements were selected for each propellant combination. Coaxial element orifices were specified for the LOX/C$_3$H$_8$ propellant combination. Impinging stream injectors were chosen for the other propellant combinations. Oxidizer enters the center of the injector where in the cases where LOX is the oxidizer, provision was made for an electrical spark ignition system. The injectors have provisions for acoustic cavities to suppress combustion instabilities.

Thrust is transmitted through the gimbal ring to the thrust mount pickup plates. These plates also serve as locators for the inlet ducts, electrical connectors, and for instrumentation connections. The gimbal assembly is located at the thrust chamber throat plane and provides the capability of gimbaling the engine through angles of ±7 degrees maximum in both the pitch and yaw axes.

The OME thruster consists of a regenerative or film cooled combustor to which is attached a radiation cooled nozzle to reduce weight and coolant requirements. Uppass cooling was selected for the regeneratively cooled chamber to simplify the ducting and to minimize volume. The regeneratively cooled portion of the thrust chambers utilize channel wall construction with an electroform nickel close-out on the outer wall. Combustion chamber lengths were selected as approximately optimum for each of the conditions analyzed.

Small amounts of film cooling were used to supplement the regenerative cooling for MMH and 50-50 fuels. Supplemental film coolant was not used with LOX/C$_3$H$_8$, LOX/RP-1 and LOX/N$_2$H$_4$ because of the high decomposition temperatures for propane and RP-1 and because of the low mixture ratio for LOX/N$_2$H$_4$.

For dump/film cooled engine the combustion chamber and nozzle, to an area ratio of 3, is insulated to maintain an outer wall temperature of 600 F. Some of the fuel entering the injector manifold is diverted to the chamber through the sleeve and dumped into the combustion chamber. The liner for the dump/film cooled combustion chamber is press fitted into the shell and utilizes channels which are constant width and constant depth.

Corrosion resistant steel was selected for the valves, injector, and regeneratively cooled chamber liner (except the O$_2$/C$_3$H$_8$ chambers for which a copper liner was chosen because of its good propellant compatibility). The higher strength of INCO 625 was used to prevent buckling of the liners in the film cooled engines. Electroformed nickel was the closeout material on regeneratively cooled chambers. Silicide coated Columbium was specified for the film cooled chamber and for all nozzles in the region of high heat flux. At lower heat fluxes (higher area ratios) titanium was used to reduce weight.

Life capabilities were determined for the regeneratively cooled and dump/film cooled thrust chambers. Each concept is limited by a different damage mechanism: the regeneratively cooled chambers by fatigue; the dump/film cooled chambers by creep.

Under most severe operating conditions, the CRES liners of the regeneratively cooled chambers were predicted to have a fatigue life of approximately 7000 cycles which, with a safety factor of 4, still exceeds the 1000 cycle requirement. Fatigue life for the copper channel wall chamber (O$_2$/C$_3$H$_8$) is much higher than for CRES. The creep analysis for the dump/film cooled chambers indicated a 75 percent damage fraction in the 15-hour required operating time including a safety factor of 4.

OME point design characteristics for the various propellants and cooling methods are listed in Table 2 for engines with a 50-inch static external exit diameter. Mixture ratios for engines using NTO/MMH and NTO/50-50 are based on equal propellant tank volumes. For the other propellants, the mixture ratio is that which yields maximum delivered specific impulse. Engine lengths are measured from the top of the oxidizer duct to the end of the radiation cooled nozzle; combustor lengths from the injector face to the throat plane. Engine inlet pressures are the pressures at the vehicle connect point and include the pressure drops through all engine components.

TABLE 3

OME POINT DESIGN CHARACTERISTICS

Propellant	NTO/50-50	NTO/50-50	NTO/MMH	NTO/MMH	O₂/MMH	O₂/MMH	O₂/C₃H₈	O₂/RP-1	O₂/N₂H₄	O₂/50-50
Cooling Method	R/F/R	D/F/R	R/F/R	D/F/R	R/F/R	D/F/R	R/R	R/R	R/R	R/R
Chamber Pressure, psia	125	125	125	125	100	100	100	100	100	100
Expansion Ratio	72	72	72	72	58	58	58	58	58	58
Mixture Ratio	1.6	1.3	1.65	1.65	1.2	1.0	2.6	2.5	0.8	1.2
Delivered I_s, sec	313.9	297.9	313.0	304.8	331.6	318.5	339.3	324.0	331.5	328.3
Engine Weight, lb	185	150	185	150	210	180	258	223	207	210
Engine Length, in.	73	70	73	71	74	72	77	86	77	72
Rad. Attach ϵ	7	3	7	3	6	3	21	5	6	6
Extension Material	Cb/Ti	Cb/Ti	Cb/Ti	Cb/Ti	Cb/Ti	Cb/Ti	Ti	Cb/Ti	Cb/Ti	Cb/Ti
Combustor Length, in.	11	8	11	9	12	10	15	24	15	10
Contraction Ratio	2	2	2	2	2	2	2	2	2	2
Liner Material	CRES	CRES	CRES	CRES	CRES	CRES	Copper	CRES	CRES	CRES
Min. Channel Height, in	.062	.025	.062	.025	.068	.025	.160	.250	.145	.071
Number of Channels	180	514	180	514	202	565	172	202	202	202
Film Coolant Flow, pct	2.9	13.5	2.0	8.4	2.6	9.4	0	0	0	2.7
Sleeve Length, in.	-	2.7	-	2.2	-	2.7	-	-	-	-
Engine Inlet Pressure Ox/Fuel, psia	169/195	169/177	169/189	169/177	138/153	138/138	138/159	138/144	138/150	138/156
Cooling Jacket ΔP, psi	21	6	16	6	14	7	20	3	11	17
Injector Ox ΔP, psia	23	23	23	23	18	18	23	23	18	18
Injector Fuel ΔP, psi	27	30	27	30	18	18	23	23	18	18

R/F/R   Regen/Film/Radiation
D/F/R   Dump/Film/Radiation
R/R   Regen/Radiation

F = 6000 lb
Dexit = 50 in.
7 Degree Gimbal
70 Percent Nozzle

The regeneratively cooled engines deliver higher specific impulse performance than the film cooled engines and have higher engine weights and fuel inlet pressures.

The effects of specific impulse, engine weights, and inlet pressure on loaded OMS weight were determined using nominal OMS weight and trade factors. The results of the cooling method comparison shown in Table indicate that the regeneratively cooled engine results in a lower OMS weights than the film cooled engine. The results of the propellant comparison for regeneratively cooled OME systems are also shown in Table 4. NTO/50-50 yields a slightly lower system weight than NTO/MMH. The lowest system weight is achieved with LOX/MMH.

1.2 TECHNOLOGICAL AND OPERATIONAL FACTORS

Chamber cooling methods and propellant combinations were also compared qualitatively with respect to complexity, reliability, maintainability, safety, development risk, and ecological factors.

Complexity

The regeneratively cooled chamber was rated as slightly more complex than the film cooled design because of the greater number of joints and manifolds and the full length double wall construction. Complexity features associated with the film cooled chamber were tighter tolerances on small channel dimensions, insulation requirements, and potential requirements for propellant sequencing at cutoff to control thermal soakback.

NTO/MMH was estimated to involve the least complexity followed closely by NTO/50-50. The high freezing point of 50-50 compared to MMH and resulting possible requirements for heaters was responsible for its lower rating. Propellant combinations using LOX as the oxidizer were significantly more complex. The primary factors increasing the complexity associated with LOX engines were the requirements for ignition and purging systems, and the complexities associated with cryogenic propellant operation. Handling RP-1 would be less complicated than the amines because of its lower vapor pressure and toxicity.

Reliability

A detailed reliability assessment of the regenerative and film cooled engines was provided. The regeneratively cooled engine was estimated to be more reliable primarily because of the redundant nature of the double wall, lower operating temperatures, the significantly greater development

TABLE 4

OVERALL OME DESIGN POINT COMPARISON OF COOLING METHODS

PROPELLANTS	NTO/MMH (MR=1.65)		NTO/50-50 (MR=1.60)		O$_2$/MMH	
COOLING	REGENERATIVE	FILM	REGENERATIVE	FILM	REGENERATIVE (MR=1.2)	FILM (MR=1.0)
I$_s$, sec	313.1	304.8	313.9	297.9	330.9	318.0
$\triangle$W$_{I_s}$, lb	Ref.	+681	Ref.	+1312	Ref.	+877
W$_{eng}$, lb	185	150	185	150	210	180
$\triangle$W$_{eng}$, lb	Ref.	-70	Ref.	-70	Ref.	-60
Max. P$_{in}$, psia	189	177	195	177	153	138
$\triangle$W$_{P_{in}}$, lb	Ref.	-71	Ref.	-106	Ref.	-105
$\Sigma\triangle$W, lb	Ref.	+540	Ref.	+1136	Ref.	+712

OVERALL OME DESIGN POINT COMPARISON OF PROPELLANT COMBINATIONS

PROPELLANTS	NTO/MMH	NTO/50-50	O$_2$/MMH	O$_2$/50-50	O$_2$/RP-1
OMS Weight, lb	27,350	27,300	27,050	27,240	27,790

R-9686

1-10

and operational experience, the lower sensitivity to contamination, and the higher performance. Simplicity was determined as the primary reliability asset of the film cooled engine.

A detailed reliability assessment of the candidate propellant combinations was also provided. The NTO/MMH and NTO/50-50 propellant combinations were determined more reliable than the propellants using LOX for the same reasons described for the complexity evaluation. In addition, the tendency of LOX propellant combinations to produce detonable gels with RP-1 and amine fuels reduced system reliability.

Maintainability

Maintainability comparisons were based on lowest maintenance and servicing (including propellants) requirements and ease of performing maintenance if required. Maintainability of the regenerative and film cooled engines were evaluated as approximately equal. Both required no scheduled maintenance.

NTO/MMH and NTO/50-50 were estimated to have approximately equal reliabilities, no scheduled maintenance, and equal ease of performing unscheduled maintenance. The lower reliability of the propellants which use LOX lowered the ranking of the LOX/RP-1 relative to the amine fuels.

Safety

Handling, testing, and operating aspects of safety were evaluated for the candidate cooling modes and propellants. The double wall features of the regenerative cooled chamber provides a safety margin, should a hot wall crack occur, not present in the film cooled engine which was considered susceptible to this failure mode due to the high operating temperatures and requirement for a coating for material compatibility.

Reliability considerations indicated a greater safety for NTO relative to LOX. The low toxicity and vapor pressure of RP-1 was a safety advantage relative to amine fuels.

Development Risk

The relative certainty of providing an OME which could meet the specified requirements with a modest development program was evaluated based on existing technology and anticipated development requirements. Because considerably more experimental data are available on technology, developmental, and operational regeneratively cooled engines compared to

buried film cooled engines, the regeneratively cooled engine was predicted to have the lower development risk.

Critical areas specified at that time (September 1972) for OME development with NTO/Amine propellants were:

1. Propellant valve cycle life and reusability

2. Combustion stability

3. Restart capability

4. Columbium coating compatibility with the shuttle duty cycle and environment

When comparing propellant combinations, NTO/MMH and NTO/50-50 had the lowest development risk because of the large available technology base. LOX/RP-1, although widely used in larger nonreusable, nonrestartable engines presented more areas where technologies applicable to the OME condition have not been adequately explored. LOX/MMH and LOX/50-50 had the smallest technology base.

Additional critical technology areas associated with LOX/RP-1 and LOX/Amine systems were defined as:

1. Ignition

2. LOX/RP-1 performance and heat flux (carbon deposition) characteristics at OME conditions

Ecology

Evaluation of the impact of production of the propellants on the earth environment was beyond the scope of the contracted study. The quantity of propellants and combustion products exhausted into space by the OME was estimated to be so small and distributed as to constitute a negligible ecological factor. Thus, only the impact of using the various propellants on the earth environment during ground test was evaluated.

The combustion products of the various propellant combinations were determined for expansion to a nozzle exit area ratio corresponding to a 50-inch diameter and a 6K thrust level. The temperature of the combustion gases at these exit conditions was less than 1000 F so that further reactions of these constituents between themselves do not take place. The two

constituents which directly affect air quality are carbon monoxide (CO) and nitrogen oxide (NO). The NO emission rate for all propellant combinations was less than the 1975 emission standard of 5 grams per horsepower hour applied to heavy duty vehicles. At the nozzle exit the carbon monoxide content of LOX/RP-1 was approximately four times the 1975 standard of 25 grams per horsepower hour. However, it was anticipated that most of this carbon monoxide would burn off and the resultant concentration to be within the standard value.

Therefore, it appeared that the emissions of all the candidate propellant combinations would be acceptable by the 1975 heavy duty vehicle standards. However, for purposes of comparison, the LOX/Amine propellant combinations produced more NO than the NTO/Amine propellant combinations and MMH produced less NO than 50-50. With respect to CO, the oxidizer appeared to be less significant than the fuel. LOX/RP-1 produced approximately twice as much CO as NTO/MMH. Actual injectors produce small amounts of finely divided unburned carbon with LOX/RP-1 which results in sooty exhaust.

Comparison

The comparison of regenerative and film cooled engines based on technological and operational factors is summarized in Table 5. Regenerative cooling was judged better considering all factors. The same considerations led to selection of NTO/MMH as the best propellant combination followed closely by NTO/50-50. The order of preference for the remaining candidates was O_2/RP-1, O_2/MMH, and O_2/50-50. The last two propellant combinations were closely ranked.

Inclusion of the performance factors shown in Table 4 served to emphasize the preference for regenerative cooling over dump/film cooling. The MMH vs 50-50 comparison was not affected. The poor performance of LOX/RP-1 led to the preference of LOX/MMH as an alternative to the NTO/Amine propellant combinations.

1.3 PROGRAM COMPARISON

Program comparison for the candidate propellants and thrust chambers were made by establishing a baseline program and determining the differences in program cost, program schedule and operational costs for the alternates. The regeneratively cooled N_2O_4/MMH Orbit Maneuvering Engine was selected as the baseline system.

TABLE 5. TECHNOLOGICAL AND OPERATIONAL COMPARISON OF COOLING METHODS

Cooling Method	Complexity	Reliability	Safety	Maintainability	Development Risk	Ecology	Overall
Regenerative Film	Simpler	More Reliable	Safer	Same	Lower Risk	Same	Better

TECHNOLOGICAL AND OPERATIONAL COMPARISON OF PROPELLANT COMBINATIONS

Propellants	Complexity	Reliability	Safety	Maintainability	Development Confidence	Ecology	Overall
NTO/MMH	Simplest	Most Reliable	Safest	Most Maintainable	Lowest Risk	2	Best
NTO/50-50	2	2	2	Most Maintainable	Lowest Risk	3	2
O_2/MMH	4	4	3	3	3	3	4
O_2/50-50	5	5	4	3	3	4	5
O_2/RP-1	3	3	2	2	2	Least Contaminants	3

Development Program

The same development program schedule was projected for the regeneratively cooled and the film cooled engines with NTO/MMH or N_2O_4/50-50. The demonstrated feasibility and hardware fabrication flow times were estimated to be approximately the same; consequently, the major differences between the programs were the hardware costs and propellant costs.

The programs for the nonhypergolic propellants all required the development of an ignition system to provide multiple restart capability. The schedules reflect a thorough DFT program for the ignition system since development of the start and cutoff sequence were critical where a restart was required. RP-1, MMH, and 50-50 contain carbon and, when combined with LOX, can form an explosive gel so that purge sequencing was required as part of the ignition sequence.

Injector and regeneratively cooled thrust chamber feasibility were assumed to be demonstrated for LOX/MMH based on test plans for this contract which were subsequently modified. The similarity between MMH and 50-50 and the significant injector performance experience with these fuels would indicate comparable program schedules and hardware cost, with the major difference being propellant costs. Basic combustion zone length and L* data would be required for the LOX/RP-1 propellant combination before the flight thrust chamber design could be released. This performance optimization and the special testing to evaluate purge effectiveness with the low vapor pressure RP-1 resulted in the longest program through qualification. The propellant costs were considerably lower for the LOX/RP-1 propellant combination.

Maintenance and Logistics

A preliminary maintenance analysis for the OME during the Space Shuttle program operational phase was performed to determine the approximate OME maintenance cost per orbiter vehicle mission duty cycle. Routine and corrective maintenance tasks were investigated as a part of the study, and labor and material costs to support each task were estimated. The routine maintenance tasks, to be performed on a scheduled basis after each flight, were identified by evaluating OME design and vehicle operational concepts. The corrective maintenance tasks, to be performed on an unscheduled basis when an OME problem occurs, and task frequency were identified from OME problem and problem rate projections. Because of the infrequency of the in-vehicle and site engine shop maintenance tasks, a factor of 1.5 was used to cover the less tangible aspects of cost.

The logistics support for the OME fall into the following categories: technical manuals, spares management, logistics engineering and technical services, training, and field engineering support. The increased complexity

of the OME when using nonhypergolic propellant increased the estimated logistics costs. It was assumed that a full-time field engineer would be assigned to the vehicle contractor facility during initial installation and checkout, and would subsequently be relocated at the launch site to support the operational program.

Program Cost and Schedule Comparison Summary

Table 6 is a summary of the program cost and schedule comparisons for the propellant combinations and thrust chambers for the OME. For this comparison, the N_2O_4/MMH propellant combination with the regeneratively cooled thrust chamber was considered the baseline program. All other program schedules, program costs and operational costs were determined as incremental values from the baseline.

As expected, the program with the least demonstrated feasibility testing, the LOX/RP-1 propellant combination with a regeneratively cooled thrust chamber, resulted in the greatest increase in cost. The other development programs with nonhypergolic propellants also cost more than the baseline.

The N_2O_4/MMH film cooled thrust chamber was the least costly program, slightly less than the baseline N_2O_4/MMH regeneratively cooled thrust chamber program, due to lower thrust chamber costs. When the propellant costs for the development program are considered, the N_2O_4/50-50 programs are the lowest in cost and the LOX/MMH programs are the highest (by 1.7 to 1.8 million dollars).

1.4   PARAMETRIC DATA

Extensive parametric engine data was generated for the range of conditions listed in Table 7. The following data were graphically presented in NASA-CR-128675, and NASA-CR-14167.

    Nozzle length
    Engine length
    Exit diameter
    Dynamic diameter (clearance for 7-degree gimbaling)
    Combustor region diameter (for installation purposes)
    Component weights
    Engine weights
    Component pressure drops
    Engine inlet pressures
    ODE and ODK specific impulse
    Boundary layer coolant requirements
    Performance losses for BLC
    Nozzle losses
    Delivered specific impulse

TABLE 6

OME PROGRAM COST & SCHEDULE COMPARISON SUMMARY

PROP.COMB.	Δ SCHEDULE		Δ MANPOWER AND HARDWARE COST		Δ PROPELLANT COST DEVELOPMENT PROGRAM		Δ MAINTENANCE COST PER FLIGHT		Δ COST, SPARES		Δ COST, LOGISTICS	
	REGEN	FILM	REGEN	FILM	REGEN	FILM	REGEN	FILM	REGEN	FILM	REGEN	FILM
N₂O₄/MMH	B.L.*	0	B.L.	-$85,000	B.L.	0	B.L.	0	B.L.	0	B.L.	0
N₂O₄/50-50	0	0	0	-$85,000	-$567,780	-$567,780	0	0	0	0	0	0
LOX/MMH	+10 Wks	+12 Wks	$1,346,000	+$1,401,000	+$282,820	+$363,520	$145(16%)	$145(16%)	$58,000	$58,000	$19,000	$19,000
LOX/50-50	+10 Wks		+$1,346,000		-$414,180		$145(16%)		$58,000		$19,000	
LOX/RP-1	+13 Wks		+$1,486,000		-$706,280		$388(43%)		$58,000		$19,000	

*Baseline

R-9686

1-17

TABLE 7. CONFIGURATIONS ANALYZED

PROPELLANTS	F, K	Pc, PSIA	O/F	ε	COOLING
NTO/MMH	6 (36 cases)	100,125,150,200	1.65,1.45,1.85	40,80,120	REGEN, FILM
	3.5 (3 cases)	125	1.65,1.45,1.85	80	
	8 (3 cases)	125	1.65,1.45,1.85	80	
	10 (3 cases)	125	1.65,1.45,1.85	80	
NTO/50-50	6 (36 cases)	100,125,150,200	1.6,1.4,1.8	40,80,120	REGEN, FILM*
	3.5 (3 cases)	125	1.6,1.4,1.8	80	
	8 (3 cases)	.125	1.6,1.4,1.8	80	
	10 (3 cases)	125	1.6,1.4,1.8	80	
LOX/MMH	6 (36 cases)	75,100,125,200	1.2,1.0,1.4	40,80,120	REGEN, FILM
	3.5 (3 cases)	100		80	
	8 (3 cases)	100		80	
	10 (3 cases)	100		80	
LOX/50-50*	6	100 (3 cases)	1.2,1.0,1.4	80	REGEN
	6	75	1.2	80	
	6	125	1.2	80	
	6	200	1.2	80	
LOX/N_2H_4**	6	100(3 cases)	0.7,0.8,1.0	58	REGEN
		75	0.8	43	
		125	0.8	73	
LOX/RP-1	6 (36 cases)	75,100,125,200	2.5,2.3,2.8	40,80,120	REGEN
	3.5 (3 cases)	100	2.5,2.3,2.8	80	
	8 (3 cases)	100	2.5,2.3,2.8	80	
	10 (3 cases)	100	2.5,2.3,2.8	80	
LOX/C_3H_8**	6	100(3 cases)	2.6,2.4,2.8	58	REGEN
		75	2.6	43	
		125	2.6	73	

* abbreviated range
** from preliminary data dump

1.5 SENSITIVITY DATA

The OME configurations were evaluated relative to the effects of propellant inlet pressure and inlet temperature. Two types of analyses were conducted. Initially feasible ranges of pressure and temperature were established based on which the engine would be designed. This range included engine calibration, nominal tank pressure variation, and effect of propellant valve malfunction. From these effects, engine mixture ratio and chamber pressure ranges were established. For the ranges established, the engines were designed to meet engine life requirements and provide adequate safety factors at the most severe off-design conditions (i.e., mixture ratio ±12 percent of nominal, chamber pressure ±10 percent of nominal, and maximum inlet temperature of 90 F).

Once the point designs were established, sensitivity plots were generated of engine mixture ratio and chamber pressure versus inlet pressure and temperature. Delivered specific impulse was determined versus the resultant mixture ratio, and inlet temperature. Both types of analyses were conducted for dump/film and regenerative cooled engines with NTO/MMH and NTO/50-50 propellants. Limited analyses were conducted for LOX/MMH and LOX/RP-1.

The requirement to design for operation at higher than nominal inlet temperatures required design compromises which resulted in the same performance degradation at nominal conditions for regenerative and dump/film cooled engines. The engine using 50-50 fuel was more sensitive than the MMH engine. The MMH fueled engine was also less sensitive to off-design chamber pressure and mixture ratio requirements and the regenertive cooled engine was less sensitive than the dump/film cooled engine.

For a fixed design, the sensitivity of mixture ratio and chamber pressure to changes in tank pressures did not depend on the type of cooling or whether the propellants were NTO/MMH or NTO/50-50. All configurations showed lower sensitivities to anticipated changes in inlet temperature compared to anticipated changes in tank pressure.

2.0   INJECTOR EVALUATION

Subscale and full-scale injectors were designed, fabricated, and tested on this contract under Tasks VI and IX. Prior and concurrent IR&D work at Rocketdyne provided additional injector design and test data. For example, an unlike-doublet element injector was fabricated and tested under IR&D. The injector indicated performance degradation with high temperature fuel and thus led to the selection of the like-doublet element type for the contract injectors. Stability model tests were also conducted under the contract and analysis and evaluation of all available OME experimental data was made. Subscale tests were reported in more detail in NASA-CR-141677 full-scale injector tests in NASA-CR-140358 and NASA-CR-141674; stability analyses and tests in NASA-CR-141676.

2.1   SUBSCALE INJECTOR ELEMENT CHARACTERIZATION

This effort was conducted under Task VI of the contract to evaluate injector configurations designed for a regeneratively cooled engine. The specific objectives of this task were: 1) to determine the optimum like-doublet element geometry for operation at conditions consistent with a fuel regener- atively cooled OME, and 2) to investigate the sensitivity of the impinging triplet element injector to hot fuels. For the like-doublet element injector, tests were conducted to determine: 1) the optimum cant angle and spacing, 2) the minimum number of elements required, 3) the possible turbulent mixing effect as a function of chamber length, 4) the influence of fuel and oxidizer temperatures on performance, and 5) the effects of chamber pressure and mix- ture ratio on C* efficiency. Like-doublet element design parameters and the configurations investigated during this program are shown in Table 8. One O-F-O triplet element injector was investigated having oxidizer and fuel orifices diameters of 0.032 and 0.057 inches, respectively.

A total of 81 tests were conducted during the program. The results of the tests on the like-doublet injectors are shown in Figs. 5 through 7. The optimum element configuration for hot fuel is indicated to be that which has an oxidizer-fuel spacing of 0.4 inches and a cant angle of 45°. For the optimum element configuration, the effects of mixture ratio, chamber pressure, and oxidizer temperature (below 100 F) are seen to be negligible. Performance was almost insensitive to fuel temperature but indicated the possibility of a slight degradation with increasing fuel temperature. The data indicated that no significant increase in performance would take place with chamber lengths greater than 10 inches so that performance was mixing limited beyond that value.

TABLE 8 . SUMMARY OF LIKE-DOUBLET INJECTOR DESIGNS

No.	Part Number	$\alpha°$	$A°$	B	C	N	d_f	d_o
1	AP73-223	60	22.5	.188	.188	3	.0289	.0332
2	AP73-224	60	22.5	.150	.178	4	.0243	.0259
3	AP73-225	60	34.0	.150	.146	4	.0243	.0259
4	AP73-226	60	45.0	.150	.114	4	.0243	.0259
5	AP73-532-011	60	45.0	.100	.417	4	.0243	.0259
6	AP73-532-021	60	34.0	.104	.437	4	.0243	.0259
7	AP73-532-031	60	22.5	.107	.458	4	.0243	.0259
8	AP73-532-041	60	45.0	.100	.265	4	.0243	.0259
9	AP73-532-051	60	34.0	.104	.285	4	.0243	.0259
10	AP73-532-061	60	22.5	.107	.306	4	.0243	.0259
11	AP73-532-011A*	60	45.0	.100	.417	4	.0243	.0289
FS-1	AP72-275	60	22.5	.188	.187	186	.0300	.0345
FS-2	AP72-369	60	34.0	.150	.140	386	.0251	.0263

NOMENCLATURE

$\alpha°$ - Impingement angle of pair

$A°$ - Inclination angle of element

B - Impingement Height

C - Impingement Distance

d_f - Fuel Orifice Dia.

d_o - Oxidizer Orifice Dia.

N - Number Elements

SECTION D-D
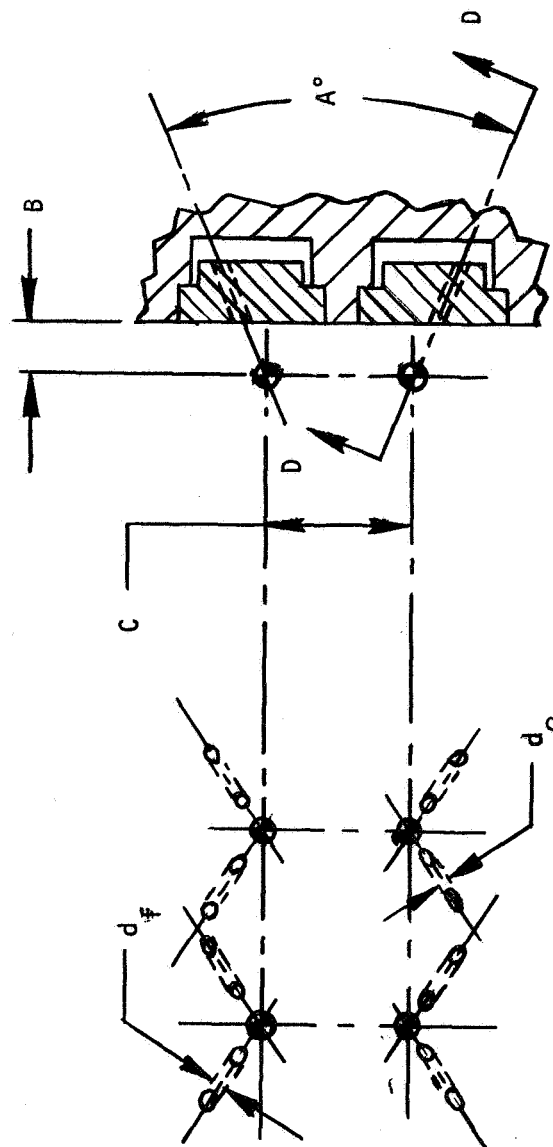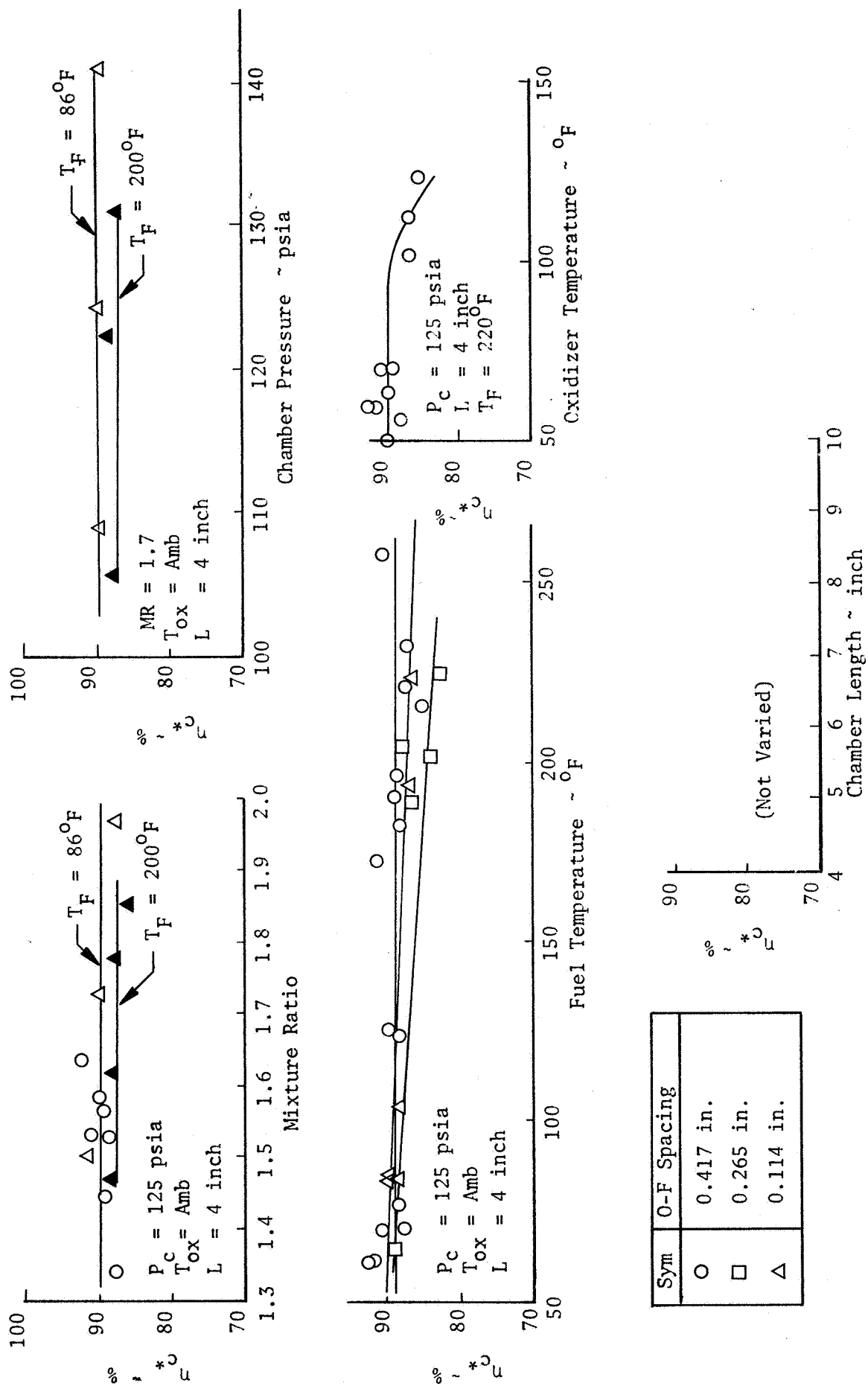
Figure 5   Summary of Experimental Results for 45° Cant Angle
Like-Impinging Doublet Injectors
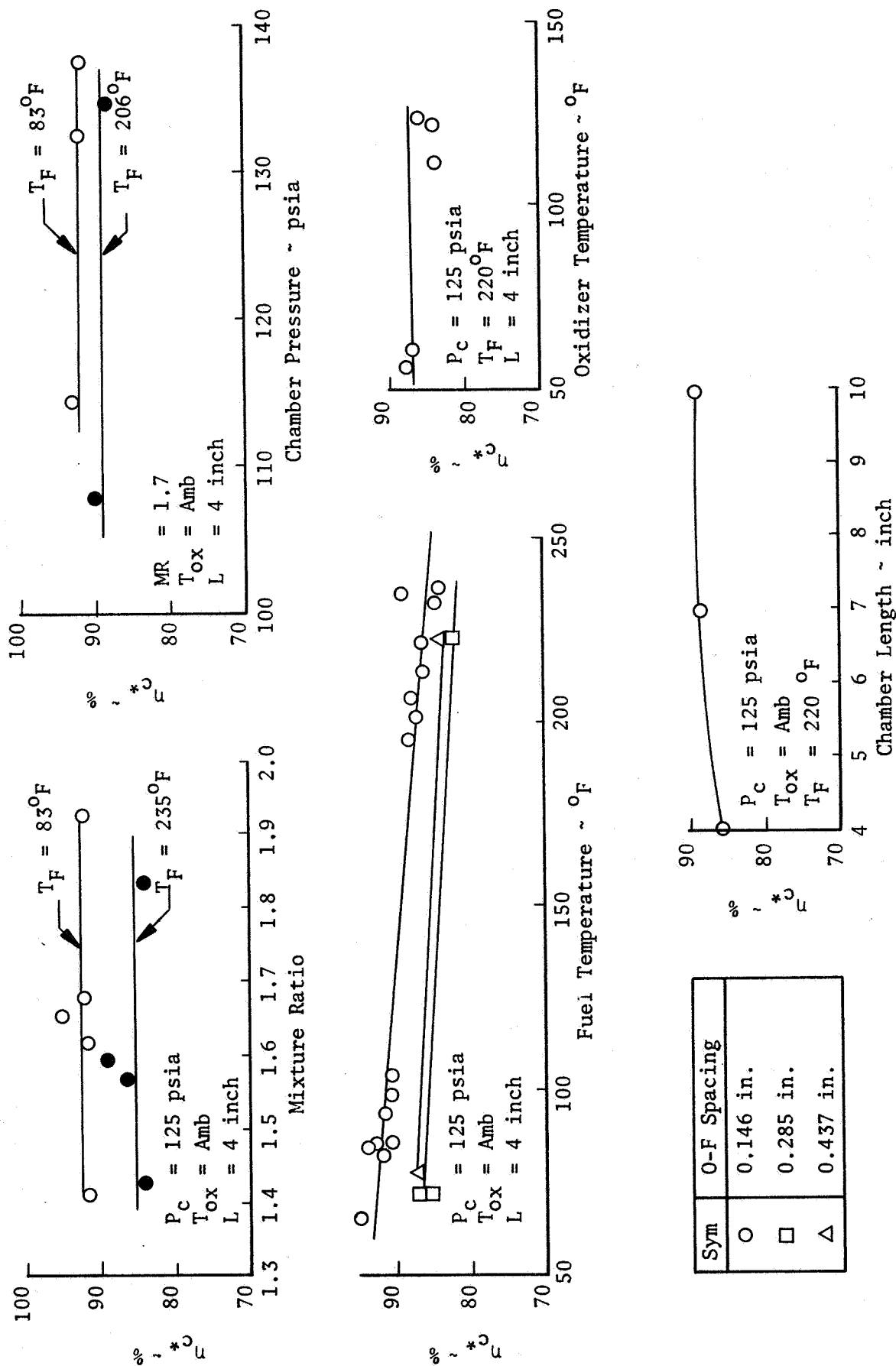
Figure 6 Summary of Experimental Results for 34° Cant Angle Like-Impinging Doublet Injectors
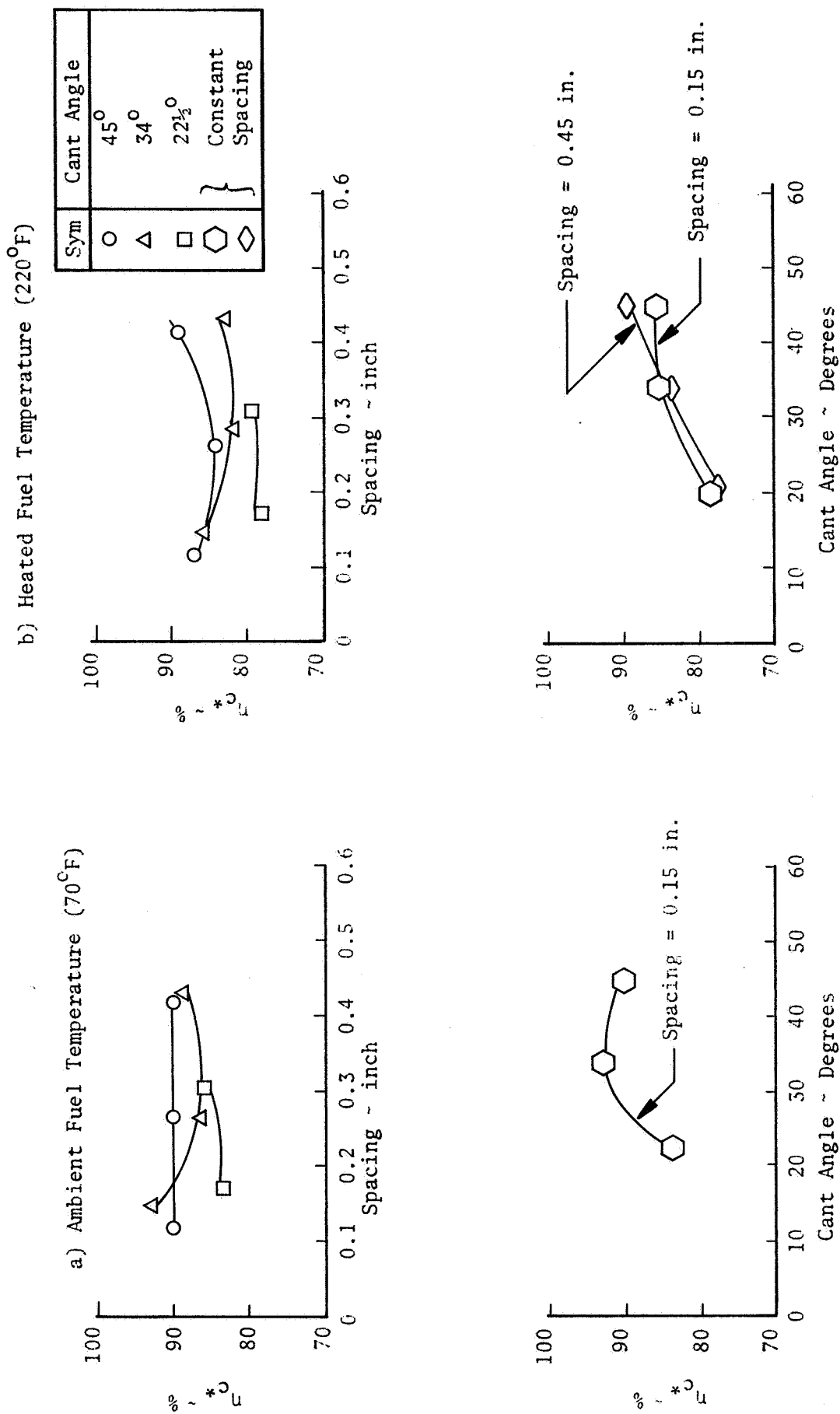
Figure 7   Effect of Cant Angle and Spacing on C* Efficiency for Like-Doublet Injector with Ambient and Heated Fuel

The triplet element test data also indicates an insensitivity to mixture ratio, chamber pressure, and oxidizer temperature as shown in Fig. 8 However, performance was more severely degraded by increasing fuel temperature then that of the like-doublet element. It appeared that the performance of the triplet element would also not increase significantly for chamber lengths greater than 10 inches.

No bombs were detonated in the chamber during these tests. However, the triplet injectors indicated low frequency (300 Hz) oscillations on almost every test. The like-doublet injectors were stable in every case with no indication of pops or oscillations.

The results of the study indicate like-doublet injectors can be designed to avoid blowapart with hot fuels. The optimum like-doublet element configuration was found to be an element with a cant angle of 45° and an oxidizer-fuel separation of approximately 0.4 inches. The performance differences observed between the various subscale configurations would be substantially reduced by inter-element mixing in a full-scale injector.

2.2   FULL-SCALE INJECTOR ELEMENT CHARACTERIZATION

Like-doublet elements were designed and fabricated for OME thrust chambers having contraction area ratios of 2 and 3. The corresponding injector diameters were 8.2 inches and 10 inches. The injector design parameters are shown in Table 8. Primary differences between the injectors, in addition to their diameters, is the number of elements and the element spacing and cant angle. In both cases, the number of elements represented a maximum number which could be conveniently fabricated for the particular element geometry and injector diameter. The spacing and cant angle for the L/D #1 injector were determined from previous injector experience. The values of these parameters for the L/D #4 injector were determined by the subscale tests.

Another important difference between these injectors is the radial sequencing of the fans. In both cases oxidizer fans impinge on fuel fans. However, for the L/D #1 injector each propellant fan is adjacent to a fan of the same propellant on its nonimpinging side. This maximizes interelement mixing for sprays which pass radially through the primary mixing zone without interaction with the opposite propellant in that zone. On the other hand, the radial sequence used with injector L/D #4 in which the fuel and oxidizer fans are radially alternated, provides maximum interelement mixing in the event of propellant blowapart in the primary mixing region.
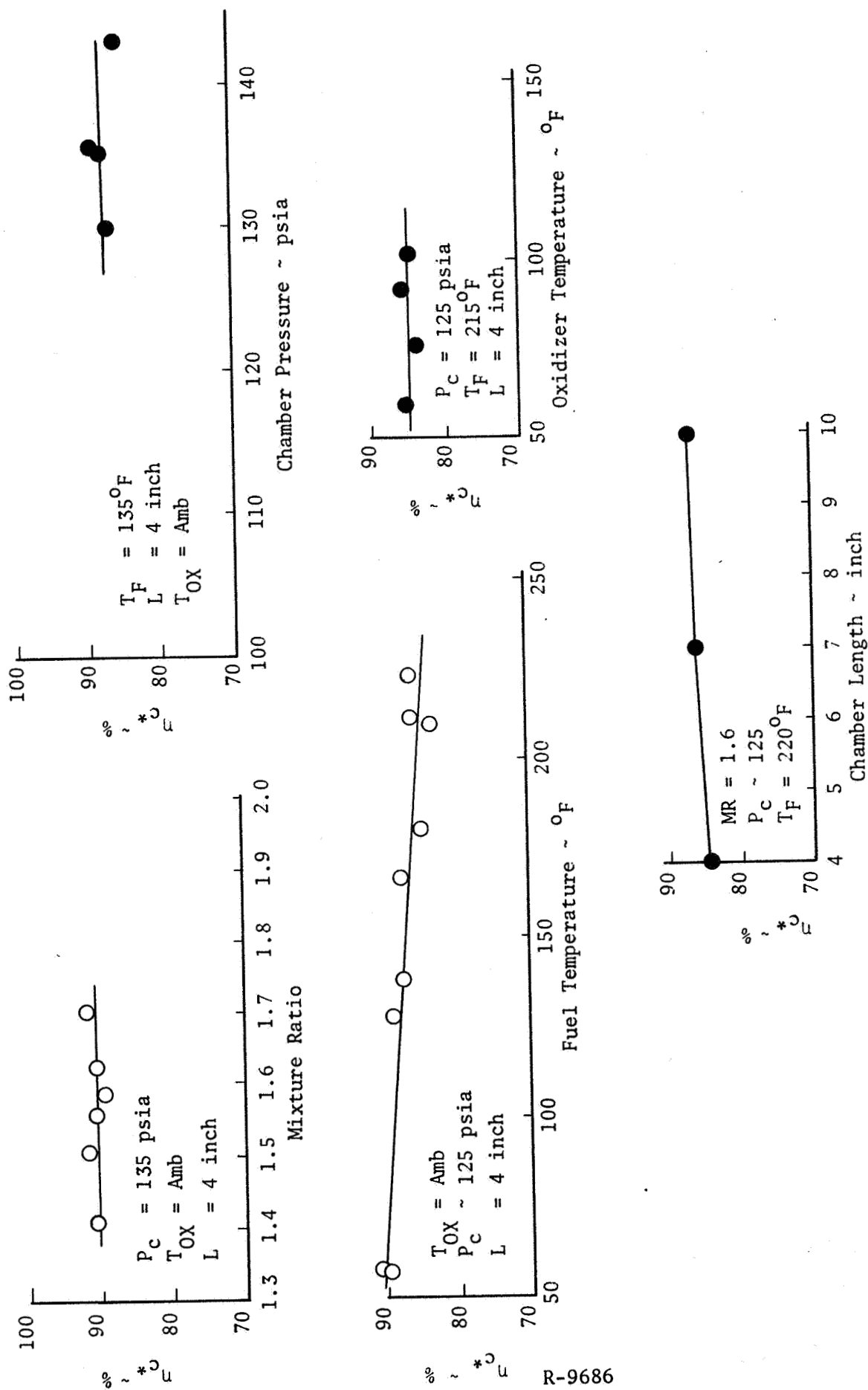
Figure 8   Summary of Experimental Results for an Unlike-Impinging Triplet Injector

R-9686

TABLE 9

LIKE-DOUBLET INJECTOR PARAMETERS

	L/D #4	L/D #1
Face Diameter, Inches	10.0	8.2
Number of Elements	229	186
Orifice Forming	EDM	EDM
Diameter of BLC Orifices (68), Inches	-	0.020
Diameter of Fuel Element, Inches	0.0294	0.028-0.033
Diameter of Oxidizer Element, Inches	0.0309	0.032-0.038
O-F Element Spacing, Inches	0.45	0.19
Impingement Height, Inches	0.101	0.188
Cant Angle, Degrees	45	22.5
Nominal Fuel ΔP, PSI	45	62
Nominal Oxidizer ΔP, PSI	55	55
Radial Sequence	O-F-O-F	O-O-F-F
Stabilization	Acoustic Cavities and Fuel Manifold Dams	Acoustic Cavities and Fuel Manifold Dams
Injector Material	321 CRES	321 CRES

Figure 9 is a photograph of the 8-inch diameter, L/D #1, injector while the 10-inch diameter, L/D #4, injector is shown in Fig.10 . Both injectors were first tested in solid workhorse thrust chambers under sea level conditions to determine performance, thermal, and stability characteristics. A typical hardware cross section is shown in Fig. 11. A combustion chamber consisted of a converging-diverging section and a cylindrical section,one or more of which were used to vary the distance from the injector to the throat. The combustion chamber sections were instrumented with thermally isolated outside wall temperature measurements. The heat flux profile was deduced from the transient temperatures recorded by these thermocouples. Bombs were detonated and high response chamber pressure measurements were made approximately three inches from the injector face to provide stability data for each injector. The initial tests on the L/D #1 injector were made with boundary layer coolant supplied by a separate manifold between the injector and combustion chamber as shown in Fig. 11. Subsequent tests on the L/D #1 injector were made with BLC supplied through orifices drilled around the periphery of the injector. No BLC was used with the L/D #4 injector.

The test programs are summarized in Table 10for both injectors. The performance test results for the L/D #1 injector are shown in Figs.12 through 14. Performance without BLC is shown in Fig. 12 to be fairly insensitive to chamber pressure, mixture ratio, or fuel temperature. The performance with BLC is shown in Fig. 13 to be approximately 1 percent lower. The performance with BLC is quite insensitive to fuel temperature, chamber pressure, or mixture ratio. The injector was tested with a combustion chamber having a smaller throat area in order to provide a contraction ratio of 3 to 1. The performance date obtained with this configuration without BLC are shown in Fig. 14. The data indicates that for a fixed injector diameter, performance would be degraded by increasing the contraction ratio.

Performance of the L/D #4 injector was virtually insensitive to chamber pressure, mixture ratio, or fuel temperature. The performance of the L/D #4 injector was expected to equal or exceed that L/D #1 because of the more optimum element configuration of the former injector. However, the results shown in Fig. 15 show the lower performance of the L/D #4 injector over the range of chamber lengths of interest. The lower performance of the L/D #4 was attributed to the radial sequencing of the elements or to oxidizer orifice hydraulic characteristics (the discharge coefficient of the oxidizer side of the L/D #4 was 0.66).

Another L/D element injector, L/D #2, having an 8-inch diameter was tested in solid wall hardware. This IR&D injector had more elements and modified element characteristics relative to L/D #1. The performance and the heat flux profile of the L/D #2 injector were similar to that of L/D #1. The L/D #2 injector was used primarily on Contract NAS9-12524.
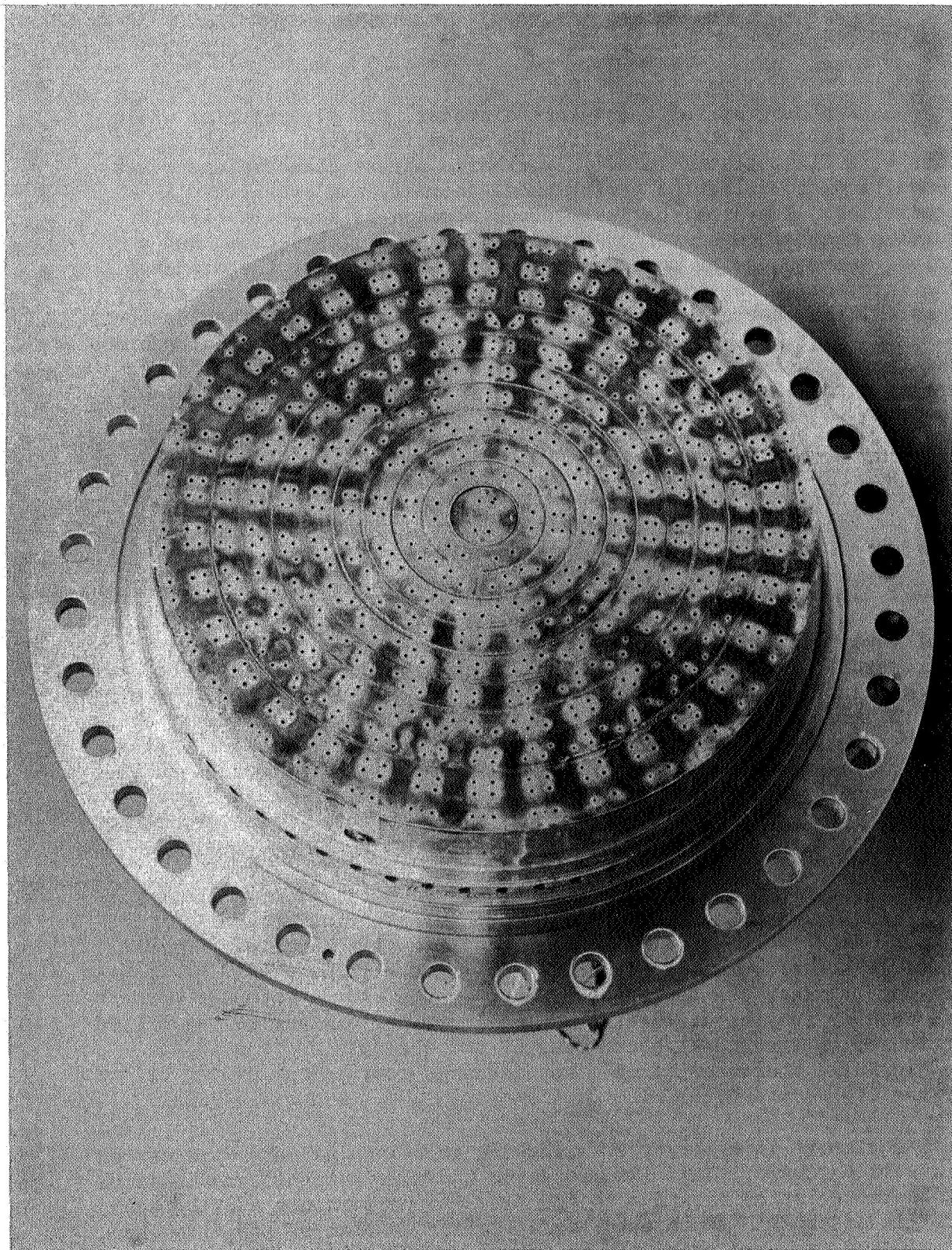
Figure 9. L/D #1 Injector
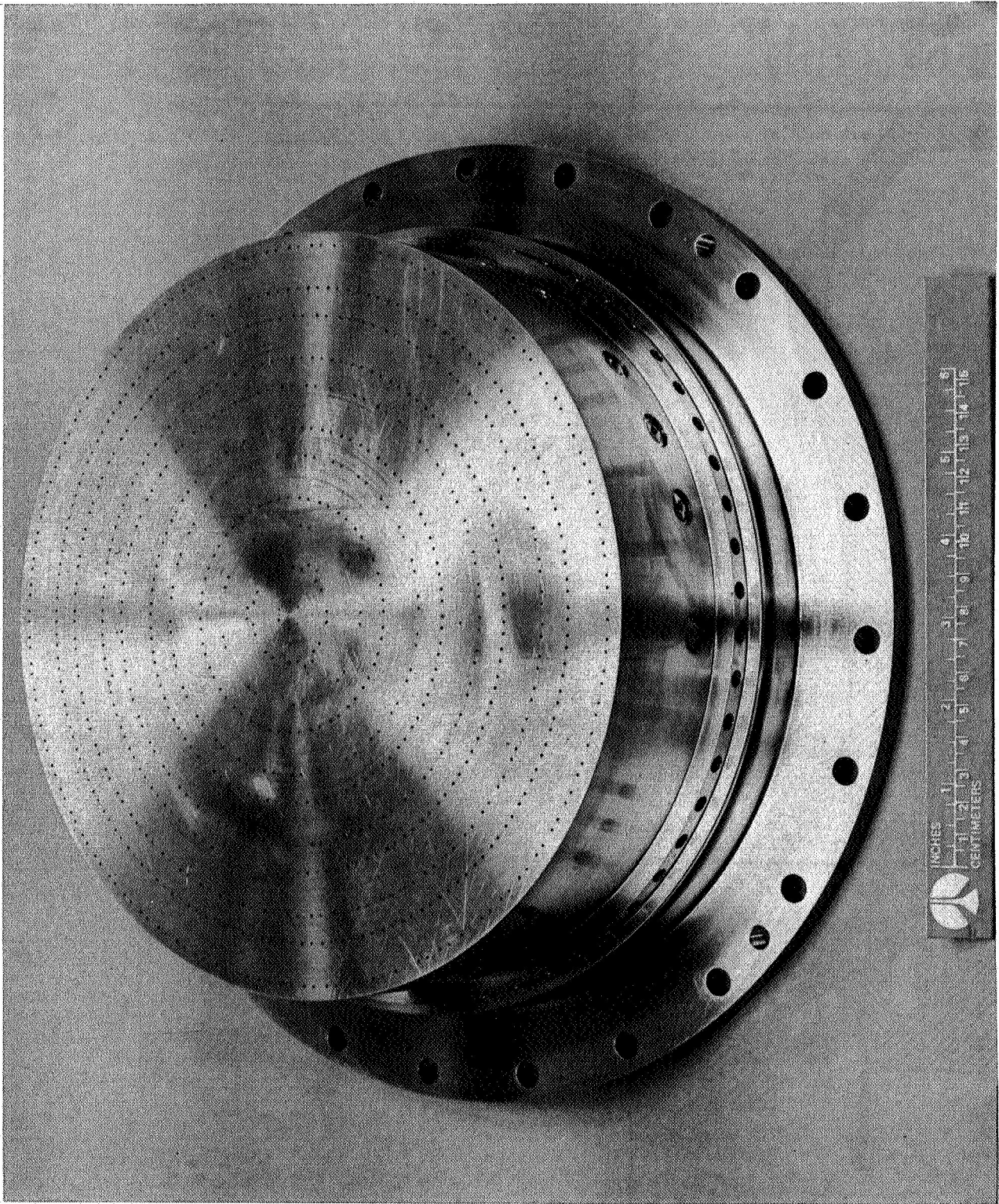
Figure 10. L/D #4 Injector
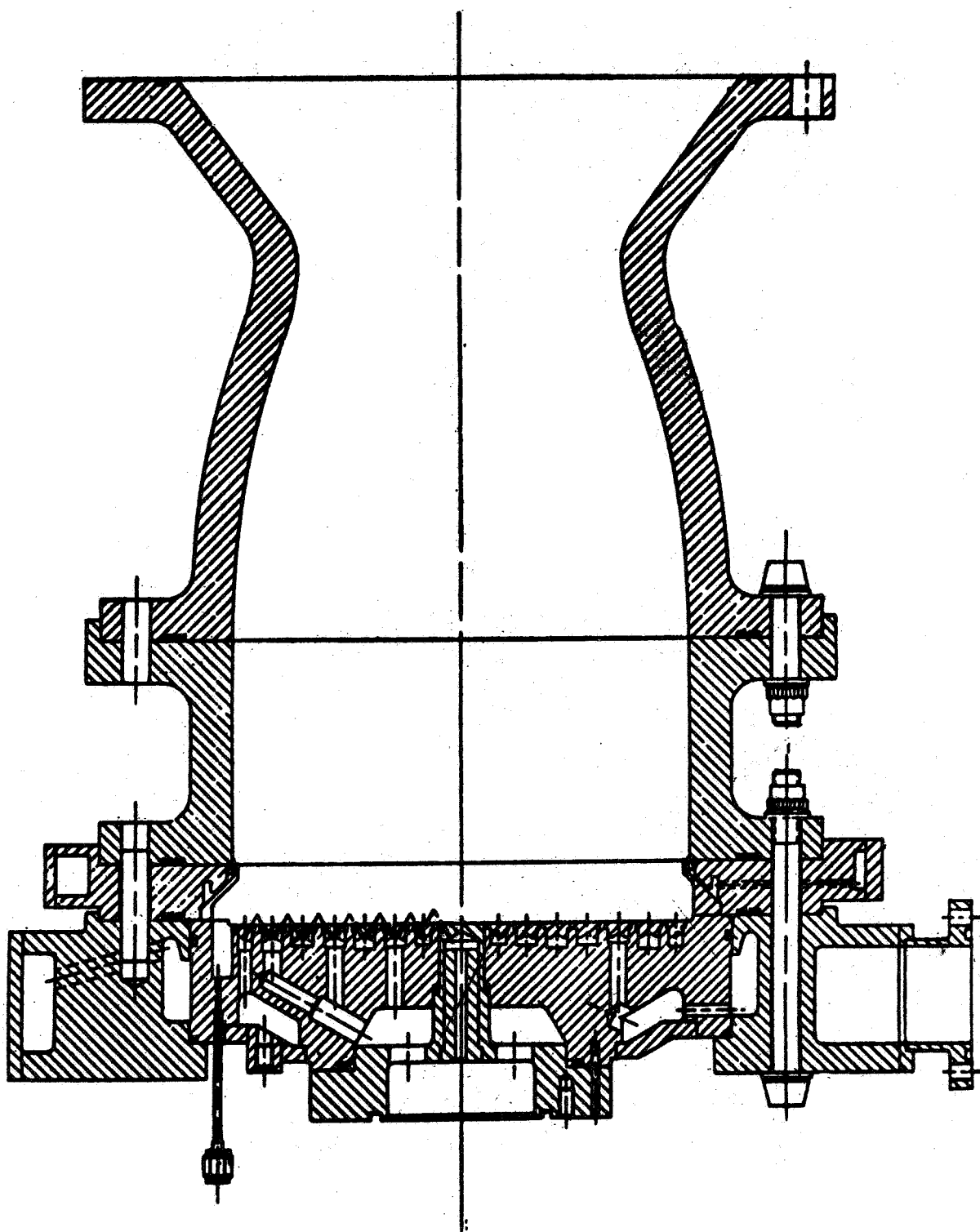
Figure 11. Uncooled Thrust Chamber Assembly

TABLE 10 FULL SCALE INJECTOR STABILITY TEST SUMMARY

Test	Dur. Sec	Pc_{NS}, PSIA	O/F	Fuel Temp., F	Comments
1	3.7	130	1.80	180	L/D #1 injector tests 1 through 18 14.8 percent acoustic cavity area, σ
2	1.1	126	1.71	190	
3	0.9	125	1.69	160	
4	5.1	140	1.55	165	
5	4.7	113	1.52	165	
6	4.7	111	1.79	175	
7	4.7	137	1.52	175	Added radial dams to injector fuel manifold
8	4.6	123	1.66	160	
9	5.0	141	1.86	165	
10	4.7	111	1.42	150	
11	4.7	136	1.44	220	Reduced σ from 14.8 to 12 percent
12	4.6	127	1.68	205	
13	4.6	140	1.80	195	
14	4.7	111	1.45	190	
15	4.6	111	1.84	175	
16	4.7	127	1.61	175	
17	4.7	143	1.65	170	
18	4.7	128	1.69	160	
19	4.7	140	1.70		L/D #4 Injector Tests 19 through 46 σ = 10 percent; effective length, ℓ, = 2.08 inches
20	3.7	134	1.84	217	
21	3.7	136	1.54	210	
22	1.6	118	1.73	162	
23	2	132	1.67	180	

TABLE 10 (Continued)

Test	Dur Sec	Pc_{NS}, PSIA	O/F.	Fuel Temp., F	Comments
24	3.6	119	1.65	187	
25	1.7	127	1.66	189	σ = 15 percent; ℓ = 1.28 inches
26	1.7	126	1.66	201	
27	4.6	140	1.80	192	ℓ = 2.12 inches
28	4.7	132	1.44	188	
29	4.6	114	1.82	189	
30	4.6	126	1.62	190	
31	4.7	140	1.61	185	
32	4.6	110	1.48	176	
33	4.6	110	1.63	188	
34	2.2	126	1.67	187	
36	4.7	125	1.62	70	
37	3.6	139	1.86	68	
38	3.7	139	1.64	65	
39	3.6	129	1.42	65	
40	4.7	125	1.69	225	Injector-to-throat distance increased from 12 to 16 inches
41	4.7	140	1.86	200	
42	4.7	140	1.54	194	
43	4.7	112	1.88	183	
44	4.7	111	1.71	194	
45	4.7	126	1.66	183	
46	4.7	140	1.70	198	
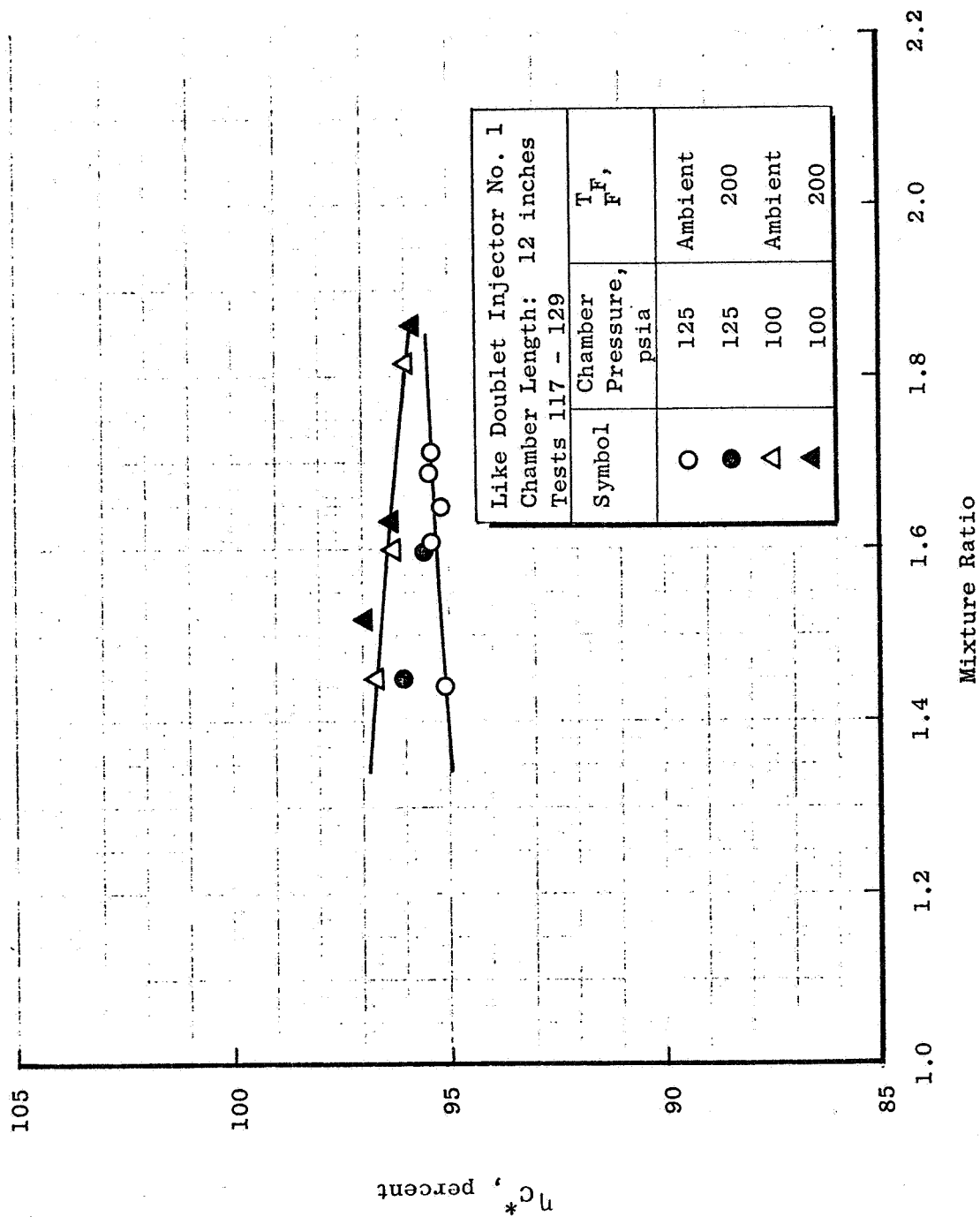
Figure 12. Characteristic Velocity Efficiency vs Mixture Ratio
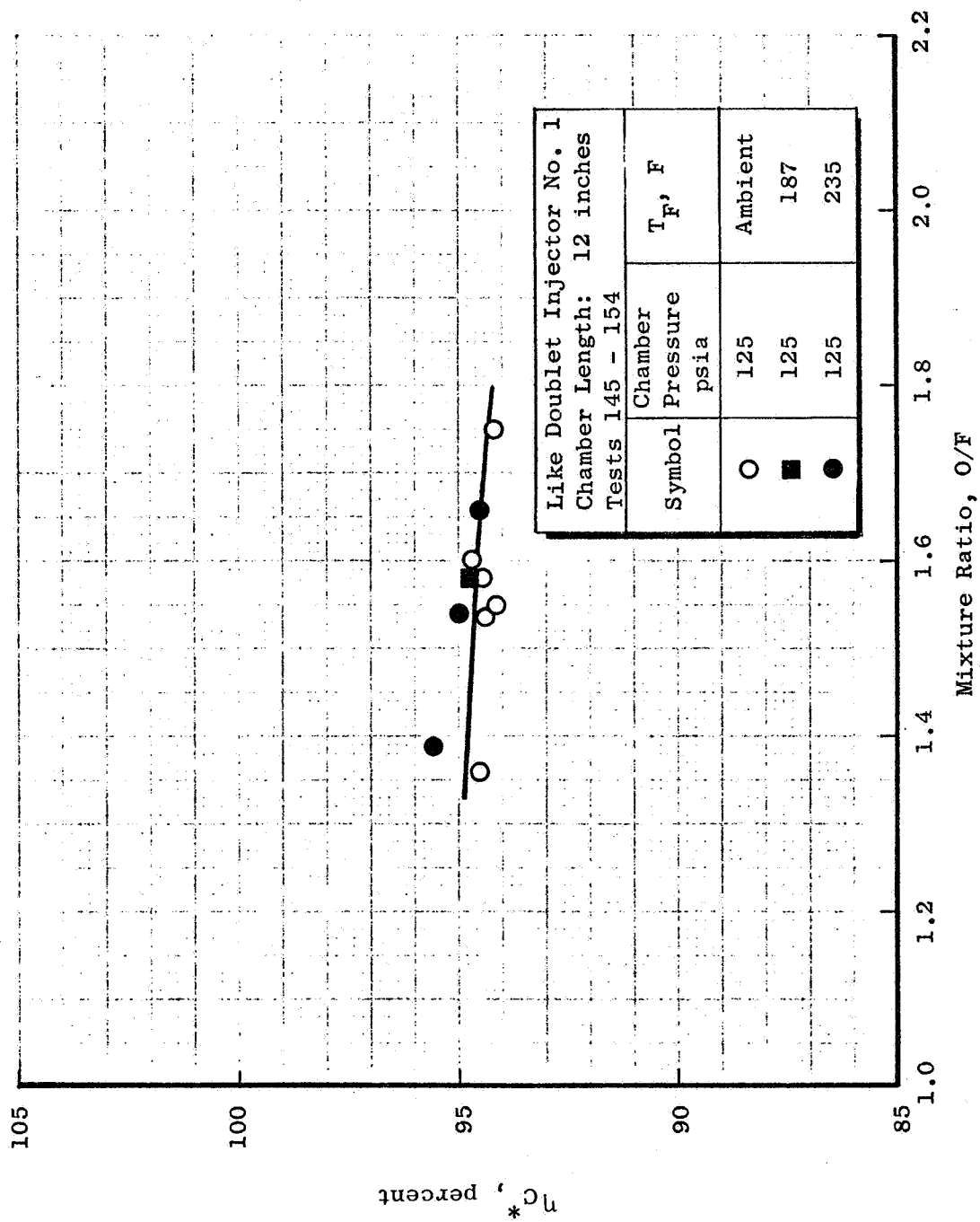
Figure 13 Characteristic Velocity Efficiency vs Mixture Ratio

Like Doublet Injector No. 1
Chamber Length: 12 inches
Contraction Ratio: 3:1
Tests 135 - 144

Symbol	Chamber Pressure, psia	T_F, F
□	180	Ambient
◼	180	200
○	150	Ambient
●	150	200
△	120	Ambient
▲	120	200

ηc^*, percent
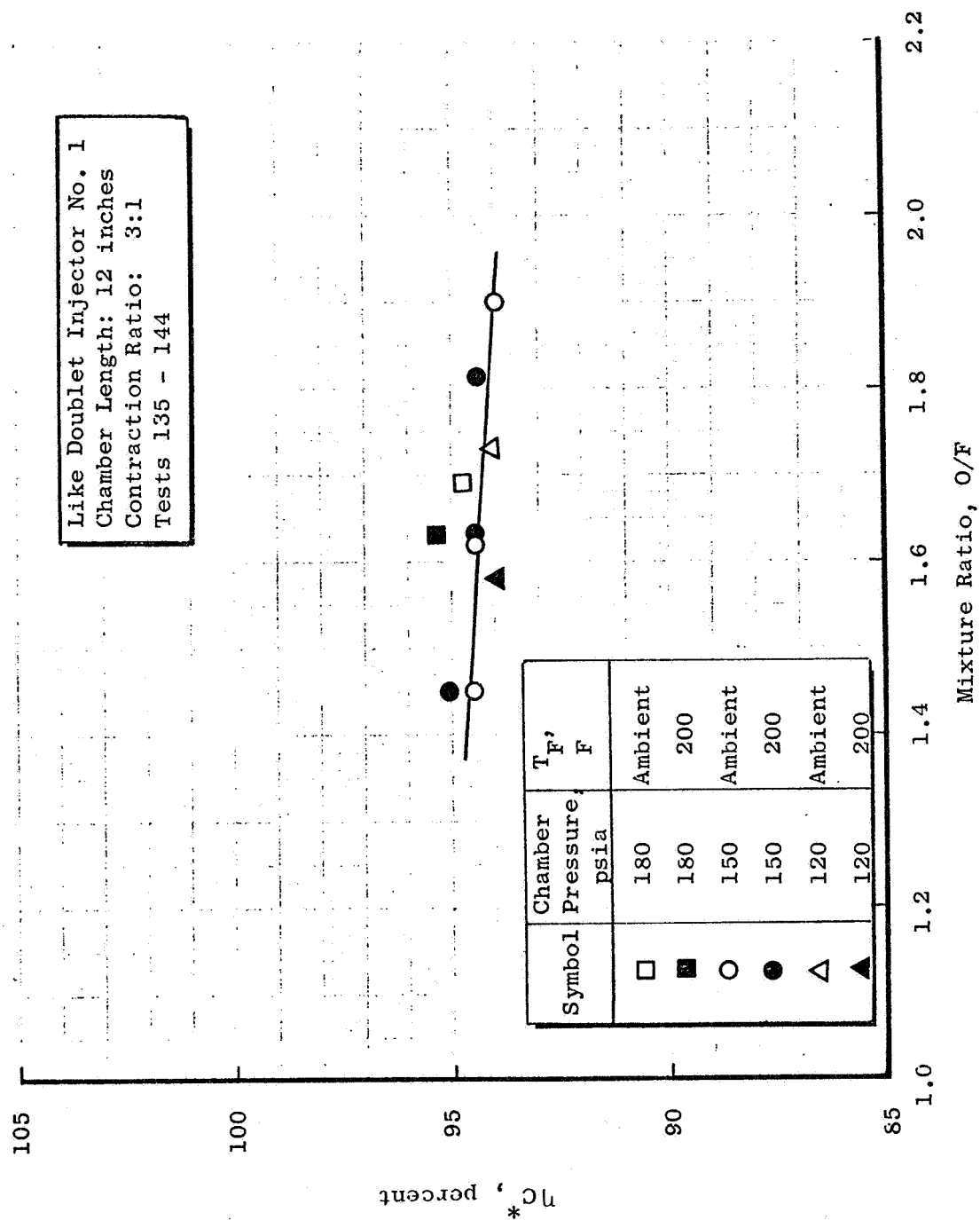
Mixture Ratio, O/F

Figure 14. Characteristic Velocity Efficiency vs Mixture Ratio

OME UNLIKE DOUBLET LOW FREQUENCY STABILITY SUMMARY

(Frequency < 1100 Hz)*

RUN	CHAMBER LENGTH, INCH	CHAMBER PRESSURE, PSIA	MIXTURE RATIO	PERCENT BLC	FREQUENCY HZ	AMPLITUDE, PEAK-PEAK, PSI	COMMENTS
96	20	132	1.48	2.72	930-1030	15-40	FROM P_C RISE THROUGHOUT
97	20	138	1.71	2.51	900-1030	15-40	FROM P_C RISE THROUGHOUT
98	20	137	1.35	2.85	900-1030	15-50	FROM P_C RISE THROUGHOUT
99	20	134	1.52	2.69	900-1030	20-40	FROM P_C RISE THROUGHOUT
100	20	112	1.52	2.73	800	10-20	LOW AMPLITUDE THROUGHOUT
101	20	99	1.61	2.68	680	15-20	FROM 1.2 SEC UNTIL SHUTDOWN
102	20	102	1.75	2.56	680	15-20	FROM 1.2 SEC UNTIL SHUTDOWN
103	20	138	1.71	2.52	890-1000	20	THROUGHOUT
104	16	94	1.65	1.25	480	20-70	INITIAL "FOOTBALL" AND FROM 2.1 SEC TO SHUTDOWN
105	16	91	1.55	1.30	480	60	FROM 1.0 SEC TO SHUTDOWN
106	16	92	1.41	1.36	490	50	NEAR END TO SHUTDOWN

* ALL UNLISTED TESTS STABLE

R-9686

2-18

OME UNLIKE DOUBLET HIGH FREQUENCY STABILITY SUMMARY
(Frequency > 3000 Hz)**

RUN	CHAMBER LENGTH, INCHES	CHAMBER PRESSURE, PSIA	MIXTURE RATIO	PERCENT BLC	FREQUENCY HZ.	AMPLITUDE PEAK-PEAK, PSI	COMMENTS
75	8	125	1.82	4.29	3000	50	FIRST TANGENTIAL MODE TRIGGERED BY LOWER FREQUENCY AT 150 MSEC FROM P_C RISE
87	12	130	1.38	2.79	3050	60	BOMB INDUCED FIRST TANGENTIAL MODE
89	12	129	1.59	2.65	3080	60	BOMB INDUCED FIRST TANGENTIAL MODE
(91)	12	SHUTDOWN	1.74	2.49	(2950)		DURING SHUTDOWN, FIRST TANGENTIAL MODE TRIGGERED BY LOWER FREQUENCY
94	12	132	1.51	4.78	3100		SELF INDUCED FIRST TANGENTIAL MODE
97**	20	138	1.71	2.51	5100		BRIEF OCCURANCE DURING LOWER FREQUENCY OSCILLATION - POSSIBLY SECOND TANGENTIAL
103	20	138	1.71	2.52	5000		BRIEF OCCURANCE DURING LOWER FREQUENCY OSCILLATION - POSSIBLY SECOND TANGENTIAL
113+	16	132	1.54	2.54	6500	30	SPONTANEOUS AT 1500 MSEC AND TRIGGERED 1100 HZ; BOTH PERSIST
115+	16	131	1.54	2.53	7000	15	SPONTANEOUS LATE IN TEST AND TRIGGERED 1100 HZ; BOTH PERSIST

*   ALL UNLISTED TESTS STABLE
** ACOUSTIC CAVITY ENLARGED PREVIOUS TO RUN 96 - NO SUBSEQUENT FIRST TANGENTIAL MODE INSTABILITY
+   HEATED FUEL TESTS

LIKE DOUBLET INJECTOR PERFORMANCE WITH FILM COOLANT

P_C = 128-133 PSIA

T_F, F	COOLANT, PERCENT
235	2.5
187	2.5
AMB	1.5
AMB	2.5

C* EFFICIENCY, PERCENT

MIXTURE RATIO
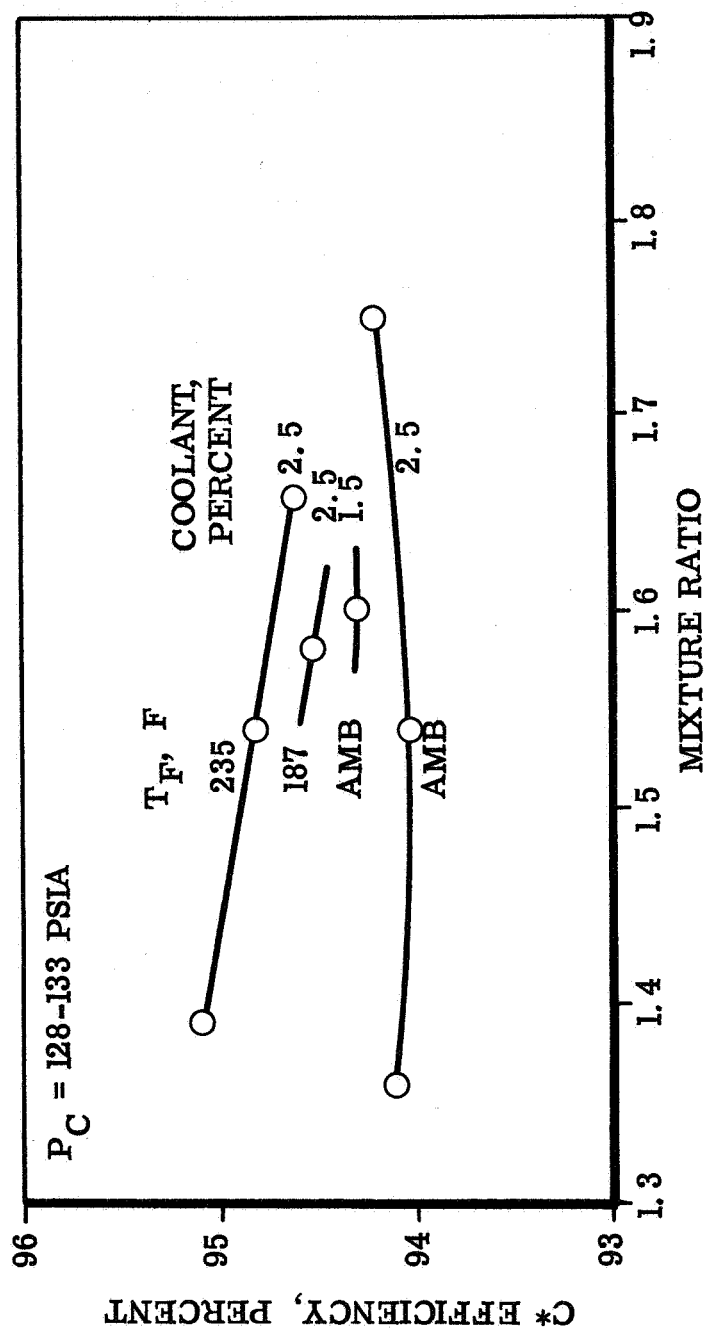
ΔP AND CONTRACTION RATIO EFFECTS

LIKE DOUBLET INJECTOR
12 IN. COMBUSTOR

HEATED FUEL
AMBIENT FUEL
HEATED FUEL
AMBIENT FUEL

$\epsilon_c = 3$

$\epsilon_c = 2$

CHAMBER PRESSURE, PSIA

η_{c*}, PERCENT

HEATED FUEL

$\epsilon_c = 3$

$\epsilon_c = 2$

AMBIENT FUEL

$\epsilon_c = 2$

$\epsilon_c = 3$

INJECTOR PLUS MANIFOLD ΔP, PSI

η_{c*}, PERCENT
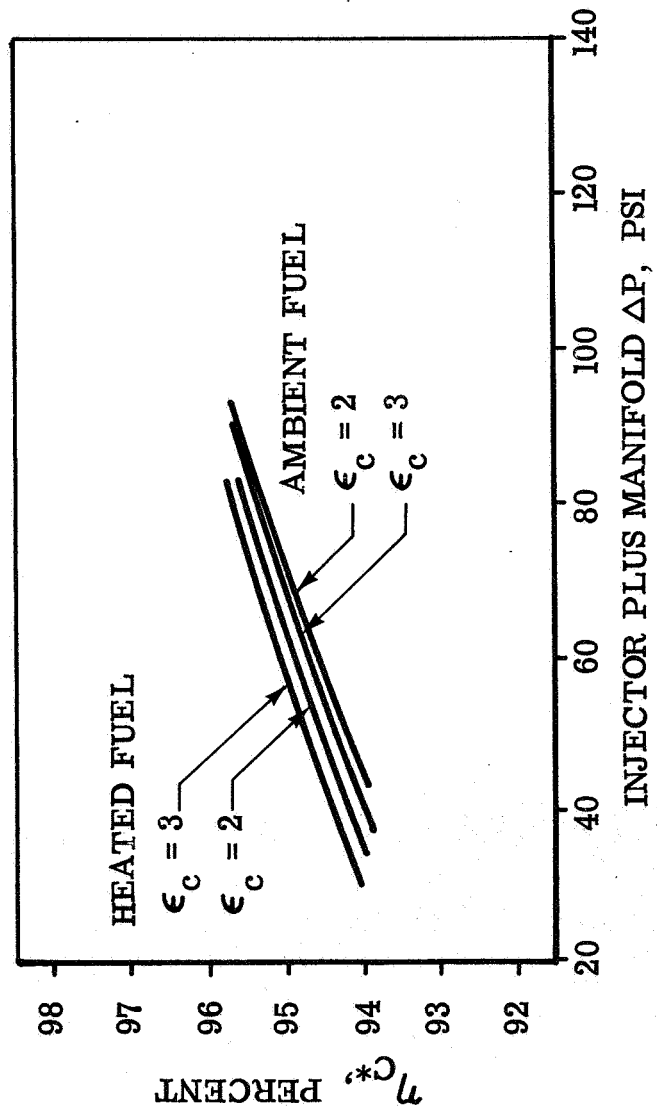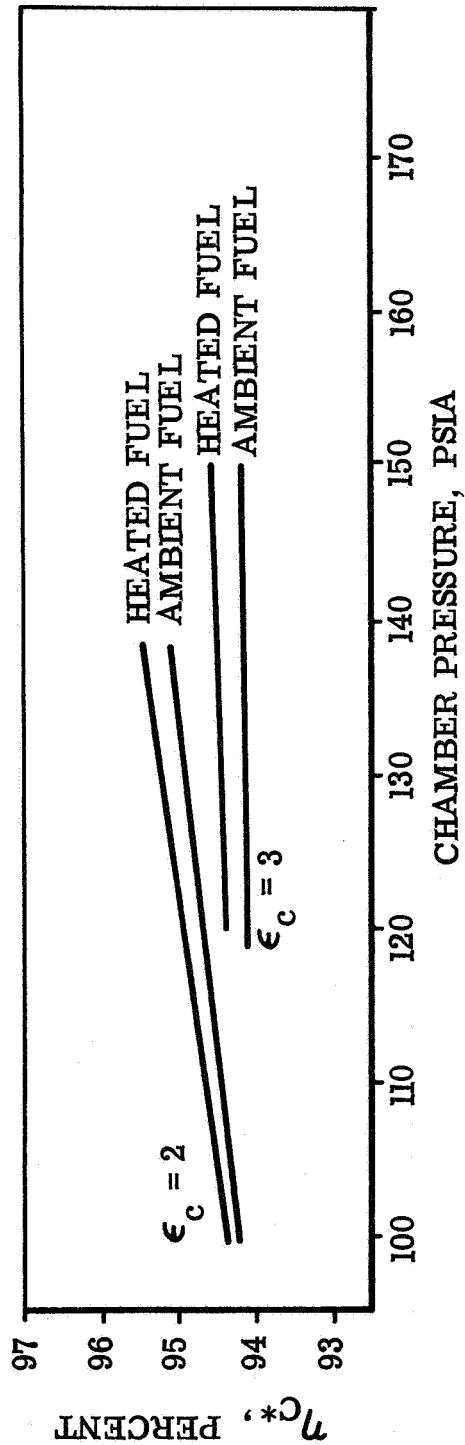
LIKE DOUBLET INJECTOR PERFORMANCE - NO FILM COOLANT

LENGTH EFFECT

$\epsilon_c = 2$
$P_c = 125$ psia
$T_f = 200F$
$L_c = 20$ in.
$\ \ \ \ \ 12$ in.

$\epsilon_c = 2$
$P_c = 125$ psia
$T_f = $ Ambient
$L_c = 20$ in.
$\ \ \ \ \ 12$ in.

TEMPERATURE EFFECT

$\epsilon_c = 2$
$P_c = 125$ psia
$L_c = 12$ in.
$T_f = 200F$
$\ \ \ \ \ $ Ambient

PRESSURE EFFECT, AMBIENT FUEL

$\epsilon_c = 2$
$T_f = $ Ambient
$L_c = 12$ in.
$P_c = 125$ psia
$\ \ \ \ \ 100$ psia

PRESSURE EFFECT, HEATED FUEL

$\epsilon_c = 2$
$T_f = 200F$
$L_c = 12$ in.
$P_c = 125$ psia
$\ \ \ \ \ 100$ psia

CONTRACTION RATIO EFFECT

$P_c = 125$ psia
$T_f = $ Ambient
$L_c = 12$ in.
$\epsilon_c = 2$
$\ \ \ \ \ 3$

MIXTURE RATIO

R-9686

2-22
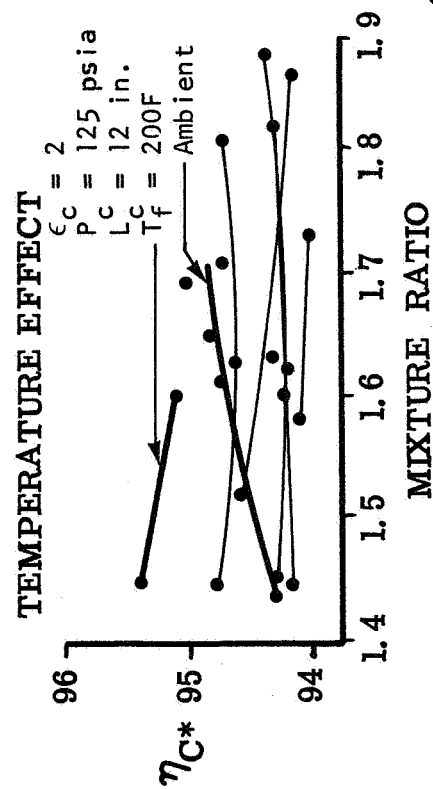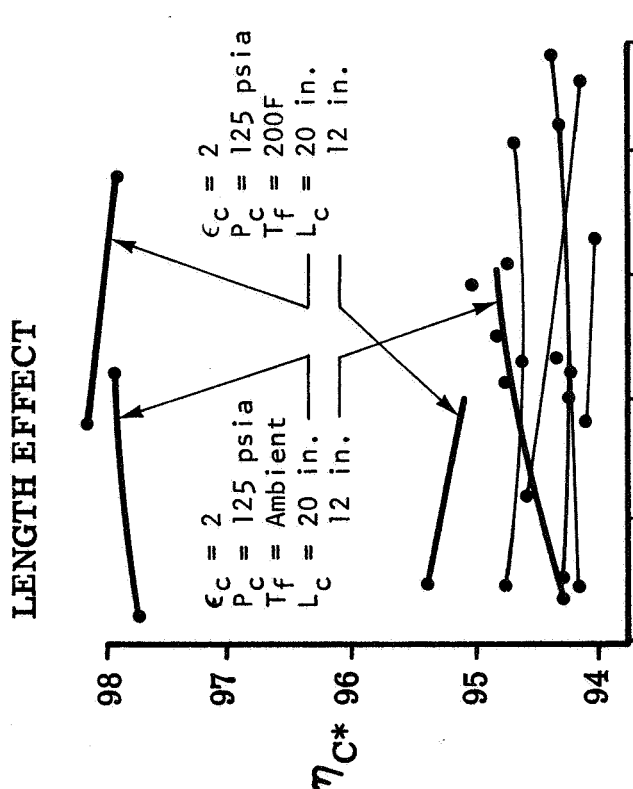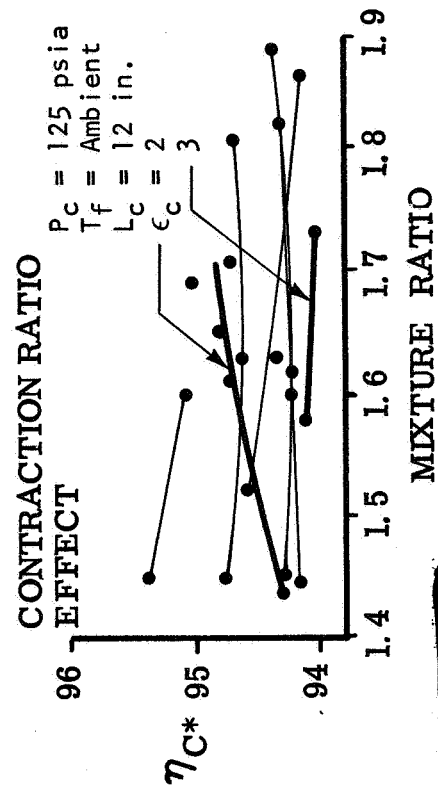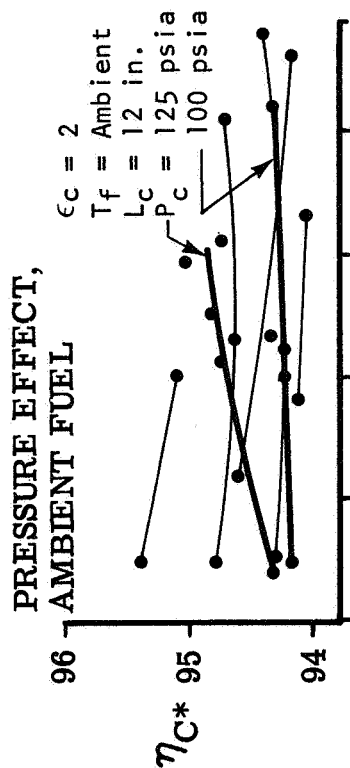
OME UNLIKE DOUBLET INJECTOR
INJECTOR PARAMETERS

	Injection Row							BLC
	1	2	3	4	5	6	7	
Oxidizer Orifice Dia.	.0355					.0355	.0464	-
Fuel Orifice Dia.	.0312					.0312	.0344	.0210
Number of Elements	4	20	32	48	60	72	80	180
Element Spacing	.644	.283	.284	.261	.267	.270	.286	.142
Rupe Number	.509					.509	.551	-
Beta Angle, °	+2.7	-2.7	+2.7	-2.7	+2.7	-2.7	+3.1	
Face Area Fraction	.010	.073	.095	.131	.167	.204	.322	
Flow Coverage								
Ideal	.010	.060	.087	.123	.159	.196	.367	
Designed	.011	.054	.086	.129	.161	.193	.367	
BLC, % of Fuel								10.6
Oxidizer ΔP	40						40	10
Fuel ΔP	45						45	-
Thrust/Element	15.6	16.1				16.1	27.5	
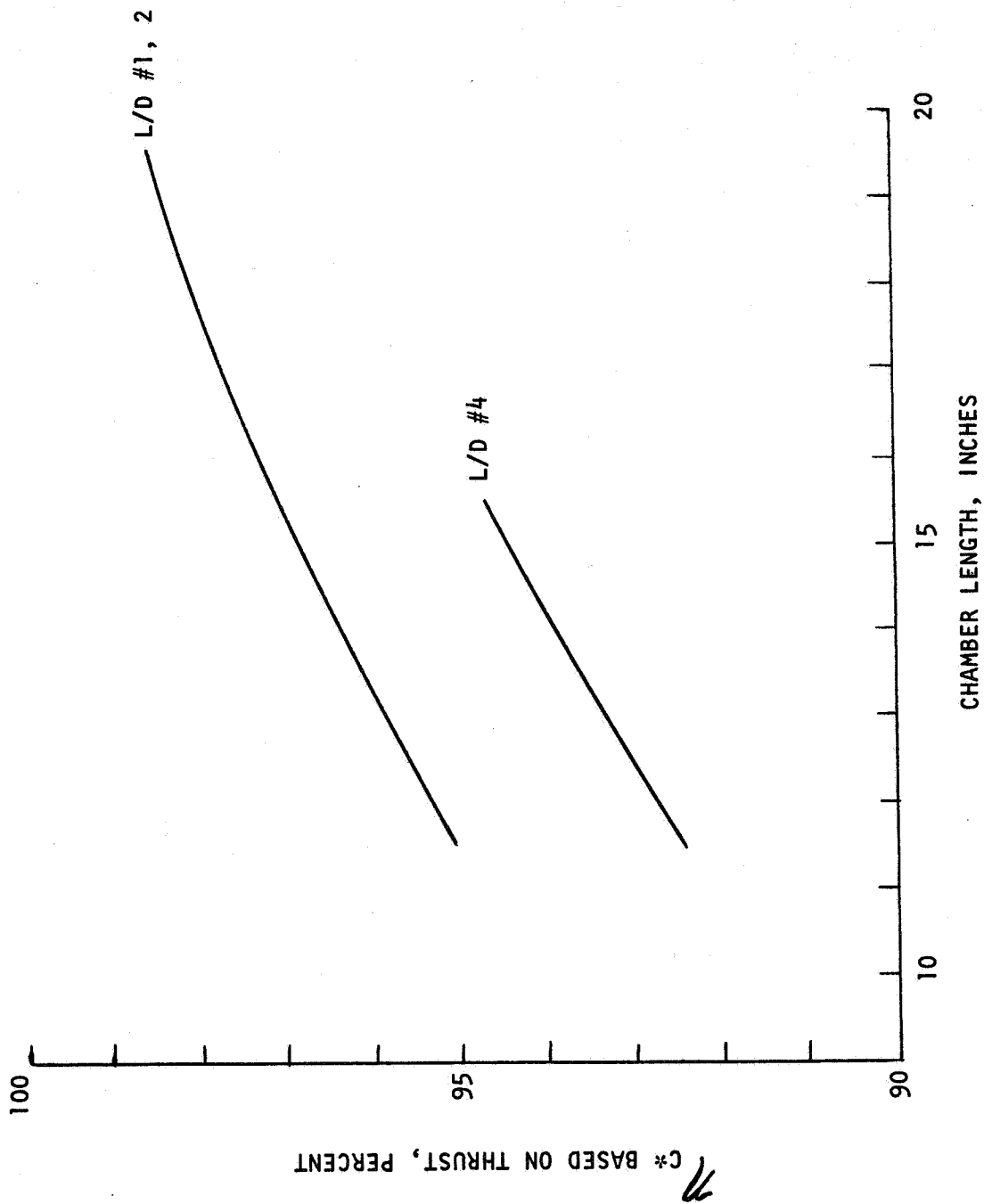
Figure 15. OME Like-Doublet Injector Performance

The heat flux data taken on the L/D #1 injector indicated a heat flux value at the throat approximately 3 BTU/in^2-sec without BLC, which reduced to 2.4 BTU/in^2-sec by the addition of 2.5 percent BLC. The heat flux in the cylindrical portion of the chamber was approximately 2.5 and 1.6 BTU/in^2-sec without and with the BLC, respectively.

The effect of combustion chamber length on the heat flux profile with the L/D #1 injector is shown in Fig.16 . The effect of lengthening the chamber was to increase the heat flux at the throat slightly and to decrease the heat flux in the cylindrical section slightly. The heat flux profile was not significantly influenced by mixture ratio or fuel temperature.

Experimental heat flux profiles for the L/D #1 and L/D #4 injectors are shown in Fig. 17   The heat flux profile between the throat and the injector for the like-doublet #4 without supplementary boundary layer coolant is lower than the profile for the L/D #1 injector with the nominal amount of BLC. The total heat load data for OME thrust chambers using these injectors is shown in Table 11. The injector-end subcooling values (the difference between the boiling temperature at injector-end conditions and the local propellant temperature) is also presented in the table. Values of subcooling for all three combinations are feasible to permit regenerative cooling of the OME thrust chamber.

In addition to the tests conducted with the solid wall thrust chambers, numerous tests were conducted with the L/D #1 injector in the demonstrator and integrated regeneratively cooled thrust chambers. Results of these tests are reported in the two sections entitled, "Demonstrator Thrust Chamber" and "Integrated Thrust Chamber." A total duration of approximately 1775 seconds was accumulated on the injector during 302 tests.
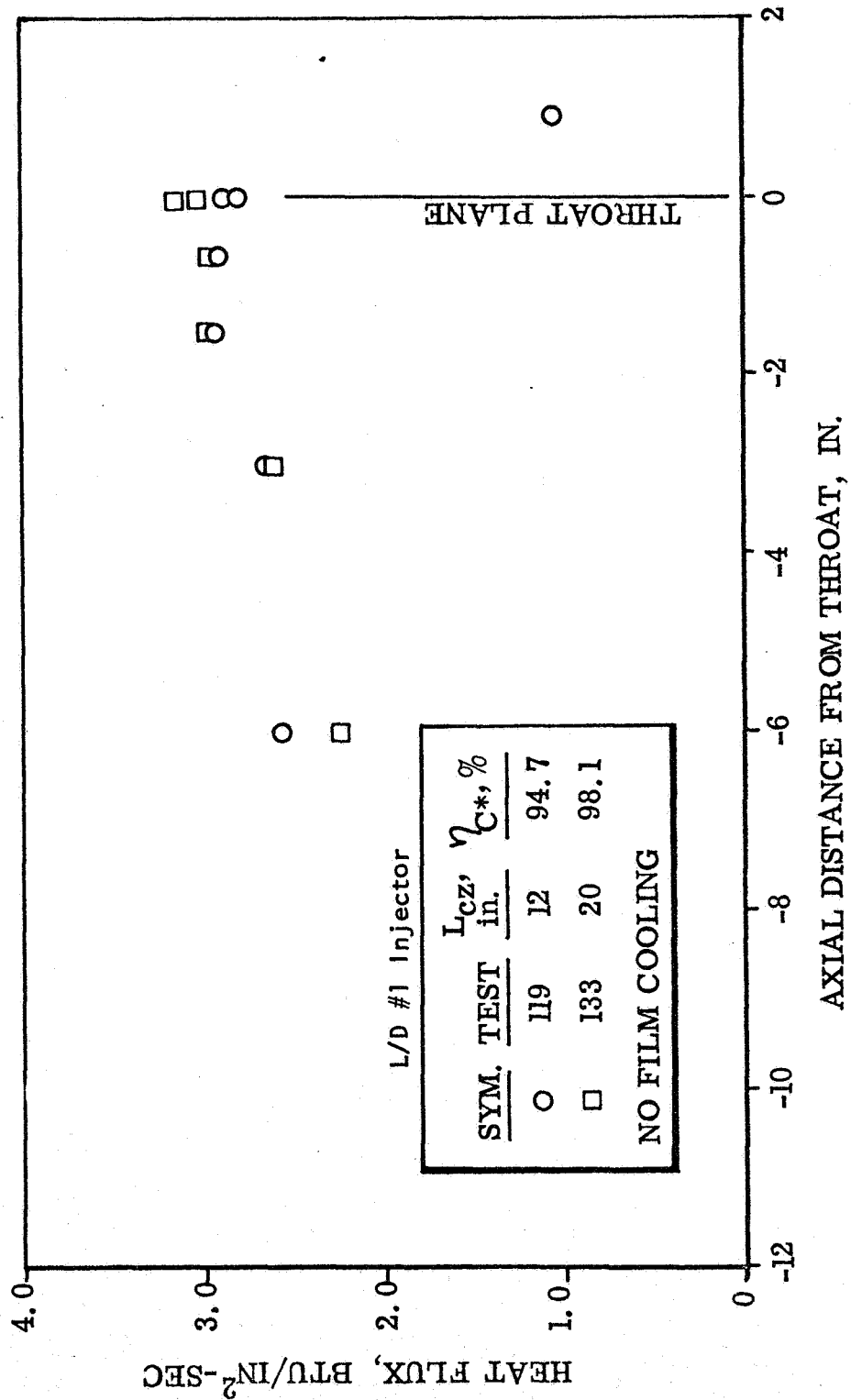
Figure 16. Effect of Chamber Length On Heat Flux
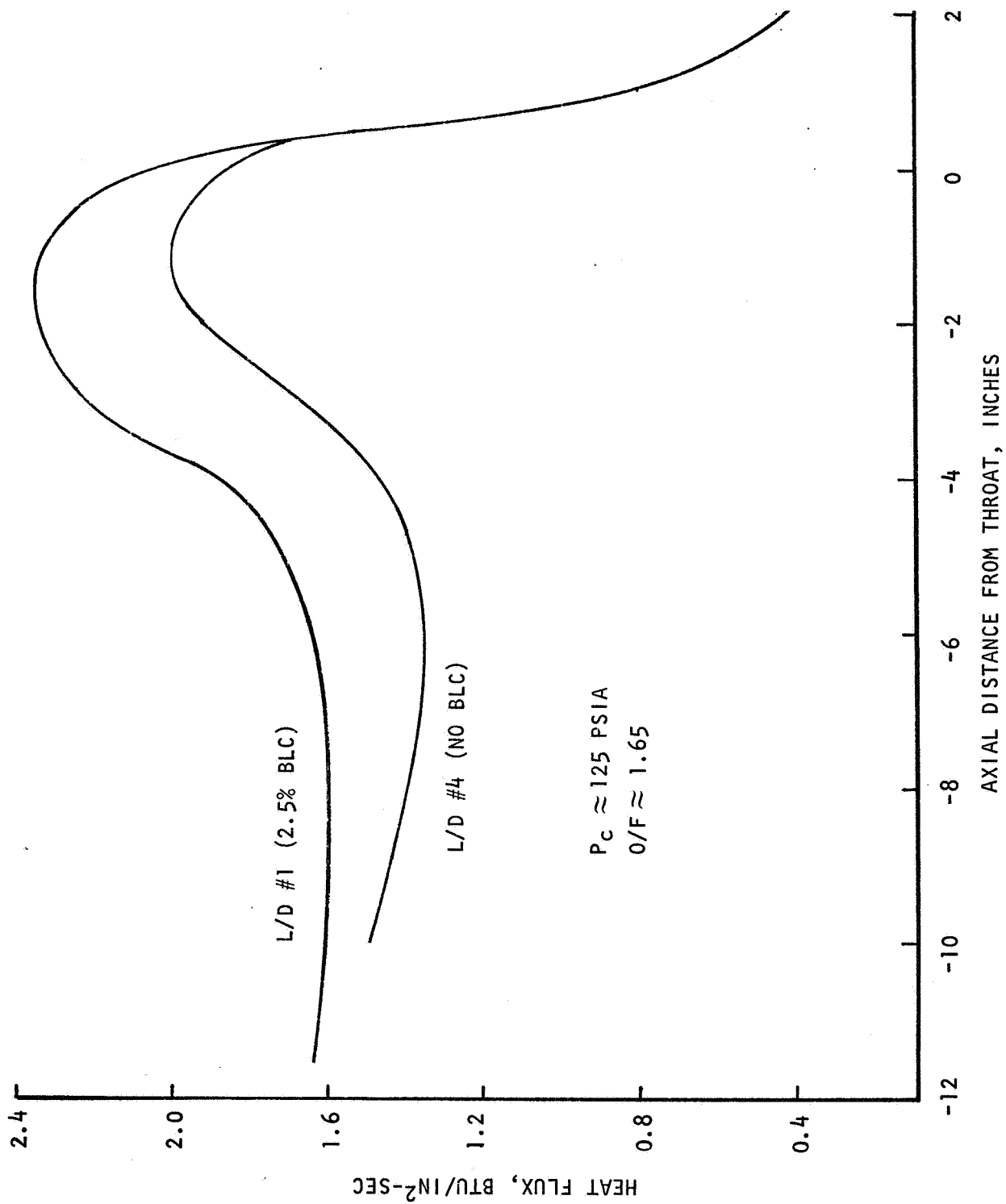
Figure 17. Experimental Like-Doublet Injector Heat Flux Profiles

The chart shows:
- Y-axis: HEAT FLUX, BTU/IN2-SEC (ranging from 0.4 to 2.4)
- X-axis: AXIAL DISTANCE FROM THROAT, INCHES (ranging from -12 to 2)
- L/D #1 (2.5% BLC)
- L/D #4 (NO BLC)
- $P_c \approx 125$ PSIA
- $O/F \approx 1.65$

TABLE 11

HEAT LOAD COMPARISON FOR LIKE-DOUBLET INJECTORS

	Chamber Length (Inches)	Heat Load (BTU/Sec)	Nominal Subcooling (F)
L/D No. 1 - Exp. With BLC	14.7	720	158
L/D No. 4 - Exp.	12.0	631	175
L/D No. 4 - Exp.	16.0	777	147

* W_F = 7.3 Lb/Sec, PIF = 180 PSIA

** Add ≈ 35 BTU/Sec for Acoustic Cavity Cooling

3.0 STABILITY ANALYSIS AND TESTS

Under Task XI of the program stability tests and analysis were conducted to
define stability characteristics of various OME chamber/injector configura-
tions and to determine the effectiveness of various accoustic cavity designs.
The effort comprised two series of full-scale stability rating tests,
bench-scale acoustic modeling tests, and analyses of data from tests conducted
by Rocketdyne and other OME technology contractors. The results were pre-
sented in NASA-CR-141676.

Test results show that the low contraction ratio (8.2-inch diameter) chamber
with injectors having like-doublet elements adequately stabilized with a
contoured entrance cavity without overlap between the chamber wall and the
inner wall of the cavity. The high contraction ratio (10-inch diameter)
chamber with the L/D #4 injector was stabilized with a similar cavity, and
this hardware combination appears more stable than the low contraction ratio
combination.

Acoustic model tests were made and the results were used to characterize the
resonance characteristics of a relatively wide range of cavity configurations.
A review of all available test data indicated that with many cavity configurations,
a 2300 to 2900 Hz mode of oscillation dominates the stability characteristics
of the 8-inch diameter chamber. This mode has not been identified fully but
is probably associated with the acoustics of the feed system with some chamber/
cavity interaction.

3.1 FULL-SCALE STABILITY RATING TESTS

Stability data was obtained for several injector/chamber/cavity configurations.
Data taken on this program was used together with data from tests conducted
under IR&D and Contract NAS9-12524, to indicate the effects of operating
conditions, chamber contraction ratio, cavity configuration, and boundary
layer coolant (BLC) on stability. The facility is described in Appendix A.

Test Hardware and Instrumentation

The previously described L/D #1 and L/D #4 injectors were used during this
program. The L/D #1 injector had been used previously for extensive non-
stability related testing, although a few stability rating tests had been
made before the BLC injection orifices were drilled in the injector. . These
tests were stable with the acoustic cavity being used. Related stability
rating tests had been made on Contract NAS9-12524 with a somewhat similar
injector, L/D #2, which showed that an acoustic cavity was required to achieve
stability.

Solid wall combustion chambers typical of that shown in Fig. 11 were used. For the tests conducted under this contract, the BLC injector was eliminated. The L/D #1 injector had 68 equispaced 0.020-inch diameter orifices near its circumference; no BLC was used for the tests with the L/D #4 injector.

The acoustic cavities were formed between the injector and removable rings, as shown in Fig.18, to facilitate modification of the cavity configurations. The acoustic cavities used for all of these tests had a contoured entrance. If difficulty had been encountered in achieving stability with this entrance configuration, testing was planned with a partially contoured entrance with overlap. The partially contoured entrance was chosen as an alternative because Aerojet had used this alternative to stabilize their engine.

In addition to the normal thrust,pressure, flow, and temperature instrumentation special temperature and high-frequency pressure instrumentation was used. The chambers were instrumented with three high frequency response pressure transducers, either Kistler model 614B/644 or PCB Piezotronics Model 123A helium and water-cooled transducers. These were located approximately 3 inches downstream from the injector face at three different angular locations. These locations (referred to fuel inlet) were 108°, 228°, and 276° for the 8-inch chamber and 12°, 108°, and 228° for the 10-inch chamber. The high frequency data were recorded on magnetic tape for subsequent analysis. The stability rating bombs were located at the same axial position and angular locations of 60° and 324°. Two cork insulated 6½ grain (6½ grains RDX and 500 milligrams lead azide) bombs were used for each firing.

Gas temperatures were measured in the acoustic cavities with exposed-junction tungsten/rhenium (W-5% Rh/W-26% Rh) or chromel-alumel thermocouples depending on the location (temperature).

8-Inch Chamber Tests

Eighteen stability tests were conducted on the 8-inch diameter chamber with the L/D #1 injector. Generally, two bombs were detonated during each of the tests which were of 5 seconds duration. Figure 19 is a typical thrust record on which the bomb detonations are clearly visible. The acoustic cavity configurations and the test conditions are listed in Table 12. The initial tests were conducted with the primary cavities having a total open area, σ, equal to 14.8 percent of the injector face area and effective cavity depth, ℓ, of 1.60 inches.

The cavities for these tests were located in a single row around the injector face, 12 equal area cavities separated by partitions. Four equally spaced cavities were tuned to suppress the third tangential and first radial modes of instability. These cavities had an effective depth near 0.78 inches and
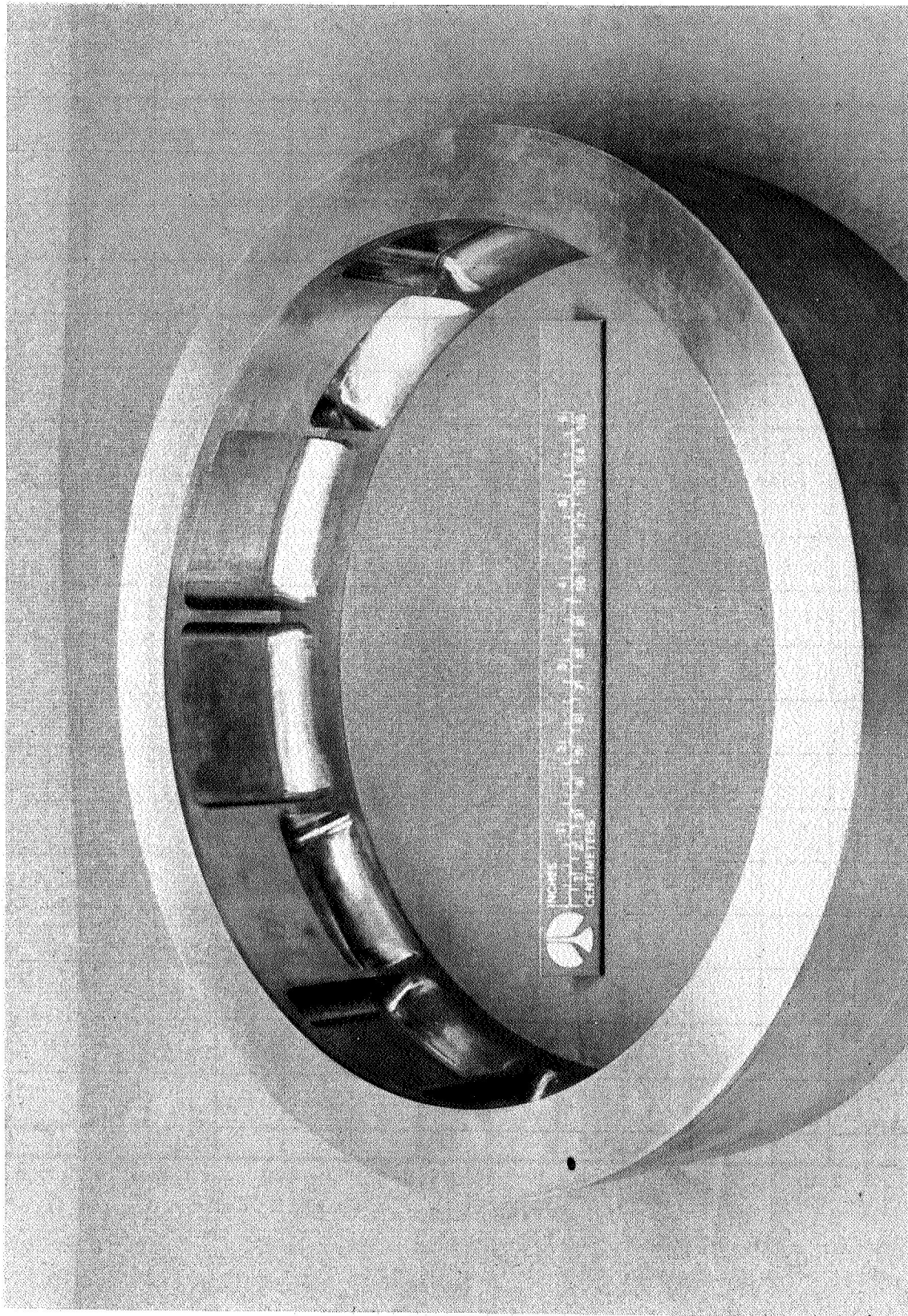
Figure 18. Acoustic Cavity Ring
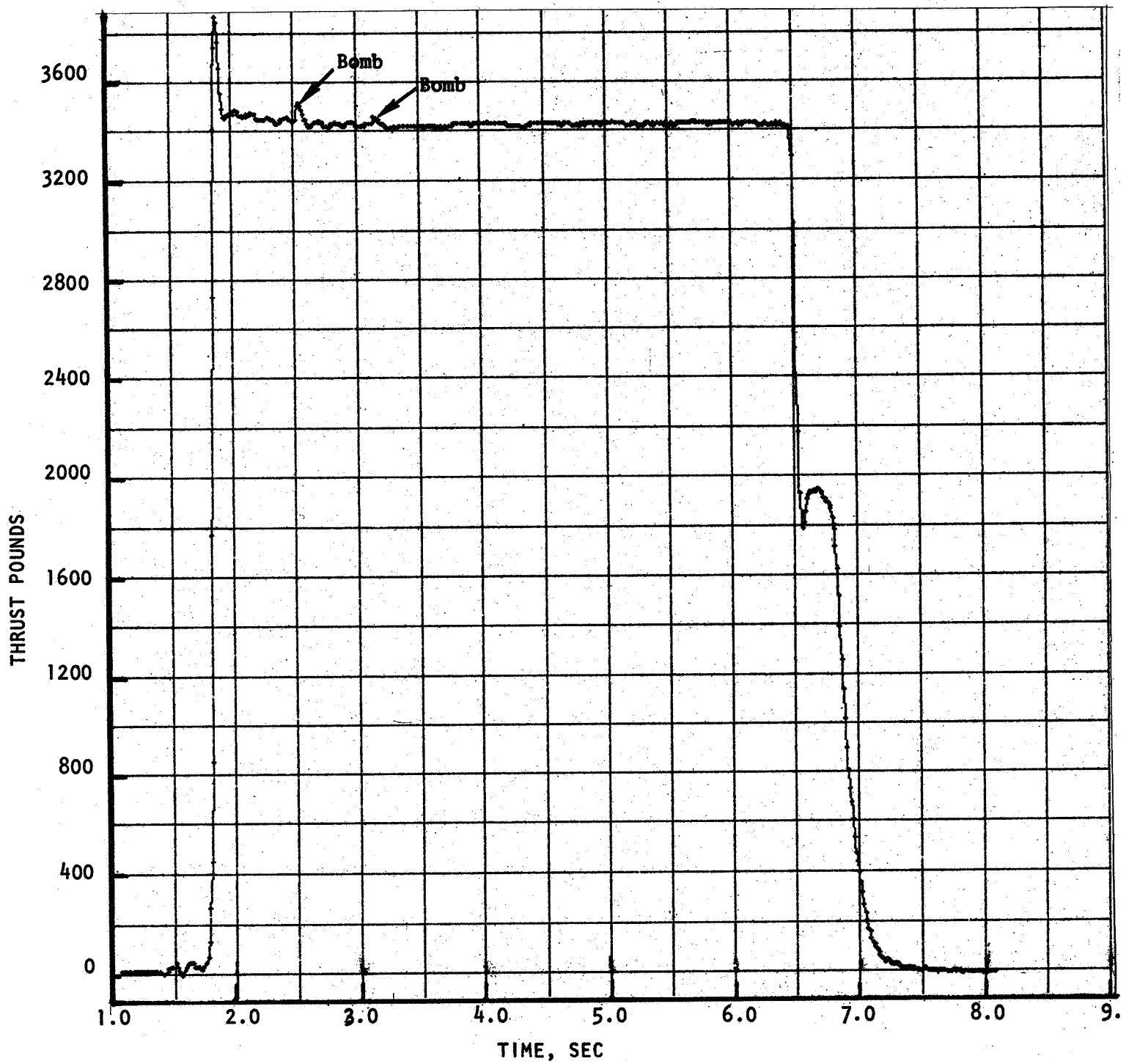
Figure 19.   Thrust Record - Test 16

R-9686

3-4

TABLE 12

SUMMARY OF STABILITY RESULTS FROM LOW CONTRACTION RATIO CHAMBER TESTS

Objective	Primary Cavity (1) σ	Primary Cavity (2) ℓ_e, in.	Secondary Cavity (1) σ	Secondary Cavity (2) ℓ_e, in.	P_c, psia	Overall Mixture Ratio	Fuel Inj. Temp., F	Maximum Damp Time, msec	Frequency, Hz	Stability
Stability of Basic Configuration	0.148	1.60	0.074	0.78	130	1.80	180	14	2330	Stable
					126	1.71	190	220	2550	Unstable
					125	1.69	160	70	2570	Unstable
					140	1.55	165	11	2300	Stable
					113	1.52	165	11		→ Stable
					111	1.79	175	12		
Evaluate Effect of Manifold Dams					137	1.52	175	12		Stable →
					123	1.66	160	13		
					141	1.86	165	15		
					111	1.42	150	14		
Stability with Reduced Open Area	0.12	1.58	0.06	0.76	136	1.44	220	11	2770	Stable →
					127	1.68	205	12	2790	Unstable
					140	1.80	195	70		Stable
					111	1.45	190	10		
					111	1.84	175	21	2790	Marginal
					127	1.61	175	10	2770	Stable →
					143	1.65	170	18	2750	
					128	1.69	160	11	2800	

(1) σ = fractional open area based on injector face area

(2) ℓ_e = effective cavity depth

R-9686

a physical depth of 0.42 inch (measured from the injector face). The remaining eight cavities were tuned to suppress the first tangential mode of instability and had effective and physical depths of ~1.60 and 1.25 inches, respectively. These effective depths were calculated from the acoustic model test results to be described below.

As shown in Table 13 two of the five tests with the initial cavity configuration were unstable (damp times exceeded 20 milliseconds) at a frequency of ~2560 Hz. A pressure record from one of these unstable tests is shown in Fig. 20. Based on initial analytical results, this 2560 Hz mode of instability was thought to be, at least possibly, associated with the acoustics of the fuel injection system. Consequently, a modification to the injector was tried in which baffles (or dams) were installed at three locations with roughly equal spacing in the annular fuel manifold on the upstream side of the injector. With this modification, the combustion chamber was found to be stable. A pressure record from one of these tests is shown in Fig. 21. The remaining tests were made with a second cavity configuration having reduced open area. Two of the eight tests made with the latter configuration had damp times in excess of 20 milliseconds. Pressure records from one stable and one unstable test are shown in Figs. 22 and 23. This cavity configuration was inadequate to prevent a 2790 Hz oscillation. The analytical results suggest that this mode is also associated with the feed system.

The temperatures are listed in Table 13 and plotted against mixture ratio in Fig. 24. The data indicate a trend of generally decreasing temperature with increasing mixture ratio. Similar results were reported in Ref. (a). The average temperature at nominal conditions was 2200 F and 2500 F for thermocouples #1 and #3 which are located at depths of 0.54 and 0.04 inches from the injector face, respectively. These temperatures agree, within the data scatter, with values obtained in Ref. (a).

The measured cavity temperatures provide an indication of the acoustic velocity existing in the cavity, which affects cavity tuning and instability suppression. Had the temperatures been different from those obtained previously, adjustments in cavity depth may have been needed to stabilize the engine. The fact that the temperatures are roughly consistent with those obtained previously, suggests the difference in method of injecting film coolant does not affect the required cavity tuning.

10-Inch Chamber Tests

Stability results from testing the 10-inch diameter chamber are summarized in Table 14. Each entry in the table corresponds to a single test with two bombs being used for each test, nominally. The cavity configurations were similar to those used in the 8.2-inch diameter chamber with contoured
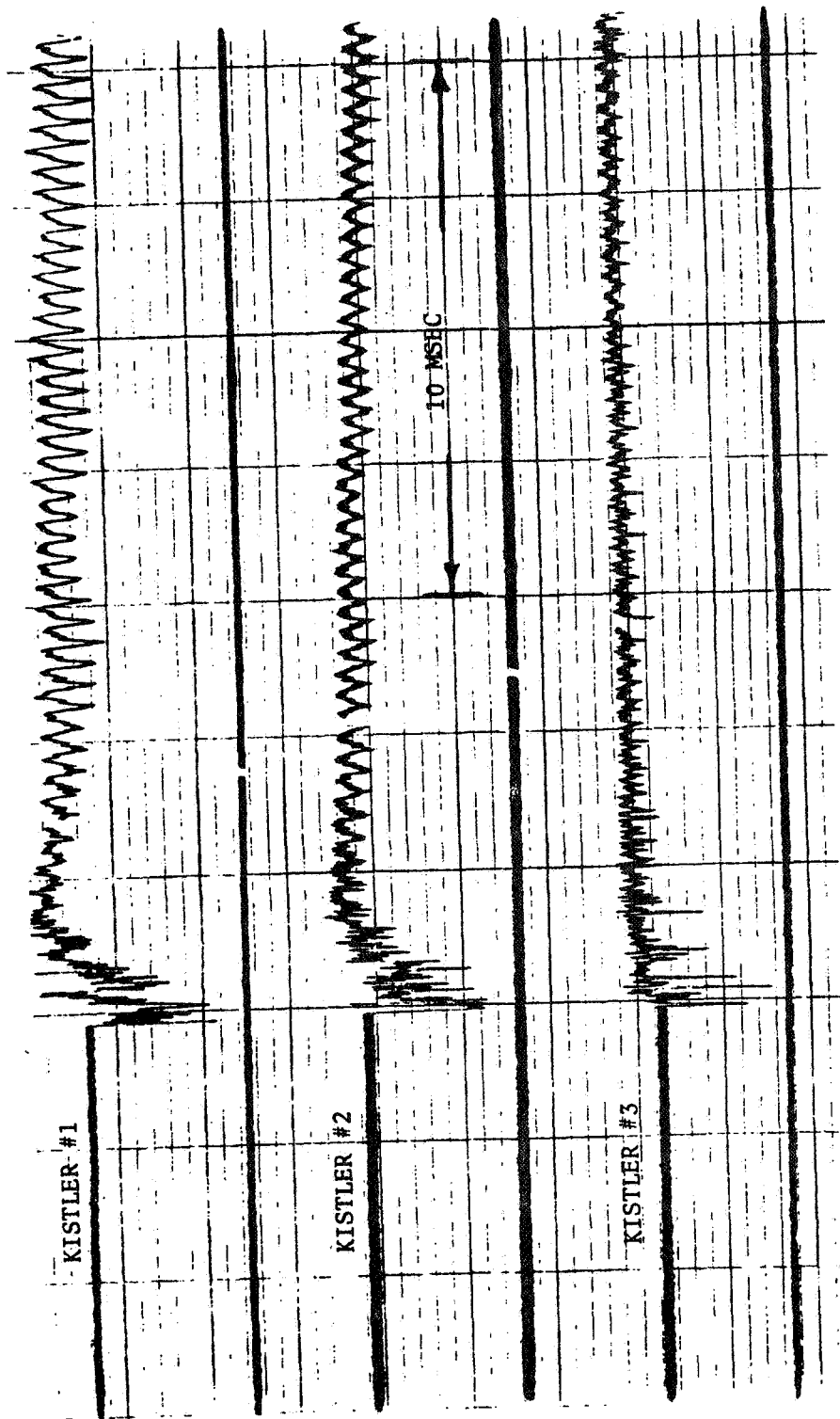
Test No. 3:   First Bomb
Cavity: 0.148 x 1.60/0.074 x 0.78 (fraction x inch)
No Manifold Dams
Frequency: = 2570
Unstable ~ 70 m sec damp time

Figure 20.   High Frequency Pressure Data
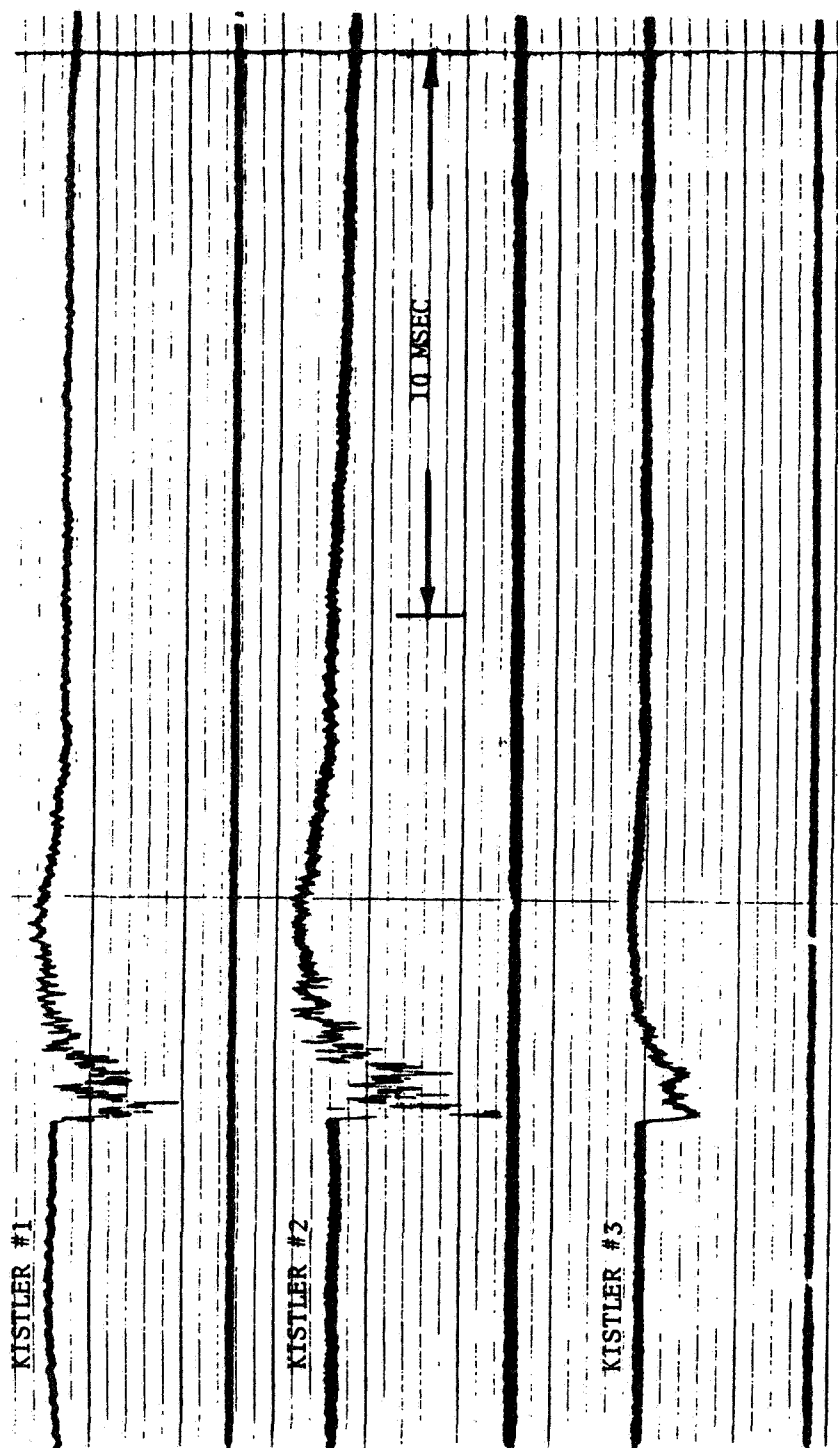
Test No. 8: First Bomb
Cavity: 0.148 x 1.60/0.074 x 0.78 (fraction x inch)
With Manifold Dams
Stable ~.13 m sec damp time

Figure 21.   High Frequency Pressure Data

10 MSEC

KISTLER #1

KISTLER #2

KISTLER #3
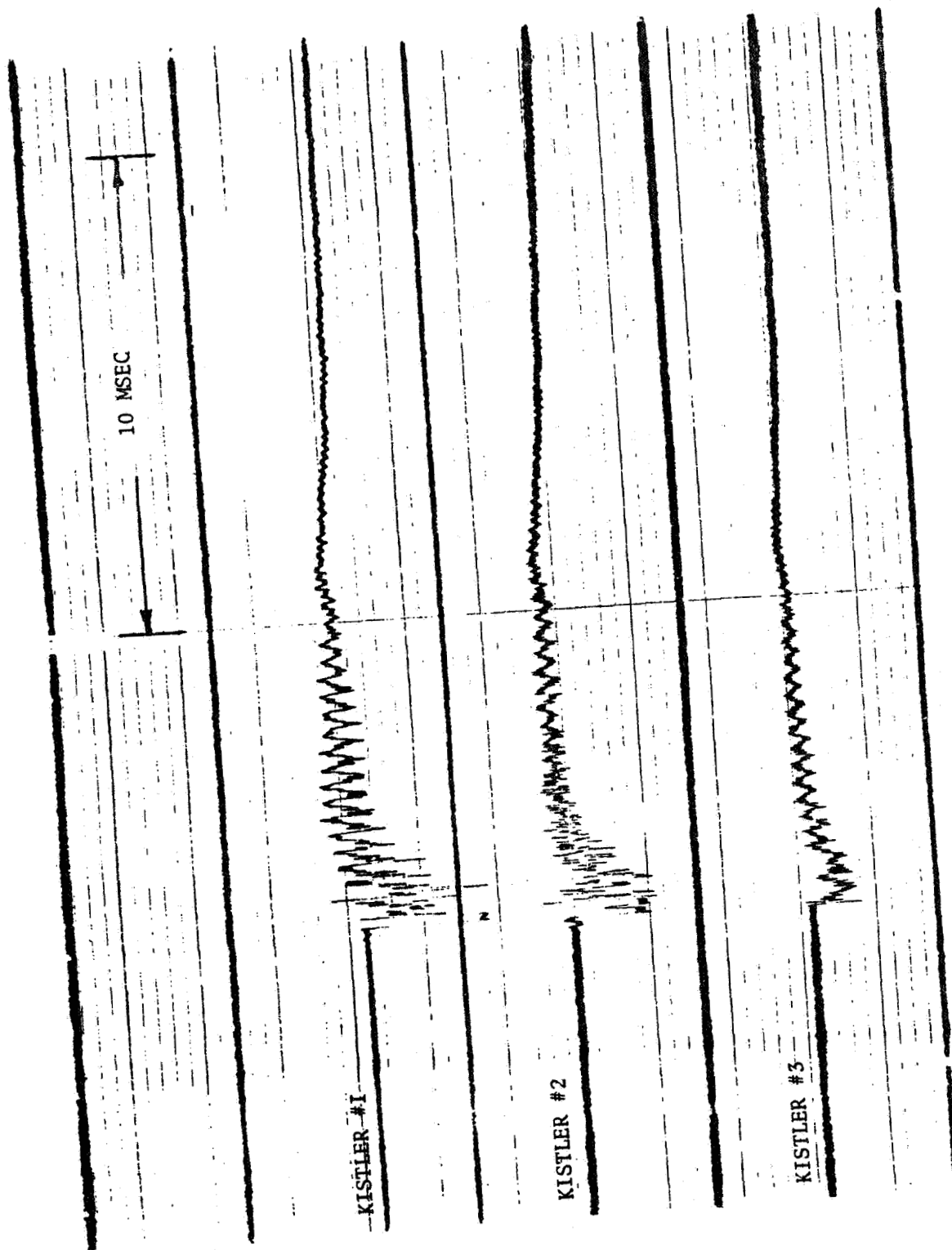
Test No. 12: Second Bomb
Cavity: 0.12 x 1.58/0.06 x 0.76 (fraction x inch)
Frequency = 2770 Hz
Stable - 12 m sec damp time

Figure 22. High Frequency Pressure Data
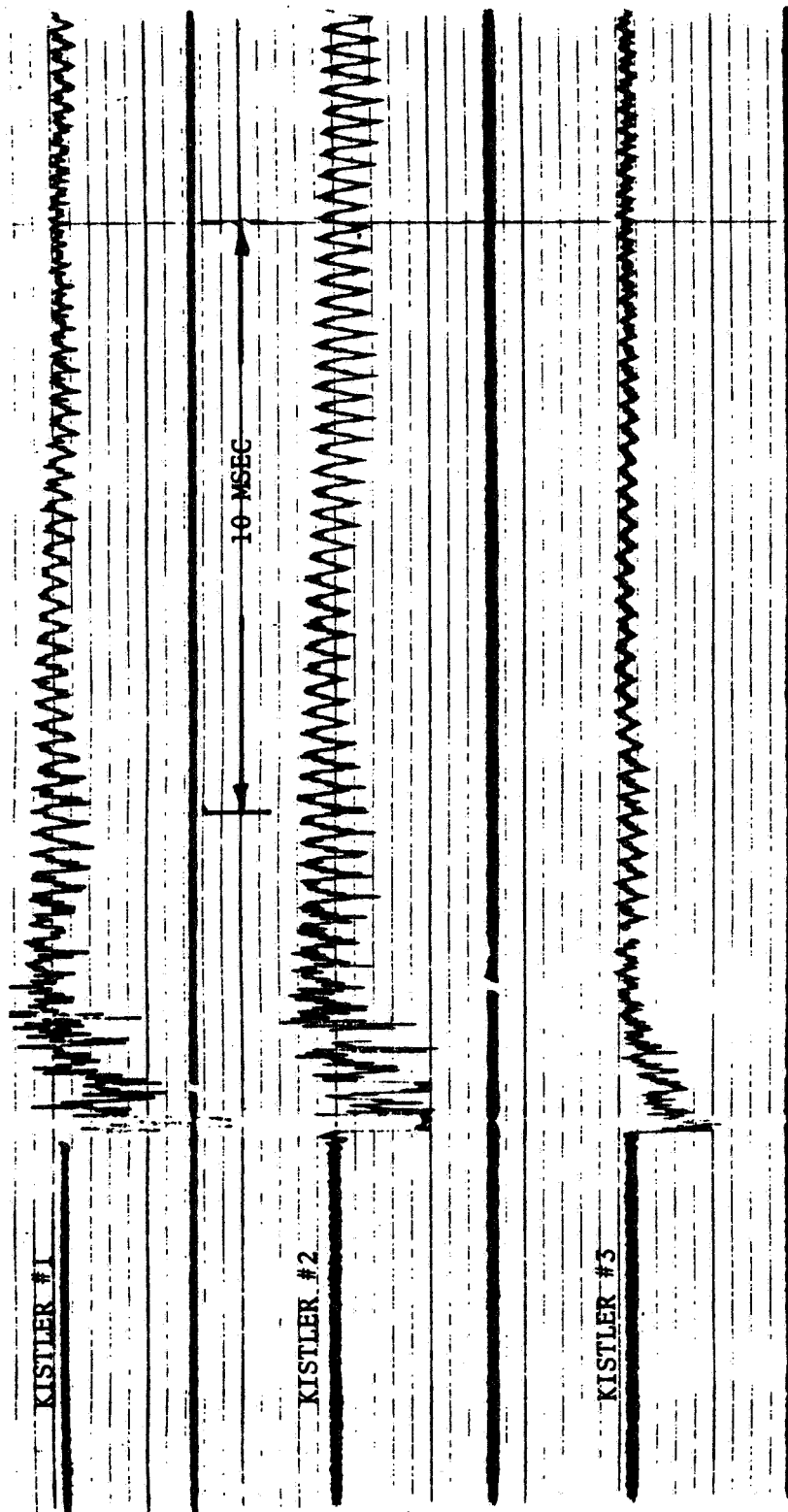
Test No. 13:   First Bomb
Cavity: 0.12 x 1.58/0.06 x 0.76 (fraction x inch)
Frequency =   2790 Hz
Unstable - 70 m sec damp time

Figure 23.   High Frequency Pressure Data

TABLE 13

ACOUSTIC CAVITY TEMPERATURES, F

| | MEASUREMENTS | | | | | | | |
| | 1 | | 2 | | 3 | | 5 | |
	@BOMBS	@C.O.	@BOMBS	@C.O.	@BOMBS	@C.O.	@BOMBS	@C.O.
TEST 1	2140	2370			2240	2340	3500	2730
TEST 2	1960							
TEST 3	1740							
TEST 4	2370	2690						
TEST 5	2310	2530						
TEST 6	1990	2200						
TEST 7	2560	2290	2400	2550	3240	3130	3140	2910
TEST 8					2660	2770	2280	
TEST 9					1200	1770		
TEST 10					1170	1660		
TEST 11					1850	2230		
TEST 12					2240	2100		
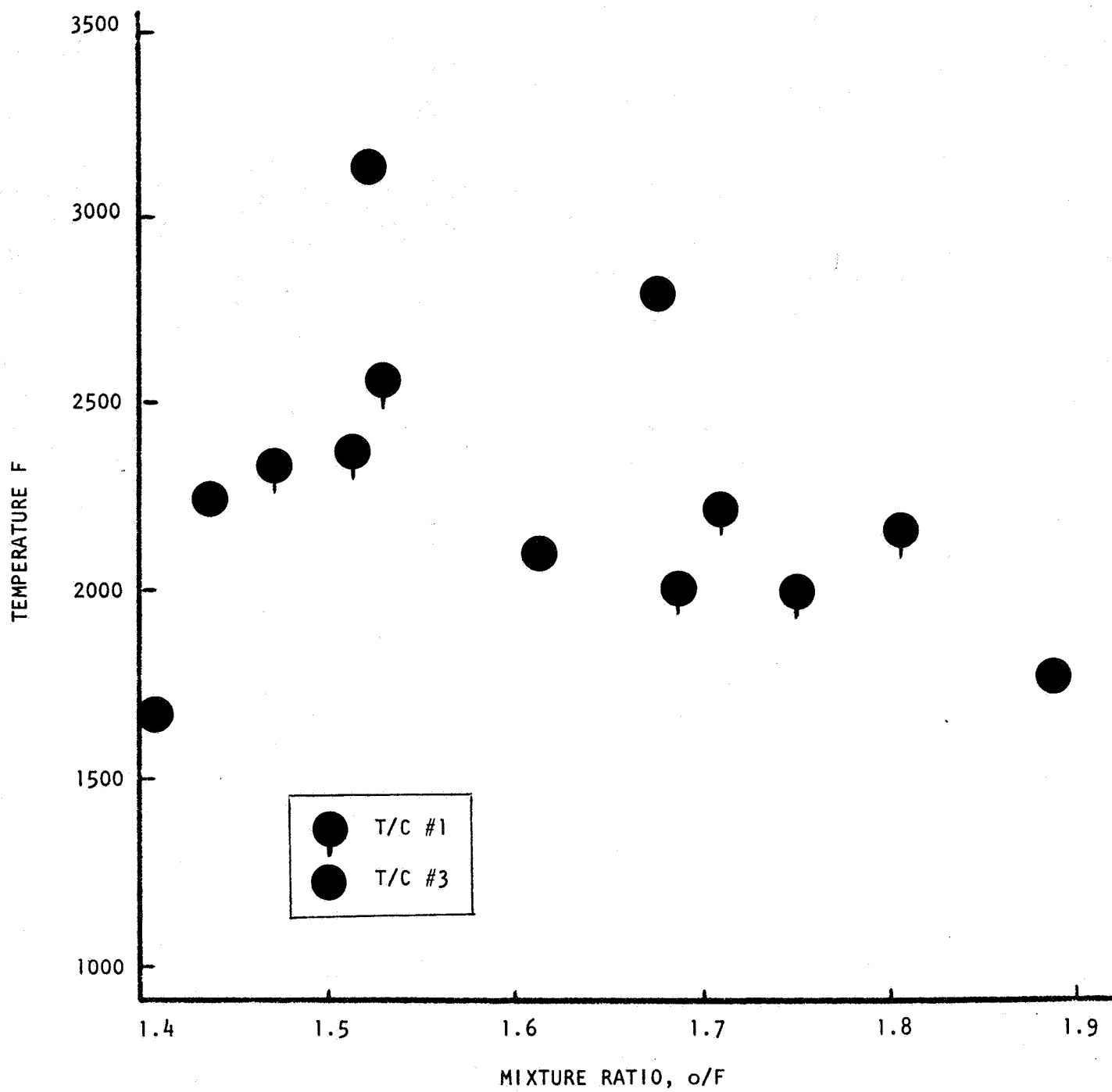
Figure 24.   Acoustic Cavity Temperature

TABLE 14

SUMMARY OF STABILITY RESULTS FROM HIGH CONTRACTION RATIO CHAMBER TESTS

Objective	Primary Cavity (1) σ	Primary Cavity (2) ℓ$_e$,in.	Secondary Cavity (1) σ	Secondary Cavity (2) ℓ$_e$,in.	P$_c$, psia	Overall Mixture Ratio	Fuel Inj. Temp.,F	Maximum Damp Time, msec	Frequency, Hz	Stability
Search for Minimum Open Area	0.099 →	2.08 →1.28			120	1.64	190	7		Stable →
					134	1.84	220	7		
					136	1.54	210	6		
					118	1.73	160	9		
Search for Minimum Depth	0.148	2.12 →	0.069 →	0.88 →	127	1.66	190	570	2640	Unstable
Confirm Stability at Nominal Depth					126	1.66	201	6		Stable →
					140	1.80	192	6		
					132	1.44	188	6		
					114	1.82	189	7		
					126	1.62	190	6		
					140	1.61	185	5		
					110	1.48	176	7		
					126	1.67	187	8		
					-	-	-	8		
					125	1.62	70	8		
					139	1.86	68	7		
Confirm Stability with Long Chamber	0.099 →	2.08 →			129	1.42	65	7		
					125	1.69	225	8		
					140	1.86	200	7		
					140	1.54	194	7		
					112	1.88	183	8		
					112	1.71	194	8		
					126	1.66	183	8		

(1) σ = Fractional open area based on injector face area

(2) ℓ$_e$ = Effective cavity depth

entrances and with 4 of 12 cavities tuned for the third tangential and first radial modes and 8 of 12 cavities tuned for the first tangential mode. The effective and physical depths of the secondary (3T/1R) cavity was 0.88 and 0.5 inches, respectively, for all tests. Testing was initiated with a 9.9 percent open area primary (1T) cavity (with effective and physical depths of 2.08 and 1.75 inches, respectively), which proved adequate to prevent instability. However, a shallow 14.8 percent open area cavity was found to be inadequate. The latter cavity had an effective depth of 1.28 inches and a physical depth of 0.9 inch. Nevertheless, subsequent testing with a deeper 14.8 percent open area cavity showed it to be adequate (physical depth of 1.75 inches). The remaining tests were made, primarily, to evaluate the effects of fuel temperature and chamber length on steady-state performance. The combustion chamber was stable during all remaining tests.

Summary of Results from Full-Scale Testing

Results from testing the 8.2-inch diameter (low Contraction ratio) chamber show that:

1. Stability was readily achieved with a contoured entrance cavity without overlap.

2. Stability was dominated by 2300 to 2800 Hz oscillation and which was improved by installing baffles (dams) in the fuel manifold.

3. The change in BLC introduction from a separate downstream injector to the periphery of the main injector did not significantly affect stability. Moreover, the stability of the L/D #1 injector appeared comparable but slightly better than that of the L/D #2 injector (described in Ref. a).

The 2300 to 2900 Hz instability data may be grouped into three sets:

1. A 2300 Hz oscillation appeared briefly during the decay transient after two bombs. The phase angles suggest a first tangential angular distribution of pressure.

2. Two sustained instabilities occurred with frequencies near 2560 Hz. The amplitude and phase data suggest a precessing and then standing first tangential type pressure distribution. The pressure node appeared to stand along the fuel inlet line. The amplitudes were ~35 to 70 psi peak-to-peak.

3. After installation of the manifold dams, multiple occurrences of
    a 2790 Hz oscillation were encountered. In each case the oscilla-
    tion damped in 10 to 70 milliseconds. The amplitude and phase
    behavior suggested, as with the 2560 Hz oscillation, that the mode
    precessed initially and then stood with the pressure node along the
    fuel inlet. Amplitudes were ~50 to 150 psi peak-to-peak.

Results from testing the 10-inch diameter (high contraction ratio) chamber show
that:

1. Adequate stability was readily achieved with a contoured entrance
    cavity without overlap.

2. The L/D #4 injector is relatively stable. Because the performance
    was somewhat low, the greater stability may not be due to the higher
    contraction ratio.

3.2 ACOUSTIC MODEL TESTING

Two kinds of acoustic model tests were made, one with relatively detailed models
of the acoustic cavities only and the second with a model of the combustion
chamber containing acoustic cavities. The tests with the detailed cavity models
were made to measure the effective acoustic depth of these cavities associated
with the entrance region. The tests with the chamber model were made to measure
the influence of the cavities on the acoustic modes of the chamber. Each kind
of model was excited with an acoustic driver and the model response was measured
with a microphone. The frequencies corresponding to maximum microphone response
were interpreted as the resonant frequencies of the models.

Cavity Model Testing

The general configuration of the cavity models is illustrated in Fig. 25 . The
model was constructed from Lucite as a three-times scale two-dimensional represen-
tation of the cavity configurations of interest. Replaceable entrance block
configurations were used to model the different cavity configurations. The
entrance to the cavity model was exposed to the room and was not contained in
another chamber.

Results from these model tests are shown in Figs. 26 through 28. The results
are shown as an effective depth, which is simply the calculated quarterwave
depth corresponding to the measured resonant frequency, as a function of physical
depth. The effective depth contribution resulting from the entrance region of
the cavity was calculated from the test results as the horizontal distance
between the line for the cavity of interest and the line for a simple quarter-
wave resonator with the same cavity width (open area).
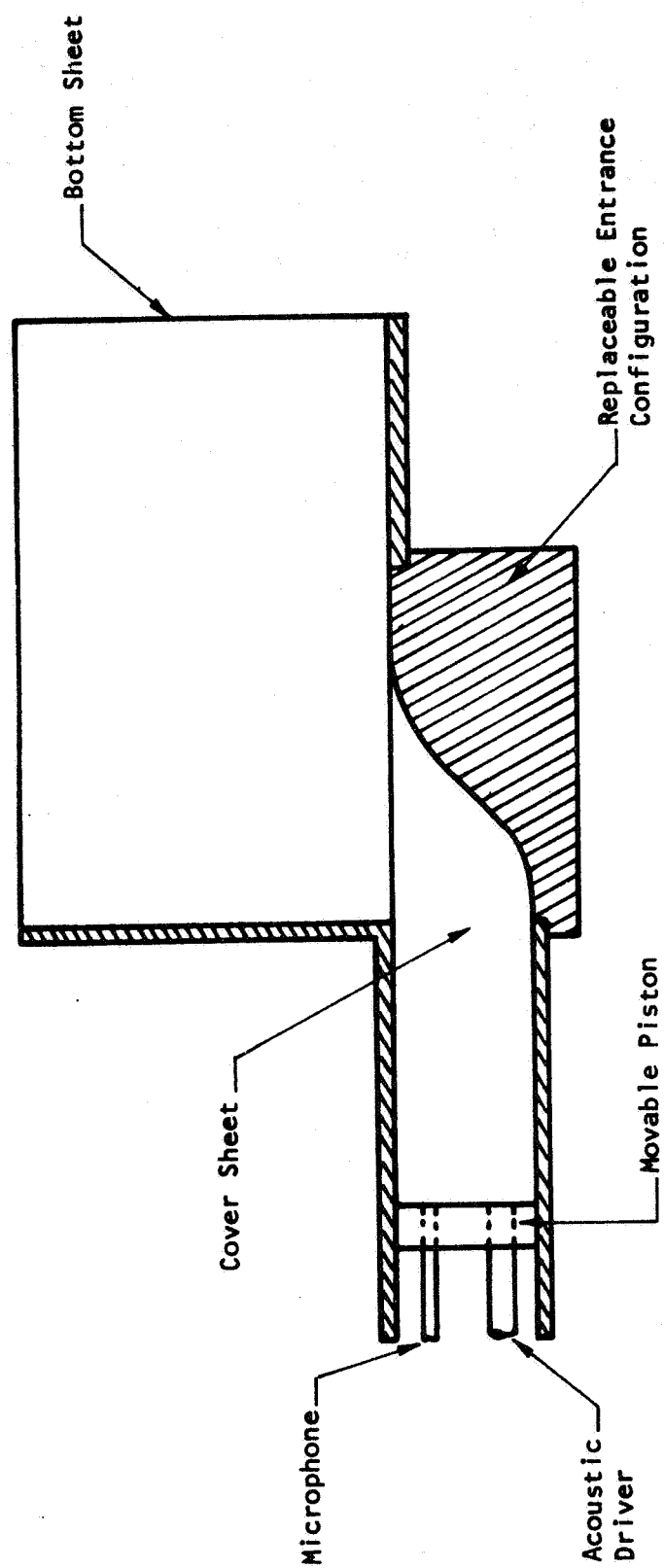
Figure 25   Schematic Diagram of Acoustic Cavity Models

CONFIGURATIONS:

Simple Quarterwave
(w = 1.5)

Rectangular
(w = 1.5)

Contoured
(w = 1.5)
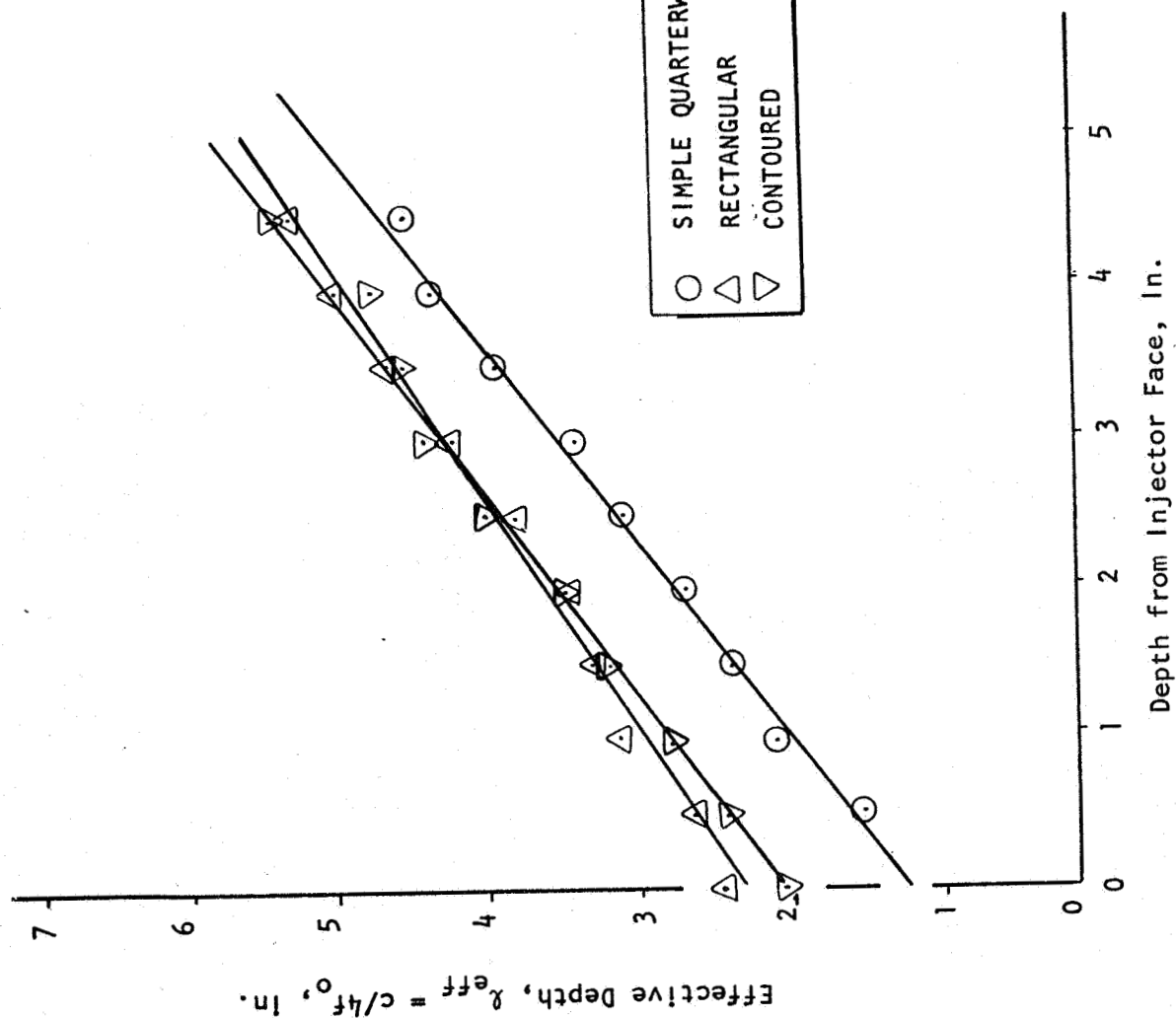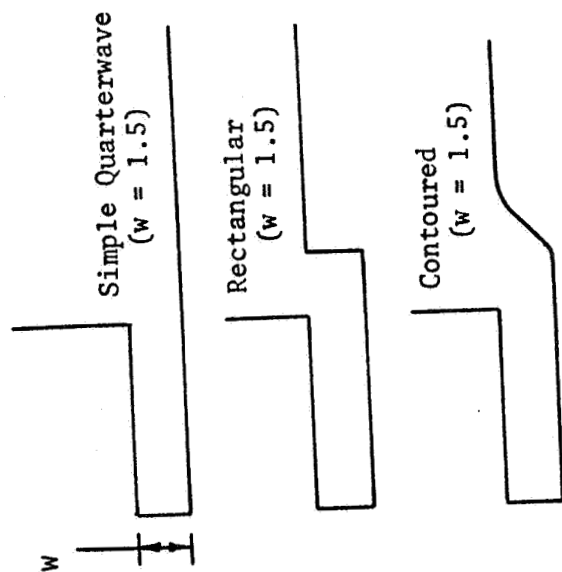
Figure 26. Acoustic Model Test Results
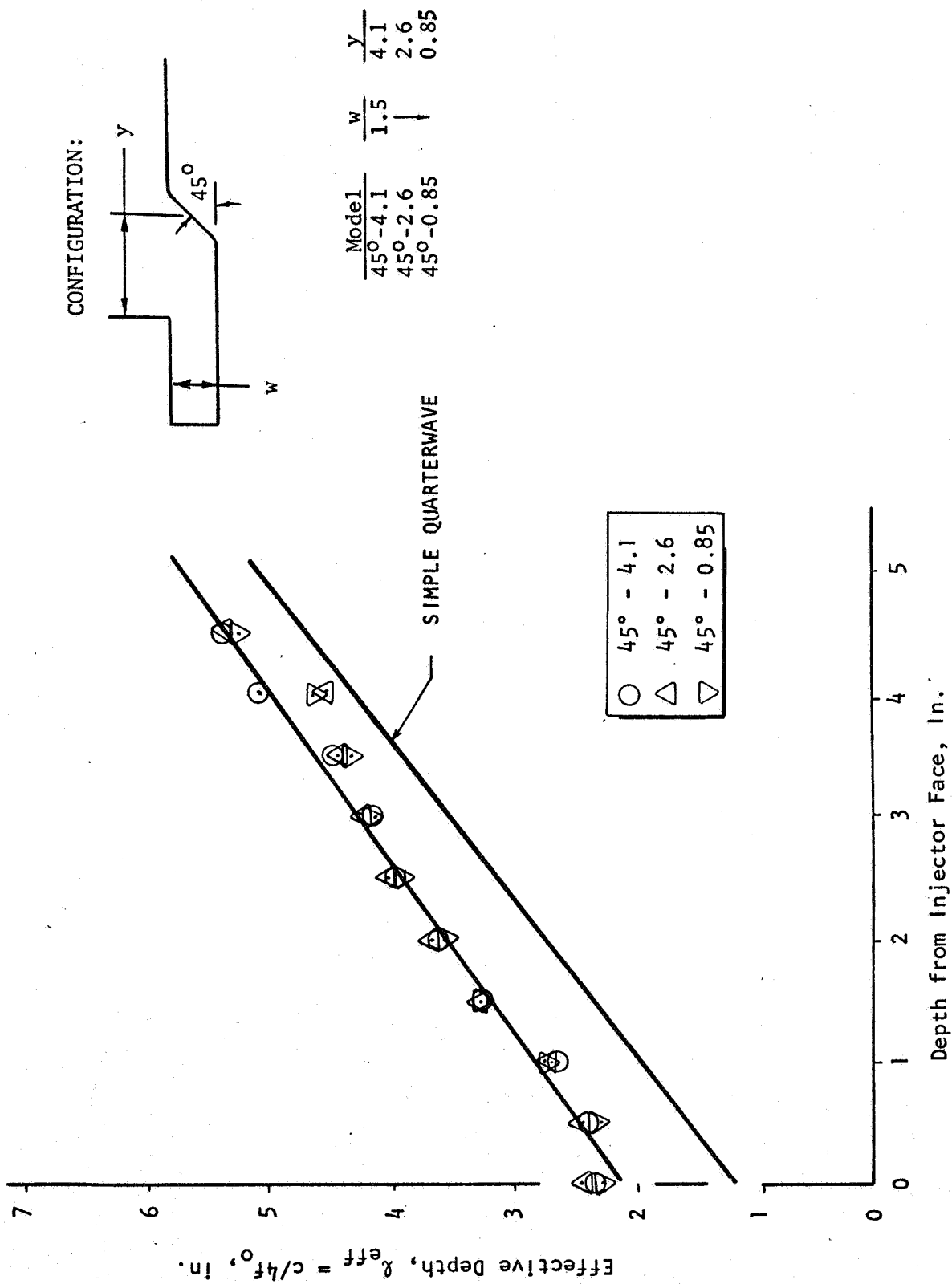
Figure 27.   Acoustic Model Test Results
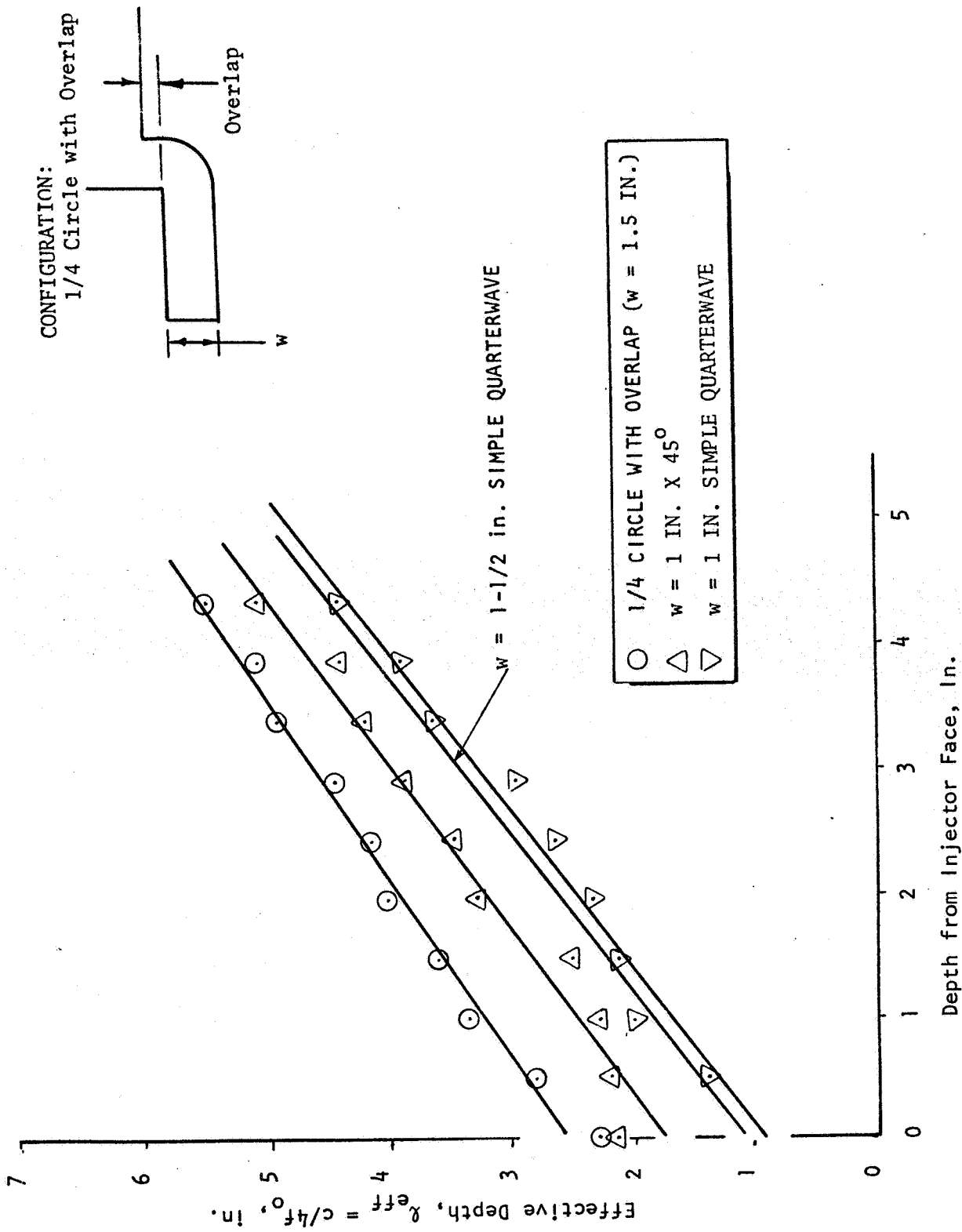
Figure 28. Acoustic Model Test Results

Because the test results appear to fall along straight lines, the depth contribution from the entrance region is also a linear function of depth, z. Employing the results from the 1 in/45° and 1½ in/45° tests the following equation for any width, w, was obtained:

$$\delta \simeq a(0.6w + 0.7) - bz(2.18w - 0.091)$$

Two significant observations may be made from the test results. First, the results shown in Fig.27 indicate the resonant frequency of the resonator is substantially unaffected by the position of the downstream portion of the cavity entrance, when varied over a range of 0.6 to 2.7 times the cavity width. Secondly, the overlap (0.2 inch) used with 1/4 circle entrance (similar to Aerojet partial contours) has apparently increased the effective depth by an amount approximately equal to the overlap; a conclusion inferred from comparison with the results for the rectangular entrance.

Chamber Model Testing

The model of the combustion chamber containing acoustic cavities, shown schematically in Fig. 29, was constructed from three concentric 1/4-inch wall Lucite tubes to form a chamber and six variable depth cavities. Employing this model, the variation of the resonant frequency of the lowest nine chamber modes with varying cavity depth was measured. The results are shown in Fig. 30, where the circular symbols correspond to measured frequencies (frequencies corresponding to response maxima). The curves in Fig. 30 correspond to predicted frequencies for each of the indicated modes. Generally, the predicted and measured frequencies agree very well.

3.3 ANALYSIS AND INTERPRETATION OF TEST RESULTS

The purposes of the analytical effort under this program were to aid design of the cavities to be tested and to aid evaluation, from the available data, of the effectiveness of acoustic cavities for suppressing instabilities. Most of the effort was directed toward assessing the significance of the 2300 to 2800 Hz oscillation experienced during testing on this and other programs.

The 2300 to 2800 Hz oscillation has been encountered repeatedly during testing of 8-inch diameter chambers at Rocketdyne and Aerojet. Rocketdyne has interpreted this oscillation as not being due to a normal chamber mode and probably associated with the acoustics of the feed system. With this interpretation, the acoustic cavity would be expected to weakly affect stability. Conversely, Aerojet has interpreted the oscillation as being due to the first tangential mode of the chamber with its frequency being suppressed by the acoustic cavity. Aerojet has tried many cavity configurations in an effort to suppress the
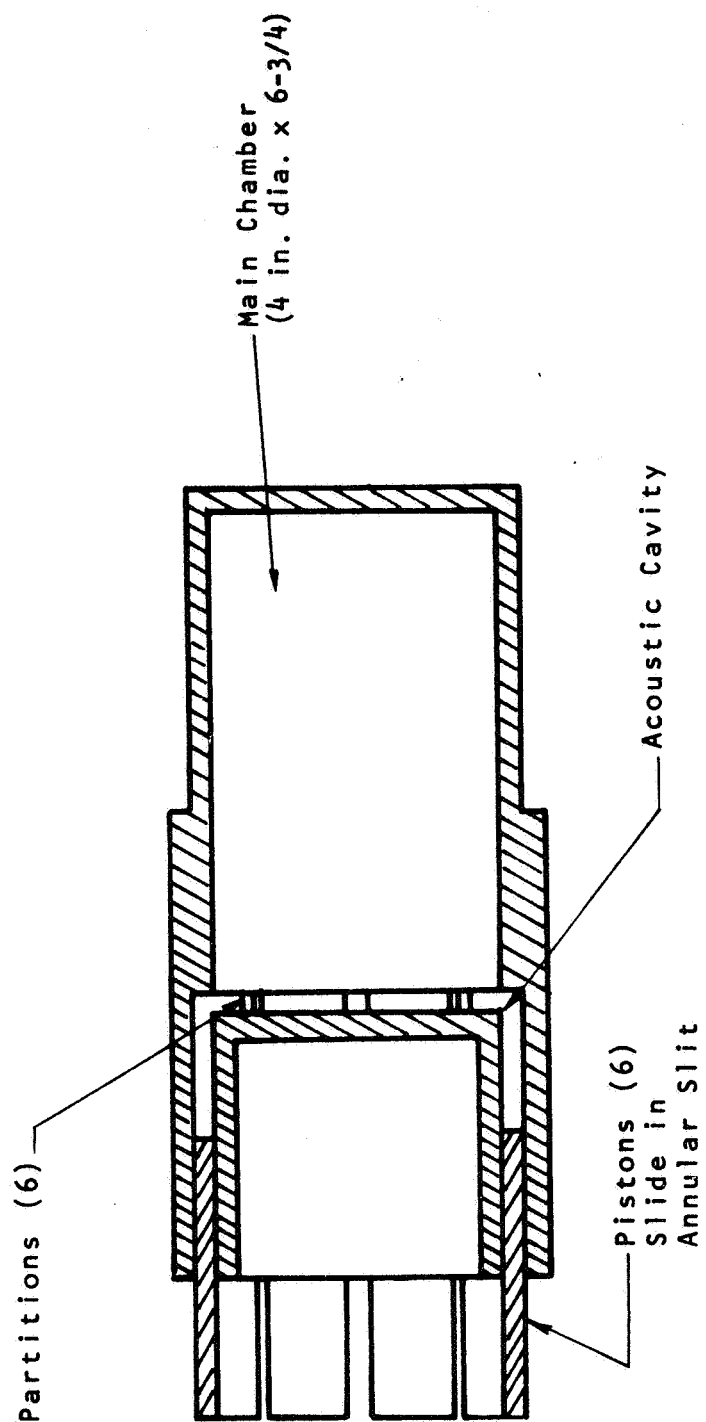
Figure 29. Schematic Diagram Of Chamber Acoustic Model

Main Chamber (4 in. dia. x 6-3/4)

Acoustic Cavity

Partitions (6)

Pistons (6) Slide in Annular Slit
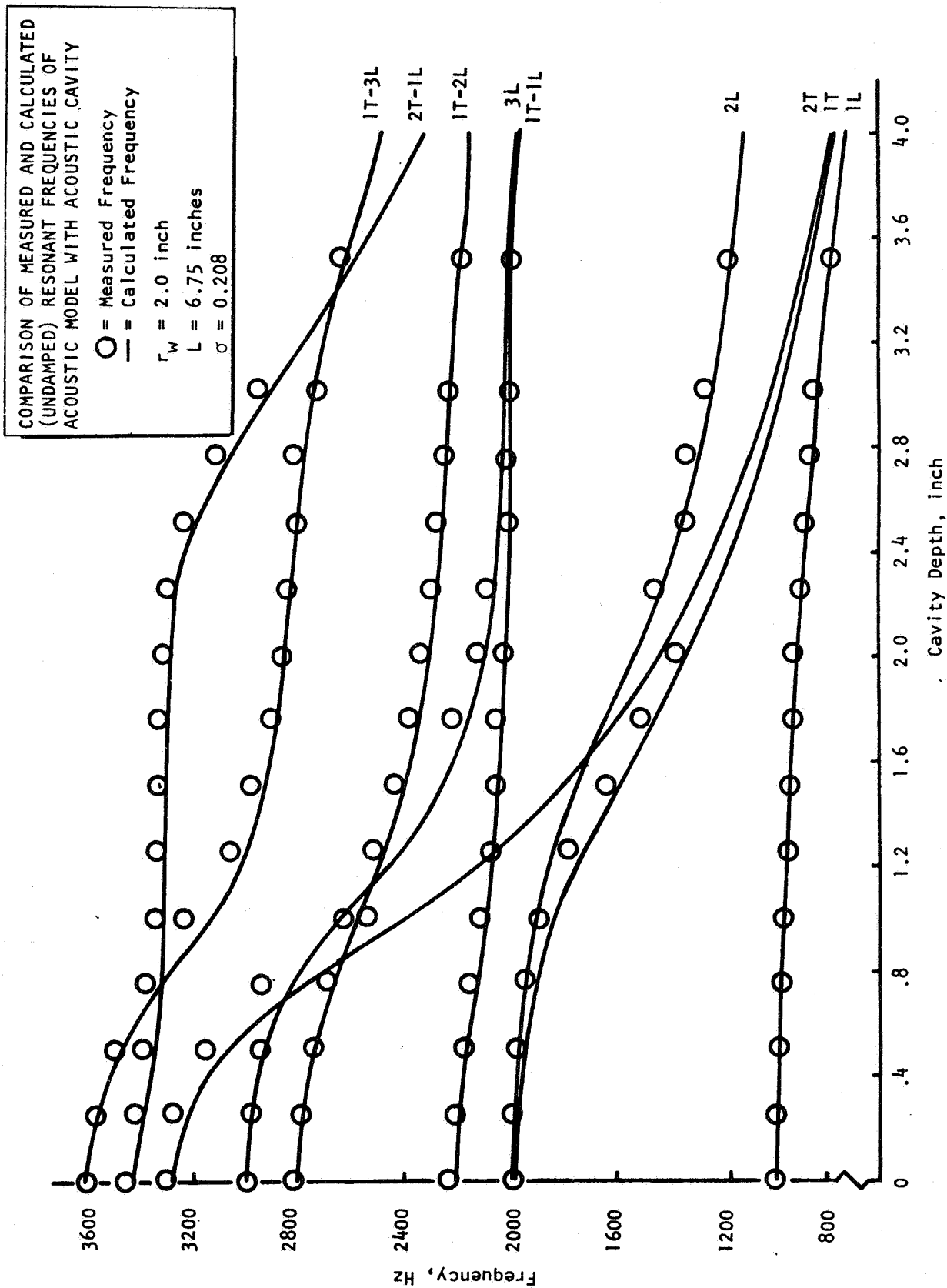
Figure 30. Results From Testing Chamber Acoustic Model

oscillation. In an effort to identify the mode or modes and clarify the implications relative to cavity effectiveness, analytical studies were made of both of these possibilities.

Observations Concerning 2300 to 2800 Hz Oscillation

Considerable testing has been done at Rocketdyne and Aerojet with 8-inch diameter chambers. The expected frequencies of oscillations may be estimated in the usual manner from the acoustic equations for a closed chamber. For the chamber used during this program, the estimated chamber mode frequencies are:

TABLE 15

EXPECTED FREQUENCIES IN ROCKETDYNE
CHAMBER WITH NO CAVITIES

Mode [1]	Frequency (Hz) [2]
1L	1631
2L	3262
1T	3194
1T-1L	3586
2T	5298
1R	6647
3T	7288

---

[1] 1L, 1T, 1R, ... denote the first longitudinal,
first tangential, first radial, ... modes.

[2] Sound velocity: 3724 ft/sec (95 percent of
theoretical shifting)

A frequency in this range was encountered during testing at Rocketdyne with an unlike-doublet injector (8.2-inch diameter chamber) but no 2600 Hz oscillation. Oscillation was observed in the range of 3000 to 3100 Hz, some higher frequencies and some in the range 480 to 1030.

During testing at Rocketdyne with the L/D #2 injector, multiple instances of 2380 to 2640 Hz oscillation were observed. This oscillation usually appeared during the damping of a bomb induced transient. It always occurred with a nominal fuel temperature of 200°F (no instances with 250°F fuel) and with a primary cavity open area fraction of 16 to 22 percent. With a smaller open area (13 percent) a 3000 Hz oscillation appeared.

During Rocketdyne testing with the L/D #1 injector, multiple instances of 2300 to 2800 Hz oscillation have been observed. However, dams in the fuel manifold eliminated the oscillation with 14.8 percent open area cavity. When the modified injector was tested in a 12 percent open area cavity, the frequency shifted to 2790 Hz from the 2560 Hz which had occurred earlier.

Aerojet has done extensive testing with an 8.1-inch diameter chamber. With platelet injectors, 2300 to 2900 Hz oscillation has occurred with a wide range of cavity configurations. Moreover, when the cavity was blocked 5200 and 6400 Hz oscillations occurred. During this testing, the contour of the cavity entrance and the amount of cavity overlap strongly influenced the instability.

Aerojet tests with a conventional like-doublet injector exhibited 2800 Hz oscillation with a shallow cavity and 3200 Hz with the cavity blocked off.

Bell Aerospace has done extensive testing with a 10-inch diameter chamber In this chamber 2520 to 2620 Hz oscillation was observed with a small open area 1T mode cavity, which corresponds to 3070 to 3200 Hz in an 8.2-inch diameter chamber.

These results suggest that when the cavity open area is insufficient, oscillation near the expected normal mode frequencies will occur, i.e., ~3000 to 3100 Hz which appears to be the first tangential mode with a slightly depressed frequency (the Aerojet platelet appeared to exhibit the second tangential and first radial modes). However, with larger open area cavities the 2300 to 2900 Hz oscillations appear with the like-doublet injectors in 8-inch diameter chambers. If these lower frequencies correspond to a first tangential mode with a depressed frequency, the frequency reduction is a much as 28 percent.

Analysis Of The Effects Of Cavities On Chamber Mode Frequencies

In an effort to assess the likelihood of the 2300 to 2900 Hz behavior being entirely or partially due to the acoustic cavities, the effects of cavities on the chamber modes were analyzed. The validity of model-predicted frequency effects was confirmed by comparison with the previously discussed acoustic model test results.

Predicted frequency variations for the first tangential and second longitudinal modes in the Rocketdyne 8.2-inch diameter chamber are shown in Fig. 31.

These calculations show that a 2300 to 2900 Hz first-tangential mode frequency is possible, but the frequency of the first tangential first longitudinal is near 3100 Hz under the same conditions. Moreover, relatively deep cavities are required (or lower sound velocities in the cavities) and the frequency should decrease with increasing cavity depth at ~800 Hz/inch. A sound velocity error ~25 to 30 percent is needed to account for the difference in predicted and actual depths. Also, the actual frequency change with increased depth is ~200 Hz/inch. In addition, a frequency change of ~50 Hz would be expected when the cavity fractional open area is increased from 0.148 to 0.12. The actual change was ~200 Hz. The disparity between the actual and predicted is too large to appear likely.

Figure 32 shows the variation of predicted damping with cavity depth for various values of the amplitude parameter $\Gamma\hat{p}/\gamma p$. The curves for $\Gamma\hat{p}/\gamma p_0 = 0.0$ correspond to the undamped case shown previously in Fig. . Thus, as damping is introduced it becomes more unlikely that a frequency of ~2600 Hz could be reached.

The foregoing analysis of cavity effects shows that frequencies of 2300 to 2900 Hz are possible as a result of cavity effects alone but very unlikely. Nevertheless, the results from full-scale testing, especially those obtained by Aerojet, show the cavity to have a significant effect under some circumstances. This observation suggests that cavity effects may interact with other effects, probably the feed system, to cause the 2300 to 2900 Hz oscillation.

Analysis of Feed/Injection System Acoustics

An indication of the possibility of feed system oscillation in the frequency range of 2300 to 2900 Hz was obtained from a calculation of the simple (uncoupled) resonant frequencies of various portions of the system.

These results suggested the need for a more thorough analysis of the feed system, allowing for coupling between the components. Therefore, such an analysis was developed. This model was obtained by solving the wave equation for the system sketched below:
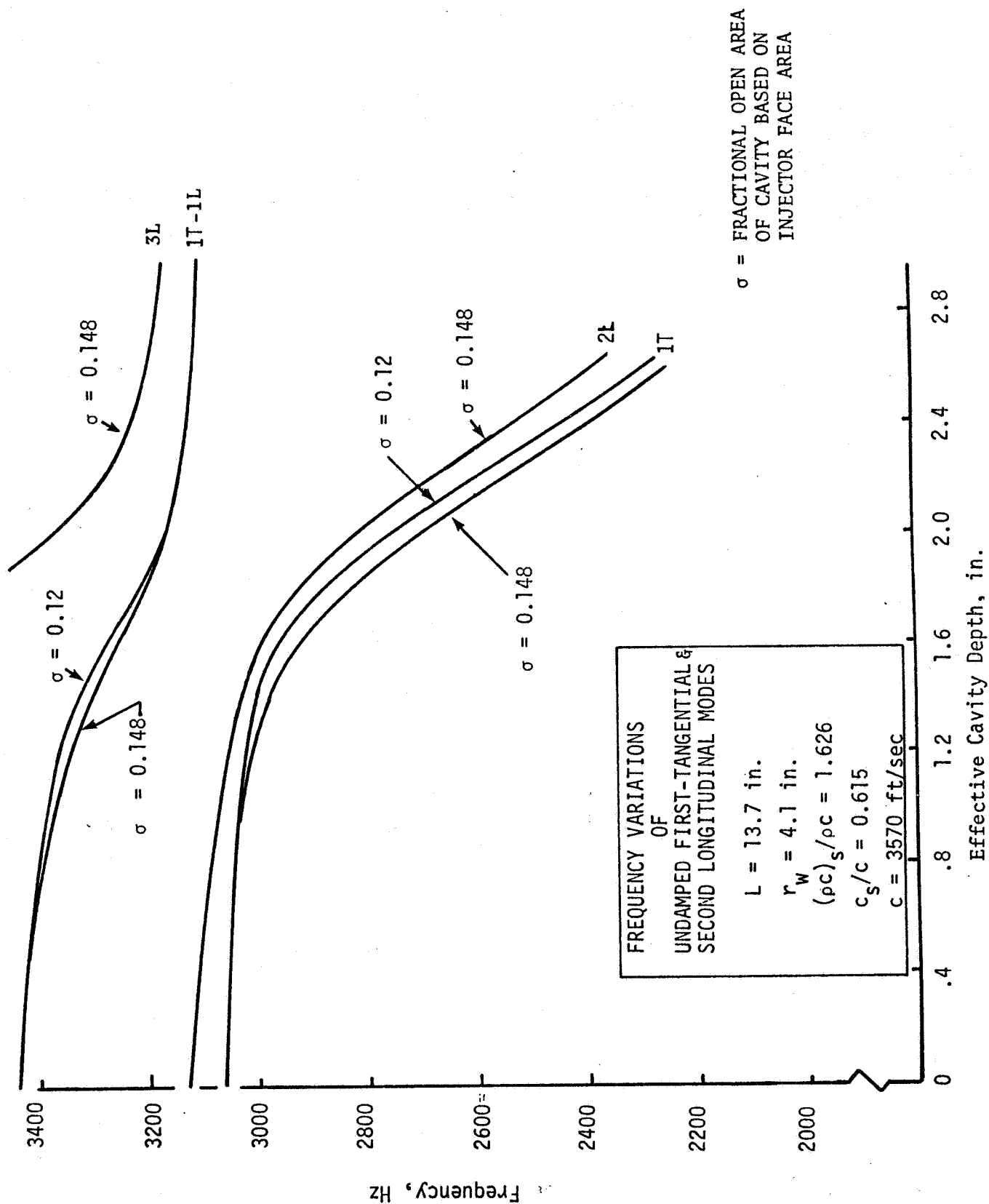
Figure 31. Predicted Frequency Variations With Cavity Depth
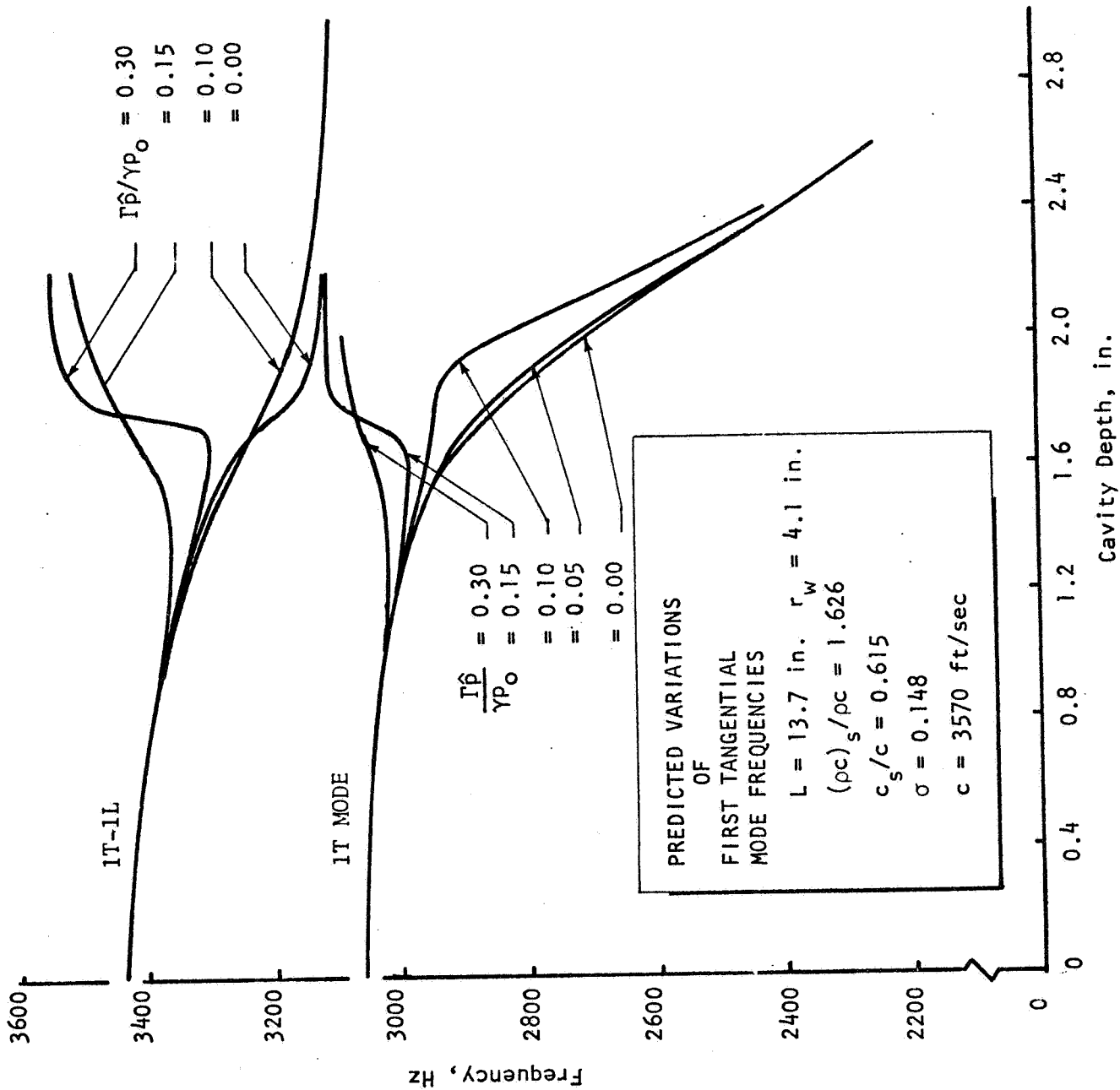
Figure 32. Variation Of Predicted Frequencies With Cavity Damping

Feed Line ———
Orifice ———
Feed Line ———
Valve ———

Manifolds

— Feed Passages

— Ring Manifolds

— Injection Orifices
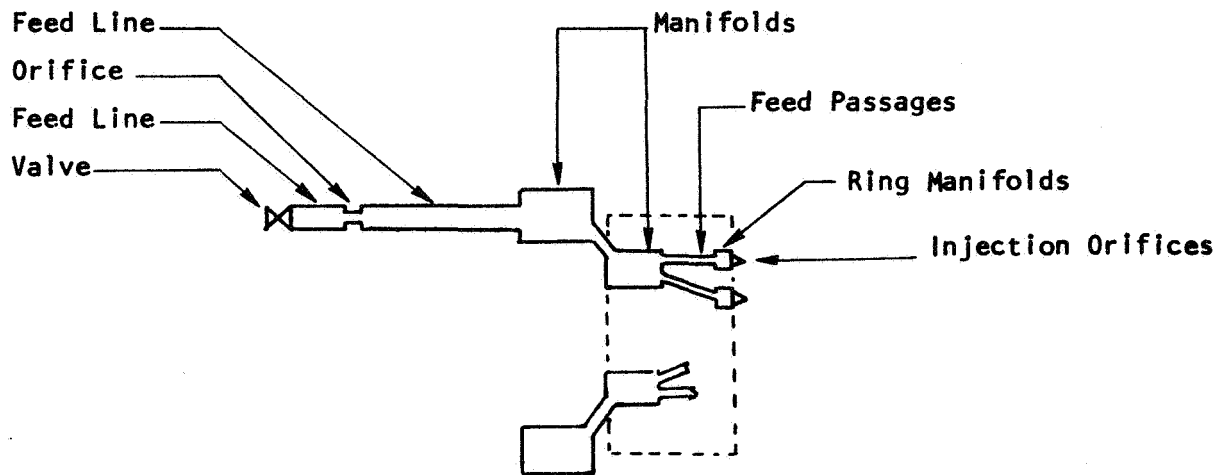
Calculations with this model for the fuel and oxidizer systems showed that a large number of modes were possible in the frequency range of interest. Although there are several modes with frequencies near those observed, the upward shift in frequency that occurred after installation of the manifold dams was not predicted. Therefore, the results from this analysis of the fuel system are not sufficient to firmly conclude the 2300 to 2900 Hz behavior is due to particular modes in this portion of the feed system. The results do show the large number of modes possible and suggest that further analysis could lead to an accurate prediction of observed behavior.

A similar analysis of the oxidizer system for purely longitudinal modes yielded results which were more compatible with the observed behavior. However, examination of the test data from this program showed clear evidence of a first tangential type of angular dependence of the pressure distribution. Thus, the results from the analysis of the oxidizer system do not permit the firm conclusion that the 2300 to 2900 Hz behavior is due to this portion of the feed system either.

Conclusions Regarding 2300 to 2900 Hz Oscillation

Results from the analysis effort do not permit the mode or modes of oscillation to be identified fully. However, it appears very unlikely that this oscillation is caused by cavity effects alone. Nevertheless, the oscillation is influenced by the cavity entrance configuration. This oscillation is also influenced by dams in the fuel manifold and, in addition, it appears to have a first tangential type of pressure distribution with the nodal position influenced by the fuel inlet position. These results suggest that the oscillation is associated with an interaction between the fuel injection system and

cavity effects. The cavity influence may result from interaction between the oscillatory jet emerging from the cavity and the injection/combustion processes of adjacent injection elements.

The available test data suggest that this mode has not occurred in the 10-inch diameter chambers.

4.0 REGENERATIVE COOLING INVESTIGATIONS

The use of electrically heated tubes and channels was shown to provide
an economical method of obtaining valuable steady-state and transient
data to assist in the design of regeneratively cooled thrust chambers.
More than 300 tests were conducted under Tasks VII, IX, and XIII of the
present contract. These tests provided data on heat flux capability of
regeneratively cooled chambers, the ability of a hot chamber to start
successfully with MMH or 50-50 fuels, and the ability of an MMH cooled
chamber to ingest helium either as discrete bubbles or in dispersed form.
Test summaries are presented in Tables 16 through 22. These investigations
are reported in detail in NASA-CR-141672, 134282 and 141560.

4.1 STEADY-STATE BURN OUT HEAT FLUX CAPABILITIES

Various types of hardware were used to simulate regeneratively cooled
thrust chamber operation. Initially, simple circular tubes such as that
shown in Fig.33 were used to obtain one-dimensional data on the heat
flux capabilities of MMH and 50-50 propellants. The steel tube was brazed
to copper terminal blocks and heated by the passage of electric current.
The test setup showing the heated tube, the electrical and propellant
connections, and the GN_2-purged box (for safety) are shown in Fig. 34.
As the heat flux (current) is gradually increased, thermocouples welded
to the outside of the tube indicate a gradual increase in temperature
until a point is reached where the transition to film boiling occurs.
At this point, the temperatures rise rapidly and the test is terminated.
This condition depends on the temperature, pressure, and the velocity of
the coolant in the tube at the downstream side of the heated tube.

These three parameters (temperature and pressure are combined in the sub-
cooling parameter) are correlated in Fig. 35 for 50-50 fuel and Fig.36
for MMH. A fair amount of scatter exists in the 50-50 data, but the MMH
data correlates the parameters fairly well. The correlation curves
derived for both the propellants were quite similar. These data were
incorporated into a two-dimensional thermal model to predict burnout
conditions and safety factors for the design of the first regeneratively
cooled OME (demonstrator) thrust chamber. The results of the heated tube
tests indicated that there was no difference in the heat flux capabilities
with saturated or unsaturated MMH.

The results of the heated tube tests were also used to design channels
having the cross-section of the regeneratively cooled chamber near the
injector-end. Figure 37 is a photograph of a typical heated channel design.
The U-shaped channel is closed out by brazing a strip of steel to the top
of the U. A copper strip brazed to the base of the U and brazed to the

TABLE 16. HEATED TUBE TEST SUMMARY

Test	Fuel	Tube I.D. in.	$\sim Q/A_2$ Btu/in^2-sec	Test	Fuel	Tube I.D. in.	$\sim Q/A_2$ Btu/in^2-sec
1	50-50	0.055	5	33	MMH	0.055	2
2		0.055	5	34			2.5
3		0.069	7	35			2.5
4		0.055	1.5	36			2.5
5			2	37			4
6			3	38			2
7			3	39			2
8			3	40			2.5
9			3	41			2.5
10			2	42			2.5
11			2	43			4
12			3	44		0.069	4
13		0.069	4	45			4
14			4	46			5
15			4	47			5
16			4	48			5
17			4	49			5
18			6	50			5
19			6	51			4
20			6	52			5
21			6	53			5
22			6	54			5
23			4	55			5
24		0.055	2	56		0.055	6
25			1.5	57			6
26			2	58			5
27			2.5	59			5
28			2.5	60			5
29			2	61			5
30			2.5	62			6
31			2.5				
32		0.069	2.5				

TABLE 17

OME HOT-START SIMULATION TESTS WITH MMH

Test	Tube Material	Initial Temp, F	Coolant Vel. (ft/sec)	Remarks
1-1	CRES No. 1	190	10	Quenched without temperature overshoot
1-2		280		
1-3		300		
1-4		630		
1-5		1000		
1-6		1200		
1-7		1340		
1-8		1200		
1-9		1070		
1-10		70		
1-11		1500		
1-12		1610		
1-13	CRES No. 2	620	8	
1-14		980		
1-15		1210		
1-16		1590		
1-17		600	5	
1-18		1030		
1-19		1210		
1-20		1600		
1-21	Electroformed Nickel	310	10	
1-22		890		
1-23		1130		
1-24		1580		
1-25		800	8	
1-26		1580	8	
1-27		350	5	
1-28		810	5	
1-29		1590	5	

NOTES: Tube dimensions = 0.25" O.D. X 0.035" wall X 4.0"

No. 1 and No. 2 are identical samples.

R-9686

TABLE 18

OME HOT-START SIMULATION TESTS WITH 50-50

Test	Tube Material	Initial Temp, F	Coolant Vel. (ft/sec)	Remarks
1-83	CRES No. 1	750	10	Quenched without temperature overshoot
1-84		1020	10	
1-85		1280	10	
1-86		1625	10	
1-87		1260	8	
1-88		1620	8	
1-89		1310	5	
1-90		1610	5	
1-91	Electroformed Nickel	646	10	
1-92		1220	10	
1-93		1600	10	
1-94		1115	8	
1-95		1600	8	
1-96		1200	5	
1-97		1620	5	

TABLE 19. SINGLE RECTANGULAR CHANNEL TEST DATA SUMMARY

	Test No.	Test Section	Heated Length (in.)	Test Type	*Adjusted Heat Flux ($\frac{Btu}{in^2-sec}$)	Helium Volume Percent @ Inlet	Coolant Velocity (ft/sec)	Remarks
1	20	4A	9.0	Checkout				
2	21			Checkout				
3	22			B.O.	1.80	0	9.7	
4	23			Froth - B.O.	1.82	0.8	12.1	
5	24				1.76	19.8	13.5	
6	25			↓	1.76	30.5	15.0	
7	26			B.O.	2.65	0	20.1	
8	27			Power Calibration	--	--	--	
9	28			B.O.	2.87	0	22.1	
10	29			Froth - B.O.	2.77	5.8	22.3	
11	30				2.87	10.4	26.1	
12	31			↓	2.90	15.8	27.8	
13	32			B.O.	3.45	0	28.0	
14	33	↓	↓	Froth - B.O.	3.57	~ 5.7	29.7	Test section failed - flow reduced too fast
15								
16	34	4B	9.0	B.O.	--	--	--	Isolation box window fogged - test terminated
17	35				--	--	--	Low heat flux - no burnout
18	36				2.07	0	13.5	
19	37				2.85	0	23.7	
20	38	↓	↓	↓	3.73	0	32.2	
21								
22	39	4B	2.5	B.O.	--	--	--	Low heat flux - no burnout
23	40				2.82	0	5.1	
24	41			↓	2.97	0	6.1	
25	42			Froth - B.O.	3.17	4.8	8.6	
26	43				3.30	12.5	11.4	
27	44			↓	3.25	39.5	13.9	
28	45			B.O.	3.80	0	13.4	
29	46			Froth - B.O.	--	--	--	Auto cut before stabilized
30	47			Froth - B.O.	3.92	6.4	15.3	Repeat Test No. 46
31	48	↓	↓	Froth Movies	--	Varied	--	Movies of various He ingestion levels
32								
33			• Adjusted for equivalent 1-D heat flux - does not include					
34			heat generation in lands or closeout					
35								

TABLE 19 (Concluded)

	Test No.	Test Section	Heated Length (in.)	Test Type	*Adjusted Heat Flux $\left(\frac{Btu}{in^2-sec}\right)$	Helium Volume Percent @ Inlet	Coolant Velocity (ft/sec)	Remarks					
1	49	4B	2.5	Checkout				Power calibration					
2	50			Checkout				Power calibration					
3	51			B.O.	2.95	0	3.8						
4	52			Froth - B.O.	3.08	19.6	9.0						
5	53			B.O.	4.35	0	16.7						
6	54			Froth - B.O.	3.83	31.6	15.6						
7	55				4.62	6.4	19.2						
8	56				4.37	5.6	17.7						
9	57			B.O.	4.45	0	17.8						
10	58			Froth - B.O.	4.35	5.7	18.0						
11													
12	59	5A	9.0	B.O.	1.55	0	15.3						
13	60				--	--	--	Auto cut before stabilized					
14	61				2.58	0	38.9						
15	62				3.26	0	55.8						
16	63				--	--	--	Auto cut before stabilized					
17	64				3.46	0	58.4						
18	65				--	--	--	Auto cut before stabilized					
19													
20	66	5A	2.5	B.O.	--	--	--	Low heat flux - no burnout					
21	67				--	--	--	Low heat flux - no burnout					
22	68				2.61	0	13.2						
23	69				3.05	0	18.8						
24	70				4.13	0	33.8						
25	71				4.72	0	43.0						
26													
27	* Adjusted for equivalent 1-D heat flux - does not include												
28	heat generation in lands or closeout												
29													
30													
31													
32													
33													
34													
35													

TABLE 20.   ROUND TUBE TEST SUMMARY

Test No.	Heated Length (in.)	Test Type	Heat Flux (Btu/in^2-sec)	Helium Volume Percent @ Inlet	Coolant Velocity (ft/sec)
1	8.9	Checkout			
2		Checkout			
3		*B.O.	1.64	.0	13.2
4			2.25	0	17.7
5			2.28	0	19.3
6	4.0		2.88	0	13.1
7			4.16	0	18.4
8			5.18	0	29.6
9			6.55	0	42.5
10		Froth B.O.	2.94	6.4	14.4
11			3.00	12.0	15.7
12			2.94	16.7	17.0
13			4.14	7.1	27.2
14			4.22	14.6	26.5
15			4.09	20.3	28.6
16			5.36	8.3	37.8
17			5.34	15.7	40.5
18			5.32	21.3	44.1
19		B.O.	5.32	0	28.4

TABLE 21. HELIUM BUBBLE INGESTION TEST SUMMARY – CIRCULAR TUBE TEST SECTION

TEST NO.	COOLANT	CRES TUBE HEATED LENGTH, IN.	HEAT FLUX, BTU/IN²-SEC	BUBBLE DURATION SEC	REMARKS
1-30	MMH	4.0	2.0	.017	
31			3.35	.017	
32			4.65	.017	T_w >1800F Burnout
33			3.25	.017	
34			3.36	.034	
35			3.05	.034	
36			2.37	.051	
37			3.05	–	
38			3.08	.051	
39			2.39	.028	
40			3.08	.028	
41			2.39	.080	
42			3.09	.081	T_w >2000F Both ends
43			2.69	.081	
44			2.89	.081	
45			3.08	.081	
46			3.12	.098	80F T_w Rise
37			3.12	.13	One inch red
48			3.15	.13	40F T_w rise
49			3.15	.13	20F T_w rise
50		2.0	3.08	.007	
51			3.10	.018	
52			3.12	.044	One inch red near outlet
53			3.06	.037	
54			3.06	.044	
55			3.04	.044	
56			3.04	.044	
57			3.04	.060	
58			3.57	.008	
59			3.57	.018	
60			3.57	.024	
61			3.57	.037	
62			3.57	.041	
63			3.59	.059	
64			3.57	.060	
65			3.57	.062	
66	SAT. MMH		3.03	.007	
67			3.03	.018	
68			3.04	.024	
69			3.04	.037	
70			3.04	.041	
71			3.04	.060	
72			3.04	.072	
73			3.04	.084	
74			3.03	.12	
75			3.04	.20	
76	50-50		3.11	.008	
77			2.31	.008	
78			3.04	.008	
79			3.10	.008	
80			3.10	.035	
81			3.10	.072	
82			3.11	.20	One inch red near outlet

# TABLE 21A. HELIUM BUBBLE INGESTION TEST SUMMARY – RECTANGULAR CHANNEL TEST SECTION

	Test No.	Coolant	*Test Section	Coolant Flowrate (lb/Sec)	**Heat Flux $\dfrac{BTU}{(in^2\text{-}sec)}$	Coolant Velocity (ft/sec)	REMARKS		
1	1-98	50-50	#1	.038	2.62	21			
2	99				2.60				
3	100				2.64				
4	101				2.60				
5	102				2.62				
6	103				2.64				
7	104				2.63				
8	105				3.24				
9	106				3.26				
10	107	↓	↓	↓	3.24	↓			
11	2-33	MMH	#2	.073	2.74	42			
12	34				2.74				
13	35				2.78				
14	36				2.73				
15	37				2.82				
16	38				2.77				
17	39				2.77				
18	40				2.73				
19	41				2.75				
20	42			↓	2.76	↓	55 F wall temp. rise		
21	43			.077	2.77	44	50 F wall temp. rise		
22	44		↓	.076	2.75	44	35 F wall temp. rise		
23	51		#3	.038	2.83	21			
24	52				2.58				
25	53				2.58				
26	54				2.58				
27	55				2.58		320 F wall temp. rise		
28	56				2.57		320 F wall temp. rise		
29	57	↓	↓	↓	2.57	↓	320 F wall temp. rise		
30									
31									
33	*Heated Length = 2.0 Inches								
34	**Adjusted Down by 13 Percent to Account								
35	for Heat Generation in Lands and Closeout								

TABLE 22. THREE-CHANNEL PANEL TEST DATA SUMMARY

	Test No.	Test Section	Heated Length (in.)	Test Type	Adjusted Q/A $\left(\frac{Btu}{in^2-sec}\right)$	Center Channel Fluid	Center Channel Flow (lb/sec)	Outer Channels Total Flow (lb/sec)	$\overline{V}$ (ft/sec)	REMARKS
1	72	Panel #1	9.0	Infinite Bubble	1.90	He	.00115	0.087	20.0	
2	73				1.99	He	.00115	0.087	20.0	
3	74			↓	1.35	He	.00115	0.050	11.5	
4	75			*P.C.	1.93	He	~.0002	0.0865	19.8	
5	76				1.35	He	~.00015	0.0485	11.1	
6	77				0.73	He	~.0001	--	--	Low MMH flow - cut before stabilized
7	78				1.35	He	~.00015	0.061	14.0	
8	79				1.36	He	~.0001	0.0645	14.8	
9	80			↓	2.00	MMH	0	0.091	20.9	No B.O.
10	81			B.O.	1.66	MMH	.021	0.041	9.8	
11	82				1.57	MMH	.020	0.040	9.5	
12	83				2.08	MMH	.031	0.060	14.3	
13	84				2.63	MMH	.044	0.0875	20.8	Fuse blown - no B.O.
14	85	↓	↓	↓	2.63	MMH	.045	0.092	21.9	
15										
16	86	Panel #3	9.0	P.C.	1.30	He	~.0001	0.083	7.4	
17	87				1.12	He	~.0001	0.060	5.4	
18	88				1.20	He	~.0001	0.087	7.8	
19	89				1.00	He	~.0001	0.060	5.4	
20	90			↓	1.17	MMH	0	0.087	7.8	No. B.O.
21	91			B.O.	1.05	MMH	.014	0.029	2.7	
22	92				1.48	MMH	.030	0.0615	5.7	
23	93	↓	↓	↓	0.98	MMH	.0185	0.0365	3.4	Auto cut failed - copper melted
24										
25	94	Panel #1	2.5	P.C.	2.47	He	~.0001	0.0655	14.0	No B.O.
26	95			P.C.	2.55	MMH	0	0.0635	13.6	No B.O.
27	96			B.O.	3.38	MMH	.0175	0.0365	8.0	
28	97	↓	↓	B.O.	3.07	MMH	.013	0.028	6.2	
29										
30	98	Panel #3	2.5	P.C.	2.18	He	~.0001	0.087	7.3	No B.O.
31	99			P.C.	2.37	MMH	0	0.080	6.7	
32	100			B.O.	2.60	MMH	.024	0.0495	4.1	No B.O.
33	101				2.38	MMH	.018	0.034	2.9	No B.O.
34	102			↓	2.45	MMH	.0135	0.0265	2.3	
35	103	↓	↓	P.C.	2.50	MMH	0	0.089	7.4	

FORM R 79-Y-3   * Plugged center channel simulation
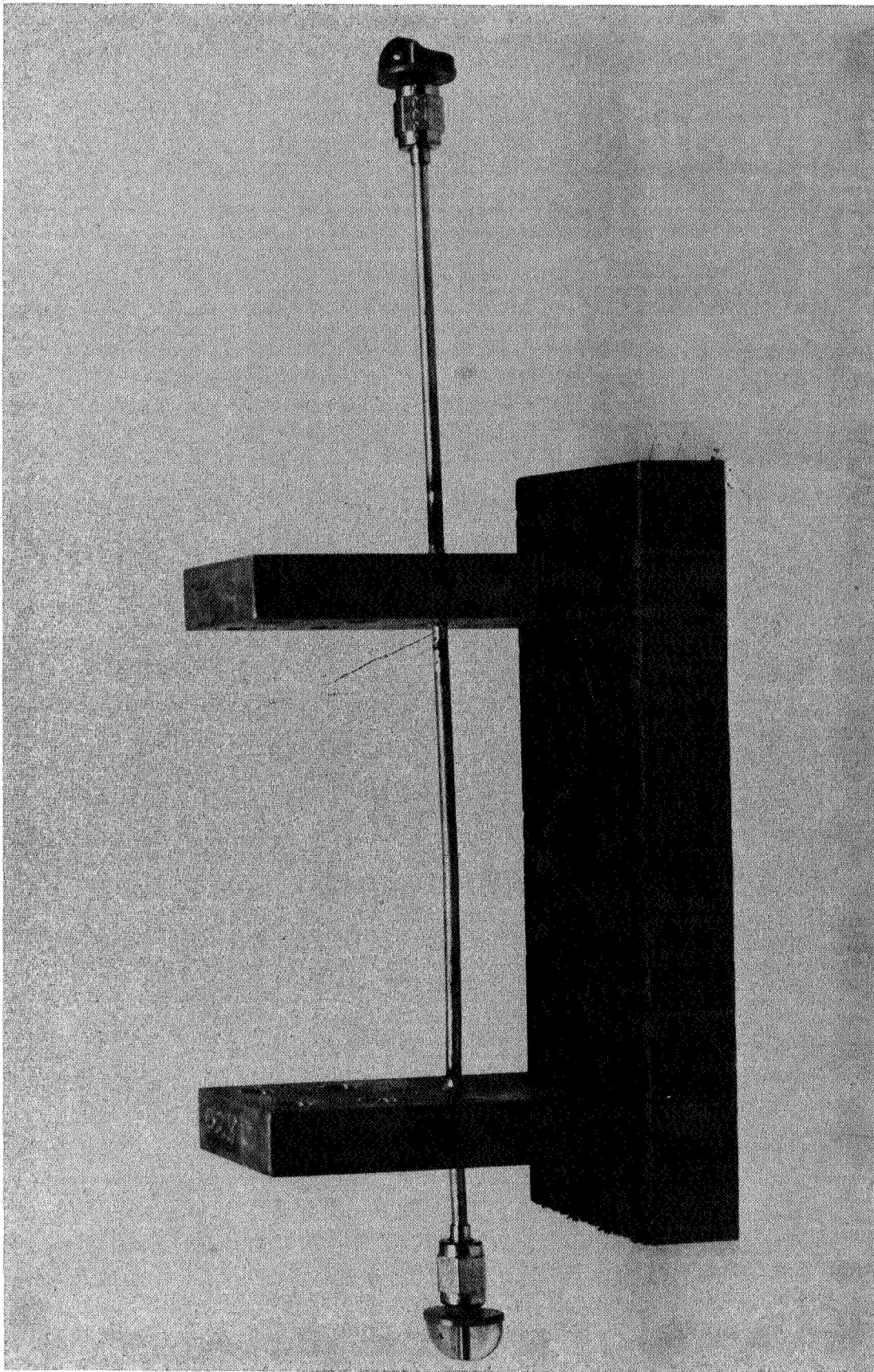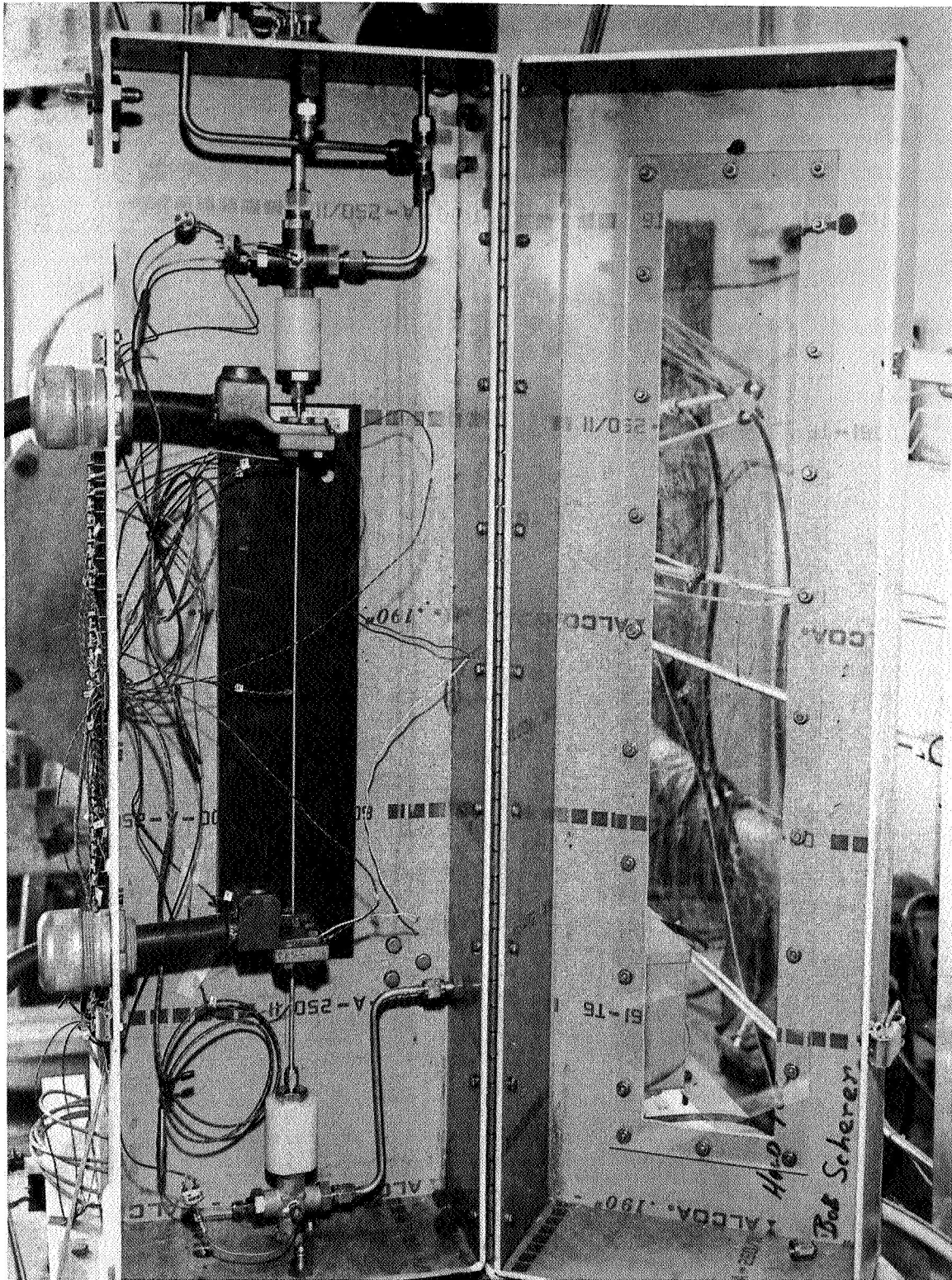
Figure 33. Heated Tube Assembly

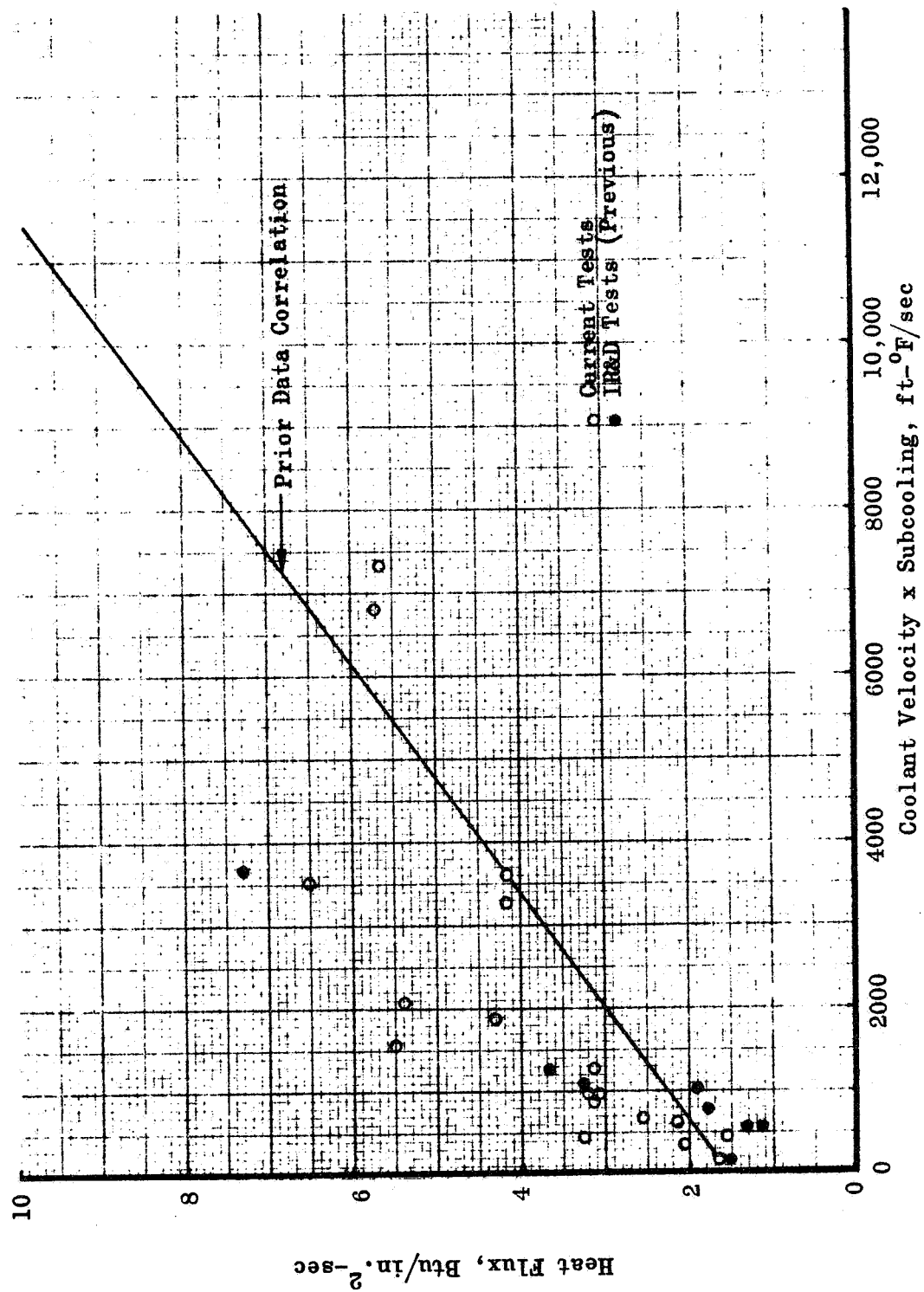Figure 34. Heated Tube Hardware And Facility

R-9686

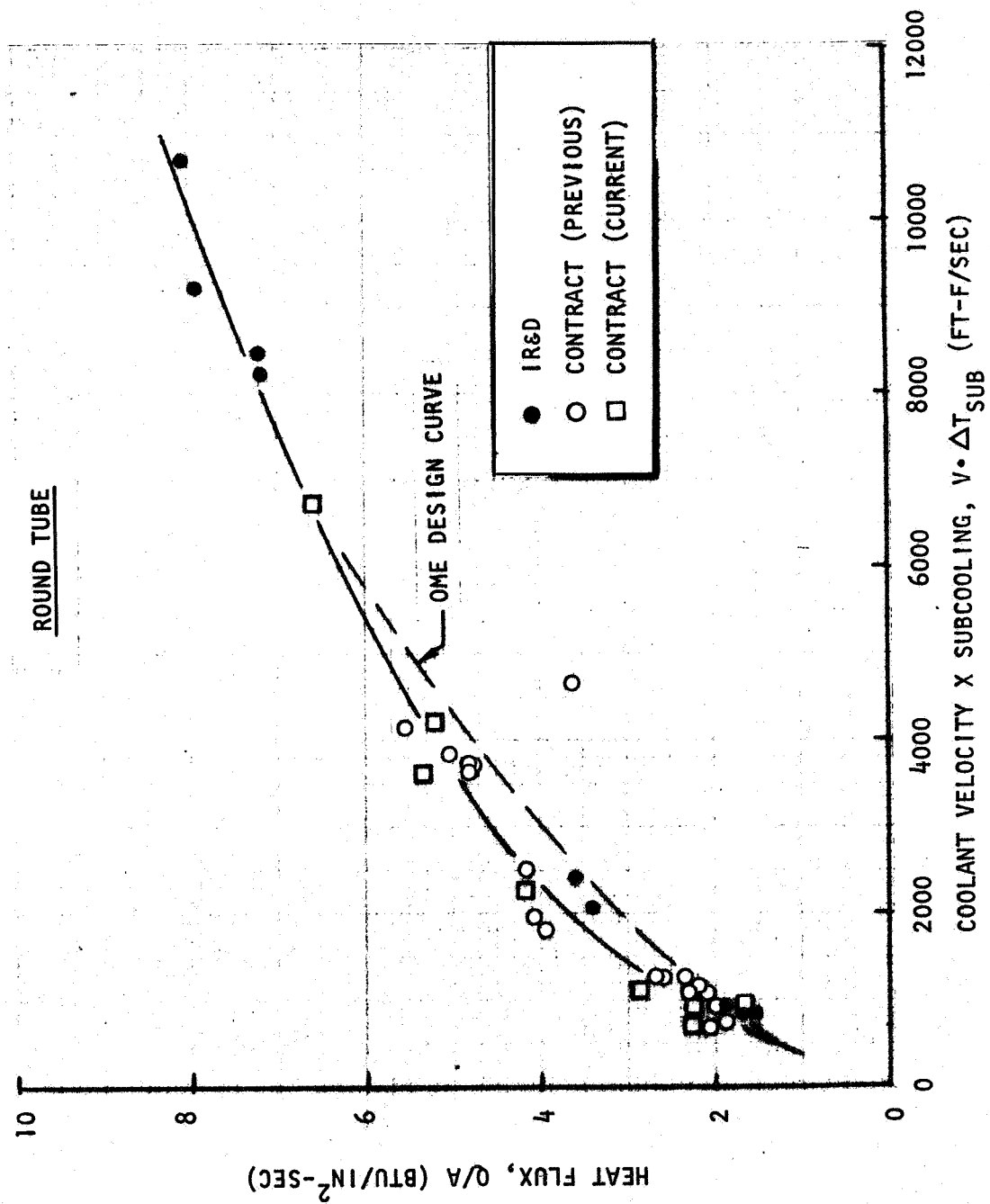Figure 35 . Experimental Burnout Heat Flux Correlation for 50-50

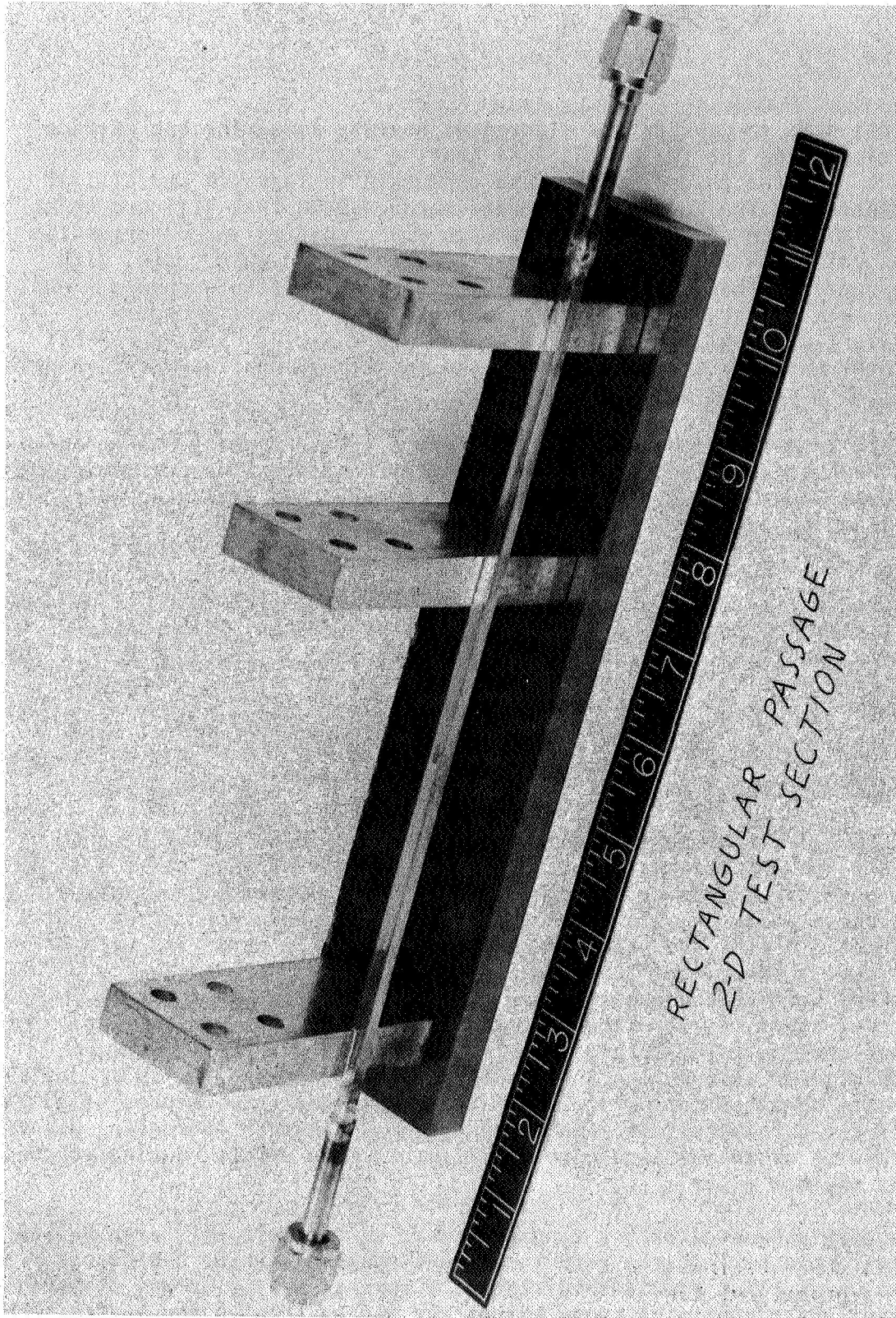Figure 36 Experimental Burnout Heat Flux Data for MMH

Figure 37. Rectangular Passage 2-D Test Section

terminal bars to provide the electrical heating along the one surface thus simulating the two-dimensional heating which occurs in a thrust chamber. Heated channel tests were conducted in Tasks IX and XIII of the contract. The results from tests conducted in Task XIII are shown in Fig. 38. The good agreement between the predicted and experimental values validates the use of the data from the round tube tests, with an appropriate thermal model, for thrust chamber design purposes. One of the sets of data shown In Fig. 38 is for the channel geometry of the flight OME designed by Aerojet. The other set of data represents a channel geometry which emphasizes the two-dimensional asymetric heating affect of a channel wall chamber.

Finally, in order to demonstrate that the single-channel tests produced valid data as compared to the multi-channel heating which occurs in a regeneratively cooled chamber, a series of tests was conducted with electrically heated panels having three channels. Figure 39 is a photograph of one of the test sections. The section is shown schematically in Fig. 40. The three bus bars provide an opportunity to test three different electrically heated lengths on the same specimen. The sandwich construction of the heated section is similar to that of the heated single-channel section. The test data shown graphically in Fig.41 illustrates the excellent agreement between data taken on single and multiple channels.

4.2 ADVERSE OPERATING CONDITIONS

The OME may be required to start with a chamber which is hot because of soak-out from a previous firing or because of the heating affects of other engines. In order to determine whether detonations or fouling would occur as a result of these starts, tests were conducted with electrically heated tubes. To simulate the materials of construction used in the OME thrust chamber, the tubes were made of electroformed nickel and CRES. The tubes were heated electrically with no propellant in the tube. The low power level required to bring the tubes to an equilibrium temperature without cooling was maintained while the coolant valve was open and coolant flowed through the tube. Coolant flow rates as low as 1/4 of the flow rate expected during start was tested at tube temperatures of up to 1600 F for both materials. No instances of detonation or fouling occurred. The results of these tests were verified, to some extent, during subsequent thrust chamber tests.

Tests were conducted with a single channel to determine if large helium bubbles could be ingested into the thrust chamber without overheating. Nominal propellant flow was initiated; a nominal heat flux was electrically applied; and a bubble of known volume was passed through the heated tube
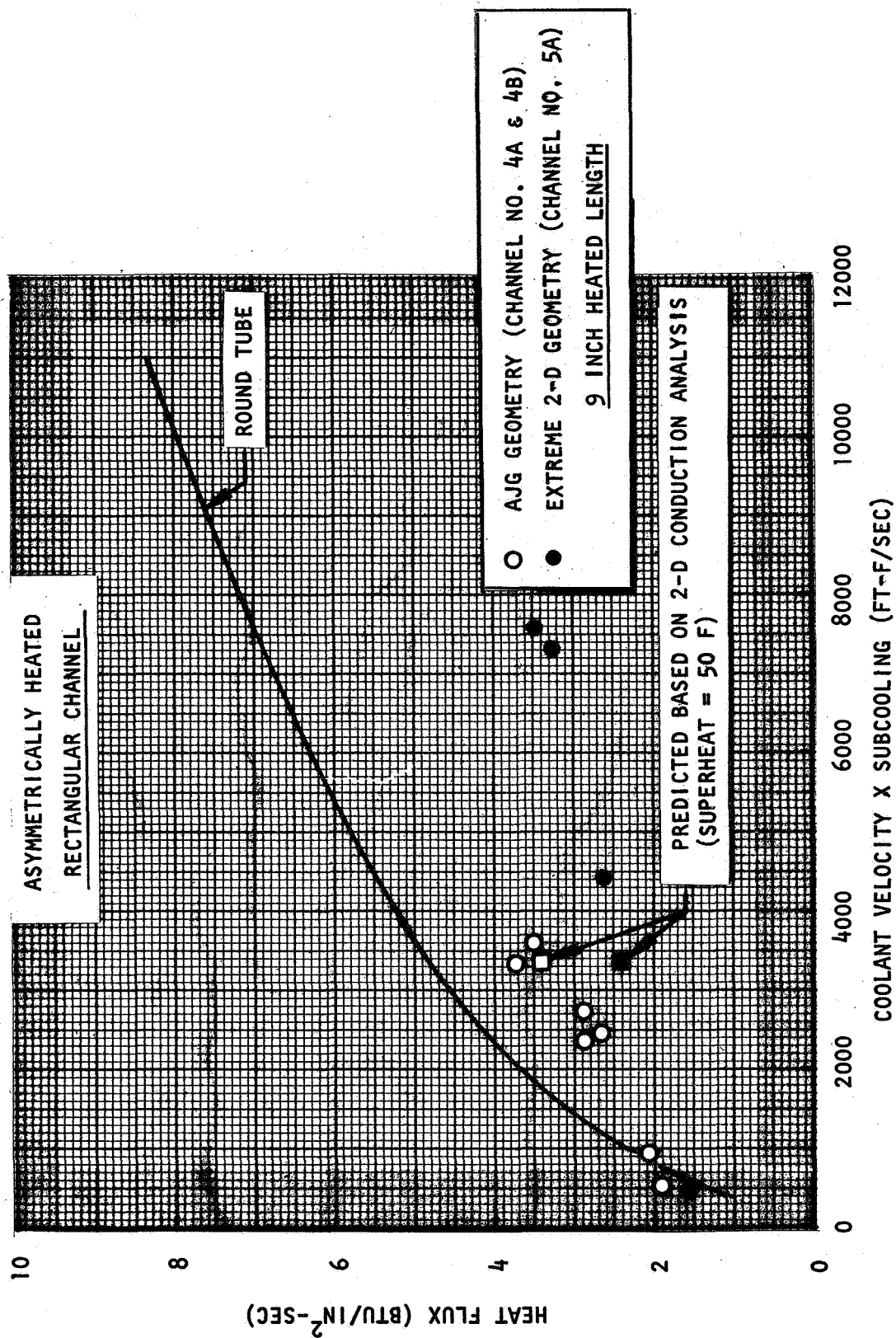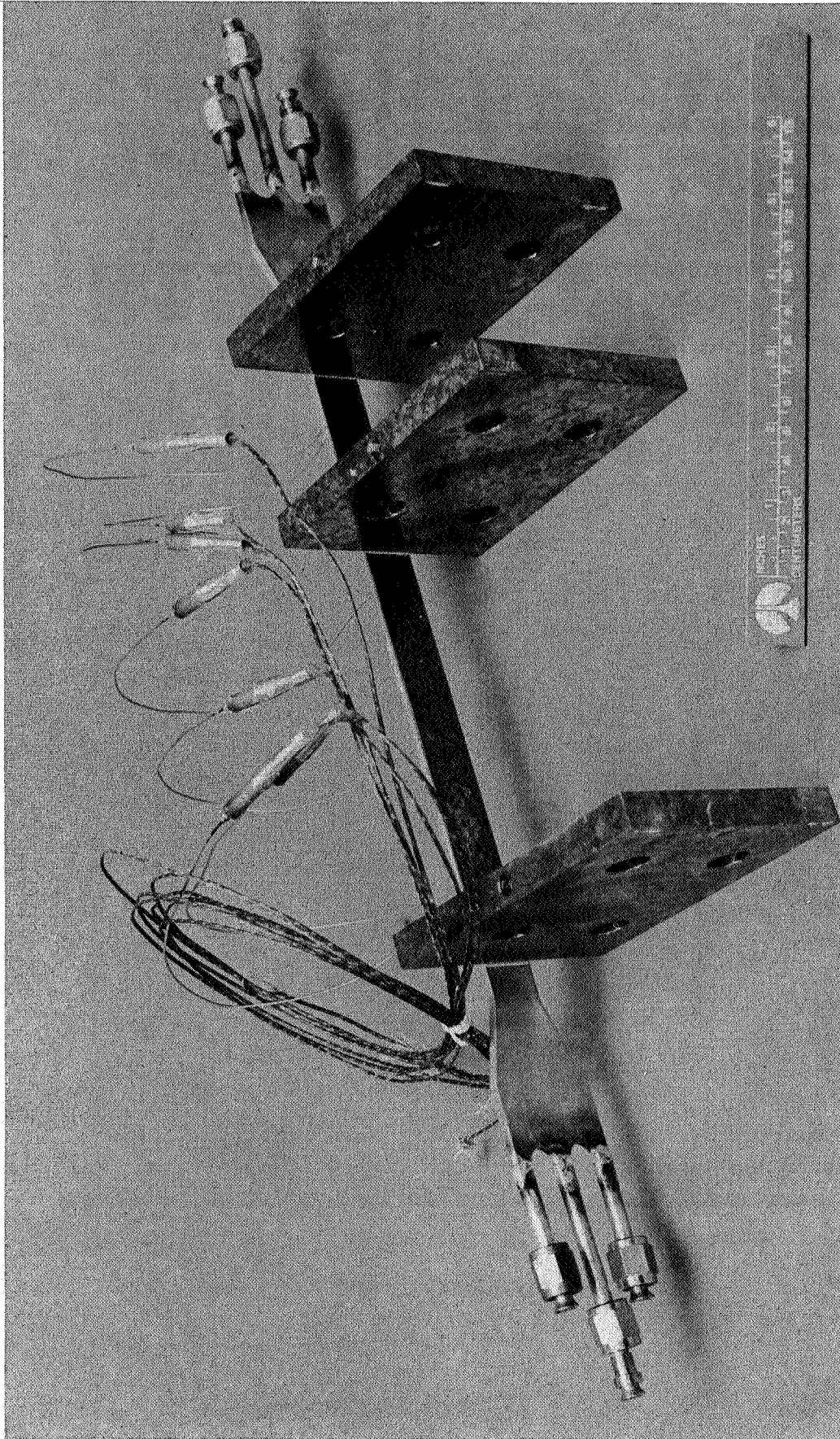
Figure 38 Experimental Burnout Heat Flux Data for MMH

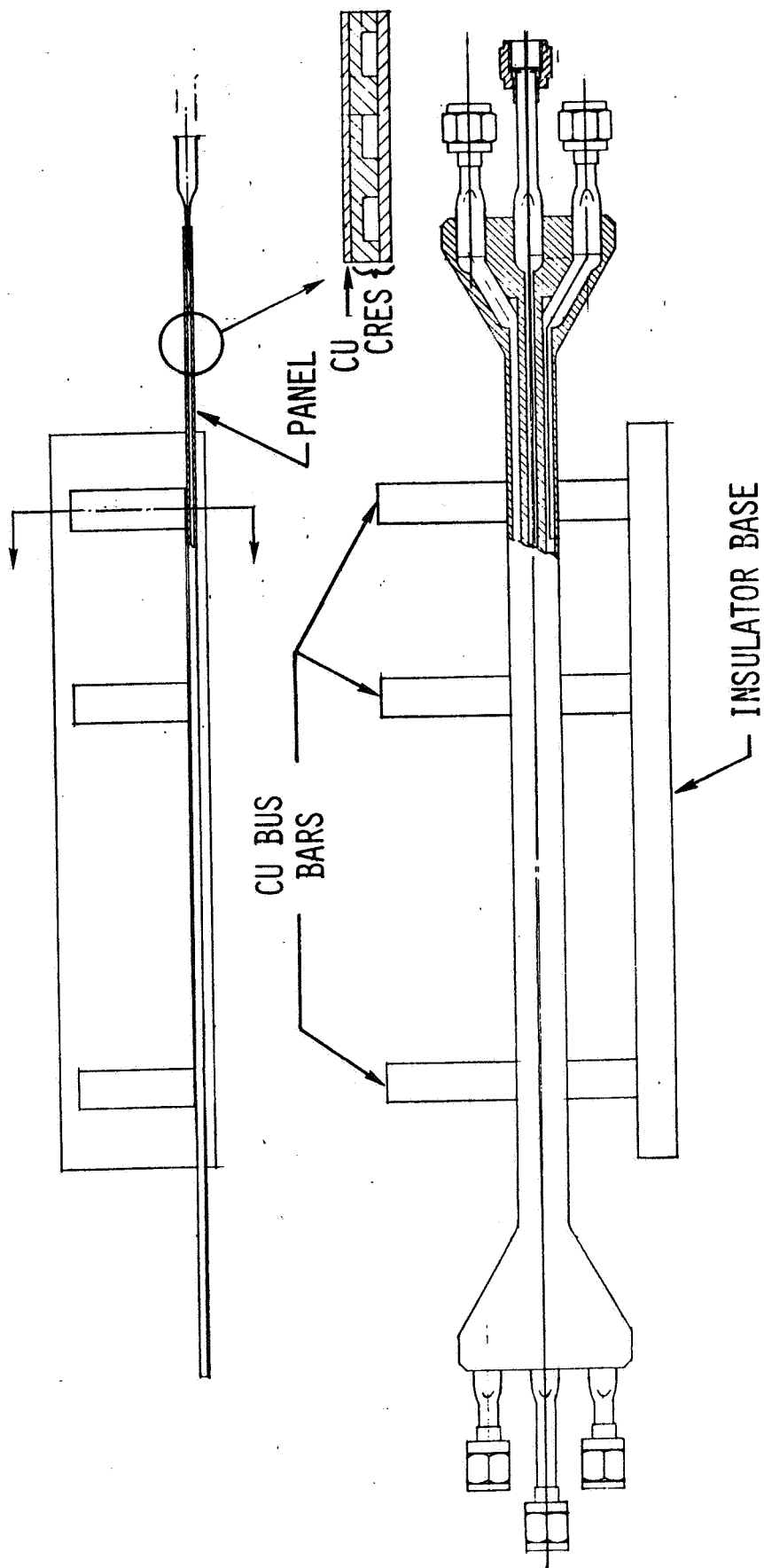Figure 39. Three Channel Panel Test Section

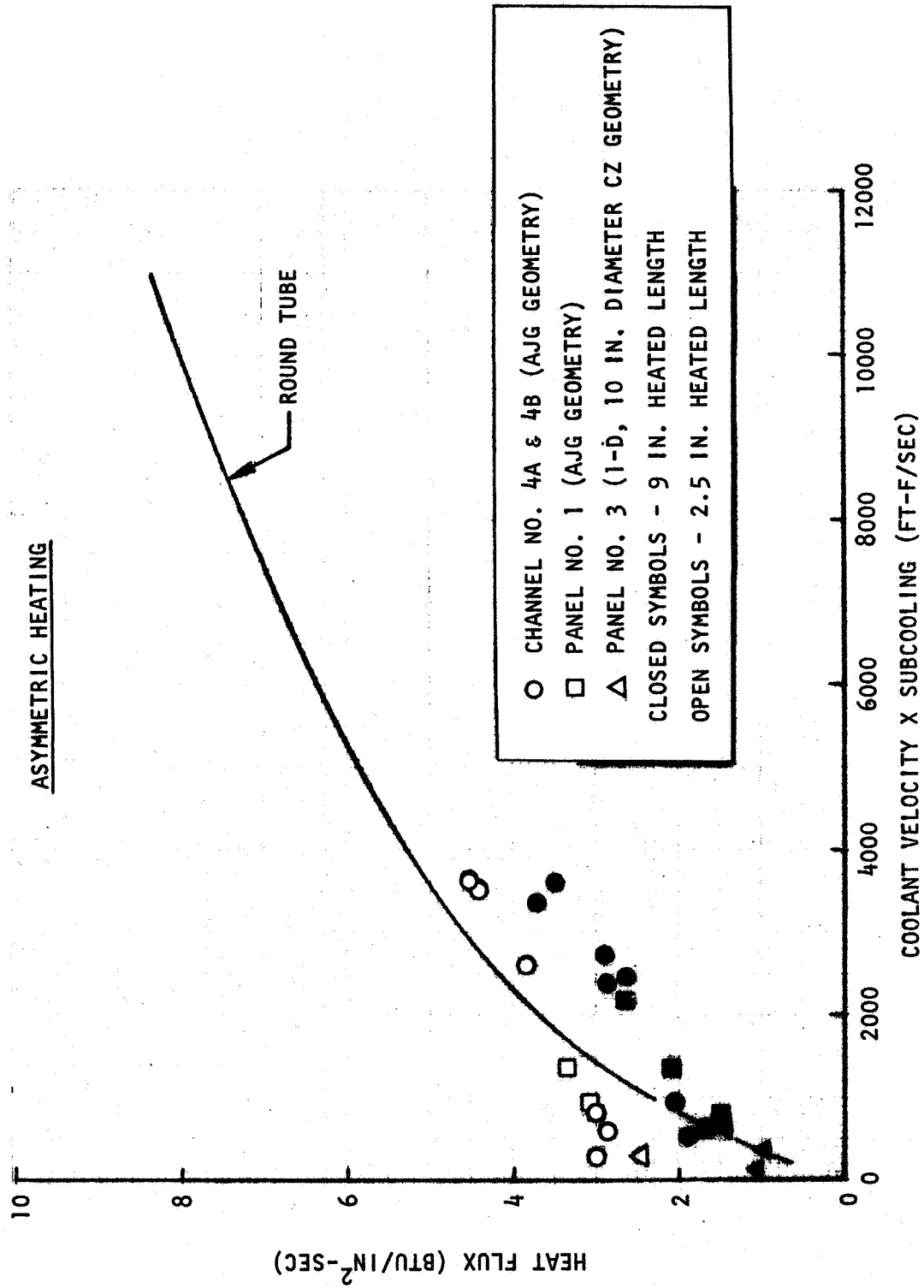Figure 40. Electrically Heated Panel 3-Channel Simulator

Figure 41 . Comparison of Channel and Panel MMH Burnout Heat Flux

and subsequently followed by a continuation of nominal coolant flow.
The temperature of the heated channel wall rose while the bubble passed
through the channel and decayed when the fresh coolant entered. No
damage occurred to the heated channel hardware even though bubbles of
durations up to 1.3 seconds were passed through the heated hardware.
Since it has been calculated that a large helium bubble would reach the
injector in approximately 0.3 seconds and result in a substantial
reduction in the heat flux, the heated channel test data indicated that
the OME thrust chamber could tolerate ingestion of a massive helium
bubble. Subsequent tests with a complete thrust chamber verified
these data.

Helium ingestion as a dispersed mixture (froth) could continue for a
relatively long time without an appreciable decrease of the heat flux.
MMH with various amounts of helium ingested in this fashion was passed
through the heated channel in order to determine whether the heat flux
correlation was affected significantly by the helium ingested in this
manner. The test results shown in Fig. 42 indicate that only a slight
reduction in the burnout heat flux capability results from ingestion of
dispersed helium in quantities as large as 40 percent by volume.

A test series was conducted with the three-channel panel to simulate
plugging of one channel on an OME thrust chamber. The center channel of
the panel was plugged on the upstream side for most cases and on the
downstream side for one test while nominal flow was maintained in the
outer two channels. No detonations occurred with either type of plugging.
The results, shown in Fig. 43 indicate a significant reduction in the
flux capabilities of the adjacent channels. The data shown can be used
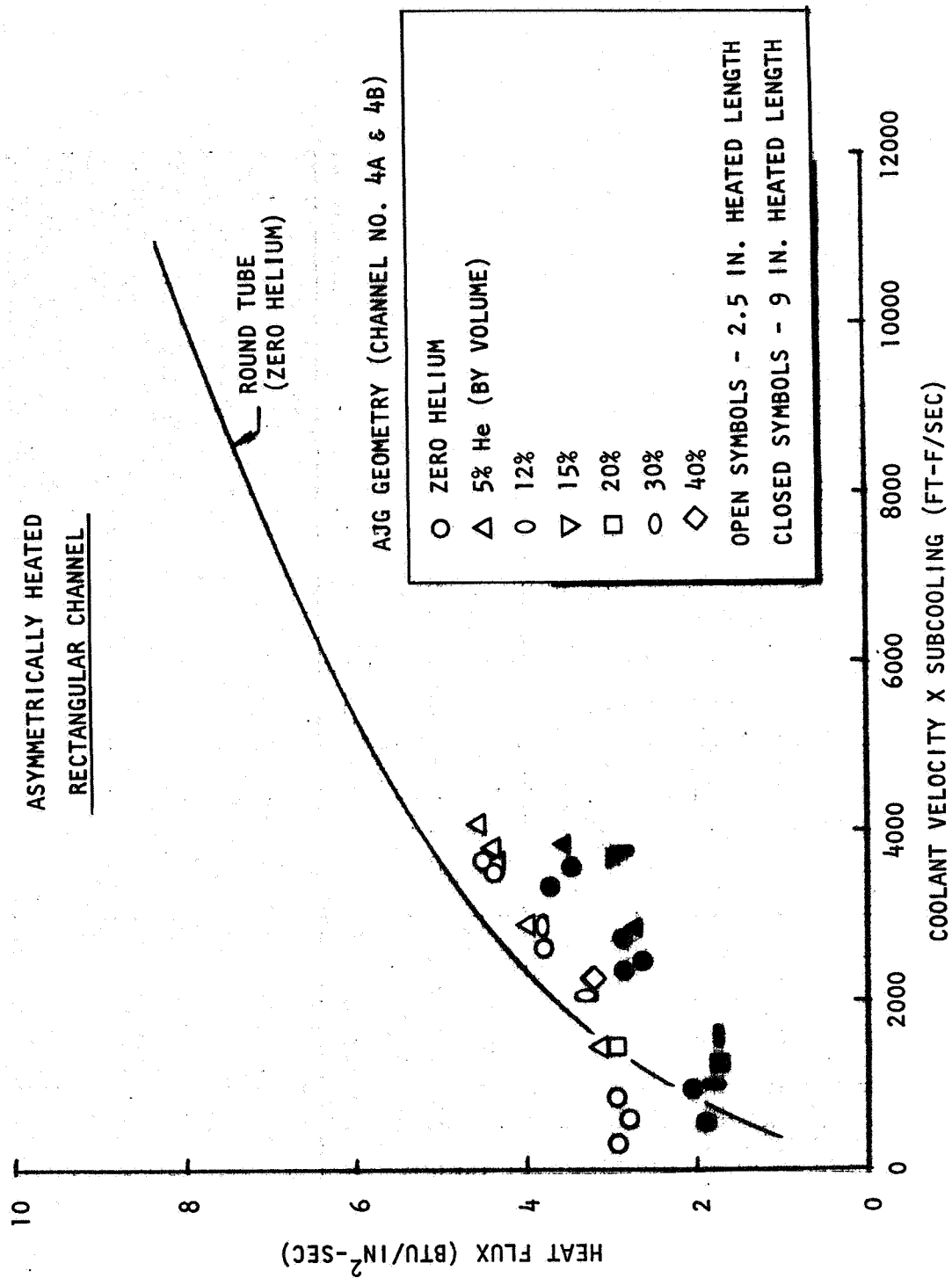to design chambers for this off-design condition.

Figure 42. Effect of Helium Ingestion on MMH Burnout Heat Flux

Figure 43. Effect of Completely Plugged Channel on Adjacent Channels Maximum Heat Flux Capability

5.0 DEMONSTRATION THRUST CHAMBER

An experimental thrust chamber was designed, fabricated, and tested in
order to demonstrate critical design, fabrication, and operating regimes
of a regeneratively cooled OME reusable thrust chamber. The results of
these demonstration chamber tests were incorporated into the design of
the integrated thrust chamber (discussed in the next section). Details
of the test program are described in NASA-CR-140321. A total of 112 tests
were run on the unit for an accumulated burn time of 1042 seconds.

5.1 DEMONSTRATOR CONFIGURATION

The demonstrator thrust chamber assembly is shown in Fig. 44. The demon-
stration chamber was designed to closely simulate the OME flight
configuration as originally envisioned. The flight configuration of the
OME thrust chamber assembly shown in Fig. 45 includes the injector, the
regeneratively cooled chamber and the radiation cooled nozzle. The radia-
tion cooled nozzle attaches at an area ratio of 7 and extends to an area
ratio of 72 which corresponds to an external exit diameter of 50 inches
at the 6000-pound thrust level for a chamber pressure of 125 psia. The
regeneratively cooled thrust chamber uses channel wall construction with
an uppass coolant circuit from an area ratio of 7 to the injector and has
a contraction area ratio of 2. The tapered contour from the injector to
the throat favors boundary layer buildup and enhances coolant character-
istics at the throat. The chamber has an integral auxiliary fuel cooling
ring which contains 180 orifices using 6.4 percent of the fuel (2.4 percent
of the propellants). This auxiliary film coolant reduces the fuel tempera-
ture rise and the resultant regenerative coolant jacket pressure drop.
The regenerative coolant channels are machined into a CRES liner and
closed out with electroformed nickel.

The injector, film coolant ring, and thrust chamber are bolted together
to allow greater flexibility during the test program. The injector and
the film coolant ring can be readily changed and the fuel flow can be
controlled separately to the injector, coolant ring, and regenerative
coolant jacket. The short radiation cooled nozzle extension has soakback
characteristics similar to that of the flight nozzle and is similarly
attached. The bolted nozzle assembly also facilitates shipping of the
(flight) engine and allows simple replacement of the nozzle if damaged
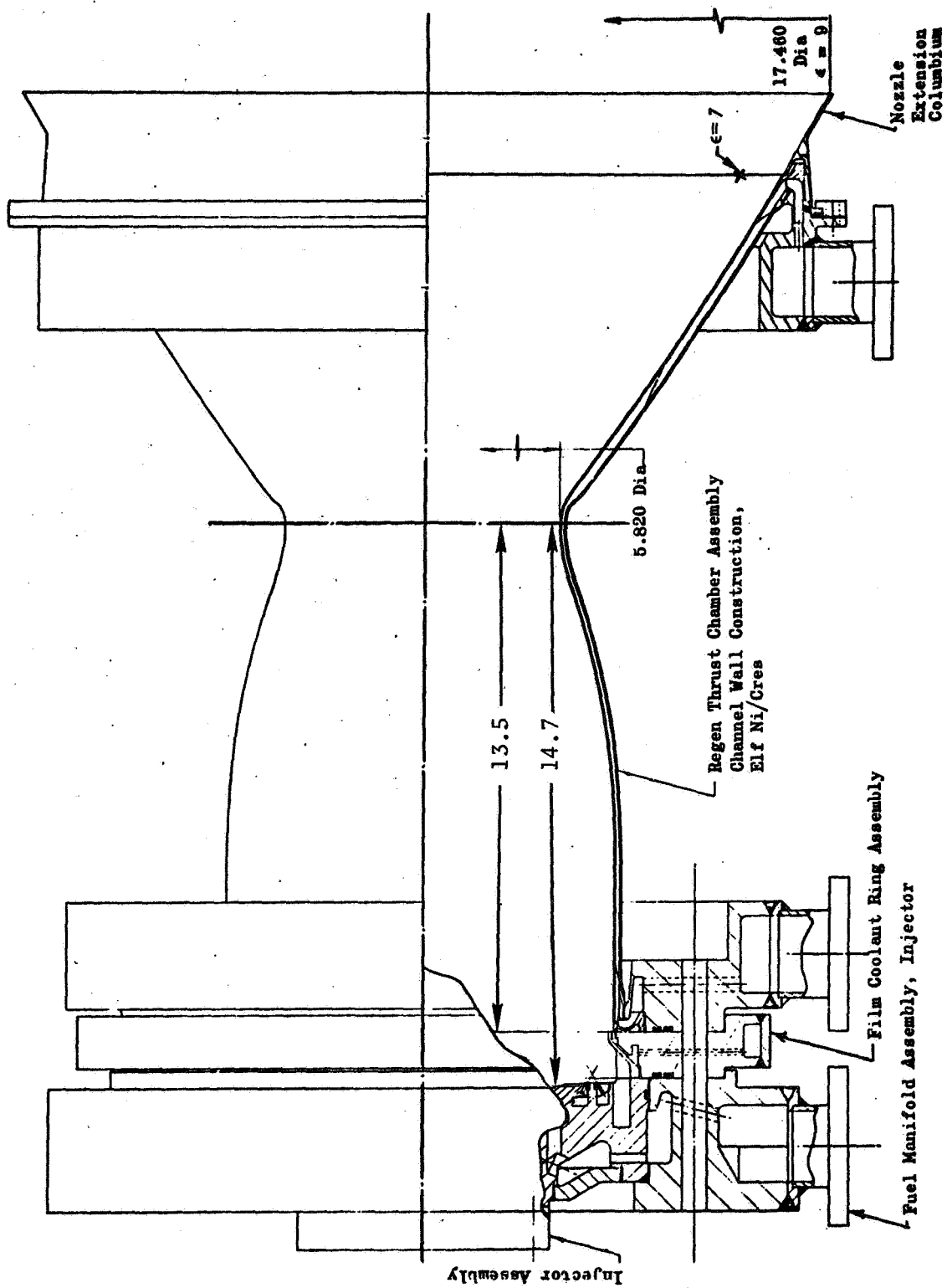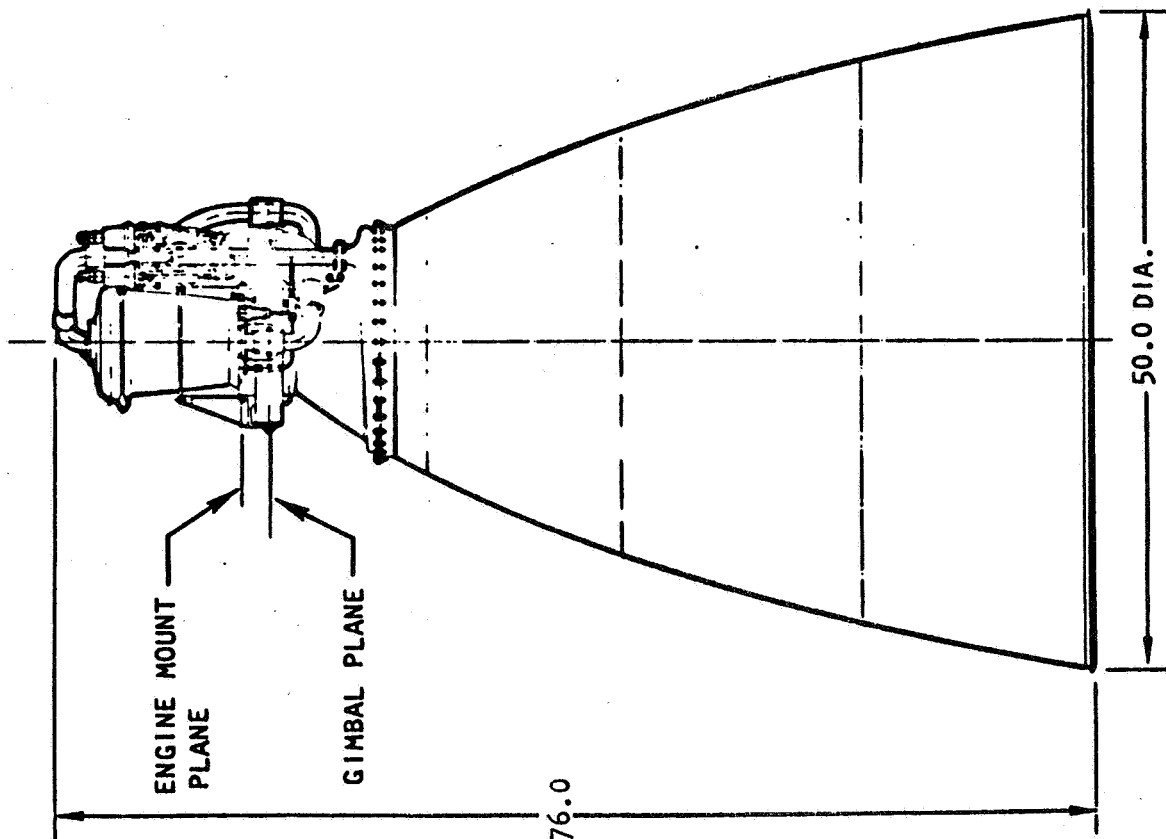during ground operations.

Figure 44. OME Thrust Chamber Assembly Demonstrator Configuration

ENGINE CHARACTERISTICS

THRUST POUNDS	6000
PROPELLANTS	N_2O_4/MMH
MIXTURE RATIO, O/F	1.65
CHAMBER PRESSURE, PSIA	125
NOZZLE AREA RATIO,	72
I_S, SECONDS	313
COOLING	
REGENERATIVE	$\epsilon = 7$
FILM, % $\dot{W}$	2.4
RADIATION	Cb/Ti SKIRT
VALVE TYPE	QUAD-REDUNDANT BALL VALVE
TVC	GIMBAL ($\pm$7 DEG)
COMBUSTION STABILITY	AC. CAV.
WEIGHT, LBS	180

ENGINE MOUNT PLANE

GIMBAL PLANE

50.0 DIA.

76.0

Figure 45. Storable OME Assembly

The CRES film coolant ring at the head-end of the flight chamber forms a part of the acoustic cavity and also directs fuel coolant from the regenerative coolant jacket to the injector. The ring is EB welded to the CRES liner and nickel is electroformed over the liner/ring assembly. The injector and manifold are then EB welded in place. All welds are inspectable and no weld is required to seal hot gases from the chamber directly.

In the demonstrator chamber, fuel flows from the regenerative coolant jacket collector manifold to the transfer manifold into the injector and film coolant manifolds by transfer tubes. Fuel from the regenerative coolant jacket is dumped during the bypass mode of operation. Double seals are used to prevent hot-gas leakage during operation of the bolted assembly. As in the flight configuration, the nickel is bonded to the CRES at all points during the electroforming operation. No weld or braze joint of the two dissimilar metals is required.

Predicted performance of both the flight and demonstrator thrust chamber assemblies are shown in Table 23 and the pressure budgets in Table 24. The coolant jacket pressure drop of the demonstrator chamber is identical to that of the flight configuration. The demonstrator fuel volumes are greater than that of the flight configuration because of the greater flexibility designed into the demonstrator to provide for injector and film coolant ring changes and to permit testing with separate flows to the coolant jacket and injector. The volume difference primarily affects the start transient and was compensated for during the demonstrator test program by sequencing of the propellant valves.

Thrust Chamber Design Detail Selection

The area ratio at which the transition from regenerative to radiation cooling is made is determined by the radiation cooling capability of the nozzle. Original heat transfer evaluation indicated the need for a high temperature refractory material such as Columbium alloy C-103 to reduce regenerative chamber heat loads. Based on an operating temperature capability of 2400 F at 10 percent overpressure, the resulting attach area ratio was determined to be about 7:1. Subsequent testing indicated reduced heat transfer rates such that either conventional materials (L-605 or CRES) could be utilized or the Columbium nozzle attached at a lower area ratio.

The chamber contraction ratio selection is based on consideration of vaporization efficiency, auxiliary film coolant flow requirements, and the attendant performance losses, pressure budget factors, and engine weight effects, as expressed in Table 25. The vaporization efficiency

TABLE 23

OME SPECIFIC IMPULSE

	FLIGHT	DEMONSTRATOR
NOZZLE AREA RATIO	72	9
TDK SPECIFIC IMPULSE (ADJUSTED FOR $\delta*$), SEC	326.7	274.8
TDK FLOWRATE (ADJUSTED FOR $\delta*$), LB/SEC	19.19	19.19
VAPORIZED MASS FLOWRATE, LB/SEC	18.84	18.84
INVISCID FLOW THRUST, LB	6128.3	5154.1
BOUNDARY LAYER THRUST DECREMENT, LB	-128.5	-58.5
THRUST CHAMBER THRUST, LB	6000	5097
THRUST CHAMBER SPECIFIC IMPULSE, SEC	312.7	265.7

TABLE 24

OME PRESSURE BUDGET

Parameter	FLIGHT CONFIGURATION OXIDIZER	FLIGHT CONFIGURATION FUEL	DEMONSTRATOR OXIDIZER	DEMONSTRATOR FUEL
$P_{Engine\ Inlet}$	211*	211*		
$\Delta P_{Feed\ \&\ Valve}$	15	16		
$P_{T/C\ Inlet}$	196	195	196	198
ΔP_{Jacket}		17		17
$\Delta P_{Inj.\ Man.}$	3	2	3	5
$\Delta P_{Inj.\ Orifice}$	62	45	62	45
$P_{Chamber(Inj.\ End)}$	131		131	
$\Delta P_{Chamber}$	6		6	
$P_{Chamber\ (Nozzle\ Stag.)}$	125		125	

* SPACE DIVISION

TABLE 25

CONTRACTION RATIO SELECTION

ϵ_C	D_{INJ}, IN.	η_{C^*VAP}	$\Delta I_{S_{vap}}$, SEC	$\%\dot{W}_C$	ΔI_{S_C}, SEC	ΔP COMB RGEN, PSI		$\Delta I_{S_{\Delta P}}$, SEC	ΔW_{ENG}, LB	ΔI_{S_W}, SEC	$\Sigma \Delta I_S$, SEC
1.5	7.1	0.986	-0.3	2.9	-0.3	12.0	21	-1.3	-15.1	+0.7	-1.2
2	8.2	0.987	Ref	2.4	Ref	6.3	17	Ref	Ref	Ref	Ref
3	10.0	0.989	+0.6	1.6	+0.3	2.8	16	+0.6	+37.2*	-1.6	-0.1

*   INCLUDES BAFFLES

CONCLUSION: $\epsilon_{OPT} \approx 2.3$, $\Sigma \Delta I_s = 0.2$ SEC ABOVE REFERENCE

RECOMMENDATION: USE $\epsilon_C = 2$ TO AVOID BAFFLES

increase as the contraction ratio is increased is based on company sponsored injector test results. Film coolant flow requirements decrease with increasing contraction ratio because of the reduced heat flux in the combustor. This effect also reduces the regenerative coolant jacket pressure drop requirements and the pressure drop of the combustion gases in the chamber decreases. Increasing the contraction ratio increases the weights of the combustor, injector, gimbal ring, and ducting. Combination of all of these effects indicates that the contraction ratio of 2 provides higher equivalent performance than either the contraction ratios of 1.5 or 3.

The natural frequency in the first tangential mode of a thrust chamber decreases as contraction ratio increases. The lower the natural frequency, the more susceptible the chamber is to acoustic instabilities and the larger the acoustic cavity must be to effectively suppress them. Thus, stability considerations tend to drive the contraction ratio to lower values. (Baffles can be installed at the expense of complexity and weight.) In order to insure stability, the contraction ratio of 2 was selected. This results in an Isp penalty of only about 0.2 sec. as compared to the optimum 2.3 contraction ratio.

The chamber length selection was based on a trade-off of performance and cooling safety factor consideration. The pertinent trade factors are summarized in Fig. 46. Overall performance variations are seen to be quite small for lengths ranging from 14 to 17 inches. The actual length selected (14.7 in) was towards the lower value in the event that heat transfer rates were higher than anticipated.

The final dimensions and contour for the regeneratively cooled demonstrator thrust chamber are shown in Fig. 47. The large contour convergent radius, R_2, was a compromise between preventing excessive reductions in the local contraction area ratio and providing a gradual turn to enhance boundary layer buildup. The throat approach radius, R_1, was selected by again avoiding large regions of low contraction area ratio while at the same time avoiding too rapid a turn at the throat which would decrease the aerodynamic discharge coefficient. The value of the downstream throat contour radius, R_3, was based on considerations of fabrication, coolant enhancement due to high curvature, and maintaining a low area in the high flux region.

The selected chamber fabrication technique was channel wall. This construction technique was determined to have greater life than double wall and lower heat load than a tube wall design (due to curved tube surface). The tube wall design also has potential hot-gas leak paths where the tubes are brazed together.
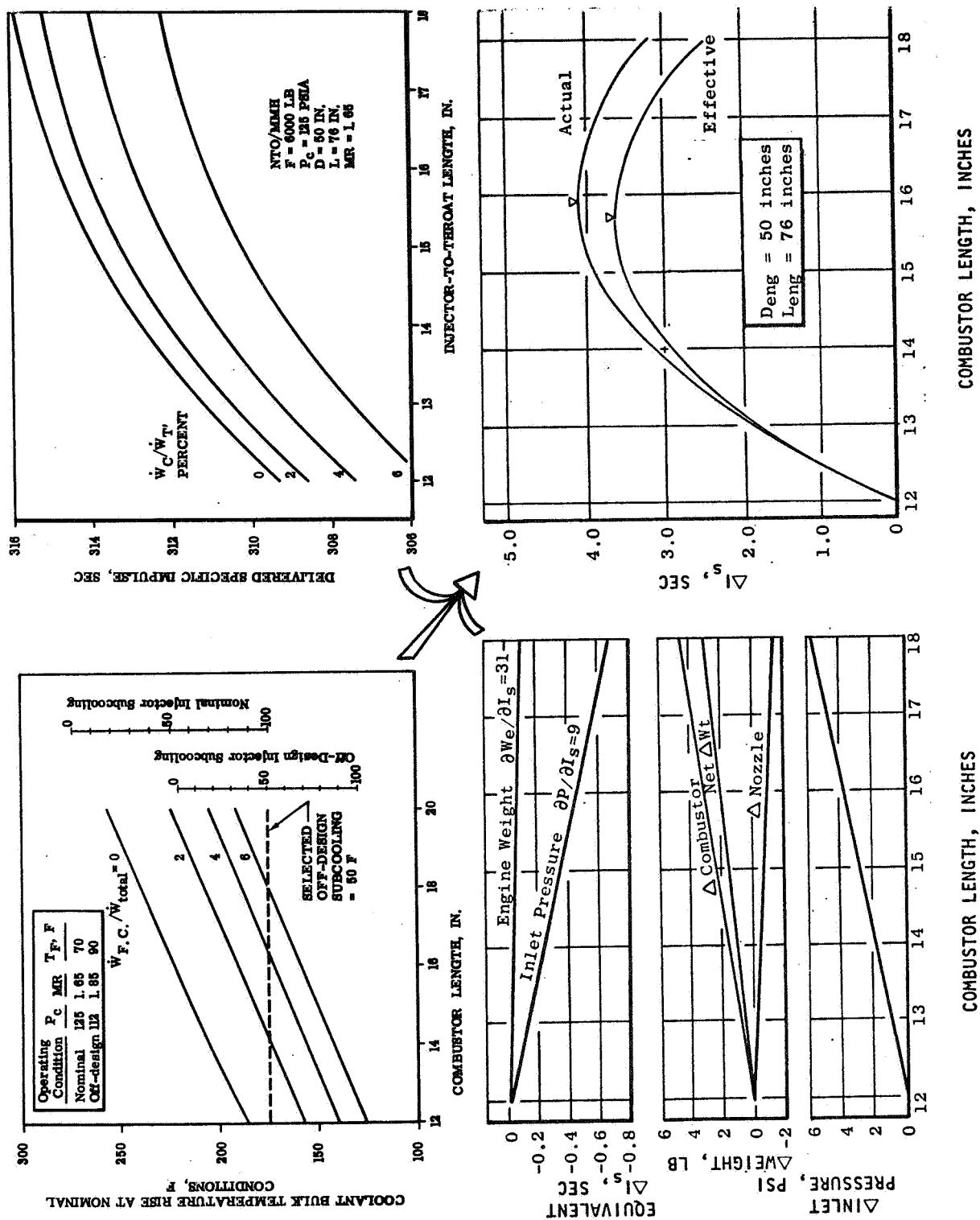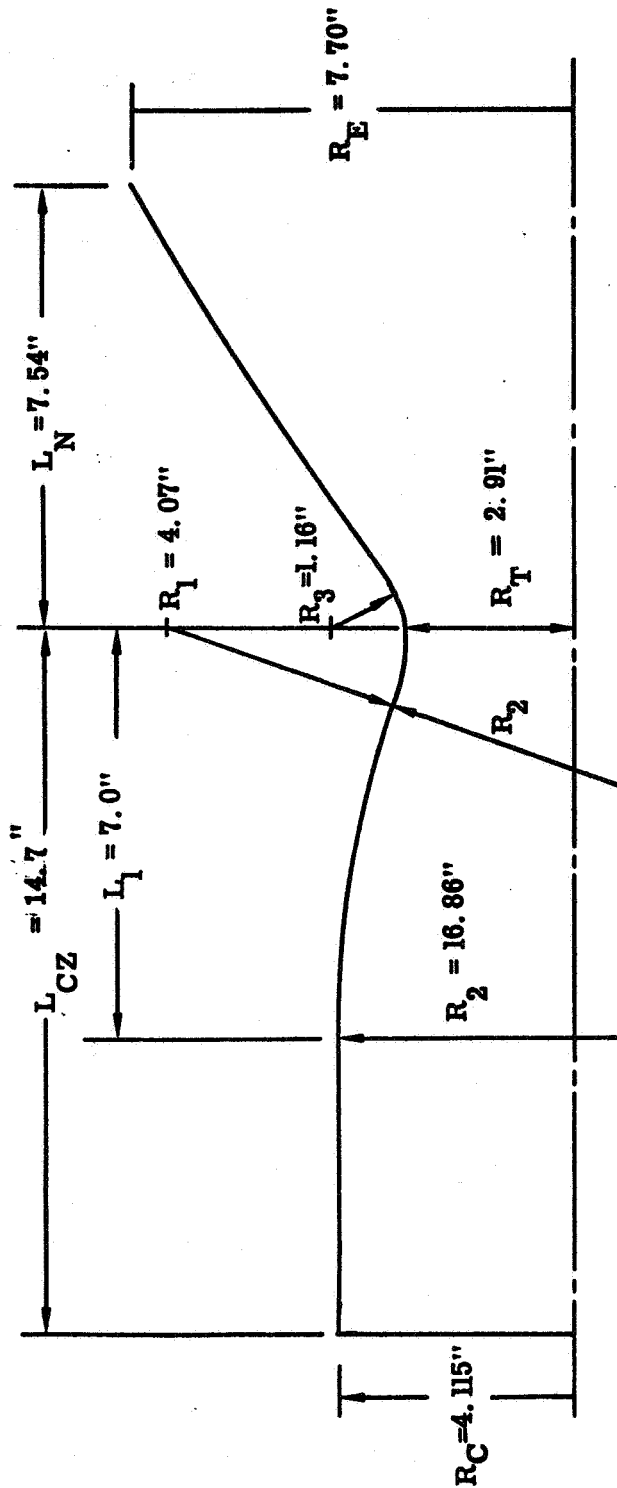
Figure 46. Demonstration Chamber Length Selection

COMBUSTOR GEOMETRY

L_1 BASED ON MINIMUM LIKELY TEST LENGTH

R_T BASED ON F=6K, P_c=125 PSIA

R_C BASED ON CONTRACTION RATIO = 2:1

R_1/R_T (= 1.4)   COMPROMISE OF HEAT TRANSFER (LOW ΣQ) AND AERODYNAMICS (HIGH DISCHARGE COEFFICIENT)

R_2/R_T SELECTED TO MINIMIZE TURNING OF COMBUSTION GASES

NOZZLE GEOMETRY

R_3/R_T (= 0.4)   SELECTED TO PROVIDE FOR POSSIBLE COOLANT CURVATURE ENHANCEMENT

L_N, R_E BASED ON RADIATION ATTACH POINT AT AREA RATIO = 7:1

NOZZLE CONTOUR: TRUNCATED 70% LENGTH PARABOLIC OPTIMUM BELL CONTOUR TO AREA RATIO = 72   BASED ON EXIT DIAMETER = 50 INCHES

Figure 47.   SS/OME Demonstrator Chamber Contour

An uppass flow circuit was selected with the coolant entering at an area ratio of 7, flowing through the throat and combustor and exiting directly into the integral manifold of the injector. This eliminates the return line and separate injector distribution manifold required in a downpass design. A one and one-half pass configuration was considered but would be somewhat more expensive to fabricate and could result in slightly higher pressure drop as compared to the single uppass design.

The selection of the number of channels and channel geometry was based on two-dimensional conduction considerations. This geometry is most critical in the injector region where the heat fluxes are reasonably high and the land width is considerably greater than at the throat portion. In order to minimize injector-end land width, it is necessary to minimize the land width at the throat and maximize the number of channels. Once these two items are specified, the resultant channel width is uniquely defined based on throat diameter.

Based on ease of fabrication, a minimum throat land width of 0.040 inches was selected. A study of the effect of number of channels on 2-D heat transfer penalty indicated that beyond 180 channels the gain was negligible. The resulting channel width was 0.060 inches.

Thermal Characteristics

The channel height profile was determined from considerations of the local coolant safety factor, MMH cooling capability (as discussed previously) and heat flux profile. In the design of the demonstrator chamber, a nominal cooling safety factor of 2 was utilized with the further restriction that this safety factor not fall below 1.5 at extreme off-design conditions. (At this time, the off-design values were T_{in} = 90 F, P_c = 112 psia and MR = 1.85.)

The channel height profile, heat flux profile and resulting pressure and wall temperature profiles are presented in Fig. 48 thru 51 at nominal condition. The final design results reflect additional constraints such as a minimum coolant velocity of 5 ft/sec, and a step change in the nozzle channel width from 0.060 to 0.120 inches to reduce channel height and nozzle weight. The coolant pressure profiles do not include inlet and outlet manifold losses estimated to be about 2 psi total.

The resultant 2-D coolant safety factor profiles are presented in Fig. 52 for both nominal and extreme off-design conditions.
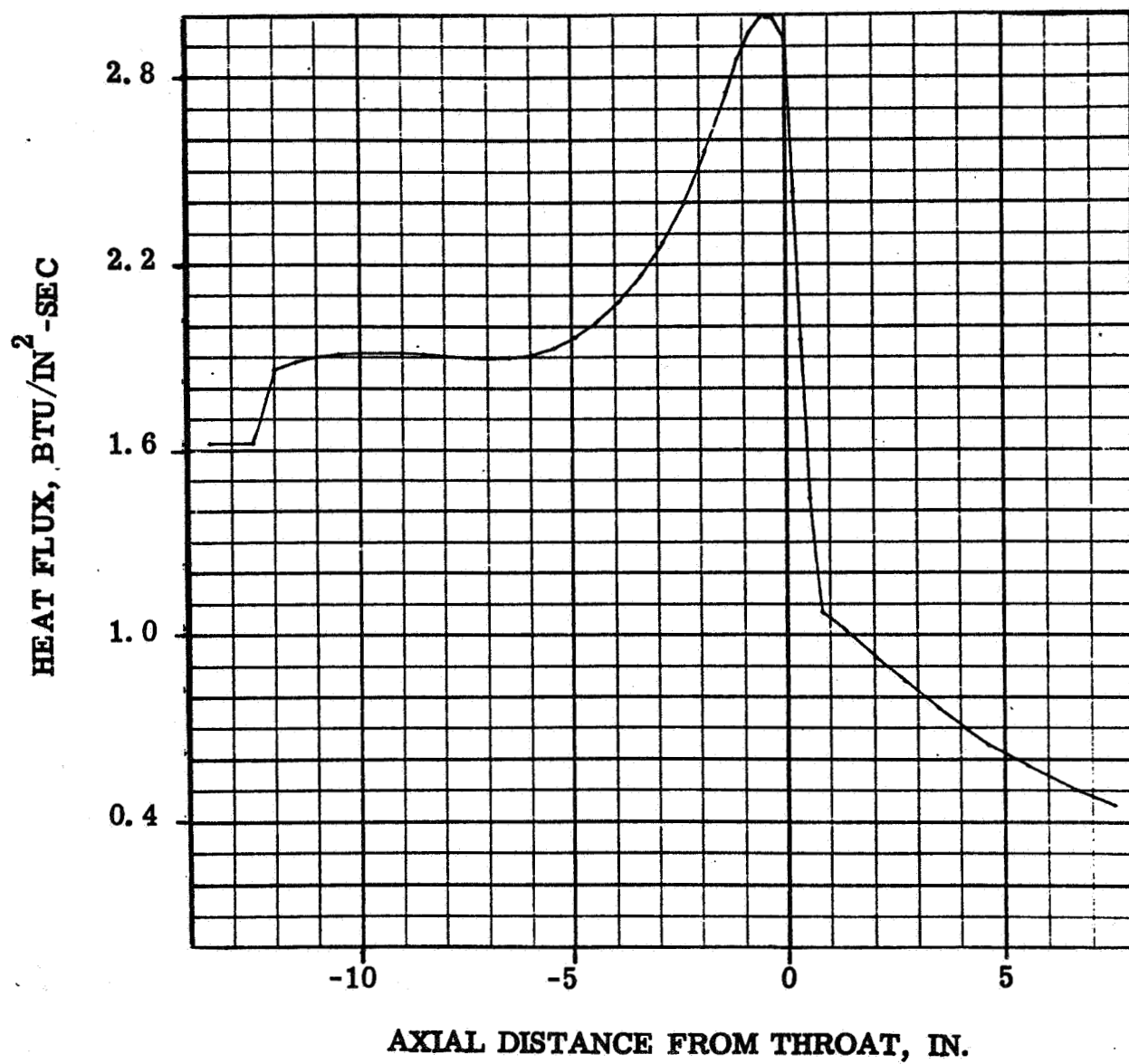
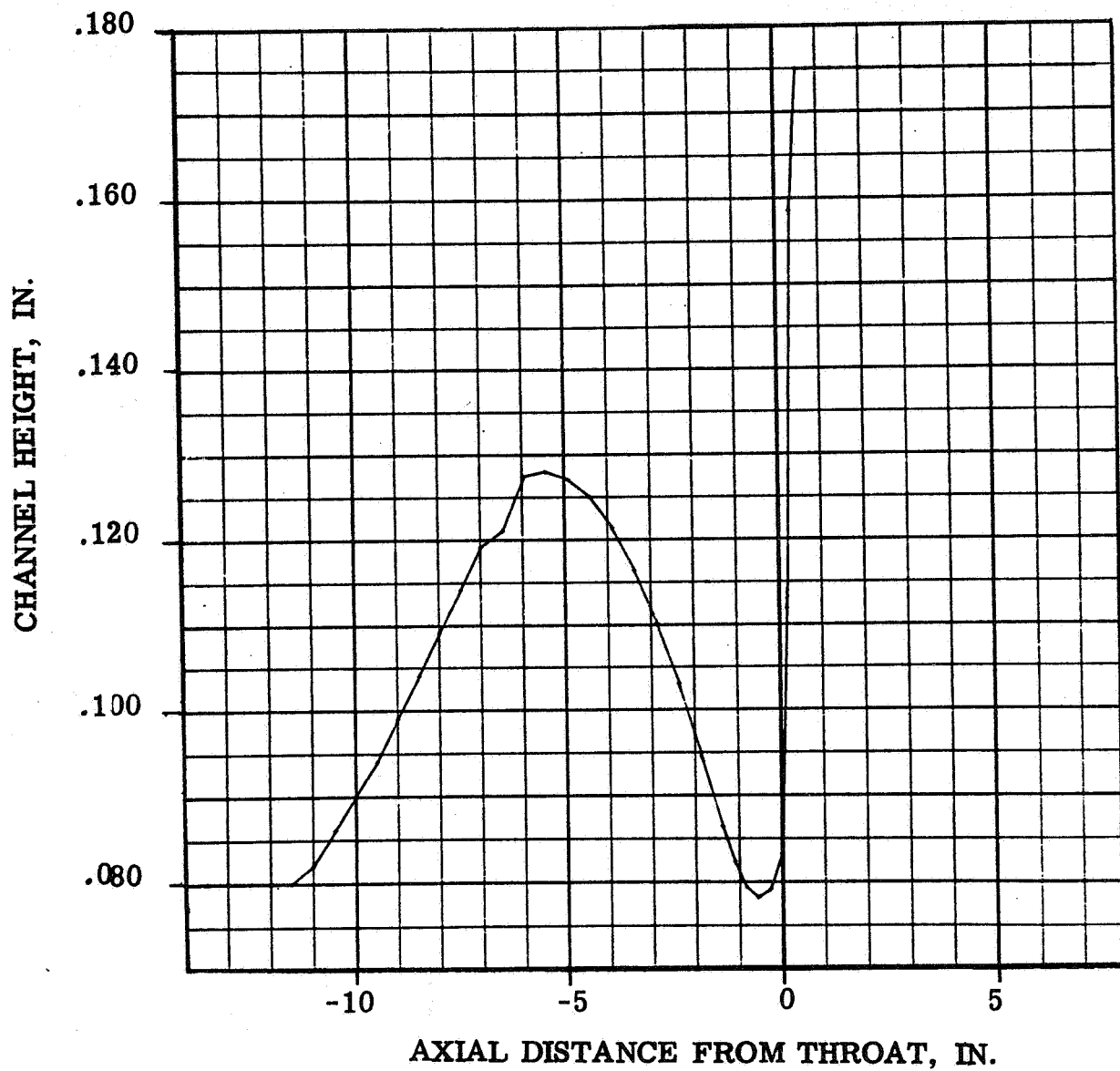Figure 48.   Demonstrator Chamber Heat Flux Profile
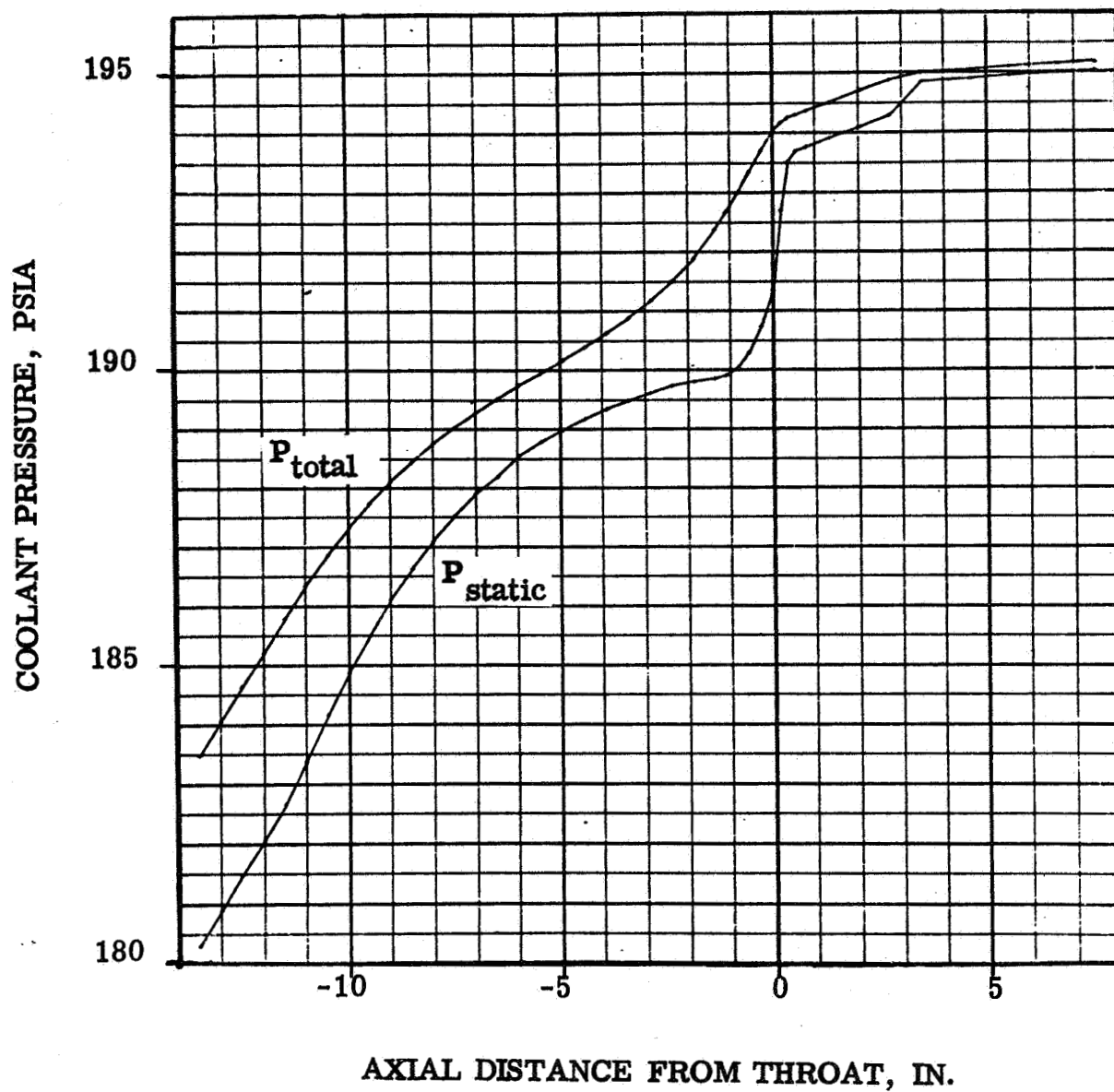
Figure 49. Demonstrator Channel Height Profile

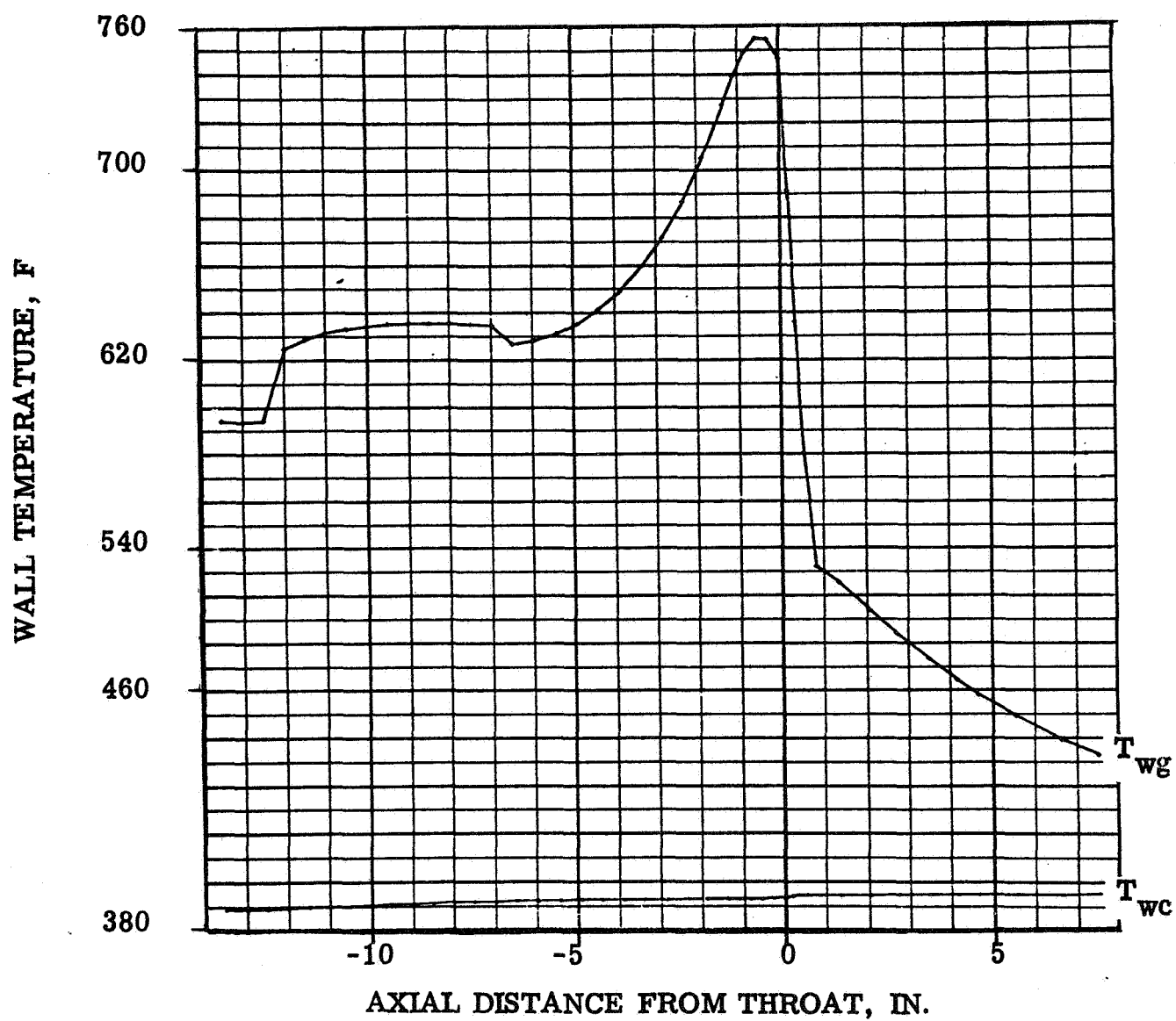Figure 50. Demonstrator Regenerative Coolant Pressure Profiles
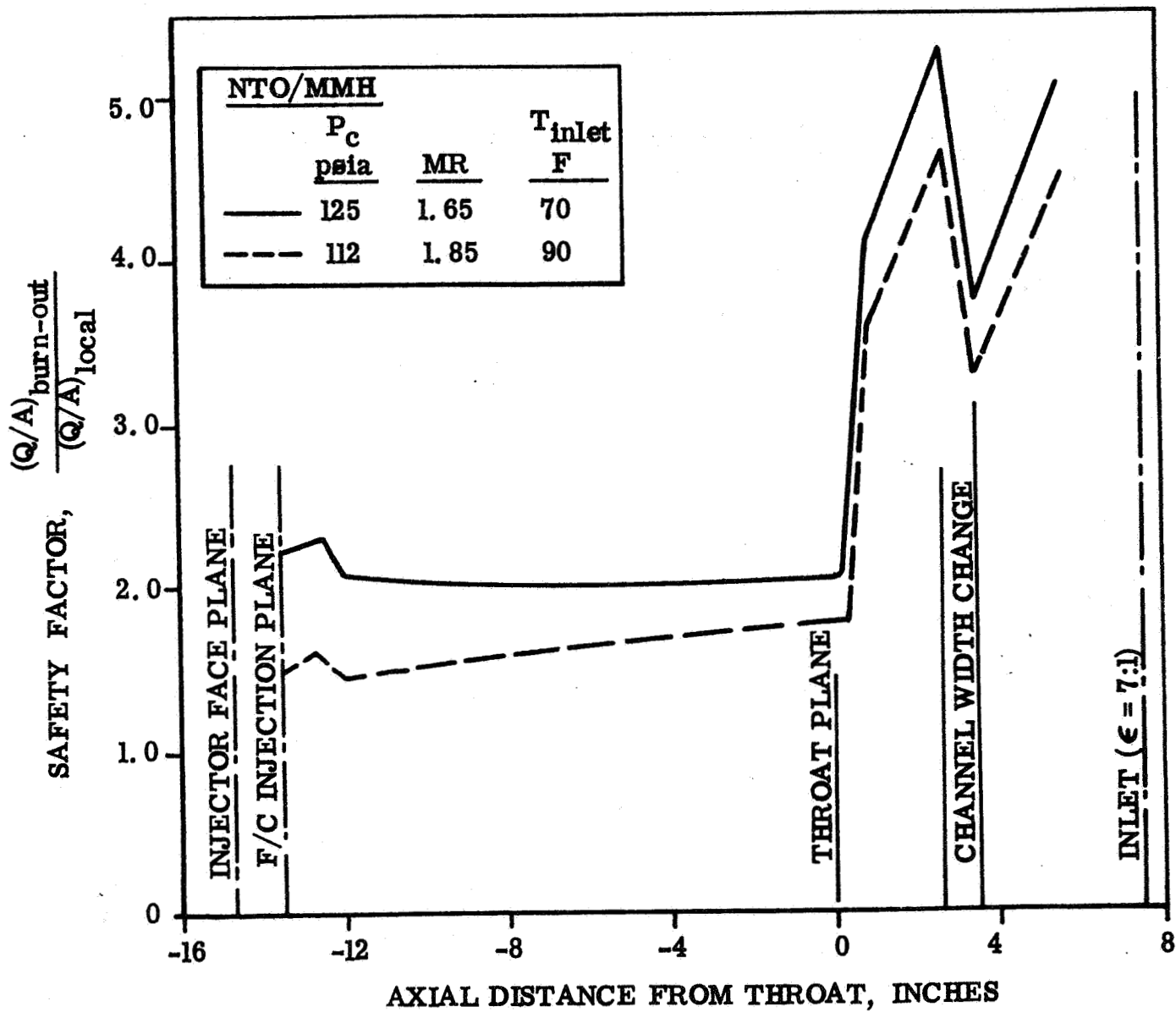
Figure 51. Demonstrator Wall Temperature Profiles

Figure 52. Coolant Safety Factor Profile

Thrust Chamber Life

The factors which enter into the thrust chamber life analysis are shown in Fig. 53. The life analysis includes the effect of both creep and fatigue damage. However, the creep damage for the regeneratively cooled engine is extremely small. For CRES at 1000 F which is considerably in excess of the wall temperature even at off-design conditions, the damage fraction due to creep is only 0.2 percent.

The Universal Slopes prediction method was utilized in conjunction with the calculated strain profile to determine fatigue life of the demonstration chamber. Details of the analysis are given in Appendix C. The strain induced into the stainless steel liner of the chamber result primarily from thermal gradients between the hot inner wall and the cold outer wall. Strains due to pressures and thrust are negligible. The strain distribution reaches a maximum of approximately 7.5 X 10-3 inches per inch slightly upstream of the throat. This results in the fatigue life profile shown in Fig. 54. The minimum life region is immediately upstream of the throat where the predicted life was approximately 7000 cycles. More recent data on strength of electroformed nickel were obtained subsequent to fabrication of this chamber. This data indicates the life to be approximately 4000 cycles. Since the required life is 1000 starts, this provides a safety factor of approximately 4 on fatigue life.

A two dimensional analysis of the nozzle and attached flange was performed in order to indicate the maximum temperatures the O-ring seal and the regenerative inlet manifold will experience during operation. These analyses indicated a maximum temperature of 2300 F, slightly below the 1 dimensional prediction. Temperatures at the inlet manifold somewhat in excess of 100 F were predicted. The minimum fatigue life of the nozzle joint was calculated to be approximately 5000 cycles.

Life analyses were conducted for all critical portions and failure modes of the radiation cooled nozzle. The most critical location for creep on the Columbium nozzle is at low area ratios where the temperature and the pressure and thrust stresses are most severe. Even under these conditions, the stress rupture time was determined to be in excess of 10^4 hours.

Transient Thermal Analysis

Start and shutdown analyses were conducted to uncover potential problem areas in the flight OME, to verify similarity between the thermal transient characteristics of the flight and demonstrator thrust chambers, and to determine the test durations required to obtain steady-state thermal conditions.

Hot wall temperature transients were determined for the regeneratively cooled thrust chamber. The transients are the same for the flight and
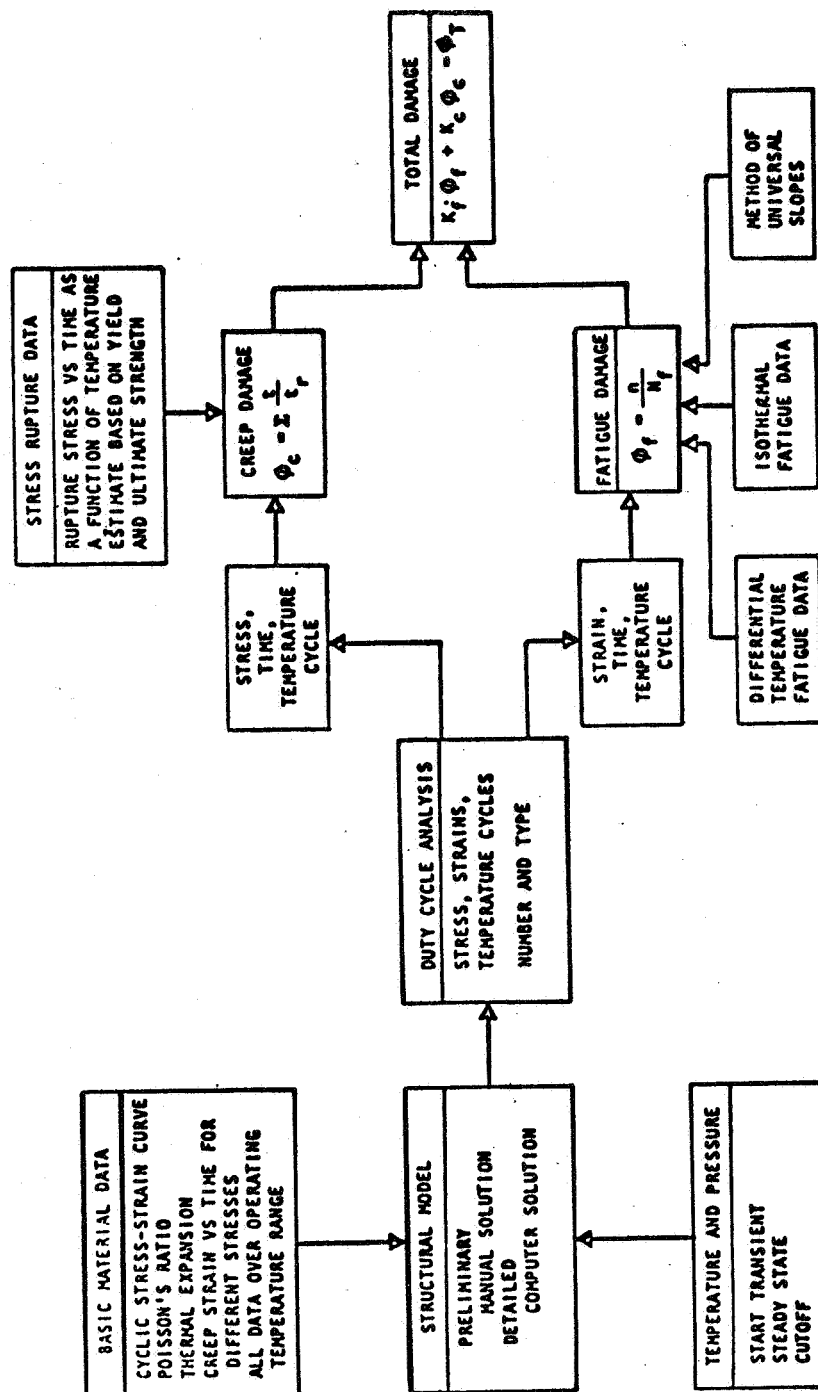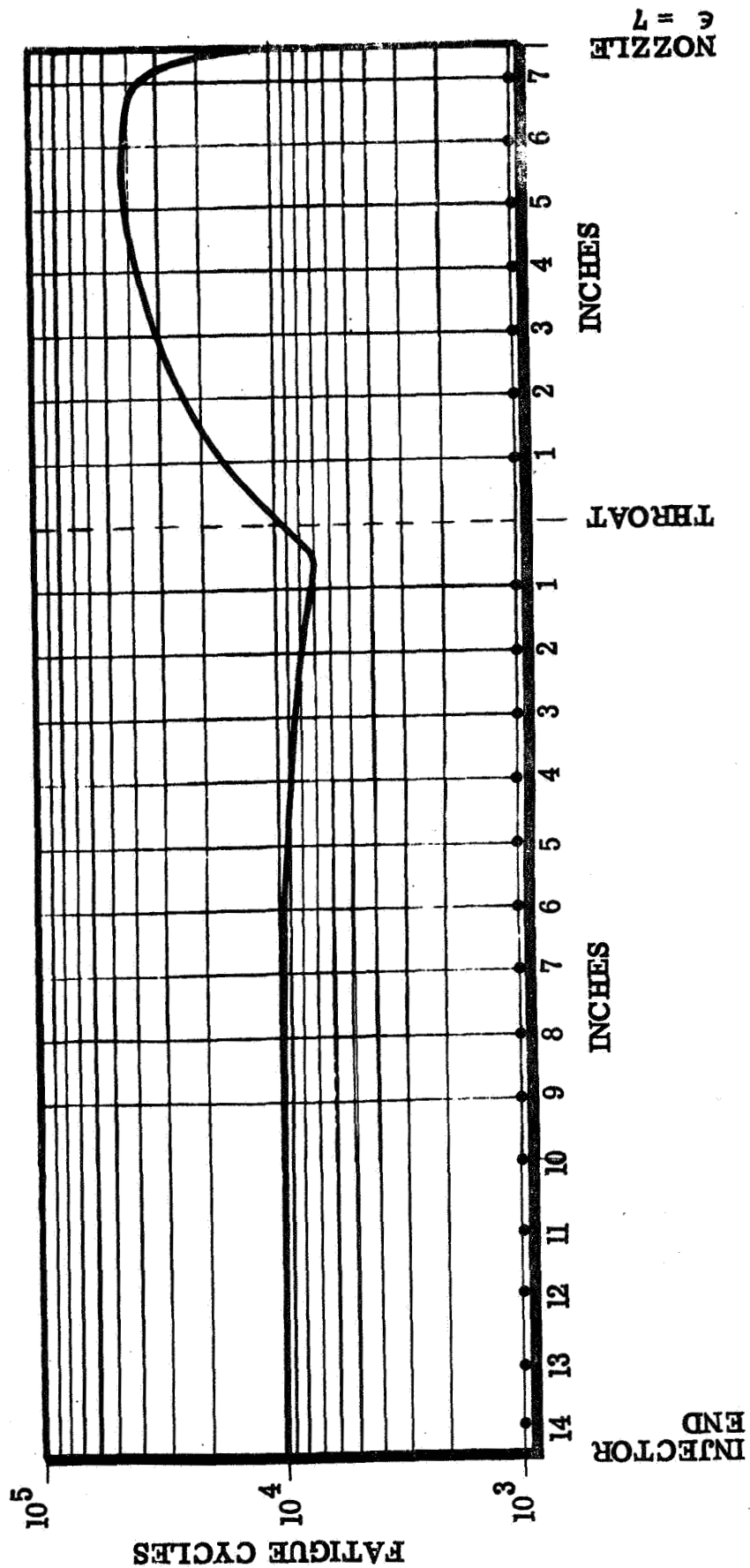
Figure 53. Engine Life Analysis

Figure 54. Thrust Chamber Cycle Life Capability

for the demonstrator chambers since channel geometry is identical. Throat temperatures stabilized within approximately 1 second while the slowest responding temperatures at the coolant inlet location are nearly stabilized in 5 seconds. Temperature transients for the flight and demonstrator nozzle extensions were also determined. In 20 seconds the maximum temperatures are nearly reached in the demonstrator nozzle. Even at 10 seconds of operation almost 90 percent of the equilibrium temperature rise has taken place. Complete equilibrium requires approximately 30 seconds. Temperature transients for the flight nozzle are somewhat more rapid. In the attachment region thermal equilibrium occurs within 20 seconds for the flight nozzle. At the exit of the nozzle (ϵ = 72) more than 60 seconds are required to reach complete thermal equilibrium.

To analyze orbital start and soakback conditions, a thermal model was constructed with assumptions delineated in Table 26. Major components of the engine were modeled and the vehicle view factors estimated from vehicle contractor drawings. Engine soakback transients immediately following shutdown were investigated. The residual fuel in the jacket is sufficient to prevent any temperature spikes at cutoff and the temperatures of all components decrease monotonically. The temperature transient for a 7-day soakout in space was also studied. Heat loss to space is balanced after approximately one day by heat gain from the surrounding vehicle. After one day, no further change in temperature takes place. All temperatures in the regeneratively cooled portion of the engine are well above the freezing point of the fuel and the injector and valve temperatures are above the freezing point of the oxidizer. Thus, no freezing problem is seen to exist during a long soak in space.

The primary concern during a start in space is that propellant will freeze through vaporization and plug injector or coolant jacket passages. To evaluate this, the start model was used to simulate a start after a long chill in a space environment. The results are shown in Fig. 55. In the analysis, the fuel temperature is calculated at various locations through the system as the fuel loses heat through vaporization and transfers heat with the surrounding materials. Initial material temperatures are based on the results of the soakout analysis. The fuel temperature decreases at first, then very rapidly begins to increase in temperature so that even at an inlet temperature of 40 F the fuel does not freeze.

The most severe freezing condition would be encountered if, after a space chill of longer than one day, the OME were fired for a short duration so that propellants primed the engine, but only a small amount of heat was generated by the firing. The results of such a condition with a one-second firing of the OME are described in Fig. 56. Components in contact with the

TABLE 26

ASSUMPTIONS FOR THERMAL TRANSIENT ANALYSES

- 40F VEHICLE – SYSTEM PRE ORBIT INITIAL TEMPERATURE
  - MODEL 049 VEHICLE – ENGINE SYSTEM CONFIGURATION

- 7 DAY RADIATION TO SPACE
  - NO SUN HEATING
  - NO EARTH ALBEDO VIEW
  - INJECTOR END ENGINE SYSTEM PARTIAL SPACE VIEW (NO RADIATION SHIELD)
  - ENGINE SYSTEM EMISSIVITY > .6

- ONE SECOND COLD START

- EVAPORATIVE CHILL OF BOTH RESIDUAL PROPELLANTS
  - 137 CU. INCHES MMH
    - FREEZES AT -62.5F
  - 22 CU. INCHES NTO
    - FREEZES AT 11.8 F
  - 5 PERCENT OF RESIDUAL LIQUID EXPELLED AS LIQUID THROUGH INJECTOR ORIFICES DUE TO TURBULENCE OF EVAPORATION
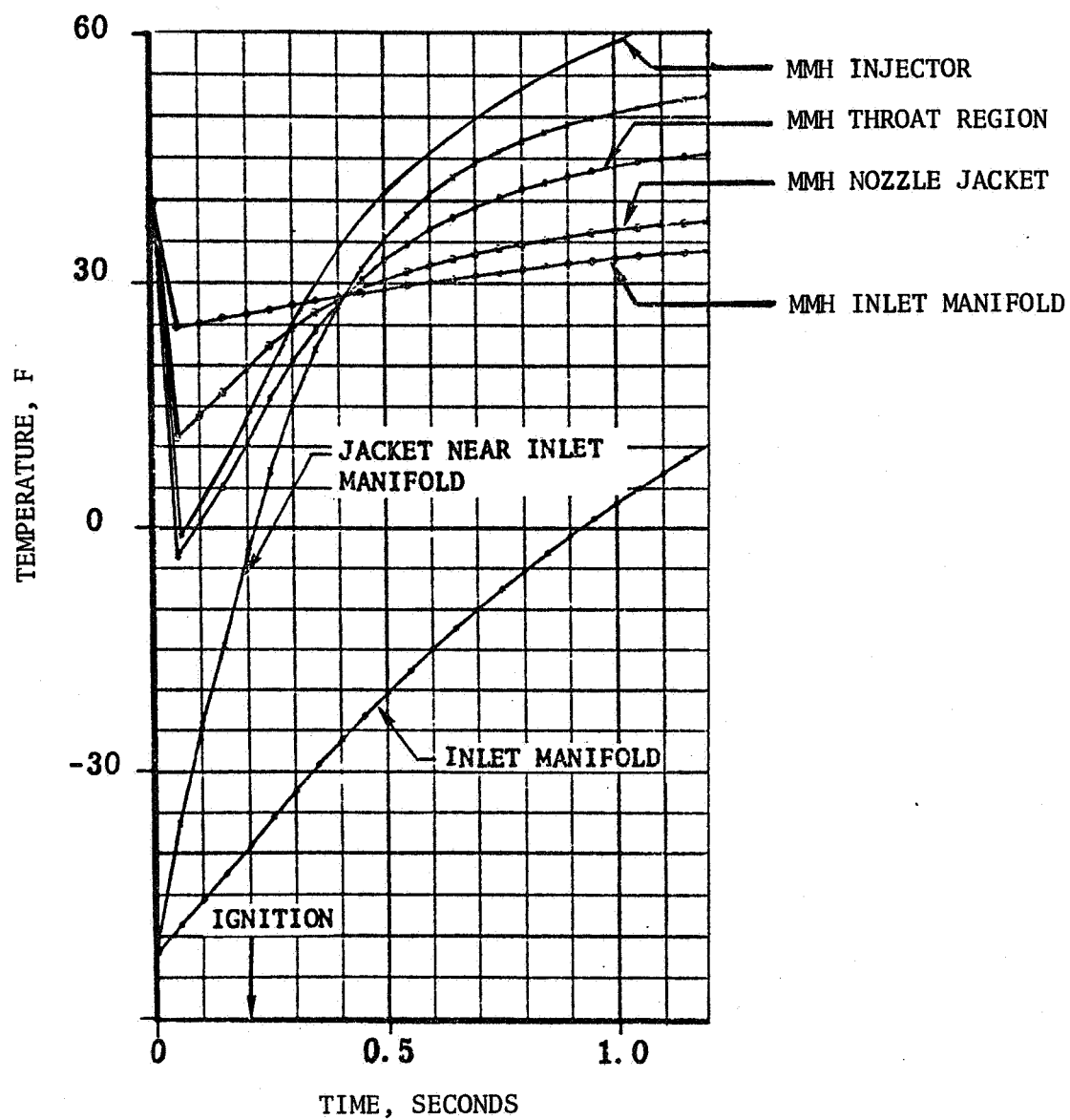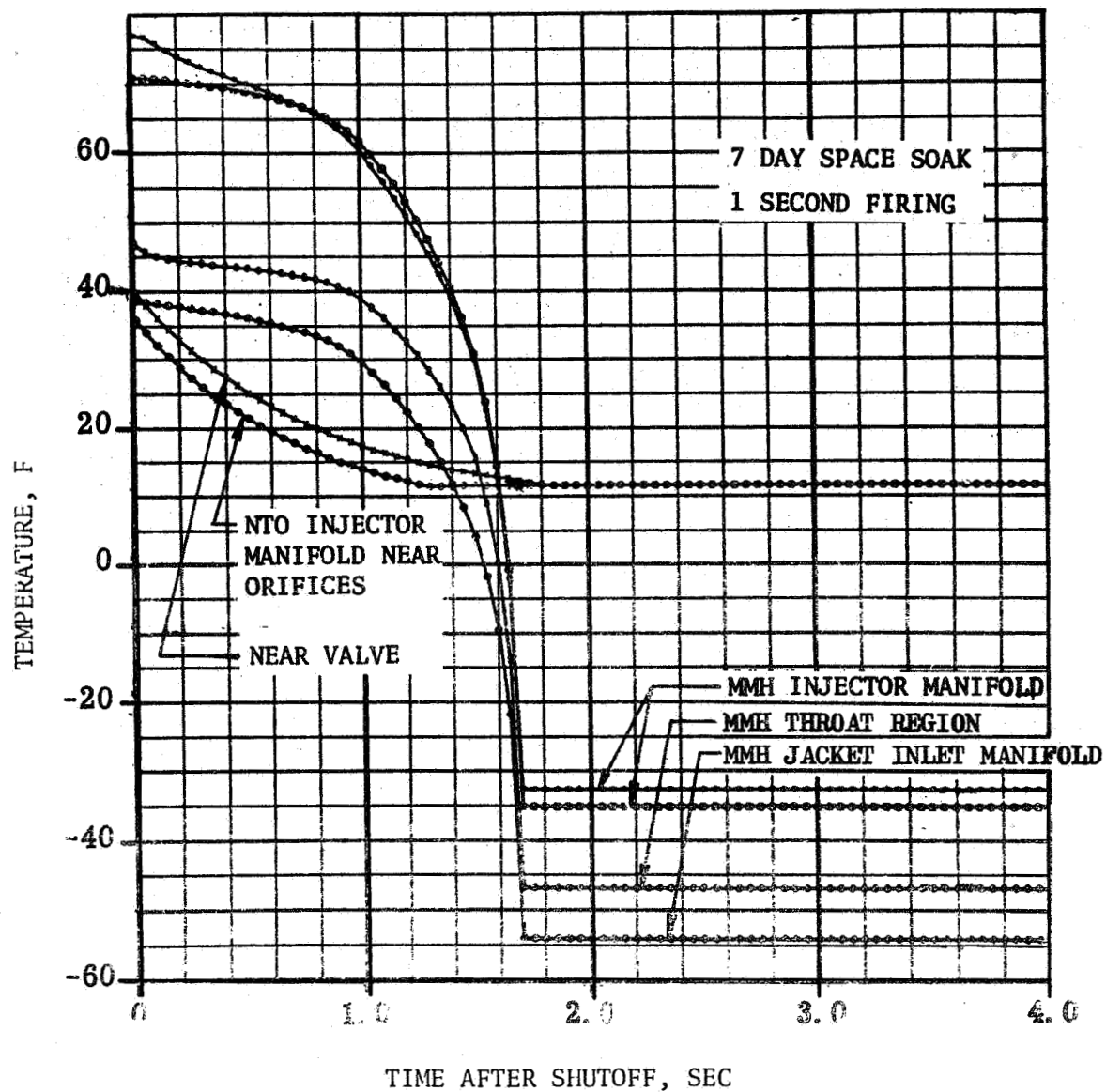
Figure 55. OME Start Following Space Chill

Figure 56   Evaporative Chill Of OME Propellants

MMH remain above the freezing point (-62 F) of the fuel. Components in contact with the oxidizer reach the NTO freezing point (12 F) indicating some degree of freezing of residual NTO and potential restart problems. None of the current mission duty cycles include such a short firing duration, but if such a requirement should develop, the condition can be improved by maintaining the NTO at warmer than 40 F or using heaters on the oxidizer feed system downstream of the engine valve.

OME Sensitivity

Sensitivity analyses were conducted to determine the effects of off-design engine inlet conditions on engine performance and safety. An engine steady-state model was used to analyze the effects of inlet pressure and temperature variations on chamber pressure and mixture ratio. The model includes variable C* effects and the pressure drops through individual components. The results of inlet pressure variations are plotted in Fig. 57 where 10 psi variations in individual tank pressure are shown to affect mixture ratio by approximately 0.1 units and chamber pressure by less than 4 psi for NTO inlet pressure variations are less than 2 psi for MMH inlet pressure variations. Inlet temperature effects are even less significant over the expected temperature ranges and particularly since the inlet temperatures are not expected to differ (between NTO and MMH) by more than approximately 10 F. The effects of these variations on performance are also shown in Fig. 57. The chamber pressure effect is seen to be negligible while the mixture ratio effect can result in performance variations of almost 2 seconds.

The effects of chamber pressure on the nominally designed regeneratively cooled thrust chamber wall temperature was investigated. The maximum wall temperature near the throat region increases from a nominal value of approximately 760 F to slightly over 900 F if the chamber pressure is increased from 125 to 200 psia. Operation is certainly safe under these conditions but the design life is slightly reduced. Variations in chamber pressure and mixture ratio affect the coolant saturation temperature, bulk temperature rise and coolant velocity. These factors, in turn, have a strong effect on the coolant safety factor. The results of a study of these effects on the demonstration chamber are summarized in Figs. 58 and 59. These results indicate the demonstrator is capable of considerable off-design operation.

Another off-design condition is the presence of gas in the propellants particularly in the fuel used to regeneratively cool the chamber. The gas may be present in solution or in the discrete gas phase. Pressurizing gas in solution constitutes no problem because the solubility of helium in MMH increases with temperature. Analysis indicated that helium in
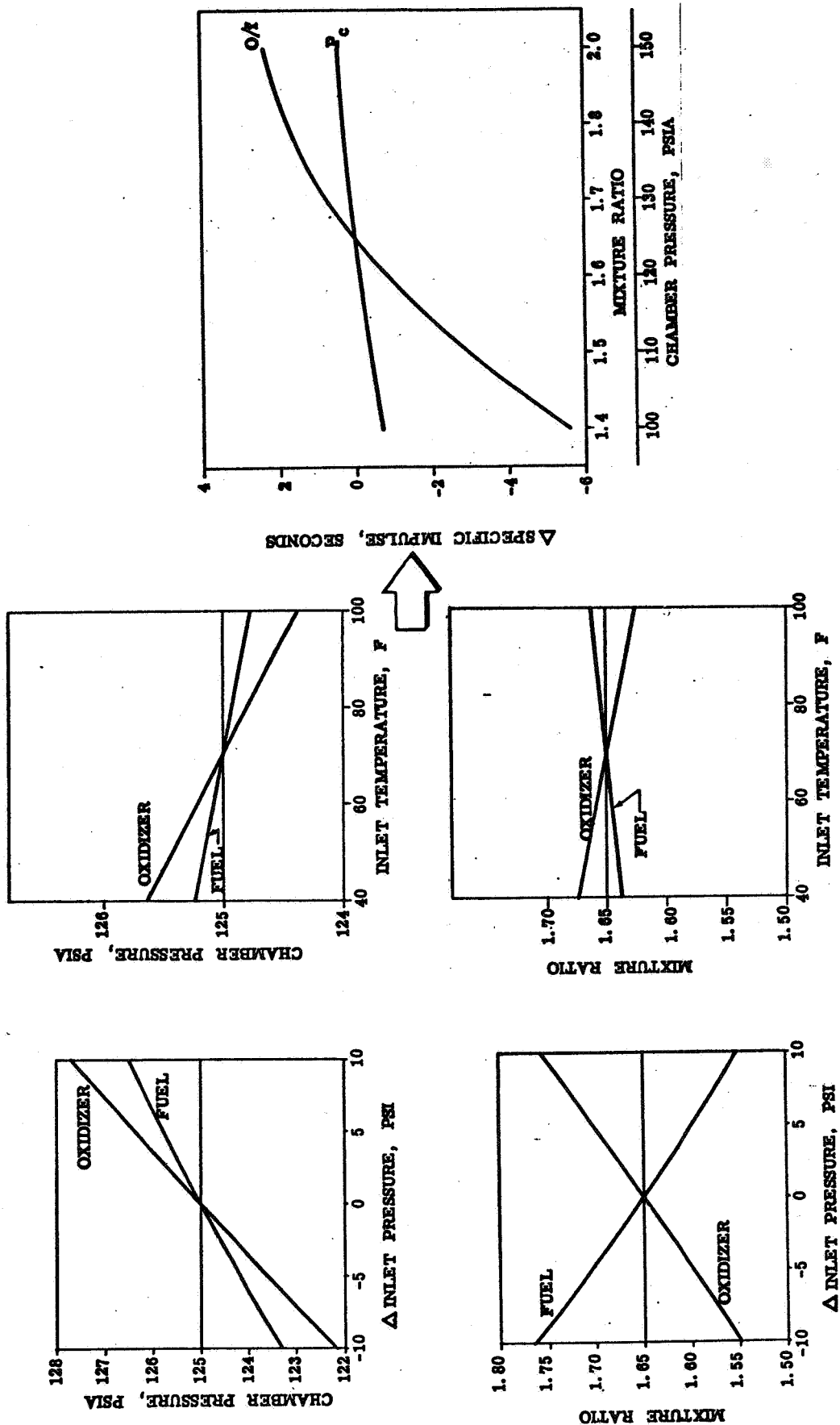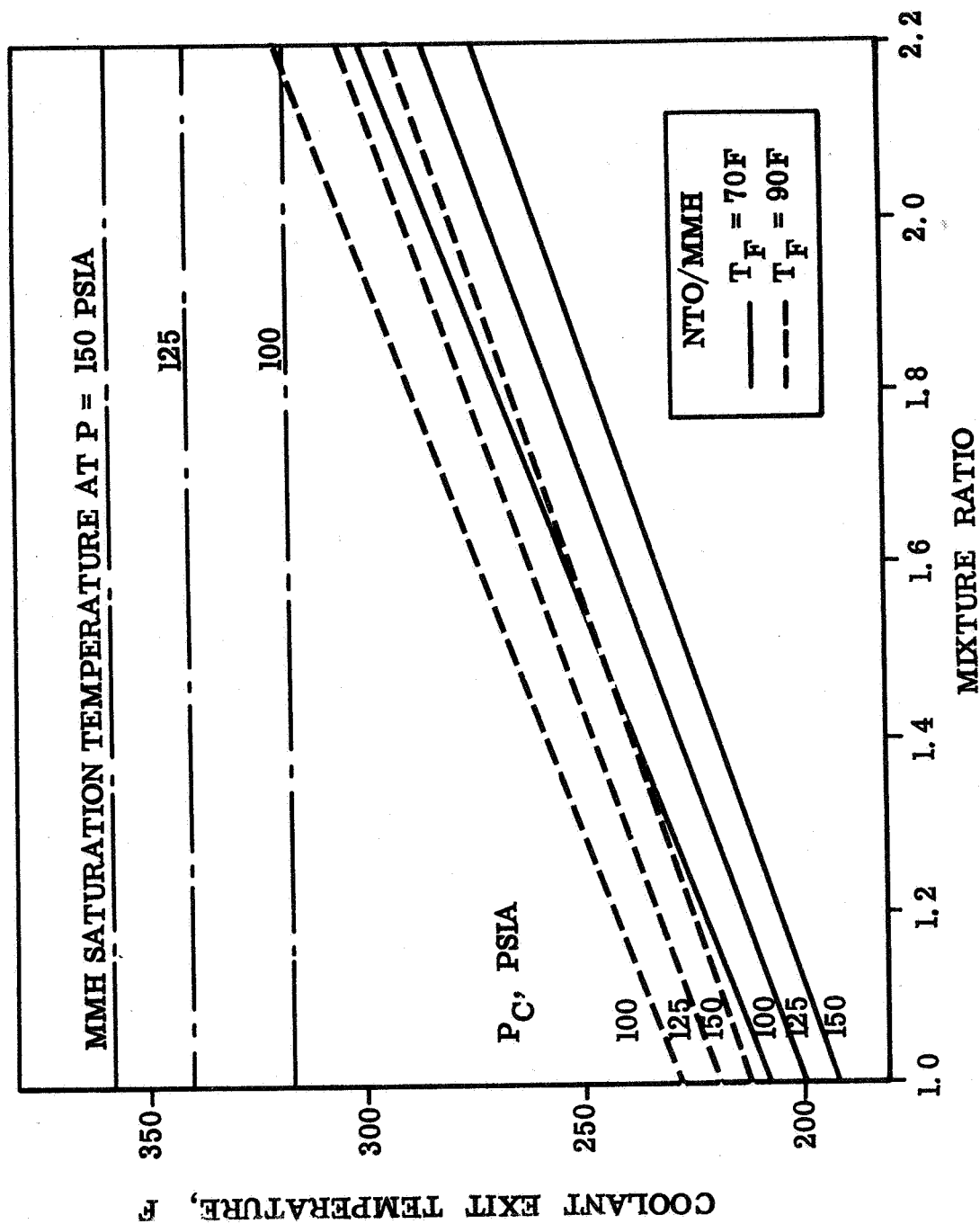
Figure 57.   Performance Sensitivity

Figure 58. Effect Of Mixture Ratio And Chamber Pressure On Coolant Exit Temperature
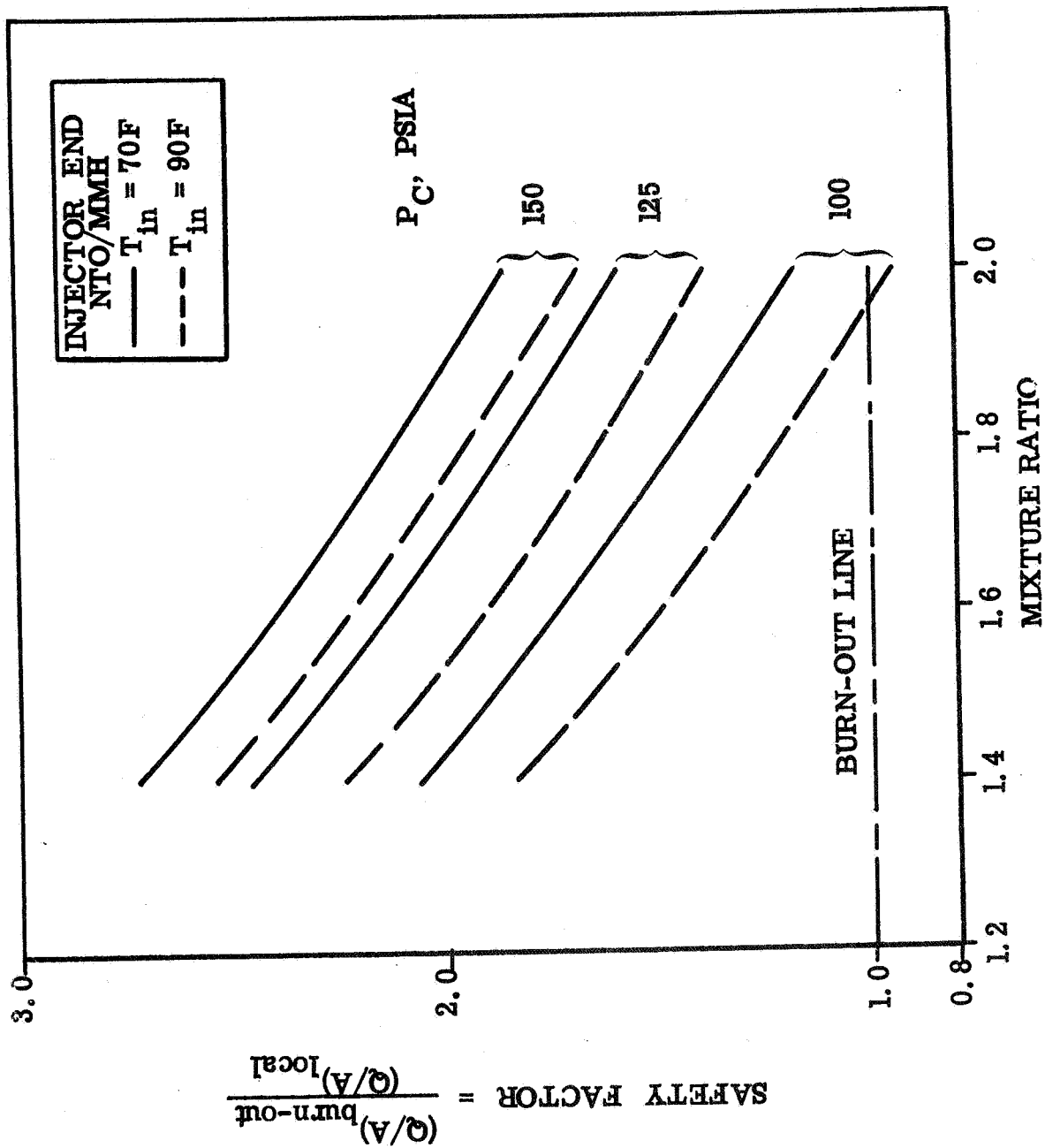
Figure 59. Off-Design Operating Capability
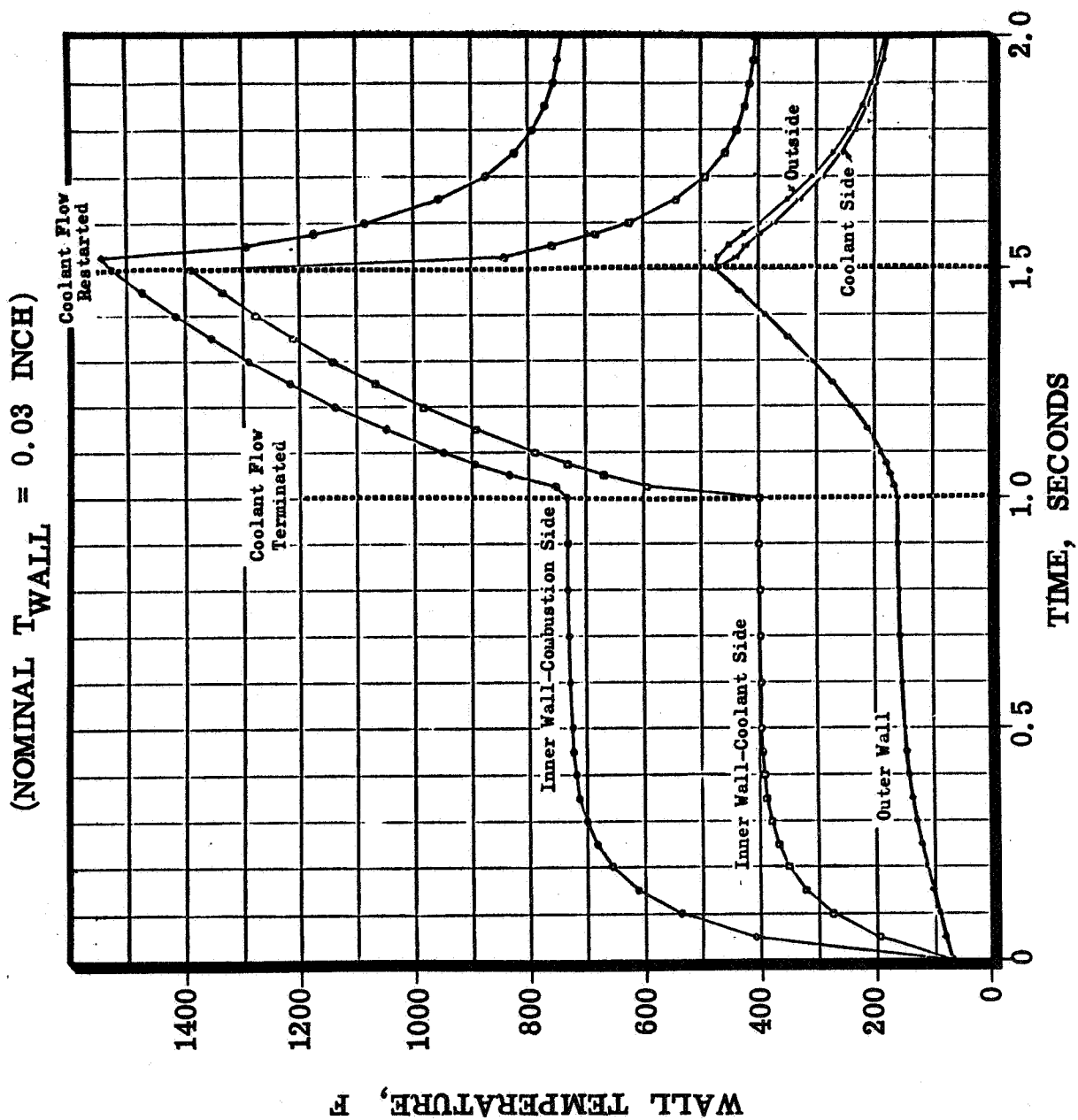
Figure 60. Wall Temperature Transients
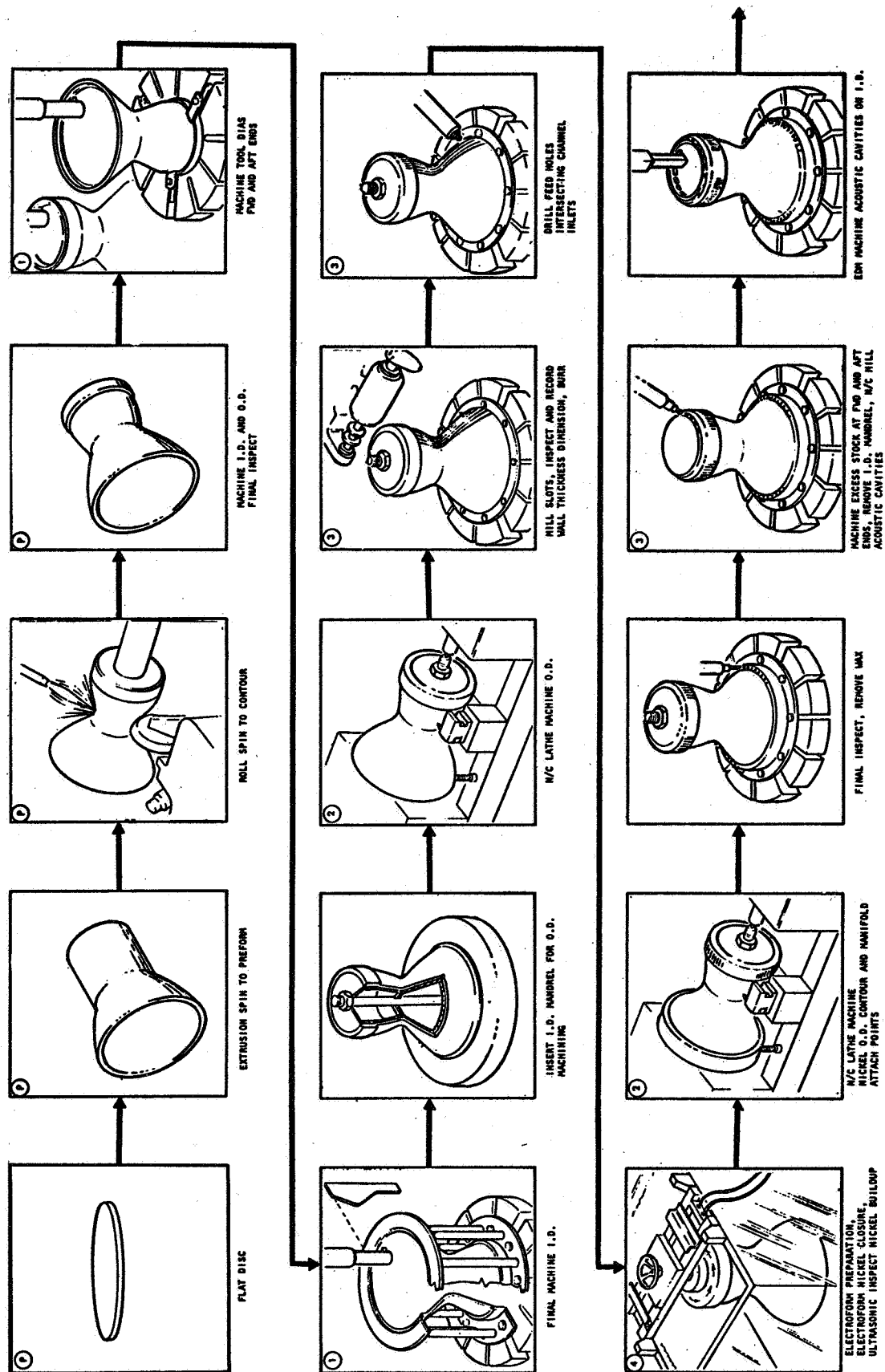
Figure 61   OME Combustor Fab Sequence
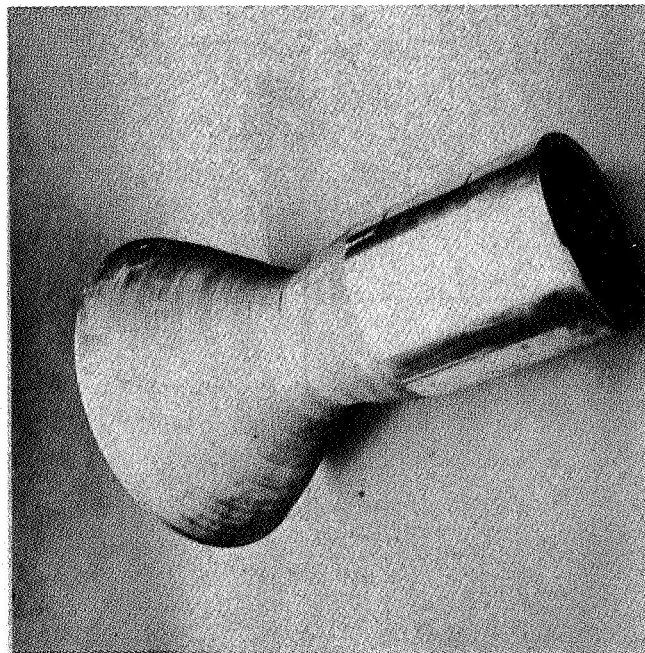
LINER MACHINING
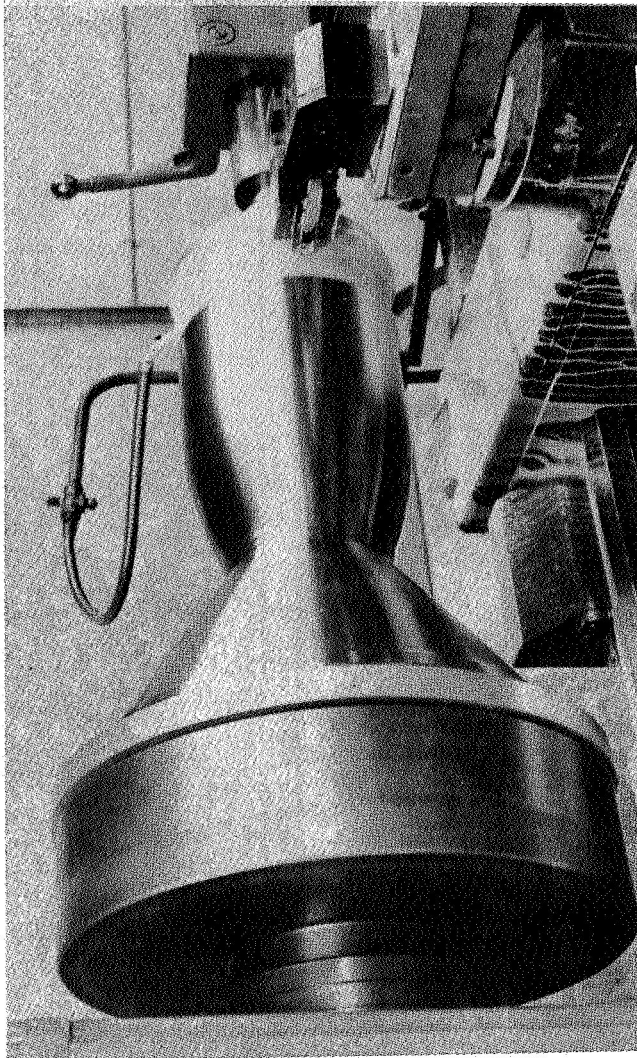
LINER SPINNING

Figure 62. Demonstration Chamber Fabrication
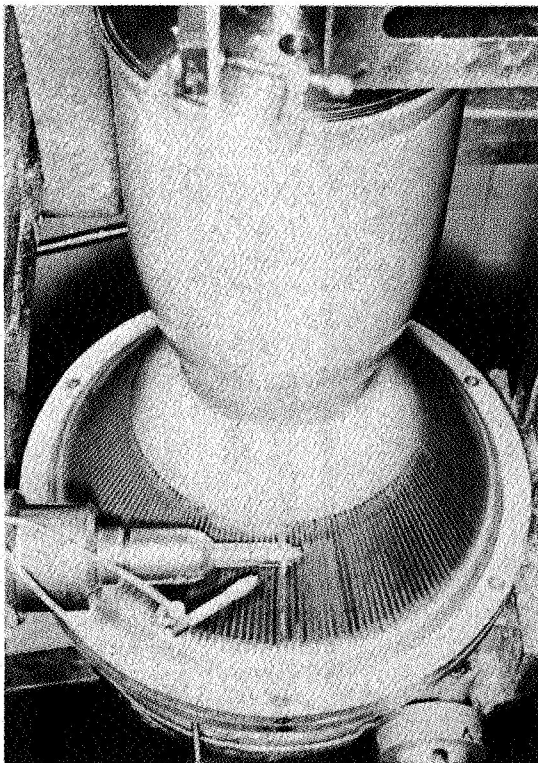
SLOTTED CHAMBER

SLOTTING NOZZLE
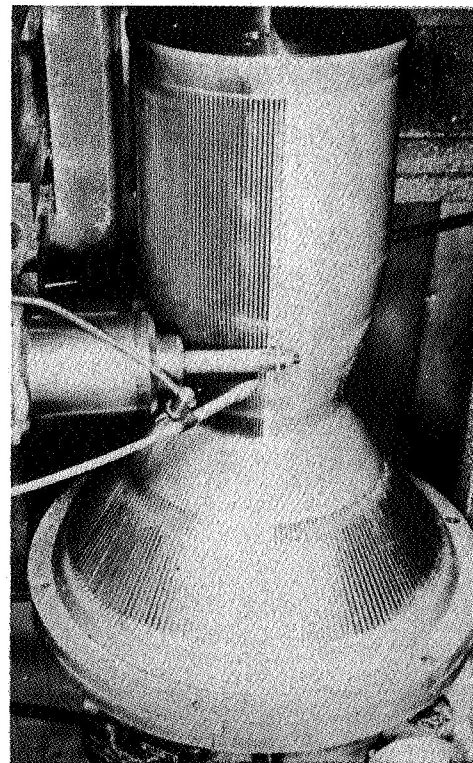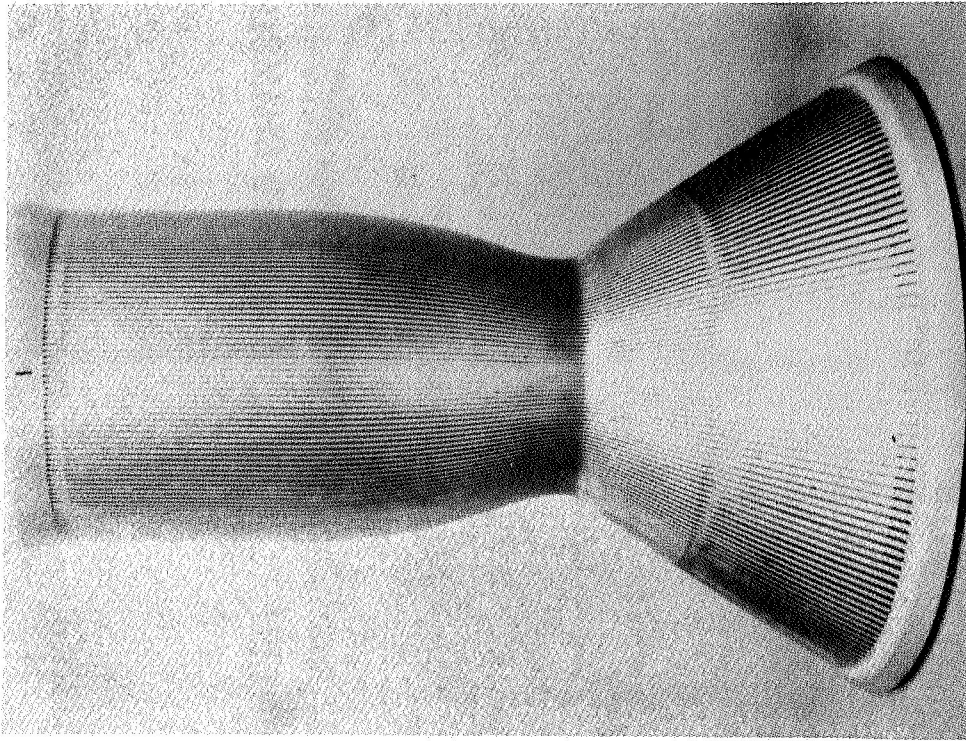
SLOTTING COMBUSTOR

Figure 63. Demonstration Chamber Fabrication

FINAL MACHINED CHAMBER

ELECTROFORMED CHAMBER

CHAMBER PREPARED
FOR ELECTROFORMING
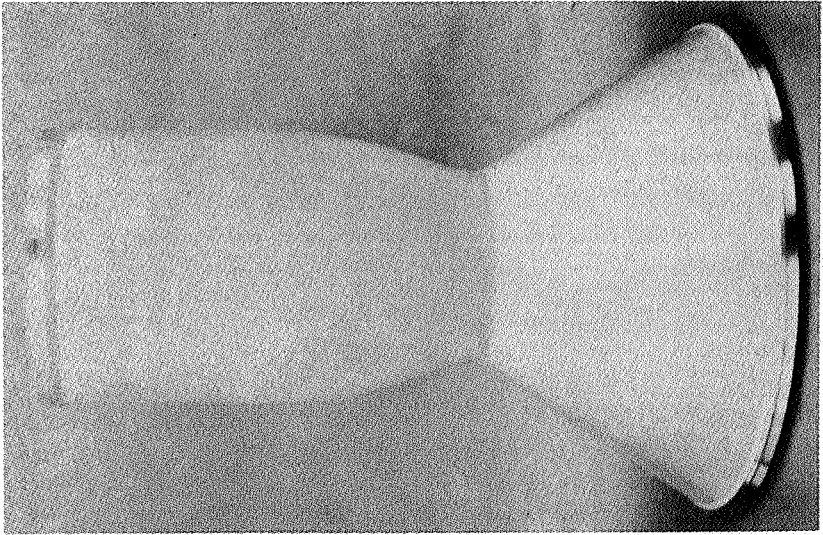
Figure 64. Demonstration Chamber Fabrication

CHAMBER ASSEMBLY COMPLETE

Figure 65. Demonstration Chamber Fabrication

solution at engine inlet pressure and temperature will remain in solution through the engine. Heated tube tests have been conducted with helium saturated MMH and indicate no effect on the burnout correlation as discussed previously.

The presence of undissolved helium in the form of a continuous bubble was studied using a 2-D channel transient conduction model. The results of this study, shown in Fig. 60, indicate a maximum wall temperature of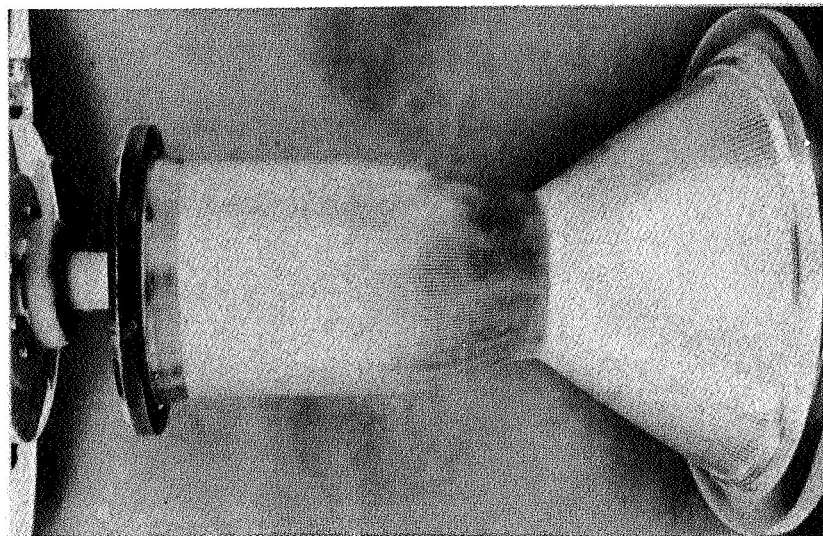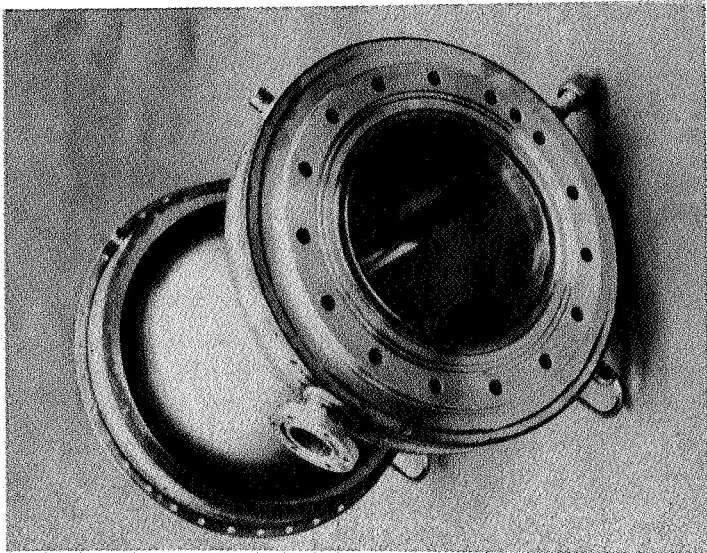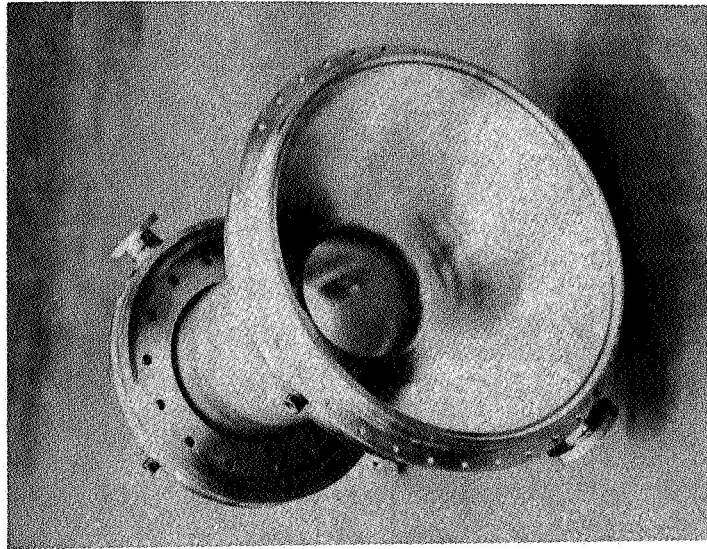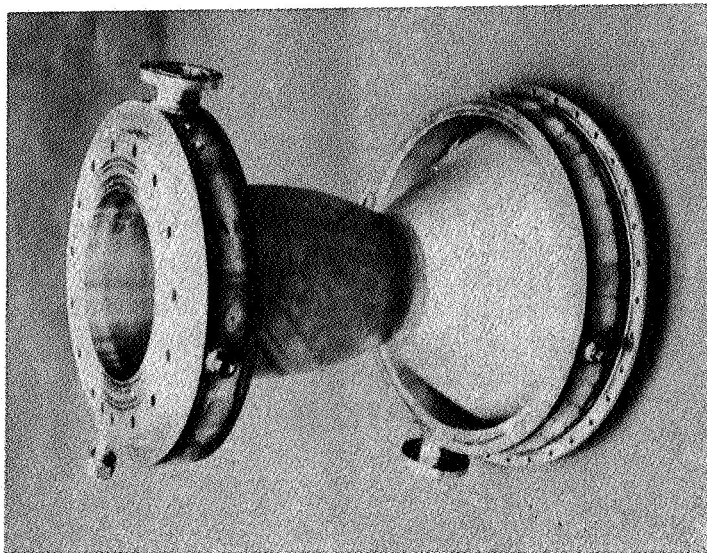 1290 F at 0.3 second after the bubble enters the chamber. Bubble duration in excess of 0.3 seconds would result in fuel depletion and combustion would cease. Structurally, the wall is actually capable of uncooled operation for almost one second. If the helium ingestion were uniformly distributed in a froth type flow, there would be some degradation in MMH cooling as discussed previously.

5.2 DEMONSTRATOR THRUST CHAMBER AND NOZZLE FABRICATION

Manufacturing Operations for the OME regeneratively cooled thrust chamber are shown schematically in Fig. 61 and pictorially in Figs.62 through 65. Fabrication of the CRES liner is begun by spinning to the approximate contour. Inside and outside contours are then machined and a light nickel electroform is applied to prepare the surface for the final electroform. Channels are then cut and their dimensions verified. Nickel electroform is applied and machined to provide an outer wall thickness of 0.030 inches. All channels are then cleaned and their flow characteristics determined. Manifolds, flanges, and ducts are machined and welded to the thrust chamber assembly. Final machining is followed by a proof and leak pressure test and a flow calibration of the completed assembly.

The nozzle extension was fabricated from a Columbium WC103 ring forging. This forging is machined to provide the 30 degree inside conical contour and the flange for attaching to the regeneratively cooled thrust chamber. After machining the nozzle is annealed and a final machining accomplished. A silicide coating is then applied and the nozzle mounted on the thrust chamber. The Thrust Chamber Assembly is shown in Fig. 66.

5.3 DEMONSTRATION CHAMBER TEST PROGRAMS

The basic objective of test programs conducted at Rocketdyne and NASA facilities (described in Appendix A) was to evaluate performance, heat flux and operating characteristics of the OME demonstrator thrust chamber assembly over the anticipated range of operating conditions. The test programs were broken down into groups of tests, called test sequences, having specific detailed objectives.
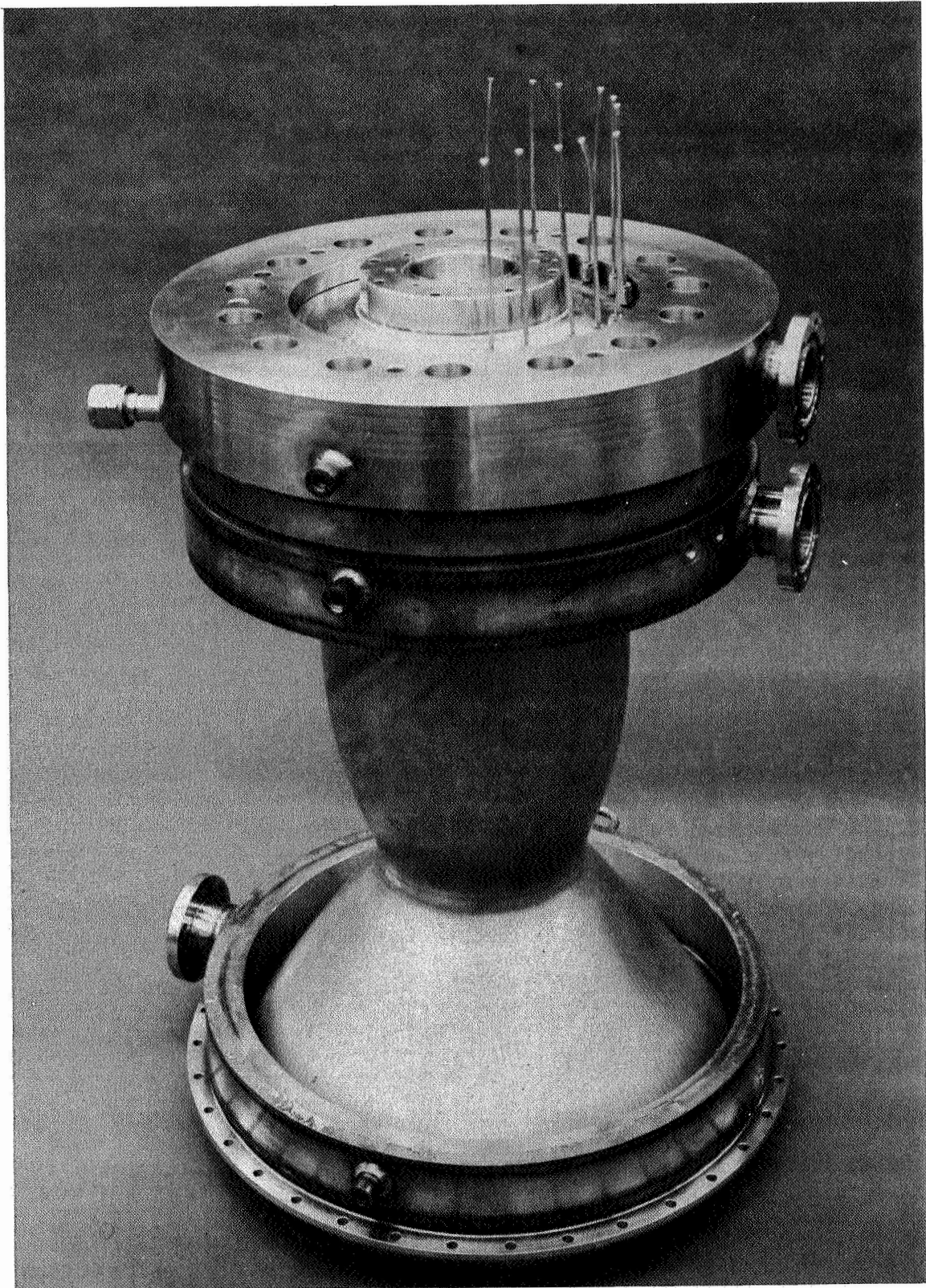
Figure 66. Demonstrator Thrust Chamber Assembly

CTL-IV Tests

A total of nine sequences were planned to be conducted at Rocketdyne's CTL-IV, of which three were completed (Table 27). A facility malfunction resulted in delay of subsequent planned tests until the WSTF test program. The L/D #1 injector was used in all sequences. Sequence 1 consisted of seven tests conducted in the bypass coolant mode with decreasing amounts of coolant, increasing duration, and increasing mixture ratio during the sequence. Sequence 2 was a series of 12 ten-second tests in the bypass cooling mode covering the complete ranges of chamber pressure (110-140 psia) and mixture ratio (1.45-1.85). The 19 tests conducted for sequences 1 and 2 in the bypass mode were generally successful except that three tests at low chamber pressure gave indications of flow separation in the nozzle rendering the thrust measurement invalid.

For Sequence 3 the engine was plumbed to the regenerative cooling config-uration and four tests were made of varying duration at the nominal conditions. These were followed by a nine test matrix covering the complete chamber pressure and mixture ratio range. Operation of these tests were successful except for three low-pressure tests, where separation again took place; and one test in which the digital data system was inoperative. The last test of this sequence was prematurely terminated at 190 seconds due to a facility malfunction which damaged the chamber and prematurely ended this phase of the test program.

The engine was mounted in a vacuum can where altitude was maintained by a LOX/alcohol hyperflow system. The engine was mounted with the nozzle exit nearly flush with a duct through which the hot gas was expelled. During the test the water cooled duct overheated and expanded against the inlet manifold of the regenerative chamber, placing a load in excess of 6000 pounds on the engine, as indicated by the thrust measurement. The test was terminated, at which time the duct collapsed and imparted a shock load on the engine inlet in excess of 10,000 pounds (thrust pegged off scale). Subsequent to this failure, the cell closure blew off due to an overpressure in the test cell.

Inspection of the chamber indicated that the outer wall was damaged locally but the hot wall did not crack. The nonaxisymmetric load caused the throat to deform one percent in diameter; and one of the channels deformed, causing a 33 percent restriction in flow area. The nickel back wall was repaired by electroforming (Fig. 67). Thermal analysis of the engine indicated that it would operate satisfactorily with the deformed channel, which effectively simulates a partially plugged channel condition.

TABLE 27

TEST PROGRAM SUMMARY

| Test Sequence	No. of Tests	Hardware Configuration	Test Purpose
Tests at CTL-IV			
1	7	L/D #1 Injector; Bypass Cooling ↓	Checkout
2	12	Same	Chamber Pressure and Mixture Ratio Survey
3		L/D #1 Injector; Regenerative Cooling ↓	Checkout
4	9	Same	Chamber Pressure and Mixture Ratio Survey
Tests at WSTF		All Regenerative Cooled	
1-1	6	L/D #2 Injector	Checkout
1-2	12	L/D #2 Injector w/o Aux Film Cooling ↓	Chamber Pressure and Mixture Ratio Survey
1-4	5	Same	Same with no Film Coolant
2-1	3	L/D #1 Injector w/o Aux Film Cooling ↓	Checkout
2-2	6	Same	Pc and O/F Survey with No Film Coolant
2-3	12	L/D #1 Injector with Aux Film Cooling ↓	Chamber Pressure and Mixture Ratio Survey
2-4	10	Same ↓	Pc and O/F Saturated Propellant
2-9	11	Same ↓	High and Low Pressure Survey
2-5	15	Same	Pc and O/F Survey with 50-50 Fuel
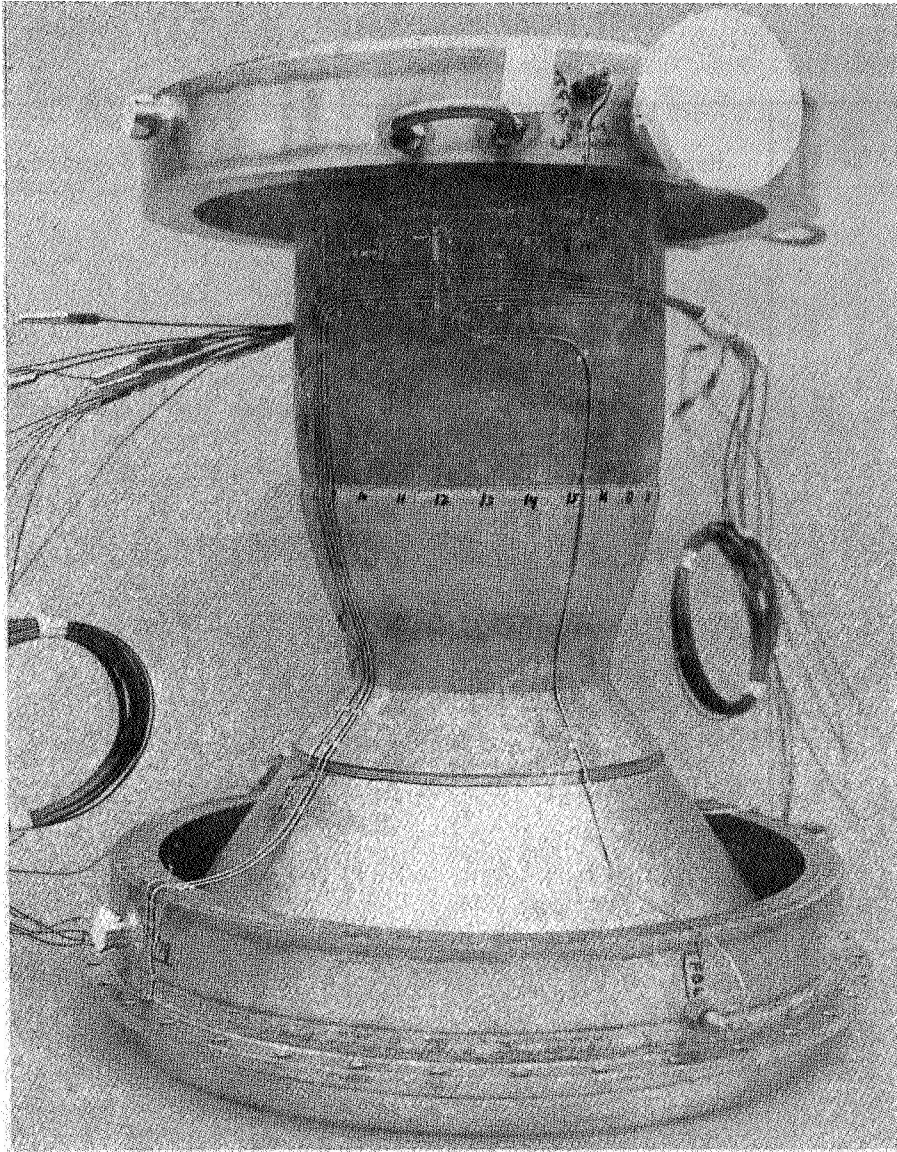
Figure 67.   Reworked Demonstration Chamber

White Sands Tests

The tests conducted at WSTF included several engine configurations (Table 27). The repaired regeneratively cooled thrust chamber shown in Fig. 67 was used for all tests. The first tests were conducted with the L/D #2 injector with the film coolant ring flowing fuel at approximately 2 percent of the total propellant flow rate. A total of six tests were conducted during the first sequence with durations ranging up to 10 seconds at nominal conditions.

Satisfactory operation of the repaired thrust chamber was demonstrated at nominal and under abnormal operating conditions. Particularly, the nominal start sequence included an oxidizer injection lead and the shutdown sequence consisted of a fuel rich shutdown. Due to a facility malfunction, an excessively fuel rich start caused by a 1½ second oxidizer valve opening delay occurred. In addition, during later tests, a slow closing oxidizer valve caused several 100 millisecond oxidizer rich shutdowns. The thrust chamber operated smoothly during these tests and the hardware was in excellent condition after the tests. Also, on two tests, the oxidizer flow meters were erratic, indicating the possibility of residual gas bubbles in the oxidizer feed system; however, no instabilities were observed in engine operation. Test data appeared to be valid on four of these checkout tests, with the exception that a small oxidizer leak in the facility could have degraded performance by approximately 1 percent. The second sequence consisted of 12 tests over the complete chamber pressure and mixture ratio range.

Posttest inspection showed that the film coolant ring had been slightly eroded and the uncooled acoustic cavity insert ring had been warped. These items are not flight configuration and were included only to permit test flexibility. In the flight hardware, film coolant will be supplied from the injector and the acoustic cavity integral with the cooled chamber.

The engine was reassembled with an uncooled spacer in place of the boundary layer coolant ring, and a series of five tests conducted to explore engine performance without boundary layer coolant. The test data indicated that fuel was leaking into the thrust chamber and posttest hardware inspection revealed that the injector indeed had become sufficiently distorted at the O-ring seal to permit massive fuel leakage to the chamber. Data analysis, delayed until after completion of this test sequence, indicated that leakage was present as early as the fifth test of the first (checkout) test sequence at WSTF.

The thrust chamber was in no way damaged during these tests, and was reassembled with the L/D #1 injector and the solid spacer ring in place of the film coolant ring. Three checkout tests and six performance survey

tests were made without auxiliary film coolant. Data from these tests indicated a variation and discrepancy in oxidizer flow. Subsequent facility checkouts after completion of the nonfilm cooled test series indicated a check valve failure allowing oxidizer leakage into a nitrogen purge line. Performance data is somewhat questionable, because the leak occurred downstream of the oxidizer flow meters.

The engine was reassembled with the repaired film coolant ring. The repair consisted of sealing the leaking area of the coolant ring and Rokide coating the surface exposed to combustion chamber gases. Twelve tests were conducted to complete a performance survey over the ranges of chamber pressure and mixture ratio. This was followed by a ten-test sequence covering the same ranges with the propellants saturated with helium at 225 psia. A series of eleven tests was then conducted with chamber pressures ranging up to 178 psia (the facility limit) to demonstrate operation of the thrust chamber at conditions near the Space Tug design for earth storable engines. The series also included tests down to 100 psia chamber pressure to simulate the blow-down conditions resulting from a vehicle pressurization system failure. Both propellants were saturated with helium at 165 psia for these tests.

The final test series was conducted with 50-50 as the fuel. The propellants were again saturated with helium at 165 psia for these 15 tests. The tests were conducted at chamber pressures ranging from 100 to 179 psia and mixture ratios ranging from 1.48 to 1.86. One test was conducted for a duration of 30 seconds. The duration was limited to 30 seconds because of the susceptibility of the film coolant ring to overheat.

After the tests, the thrust chamber and injector were in excellent condition, while the film coolant ring was again slightly eroded in three places.

5.4   DEMONSTRATION CHAMBER TEST RESULTS

The test conditions and a steady-state data summary for all the tests conducted on the regeneratively cooled demonstration thrust chamber are summarized in NASA-CR-140321. A total of 112 tests was conducted for a cumulative duration of 1042 seconds. Chamber pressures ranged from 100 psi to almost 180 psi and mixture ratios from 1:4 to 1:9. Figure 68 is a graphic presentation of the distribution of chamber pressure and mixture ratio points tested during the program.

Start And Shutdown Characteristics

The thrust and chamber pressure transients depend on valve sequencing, facility and engine flow resistance, facility and engine volumes, ambient
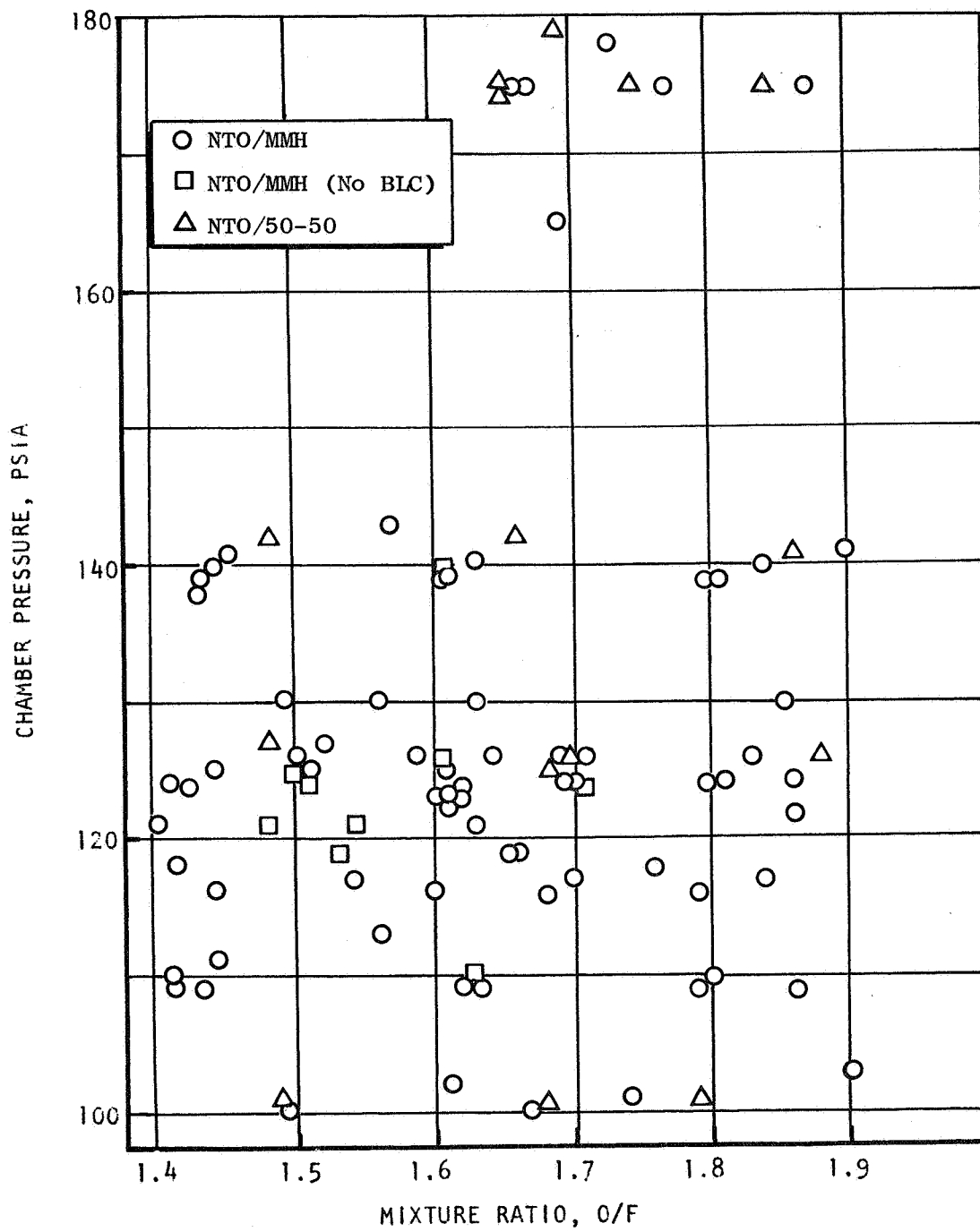
Figure 68 Demonstrator OME Thrust Chamber Operating
Conditions

pressure, and steady-state operating conditions. Some oscillating of the servo controlled fuel throttling valve at the CTL-IV facility generally occurred distorting the start transients, so that the transients demonstrated at the White Sands Test Facility are more typical of vehicle operation. A typical start sequence for the demonstration chamber with the L/D #1 injector is shown in Fig. 68A.

First major rise in the oxidizer injector pressure leads the fuel injector pressure rise by approximately 300 milliseconds. There is no overshoot in chamber pressure, although some damping of the trace is probable due to the configuration of the tube from the chamber to the transducer. The thrust overshoot is approximately 60 percent of the steady-state value and the oxidizer pressure overshoot is approximately 30 percent of its steady-state value.

The start transient for a similar oxidizer lead with the No. 2 like-doublet injector is similar to the transient characteristics of L/D #1 injector. The injector/thrust chamber combinations tested in this program have demonstrated the ability to start safely over a range of propellant inlet conditions and sequences, which allows considerable flexibility in design of flight valve and ducting configurations.

The oxidizer valve was scheduled to close prior to the fuel valve so that the heat input to the regeneratively cooled jacket would decay before the coolant flow decayed. In the typical shutdown transient shown in Fig. 68B, the oxidizer injection pressure decayed slightly before the fuel injection pressure as planned. Due to a facility malfunction on Test 1-1B-3, the fuel valve closed approximately 100 milliseconds before the oxidizer valve closed, resulting in an oxidizer-rich shutdown. However, posttest inspection indicated no hardware damage resulted from this shutdown. Not only was the thrust chamber undamaged by this shutdown sequence, but the shutdown transient data indicated that severe exothermic overheating of the fuel did not occur.

The heat sink capability of the channel wall design is sufficient to tolerate oxidizer rich shutoffs of this magnitude. Since chamber pressure and, consequently, heat flux, decay significantly with the reduction of fuel injection pressure, it is probable that even longer oxidizer rich shutdowns could be tolerated.

Stability Characteristics

No high or low frequency instability was recorded over the entire range of chamber pressures and mixture ratios tested with either MMH or 50-50 fuels with either the L/D #1 or L/D #2 injector. All configurations relied

Fire Switch

Axial Accelerometer

Oxidizer Injection Pressure
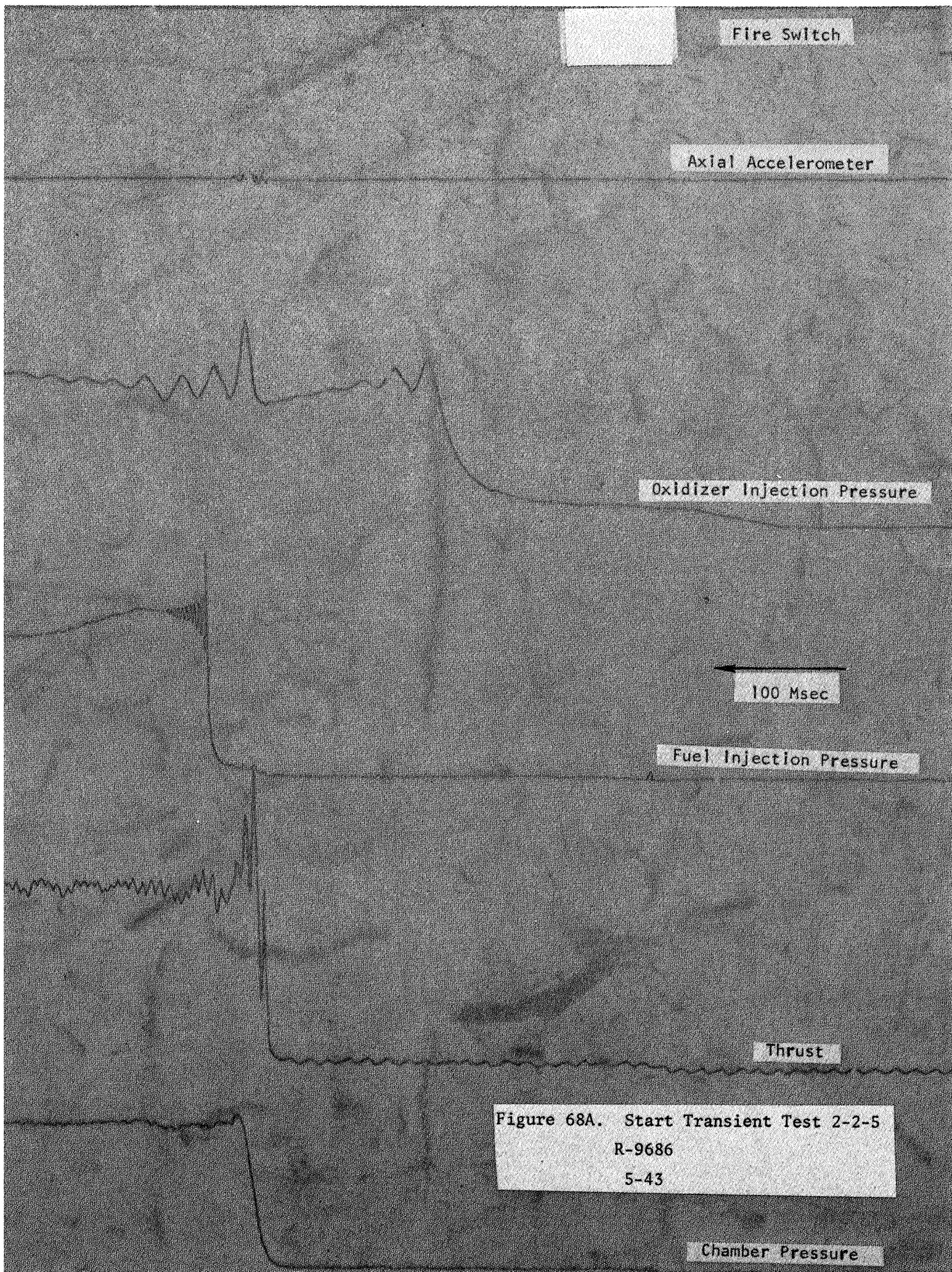
100 Msec

Fuel Injection Pressure

Thrust

Figure 68A. Start Transient Test 2-2-5
R-9686
5-43

Chamber Pressure

Fire Switch

Axial Accelerometer

← 100 Msec

Oxidizer Injection Pressure

Fuel Injection Pressure

Thrust

Chamber Pressure

R-9686

5-44

Figure 68B. Shutdown Transient Test 2-2

on acoustic cavities without baffles to maintain stable operation.
Axial accelerometers installed on the engine thrust mount typically
showed disturbances of 10-20 g's RMS at start and no significant activity
during the tests.

Performance Characteristics

Performance is summarized for all tests in the Demonstration Chamber
Test Data Dump. The method of calculating performance from the test data
is described in Appendix B. Performance is shown in Fig. 69 versus
mixture ratio for the tests with unsaturated NTO and MMH using the L/D #1
injector at CTL-IV and WSTF. Performance on the tests at nominal condi-
tions with 2 percent auxiliary film coolant at CTL-IV averaged approximately
310 seconds. A one percent improvement in injector performance is predicted
with minimum development. Performance measured at WSTF was slightly over
308 seconds at nominal conditions. The deformed nozzle (as a result of
the CTL-IV malfunction) may have resulted in a slight performance degrada-
tion at WSTF.

The WSTF data shown in this figure were taken on tests of 7 seconds
duration (the 2-3 test sequence). Tests at WSTF indicated a trend of
increasing performance with durations even beyond 10 seconds. On a long
duration test, the performance increase between data slices taken at 7
seconds and 30 seconds (the duration of the test) was greater than 1½
seconds. Performance increases of 0.2-0.5 seconds between the 7 and 10
second data slices were typical for test series No. 2. The reason for
the performance variation with time at WSTF is not clear at this time.
One long duration test with data was conducted at CTL-IV. Thermal data
indicate failure of the supplemental film coolant ring began approximately
25-30 seconds into the test. Performance data from 5-20 seconds does not
indicate a significant performance increase during this time. Also,
performance measured on the shorter duration tests at CTL-IV were in
good agreement with the data from this longer test as shown in Fig.69 .

As shown, the performance at nominal conditions agrees within 1/2 percent
at the nominal conditions between the two test facilities. Longer duration
tests at WSTF may result in nearly perfect agreement of specific impulse
measurements between the facilities at a value of 310 seconds. Theoretical
and measured performance and losses are shown in Table 28.

The variation of performance with chamber pressure and mixture ratio
measured at WSTF over the ranges for which the demonstrated was designed
is shown in Fig. 70 for unsaturated propellants and approximately 2 percent
film cooling. An increase in performance of approximately 1-second occurs
at the upper end of the nominal operating range of the OME (P_c = 140 psia,
o/f = 1.8), compared to performance at nominal conditions. Peformance
decreases by approximately 3 seconds operating at a chamber pressure of
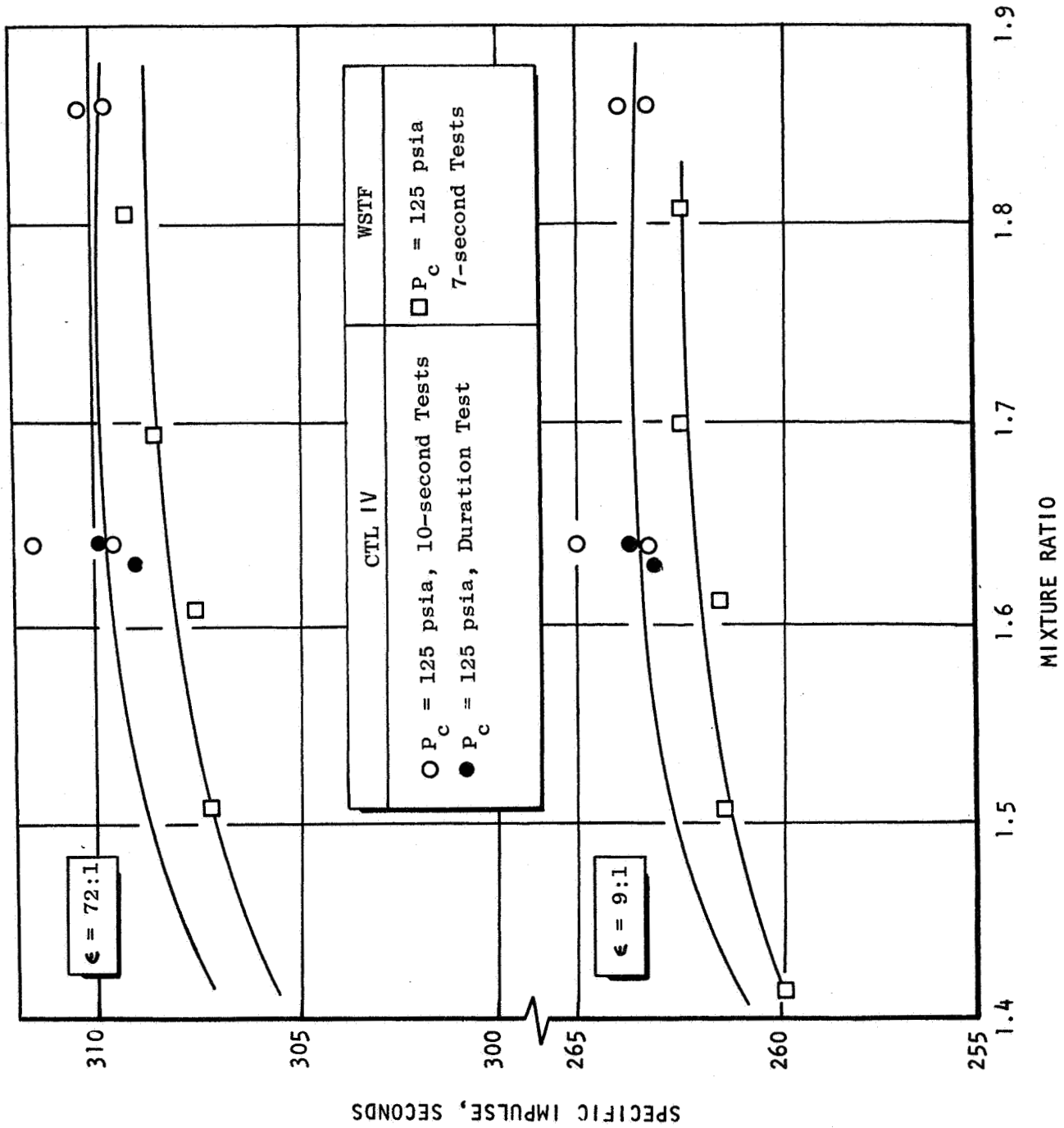
Figure 69 . Comparison Of Performance Measured At CTL-IV and WSTF

TABLE 28

OME SPECIFIC IMPULSE SUMMARY

	FLIGHT SYSTEM AT ϵ = 72	TEST SYSTEM AT ϵ = 72	TEST SYSTEM AT ϵ = 9
ODK SPECIFIC IMPULSE, SEC	332.6	332.6	302.4
DIVERGENCE EFFICIENCY	0.985	0.985	0.915
COMBUSTION EFFICIENCY	0.974	0.965*	0.965*
REGEN HEATING EFFICIENCY	1.006	1.005	1.005
IMPURITY FACTOR	0.998	0.998	0.998
DRAG LOSS, SEC	-6.5	-6.5	-3.0
STRATIFICATION LOSS, SEC	-1.0	-1.0	-1.5
DELIVERED SPECIFIC IMPULSE, SEC	312.9	309.6	263.3

* L/D #1 INJECTOR BASED ON SOLID WALL CHAMBER TESTS
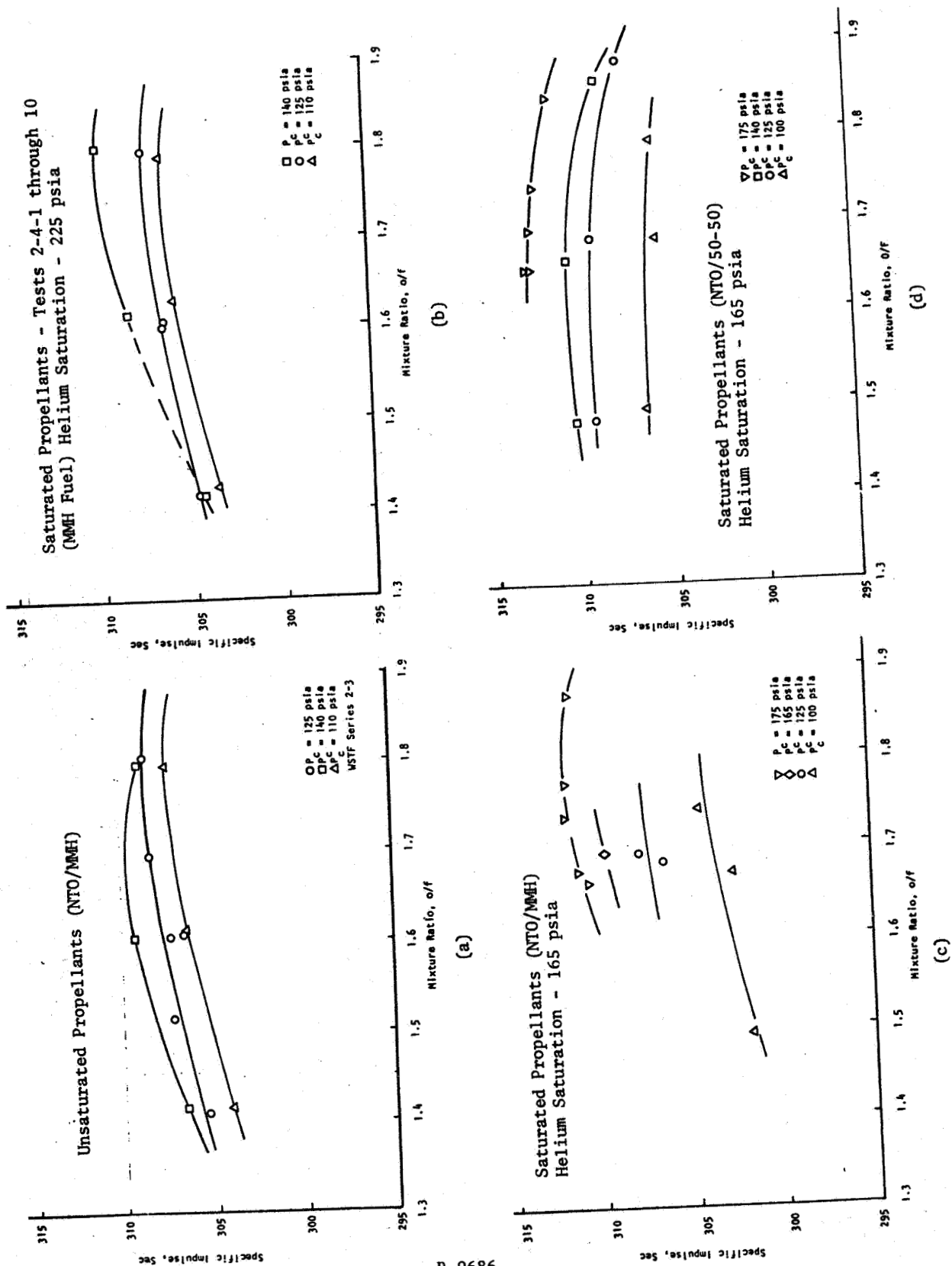
Figure 70. OME Engine Performance

110 psi and a mixture ratio of 1.45. Performance data measured at CTL-IV at off-design chamber pressures did not show the trend. Low pressure data was invalid due to nozzle separation. High pressure data indicated a slight pressure loss.

Performance with NTO/MMH and the L/D #1 injector without film coolant was determined at WSTF during test sequence 2-1. During these tests, a facility oxidizer leak occurred at the start of each test and decayed during the test. This leak decreased performance to an unknown extent and is probably responsible for erratic performance on the first few tests of the series. The data also appear questionable when compared to subsequent tests with film coolant in which the performance was as high or higher than the tests without film coolant.

Performance with helium saturated propellants is shown in Figs.69b and 69c. A performance penalty of approximately 1-second results under nominal operating conditions. The shape of the measured performance curve at 140 psia chamber pressure and 225 psia saturation pressure appears to be more sensitive to mixture ratio compared to the rest of the data. However, the point at nominal mixture ratio is consistent with all other data.

Operating at a chamber pressure of 175 psia would increase the performance by about 4 seconds. An OME derivative used for a Space Tug application would operate at a chamber pressure of approximately 240 psia and would have a significantly higher area ratio. The 100 psia test conditions simulate the effect of vehicle pressurization system failure. A performance loss of over 1 percent occurs under these conditions relative to performance at the design point.

The performance of NTO with helium saturated 50-50 fuel and the #1 like-doublet injector is shown in Fig. 69d. The nominal mixture ratio for this propellant combination is 1.60 for equal tank volumes. At this mixture ratio and a chamber pressure of 125 psia, a performance level of approximately 310 seconds was measured. These tests were of 7 seconds duration.

Operating at a high mixture ratio with this propellant combination results in a performance loss (rather than a performance gain as was the case with NTO/MMH). It was predicted analytically and shown in NASA-CR-128675, the Data Dump for Task I and II, that both ODK and delivered Is for NTO/MMH peaks at a higher value of o/f than for NTO/50-50. Figures 46 and 47 of the same reference indicate NTO/50-50 performance to be 2.2 seconds higher than NTO/MMH at 1.6 and 1.65 o/f, respectively. A gain of approximately 1 second in performance occurs at a chamber pressure of 140 psia. Performance sensitivity to chamber pressures is approximately the same as with the NTO/MMH combination, as shown in Fig. 71 which summarizes the WSTF data.
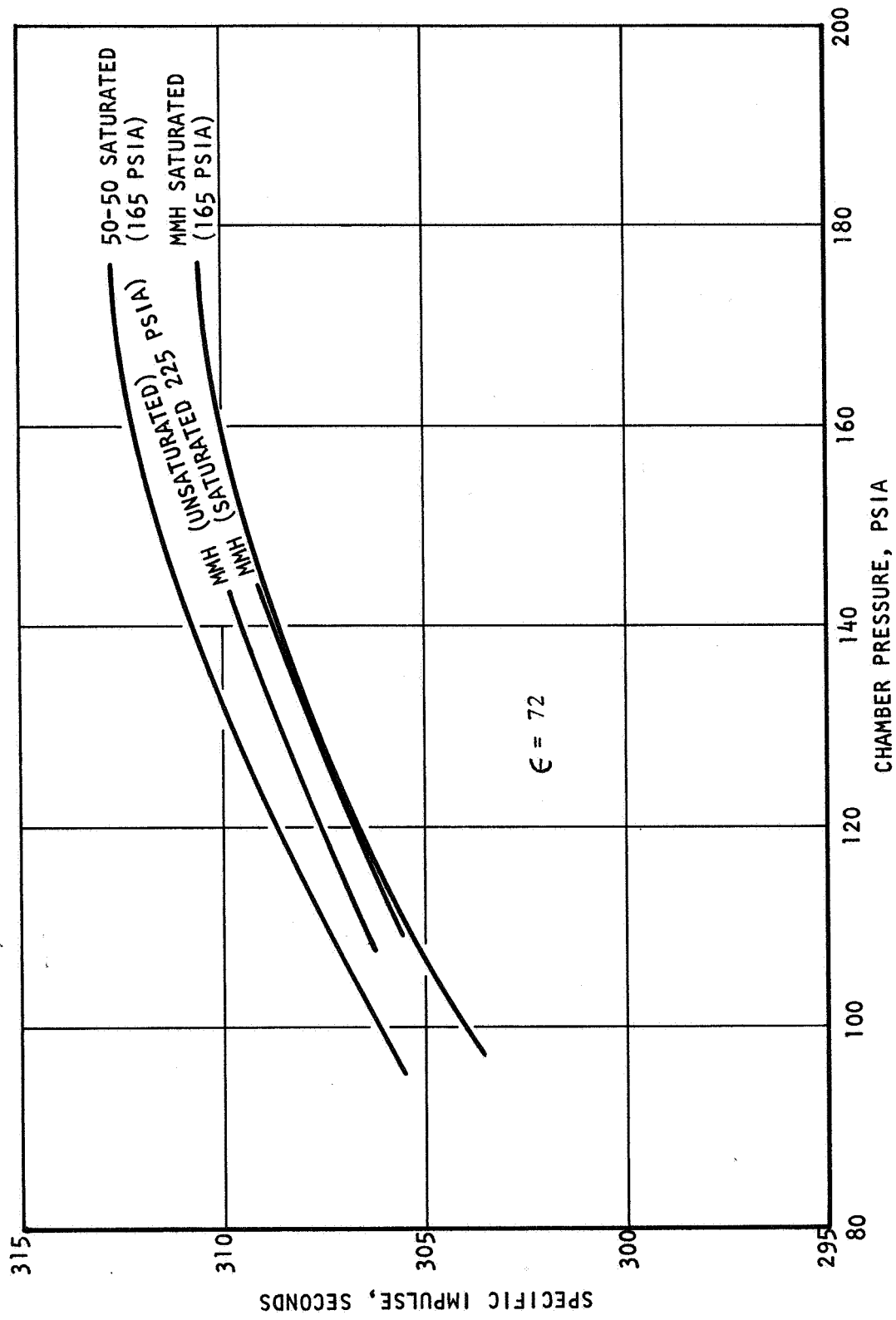
Figure 71   Summary of OME Performance Measured at WSTF

The L/D #2 injector was tested at WSTF during Series 1. Fuel leakage rendered most of the data unusable. The remaining data are questionable because of a possible oxidizer leak in the facility and the short durations (in view of the transient performance measured on longer duration tests) of these tests. The results indicate performance equal to or lower than the L/D #1 injector. Previous comparisons of these injectors during a company sponsored program at Rocketdyne indicated slightly higher performance for the L/D #2 injector.

Thermal Data

Thermal data taken during the tests at both facilities consisted of fuel bulk temperature rise, regenerative chamber back wall temperatures, and radiation cooled nozzle temperatures. These data, together with the data generated during the heated tube tests under this contract, were used to provide an indication of the safety margin at which the thrust chamber and nozzle were operating.

Bulk Temperature Rise and Heat Load

Coolant inlet and outlet temperatures, ΔT's, and the heat load for all tests are tabulated in the Demonstrator Test Data Dump. Fuel inlet and outlet temperatures were each measured in three locations. Three bulk temperature rises were calculated based on the three outlet temperature thermocouples. The inlet temperature thermocouple TFB-6 was used as the reference temperature for all three ΔT's because of its proximity to the inlet and general agreement with the fuel flowmeter temperature thermocouple. Temperature rises calculated in this manner generally agree with each other within 5 percent for the bypass cooled tests at CTL-IV and within 10 percent for the regeneratively cooled tests at the same facility with ΔT_3 generally exhibiting the lowest value and ΔT_2 the highest.

The three coolant temperature rise measurements taken at WSTF generally agreed within 5 percent except for the last half of the last test series, 2-5 (NTO/50-50), on which ΔT_1 and ΔT_3 generally agreed within 6 F, while ΔT_2 was about 15 F higher. The data fit for these latter tests was improved by basing ΔQ on ΔT_1 and ΔT_3 only for these cases.

The response of the coolant bulk temperature at the outlet for a typical cold-start test at CTL-IV indicated that two of the three outlet temperatures reach steady-state conditions in approximately 5 seconds, while the third requires almost 9 seconds to reach steady state. However, even the slow responding measurement reached approximately 96 percent of steady-state value in 5 seconds. Most tests were about 10 records duration with the last test at CTL IV about 180 seconds. Typical average outlet bulk temperature transients measured at WSTF are shown in Fig. 72 . Most tests at
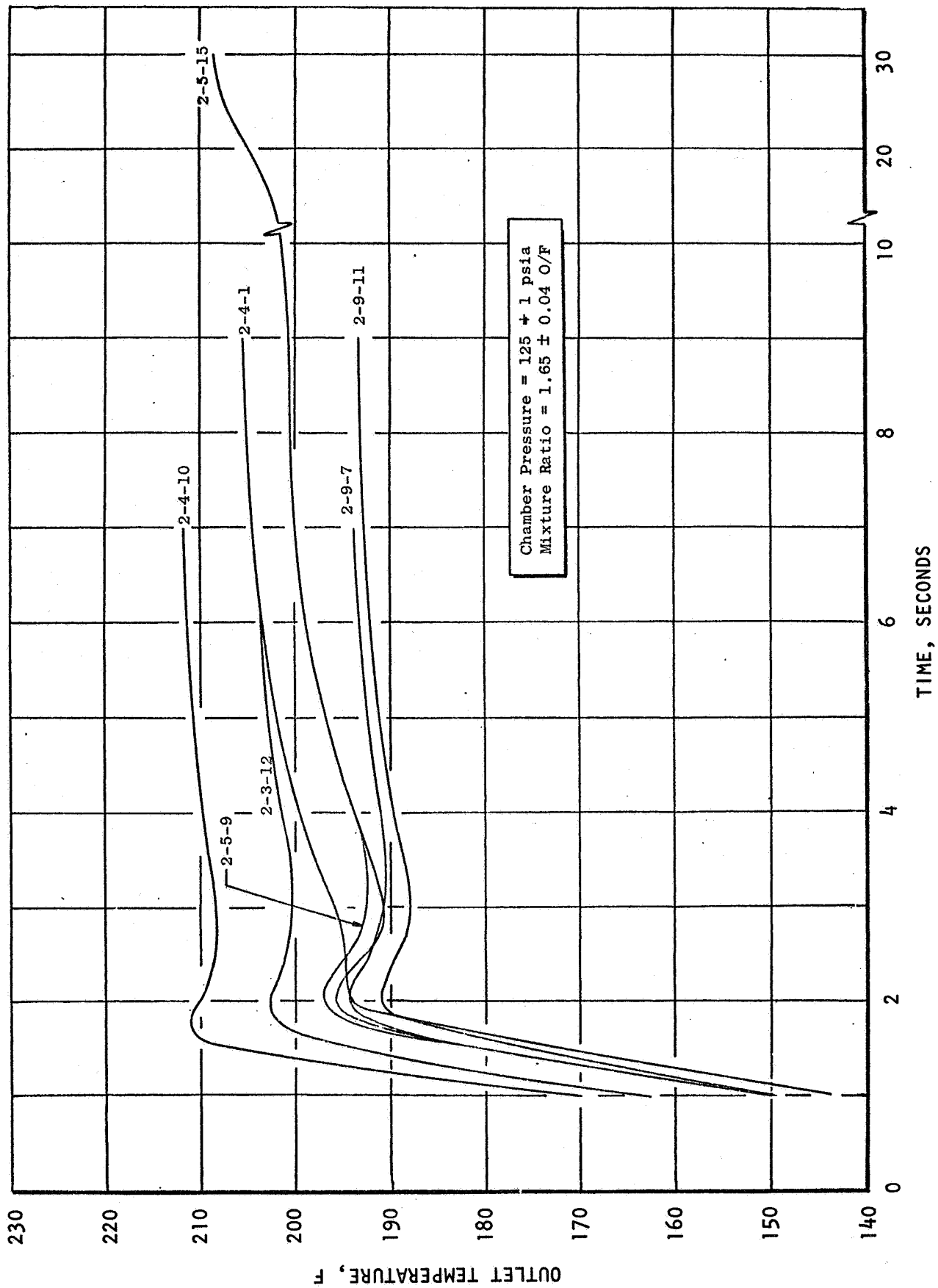
Figure 72 . Outlet Bulk Temperature Transient at WSTF

WSTF were approximately 6 to 10 seconds duration. The bulk temperature response time for these tests was approximately 6 seconds. One test was of 30-seconds duration. The temperature transient for this test, also plotted in Fig. 72, indicates a similar transient for the first 7-10 seconds; but subsequently, this temperature continues to rise gradually, so that the heat load measured at 7 seconds is approximately 4 percent less than the heat load at 30 seconds. Thus, the heat loads reported based on WSTF data may be four to five percent below the steady-state value. A significant part of the transient at both facilities may be due to the massive exit manifold which would not be present on the flight chamber. A flight type exit manifold was incorporated into the integrated chamber, which is discussed later.

The average values of the ΔT's were multiplied by the fuel flowrate through the jacket and the specific heat of the fuel to determine the heat absorbed by the fuel. In Fig. 73 the heat loads are plotted versus chamber pressure for the bypass cooled tests at CTL-IV with coded symbols to denote mixture ratio ranges. These data follow the predicted variation with P_c to the 0.8 power. However, the measured absolute values of the heat load were approximately 10 percent lower than the predicted values which were based on heat sink chamber test data. The effect of mixture ratio could not be distinguished except at the lowest mixture ratio conditions (o/f = 1.4 - 1.44).

The heat load results for the regeneratively cooled tests are summarized in Fig. 74 for all test conditions at both CTL IV and WSTF. The resulting curves for all test conditions follow an approximate 0.8 power of P_c relation which is as would be predicted. The regeneratively cooled chamber length was 13.5 inches.

Both the predicted and measured heat loads of the regeneratively cooled chamber at CTL IV are higher than the corresponding results with the separate coolant circuit due to the reduced effectiveness of the heated boundary layer coolant. The experimental regnerative cooling heat loads are about 15-20 percent less than predicted. The WSTF test results with 2 percent BLC indicate approximately a 5 percent lower heat load as compared to CTL IV results. This is within the data scatter of both facilities.

The WSTF tests at nominal BLC were conducted with both unsaturated and helium staurated propellants. No difference in heat load was noted in these tests due to propellant saturation.

The results of the zero BLC tests conducted at WSTF indicate that the use of 2 percent fuel film coolant reduces the heat load by about 20 percent. This is in agreement with the theoretical prediction of film cooling effectiveness. Negligible effect of mixture ratio on heat load
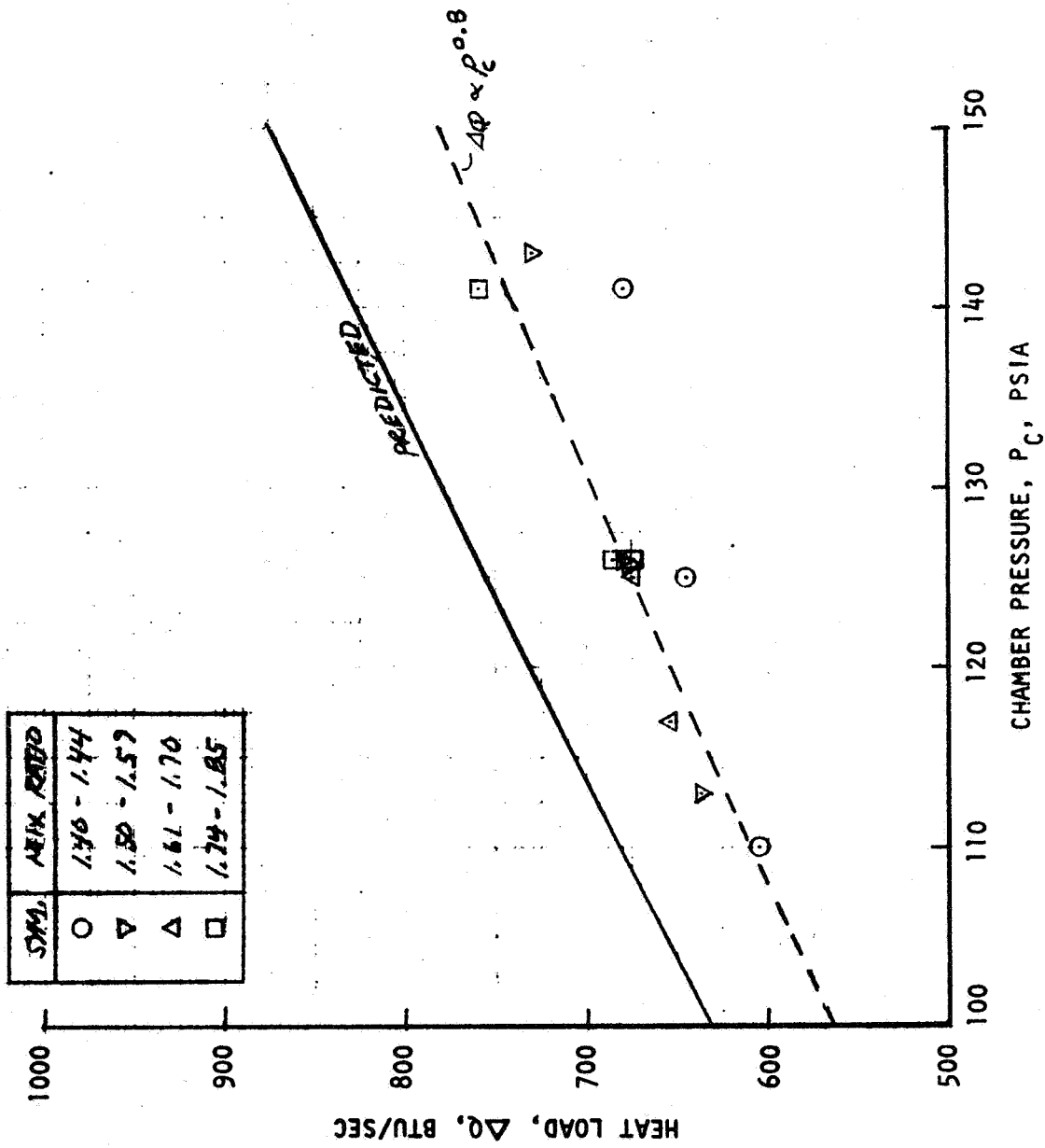
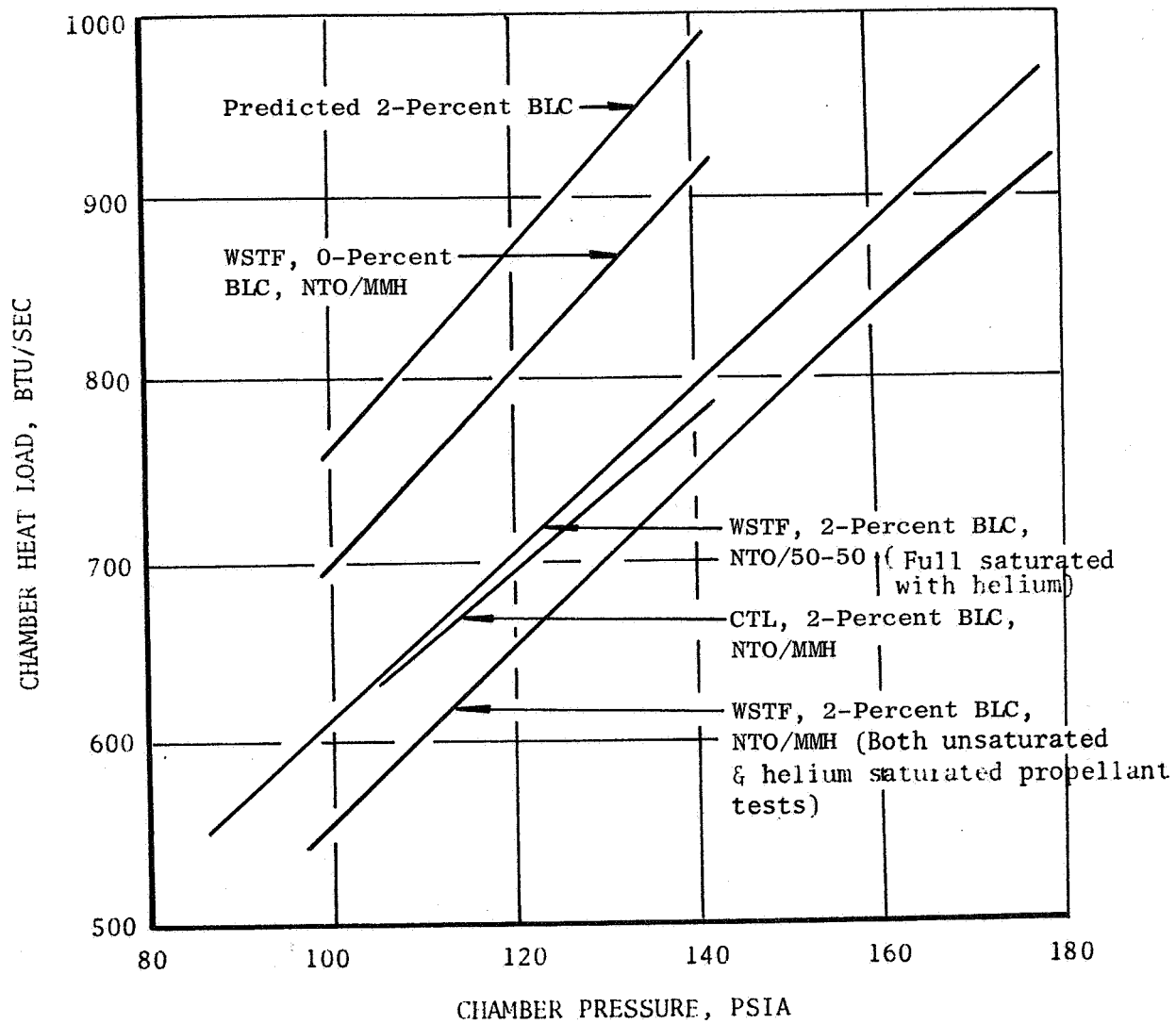Figure 73. OME Chamber Integrated Heat Load Separate Coolant Circuit

Figure 74. Summary of Demonstrator Heat Load Data

was noted in the limited tests with zero film cooling which is also in agreement with theoretical prediction.

The NTO/50-50 tests at WSTF were conducted with helium saturated fuel. The resulting heat load is approximately 6 percent higher than corresponding results at WSTF with NTO/MMH.

The effect of mixture ratio on heat load for all tests with BLC was found to be almost negligible. There appeared to be a slight trend of increasing heat load with increasing mixture ratio. The variation was less than ±5 percent about nominal which is actually within the data scatter of the test facilities.

The experimental results were used to predict minimum coolant safety factors for the demonstator chamber at both nominal and off-design conditions. These factors are summarized in Table 29.

No useful thermal data were obtained with L/D #2 injector because of the brief duration of some of the tests and the facility and engine leakage which occurred on the longer tests.

Back Wall Temperatures

Back wall temperatures were measured on the thrust chamber to indicate steady-state values during operation and also values at the start of each test. Steady-state values are significant in that the OME is required to operate at maximum back wall temperature of less than 600 F. The starting temperature of the back wall indicated values to which the back wall could be safely heated by soakback or other external heat inputs prior to start. The steady-state back wall temperatures for each test were presented in the Demonstrator Test Data Dump.

Back wall temperatures for a start from ambient conditions; i.e., the first test series, are shown in Fig. 75 for a typical test conducted at WSTF. As would be expected, the response is more rapid in the higher heat flux regions. The throat responds in about 3 sec; the injector-end in about 5 sec; and the nozzle region in about 8 sec. The multiple curves for each region indicate data taken at the various circumferential locations. Back wall temperatures on a hot start test at CTL-IV are shown in Fig. 76. Circumferential variations in the initial temperatures of over 50 degrees were sometimes noted as a result of the horizontal orientation of the engine, variations in soakback, and possibly local blowback in the altitude cell. The injector end, typically, experienced on hot-test prestart temperatures. In the most extreme case, the starting temperature was over 400 F. No abnormalities were exhibited during the start transient on these tests.

TABLE 29

THERMAL SAFETY FACTORS BASED ON EXPERIMENTAL DATA

Propellant	Safety Factor (1-D)	
	Nominal	Off-Design**
NTO/MMH with 2% BLC	3.5	2.8
NTO/MMH with no BLC	2.0	1.4
NTO/50-50 with 2% BLC	3.0	2.2

* P_c = 125 psia; $T_{bulk\ in}$ = 70F; o/f = 1.65 (MMH), 1.60 (50-50);
  Fuel Injector $\triangle P$ = 45 psi

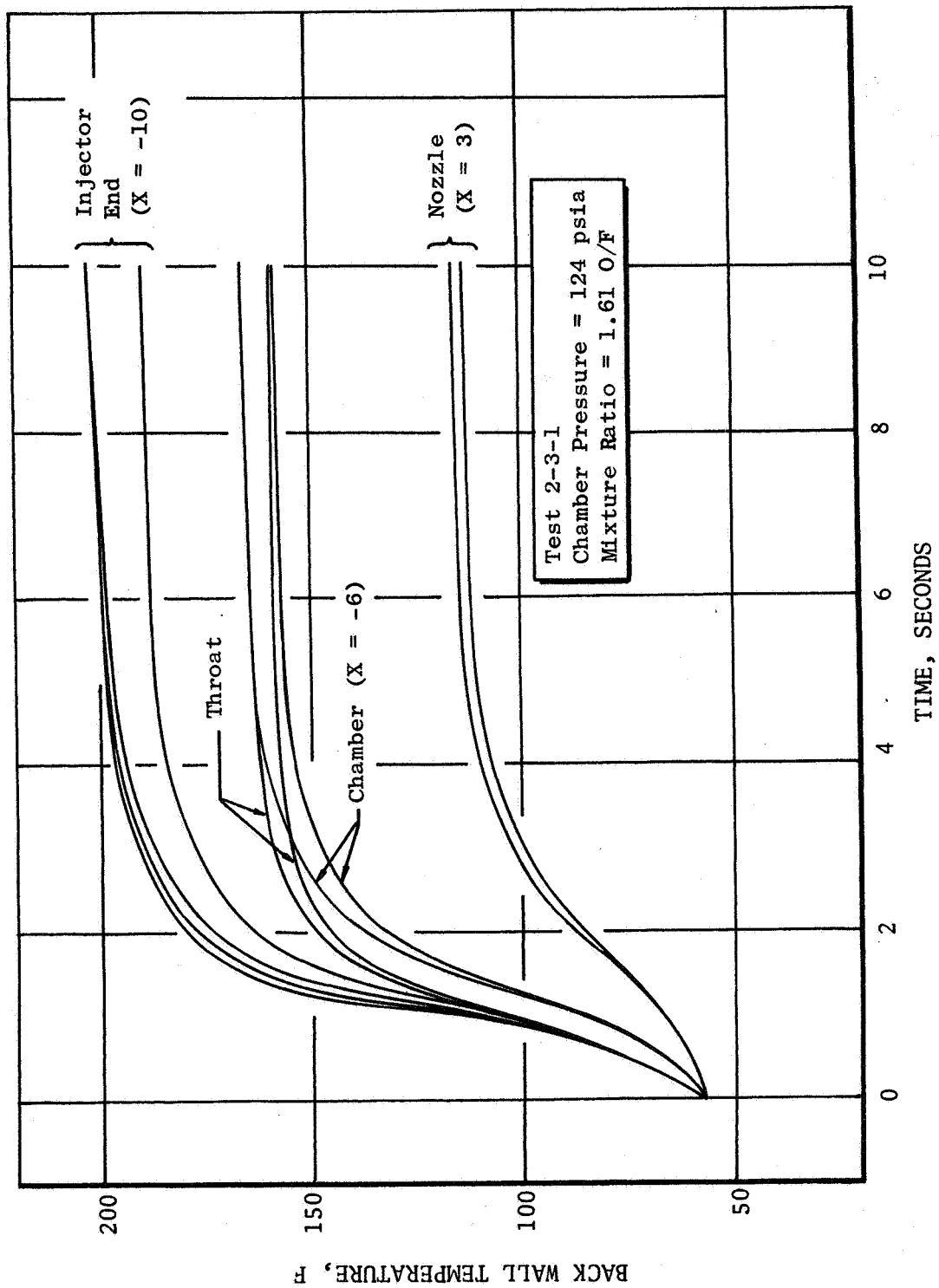** P_c = 120 psia; $T_{bulk\ in}$ = 100F; o/f = 1.84 (MMH), 1.79 (50-50);
  Fuel Injector $\triangle P$ = 36 psi

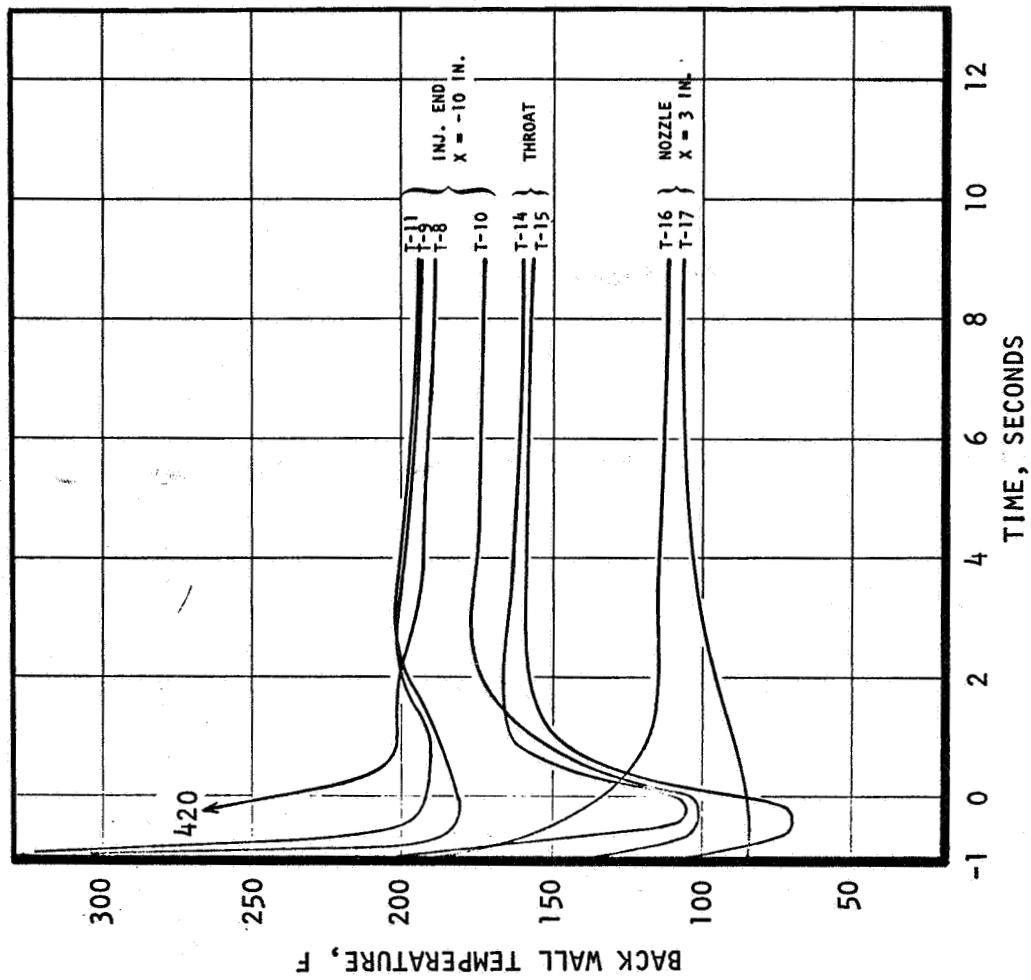Figure 75 Typical Cold Start Transients at WSTF

Figure 76 Regeneratively Cooled T/C Backwall Temperature Response

Hot start transients at WSTF generally did not exhibit as high a starting temperature at the injector-end as was recorded at CTL-IV. This is probably due to the differences in procedures between tests at the two facilities. At WSTF the engine was purged between tests. The ability of the thrust chamber to start without purges between firings was demonstrated at CTL-IV by purging only after a test series was completed. Heat from soakback and blowback resulted in high temperatures after shutdown on these tests.

Experimental steady-state back wall temperature measurements at nominal and off-design operating conditions are compared with the analytically predicted outer profile in Figs. 77 and 78. Since the actual heat load was experimentally determined to be about 25 percent lower than predicted, the analytical back wall temperature profile was based on a heat flux profile which was 25 percent below the originally predicted profile. The off-design case exhibits higher back wall temperatures due to increased coolant bulk temperature resulting from the higher mixture ratio.

In the combustion zone the measured temperatures are about 15-20 F lower than predicted outer surface values. The temperatures are, however, above the predicted bulk temperature which they must be in actuality. In the nozzle region (x = 3.0 inch) the measured temperature also appears approximately 10 F lower than predicted although the fact that the measurement was made near the region of the step change in channel width tends to complicate the results. Longitudinal conduction would tend to smooth the temperature profile in this region, thereby, making measured and predicted results in better agreement for the 75 F inlet temperature case.

In the throat region, the measured temperatures are about 20 F higher than predicted. Theoretical analysis indicates this temperature increase is most likely associated with a decrease in the coolant film coefficient along the closeout surface due to throat region curvature. The somewhat higher back wall temperature could tend to increase chamber life due to a decreased temperature differential between hot wall and closeout.

Radiation Nozzle

Limited experimental data on steady-state operation of the short Columbium radiation nozzle extension exists since nearly 30 seconds test duration is required to achieve equilibrium temperatures. A single 30-second test at CTL IV with NTO/MMH indicated a maximum steady-state temperature of about 1900 F. A similar test at WSTF with NTO/50-50 propellants indicate maximum nozzle temperature of about 1600 F as shown in Fig. 79.
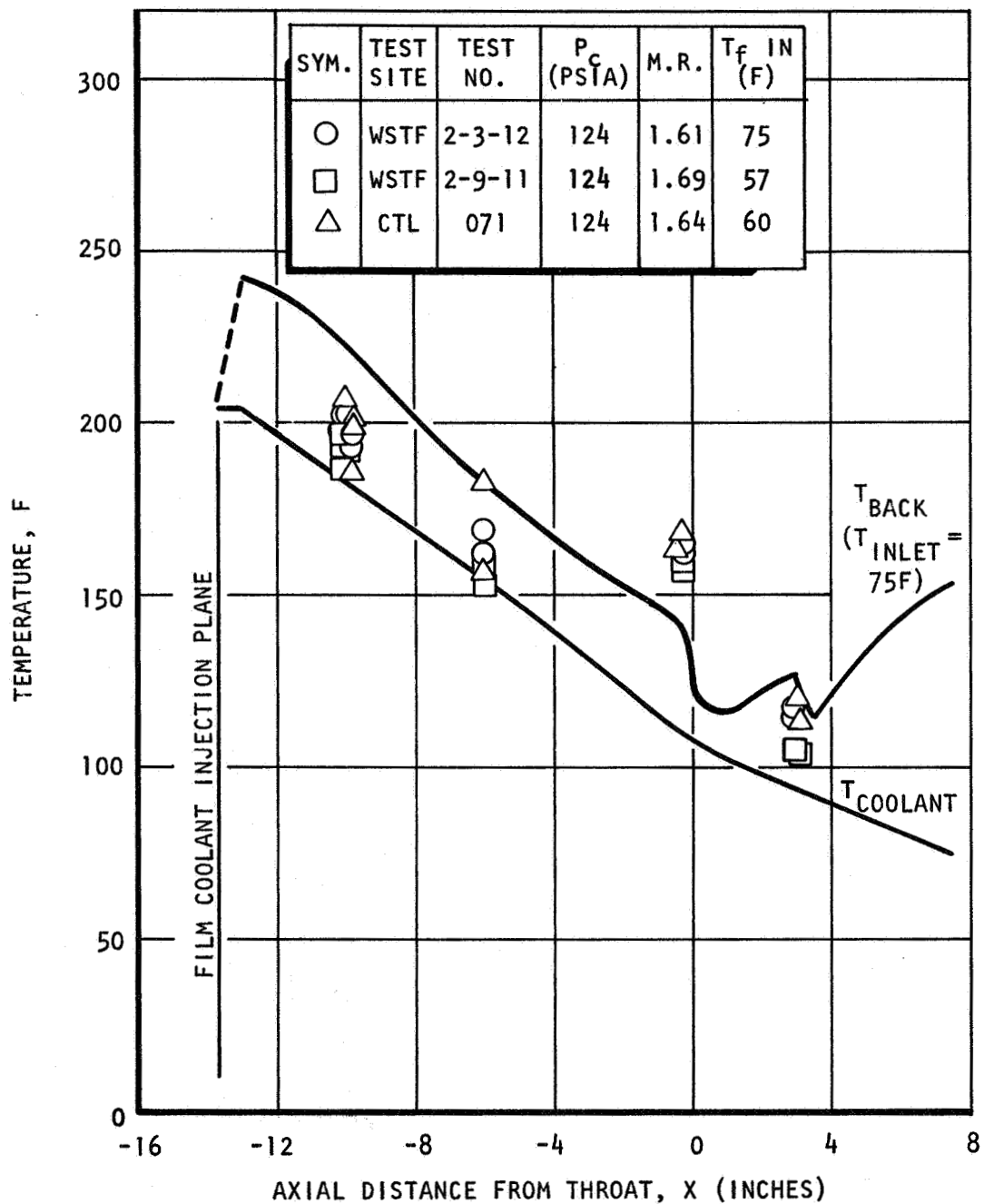
Figure 77   Back Wall Temperature Profile for the OME
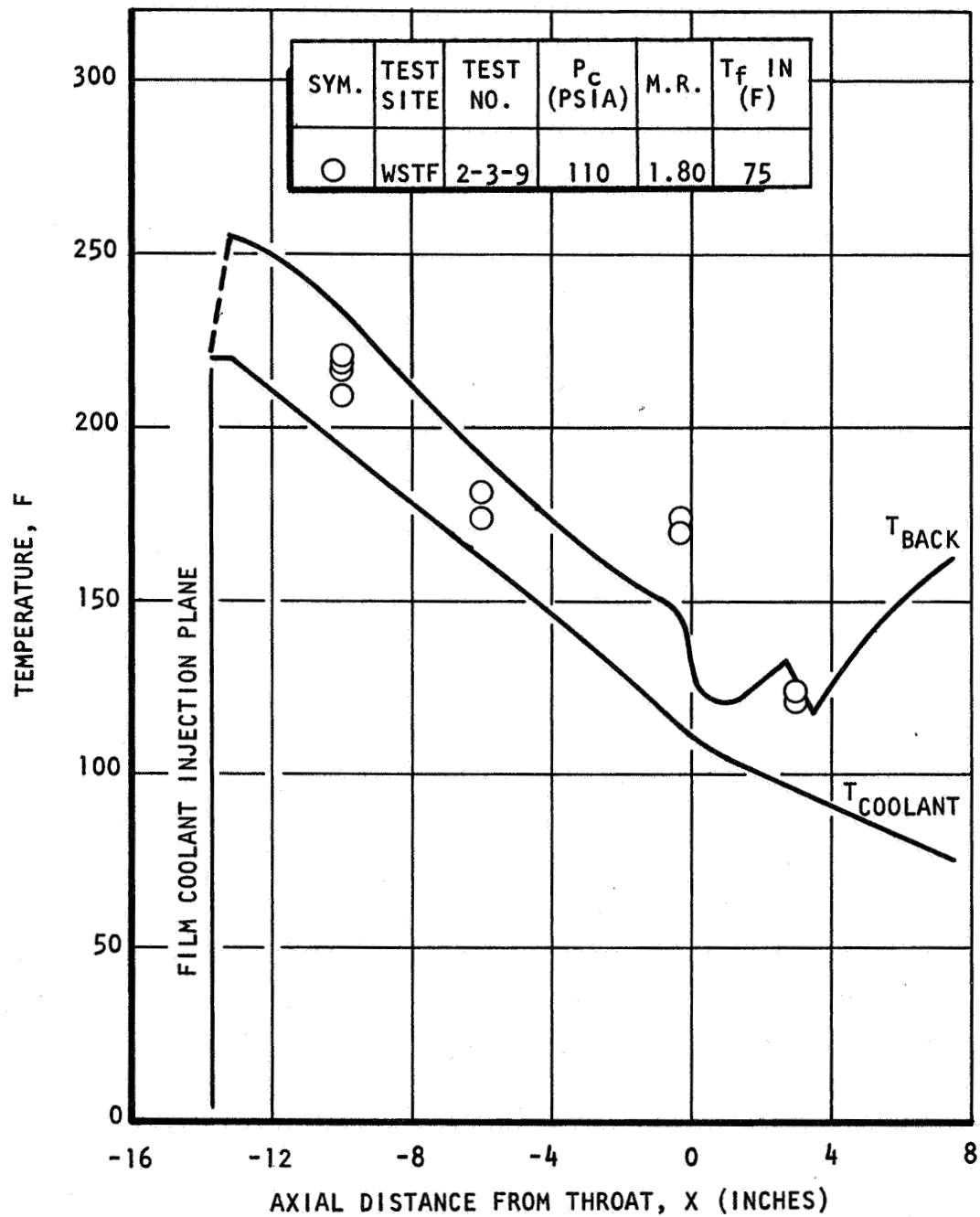Demonstrator (Nominal Conditions)

Figure 78 Back Wall Temperature Profile for the OME
Demonstrator (Off-Design)
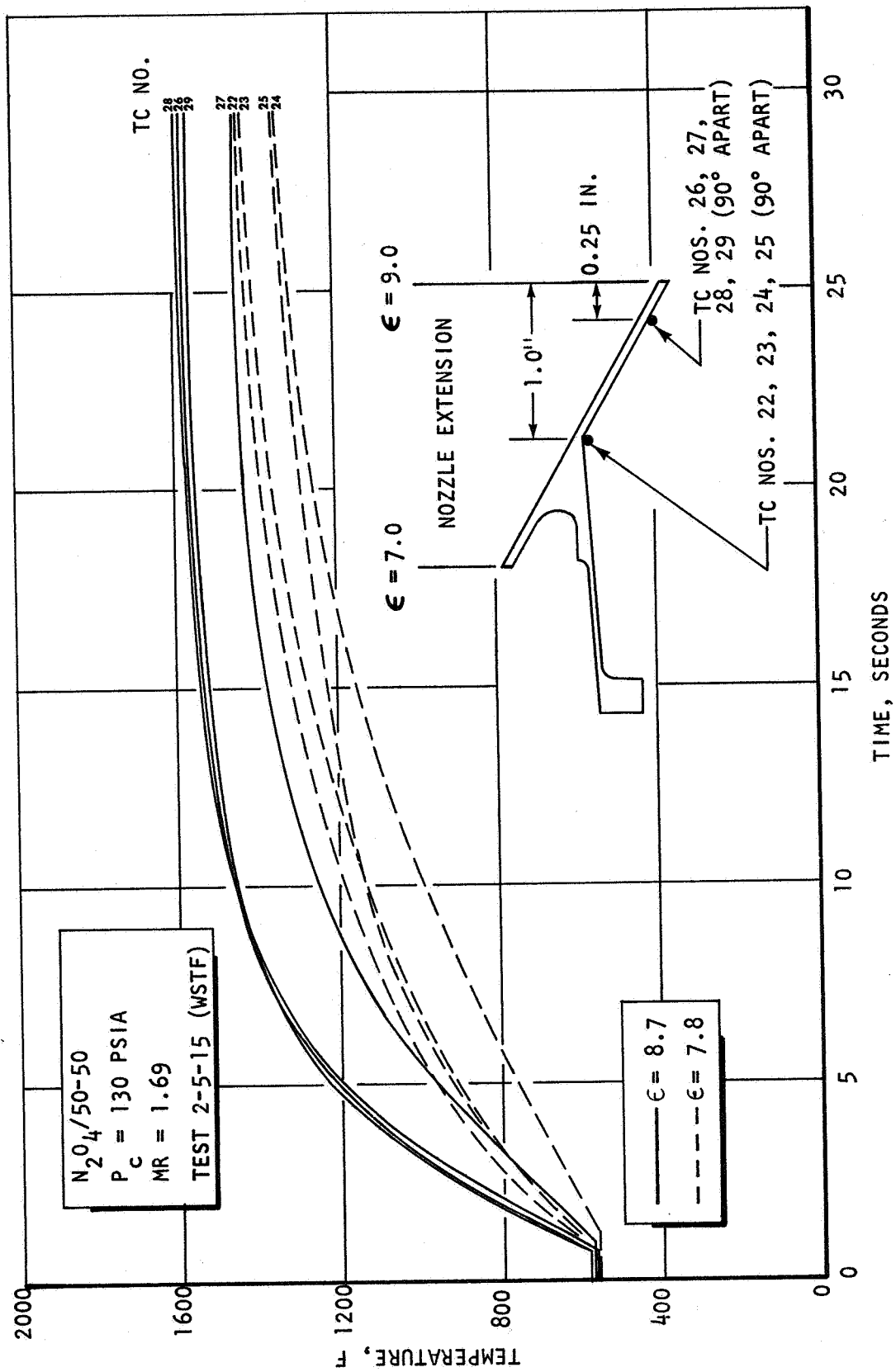
Figure 79 Radiation Cooled Nozzle Temperature Transients

A comparison of nozzle transient temperatures for MMH and 50-50 tests at shorter times (∿10 seconds) indicate lower nozzle temperatures with NTO/MMH propellants. The higher nozzle temperatures at CTL IV may be due to facility blowback and/or possible nozzle flow separation.

The predicted nozzle temperature of about 2200-2300 F for the short extension is considerably higher than the experimental values. It appears that film cooling carryover downstream of the throat results in significant reduction of the radiation nozzle temperature. This is an important result since it permits the use of a more conventional nozzle extension material with possibly significant cost savings.

Coolant Jacket ΔP

The regenerative jacket pressure drop versus flowrate is shown in Fig.80. Inlet and outlet pressures were measured at the same locations in the manifolds of both facilities, and were therefore comparable with the predicted pressure drop which did not include manifold losses. The pressure drops for the regeneratively cooled tests at CTL-IV are seen to be approximately 1-2 psi below the predicted values, while data taken at WSTF was approximately 1-2 psi above the predicted value.

Pressure drops were also calculated by subtracting the fuel injection pressure from the regenerative coolant jacket inlet pressure. This ΔP includes the jacket exit manifold and crossover passage pressure drops. A much better consistency between these data from the two facilities was obtained implying that a discrepancy exists between the coolant jacket exit pressures. The ΔP from the coolant jacket exit to the fuel injector was examined and found to be low (generally <2 psi) and sometimes negative based on WSTF data compared to 3-6 psi based on CTL-IV data. The CTL IV data therefore appears more credible. However, at each facility, the ΔP values were obtained by subtracting absolute pressure measurements (∿200 psia) so that such variations are within instrumentation accuracies. More precise pressure drop data should be obtained by using a differential pressure transducer or by low pressure flow calibration tests.

Figure 80   Coolant Jacket Pressure Drops

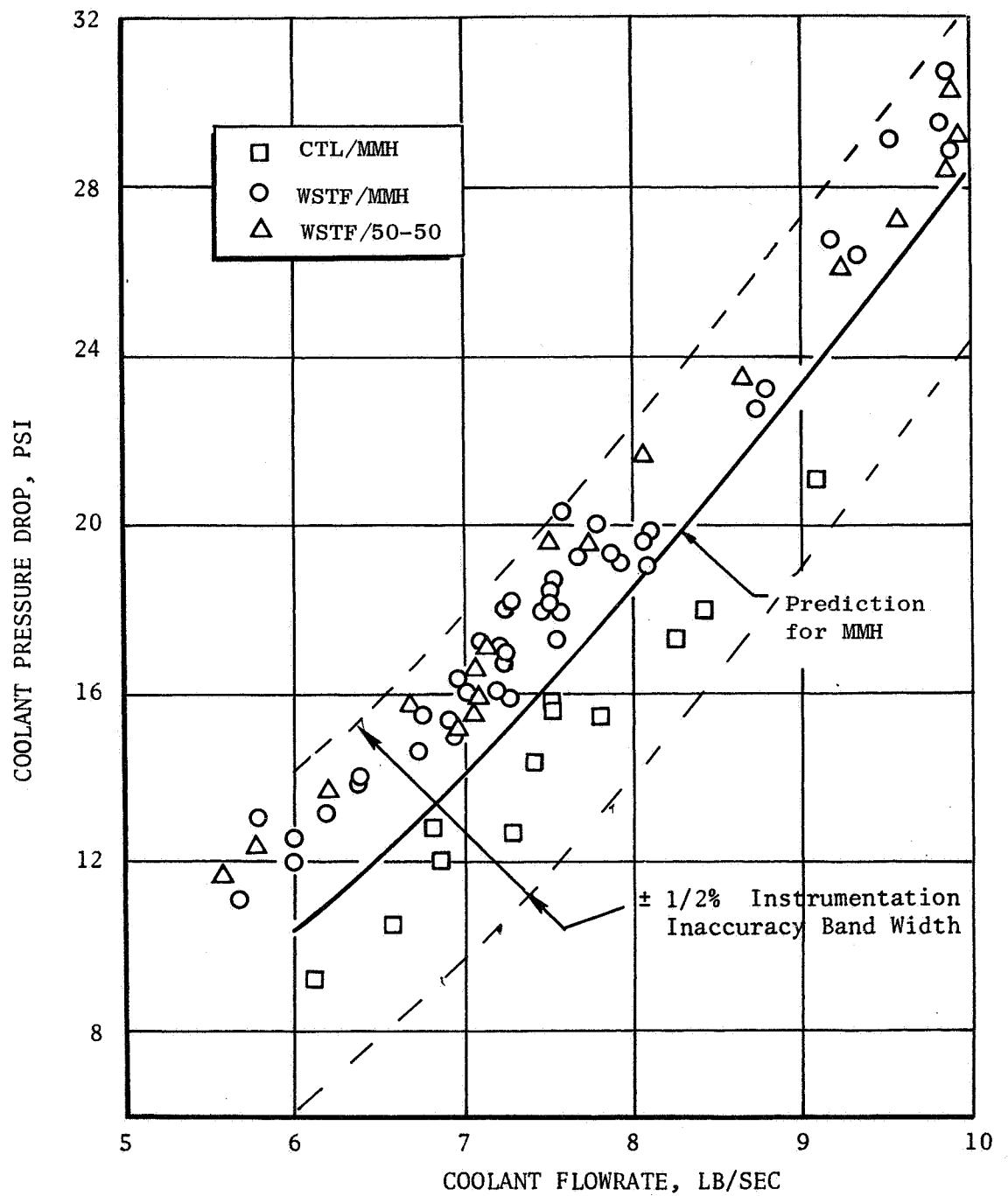# 6.0 INTEGRATED THRUST CHAMBER

6.1 DESIGN DESCRIPTION

The demonstration chamber discussed previously was utilized to investigate effects of film and regenerative coolant flowrates and as such incorporated a separate film coolant injection ring and primary injector distribution manifold. The results of the demonstrator chamber tests were utilized to aid in designing a nearly flight type OME chamber in terms of the head end configuration. In this chamber the acoustic cavity dams are integral with the chamber and are regeneratively cooled. The coolant channels feed directly into the injector and no separate fuel injection manifold is required. This design configuration is referred to as the integrated thrust chamber (ITC) to differentiate it from the demonstration chamber.

The basic design characteristics of the ITC are summarized in Table 30. The internal contour of the ITC is essentially the same as the demonstrator in terms of injector-to-throat length (14.7 inches) and contraction ratio (2:1) based on the selection criteria discussed previously. The inlet manifold and nozzle attachment are identical to the demonstrator configuration. The primary differences between the two chambers are: 1) head-end configuration, 2) film coolant injection technique, and 3) coolant channel geometry.

Head-End Configuration

The head-end configuration of the ITC is depicted in Fig.81 for the various dual-mode acoustic cavity arrangements. The basic flight (welded) configuration is also shown for comparison purposes. It is apparent that the only difference between the flight version and the ITC is the bolt flange to facilitate testing. The ITC could be readily converted to a flight configuration by machining off the flange and welding the injector directly to the chamber.

The acoustic cavities are integral with the chamber and regeneratively cooled (along with the dams) as shown in Fig.81 . The use of regeneratively cooled cavities and dams essentially eliminate the overheating problems incurred during the demonstrator tests wherein the cavity regions downstream of the injector were convectively cooled with the film coolant before injection. (This section of the acoustic cavities were part of the separate film coolant ring utilized in the demonstrator tests).

The regenerative coolant from each channel is fed directly into the injector. The chamber, therefore, acts as an injector distribution manifold. This simplifies the injector design and reduces the overall coolant pressure drop.

TABLE 30

INTEGRATED THRUST CHAMBER ASSEMBLY CHARACTERISTICS

INJECTOR

    MATERIAL   321 CRES
    PATTERN   MULTI-ELEMENT LIKE-DOUBLET
    DIAMETER   8.1 INCH
    STABILITY AIDE   MULTI MODE ACOUSTIC CAVITY
                                       IT   - 8 CAVITIES 0.5 WIDE X 1.15 DEEP
                                       IR,3T - 4 CAVITIES 0.5 WIDE X 0.42 DEEP

COMBUSTOR

    MATERIAL   321 CRES HOT WALL, ELFNI CLOSEOUT
    CONTRACTION RATIO   2:1
    LENGTH   14.7 INCH
    CONTOUR   TAPERED FROM 7 INCH UPSTREAM OF THROAT

NOZZLE

    REGEN SECTION MATERIAL   321 CRES HOT WALL, ELFNI CLOSEOUT
    REGEN SECTION EXPANSION RATIO   TO 7:1
    NOZZLE EXTENSION MATERIAL   SILICIDE COATED COLUMBIUM
    NOZZLE EXTENSION EXPANSION RATIO 7:1 to 9:1
    CONTOUR   70 PERCENT BELL

COOLANT

    CIRCUIT   UP-PASS
    NUMBER OF COOLANT CHANNELS   120
    COOLANT PRESSURE DROP   16 PSID
    COOLANT BULK TEMPERATURE RISE   178 F (ANALYTICAL PREDICTION)
    AUXILIARY FILM COOLANT   2 PERCENT TOTAL PROPELLANT
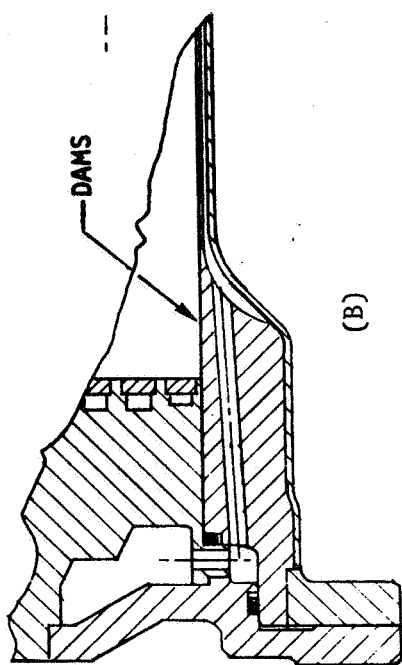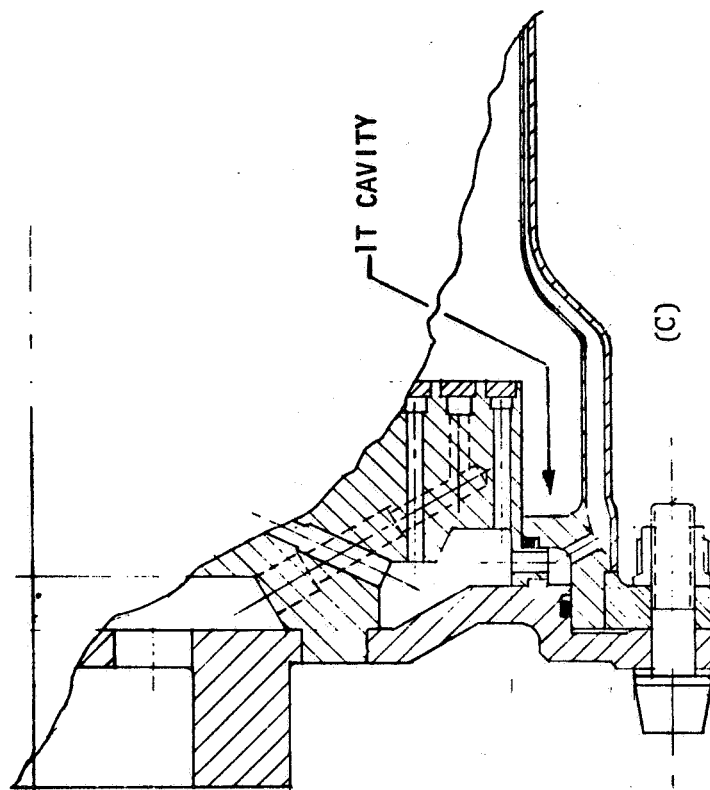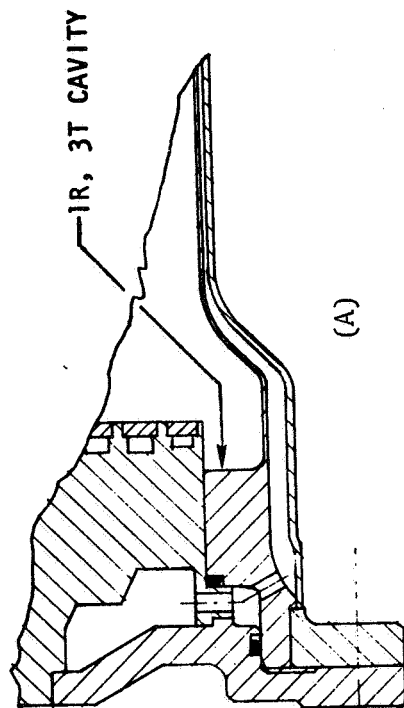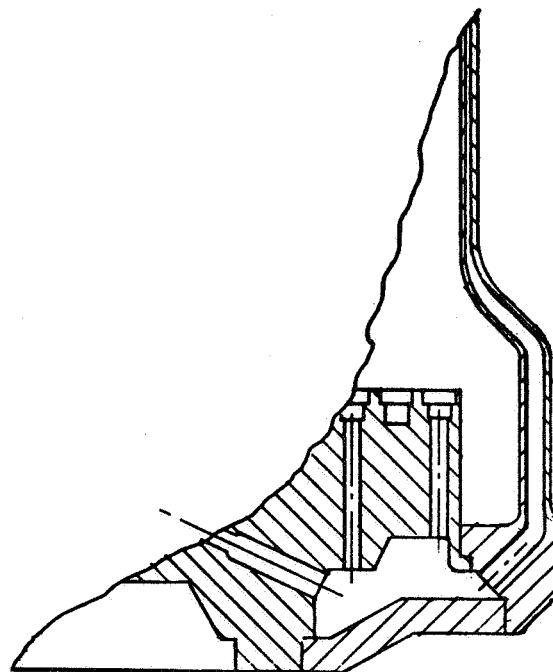
Figure 81. Injector/Thrust Chamber Interface Comparison

Film Coolant Injection Technique

Various film coolant injection techniques were considered for the ITC as shown in Table 33. The reduced heat loads encountered in the demonstrator tests made it feasible to consider the simpler, though potentially less efficient, technique of injecting the film coolant from the primary injector across the acoustic cavities onto the wall.

Based on a nominal fuel film coolant flowrate of 2.3 percent of total propellant flow, as determined from demonstrator tests, a minimum injection orifice diameter of 0.020 inches (to prevent possible plugging) and a fuel ΔP = 45 psi, the required number of injection orifices was determined to be sixty.

Channel Geometry

A more detailed channel geometry optimization was performed for the ITC in an attempt to reduce the required number of coolant channels. A reduction in number of channels is desirable from a cost standpoint and to make the chamber design more compatible with the reduced number of film coolant injection orifices.

Coolant channel design is strongly dependent on local heat flux level and specified safety factor. The selected heat flux profile was that utilized in the design of the demonstrator chamber (Fig.48). Although the demonstrator experimental heat loads were about 20-25 percent lower than predicted it was felt that the potentially less efficient film coolant injection technique utilized in the ITC could offset this gain.

The safety factor ground rule used in the ITC design was a minimum value of 1.5 (ratio of MMH burnout capability to local imposed heat flux level) at extreme off-design conditions. The off-design conditions were a chamber pressure of 120 psia, mixture ratio = 1.84 and a propellant inlet temperature of 100°F. The rationale leading to these off-design conditions is summarized in Table 32.

The effect of number of channels on channel geometry for a constant channel width design is presented in Fig.82. The maximum channel width and injector end land width parameters are purely geometric and dependent on minimum throat land width as well as number of channels. The minimum channel height results from consideration of 2-D conduction effects in conjunction with heat flux level and desired safety factor. It is apparent that decreasing the number of channels results in increased channel width and injector-end land width. The increased land width at the injector end results in a 2-D conduction penalty with resultant increased velocity and reduced channel height.

TABLE 31

AUXILIARY FILM COOLANT DESIGN OPTIONS

INJECT FROM CHAMBER - OME DEMONSTRATION CHAMBER TECHNIQUE (TASK V TESTS)

    ADVANTAGE - HIGH COOLING EFFICIENCY

    DISADVANTAGE - COMPLEX CHAMBER DESIGN

INJECT FROM INJECTOR - OME INTEGRATED CHAMBER TECHNIQUE (TASK XII TESTS)

    ADVANTAGE - SIMPLE DESIGN

    DISADVANTAGE - POTENTIALLY LOWER COOLING EFFECTIVENESS
        (JUMP ACOUSTIC CAVITY)

        - FEWER INJECTION ORIFICES (0.020 MINIMUM
          DIAMETER, 45 PSID ΔP)

INJECT FROM CAVITY DAMS

    ADVANTAGE - SIMPLE DESIGN, LARGER AND FEWER INJECTION HOLES

    DISADVANTAGE - REQUIRES COLD FLOW INVESTIGATION TO DEFINE
        FLOW PARAMETERS PRIOR TO INCORPORATION
        INTO CHAMBER

NO FILM COOLANT - OME DEMONSTRATION CHAMBER TESTS (TASK VIII TESTS)

    ADVANTAGE - SIMPLEST DESIGN, MAXIMUM PERFORMANCE

    DISADVANTAGE - HIGHER INLET PRESSURE REQUIRED

TABLE 32

OME CHAMBER CONDITIONS FOR MINIMUM SAFETY FACTOR

(SERIES TANK FEED SEPARATE REGULATORS)

● INLET CONDITIONS:

FUEL TEMPERATURE	100F
OXIDIZER TEMPERATURE	90F
FUEL PRESSURE*	198 PSIA
OXIDIZER PRESSURE*	211 PSIA

* RESULTING FROM: SERIES FEED
PRIMARY OXIDIZER PRES. REG. FAILURE
FUEL PRES. CHECK VALVE FAILURE

● ENGINE CONDITIONS:

+2 PERCENT O/F CALIBRATION TOLERANCE

-1 PSIA P_C CALIBRATION DEVIATION, NO VALVE FAILURE
(INCREASE SAFETY FACTOR)

● RESULTING OPERATING CONDITIONS:

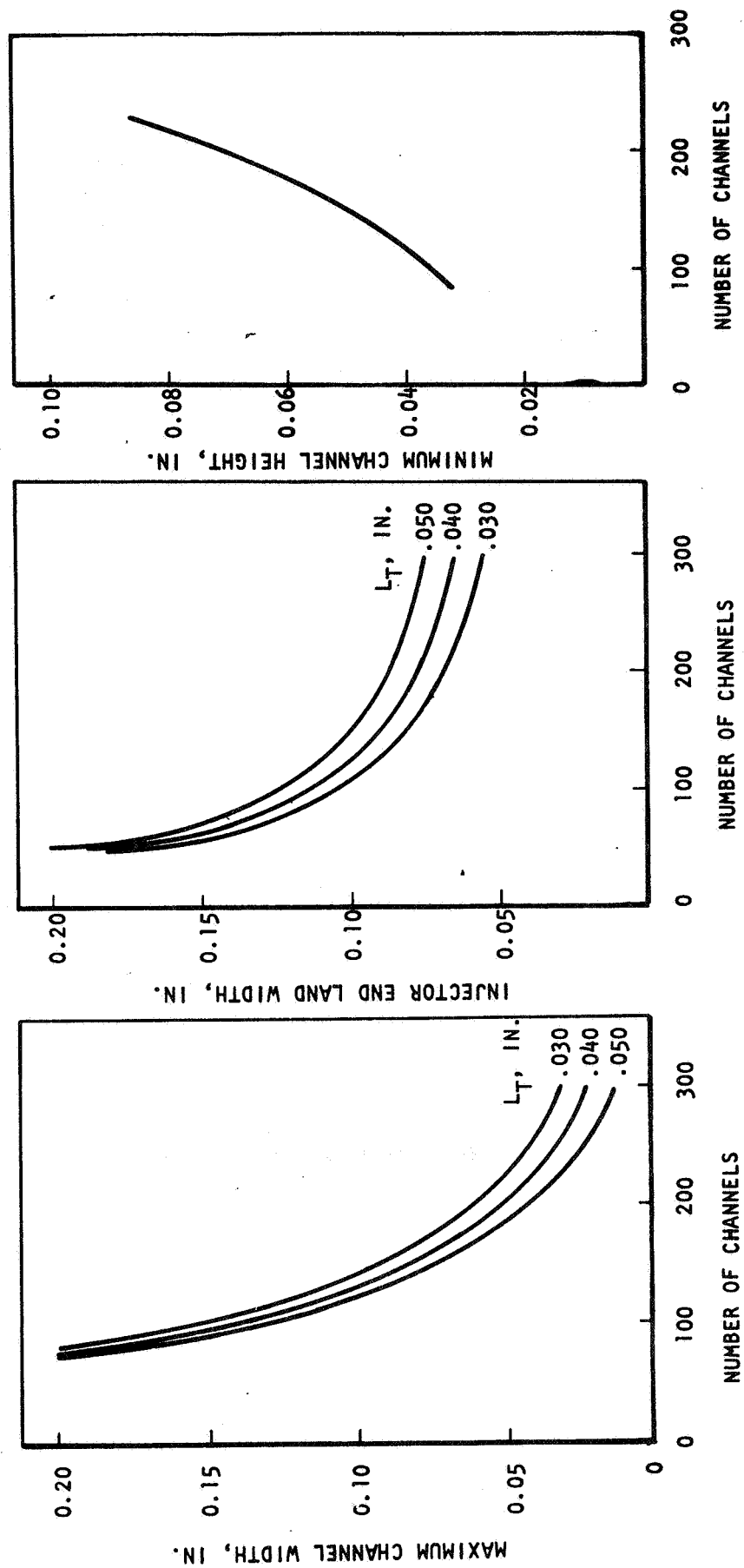|	
THRUST, LB	5860
CHAMBER PRESSURE, PSIA	120
MIXTURE RATIO, O/F	1.84
SAFETY FACTOR	1.5

Figure 82. Effect of Number of Channels On Channel Geometry

The effect of number of channels on chamber pressure drop and weight are presented in Fig.83. Fewer channels result in increased pressure due to higher velocity requirement as discussed previously. A very large number of channels (>200) also tends to increase pressure drop due to the hydraulic diameter effect of small channels. Increased number of channels also increases weight due to the increased channel (and land) heights. Converting pressure drop to equivalent OMS weight indicates an acceptable range of about 110 to 220 channels for a 10 lb equivalent weight penalty.

The selected number of channels for the ITC was 120. The final selection was based on consideration of the number of film coolant injection orifices. The use of 120 coolant channels in conjunction with the 60 film coolant orifices provides for symmetrical coverage of the coolant channels.

ITC Thermal Design Results

The predicted ITC operating temperature profiles at nominal conditions is presented in Fig. 84. The maximum gas-side wall temperature is less than 800^oF.

The ITC predicted coolant safety factor profiles at nominal and off-design conditions are presented in Fig.85 for both 1-D and 2-D thermal conduction analysis assumptions. In the nozzle region the safety factor is considerably in excess of the minimum specified. This is due to a minimization of nozzle channel height to reduce weight. (There is a negligible pressure drop penalty in the nozzle region due to low heat flux levels). This high nozzle safety factor should be sufficient to permit sea level tests with nozzle flow separation.

Thermal transients, including space chilldown and chamber soakout conditions, are essentially the same for the ITC as discussed previously for the demonstrator chamber.

Performance sensitivity studies of the ITC were conducted as discussed in the demonstrator section of the report. The results are essentially the same and were summarized in Fig. 57.

ITC Fatigue Life and Strength

The fatigue life of the ITC was determined using the techniques discussed previously. The hot-wall thickness and operating temperatures of the ITC are essentially the same as the demonstrator. Recent data on the strength of as-deposited electroformed nickel, however, indicate much higher nickel strength than originally supposed. This higher

Figure 83. Effect of Number of Channels On Weight
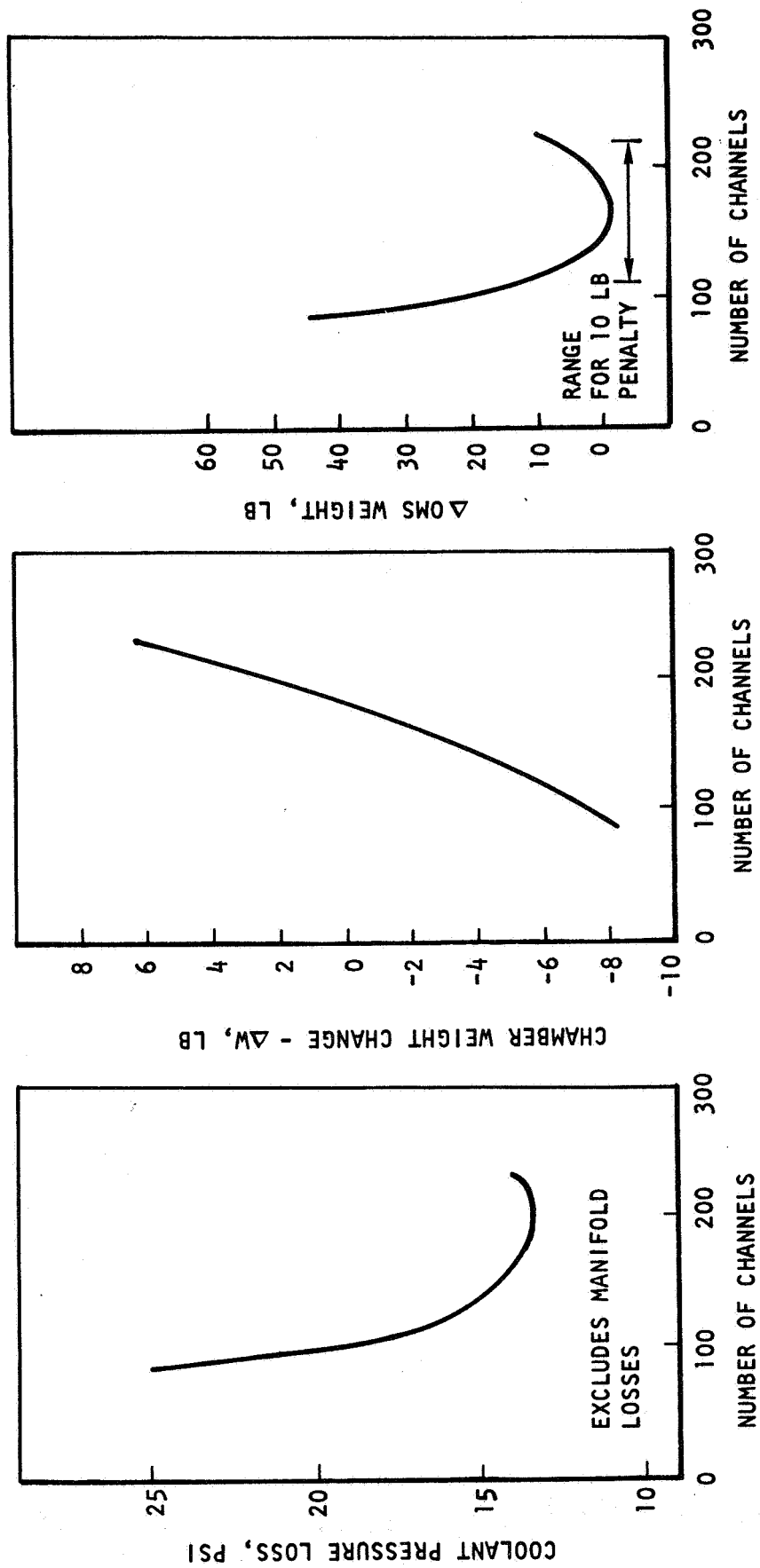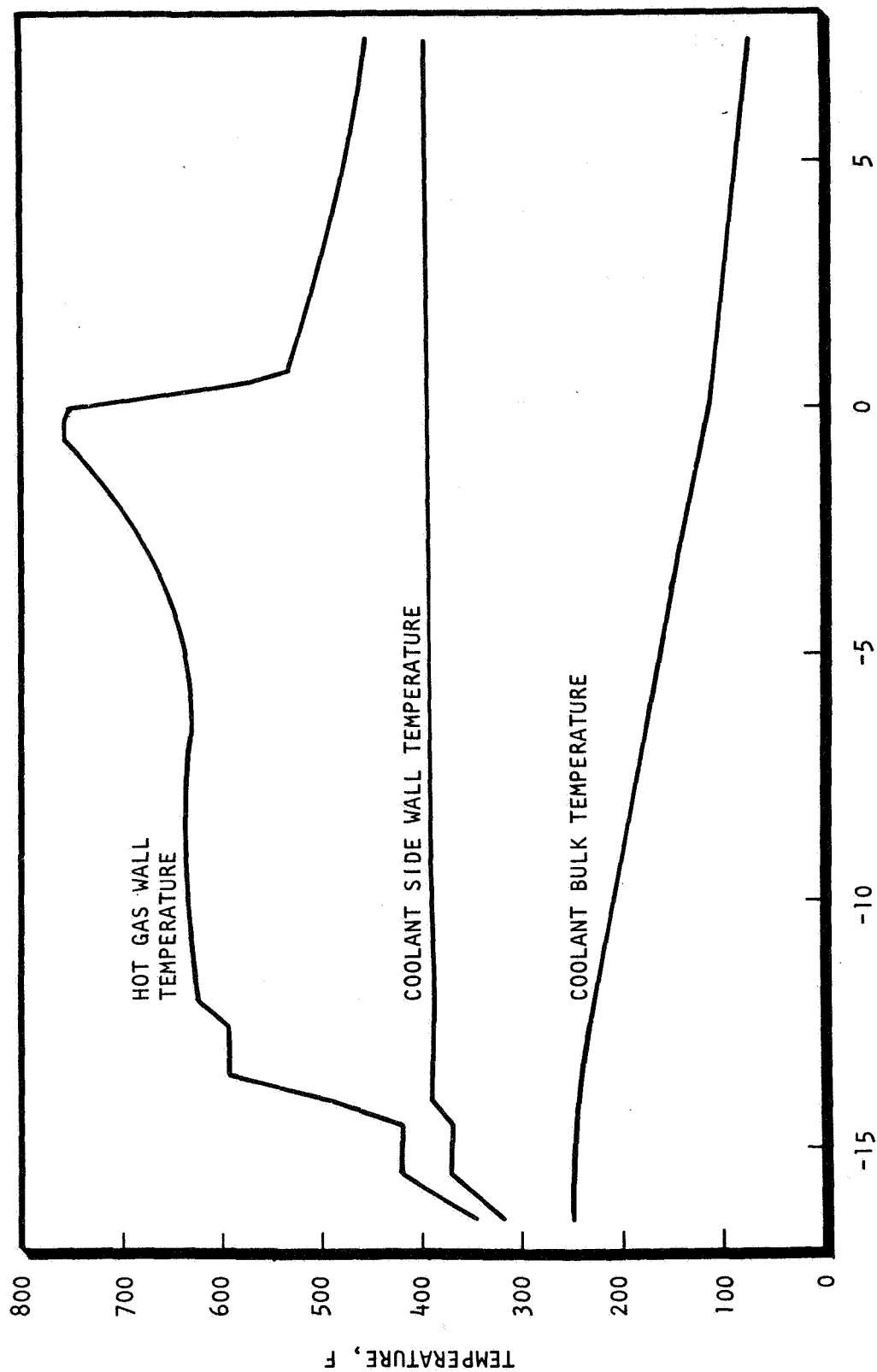
CHAMBER TEMPERATURE PROFILES

HOT GAS WALL
TEMPERATURE

COOLANT SIDE WALL TEMPERATURE

COOLANT BULK TEMPERATURE

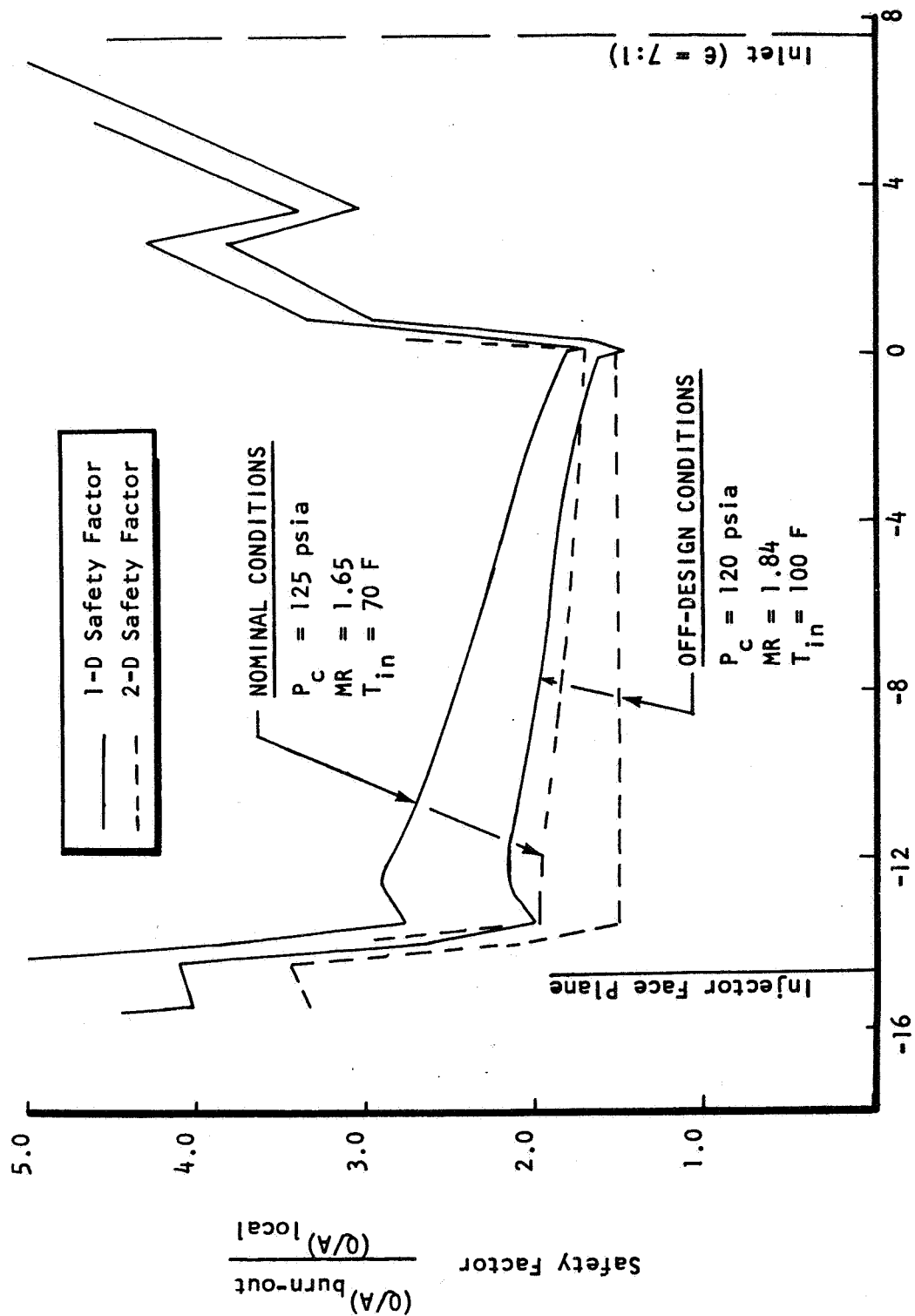Fig. 84 AXIAL DISTANCE FROM THROAT, INCHES

TEMPERATURE, F

Figure 85. OME Chamber Safety Factor Profile

R-9686

6-11

strength results in less yielding of the nickel and a greater load imposed on the CRES hot wall with resultant fatigue life reduction. To off-set the higher nickel strength somewhat, the nickel closeout thickness at the throat was reduced to 0.025 inch. The predicted minimum fatigue life for the ITC is about 5000 cycles (1250 cycles with safety factor of 4) which is still in excess of that required. The ITC fatigue life profile is shown in Fig. 86. The ITC fatigue life could be increased substantially by annealing the nickel.

The nickel strength curve is presented in Fig. 87 where it is seen that the design hoop stress safety factor is about 6.8 based on yield and about 10 based on nickel ultimate strength.

6.2 THRUST CHAMBER FABRICATION

The fabrication of the ITC is essentially the same as that shown for the demonstrator chamber. The single major difference is the electric discharge machining of the acoustic cavities in the head-end of the ITC. The resulting head-end geometry of the ITC is shown in Fig. 88.

6.3 INTEGRATED THRUST CHAMBER TEST PROGRAMS - PHASE I

The integrated thrust chamber shown in Fig. 89 was tested in two phases at White Sands Test Facility. (See Appendix A for facility description). Phase I tests were concerned primarily with the steady-state stability, thermal, and performance characteristics of the ITC with additional limited tests to determine transient characteristics. The results were reported in NASA-CR-134256 and NASA-CR-140250.

A total of 40 tests were conducted during Phase I on the integrated thrust chamber with the like-doublet No. 1 injector and 72:1 area ratio heat sink/radiation nozzle. The total duration accumulated during these tests was 445 seconds. A test summary is presented in Table 33.

The tests were broken down into groups of tests called test sequences, having specific detailed objectives. The first sequence consisted of three tests of increasing duration and mixture ratio. The objective of this first test series was to check out the engine facility and instrumentation. The objective of the second test series was to determine the engine operating characteristics with ambient temperature unsaturated propellants. A relatively long oxidizer lead was used for these ten tests.
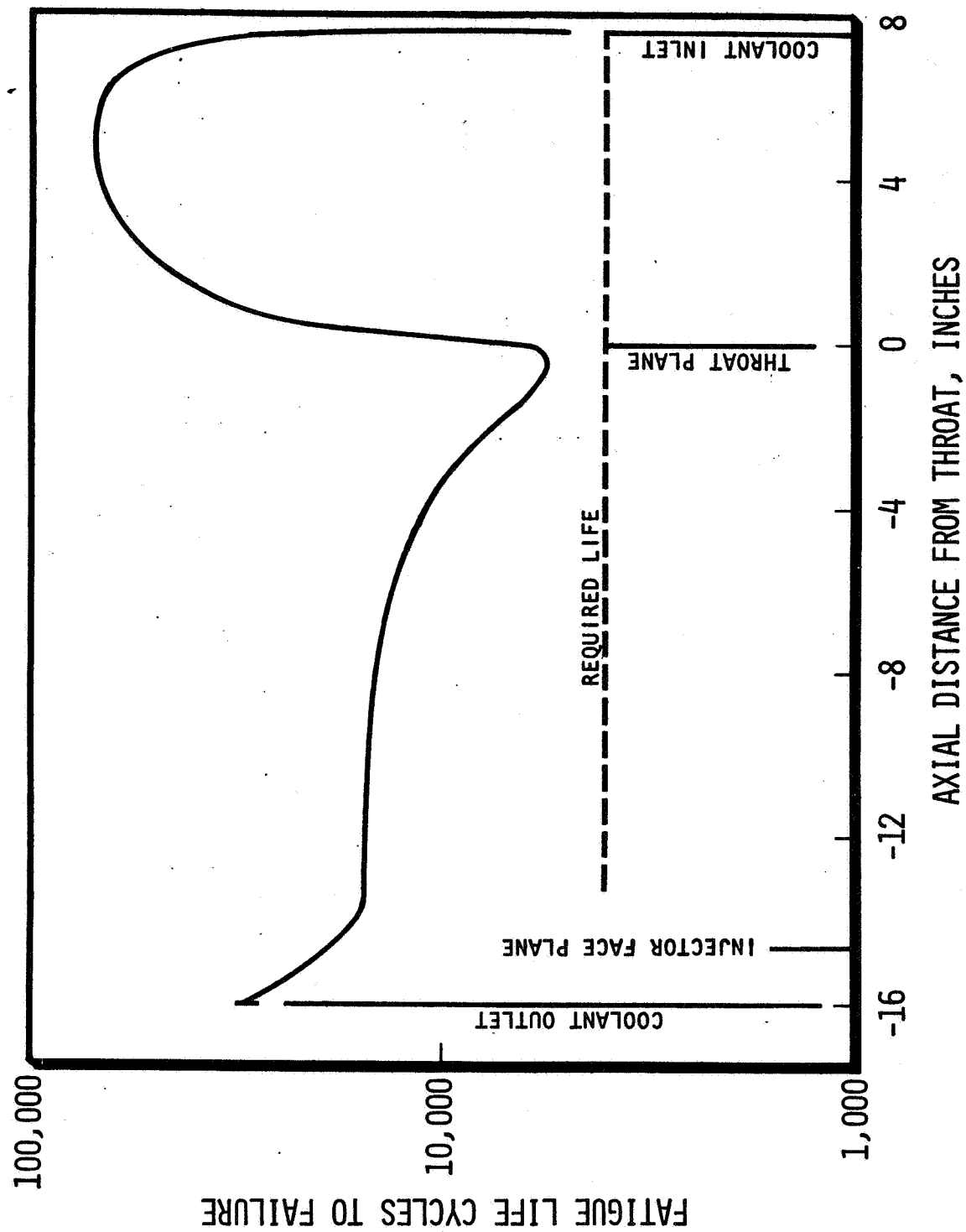
Figure 86. Chamber Cycle Life Capability

MATERIAL PROPERTIES FOR AS-DEPOSITED ELECTROFORMED NICKEL
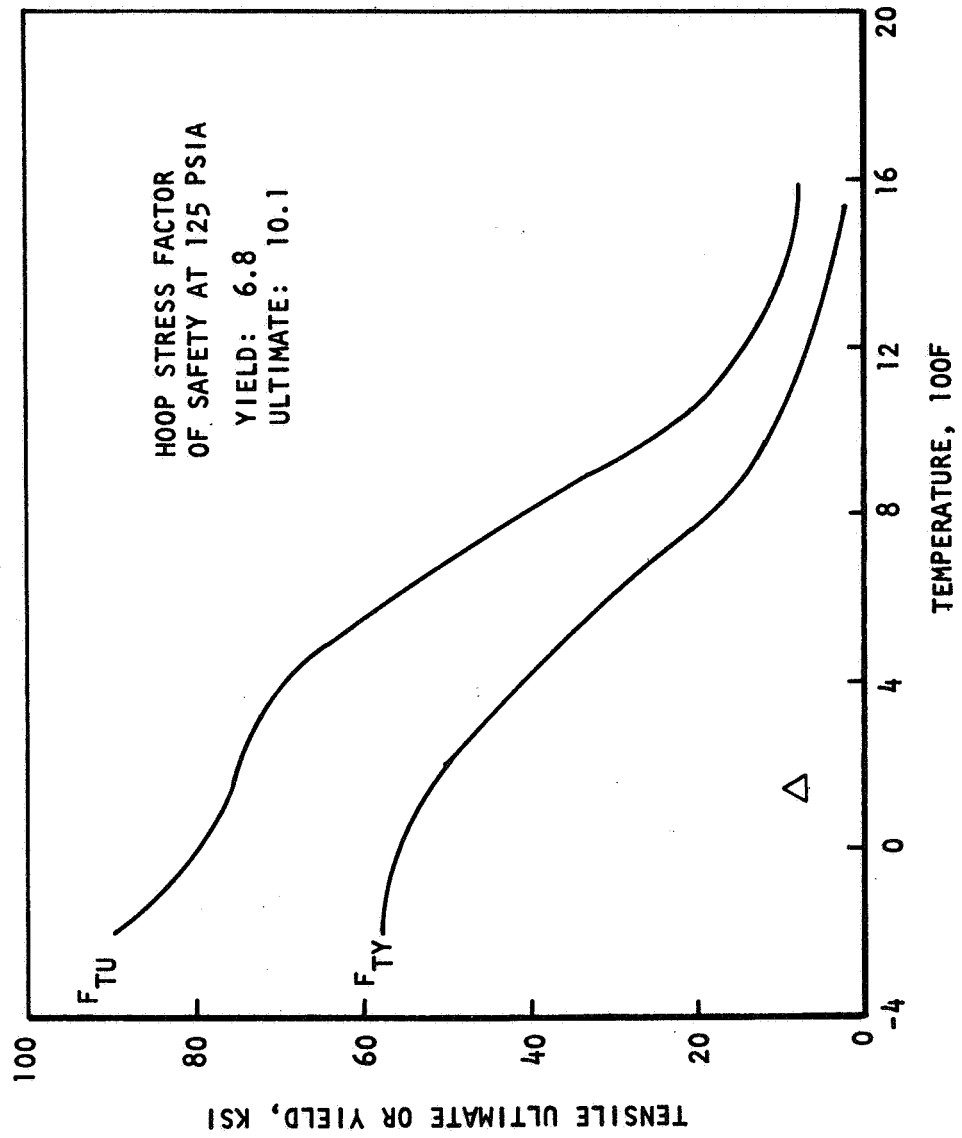
Fig. 87
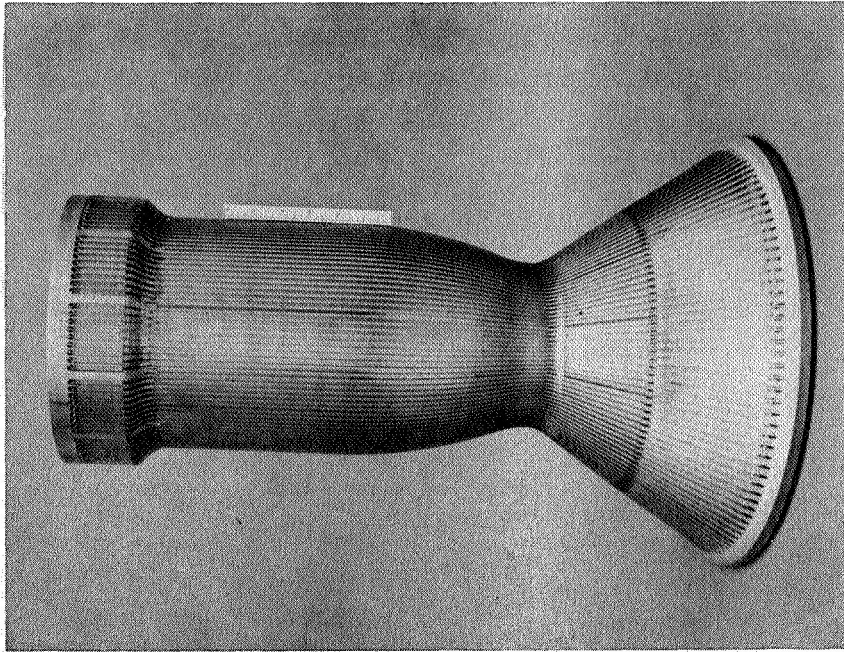
Figure 88. Slotted Liner Prior to Electroform
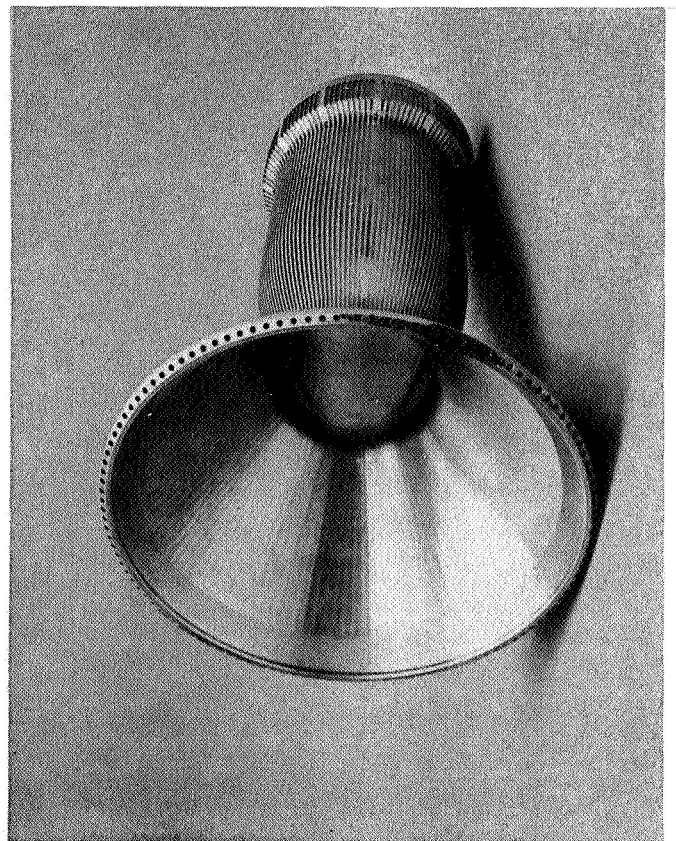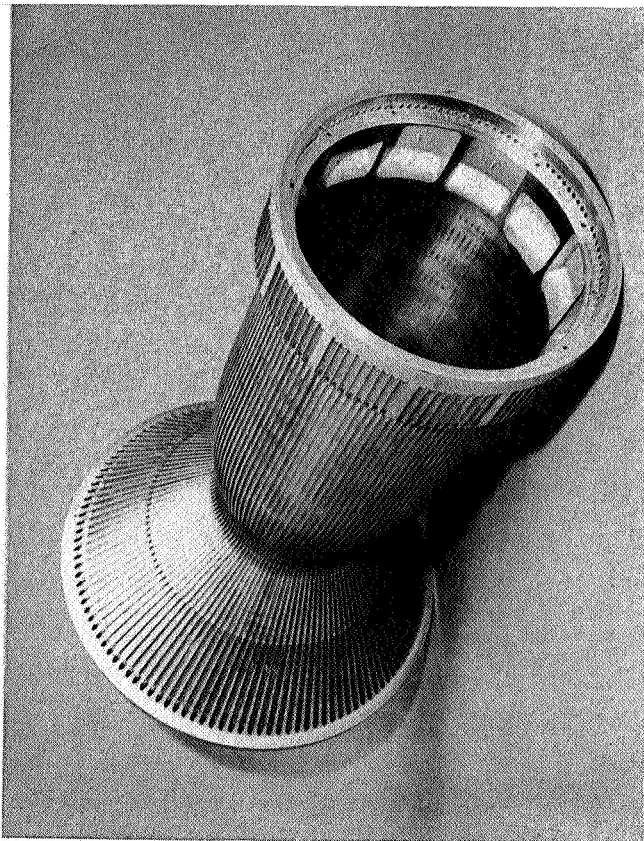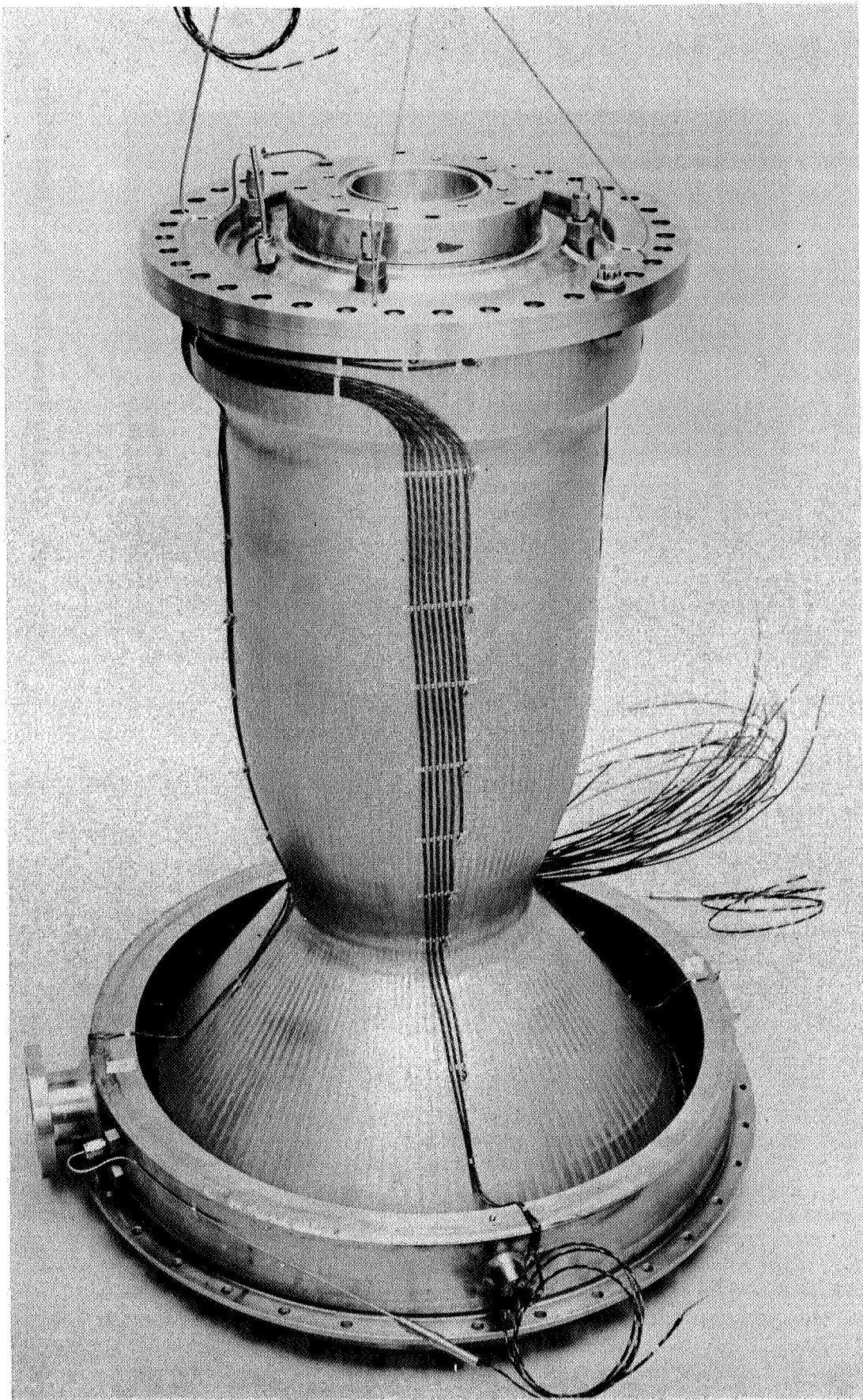
Figure 89. Regeneratively Cooled Thrust Chamber

R-9686

TABLE 33 INTEGRATED THRUST CHAMBER PHASE I TEST SUMMARY

TEST	NOM DUR SEC	$P_{C_{NS}}$ PSIA	O/F
Checkout			
1-1	3	117	1.372
1-2	5	117	1.464
1-3	10	116	1.465
Unsaturated Propellants			
2-1	10	124	1.667
2-2	10	126	1.858
2-3	10	141	1.466
2-4	10	142	1.656
2-5	10	142	1.844
2-6	10	111	1.485
2-7	10	112	1.670
2-8	10	112	1.871
2-9	10	126	1.470
2-10	10	126	1.671
Saturated Propellants			
3-1	10	125	1.657
3-2	10	124	1.865
3-3	10	140	1.452
3-4	10	139	1.652
3-5	10	140	1.843
3-6	10	109	1.439
3-7	10	110	1.682
3-8	10	109	1.864
3-9	10	125	1.460
3-10*	10	126	1.654

*Followed by 30 minute vacuum soak

R-9686

TABLE 3.3 INTEGRATED THRUST CHAMBER PHASE I TEST SUMMARY (Cont'd)

TEST	NOM DUR SEC	$P_{C_{NS}}$ PSIA	O/F
Hot (100F) Propellants			
4-1	30	122	1.658
4-2	10	138	1.449
4-3	10	138	1.643
4-4	10	137	1.874
4-5	10	109	1.438
4-6	10	110	1.595
4-7	10	109	1.855
4-8	10	124	1.457
4-9	10	124	1.846
4-10*	10	126	1.649
Thrust Limits			
5-1	44	124	1.658
5-2	33	149	1.650
5-3	40	100	1.667
5-4*	10	125	1.664

*Followed by 30 minute vacuum soak

Sequence 3 consisted of ten tests conducted with ambient temperature propellants saturated with helium at 225 psia. A 30-minute vacuum soak was conducted after the last test in this series. Sequence 4 was conducted with unsaturated propellants heated to 100F. A vacuum soak was again accomplished after the last of the ten tests in this sequence. The fifth and final sequence consisted of four tests with unsaturated ambient temperature propellants. The highest and lowest anticipated thrust levels were tested during this sequence. A vacuum soak was accomplished after the first test of this sequence. The test conditions are summarized in Table 33. A total of 40 starts and 445 seconds duration were accumulated.

The test program was conducted without any major difficulties. Minor difficulties arose during the second test series, when the extended oxidizer lead programmed on that series resulted in triggering a safety device which shut the engine down for failure to establish full chamber pressure within specified time increment. The time increment was reset commensurate with the valve lead and testing proceeded. Also during the fifth test sequence, failure to reset the low-chamber-pressure safety device resulted in a premature shutdown on the test programmed for a low-chamber pressure. Again, the device was reset and testing proceeded. All steady state data appeared to be valid. However, the engine ports for measuring the fuel and oxidizer injection pressures were undersized so that the transient data obtained for these measurements is of limited value.

After the Phase I test program, the thrust chamber and injector were disassembled and inspected and found to be in good condition. The injector was dye penetrant checked to verify the structural integrity of the ring/land welds. The thrust chamber was water flowed and the emerging streams observed to provide a visual estimation of uniformity of flow feed. The flow appeared approximately uniform with a bias of approximately 5 to 10 percent higher flow in the area opposite the coolant inlet manifold. (This agreed with the circumferential variation in coolant outlet temperature observed in hot firing data). The acoustic cavity dams were very slightly eroded at a level corresponding to just downstream of the injector face. Although the chamber was useable without modification, the eroded portions of the dams were machined clean in order to reduce the probability of future erosion and to provide a surface upon which further erosion would be more clearly visible if it occurred during Phase II testing.

Thrust Chamber Performance Characteristics

The thrust chamber performance characteristics and operating parameters were summarized in the NASA-CR-134256 .   The variation of specific impulse with chamber pressure and mixture ratio is shown in Fig.90 for both saturated and unsaturated propellants. Performance peaks at a mixture ratio of approximately 1.8 and increases with chamber pressure.

The data curve from the demonstrator thrust chamber series is also shown in Fig.90 and indicates 1 to 2 seconds lower performance at the higher mixture ratios. This curve represents data taken mostly on ten-second duration tests, and it was concluded in the report summarizing that test program that the performance could be low because of the nonequilibrium temperature conditions in the hardware. In fact, based on the results of a long duration test with the demonstrator thrust chamber, using an alternate fuel, the performance under nominal conditions was predicted to be approximately 310 seconds. The data shown for the demonstrator thrust chamber were based upon analytic extrapolations to ϵ = 72 of data taken with a 9:1 expansion area ratio nozzle. The good agreement affirms the validity of the analytical extrapolations.

A comparison of the performance with saturated and unsaturated propellants (Fig.91) indicates that there is no discernible difference in performance with the propellant in either condition. The saturated propellant tests were conducted with both the fuel and the oxidizer saturated with helium at 225 psia. Performance was only slightly improved by heating propellants to 100F, as indicated in Fig.91. The performance improvement appeared to be greater at the lower mixture ratios and was, at most, one second.

Injector and jacket pressure drops are plotted in Fig.92. The pressure drops were determined by subtracting absolute pressure measurements so that accuracy in the order of 1-2 psi might be expected. Excellent correlation was shown on the oxidizer injector pressure drop clearly defining the difference between data taken with ambient and with 104F oxidizer. The correlation on the fuel side was good, but the data had slightly more scatter probably because of the effects of variations in the fuel temperature rise in the coolant jacket. The effect of hot fuel at the chamber inlet can still be seen clearly. Fuel jacket pressure drop appeared consistent on the first test of each sequence (test 2-1B was actually the third test of the sequence, preceded by two tests of approximately 1/4-second duration), but was erratic thereafter. Oxidizer and fuel pressure drops at nominal conditions were 56 and 61 psi, respectively. Injector pressure drops for both propellants increase by approximately 4 psi when the inlet temperatures are increased to 100F. Coolant jacket pressure drop was 15 psi at nominal conditions with no significant change at 100F inlet temperature. A pressure drop summary for the thrust chamber assembly is shown in Fig.93 .
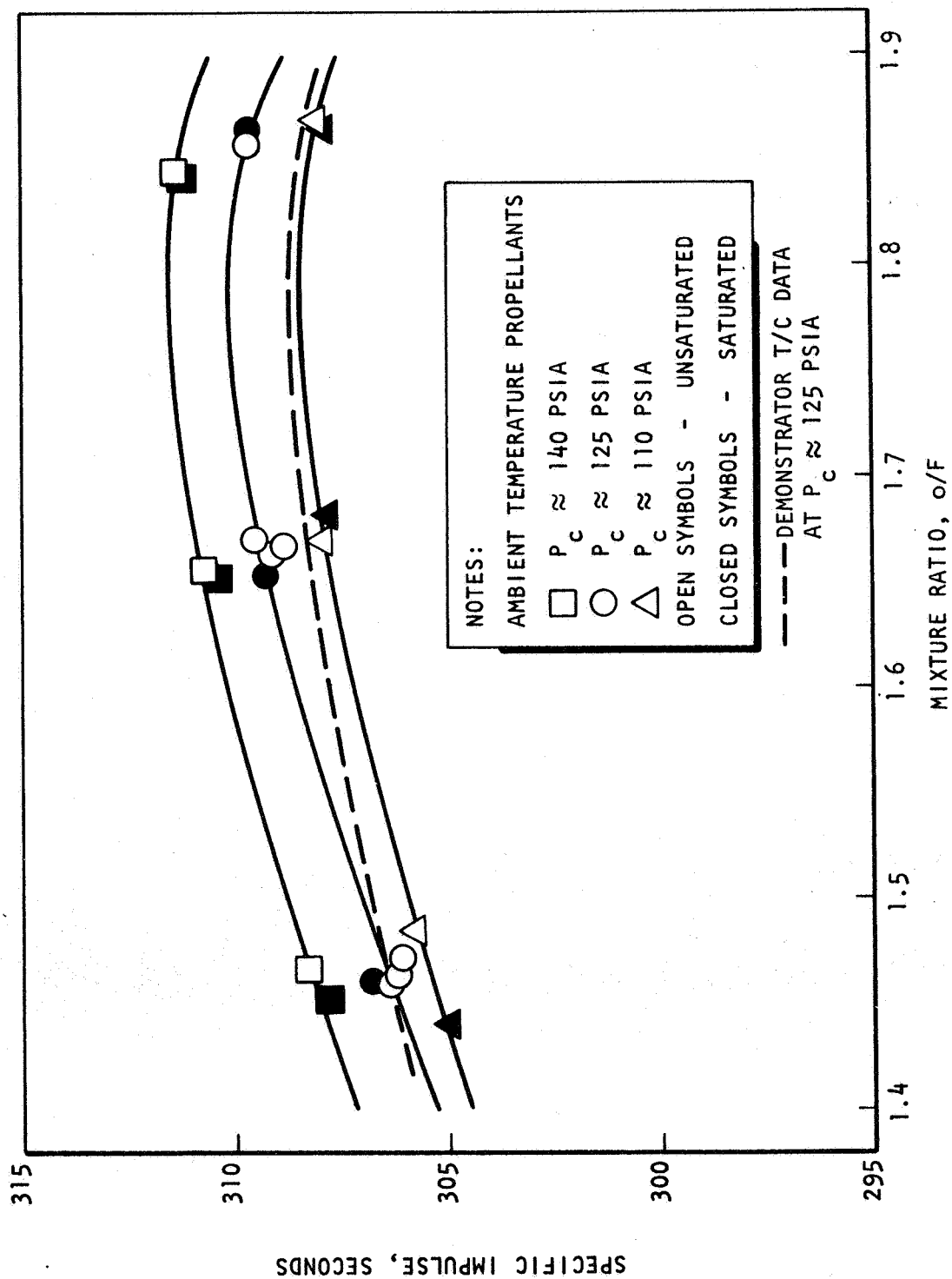
Figure 90. Integrated Chamber Performance With Ambient Temperature Propellants
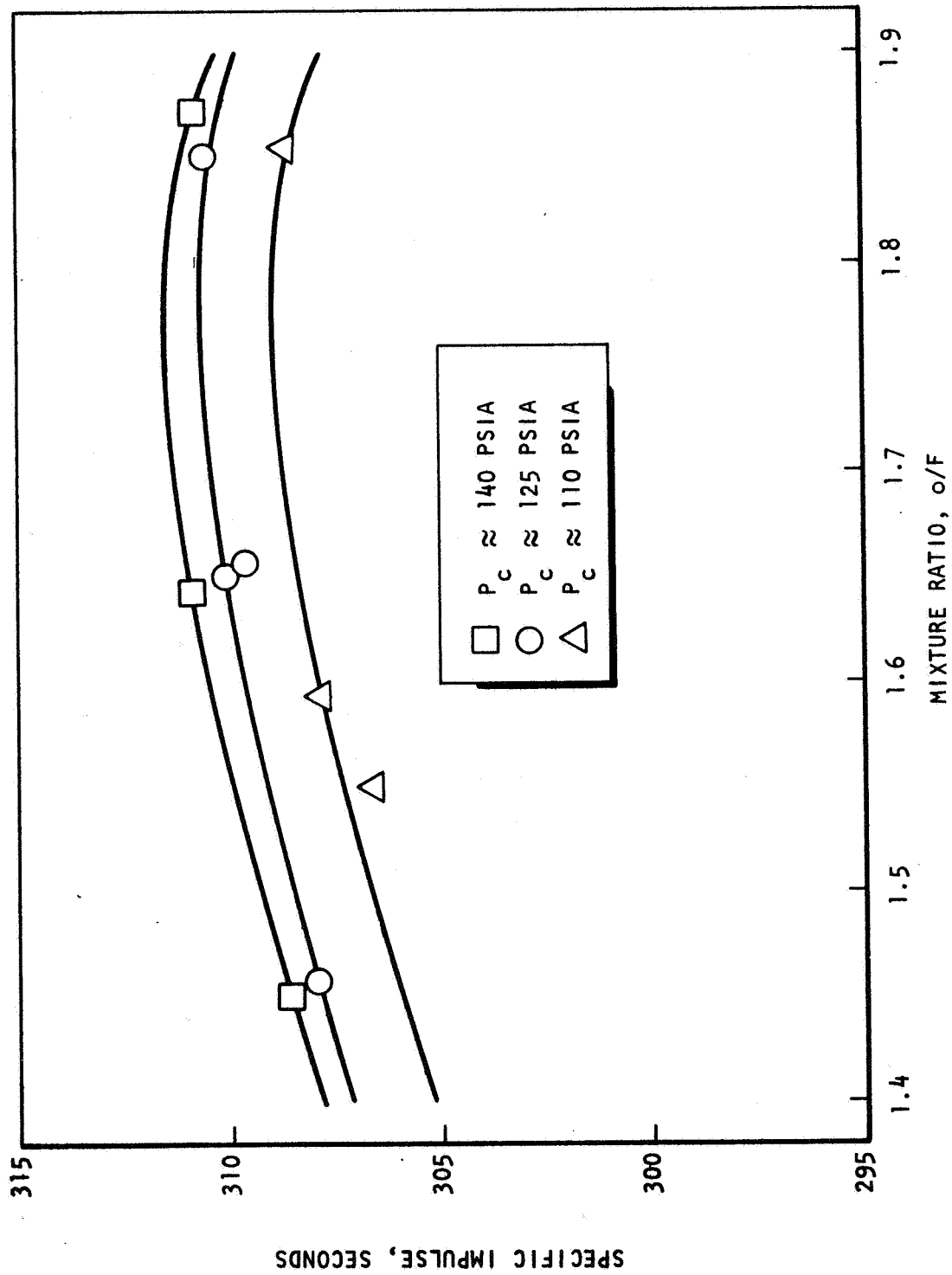
Figure 91   Integrated Chamber Performance With Unsaturated Heated Propellants

Figure 92. Pressure Drop Correlations
R-9686

FUEL
INLET P   208* PSIA

INLET
MANIFOLD ΔP   1 PSI

CHANNEL
ΔP   14 PSI   } TOTAL CHAMBER ΔP = 15 PSI

OUTLET
MANIFOLD ΔP   0 PSI

INJECTOR INLET P   193* PSIA

INJECTOR
MANIFOLD ΔP   1 PSI

INJECTOR
ORIFICE ΔP   60 PSI   } TOTAL INJECTOR ΔP = 61 PSI

OXIDIZER
INLET P   188* PSI

INJECTOR
MANIFOLD ΔP   4 PSI

INJECTOR
ORIFICE ΔP   55 PSI   } TOTAL INJECTOR ΔP = 56 PSI

INJECTOR END P = 132* PSIA

COMBUSTOR ΔP   7 PSI

NOZZLE STAGNATION P = 125 PSIA

* MEASURED PRESSURES

Figure 93   Integrated Thrust Chamber Assembly Pressure Drops

Thermal Data

Thermal data taken during the tests at WSTF consisted of fuel bulk
temperature rise, regenerative chamber back wall temperature, and
steel heat sink nozzle temperature transients. These data, together
with the data generated during the heated tube tests under this con-
tract, were used to provide an indication of the safety margin at
which the thrust chamber was operating. Nozzle equilibrium tempera-
tures were predicted based on the heat sink nozzle transients in con-
junction with previous columbium nozzle tests with the demonstrator
chamber.

Bulk Temperature Rise and Heat Load. Coolant inlet and outlet tempera-
tures, ΔT's, and the heat load were tabulated in the NASA-CR-
report for each of the 35 tests which were of sufficient duration to
obtain thermal data. Fuel inlet and outlet temperatures were each
measured in three circumferential locations. The inlet temperature
measurements were made in the coolant inlet manifold. The outlet
temperatures were measured in the injector fuel distribution passages.
The three bulk temperature rises generally agreed within 8 percent.

The response of the coolant outlet bulk temperature and coolant ΔT for
a typical cold-start test is presented in Fig.94. The ΔT values achieve
nearly steady-state conditions in about 20-25 seconds. Ninety percent
of the final value is achieved in about 10 seconds. The long duration
to achieve final steady-state conditions is due primarily to the time
required for the massive (non-flight-weight) inlet manifold to reach
equilibrium with the fuel inlet temperature. Subsequent tests achieve
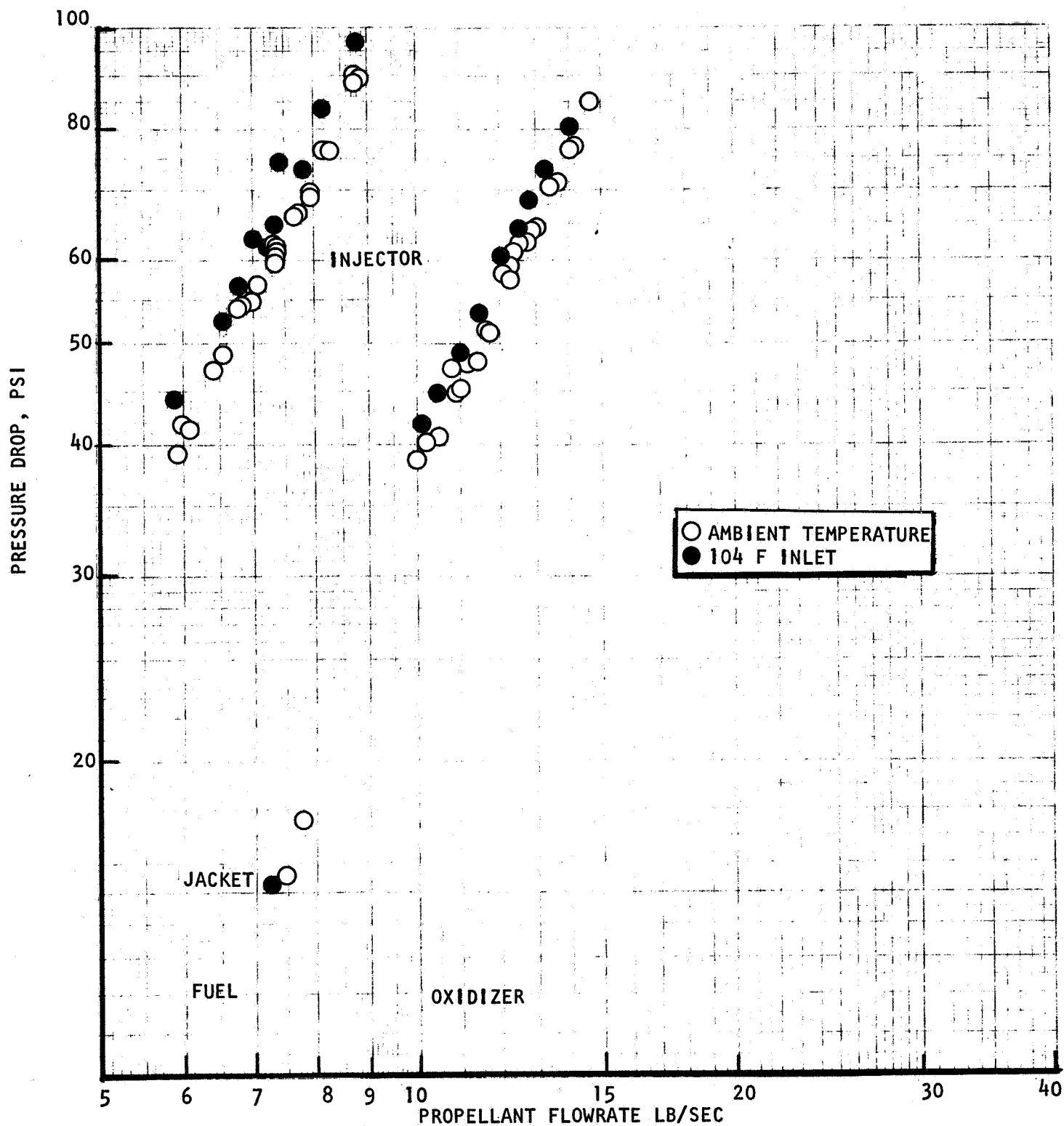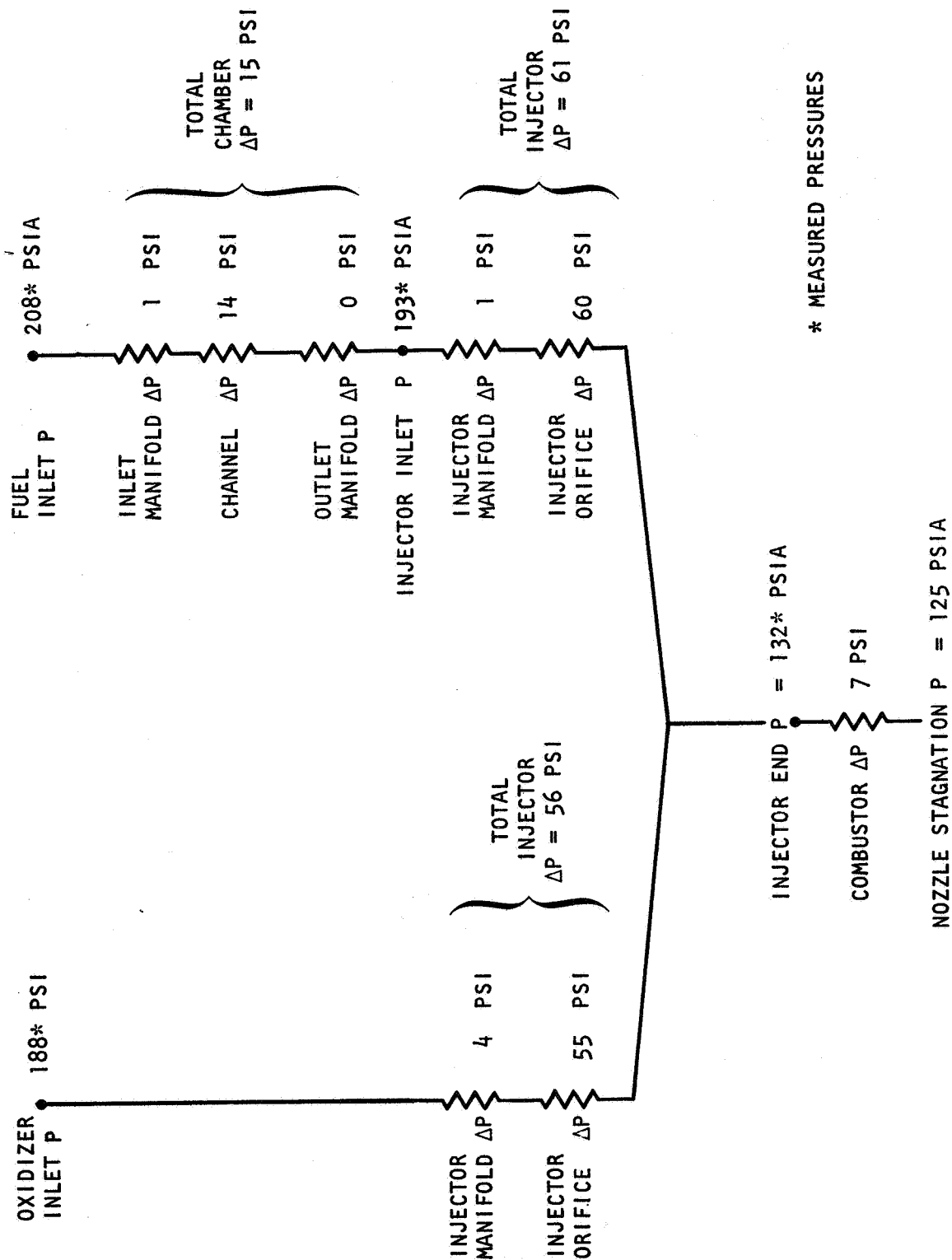steady-state conditions in less than 10 seconds as noted in Fig.95 for
a typical hot-start condition.

The average values of the ΔT's were multiplied by the fuel flowrate
through the jacket and the specific heat of the fuel to determine the
heat absorbed by the fuel. The heat loads for ambient propellants
(both saturated and unsaturated) are plotted versus chamber pressure in
Fig.96 , with coded symbols to denote approximate mixture ratio. These
data follow the predicted variation with Pc to the 0.8 power. The
effect of mixture ratio on heat load appears negligible, which is con-
sistent with heat transfer theory for the range of mixture ratios tested.
Helium saturation also does not appear to effect chamber heat load.

The best-fit line of the demonstrator heat load test results is also
presented in Fig.96 for comparison with the ITC heat loads. The ITC
heat loads are about 12 percent higher than for the demonstrator chamber,
even though a slightly higher supplemental film coolant flowrate (2.7 vs
2.0 percent) was utilized in the ITC. The primary reason for the
increased heat load is due to the less efficient, but much simpler,
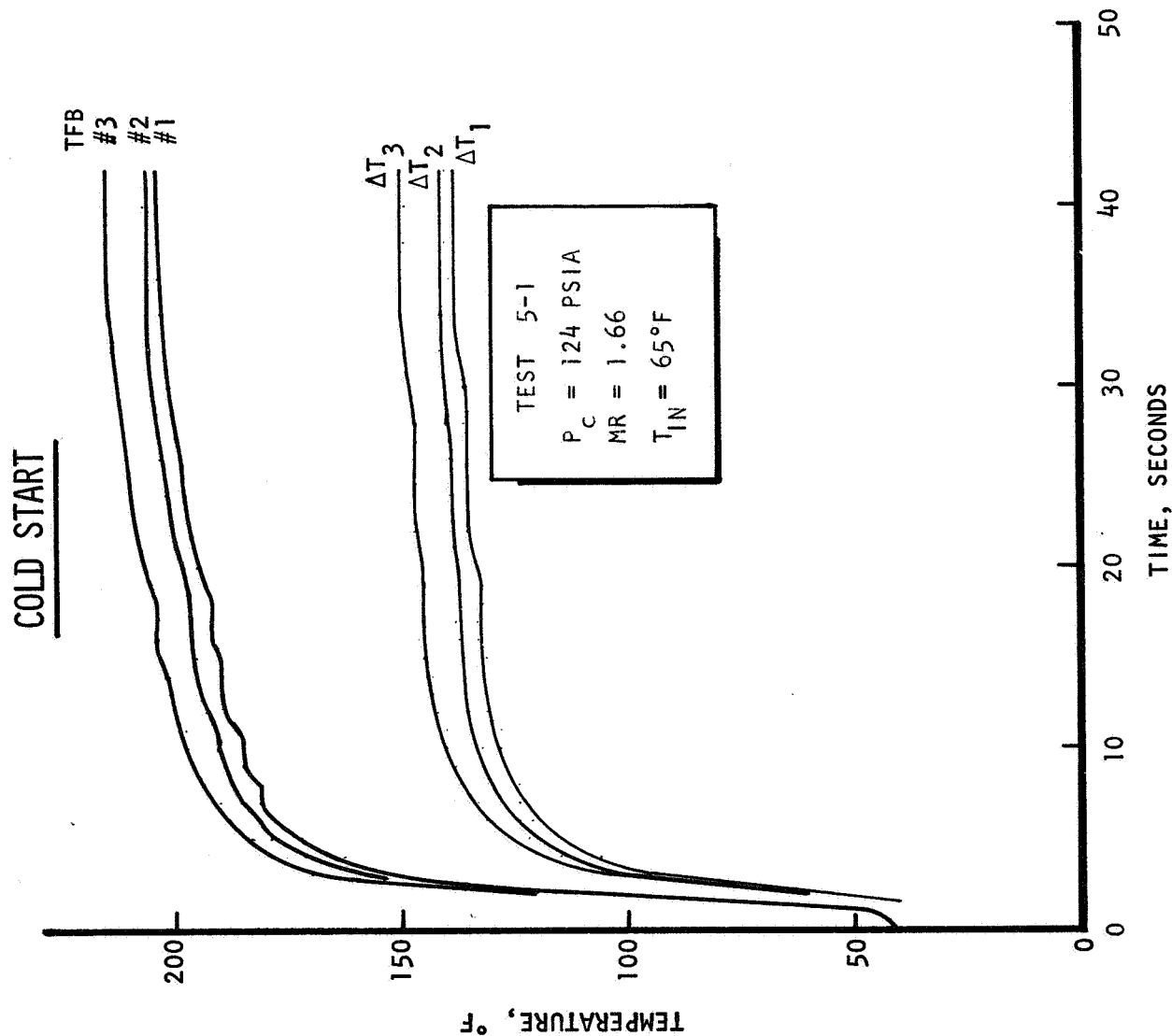method of film coolant injection employed in the ITC design. In the ITC

Figure 94. Typical Outlet Bulk Temperature and Temperature Rise Transients For The Integrated Thrust Chamber
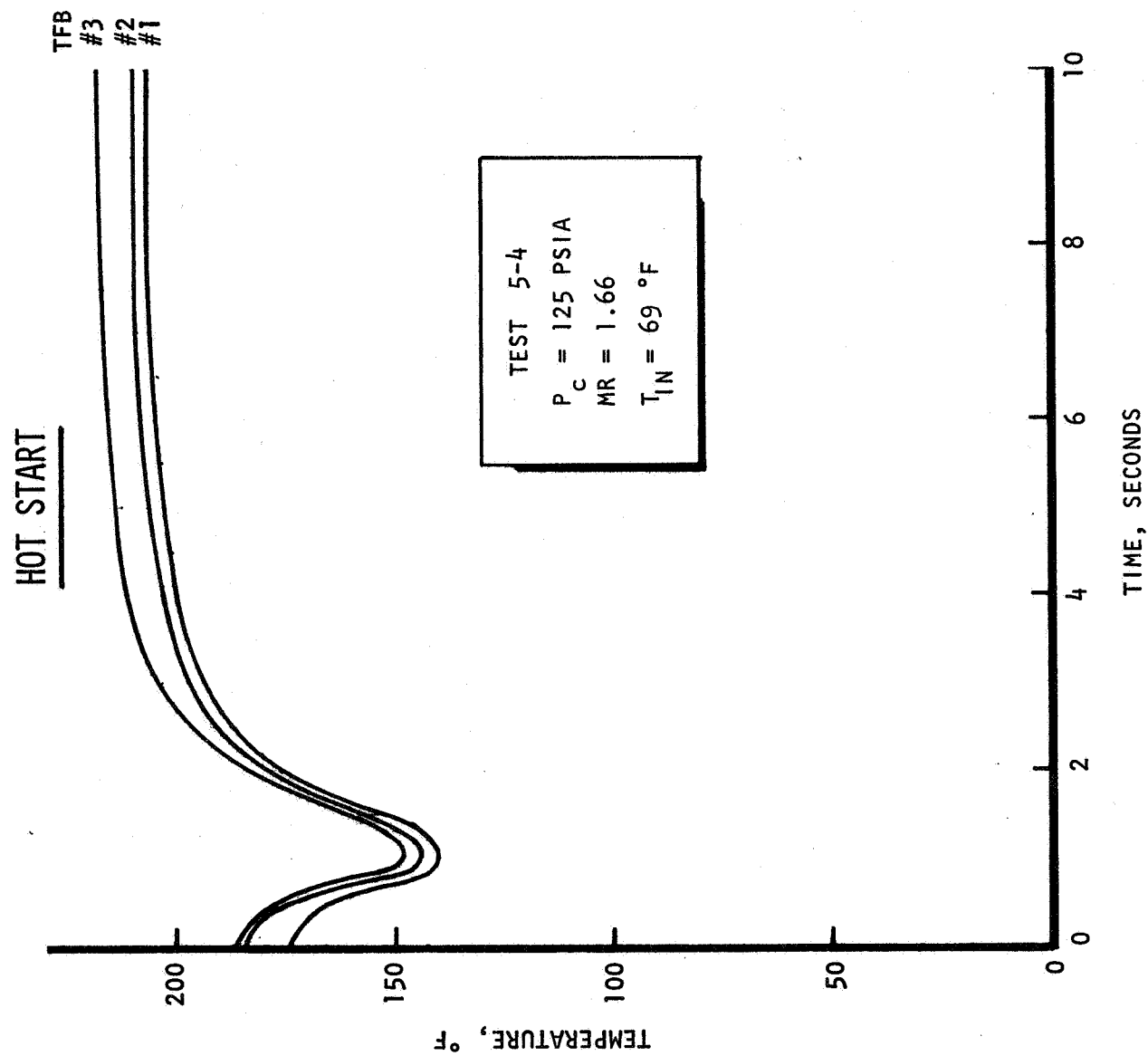
Figure 95. Typical Outlet Bulk Temperature Transient, Integrated Thrust Chamber
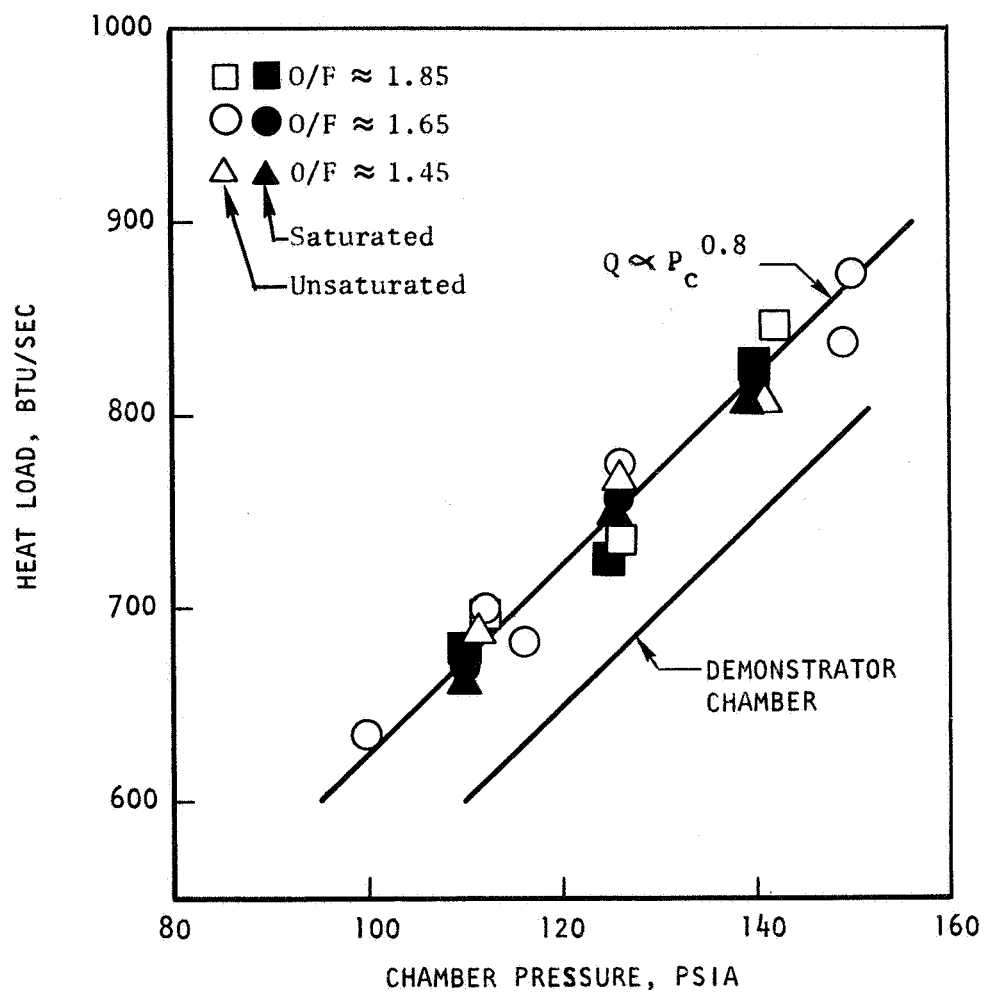
Figure 96. Integrated Chamber Heat Load With Ambient Propellants

design, the film coolant is injected from the primary injector across
the acoustic cavities onto the chamber wall. The demonstration
chamber utilized a separate film coolant ring, which injected the film
coolant directly along the wall without having to jump the acoustic
cavities.

An additional factor in the ITC design is that the acoustic cavities
are regeneratively cooled. It is estimated that about one-third of
the increased ITC heat load can be attributed to regenerative cooling
of the acoustic cavities.

The effect of hot propellants ($\simeq$100F) on chamber heat load is compared
with the ambient propellant test results in Fig.97. There appears to
be a very slight reduction in heat load, although the difference is
essentially insignificant.

Back Wall Temperatures. Back (outer surface) wall temperatures were
measured in numerous locations on the ITC (see Fig.98) to indicate
steady-state operating values, as well as start and soakout temperature
characteristics.

Typical back wall temperature response from a cold start (i.e., first
in a test series) is presented in Fig.98. As would be expected, the
response is more rapid in the higher heat flux regions, such as the
throat. An initial apparent steady-state temperature level is achieved
in less than ten seconds for the various back-wall temperatures depicted.
The back-wall temperatures continue to rise slowly from this time as the
fuel inlet temperature increases due to inlet manifold heating and a
rise in the propellant inlet temperature. Final steady-state tempera-
tures are achieved in about 30 seconds from start of test.

Typical hot start back-wall temperature transients are presented in
Fig.99. There is an initial cooling down of the back-wall as the coolant
flows through the channels before combustion gas heating diffuses
through the walls into the coolant and back-wall region. Steady-state
back-wall temperatures are readily achieved in about 5 seconds or less
under hot-start conditions. Maximum nickel back-wall temperatures
after soakout and prior to restart were, in general, less than 300F.

Steady-state back-wall temperatures are utilized primarily as an indi-
cation of circumferential heat load uniformity. These measurements are
relatively insensitive to local heat flux level and tend to reflect
integrated heat load along a channel in that back-wall temperatures
are strongly influenced by the local bulk temperature. In general,
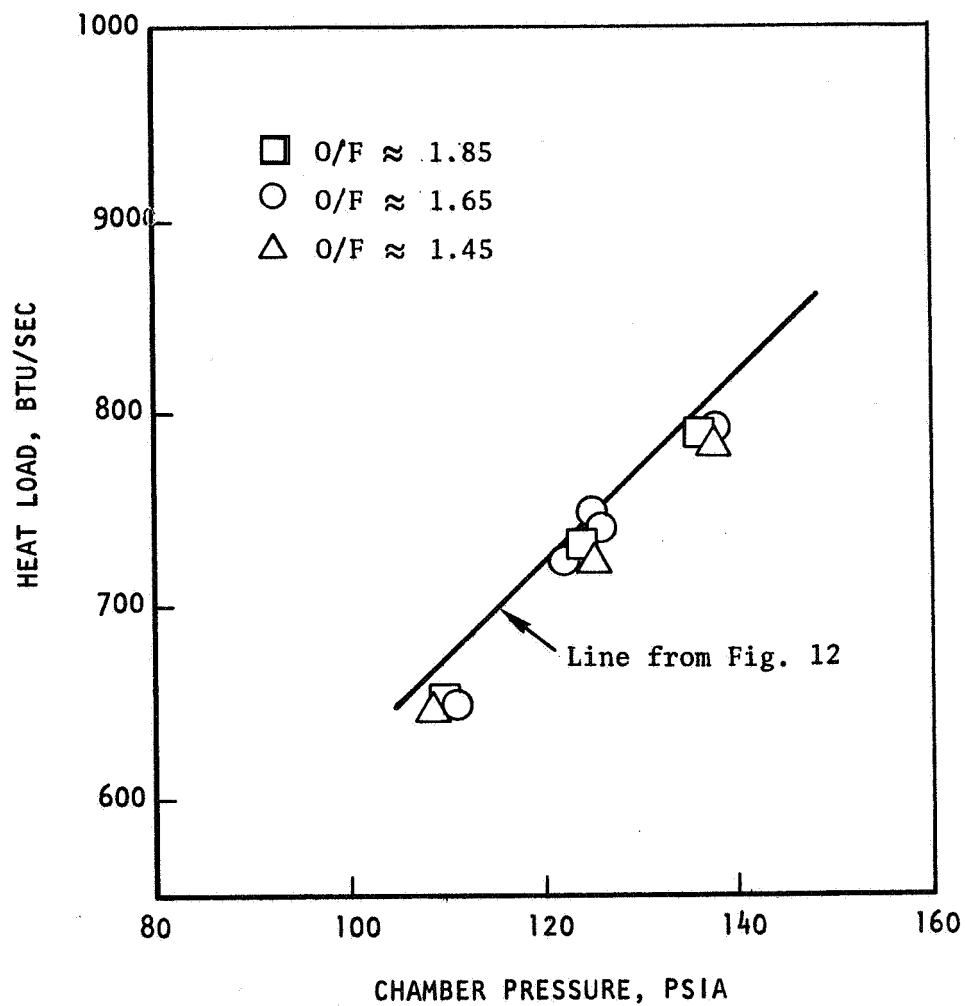circumferential variation in back-wall temperatures were less than

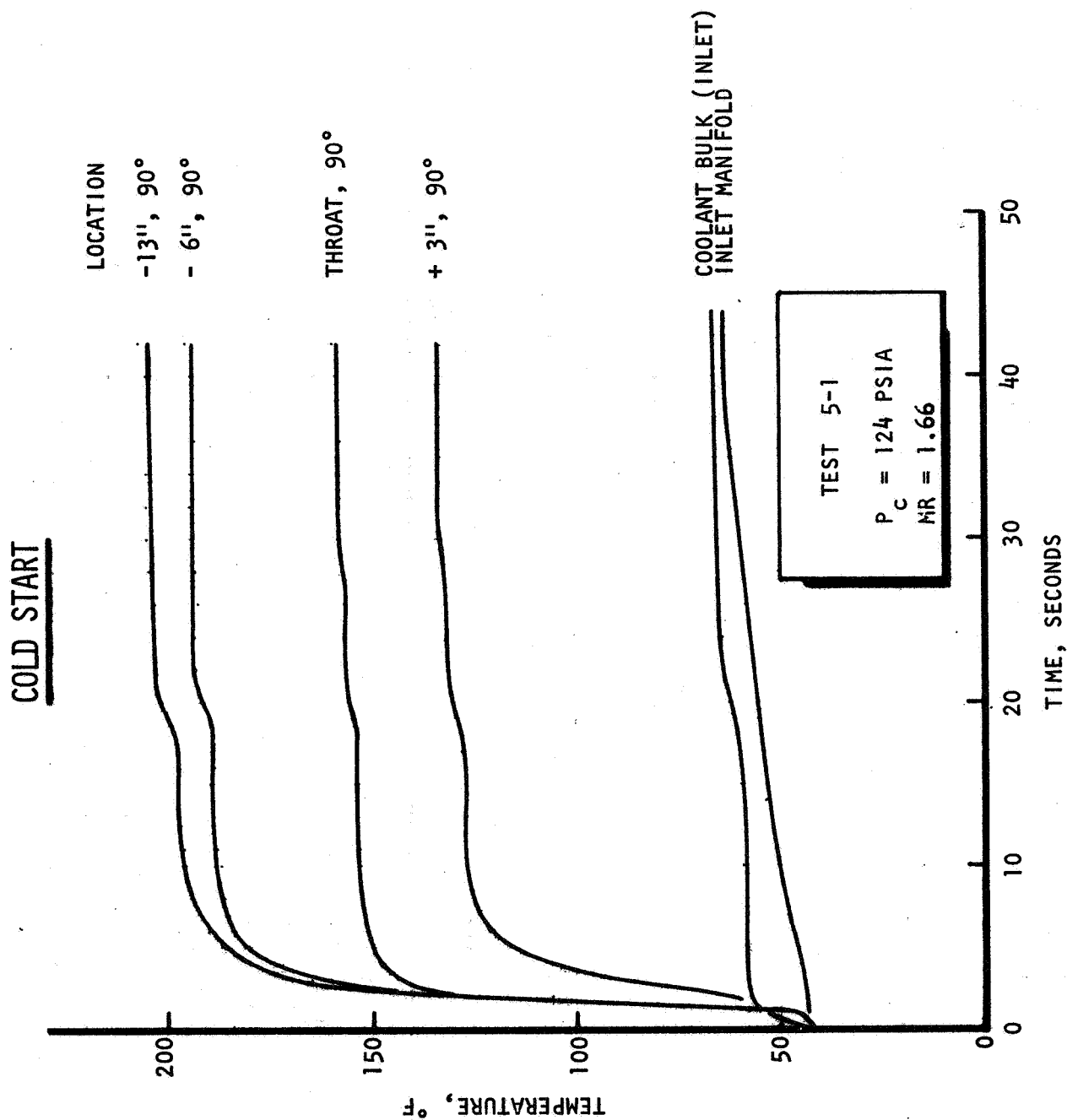Figure 97   Integrated Chamber Heat Load With 100F Propellants

Figure 98   Typical Backwall Temperature Transients for the Integrated Thrust Chamber
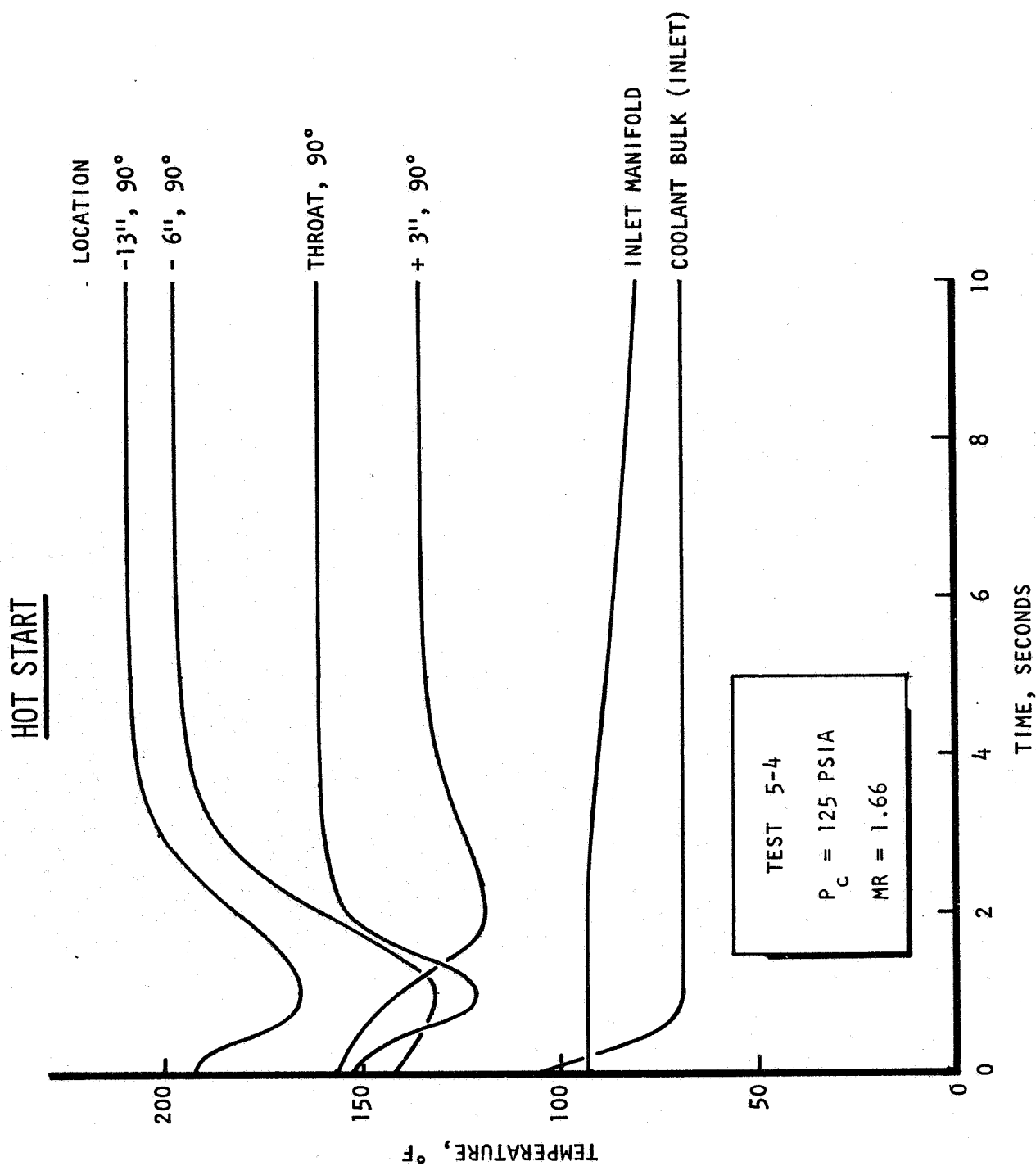
Figure 99 Typical Backwall Temperature Transients for the Integrated Thrust Chamber

10F, except at the throat and injector end/acoustic cavity regions, where differentials of 15 to 20F occurred. The injector end region is strongly affected by film cooling impingement and surface coverage, and resultant large heat flux variation can affect back-wall measurements.

A plot of back-wall temperature distributions is presented in Fig. 99 for a typical test at nominal operating conditions. The maximum and minimum values are denoted, as well as average back-wall temperatures. It is apparent that the back-wall temperatures increase rather uniformly from slightly upstream of the throat to a point 10 inches upstream of the throat. The temperature thereafter remains essentially constant to the end of the chamber. This latter factor implies a very low rate of heat input in this region as would be accounted for by a liquid film coolant. It appears therefore that from the point of film impingement on the wall (X = 13.7 in.), the film liquid length persists to a point approximately 10 inches to 11 inches upstream of the throat. This is corroborated somewhat by visual posttest inspection, wherein bright, clean metal surfaces existed for distances of about 2 inches to 4 inches downstream of the point of film coolant impingement. Such surfaces indicate the likelihood of cool under composed liquid MMH along the wall.

The theoretical film coolant model was utilized with varying input liquid lengths in order to match the total ITC measured heat load. The heat load was matched assuming MMH decomposition at a point approximately 10.5 inches upstream of the throat, which is consistent with the above observations. The resulting analytical back-wall (2-D analysis) and coolant bulk temperature profiles are included in Fig. 100 for comparison with experimental results.

In general the predicted back-wall temperatures are about 15 to 30F higher than experimental data in the combustion zone upstream of the throat. The general slope of the experimental back-wall data and predicted bulk temperature profile agree quite well in the combustor region. In the nozzle region (X = +3 in.) the measured back-wall temperatures agree favorably with the predicted value, although the fact that the measurement was made near the region of the step change in channel width tends to complicate the results.

In the throat region of the chamber, the average measured temperatures are about 20F higher than predicted. The data scatter of the four throat measurements is also, in general, greater than for other chamber locations, being about a 20F maximum temperature difference, rather than 5 to 10F. These results are similar to those noted previously for the
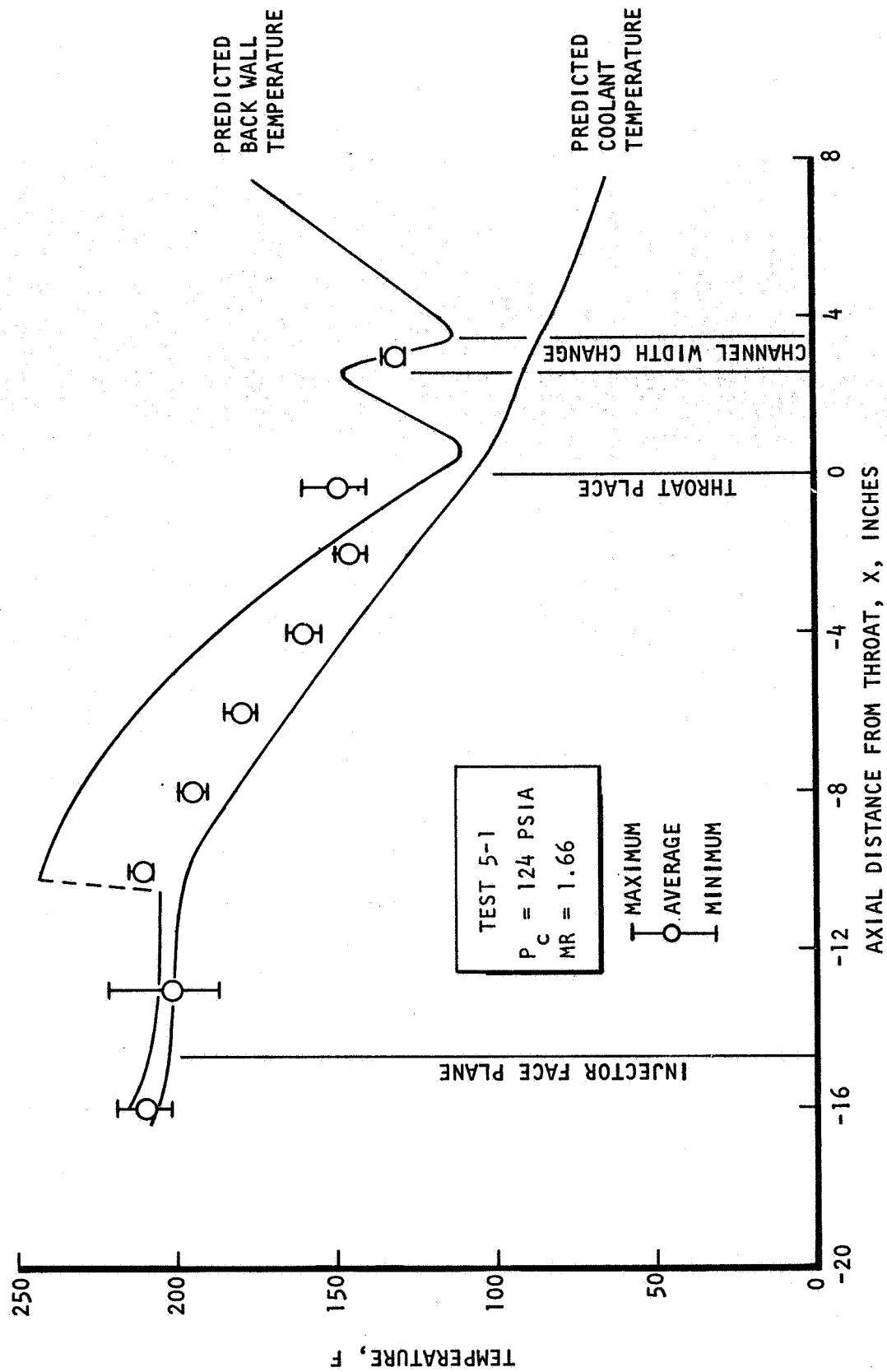
Figure 100 Integrated Thrust Chamber Back Wall Temperature Profile

demonstrator chamber tests. These differences believed due to throat region curvature effects on coolant convective coefficient along the closeout wall surface as discussed in the demonstrator section of the report.

Heat Sink Nozzle. The ITC chamber tests were conducted with a full 72:1 area ratio CRES heat sink nozzle to obtain accurate performance information. Wall temperature measurements at various locations were recorded during the ITC tests. Typical temperature response data for the CRES nozzle are presented in Fig.101 Test cut-off was based on maximum nozzle temperatures of about 1400-1500F.

There is good agreement between the two circumferential measurements except at lower area ratios where temperature differences of 100 to 150F occur. The reason for this difference may be attributed to uneven film cooling carryover effects.

Of primary significance, however, is the fact that nozzle heating rates are apparently about one-half the predicted value. A detailed transient thermal analysis was conducted, varying film convective coefficients and film temperature, in order to match the experimental transient response. The results of this analysis are shown in Fig.102 The estimated film temperature of 3300F is about 1000F lower than utilized for the original "dry-wall" analysis. This indicates a region of fuel rich gas adjacent to the wall which persists downstream of the throat. The single most significant conclusion to be drawn from the heat sink nozzle tests, is that the use of a refractory material is unnecessary at the current attach point. The use of an L-605 type nozzle extension appears quite feasible which should result in considerable cost saving to the OME engine concept. Alternatively, the columbium nozzle could be attached to a lower area ratio with an attendant reduction in engine weight and regenerative coolant heat load.

Start Sequence Variations

Three different propellant valve opening sequences were used during the program. The propellant control valves were set so that the oxidizer propellant valve reached the full open position nominally 50 ms before the fuel valve reached its full open position for test series 1-1. The oxidizer valve lead was reset for approximately 250 ms on test series 1-2 and for 150 ms on test series 1-3, 1-4, and 1-5. Considerable variation in the oxidizer valve lead (198-307 ms) occurred from test to test on series 1-2.

Figure 101 Steel Nozzle Temperature Response

Figure 102   Comparison of Modified Analysis with the
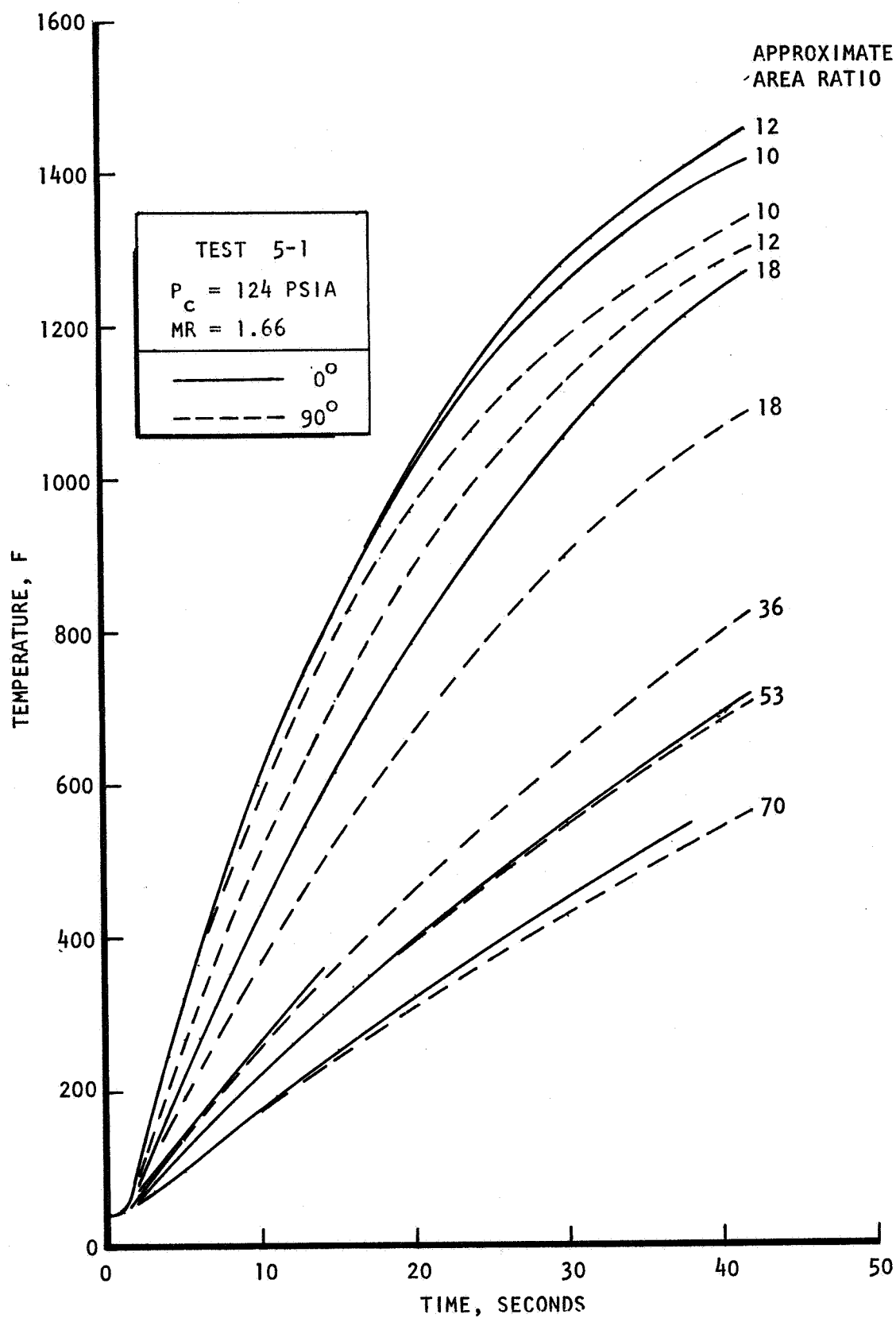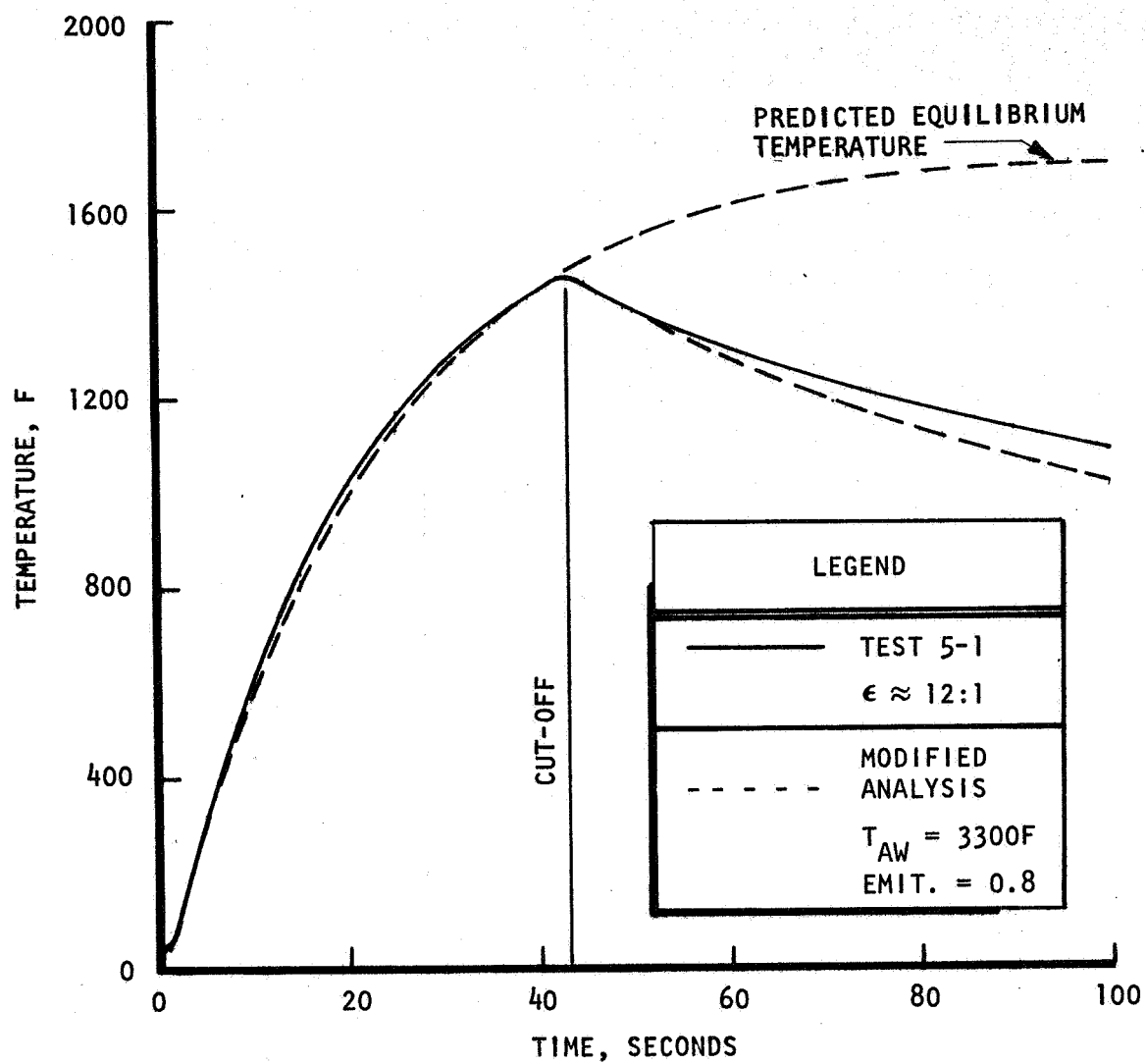Experimental Temperature Response of the
CRES Heat Sink Nozzle

Oxidizer valve lead, oxidizer injection lead, thrust and Pc over-
shoots, and maximum 'g' levels are summarized in Table 34. On the
first two tests (1-1-1 and 1-1-2), the load cells were overloaded so
that the actual value of the overshoot cannot be specified. The fuel
and oxidizer injection pressure measurements had poor response.
Injector priming was inferred from the engine interface pressure
measurements (upstream of the propellant valves) which were quite
responsive. This procedure was also justified by the good correlation
between oxidizer injection lead, determined in this manner, and
oxidizer valve lead. Chamber pressure began to rise simultaneously
with thrust but the chamber pressure overshoot appears to be damped and
did not correlate well with thrust overshoot or 'g' level.

Accelerometers always indicated the highest 'g' level on the first test
of each series and the thrust overshoots were also the highest on these
tests (except series 1-4). This phenomenon could be associated with
incomplete purging between tests or with cold hardware on the first
test. The cold hardware is most likely responsible because the purging
procedures are quite thorough. Furthermore, tests 1-2-1A and 1-2-1B
were very short duration tests (≃1 sec) on which the hardware did not
have an opportunity to warm up and the thrust overshoots and 'g' loads
were relatively severe on tests 1-2-1B and 1-2-1, each of which was con-
ducted within 1-3 minutes of the previous test.

Typical start transients from the fourth test in a series (Test 5-4) are
shown in Fig.103and104. The oxidizer valve opening times for tests 1-5-1
and 1-5-4 were 40 and 50 milliseconds respectively. The fuel valve
openings for tests 1-5-1 and 1-5-4 were 140 and 95 milliseconds
respectively. The fuel and oxidizer interface pressure transients re-
flect these valve times. The most significant differences between the
traces for the first and fourth tests are that the injection pressures
and chamber pressure for the last test are slightly higher than for the
first tests during the low pressure part of the transient tests, imply-
ing that the warm hardware has vaporized some of the propellants enter-
ing the injector and chamber.

Thrust chamber temperatures for the first and last tests of each sequence
are summarized in Table 35. The included MMH saturation data indicates
that very little vapor pressure would be generated by the hardware heat-
ing the fuel to the temperatures indicated for the first tests. However,
vapor pressures corresponding to the thrust chamber temperatures
measured near the injector end prior to the start of the last tests
could be as high as 60 psia. These pressures could reduce the fuel flow-
rate somewhat. But more significantly, the vaporized fuel could provide
a smoother ignition with the oxidizer. Corresponding temperature data

TABLE 34
INTEGRATED THRUST CHAMBER TRANSIENT DATA

TEST NO.	OX VALVE LEAD, MS	P_c OVER-SHOOT,%	F OVER-SHOOT,%	ACCELER-OMETER,g	OXIDIZER INJECTION LEAD, MS
1-1-1	50	37	>110	43	132
1-1-2	44	37	>110	18	108
1-1-3	43	33	98	10	55
1-2-A	198	35	~90	37	258
1-2-B	218	23	~90	29	248
1-2-1	248	24	84	37	293
1-2-2	250	25	70	18	305
1-2-3	248	25	77	14	282
1-2-4	263	29	77	13	303
1-2-5	270	25	70	15	337
1-2-6	270	32	67	17	323
1-2-7	288	35	80	9	340
1-2-8	307	31	65	13	367
1-2-9	328	28	93	12	362
1-2-10	346	32	89	12	379
1-3-1	147	21	72	27	199
1-3-2	151	19	45	13	227
1-3-3	147	15	72	16	204
1-3-4	145	16	66	13	215
1-3-5	146	17	62	12	223
1-3-6	144	17	43	19	212
1-3-7	147	25	54	16	219
1-3-8	146	22	44	16	227
1-3-9	142	19	58	9	202
1-3-10	141	23	61	14	205

TABLE 34 (Continued)

INTEGRATED THRUST CHAMBER TRANSIENT DATA

TEST NO.	OX VALVE LEAD, MS	P_C OVER-SHOOT,%	F OVER-SHOOT,%	ACCELER-OMETER,g	OXIDIZER INJECTION LEAD, MS
1-4-1	188	19	67	28	222
1-4-2	153	9	75	17	199
1-4-3	142	16	73	9	199
1-4-4	145	19	73	10	207
1-4-5	150	22	61	9	217
1-4-6	153	20	54	9	227
1-4-7	155	24	54	13	240
1-4-8	150	28	70	14	213
1-4-9	150	29	66	10	228
1-4-10	142	18	65	12	215
1-5-1	170	37	95	36	210
1-5-2	130	42	59	13	190
1-5-3	145	42	72	6	241
1-5-4	145	26	86	12	223
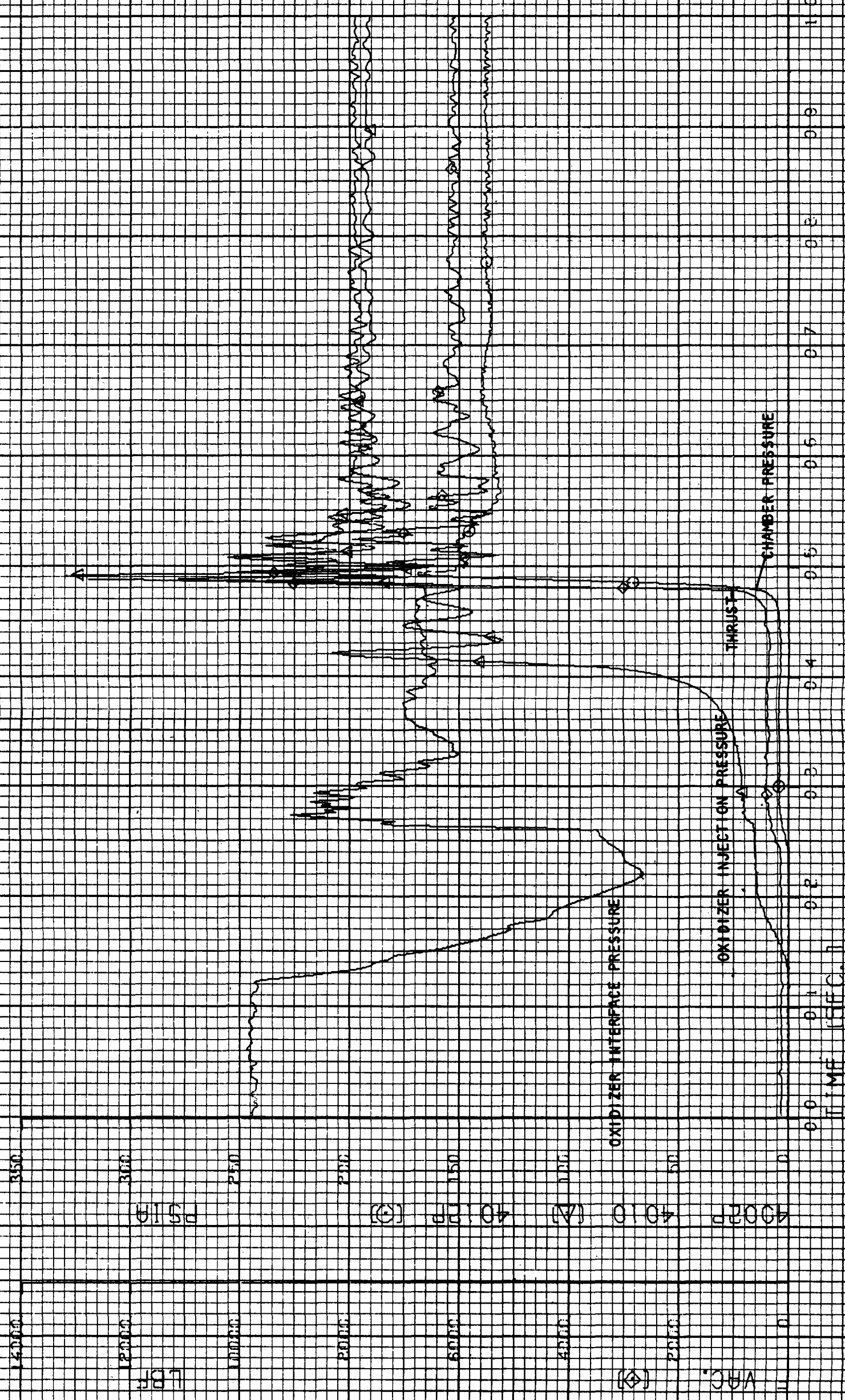
Figure 103 Oxidizer Transients on Test 1-5-4

R-9686/6-41
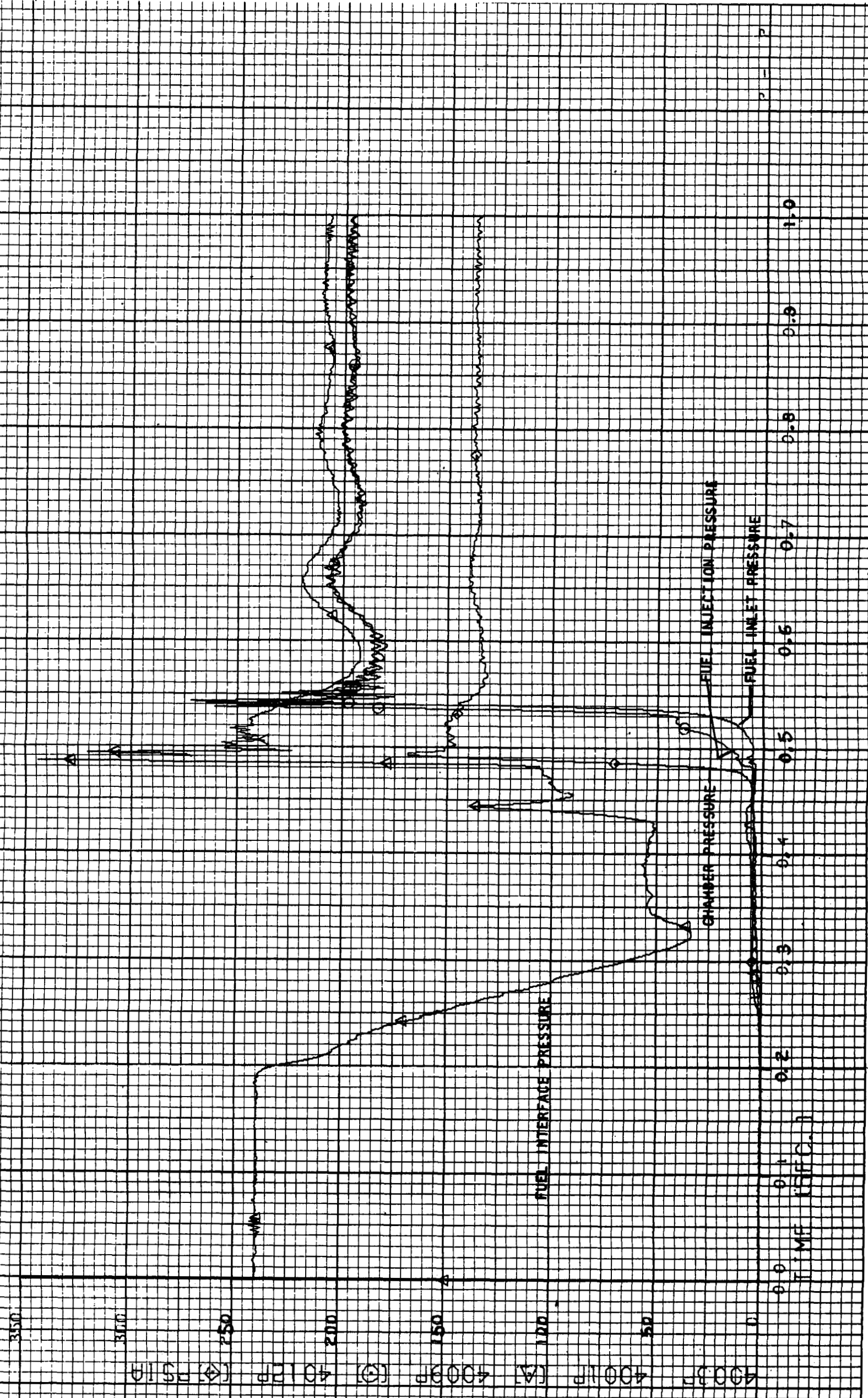
Figure 104 Fuel Transients on Test 1-S-4

R-9686/6-42

TABLE 35

PRETEST THRUST CHAMBER TEMPERATURES

	PRETEST AVERAGE TEMPERATURES, F									
	Metal Temperatures Located at								Coolant @ Inlet	Coolant @ Injector
Test	-16 In	-13 In	-8 In	-4 In	0.3 In	+3 In	Nozzle Flange	Nozzle @7.2 In		
1-1	60	60	60	60	60	60	60	50	50	60
1-2	90	90	70	60	70	70	80	150	80	100
1-3	200	180	130	130	130	130	100	300	100	130
2-1B	50	50	60	60	60	60	70	70	60	50
2-10	210	140	120	120	140	130	210	780	90	130
3-1	60	60	60	60	60	60	60	60	60	60
3-10	240	160	120	170	140	130	190	1000	90	150
4-1	50	50	50	50	50	50	50	50	50	50
4-10	270	200	160	170	160	160	210	810	100	210
5-1	40	40	40	40	40	40	50	40	40	40
5-4	200	170	140	150	140	150	100	500	100	180

NOTE: MMH Saturation Data

T_{sat}, F	270	200	90	40
P_{sat}, psia	60	20	3	<1

R-9686

were not measured on the oxidizer side of the engine. However the
higher injection pressures imply that the oxidizer also was subject
to vaporization on latter tests in each sequence.

Although the correlation between the thrust overshoot and oxidizer
injection lead was only loosely defined it appears that the overshoot
would be minimized by an oxidizer lead of 150 to 250 ms.

Post-Firing Thermal Transients

The last tests of sequences 3, 4, and the first test of series 5 were
followed by thermal soakout in vacuum for a period of approximately
one-half hour. On sequence 3 the soakout was initiated without any
purge after the test. On sequences 4 and 5 a brief (1 second) purge
of fuel and oxidizer was accomplished in order to simulate the propel-
lant depletion which would occur under zero 'g' flight conditions.
Three significant events occurred during the transients. During the
first two to five seconds after shutdown, inside and outside wall
temperatures equilibrate with the result that certain back-wall
temperatures reach a maximum in this period and then decay. At about
20 to 80 seconds propellant fuel depletion in the jacket is indicated.
In about 30 minutes all hardware temperatures have reached their maxi-
mum soakout values.

Nickel backwall, inlet manifold and flange, and nozzle shutdown tempera-
ture response plots are presented in the Task XII Data Dump. A typical
plot of nickel backwall temperatures at the zero degree circumferential
location (90 degrees clockwise from the coolant inlet viewing aft) after
test 1-3-10 (no purge) are shown in Fig. 105. The break in the data from
62 to 82 seconds is the result of instrumentation calibrations being
taken at that time. Cut-off occurred at 10 seconds. Wall temperatures
generally peak 2 to 3 seconds after cut-off as a result of the inner and
outer walls reaching equilibrium. Wall temperatures at the injector-
end peak more slowly because of the influence of the acoustic cavity
dams and the thicker liner in this region. The maximum temperature
recorded at this time period on any of the soakout tests was less than
375F. The thrust chamber can be safely restarted at these temperatures
based on the results of the electrically heated tube tests conducted
under Task IX of the contract. Under this task starting conditions
were simulated with tubes as hot as 1600F with no adverse effects.

0 DEGREE LOCATION

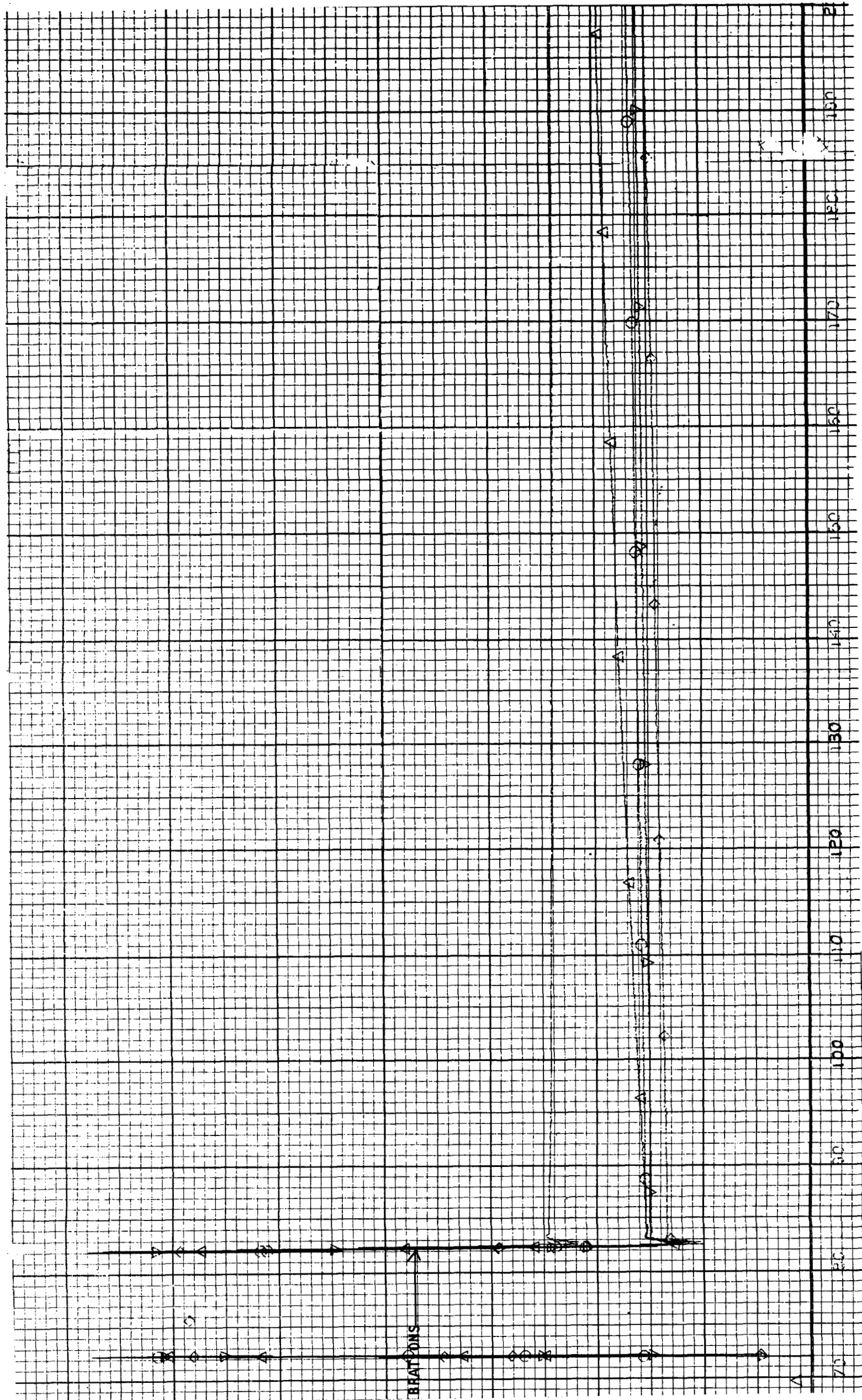MMH BOILING TEMPERATURE

CAL

TIME (SEC)
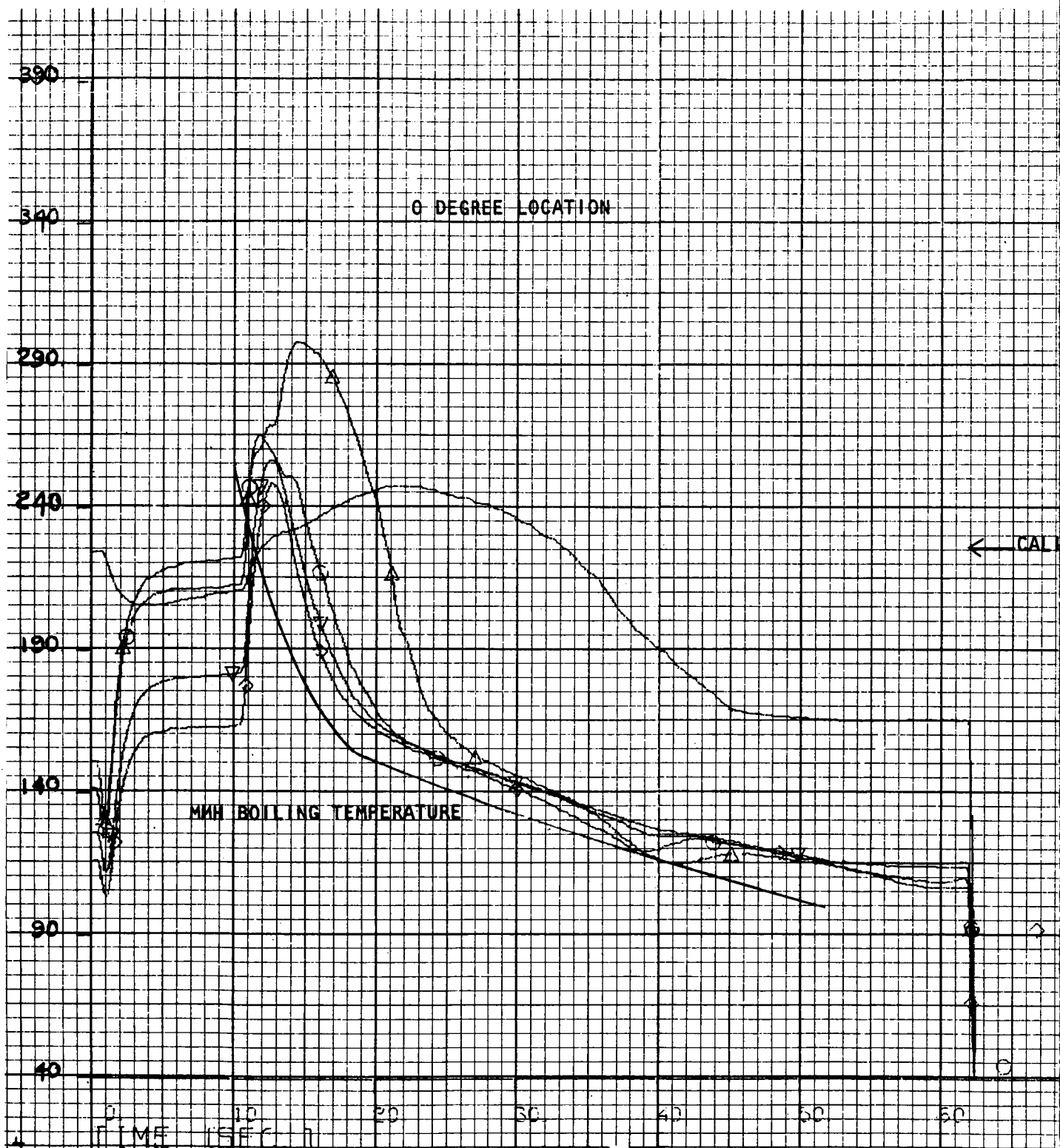
Fold-Out #1

Figure 105. Nickel Wall Temperatures (Forward Region)

6-45

FOLD-OUT #2

After the inner and outer walls come to equilibrium, the wall (inner and outer) is heated by soakback from the radiation-cooled nozzle and the injector and is cooled by residual fuel in the jacket, inlet manifold, and line. The volume of fuel in the injector and coolant channels is approximately 60 inches^3 and the volume of the inlet manifold and line to the valve is approximately the same. The shapes of the backwall temperature transients do not indicate an orderly boiling down past each axial station in the jacket. Either all the fuel in the jacket is discharged in the first few seconds or violent boiling bathes the walls with froth independent of axial location.

The MMH boiling temperature curve is superimposed on Fig. 106 based on measured pressure. The accuracy of the pressure measurement is in the order of 1 psi which corresponds to a 10F accuracy in the boiling temperature at the lower pressures. After the initial transient, the wall temperatures are generally 10 to 15F above the boiling temperature implying that any fuel in the channels would be boiled at all locations. The divergence between the wall and boiling temperature curves could be the result of decreasing quantities of MMH percolating up the channels. A bias of 1 psi in the inlet manifold pressure measurement could also cause the divergence. However, at 60 seconds (50 seconds after shutdown) some of the wall temperatures reach minimum values and begin to rise indicating the onset of depletion of MMH. All wall temperatures (except at station 16, the injector end) were rising by the time calibrations were completed at 73 seconds after shutdown. This implies essentially complete propellant depletion from the channels. Wall temperature profiles at T = 83, 200, 600, and 1200 seconds plotted in Fig. show the effects of thermal inputs from the injector and nozzle. The nozzle is the primary heat source during the latter period of the soakout. Regenerative chamber wall temperatures do not exceed the initial peak value at 1200 seconds all the radiation nozzle temperatures are less than 300F and decreasing.

The flange temperature and the three inlet manifold fuel temperatures were utilized to estimate propellant depletion time. As propellant boils off in the manifolds, the closed tip thermocouples are uncovered and heated by conduction from the warm inlet manifold and nozzle extension. Table 36 is a summary of the fuel depletion times based on the fuel inlet temperature transient data for each of the soakout tests and the associated significant conditions for each test.
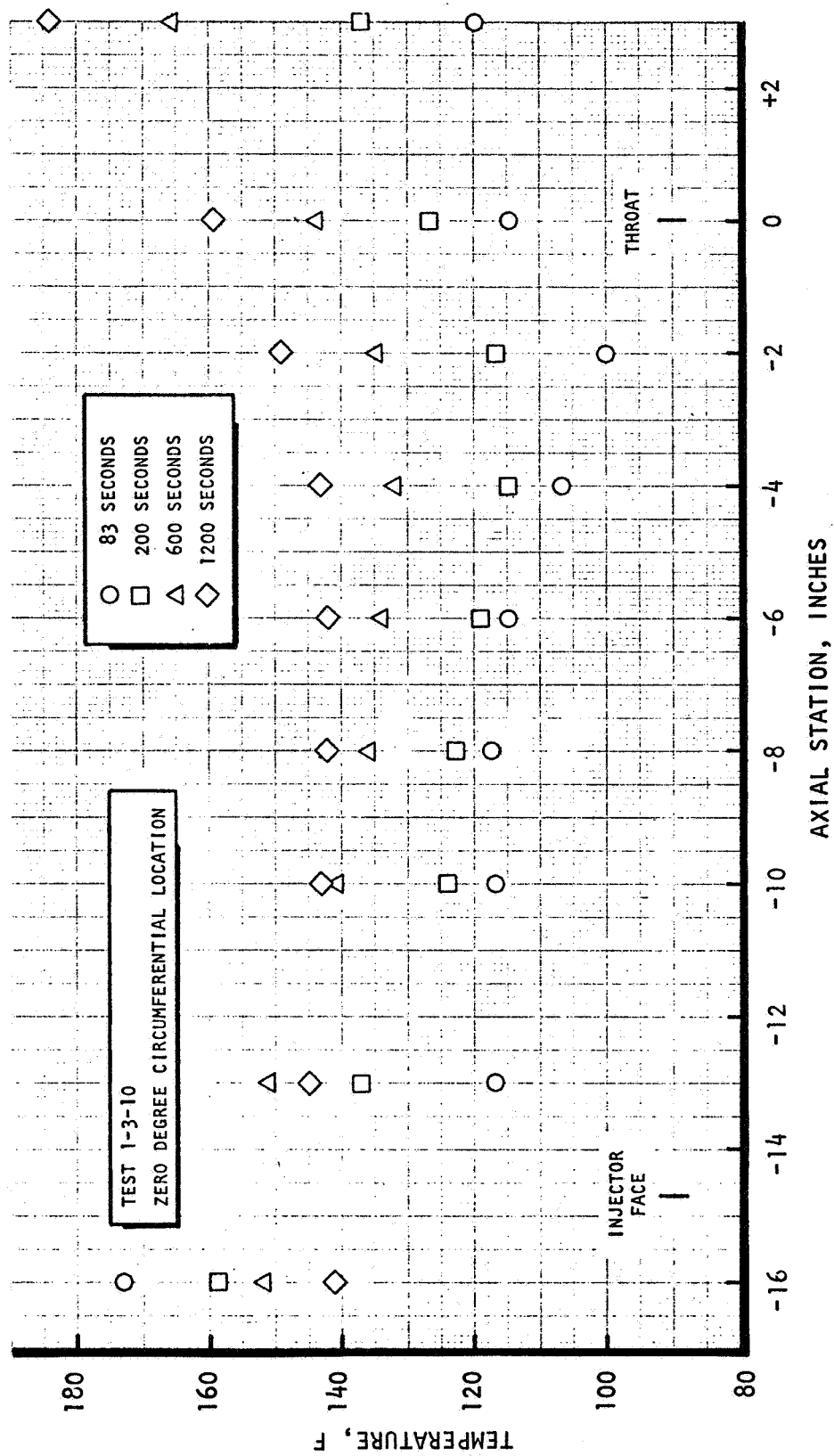
Figure 106 Regenerative Chamber Wall Temperature Profiles

TABLE 36. PROPELLANT DEPLETION SUMMARY

Test	1-3-10	1-4-10	1-5-1
Depletion Time, sec After Shutdown	60	25	60
Fuel Inlet Temperature, F At Shutdown	65	105	65
Regen Flange Temp, F At Shutdown	190	210	50
Posttest Purge	No	Yes	Yes

The depletion time on test 1-4-10 was significantly shorter than on test 1-3-10 which can be attributed to the higher fuel temperature and the brief posttest purge. Fuel depletion times were about the same for 1-3-10 and 1-5-1 despite the posttest purge on test 1-5-1. It appears that the effect of the purge was offset by the colder regenerative chamber flange temperature. The flange temperature does not change significantly during the tests but does increase between tests because of soakback from the nozzle as indicated by the data in Table 37.

Temperatures after 20 minutes of vacuum soakout are tabulated in Table 38. All temperatures were less than 350F at this time for all three tests. The maximum temperature difference measured on the regenerative chamber wall was 60F. The regenerative chamber flange temperature on test 1-3-10 appears low but is based on two measurements which agree within 4F. The highest temperature at this time was 340F on the radiation nozzle. Although the nozzle operating temperature for the flight hardware is greater than that tested, the nozzle wall thickness of the flight hardware is significantly less (.030 vs .125 inches) so that heat transfer to the regenerative chamber should be no greater in the flight configuration.

6.4 ITC TEST PROGRAMS - PHASE II

The primary objective of the Phase II test program was to investigate the OME start, shutdown, and restart characteristics to determine if restrictions of the mission-duty cycle exists for the current configuration of the OME. Secondary objective was the investigation of OME thrust chamber operating characteristics at very low chamber pressures typical of propellant tank blowdown operation and without supplementary boundary layer coolant.

TABLE 37. SOAKOUT TEMPERATURES AT 1200 SECONDS

Location	Temperature*, F		
	Test 1-3-10	Test 1-4-10	Test 1-5-1
-16 In	144	184	135
-13 In	145	190	127
-10 In	142	187	154
-8 In	141	184	155
-6 In	141	182	157
-4 In	142	181	157
-2 In	147	185	160
Throat	159	193	166
+3 In	186	219	186
Inlet Manifold	208	233	187
Regen Flange	126	225	209
Near Rad. Flange (7.2 In)	254	307	246
Radiation Nozzle (7.8 In)	265	324	256
Max. Rad. Nozzle Temp.	285	340	292

*Circumferentially averaged

TABLE 38 METAL TEMPS AT O DEGREE LOCATION

Test	Regen. Flange		Nozzle @ 7.2 In*		Nozzle @ 7.8 In.	
	-1 Sec	10.5 Sec**	-1 Sec	10.5 Sec	-1 Sec	10.5 Sec
1-3-1	60	60	60	250	60	670
-2	80	81	390	460	610	1010
-3	95	95	520	570	750	1080
-4	115	116	640	680	930	1210
-5	134	133	720	750	1030	1300
-6	137	135	650	670	890	1100
-7	152	152	690	710	970	1190
-8	170	169	740	760	1050	1250
-9	173	171	700	720	960	1180
-10	188	188	740	770	1050	1260
1-4-1	51	53	50	600	50	1200
-2	78	77	600	640	870	1160
-10	214	213	800	830	1140	1310
1-5-1	47	50	44	760	41	1360
-2***	73	74	180	830	180	1280

NOTES: *0.2" from flange of radiation nozzle
**30 Sec for Test 1-4-10 & 43 Sec for 1-5-1
***Long delay & aborted test between 1-5-1 & 1-5-2

A total of 116 tests and 744 seconds were accumulated during Phase II of the Integrated Thrust Chamber Test Program. All of the tests were conducted with the electroformed regeneratively cooled thrust chamber and the like-doublet No. 1 injector. Most of the tests were conducted with the heat sink/radiation cooled nozzle having an area ratio of 72 to 1. Tests at lower chamber pressure and tests with zero boundary layer coolant were conducted with a radiation cooled nozzle having an area ratio of 9 to 1. Including previous tests, the integrated thrust chamber has been fired 156 times for a total duration of 1190 seconds and the No. 1 like-doublet injector has been fired 284 times for a total of duration of 1695 seconds.

The tests were broken down into groups of tests called test sequences each having specific detailed objectives or test conditions. The number of tests in each sequence and the objectives of the sequence are shown in Table 39. A summary of the most significant conditions for each test is presented in Table 40. As noted, all tests of sequence 1 through 6 (except 1-1 and 1-2) were conducted at approximately nominal chamber pressure and propellant mixture ratio.

A series of tests (sequence 1) were conducted with various posttest purge and flush sequences to determine how the engine might be returned to ambient temperature between multiple tests. It was decided that no flush or purge would be used between tests in order to avoid possibility of contaminating the engine. A brief series of tests were conducted wherein the fuel valve signal delay time (relative to the oxidizer valve signal) was varied from 100 milliseconds to 0 milliseconds. No significant change in pressure or thrust overshoots or 'g' level at start resulted from these variations.

Hot engine restart tests (sequence 4) were conducted by firing the engine until it reached thermal equilibrium and then shutting down for various coast periods ranging from 1 to 180 seconds. These tests were conducted with ambient temperature propellants and with cold (approximately 45F) propellants. This series of conditions resulted in starting the engine with no propellants in the manifold, residual fuel only in the engine, and both residual oxidizer and fuel in the engine. One 1500 g spike was recorded at oxidizer prime with no engine damage. A 530 g start was also recorded but could not be repeated. All other starts had acceleration spikes of less than 130 g. Accelerations of 15-40 g's were recorded with normally operating valves at ignition. Thrust overshoots as high as 160 percent were recorded. No damage was done to the thrust chamber.

TABLE 39. INTEGRATED CHAMBER TEST PROGRAM SUMMARY - PHASE II

Sequence	Tests	Purpose
1	12	Checkout, posttest purge & flush effects, performance
3	35	Valve sequencing, hot engine restart, soakout, fuel depletion
4	13	Warm engine restart, soakout
5	15	Hot engine restart with cold propellants, soakout
6	17	Ambient engine restart, soakout
7	14	Performance, thermal low P_c operation
8	10	Performance and thermal without BLC
Total	116	745-Sec duration

TABLE 40

TEST CONDITIONS

Test Seq. No.	Ox. Valve Lead, msec	Duration sec.	Comments
1-1*	100	1.0	Targeted P_c and o/F 125 psia and 1.5 respectively for tests 1-1 and 1-2; 125 psia and 1.65 for subsequent tests. Posttest water spray (38 sec) alcohol flushing (42 sec) and GN_2 purge.
1-2	100	3.1	Restarted immediately after above procedures. Five-minute posttest soak.
1-3*	100	1.0	Restarted without purges after soak. Posttest water spray, alcohol flush, and GN_2 purge to cool engine.
1-4	100	0.14	Restarted after above procedures. Hard start and CSM shutdown.
1-5*	100	0.3	One minute of purge (cycling) posttest, then restart.
1-6	100	0.3	One minute posttest purges, then restart.
1-7	100	0.3	One minute of posttest purge, then restart.
1-8	100	0.3	One minute of posttest purge, then restart.
1-9	100	1.3	One minute of posttest purge, then restart.
1-10	100	0.3	One minute of posttest purge, then restart.
1-11	100	0.3	15 sec. posttest purge, 8 sec. alcohol flush, 100 sec GN_2 purge, then restart.
1-12	100	35.6	18 sec. posttest GN_2 purge, 30 sec. alcohol flush, 40 sec. purge, 5 min. soak.
3-1*	100	0.3	One-minute posttest purge.
3-2	100	0.3	One-minute posttest purge.
3-3	50	0.3	One-minute posttest purge.
3-4	0	29.3	Simultaneous propellant valve signals for this and subsequent tests. No posttest purge.

*First test of a vacuum period.

R-9686

TABLE 40. TEST CONDITIONS (Continued)

Test Seq. No.	Duration Sec.	Pretest Coast Time, Sec.	Comments
3-5	14.3	180	No posttest purge.
3-6	4.3	120	2 min. posttest purge (including upper nozzle external purge).
3-7*	32.0		No posttest purge after this and following tests, except each day's testing or as noted.
3-8	14.7	60.1	
3-9	9.9	30.0	
3-10	9.8	35.5	
3-11	4.8	21.1	
3-11A	4.8	53.6	
3-12	4.8	9.9	Hard start.
3-13	4.8	10.0	
3-14	4.8	4.9	
3-15	4.8	2.0	
3-16	4.8	1.1	
3-17	4.8	1.2	30 min. vacuum soak.
3-18*	0.15		No tape data during posttest soak.
3-18A*	0.15		Pretest purge. Hard start at Ox. injector prime. 10 min. posttest soak.
3-18B*			Injector rotated. 6 Ox. valve on-off cycles.
3-18C	0.94		30 min. posttest soak.
3-19*	31.7		Ox. valve changed.
3-20	9.8	25.2	
3-21	9.8	24.4	
3-22	4.8	18.1	
3-23	4.8	12.5	Fuel depletion and helium injestion.
3-24*	31.8		
3-25	4.8	16.0	
3-26	4.8	16.3	
3-27	4.8	11.3	
3-28	4.8	11.3	
3-29	4.8	29.2	

*First test of a vacuum period.

TABLE 40. TEST CONDITIONS (Continued)

Test Seq. No.	Duration Sec.	Pretest Coast Time, Sec.	Comments
3-30	4.8	5.4	
3-31	4.8	5.0	
3-32	4.8	2.0	
3-33	4.1	2.0	3 minutes posttest soak
4-1*	1.0		
4-2	1.0	179.8	
4-3	1.0	120.8	
4-4	1.0	61.2	
4-5	1.0	31.2	
4-6	1.0	16.1	
4-7	1.0	9.0	
4-8	2.9	4.6	
4-9	1.1	0.3	
4-10	1.1	0.7	
4-11	1.0	13.8	
4-12	1.0	30.1	
4-13	0.4	44.8	30 min. posttest soak.
5-1*	31.8		Cold propellants for sequence 5.
5-2	17.7	181.0	
5-3	14.7	121.2	
5-4	11.8	61.3	
5-5	8.7	31.3	
5-6	4.8	15.5	
5-7	4.8	9.9	
5-8	4.8	4.4	
5-9	4.8	2.0	
5-10	4.8	1.6	
5-11	4.8	20.3	
5-12	10.8	46.3	
5-13	13.8	91.2	
5-14	4.8	31.1	
5-15*	0.15		Posttest soak.
6-1*	0.16		Ambient propellants for sequence 6.
6-2	0.18	180.7	

*First test of a vacuum period.

TABLE 40. TEST CONDITIONS (Continued)

Test Seq. No.	Duration Sec.	Pretest Coast Time, Sec.			Comments
6-3	0.20	119.7			
6-3A	0.18	55.9			
6-4A	0.20	15.7			
6-5	0.20	60.8			
6-6	0.20	31.1			
6-7	0.25	6.3			
6-7A	0.26	5.1			
6-8	0.27	2.5			
6-9	0.16	(14 min.16 sec.)			
6-10	0.23	5.2			
6-11	0.20	45.4			
6-12	0.16	2.7			
6-12A	0.17	3.1			
6-12B	0.16	7.6			
6-13	0.04	45.9			10 minute posttest soak.
			P_c, psia	O/F	Comments
7-1*	9.7		125	1.45	Cold fuel, ambient ox., 9:1 nozzle for seq. 7 & 8.
7-2*	9.7		125	1.65	
7-3	9.7		100	1.65	
7-4	9.7		100	1.45	
7-5	9.8		125	1.45	
7-6	9.8		125	1.85	Posttest purges on tests 6-13
7-7	34.7		125	1.65	
7-8	4.7		80	1.65	
7-9	4.7		70	1.65	
7-10	4.7		60	1.65	
7-10A	4.7		70	1.45	
7-12	4.7		60	1.45	
7-13	4.7		60	1.65	
7-14	9.7		125	1.65	30 min. posttest coast.
8-1*	33		125	1.8	Injector BLC orifices plugged for sequence 8.
8-2	10		140	1.75	
8-3	10		140	1.55	
8-4	10		125	1.55	
8-5	10		110	2.0	
8-6	10		109	1.6	
8-7	10		135	2.0	
8-8	10		109	1.5	
8-9	10		106	2.0	
8-10	10		126	1.8	30 min. posttest soak.

* First test of a vacuum period.

A series of tests (sequence 5) was conducted with coast times ranging from 0.3 to 180 seconds wherein the engine was fired 1 second each time between coast periods. This was termed a warm-engine start and represents the minimum firing duration required of the OME. Maximum 'g' levels at start and thrust overshoots were only 20 g's and 120 percent, respectively. These tests were conducted with ambient temperature propellants.

A final series of restart tests (sequence 6) was conducted with the engine being fired for a duration of only 0.2 seconds between coast periods. The coast periods ranged from 2.5 seconds to 14-1/4 minutes. Maximum 'g' levels were about 20 g's at ignition for all coast times. However, acceleration spikes as high as 180 g's occurred at oxidizer prime (before ignition) for long coast times. The maximum thrust overshoot of 150 percent occurred at a coast time of 2.5 seconds but there was considerable scatter in the data. Ambient temperature propellants were used.

No hardware damage was incurred as a result of any of these tests which indicated that the OME can be safely restarted without any limit on the coast time.

A series of tests (sequence 7) of 5-second durations were conducted with unsaturated propellant at lower than nominal chamber pressure to investigate engine operating characteristics under propellant tank blowdown conditions. Tests at 80 and 75 psia chamber pressure resulted in chugging at start which damped out during the tests. At 65 psia chamber pressure, the chug persisted throughout the test. The chugging occurred at frequencies of 115 to 310 Hz and did not appear to be detrimental to the engine. The test results indicate that under conditions of smoothly decaying tank pressures and unsaturated propellants the engine could probably blowdown to approximately 65 to 75 psia chamber pressure without chugging.

A fuel depletion test was conducted for a duration of 4.5 seconds. The test was started with very little fuel in the fuel tank and ended with an indicated mixture ratio of 4.4 although assessment of the mixture ratio is difficult because the test data indicate that slugs of helium were also entering the thrust chamber. After the test, the thrust chamber was observed to have a number of blue streaks in the combustion zone particularly in the converging section. A dye penetrant test on the thrust chamber did not indicate any cracks or leaks and testing was continued.

Supplementary boundary layer coolant is supplied to the thrust chamber by orifices in the periphery of the injector. These orifices were

plugged for one sequence of tests (sequence 8) which were conducted over a range of chamber pressures and mixture ratios. Comparison of these test results with results of the Phase 1 tests indicate that at nominal conditions a performance gain of approximately 1.5 seconds I_s results from the elimination of the BLC. Concurrently, the heat load to the regeneratively cooled chamber increased by approximately 26 percent which would result in a safety factor of 1.2 at off-design conditions (P_c = 120 psia, O/F = 1.73, T_f = 100F).

No hardware damage resulted from these latter series of tests. The injector and chamber are usable for further testing if required.

Start Transients

Facility and engine ducting were configured to simulate, as far as possible, the volumes and lengths of the current Orbit Maneuvering System propellant feed system. A brief investigation of the effects of propellant valve sequencing on start transient characteristics was made during the first four tests of Sequence 3. These tests also provide a comparison of the first start transient of a vacuum period with subsequent starts. Previous experience had indicated, in general, slightly higher g-loads at start on the first tests. Therefore, the first and second tests were both conducted with the fuel valve opening signal delayed 100 msec relative to the oxidizer valve signal. The delay was reduced to 50 msec on the third test and to 0 msec (simultaneous signals) on the fourth test. Figure 107 is a reproduction of a typical oscillograph derived from the analog tape for Test 2 of Sequence 3. Comparison of the start transients for Tests 1 and 2 indicated a more gradual oxidizer injection pressure rise at oxidizer prime and a complete absence of pressure surges at ignition in the oxidizer injection pressure on the first test. The data indicated a hard liquid system for the second test and the presence of some gas in the system for the first test.

The fuel injection pressure transients also indicated a more gas-free system on the second test by virtue of the more regular and higher frequency oscillation which occur during the priming transient. Gases in the fuel at ignition would lead to the smoother transient indicated in thrust for the first test. The thrust transient on the first test indicated a more rapid rise to a low thrust value than on the second test. This rise was accompanied by accelerometer activity not present on the second test. The engine was purged completely before each of these tests so it is presumed that no propellants existed downstream of the propellant valves in either case. It therefore appears that small amounts of gas existed in the propellant feed system upstream of the valves on the first test and that the second test is therefore a more typical start.

├─10 MS─┤

THRUST

ACCELEROMETER

FUEL INTERFACE PR.

OXID. INTERFACE PR.

FUEL INJECTION PR.

OXID. INJECTION PR.

CHAMBER PR.

FOLD-OUT #1

FIGURE 107 START TRANSIENT FOR TEST IHT1-3-2

R-9686
6-59

FOLD-OUT #2

A comparison of the start transients of Tests 2 and 4 indicated that simultaneous signalling of the propellant valves on Test 4 moved the oxidizer injection prime point much closer to the fuel injector prime point, but the effect on the ignition characteristics is not significant for this range of oxidizer leads. The reason for this is that the oxidizer injection prime transient is completed by the time the fuel injection transient and ignition occurs even with simultaneous valve signals. In fact, the shape of the transient indicated that fuel injector prime could occur 20 to 30 milliseconds earlier without significantly affecting the ignition characteristics. However restart characteristics could be affected because short coast times tend to reduce the oxidizer lead even further. Thrust overshoot and accelerometer data tabulated in Appendix A of the Task XII-Phase II Data Dump indicate that these characteristics did not vary much between Tests 3-2 through 3-4.

The start transient for Test 3-18A is shown in Fig.108. The high acceleration spike on this test occurred not at ignition but at the time the oxidizer injector primed. The ±2000 g accelerometer (not recorded in Fig.108) indicated 1500 g at that time. The high value of the spike in oxidizer injection pressure at prime implies a detonation in the oxidizer dome at this time. (The instrumentation is nearly saturated so that the actual value of the spike is even higher than indicated). It is suspected that the dome was contaminated even though the injector was purged before the test.

An accelerometer spike of lesser magnitude occurred at ignition. The magnitude of this pike was more typical of values recorded at the start of a first test of a vacuum period. Note the wide variation in accelerations recorded by accelerometers at different locations on the chamber. As an indication of the physical significance of the magnitudes of these acceleration, it is noted that a light tap with a hammer on the injector dome resulted in accelerations of up to 500 g's.

Engine Shutdown and Soakout Characteristics

A typical shutdown transient after a long duration test without posttest purges is shown in Fig.109. Approximately 0.6 seconds after the shutdown signal considerable accelerometer activity begins and lasts for up to several seconds. Because of this phenomenon, it was difficult to evaluate g-loads at restart for test with coast durations less than 5 seconds. Posttest accelerometer readings of several hundred g's were occasionally recorded. "Football" type oscillation of 2400 Hz were frequently encountered on one of the accelerometers whereas the data from the other 3 accelerometers was fairly random.

START SIGNAL

TIME →   10 MSEC
|—|

CHAMBER PRESSURE

TEST IHT 1-3-18A

ACCELEROMETER 4097D ±1000 'g' DOME

ACCELEROMETER 4008D ±200 'g' FLANGE

OXID. INJECTION PRESS

FUEL ISOLATION VALVE POSITION

ACCELEROMETER 4007D ±200 'g' DOME
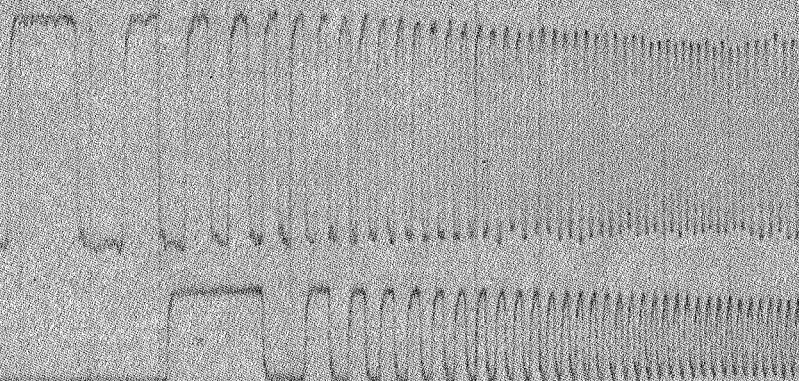
OXID ISOLATION VALVE POSITION

FUEL INJECTION PRESS.

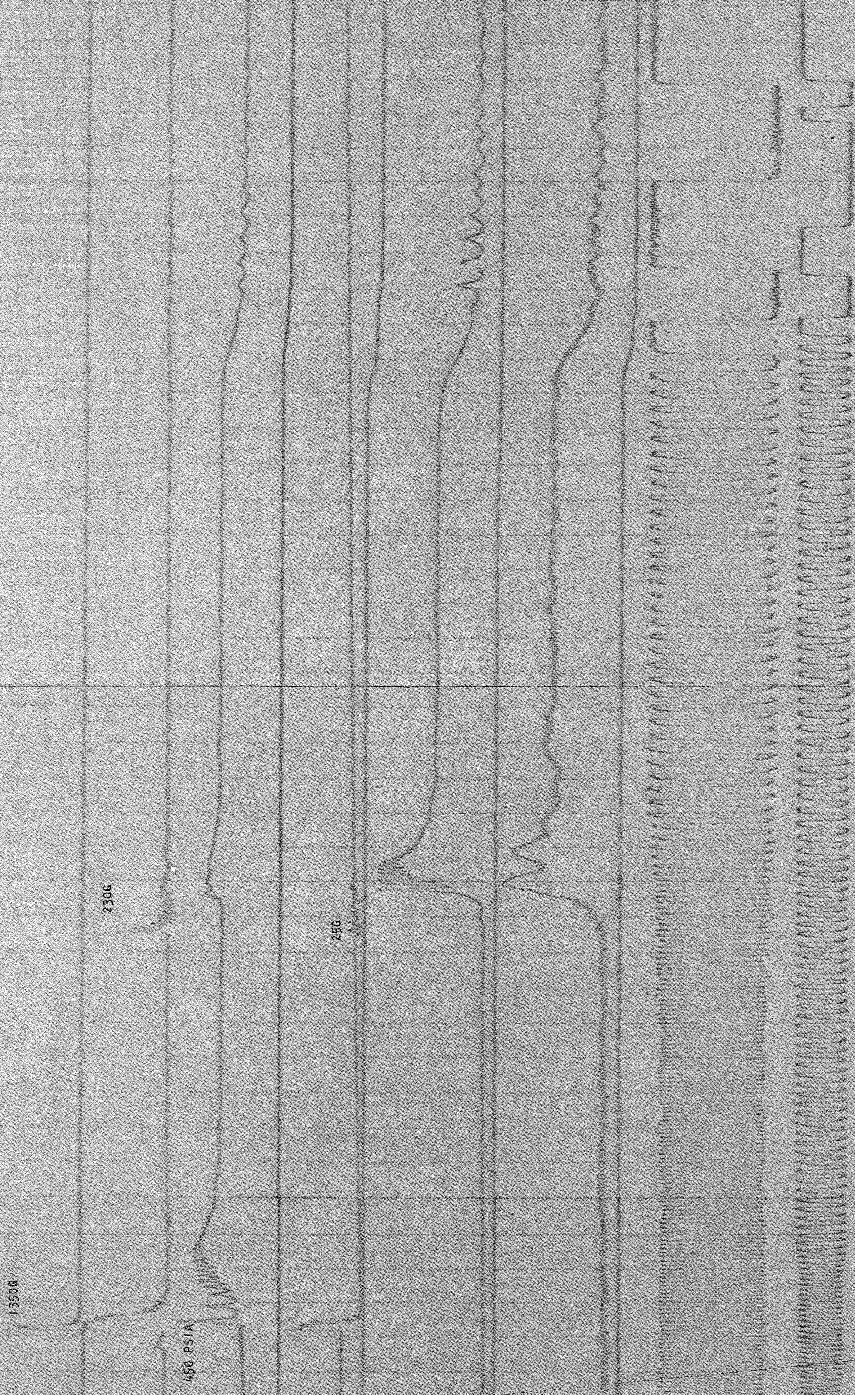FUEL SHUTOFF VALVE POSITION

THRUST

OXID. SHUTOFF VALVE POSITION

FUEL FLOW

OXID. FLOW

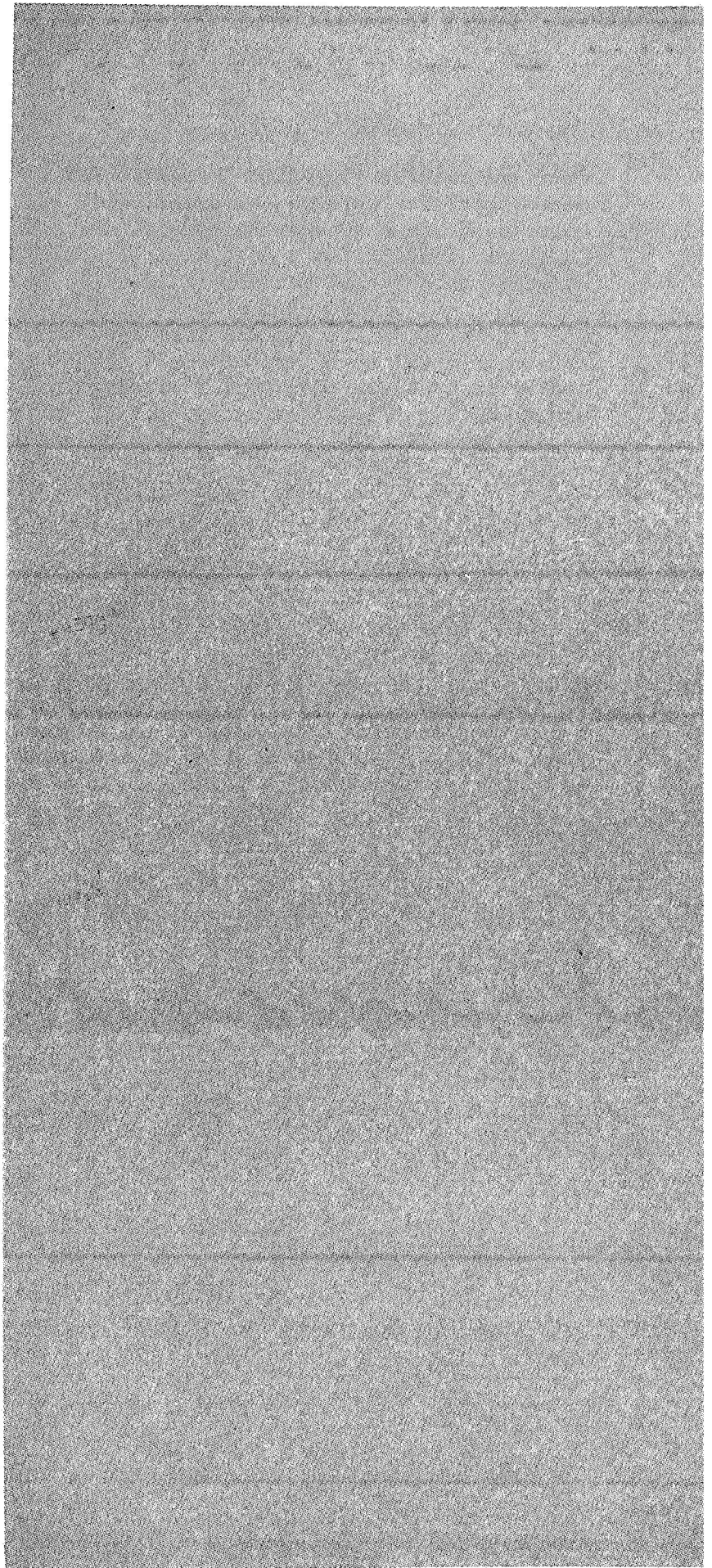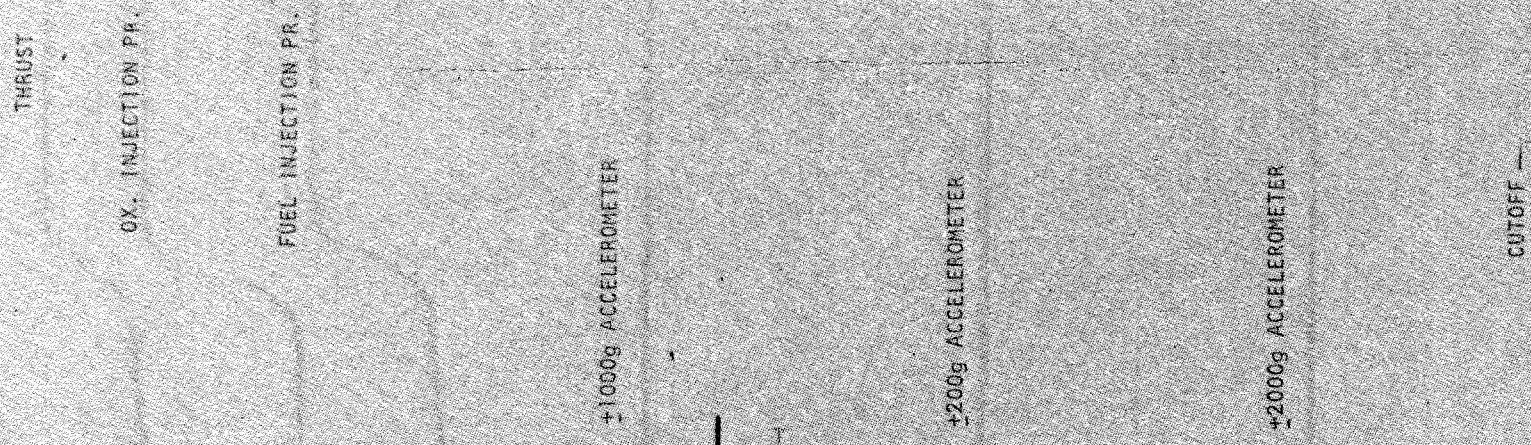START SIGNAL

FOLD-OUT #1

FIGURE 108 TEST IHT1-3-18A

1350G

230G

25G

450 PSIA

R-9686
6-61/6-62

FOLD-OUT #2

FOLD-OUT #1

FIGURE 109 SHUTDOWN TRANSIENT FOR TEST 1HT1-3-4

THRUST

OX. INJECTION PR.

FUEL INJECTION PR.

±1000g ACCELEROMETER

TIME
100 MS

±200g ACCELEROMETER

±2000g ACCELEROMETER

CUTOFF

R-9686
6-63

FOLD-OUT #2

Fuel and oxidizer injection pressures at the beginning of the acceler-
ometer activity were in the order of 40 and 20 psia respectively, which
corresponds to a saturation temperature of 240F for MMH and 60F for NTO.
On short duration tests such as 3-18 and 3-18A which were of 0.15-second
duration no posttest accelerometer activity occurred.

On Test 3-18C, which was 0.9-second duration, accelerometer activity did
not occur until approximately 1.2 seconds after shutdown and was signifi-
cantly less severe than that following long-duration tests. Sequence 4
was a series of 1-second duration tests with varying coast times.
Accelerometer activity began 1.4 seconds after shutdown for the first
tests and occurred at progressively shorter times, such that, at the
latter tests the activity was commencing at 0.5 seconds after the shut-
down signal.

Sequence 6 included a series of 16 tests of approximately 0.2-second
duration. The only posttest accelerometer activity recorded during this
test sequence was after Test 8 which was the longest duration (0.27 sec)
test of the series. The activity was quite mild and occurred 1.7 seconds
after the shutdown signal. The posttest value of the regenerative thrust
chamber wall temperature was the highest on Test 8. At the time the
accelerometer activity occurred, the highest temperature was 235F
measured at the -8 inch station on the chamber. Fuel injection pressure
at this time was approximately 20 psia corresponding to a saturation
temperature of 200F. Coolant inlet manifold temperatures were quite cool
averaging approximately 50F.

Thus, it appears that the posttest accelerometer activity depends upon
the engine temperature at shutdown which, in turn, is a function of the
test duration.

The accelerometer activity may be due to violent boiling of MMH in the
regenerative coolant jacket or NTO in the injector. However, a more
probable source of the effect is suggested by the following data (all
times referred to the shutdown signal).

Test IHT 1-	Time of Accelerometer Activity, Sec.	Time of Purge Initiation, Sec	
		Oxidizer	Fuel
3-4	0.6 to 4.6	None	None
3-5	0.7 to 4.6	None	None
3-6	0.7 to 3.6	2	7
1-12	0.7 to 2.7	2	7
7-6, 7-7	None	-1	-1

These tests were all of sufficiently long duration (>5 sec) to heat the
engine. When the oxidizer purge only was initiated manually approximately
2 seconds after the shutdown signal, the duration of the accelerometer
activity was significantly reduced. When the purges were initiated dur-
ing the shutdown transient (by setting the purge pressures lower than
steady-state injection pressures prior to the shutdown signal) the
characteristic accelerometer activity did not occur. This suggests that
for an unpurged hot engine shutdown, the oxidizer drains out of the duct
while fuel boils out of the chamber jacket giving rise to sporadic low-
level combustion and popping. The oxidizer purge blows the NTO out of
the duct rapidly and eliminates the low-level combustion. With a cold
chamber (firing times ≤ 0.2 sec) the fuel comes out of the jacket very
slowly so that the oxidizer simply drains out of the injector and cham-
ber without combusting. Although the accelerometer activity is quite
pronounced after cutoff the effects are not manifested in either thrust
or injector pressures (the chamber pressure measurement did not have
rapid response characteristics) and are probably not harmful to the
engine.

Figures 110 and 111 represent typical soakout transients at selected loca-
tion for an engine which has been fired long enough to have reached
thermal equilibrium. The test shown was a 5-second test after a hot
engine restart. Regenerative chamber outer wall temperatures at the
-16 inch location, behind acoustic cavities, are shown in Fig. 108 .
The wall at this point receives heat inputs from the acoustic cavity
dams and the injector and is cooled by MMH being boiled in the jacket.
The heat inputs at first predominate and the temperature rises for
approximately 40 seconds, after which the cooling injector and cavity
dams cannot keep up with the cooling capability of the MMH and the
temperature again decays. When the MMH is depleted to the point that
liquid can no longer percolate up the channel to cool this region, the
temperature again rises in response to the injector heat input, reaches
a maximum, and decays as heat is transferred to the rest of the chamber
and the environment. The maximum temperature at this location was less

SUBSYSTEM 6K OME   SERIES RD/IHT 1 - 3
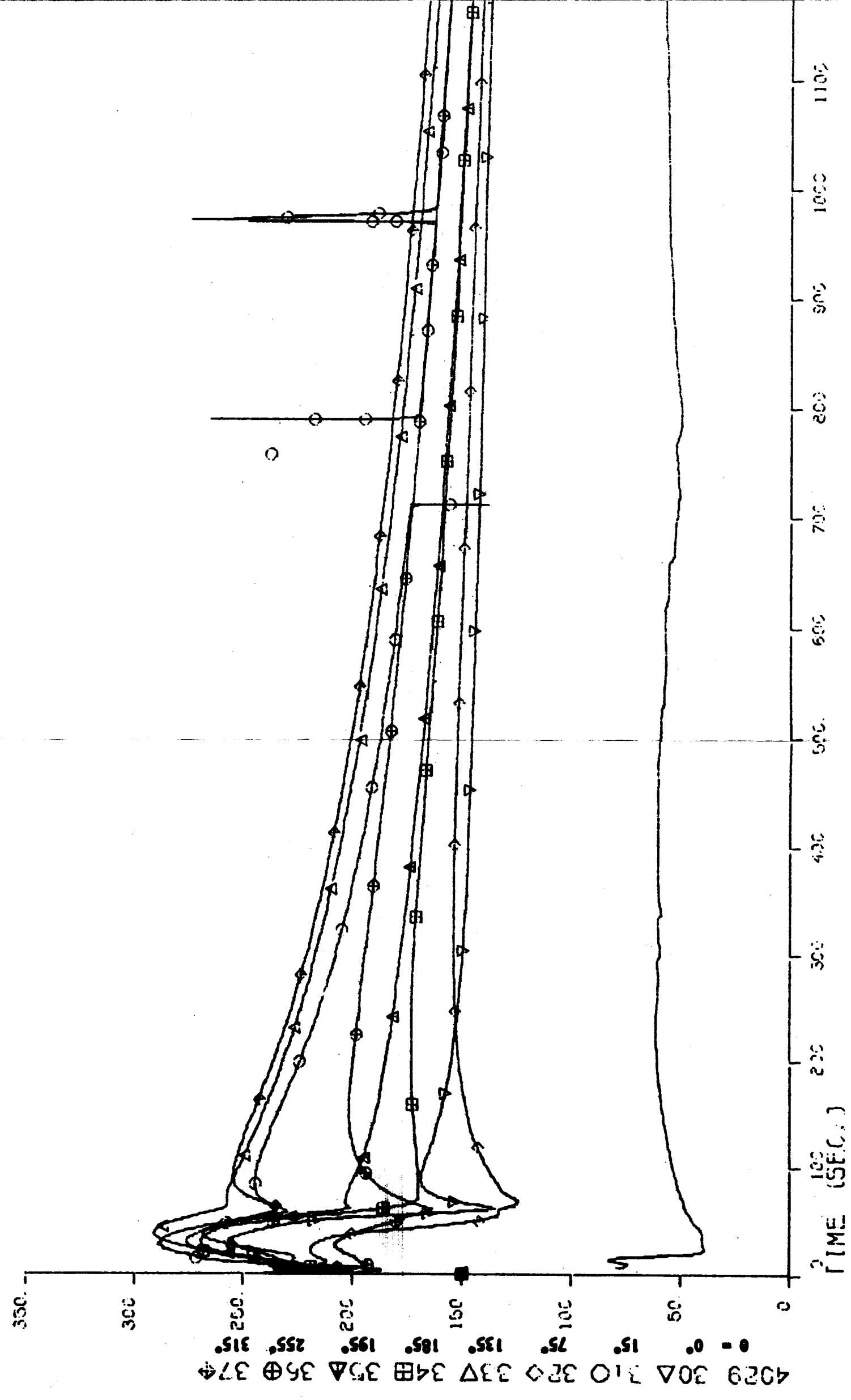
TEST 17   RUN 1

FOLD-OUT #1

FIGURE 110 NICKEL WALL TEMPERATURE AT X = -16 INCHES
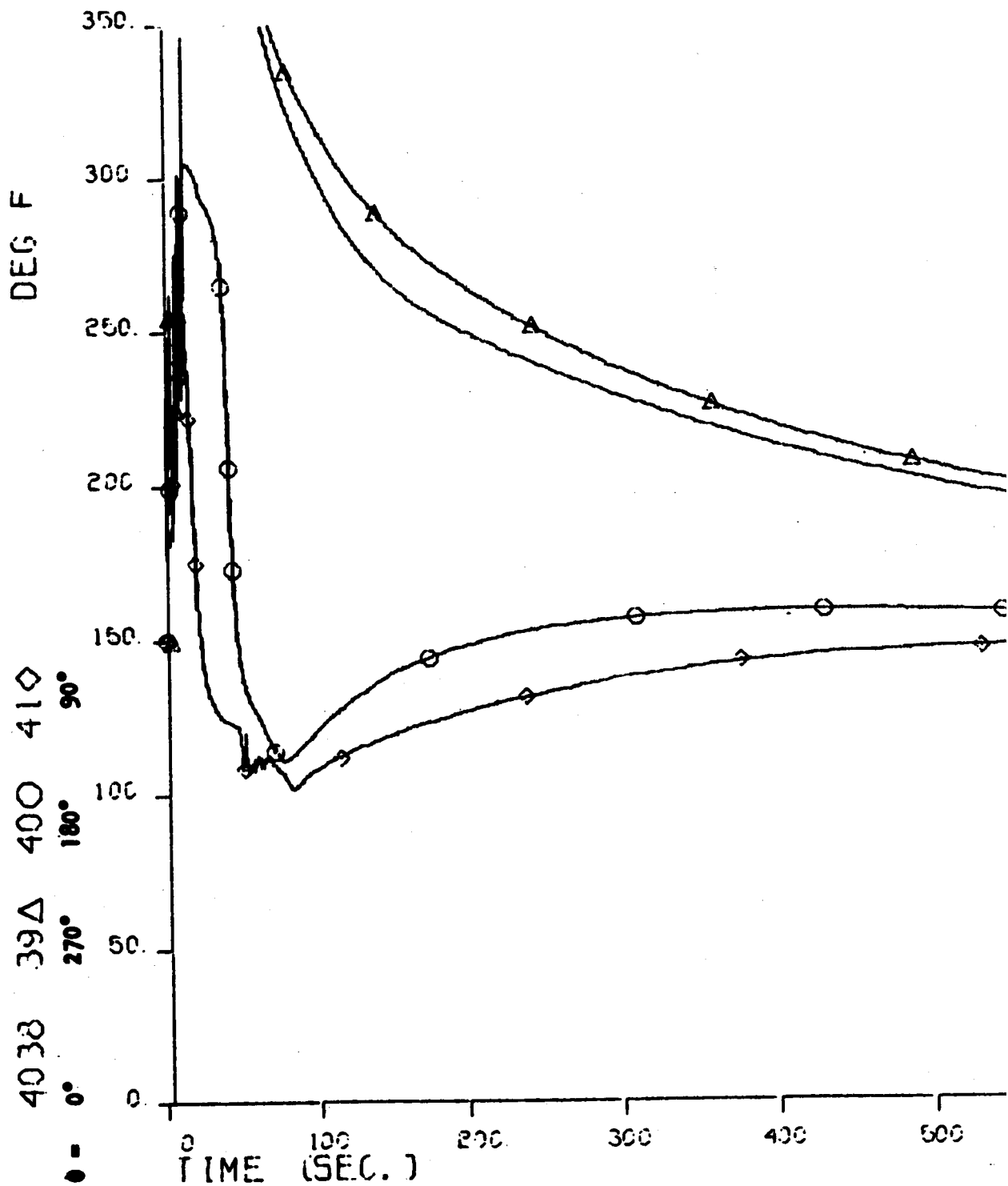
OX. DUCT

1200   1300   1400   1500   1600   1700   1800
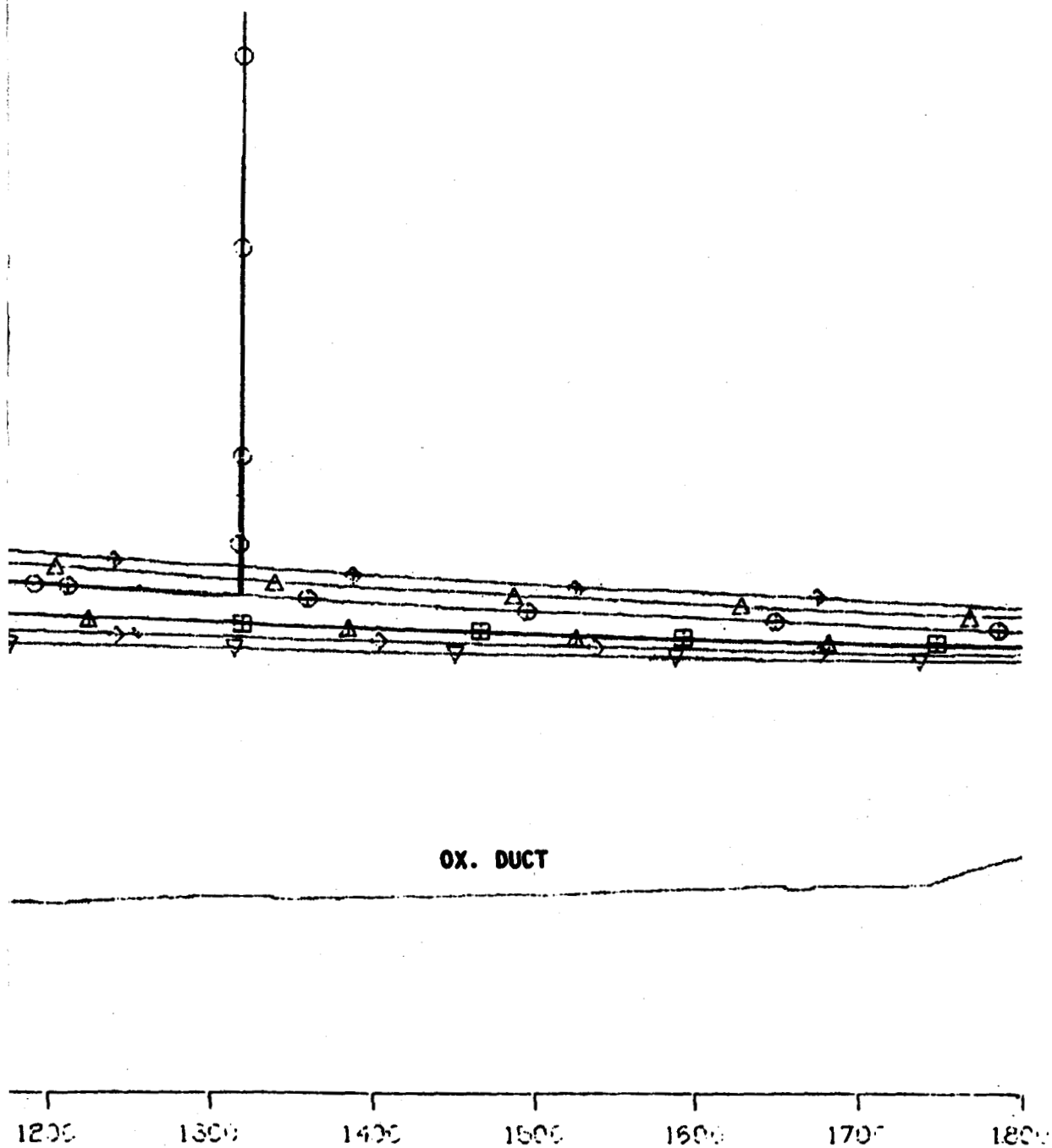
FOLD-OUT #2   R-9686
                     6-66

SUBSYSTEM 6K OME   SERIES RD/IHT 1 - 3

TEST 17   RUN 1

DEG F

TIME (SEC.)

FOLD-OUT #1

FIGURE 111 NICKEL WALL TEMPERATURE AT X = -13 INCHES
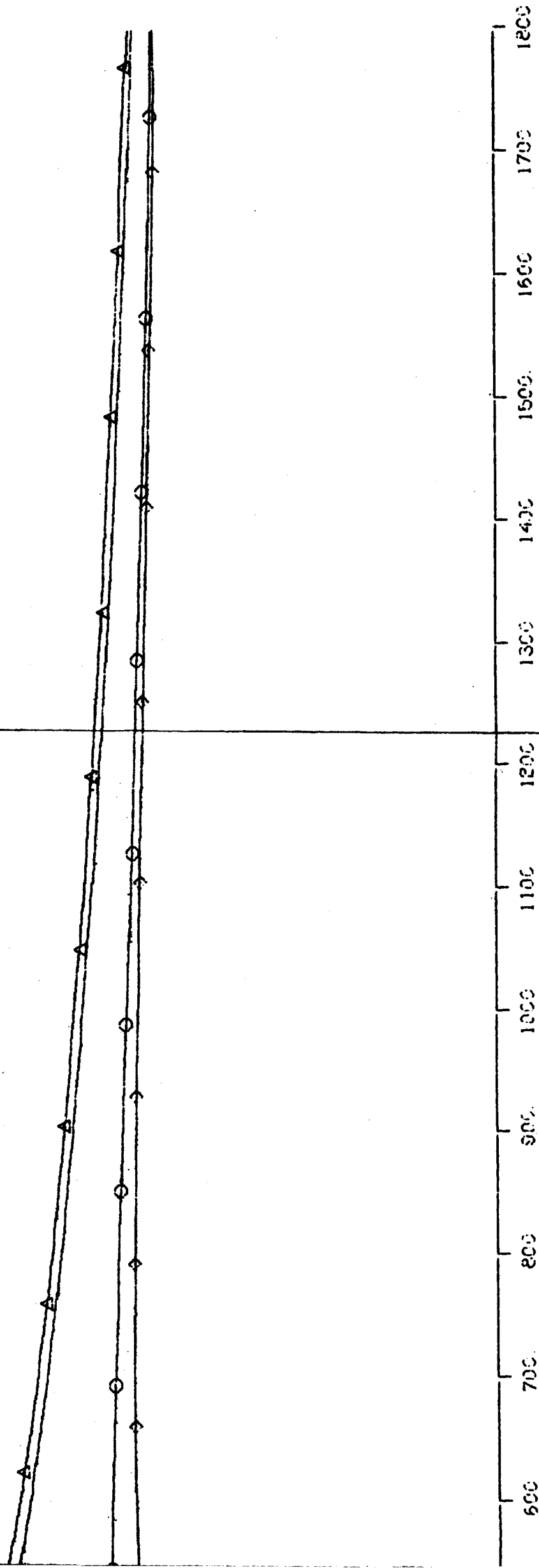
R-9686
6-67

FOLD-OUT #2

than 300F, well below the decomposition temperature of MMH.

The back wall temperatures at the -13 inch location are plotted in Fig. 111. The upper two curves indicate that the cooling effect of the MMH is not being felt at these locations. The maximum temperature reached on this test at this location was 445F, the highest on the regenerative chamber wall. That the chamber can be safely started with channel wall temperatures much higher than this value has been demonstrated in the heated tube test program of Task IX.

Temperatures at the coolant inlet are plotted in Fig. 112. After shutdown the temperatures generally indicate a constant temperature value until approximately 60 seconds after which they decay at the same rate. As the coolant is exhausted at each thermocouple, the thermocouple is heated by the surrounding metal and indicates an increasing temperature. The minimum values therefore indicate the time of fuel depletion at each thermocouple location. The thermocouple measuring the temperature indicated by the curve coded with a triangle is near the top of the inlet manifold and is depleted very soon. The other thermocouples are further down in the manifold. One thermocouple, indicated by the data coded with a diamond, is faily close to the lowest point in the inlet manifold and, thus, its turnaround point indicates nearly complete depletion of fuel in the manifold. This occurs at 95 seconds or approximately 90 seconds after cutoff.

A summary of propellant depletion times and conditions for typical vacuum soakout tests is given in Table 41 . The fuel and oxidizer interface temperatures are measured upstream of the valves and are given at the start of the firing as indications of propellant temperatures during the test. Test durations quoted are the durations during which the thrust exceeded approximately 90 percent of the steady-state value. The fuel inlet thermocouples measure the temperature of the fuel at the lowest elevation in the system. The fuel depletion times were determined as the time when inlet thermocouples indicated a minimum in temperature. That minimum temperature and its corresponding saturation pressure are also tabulated. For comparison the actual measured pressure, determined by averaging the low-pressure-range fuel inlet and fuel injection pressures at that time, is also presented.

The lowest elevation in the oxidizer system is in the inlet duct near the engine inlet. The oxidizer inlet duct generally drains down from the valve into the engine with a very small puddling capability at the above mentioned location. Thermocouples are welded to the top and bottom of the duct at this location. The oxidizer depletion time is taken as the time at which the bottom thermocouple indicates a minimum value. The value of that minimum and the injection pressure measured at that time are also tabulated.
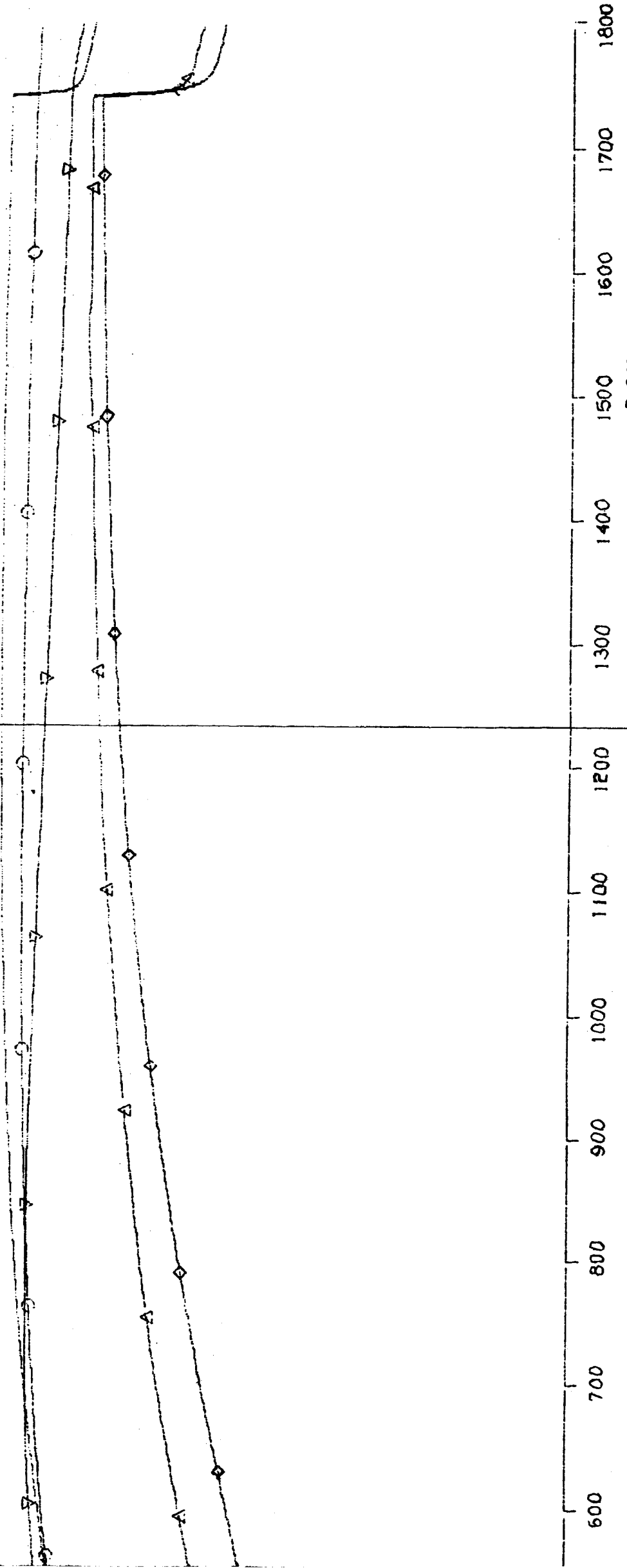
SUBSYSTEM 6K OME   SERIES RD/IHT 1 - 3
TEST 17   RUN 1
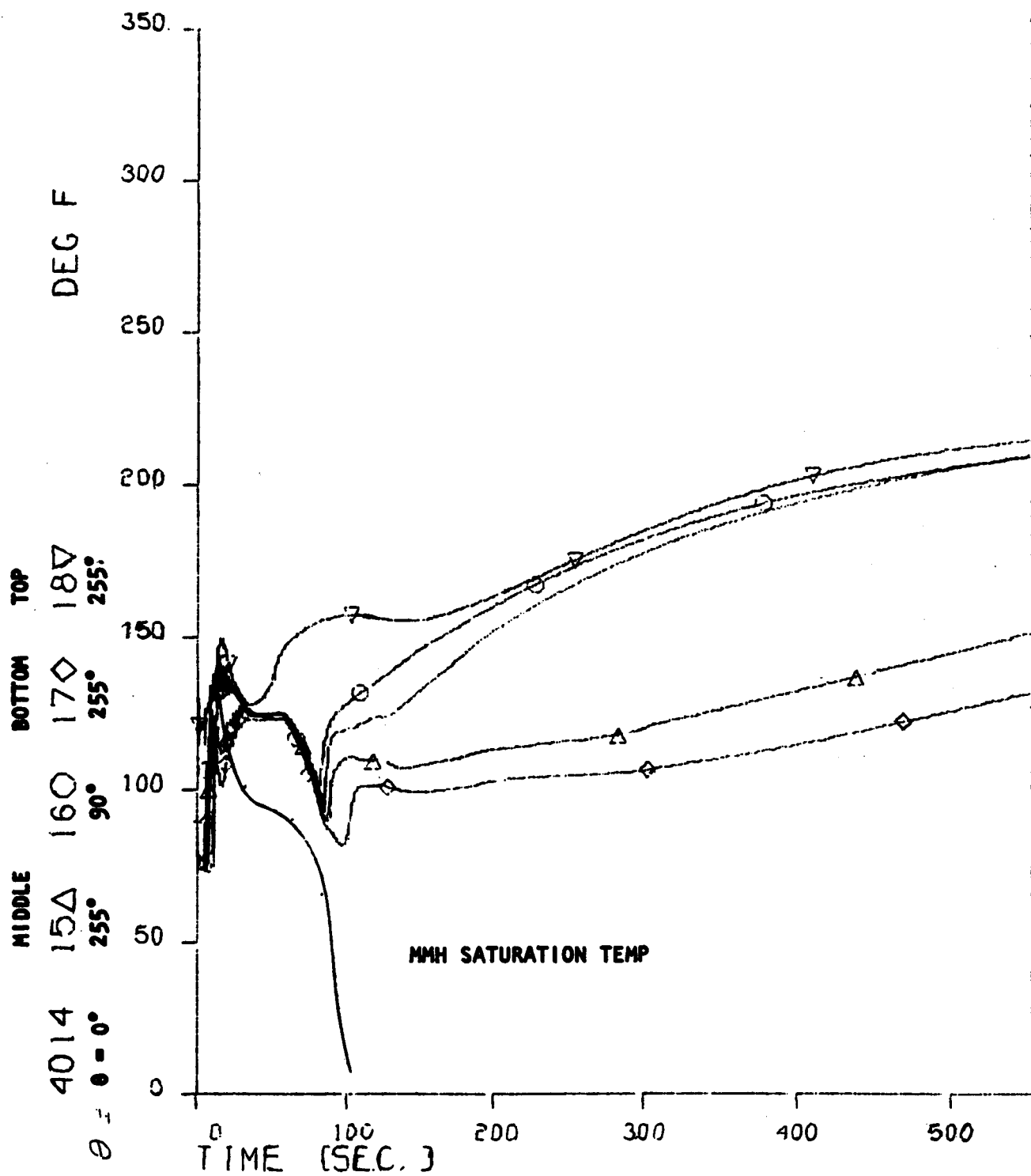
FOLD-OUT #1

FIGURE 112 COOLANT TEMPERATURE AT INLET

R-9686
6-69

FoLD-OuT #2

TABLE 41

PROPELLANT DEPLETION TIMES

| Test | Test Duration Sec | Fuel Interface Temp., F | Conditions at Fuel Depletion | | | | Ox. Interface Temp., F (@ t = 0 sec) | Ox. Depletion Time, Sec. | Min. Ox. Duct Temp. F | Meas. Ox Press. @ Depletion, psia |
			Time, Sec.	Inlet Temp., F	P_{SAT}, PSIA	Measured Press. Psia				
3-17	4.8*	74	90	82	1.3	0.7	74	12	40	4.5
3-18C	1.0	70	180	60	0.6	0.3	68	11	29	3.9
7-14	10*	44	300	65	0.7	0.7				
3-18A	0.15	54	600**	47	0.4	0.2	66	12	24	0.9
5-15	0.15	44	3700**	38	0.3	0.3	45	12	13	4.0
6-13	0.04	73	-	64***	0.7	0.3	78	10	13	1.0
6-4A	0.20						78	12	11	3.1

*Engine hot from previous firings

**Very shallow minimums

***At end of 10-minute soak

Tests 3-17 and 3-18C were conducted with nearly ambient-temperature propellants. Test 3-16 was the last of series of hot-engine restart tests so that the engine was at thermal equilibrium after this test. Test 3-18C was a single one-second duration test corresponding to the current minimum required burn time of the OME. A comparison of the fuel depletion times of these two tests indicates that there is a factor of two in depletion times between the currently specified conditions which lead to the engine at its hottest and coldest temperatures. When a hot-engine soakout was conducted with cold fuel (Test 7-14) 300 seconds were required to deplete the fuel. No vacuum soakout tests were conducted after the engine had been fired for one second with cold fuel. However, using the previously noted factor of two in fuel depletion times for hot-engine and one-second tests with ambient fuel, it is estimated that fuel depletion will occur within 10 minutes after a one-second firing with cold fuel.

Test 3-18A, 5-15 and 6-4A were typical of short-firing bursts which might be the result of a premature shutdown signal. The posttest fuel temperature transients associated with these tests were very gradual because of the cold fuel and engine hardware making the actual depletion time difficult to determine. It appears that under these conditions, fuel can be retained in the engine for periods of 10 minutes to an hour after shutdown. The longer depletion time on Test 5-15 is probably the result of the colder fuel even though the engine hardware was somewhat colder on Test 3-18A.

One test (6-13) was conducted for an extremely short-firing time of 0.04 seconds in order to determine whether freezing of the propellants would occur with a firing duration so short as to input practically no heat into the chamber. The 10 minute vacuum soak period was not sufficiently long to determine minimum fuel temperatures. However, the temperatures were sufficiently high (70F) and falling at so slow a rate as to indicate that freezing of the fuel was not a likelihood.

In all cases, the measured pressures at the fuel inlet and injector were lower than saturation pressure at the time of depletion. This provided additional evidence of the absence of fuel in the system at that time.

Very little oxidizer accumulates in the system as is evidenced by the 10- to 12-second oxidizer depletion times for all of these tests. The relative depletion times of the fuel and oxidizer indicate that engine restarts between approximately 10 to 100 seconds after shutdown would result in a start with residual fuel only in the engine. A series of oxidizer valve only cycling tests were conducted during the program with 70F oxidizer. The duct temperatures always remained above 17F during the post flow soakout periods.

Fuel duct temperature transients were somewhat difficult to evaluate because of the thermal input from the radiation cooled nozzle. Well-defined minimums and the temperatures of the bottoms of the fuel duct near the valve and near the chamber inlet imply the presence of fuel in the duct for as long as 170 seconds after the firing.

The regenerative coolant inlet manifold is cooled during the soakout by vaporizing MMH and is heated primarily by the radiation cooled nozzle through the connecting flange. The inlet manifold reaches thermal equilibrium after approximately 30 minutes of vacuum soak after a hot-engine shutdown. The equilibrium temperatures at the zero and 90° circumferential locations is approximately 225F. The equilibrium temperature at the 180° location is approximately 190F. The minimum in the temperature transient of the fuel inlet manifold is related to fuel depletion but cannot be used to define the exact time of fuel depletion because of the massive nature of the inlet manifold.

Test Sequences 1 through 6 were run with the full length, $\epsilon = 72$, nozzle in order that the thrust overshoot might be correctly simulated. This nozzle is more massive than the flight type nozzle. The columbium nozzle, although only an $\epsilon = 9$ nozzle, was designed by thickness control to simulate the early soakout transients of a flight type nozzle. Test Sequences 7 and 8 were conducted with this columbium nozzle.

The nozzle surface and fuel inlet manifold skin temperature soakout transients are shown in Fig. 113 for Test 7-14. In comparison with the steel nozzle, the nozzle temperature decay is much more rapid. However, the affect on the fuel inlet manifold skin temperature for the first 100 to 200 seconds is quite similar. For the steel nozzle, the average inlet manifold temperature at 150 seconds is approximately 25F higher than the pretest value. For the columbium nozzle, the posttest value is approximately 15F higher than the pretest value. Thus, the thermal inputs from the steel nozzle to the fuel inlet manifold are similar to thermal inputs which may be expected from a flight type nozzle during the early soakout transient.

The steel nozzle temperature after a 1-second firing does not heat up significantly and causes very little temperature rise in the inlet manifold during the soakout transient.

Restarts

The objective of this phase of the testing was primarily to evaluate the restart capabilities of the OME and determine whether any limitations of the presently specified duty cycle exist.
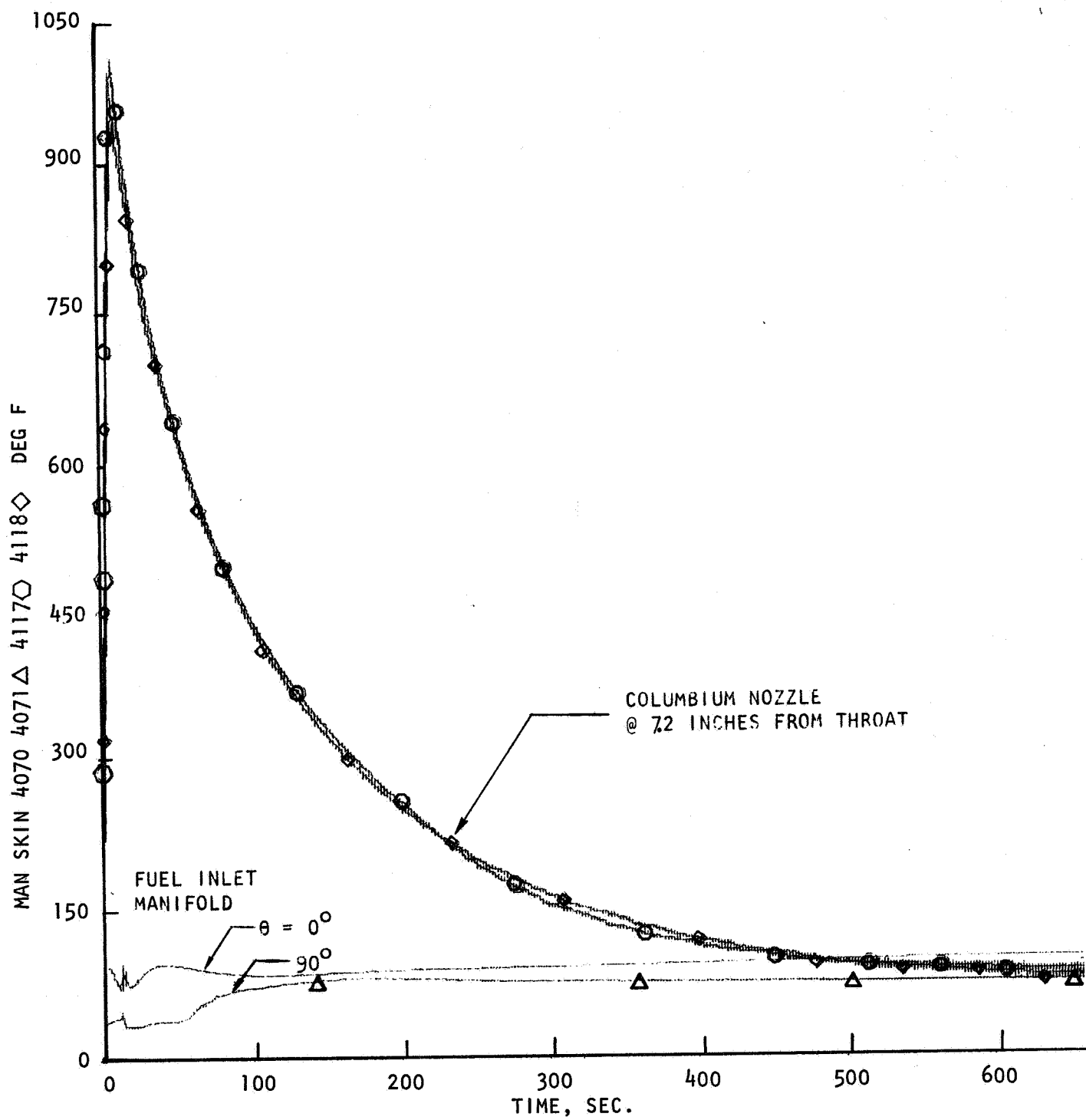
Figure 113. Columbium Nozzle and Fuel Inlet Manifold Temperatures

Conditions which were considered possible problem areas before the test program were: 1) high and low propellant and hardware temperature which might result in fuel decomposition or oxidizer freezing respectively, and 2) inversion of the nominal oxidizer lead (due to more rapid draining of the oxidizer out of the engine between restarts) which might have an adverse effect on thrust and pressure overshoots and acceleration spikes.

The test program was therefore accomplished with engine and propellant temperatures and coast times selected to generate those conditions which would be most conducive to the aforementioned potential problems.

Potential Freezing and Overheating Conditions. The oxidizer cooling effects were alluded to in the discussion of the posttest shutdown transients. The most severe conditions tested to aggravate this potential problem were the tests conducted in Sequence 6. These tests were approximately of 0.2 seconds duration so that very little heat was added to the engine and the hardware was cooled by evaporation. The test conditions and effects on the oxidizer system and chamber pressure are tabulated for Sequence 6 tests in Table 41 . As previously noted, the minimum oxidizer duct temperature occurs at approximately 10 seconds after shutdown. Therefore, those tests which have shorter coast durations than 10 seconds do not reach the minimum duct temperature. The data indicates that the duct temperature reaches the freezing point of NTO between some of the tests. However, no significant effect on oxidizer injection pressure or chamber pressure for the subsequent test was noted indicating that very little freezing of the NTO occurs during the coast period. Figure 112 is a plot of the oxidizer duct temperature transient after a 16-second coast period. The short period of oxidizer flow (approximately 0.2 seconds) is sufficient to warm the duct to 50F.

From these data it appears that repetitive tests of even 0.2 seconds duration (the currently required minimum firing duration is 1.0 seconds) would not result in significant icing of the oxidizer system with ambient temperature propellants and >1 second between tests. The only tests of greater severity which could have been imposed would be to have conducted the cycling test with 40F oxidizer at higher simulated altitudes. However, the data in Table 42 indicates that oxidizer temperature had little effect on oxidizer depletion time or minimum duct temperature as can be seen by comparing the values tabulated for Tests 5-15 and 6-4A. It therefore appears that repeated cycling even with 40F oxidizer would not cause significant freezing of the NTO.

Freezing of MMH between firings does not appear to be a problem at all. The data in Table 42   indicate that for engine firings ranging from 1 second to maximum burn durations the MMH soakout temperature will be

TABLE 42

OXIDIZER COOLING EFFECTS

Test IHT1-6-	Firing Dur., Sec	Coast Dur., Sec	Minimum Oxid. Duct Temp., F	Oxid. Inj. Press., Psia	Chamber Press., Psia
1	0.16			185	130
		181	13		
2	0.18			185	135
		20	15		
3	0.20			183	133
		56	13		
3A	0.18			184	133
4A	0.20			182	133
		61	11		
5	0.20			183	134
		31	12		
6	0.20			186	134
		6.3	30		
7	0.25			184	135
		5.1	42		
7A	0.26			184	134
		2.5	59		
8	0.27			185	137
		856	15		
9	0.16			186	134
		5.2	49		
10	0.23			184	135
		45	16		
11	0.20			185	134
		2.7	55		
12	0.16			188	138
		3.1	59		
12A	0.17			185	138
		7.6	33		
12B	0.16			185	136
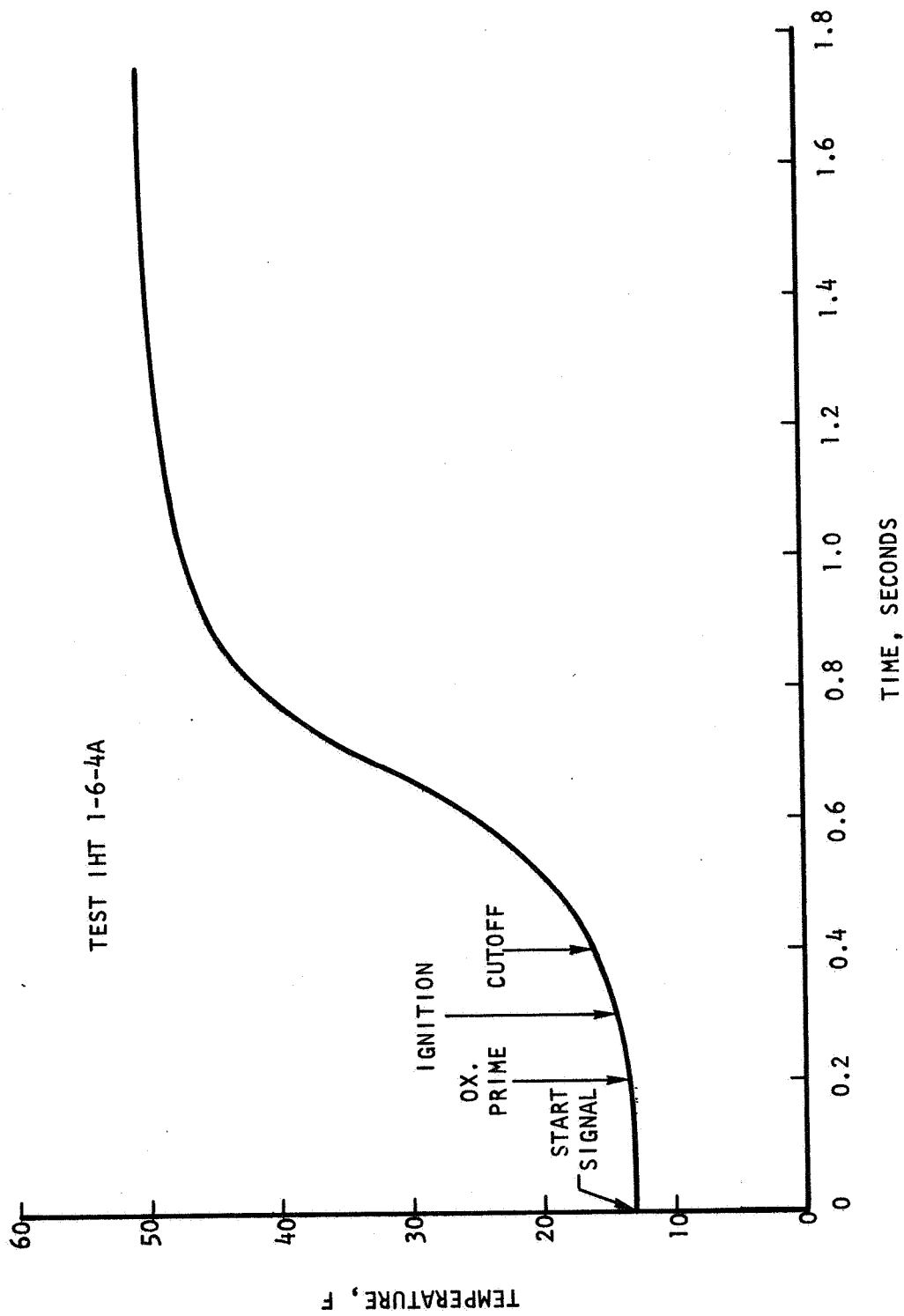
Figure 114 Oxidizer Duct Temperature Transient

approximately ambient. The MMH soakout temperatures even after very short duration firings are very far removed from the freezing point.

It was demonstrated that the thrust chamber could start with a hot regeneratively cooled jacket on Sequence 3. The engine was started with chamber wall temperatures approaching 400F several times. This substantiates the results of the heated tube tests conducted under Task IX of this contract. Test 3-23 was a fuel depletion test in which wall temperatures soaked out to values exceeding 500F (the instrumentation limit) with no indication of explosive decomposition or fouling of the channels.

Restart Transients. Pretest values of engine and propellant temperatures and pressures are summarized in Table X of the Task XII-Phase II Data Dump for the restart test sequences. Consistent values of the propellant interface pressures indicated that the facility was always set up to deliver the same engine inlet conditions. The most significant deviations in the interface pressures occur during the very short coast times when the system was still experiencing some pressure transients from the previous shutdown. Tank pressures were more nearly constant even for these conditions. The restart tests may be grouped into hot engine restarts, where the engine is at equilibrium temperature at shutdown; warm engine restarts, where the engine has been fired to 1 second prior to shutdown; and near-ambient engine restarts where the engine has been fired only a few tenths of a second prior to shutdown.

Ideally, the test program would be conducted by bringing the engine and all components to a uniform temperature, firing the engine, coasting the prescribed time period, restarting the engine, and returning the complete engine to the required temperature prior to the next test. Returning the engine to a specified temperature involves considerable time. The purging and flushing operations conducted in Sequence 1 indicated that the purges were not very effective in bringing the hardware rapidly to a uniform temperature and that the flushes could be a source of contamination. It was decided, therefore, not to condition the engine between tests.

Typical thrust overshoot and accelerometer data are shown in Fig.115as a function of oxidizer lead for the hot restart tests. These results were utilized in conjunction with the Sequence 3 tests to determine thrust overshoot and accelerations as a function of coast time. (The oxidizer valve was erratic during this test sequence and a direct correlation between coast time and thrust overshoot could not be obtained).
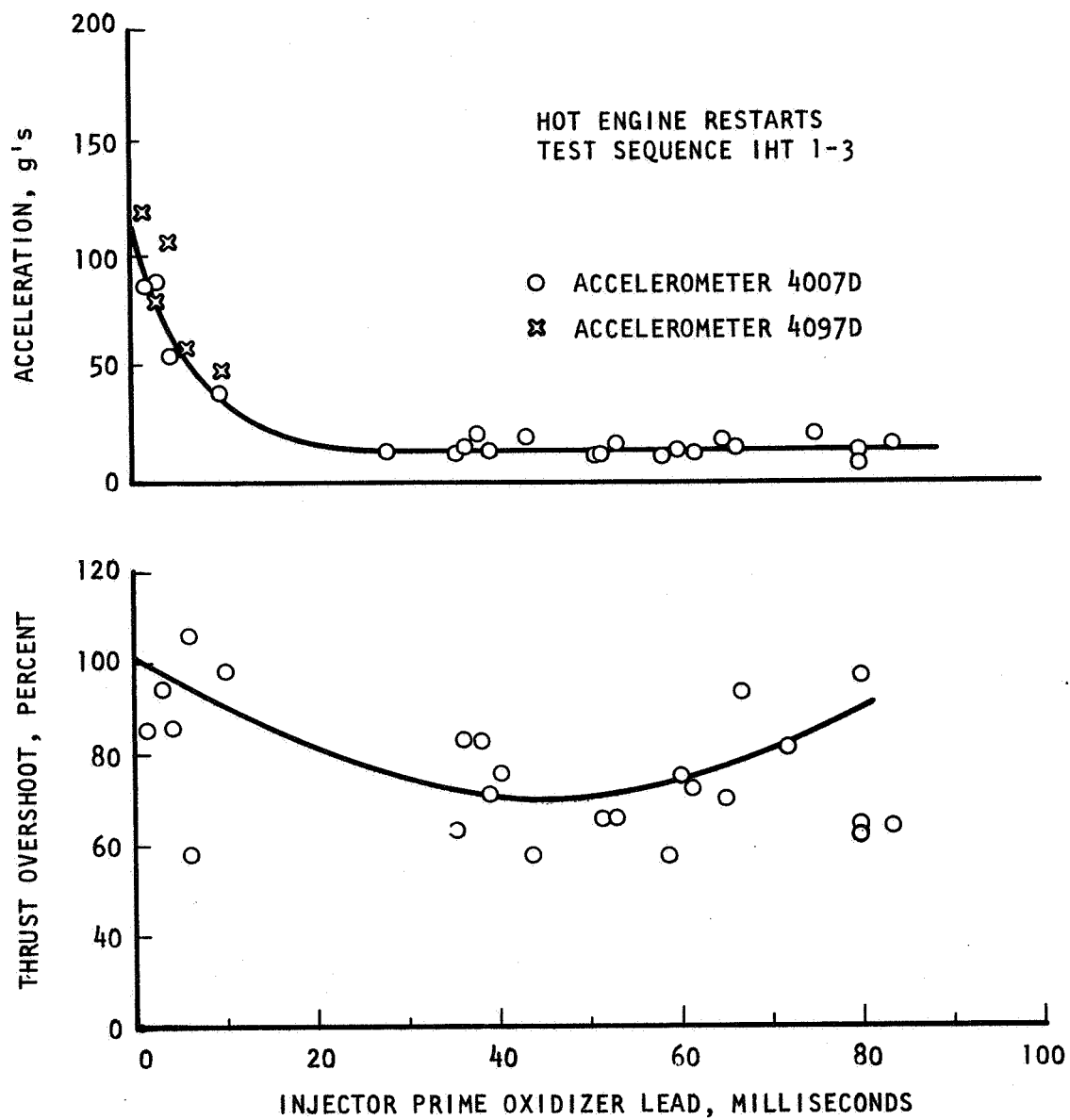
Figure 115 Accelerations and Thrust Overshoots Vs Oxidizer Lead

Thrust overshoot and accelerometer results for the various start condi-
tions are presented in Figs. 116-119 as a function of coast time. Thrust
overshoots vary from 70 percent for short-coast time to 130 percent
for long-coast times. These values can be reduced possibly by reducing
the valve opening rates. On the previous (Phase I) test program with
the same thrust chamber assembly, using facility valves, thrust over-
shoots were in the order of 70 percent for a 200 msec oxidizer injec-
tion pressure lead.

The injector priming characteristics for the four types of starts
investigated are summarized in Figs. 120-123. It should be noted that the
derived injector oxidizer lead time versus coast time curve indicates
that no matter what the coast time, the oxidizer lead would be 25 milli-
seconds or greater. This is the result of the rapid priming of the
oxidizer system relative to the priming of the fuel system. Even for
the case of a 10-second coast period where the propellant depletion data
indicated that no oxidizer remained in the system while significant
amounts of fuel did exist, the oxidizer system refilled completely in
a shorter time than that required to fill the fuel side. Thus, the
higher accelerations related to the short oxidizer leads experienced
during Test Sequence 3 would not exist in a system wherein the valves
operated simultaneously. Accelerations in the order of 15 g's would
result for all coast times.

Throttling Tests

Test Sequence 7 included a series of tests the purpose of which was to
determine the level to which chamber pressure could be reduced before
chugging would occur and the effect of mixture ratio on this minimum
pressure level. Discrete 5-second tests were conducted (as opposed to
continuous blowdown tests) to minimize facility hyperflow time. Cold
fuel (40F) was used to enhance the regenerative coolant safety factor
at low chamber pressures. Propellants were not saturated with helium
for Sequences 7 and 8.

These tests (7-7 through 7-14) were conducted with unsaturated propel-
lant using the facility feed-system configuration which simulates the
OMS. Tests 7-2 and 7-4 were moderately low-pressure tests conducted
with the external facility propellant tanks. Based on the stiffness
factor, $\sqrt{\Delta P / \dot{w}}$ (where ΔP is the difference between propellant tank and
chamber pressures, and $\dot{w}$ is the propellant flowrate) the feed system
using external oxidizer tanks is 3 percent stiffer than the OMS simu-
lated system and the feed system using external fuel tanks is 8 percent
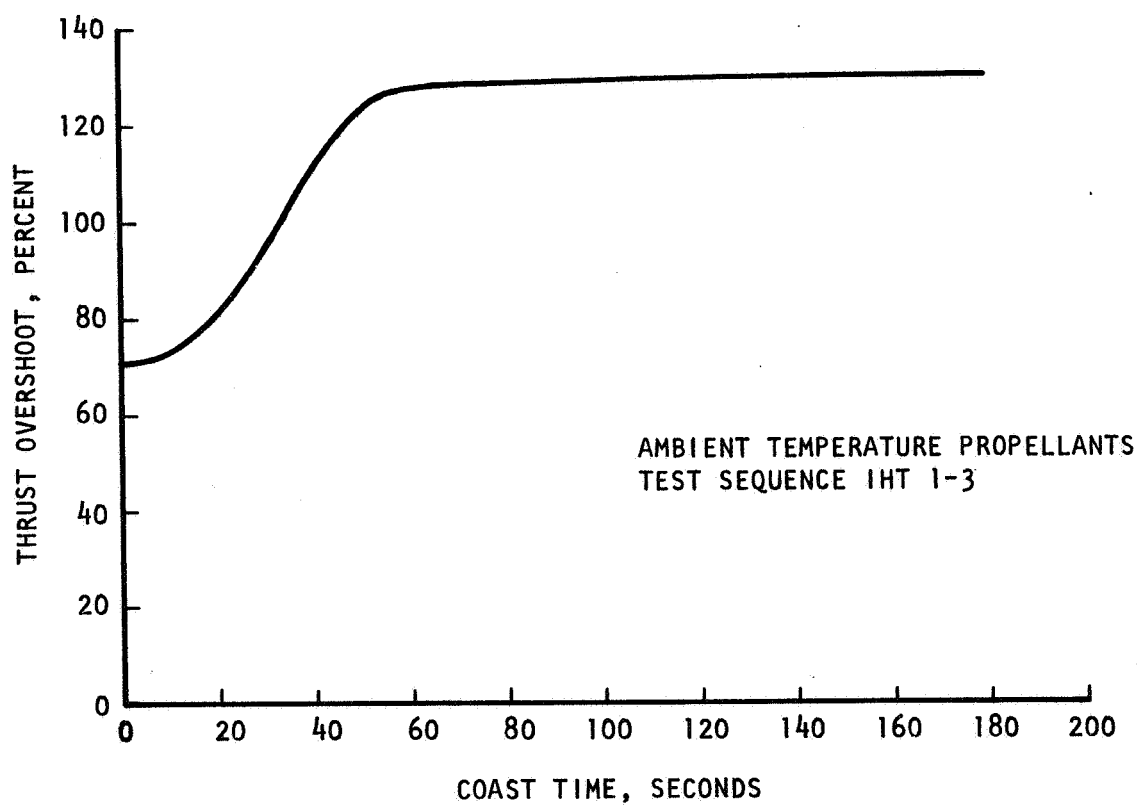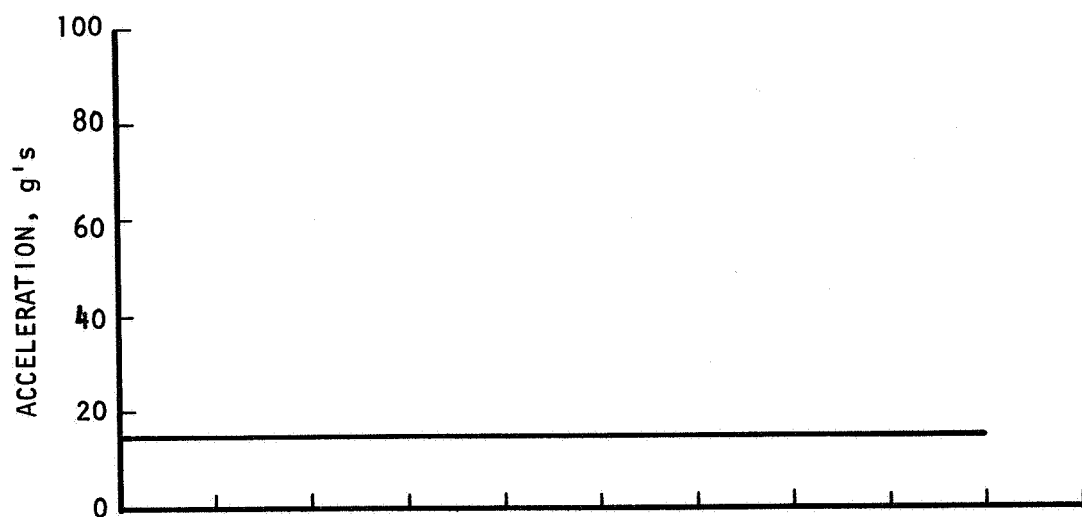stiffer than the corresponding OMS system.

Figure 116   Accelerations and Thrust Overshoots For Hot Engine
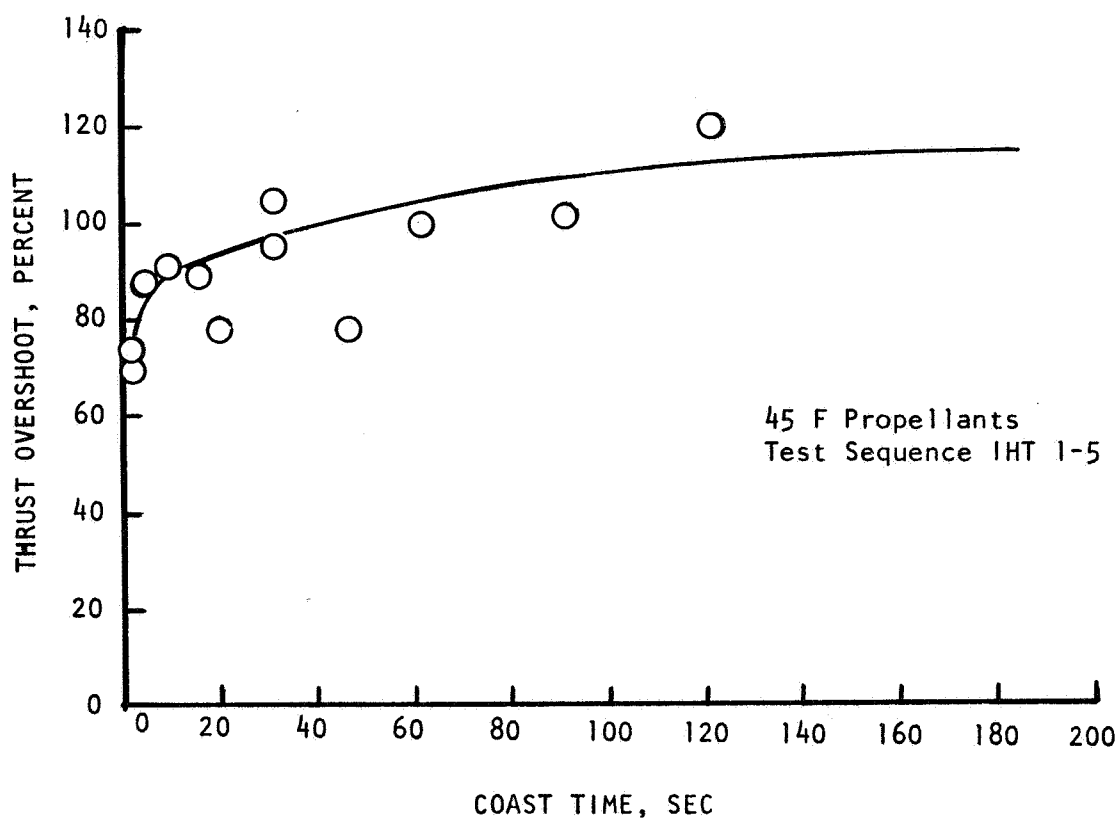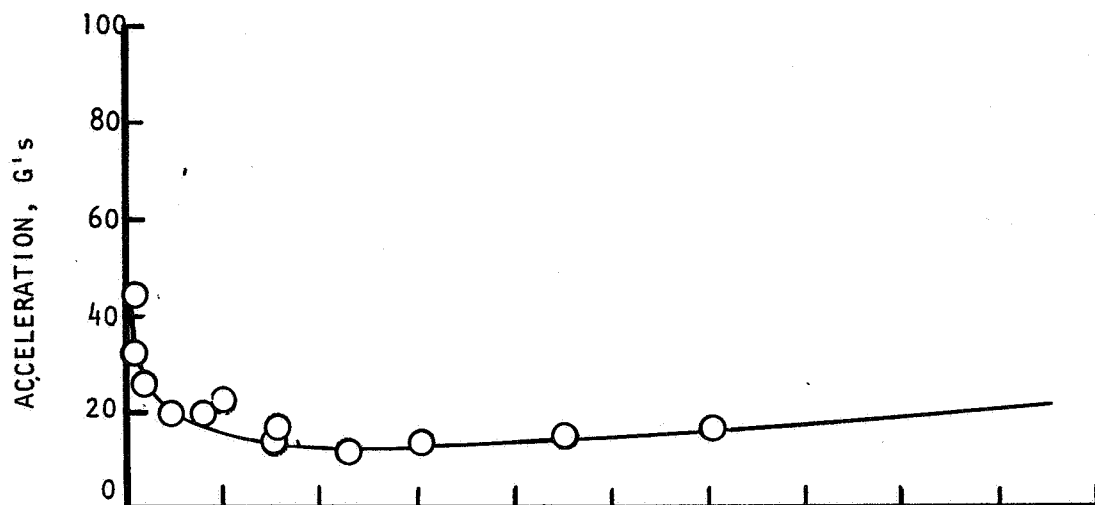Restarts

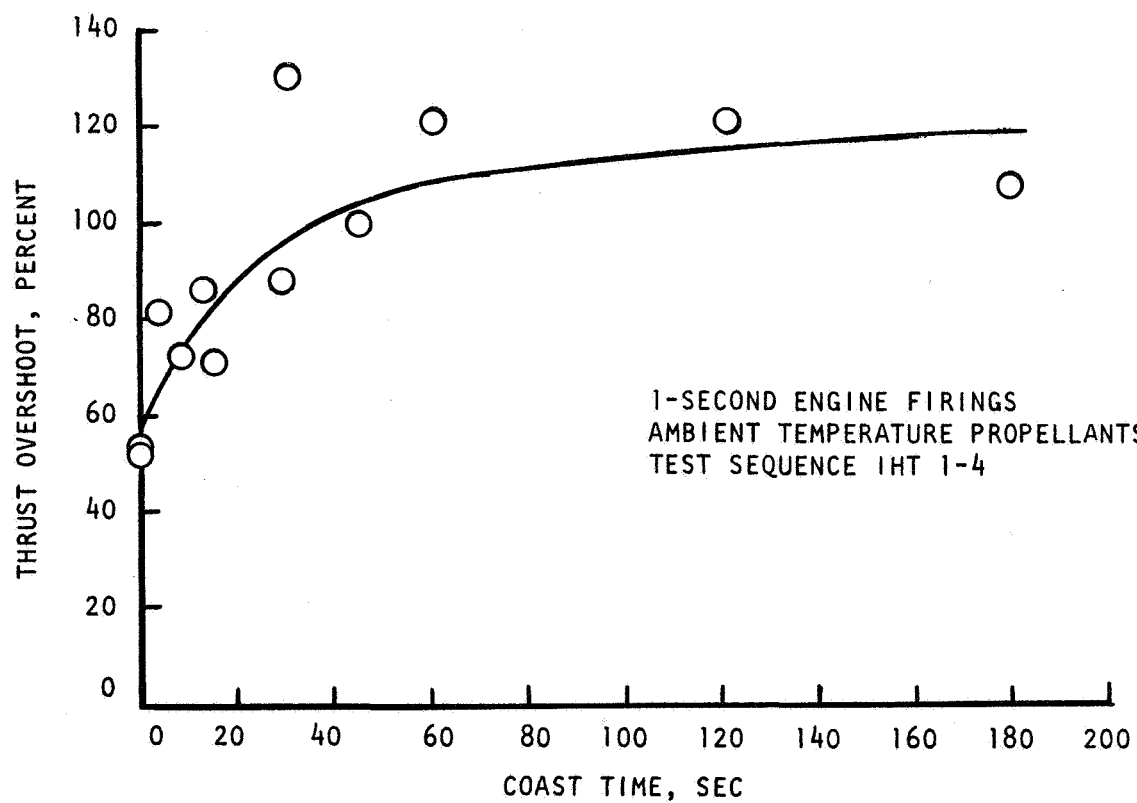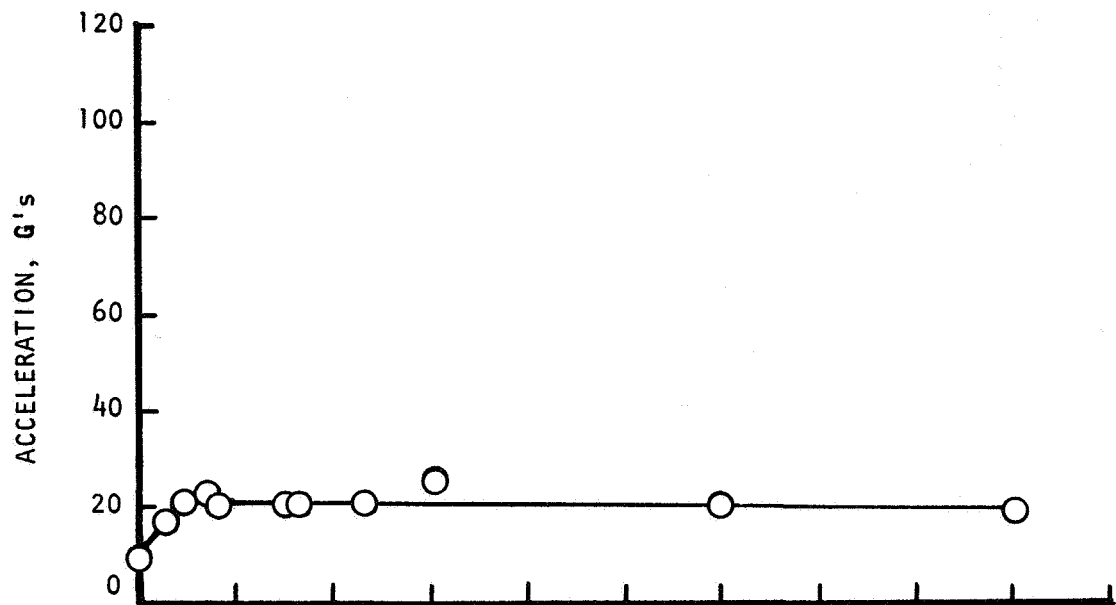Figure 117 Acceleration And Thrust Overshoot For Hot-Engine Restarts

Figure 118 Acceleration and Thrust Overshoot Data for Warm
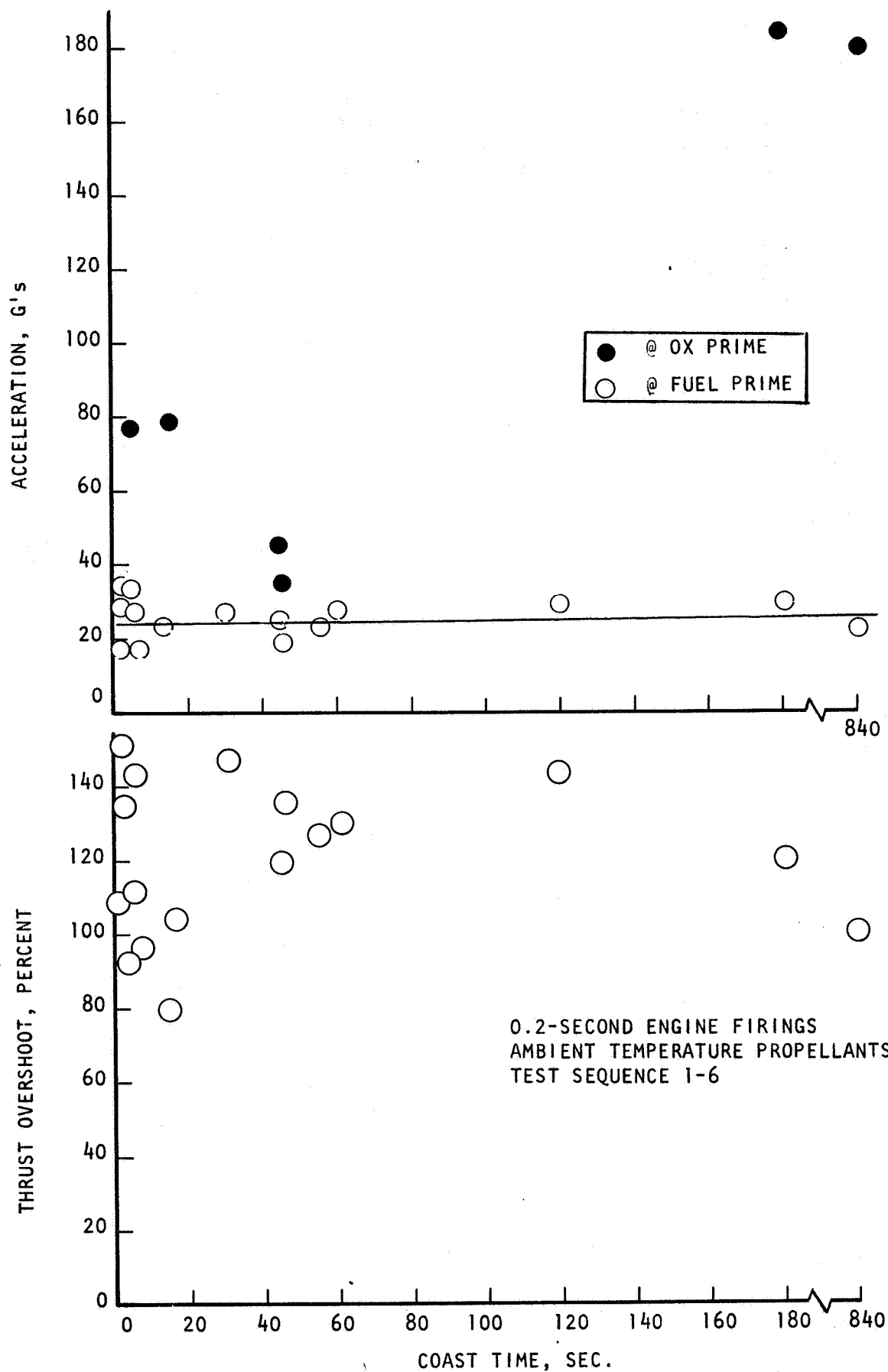Engine Restarts   R-9686

Figure 119   Accelerations And Thrust Overshoots For Ambient Engine Restarts
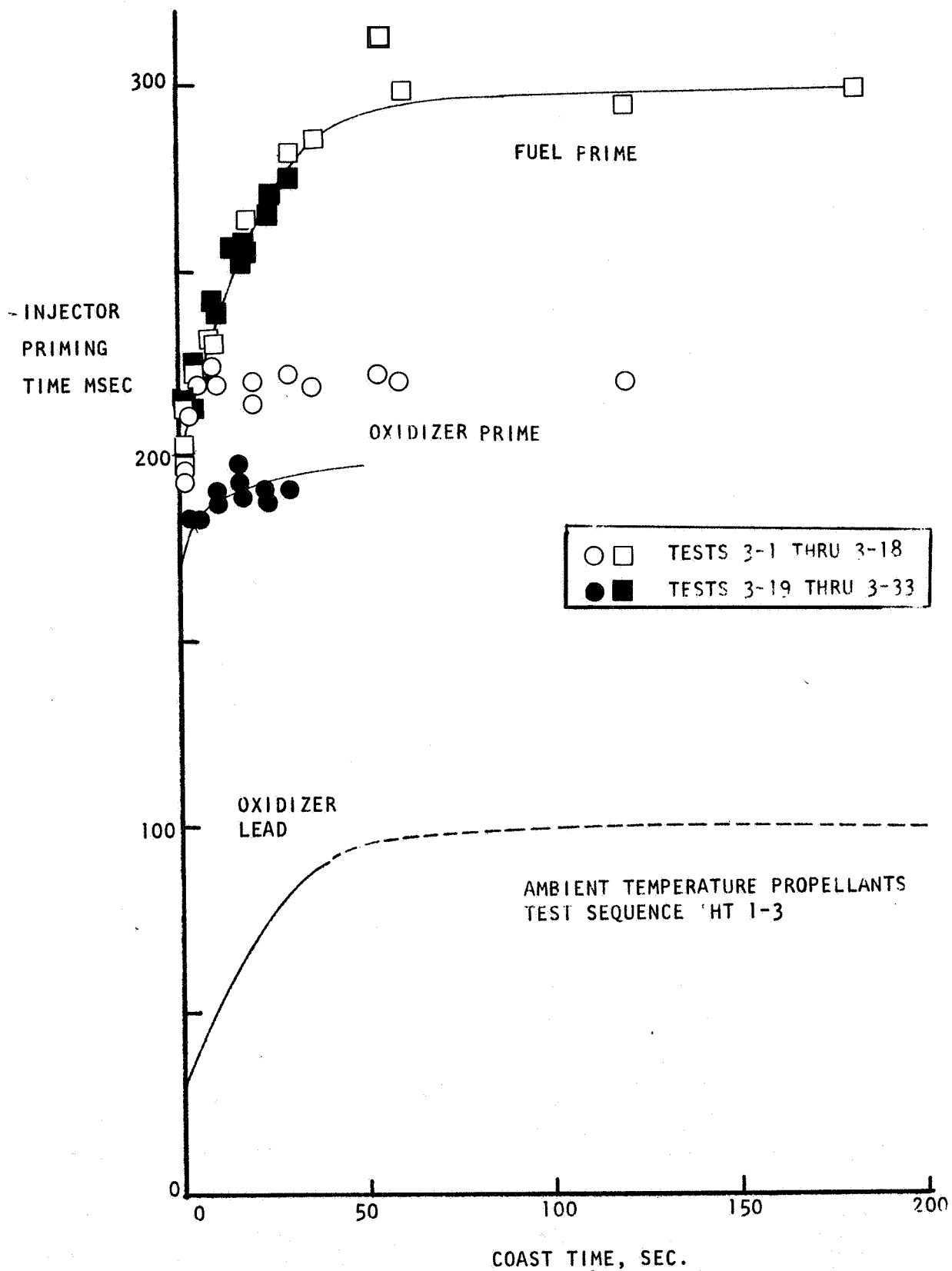
R-9686

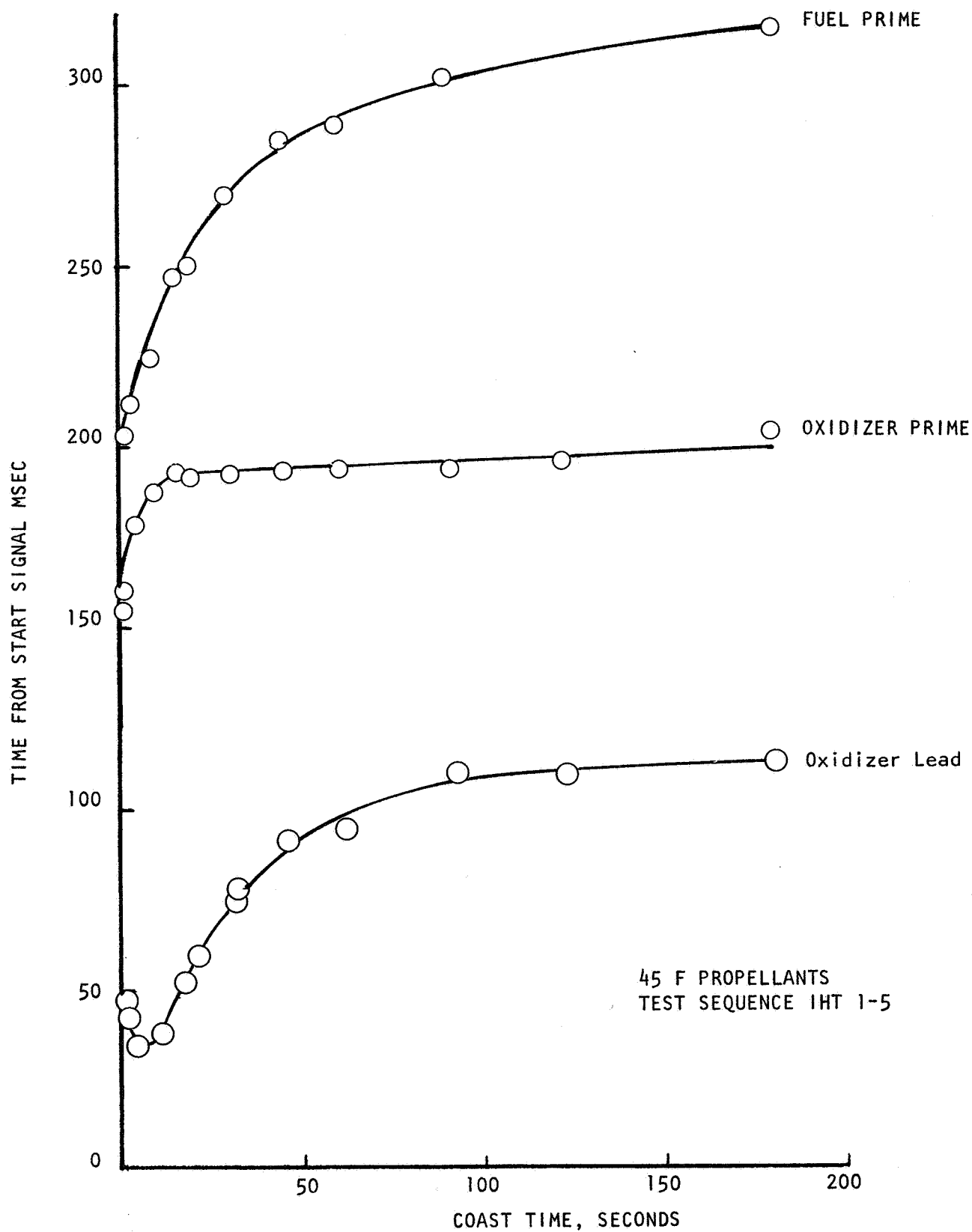FIGURE 120 INJECTOR PRIMING TIMES FOR HOT ENGINE RESTARTS

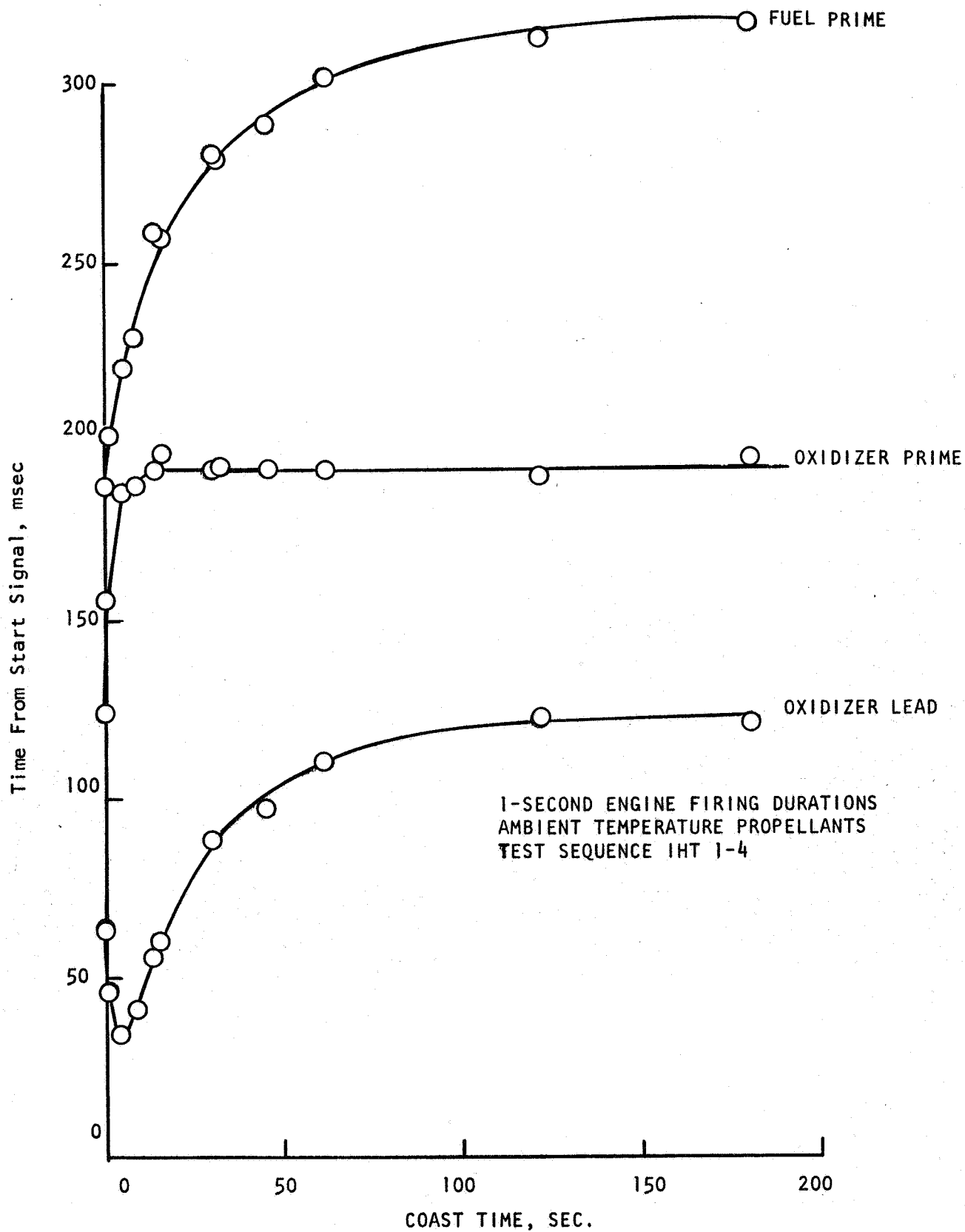FIGURE 121   Injector Priming Times - Hot Engine With Cold Propellants

R-9686

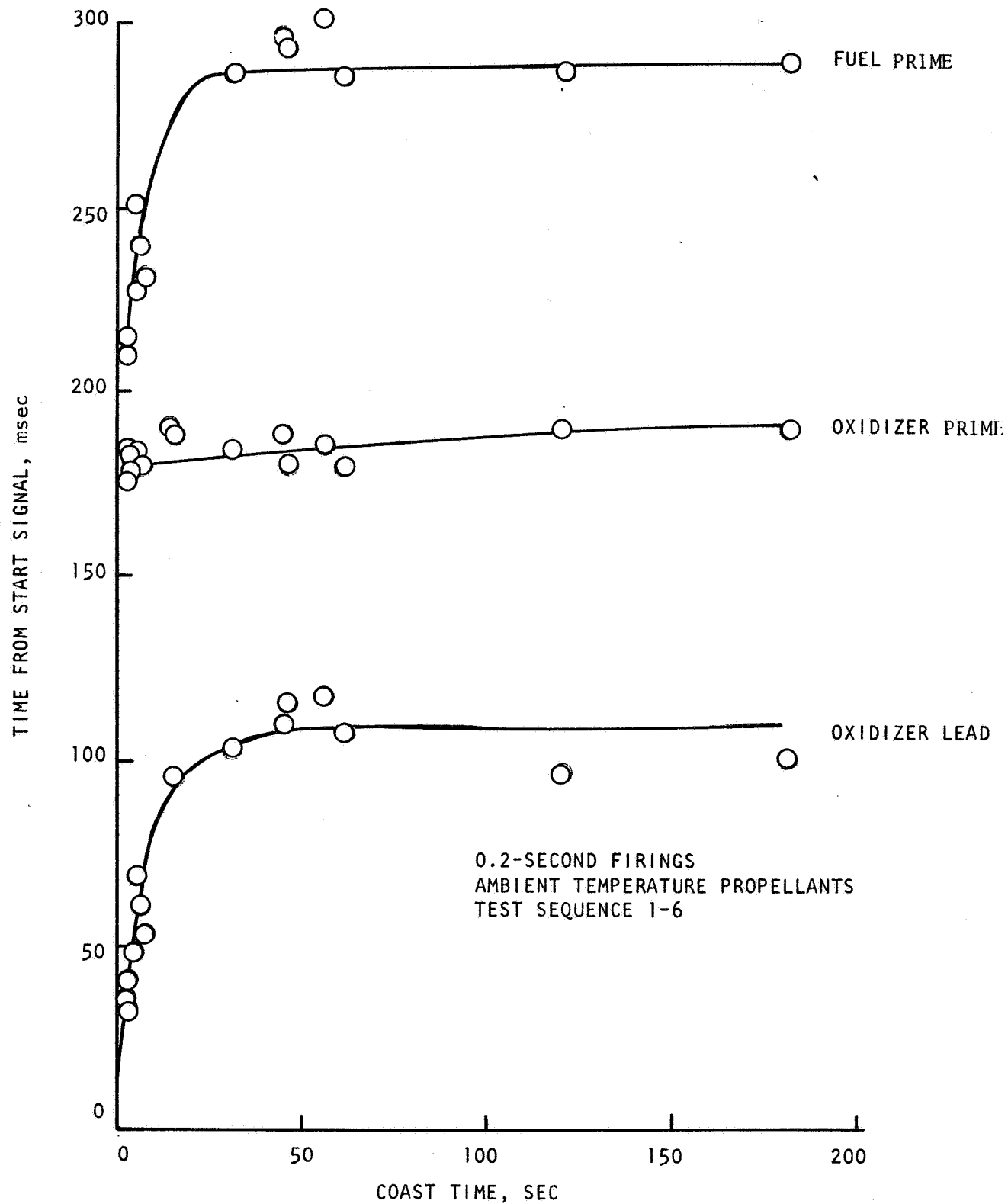Figure 122 Injector Priming Times For Warm Engine Restarts

Figure 123 Injector Priming Times For Ambient Engine Restarts

The range of chamber pressures, propellant flowrates, and mixture ratios tested is shown in Table 43. Measured and predicted injector pressure drops are tabulated. The measured pressure drops are the values recorded when no significant oscillations were occurring during the test. Predicted values are all referred to the measured values of Test 7-7 and ratioed according to the square of the flowrates. The difference between the measured and predicted pressure drops particularly at lower pressures may be the result of subtracting two high pressure measurements (injection and chamber pressures) to obtain a ΔP although the discrepancy is greater than would be expected from instrumentation inaccuracies. Values of injector ΔP divided by Pc are also tabulated based on the predicted pressure drops. Tests were conducted with values as low as approximately 0.2 on each side of the injector.

Chug frequencies of 200-300 Hz were noted. **Oscillations at two frequencies were indicated during the early portions of some of the tests. The lower frequency persisted for less than a second after start.**

Heat load data for the throttling tests are shown in Fig.124. The data taken on the 10-second duration tests at nominal pressure agree quite well with the data from the previous Phase I test effort. The data from the 10-second tests indicated that the value of the heat load measured at 10 seconds was approximately 60 BTU per second higher than the value measured at 5 seconds. The throttling tests were of 5-second duration. The values recorded at this time are plotted in Fig.124. Raising the plotted values by 60 BTU per second results in very good agreement with the Phase I data. Therefore it appears that no adverse thermal effects occur during chugging operation. The chug frequencies are high enough so that cyclic effects almost completely damp out across the chamber wall. Cycle life is probably degraded to a small extent by the chugging.

Chugging was not evident as the chamber pressure was reduced from test-to-test until Test 7-8 where a chamber pressure of 84 psia was obtained for steady state. On this test, chugging occurred for approximately 0.6 seconds after ignition at a frequency of about 300 Hz as shown in Fig. 125. As the chamber pressure was reduced on the successive tests, the duration of the chugging increased until at a chamber pressure of 68 psia chugging continued throughout the test. When the chamber pressure was increased on the next test to 73 psia and the mixture ratio was decreased to 1.5, continuous chugging occurred for 1.6 seconds but continued sporadically throughout the remaining duration of the test. Variation of the mixture ratio to 1.6 and 1.9 at $\approx$67 psia chamber pressure on the next two tests resulted in small changes in the chug amplitude.

TABLE 43

INTEGRATED CHAMBER LOW-PRESSURE TESTS

	7-3	7-4	7-7	7-8	7-9	7-10	7-10A	7-11	7-12	7-14
CHAMBER PR., PSIA	99	100	126	84	76	68	73	66	68	126
MIXTURE RATIO, O/F	1.67	1.46	1.68	1.7	1.8	1.8	1.5	1.6	1.9	1.66
FLOWRATE, LB/SEC										
OX	9.79	9.32	12.4	8.29	7.41	6.34	6.78	6.02	6.57	12.2
FUEL	5.86	6.41	7.39	4.72	4.10	3.48	4.53	3.79	3.40	7.39
MEASURED INJ. ΔP,*										
PSI OX	31	26	56**	19	11	-	-	-	-	51
FUEL	41	48	57**	18	10	-	-	-	-	52
PREDICTED INJ. ΔP,										
PSI OX	36	32	56**	24	20	15	17	13	16	54
FUEL	38	45	57**	23	17	12	21	15	12	57
PREDICTED $\Delta P/Pc$ OX	.36	.32	.44	.29	.26	.22	.23	.20	.24	.42
FUEL	.38	.45	.45	.28	.22	.19	.29	.23	.18	.43
CHUG DURATION, SEC	0	0	0	0.6	2.1	4.7	1.6***	4.7	4.7	0
FREQUENCY, HZ	-	-	-	310	270	115/230	280	230/280	240/270	-
PK/PK AMPLITUDE,										
PSI OX	-	-	-	290	370	200	250	180	160	-
PSI FUEL	-	-	-	80	60	100	80	70	100	-
LB THRUST	-	-	-	1400	1700	3300	1300	3500	3500	-

*DURING STABLE PART OF TEST   **REFERENCE   ***SPORADIC THROUGHOUT TEST
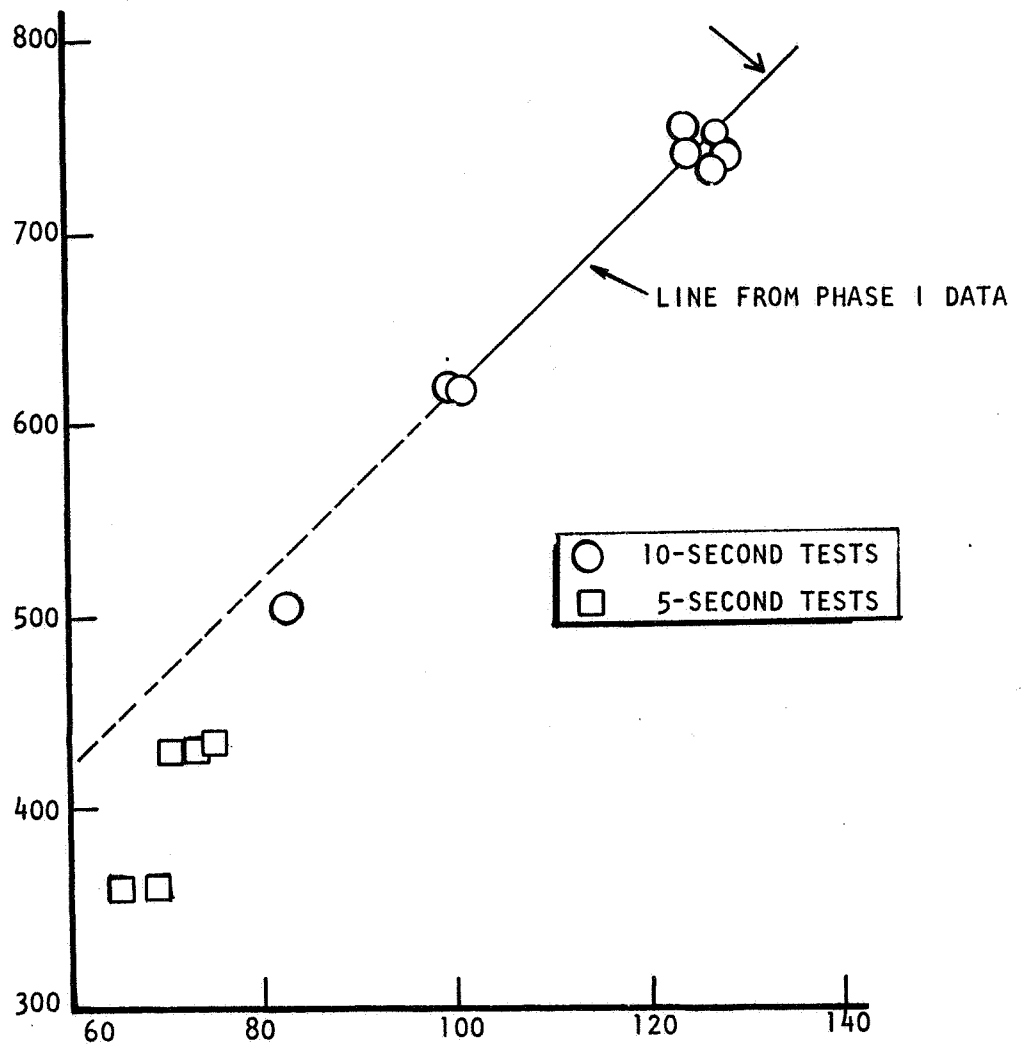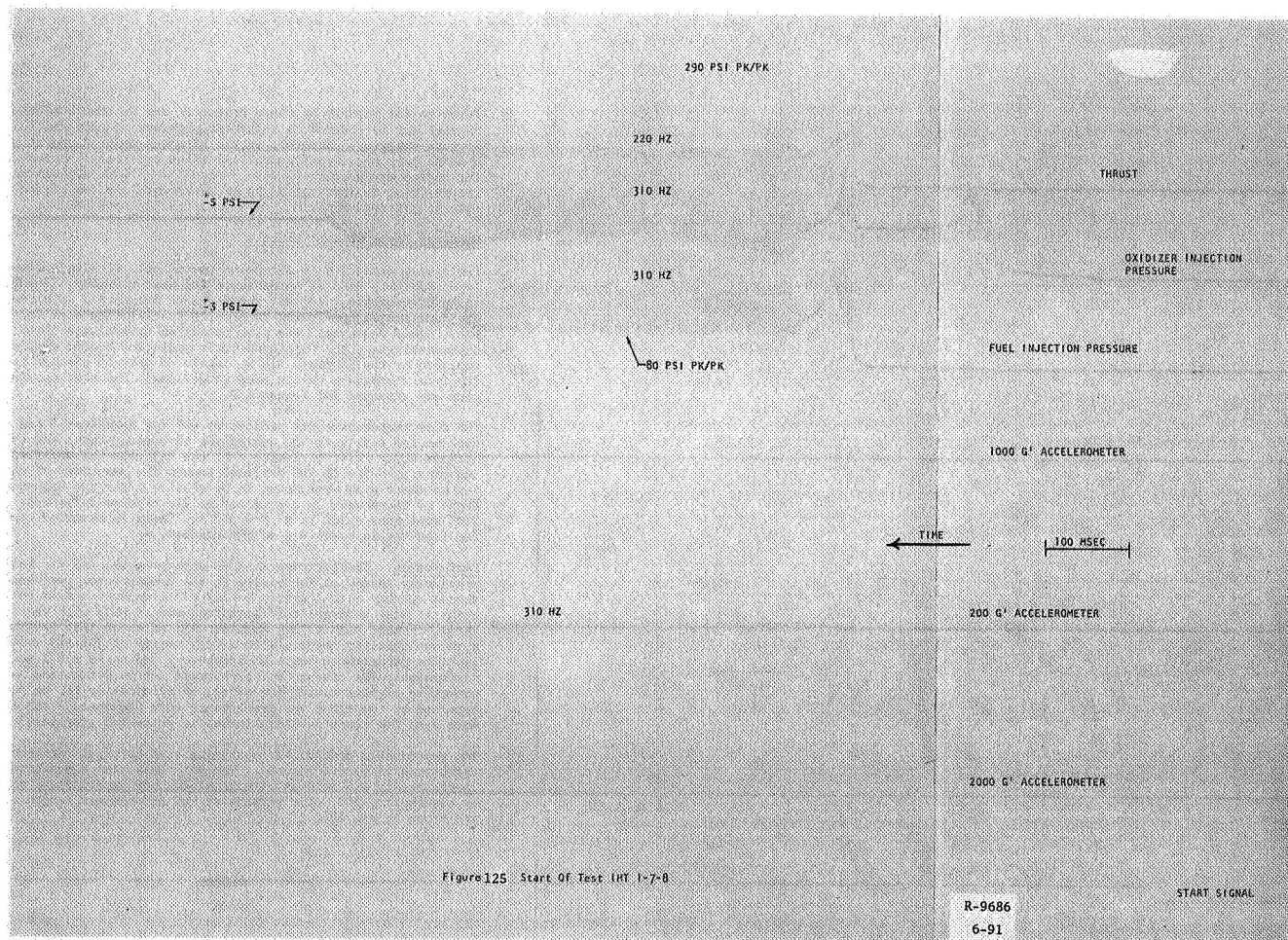
Figure124. Heat Load During Throttling

290 PSI PK/PK

220 HZ

310 HZ

±5 PSI

310 HZ

±3 PSI

80 PSI PK/PK

THRUST

OXIDIZER INJECTION PRESSURE

FUEL INJECTION PRESSURE

1000 G' ACCELEROMETER

TIME

100 MSEC

310 HZ

200 G' ACCELEROMETER

2000 G' ACCELEROMETER

Figure 125 Start Of Test IHT 1-7-0

START SIGNAL

R-9686
6-91

Based on the results of these tests, it may be concluded that the chamber can be started to a chamber pressure of approximately 90 psi without chugging. However, in the blowdown mode of operation (where chamber pressure decays gradually) if no external disturbances occur, the engine may be throttled to perhaps 65-75 psia without chugging. The chugging did not appear to be detrimental to the engine over the several 5-second duration tests conducted in this program.

Boundary Layer Coolant Effects

Tests were conducted to determine the effects of elimination of boundary layer coolant, BLC, on performance and heat transfer. The first seven tests of Sequence 7 and all the tests of Sequence 8 were conducted with the feed system configured to provide precise flow data for BLC comparison. Since Sequence 7 was also conducted to evaluate throttling characteristics, the high area ratio radiation cooled nozzle was replaced by the shorter, $\varepsilon = 9$, nozzle to prevent chamber damage resulting from vibrations during deep throttling. The same nozzle configuration was retained for Sequence 8.

The fuel temperature was reduced to 40F for Sequences 7 and 8 to enhance the cooling safety factor during the throttling tests and the tests without BLC. Prior to Sequence 8, the injector was modified by inserting pins into the 68 BLC orifices around the periphery of the injector. Ten of these pins were found to be missing after the Sequence 8 tests. Eight of these were in the sector of the chamber defined by 0 = 70 to 110° (the fuel inlet is at 0 = 270°). Theta is measured clockwise viewing from the injector end of the chamber.

Performance. The injector used in this program, L/D #1, had been previously tested at Rocketdyne in the demonstrator regeneratively cooled thrust chamber with a nozzle having a 9:1 expansion area ratio, at WSTF with the same hardware configuration, and at WSTF with the integrated thrust chamber with a 72:1 nozzle. All of these test programs indicated a vacuum specific impulse with a 72:1 nozzle of 309-310 seconds. The baseline performance tests on Sequence 7 indicated a 2-3 second lower performance, the reason for which could not be determined. However, the objective of determining the effect of eliminating BLC on performance was obtained by comparing the performance data Sequences 7 and 8. Performance data for these two test series is presented graphically in Fig.126.

The performance penalty for operating with 40F fuel (instead of 70F) was calculated to be 0.3 seconds. The data indicates a performance gain of approximately 1.5 seconds at nominal chamber pressure and mixture ratio by eliminating BLC. The effects of BLC and chamber length on performance are shown in Fig.127.
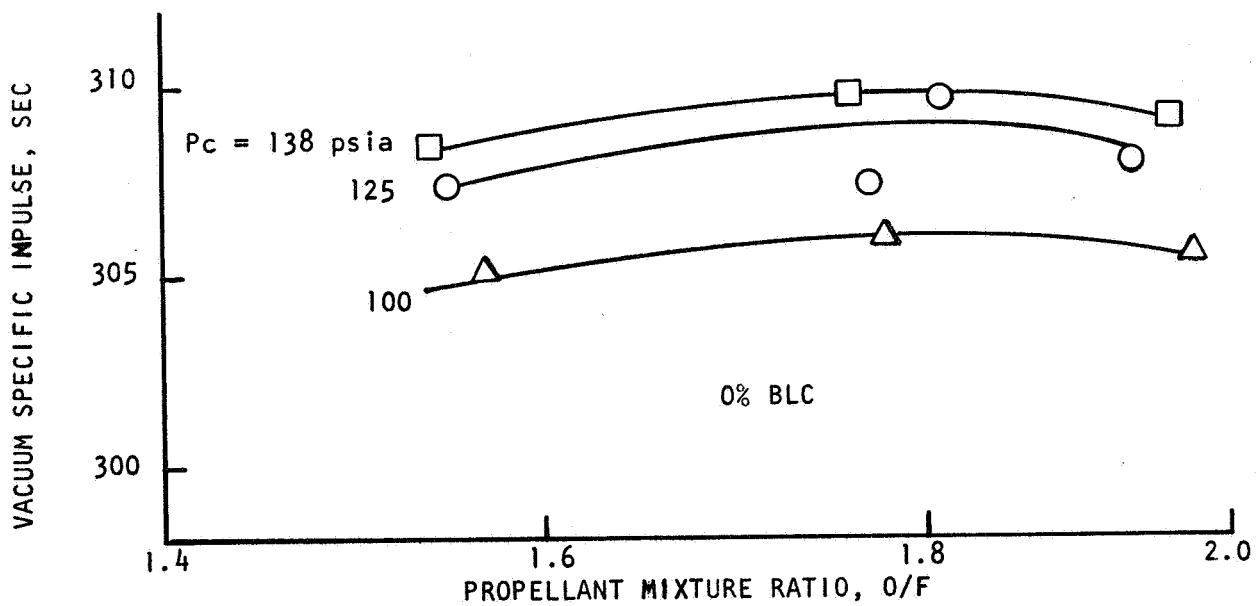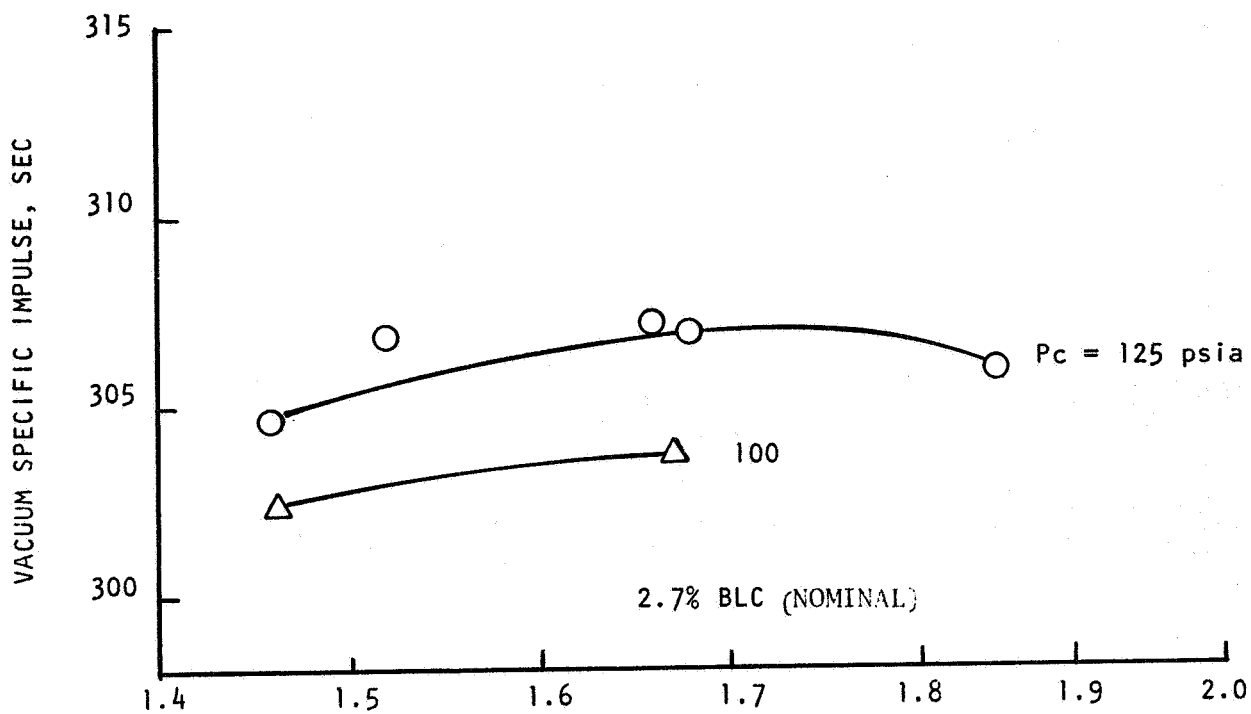
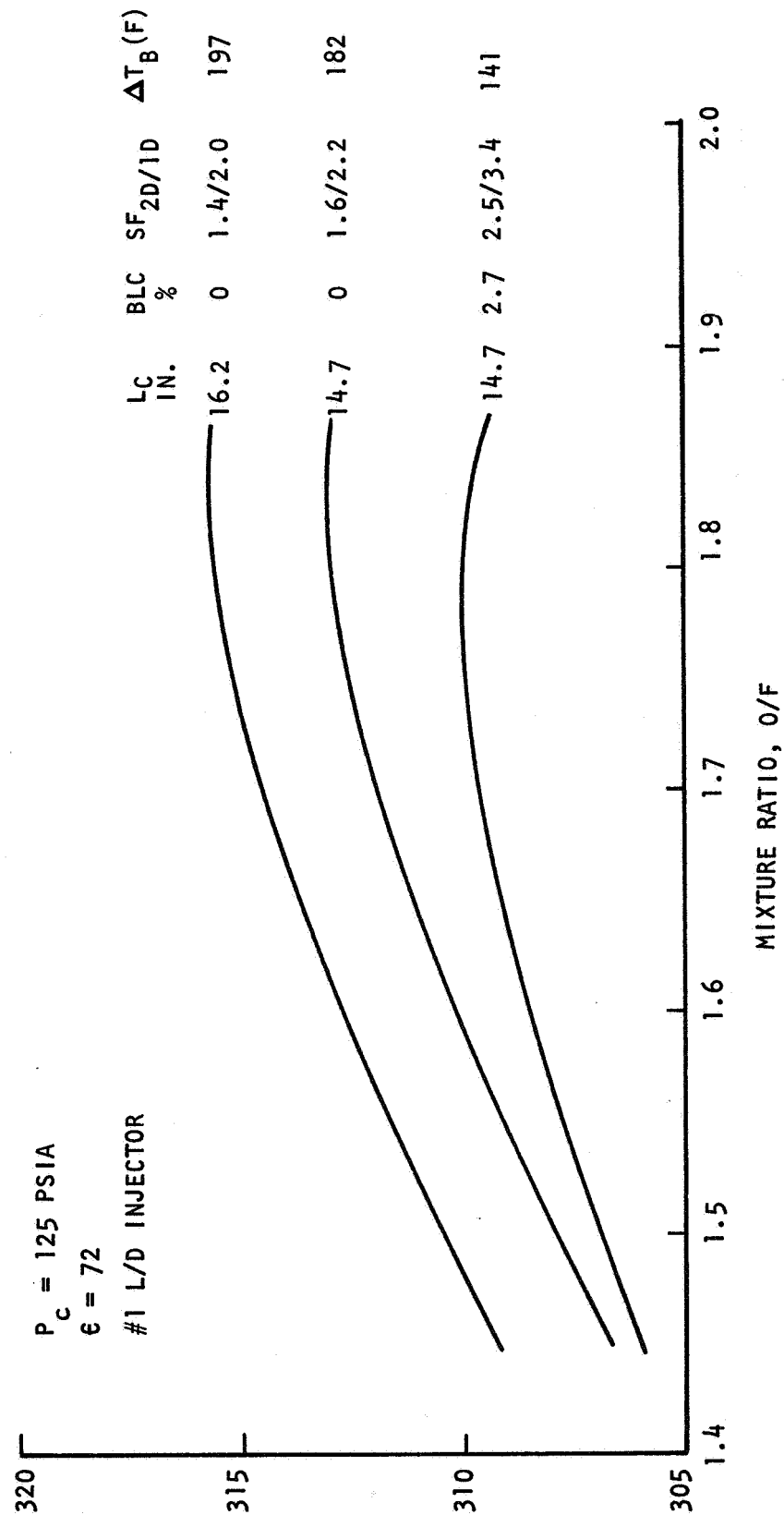Figure 126   Performance With and Without Boundary Layer Coolant

Figure 127 OME Performance With #1 L/D Injector

Thermal Data. Thermal data taken during the Phase II test series at WSTF were the same as in Phase I and consisted of fuel bulk temperature rise, regenerative chamber back wall temperature, and steel heat sink nozzle temperature transients or columbium radiation cooled nozzle temperature response and equilibrium values. These data, together with the data generated during the heated tube tests under this contract, were used to provide an indication of the safety margin at which the OME Integrated Thrust Chamber (ITC) was operating both with and without supplemental boundary layer cooling (BLC). Radiation equilibrium temperatures for a full size (ε = 72:1) columbium nozzle with and without BLC were predicted based on the results of tests with the short demonstrator columbium nozzle ($7 \leq \varepsilon \geq 9$) in conjunction with the full size steel heat sink nozzle temperature transients.

A comparison of the coolant outlet temperature response with and without BLC are presented in Fig.128 and 129 for cold and hot start conditions respectively. It is apparent that deletion of boundary layer coolant results in a significant increase in regenerative coolant outlet temperature as would be expected.

A comparison of the relative heat loads as a function of chamber pressure is given in Fig.130. The nominal BLC condition reduces the heat load by about 22 percent. Most of this reduction occurs in the cylindrical section of the combustor near the injector end as will be shown later. This is in agreement with analytical predictions. The non-film-cooled chamber results, however, are lower than originally predicted due most likely to the fuel rich outer region inherent in the L/D #1 injector design. Mixture ratio effects are seen to be negligible which is in accordance with analytical predictions.

Back (outer surface) wall temperature response curves for zero BLC are similar to the nominal BLC results except, of course, the final values reflect the higher heat loads.

A notable difference between the tests with and without BLC is that the soakout temperatures prior to restart are in excess of 500F at the x = -13 inch location without BLC. This compares to a value of about 300F when supplemental BLC is utilized. The head end obviously operates hotter without BLC as would be expected due to higher operating back wall temperatures (due to higher bulk temperature) and hot-gas wall temperature (due to increased local heat flux). The acoustic cavity and dams probably also operate at higher temperatures and contribute to the higher soakout temperatures.
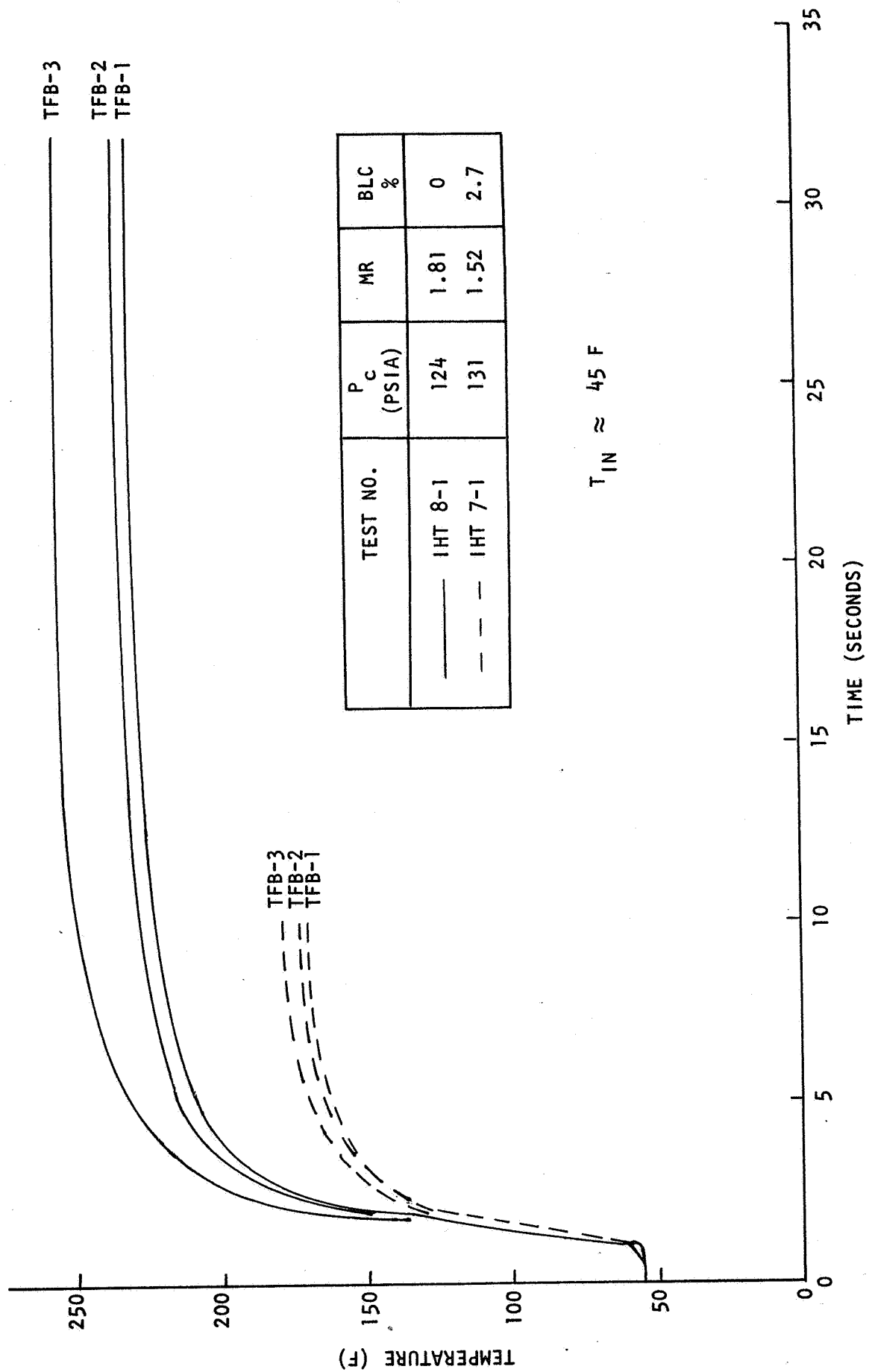
Figure 128 Typical Outlet Bulk Temperature Response - Cold Start
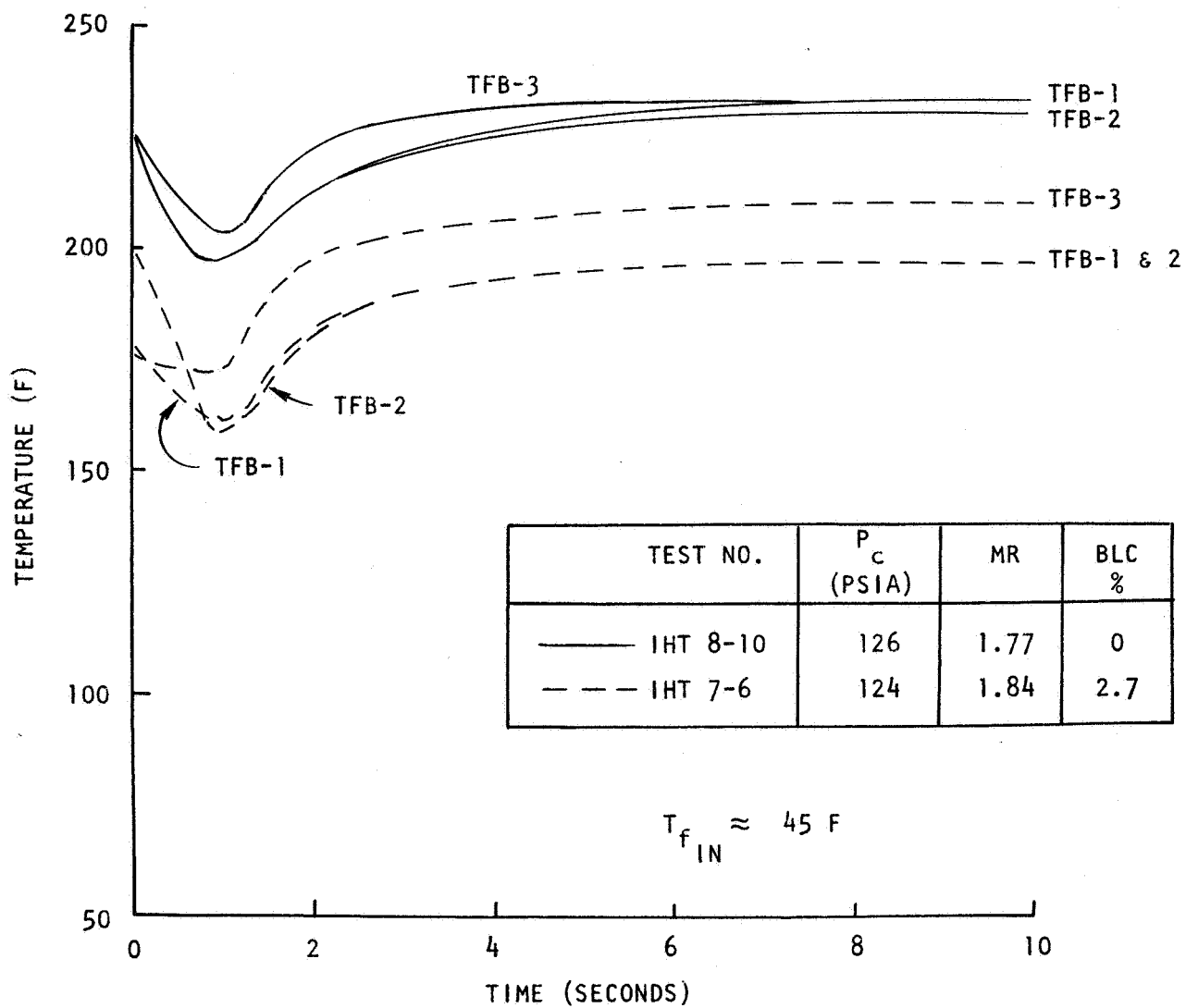
Figure 129   Typical Outlet Bulk Temperature Response -
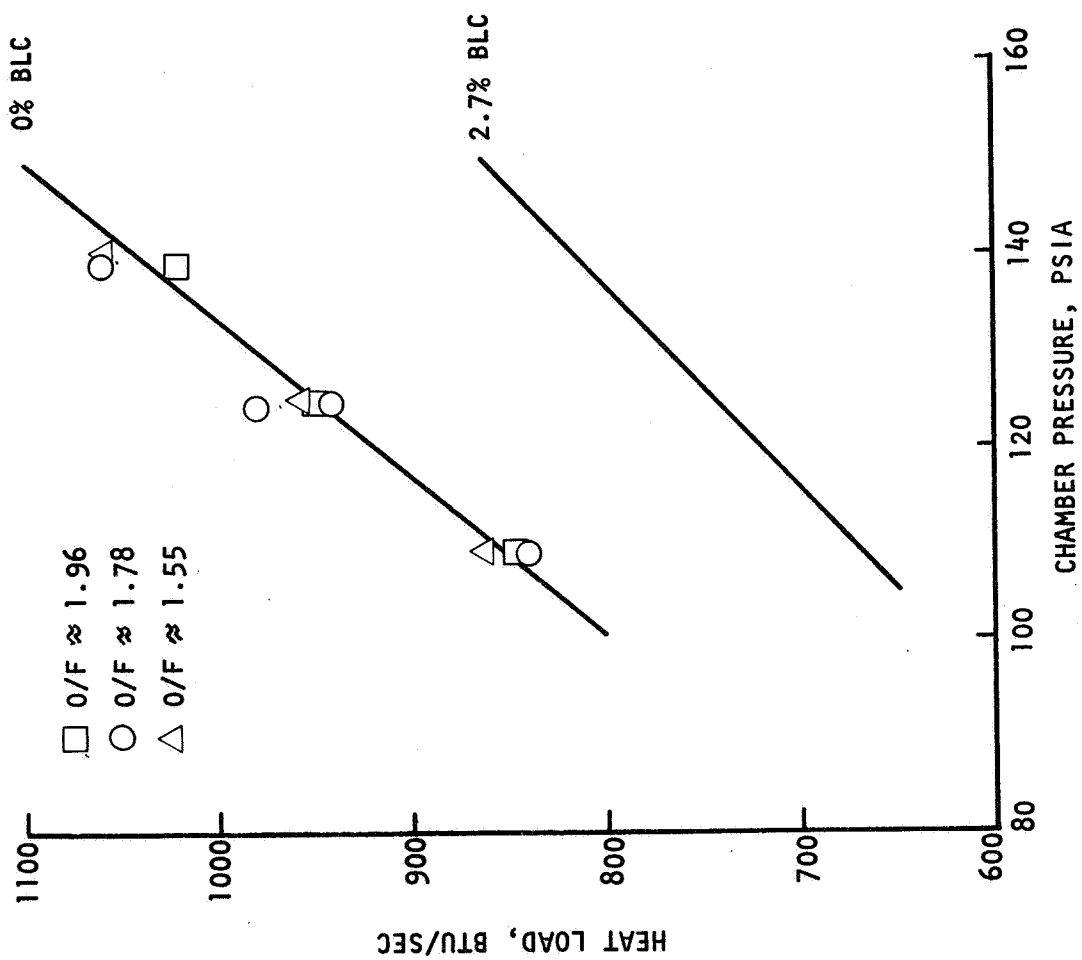   Hot Start

Figure 130 Effect of Boundary Layer Coolant on Regenerative Chamber Heat Load

Steady-state back wall temperatures are utilized primarily as an indication of axial heat load distribution and circumferential heat load uniformity. These measurements are relatively insensitive to local heat flux variations and tend to reflect integrated heat load along a channel in that back wall temperatures are strongly influenced by the local bulk temperature.

A comparison of the average back wall temperature profile with and without BLC is presented in Fig.131. The effect of BLC is seen to be small from the regenerative coolant inlet to a point about 8 inches upstream of the throat. The primary effect of BLC occurs in the region extending from the injector to about 10 inches upstream of the throat.

In the case of film cooling, the back wall temperatures are relatively flat or decreasing in going from X = 8 inches to the injector end. This would indicate a combination of reduced heat flux level and relatively constant bulk temperature resulting from the lower heat flux. Without BLC, however, the back wall temperatures continue to increase right up to injector end and decrease only in the acoustic cavity region. This would indicate a relatively constant heat flux and increasing regenerative coolant bulk temperature in the cylindrical region. Reduced heat flux level in the acoustic cavity accounts for the reduced back wall temperature in that region.

In general, circumferential variations in back wall temperatures were less than 10F in the nozzle and throat region. The variation appears to increase significantly to about 30 to 40F in the combustor/injector end region both with and without film cooling. This variation would amount to about $\pm$10 percent difference in heat load to the regenerative coolant.

Comparison of the average acoustic cavity back wall temperatures (measured at 8 circumferential locations) with the average outlet bulk temperature give agreement within about 1 to 2F in most cases. This would indicate that these acoustic cavity region measurements are essentially equivalent to local coolant bulk temperatures (due to very low heat flux levels) and can be utilized to indicate nonuniformity of circumferential heat load. Based on the results of the 10 nonfilm cooled tests, the average circumferential variation range in heat load was +10 percent and -12 percent.

A typical plot of back wall temperature distribution without BLC is presented in Fig.132for the test conditions as noted. (Thermocouples at the 270 degree location 4 inches to 13 inches upstream of the throat were inadvertently installed over mid-land rather than mid-channel and are not included due to the resulting higher recorded temperatures).
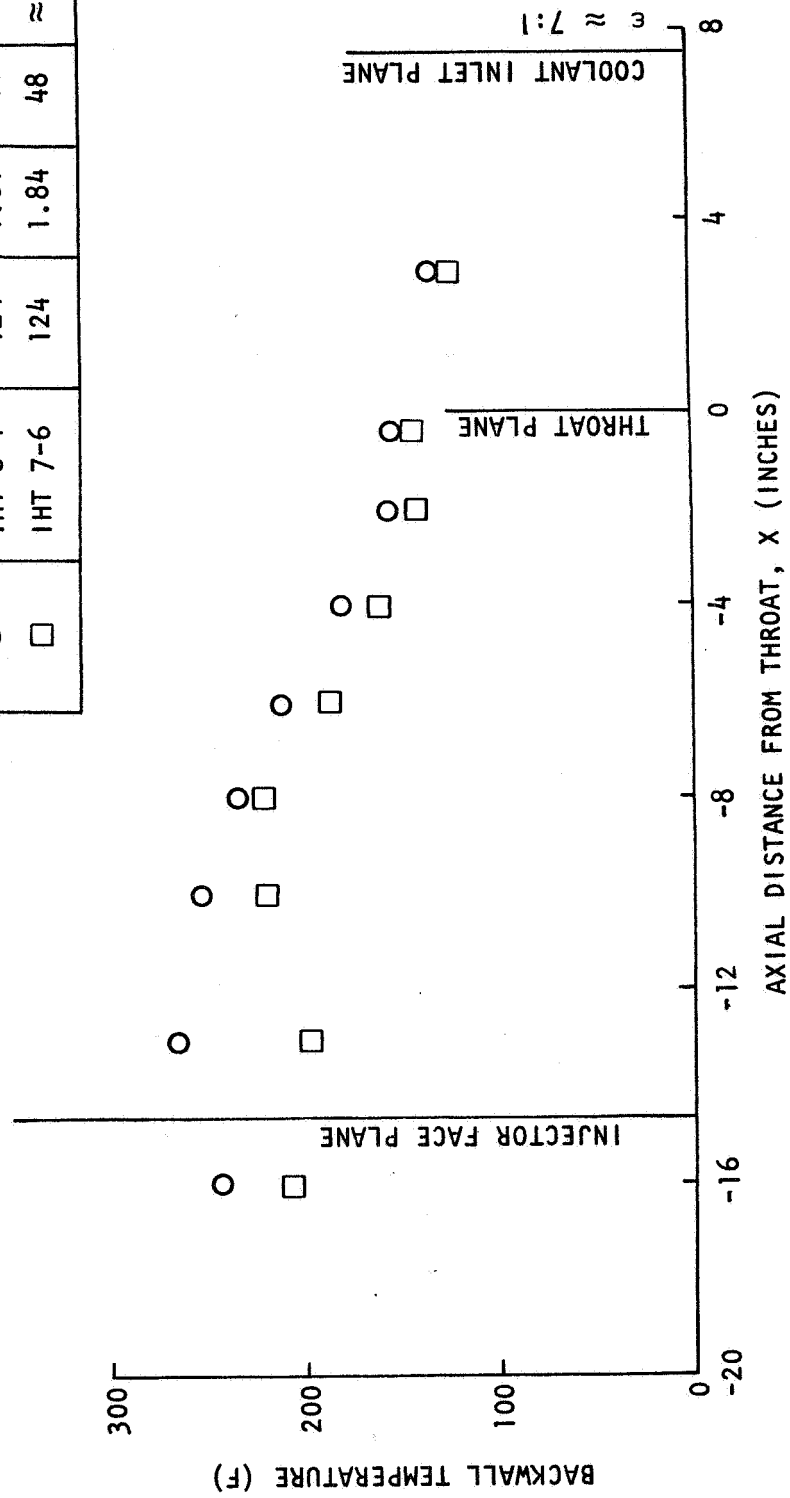
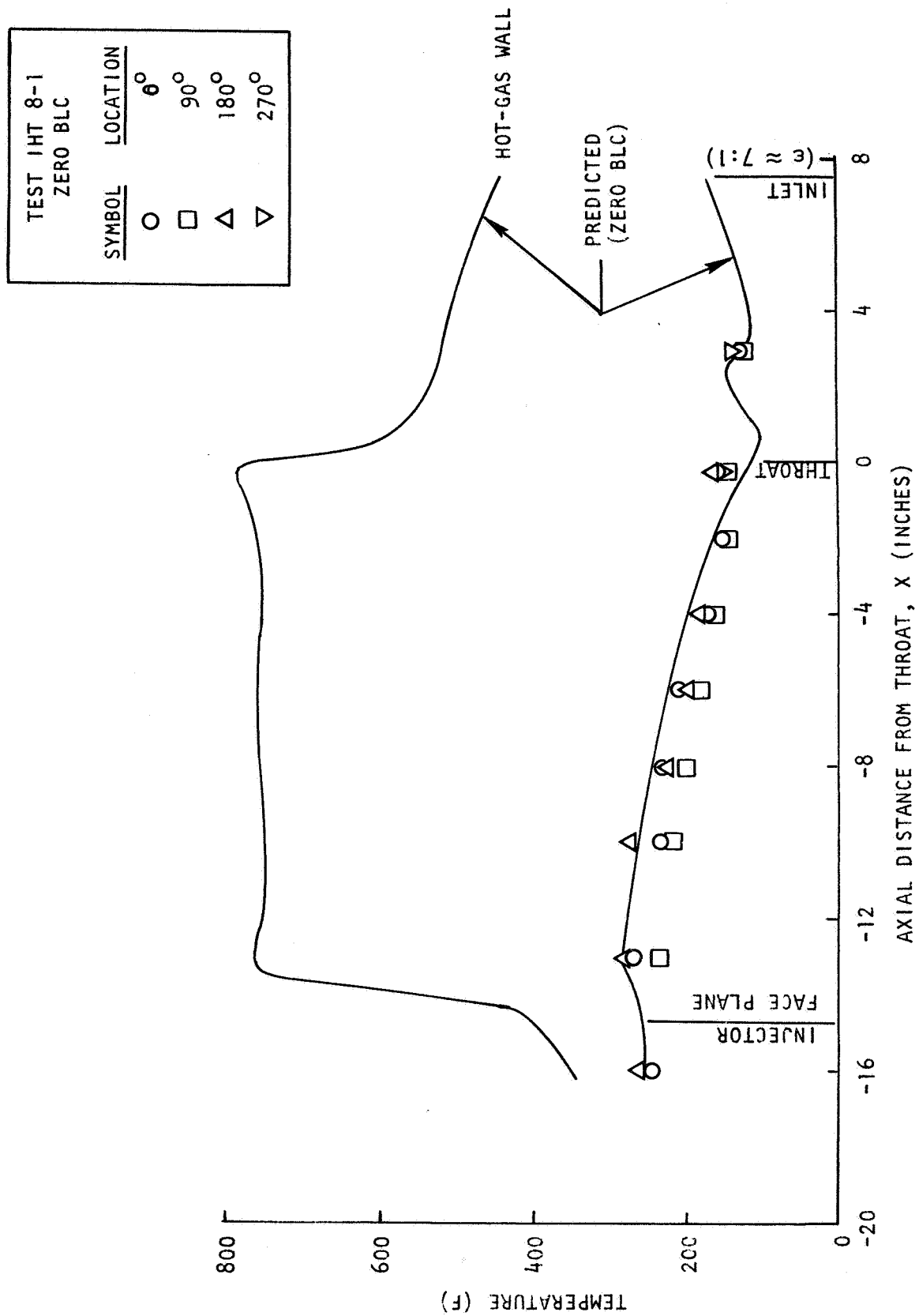Figure 131   Effect of Supplemental Film Coolant on Backwall Temperature Profile

Figure 132. Wall Temperature Profiles Without Supplemental Film Coolant

The predicted back wall and hot gas wall temperature profiles are also presented for comparison. The predicted values are based on a boundary layer analysis (without film cooling) with a slight adjustment ($\simeq$ 4 percent reduction) in order to match the total integrated heat load. The experimental and predicted back wall temperature profiles appear to be in relatively good agreement. The predicted maximum hot gas wall temperature is about 780F without BLC compared to about 740F with BLC.

Test Sequences 7 and 8 were conducted using the columbium radiation cooled nozzle. The nozzle attaches to the ITC at an area ratio of 7:1 and extends to an area ratio = 9:1. The latter dimension was selected based on compatibility with the diffuser utilized during earlier tests at Rocketdyne's facility. The 0.050-inch wall thickness was selected to simulate soakback conditions after shutdown. The wall thickness has a negligible effect on radiation equilibrium temperature. Typical temperature response data for tests with and without BLC are presented in Fig.133. It is apparent that there is a definite increase in equilibrium wall temperature for the test with no supplemental film coolant. This essentially proves that there is film coolant carry-over downstream of the throat.

The use of full-size columbium nozzle (ε =72:1) would result in a wall temperature increase of about 90F in each case due to a reduced view factor out of the nozzle exit plane. The resulting maximum equilibrium temperature for a full-size columbium nozzle are, therefore, 1800F and 1630F without and with BLC, respectively. The latter value compares favorably with the 1700F predicted based on theoretical extrapolation of the CRES heat sink nozzle test results as discussed in the Phase I section. The slightly lower temperature achieved by the columbium nozzle is due to the high emittance ($\simeq$0.9) coating utilized for oxidation protection.

These results support the previous (Phase I) conclusion that the use of a refractory material is unnecessary at the current attach point with or without supplemental BLC. The use of an L-605 type nozzle extension appears quite feasible which should result in considerable cost saving. Alternatively, the columbium nozzle could be attached at a lower area ratio ($\simeq$3:1) with an attendant reduction in engine weight and regenerative coolant bulk temperature rise ($\simeq$20F).

Safety Factor and Fatigue Life

A primary purpose of the OME Reusable Thrust Chamber Test program (both chamber and heated tube tests) was to obtain data which would improve estimation of the OME regenerative coolant safety factor profile and, indirectly, fatigue life capability. This was accomplished by modifying
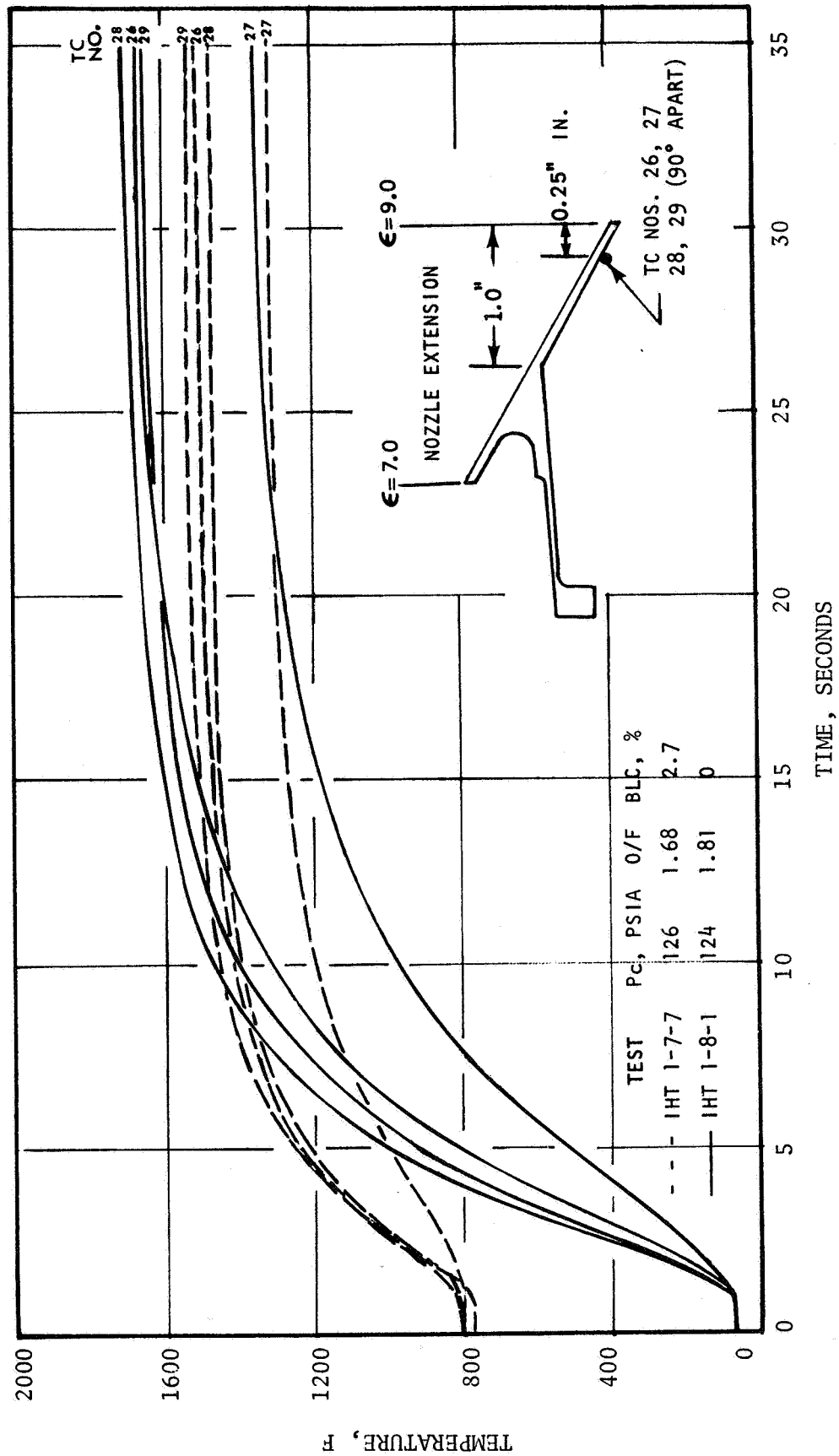
Figure 133. Radiation Cooled Nozzle Temperature Transients

the analytical models to fit the thermal data and then utilizing these
models to predict heat flux and wall temperature profiles.

The resulting predicted heat flux profiles at nominal operating condi-
tions are presented in Fig. 133A with and without BLC. The film cooling
model indicates a liquid film persists about 3 inches downstream of the
point of impingement on the wall. The heat flux in this region is
negligible since the film and regenerative coolant temperatures are
nearly the same. The case without BLC indicates a nominal heat flux of
2 BTU/in-sec throughout the cylindrical combustor region.

The resulting safety factor profiles based on 2-D conduction effects is
presented in Fig.134 for current off-design conditions (Pc = 120 psia,
MR = 1.73 and T_{in} = 100F). The coolant safety factors are similar in
the throat and nozzle region. There is a marked difference in safety
factor in the combustor region, particularly near the injector end.
The case without BLC results in a minimum safety factor of about 1.2 due
to a combination of high coolant bulk temperature (reduced subcooling)
and comparatively high heat flux level. The use of film coolant markedly
increases the safety factor at the injector end due to greatly reduced
heat flux level in the region of minimum subcooling. In addition, the
maximum coolant bulk temperature is decreased which further enhances the
safety margin.

It should be pointed out that the ITC was not originally designed to
operate without BLC. The minimum safety factor could be raised to a
value of about 1.5 simply by increasing the coolant velocity in about
the last 2 inches of the cylindrical section. This would result in an
increased pressure drop of about 2 psi.

The cyclic fatigue life profiles were calculated at nominal operating
conditions using the predicted wall temperatures. The results, with and
without BLC, are presented in Fig.135. The minimum predicted life occurs
in the region slightly upstream of the throat and is about 4800 and 4400
cycles for operation with and without BLC, respectively. Application of
a life safety factor of 4 would indicate a life capability in excess of
the required 1000 cycles for either operating condition.

The life cycle capability of the two operating conditions differs the
most in the combustor region due primarily to the difference in hot wall
temperatures.

It should be mentioned that a major restriction to the ITC fatigue life
is due to the extremely high strength nickel ($\simeq$ 66,000 psi yield) as
electrodeposited at Rocketdyne. By simply annealing the nickel, the
chamber fatigue life can be increased since the thermal load would be
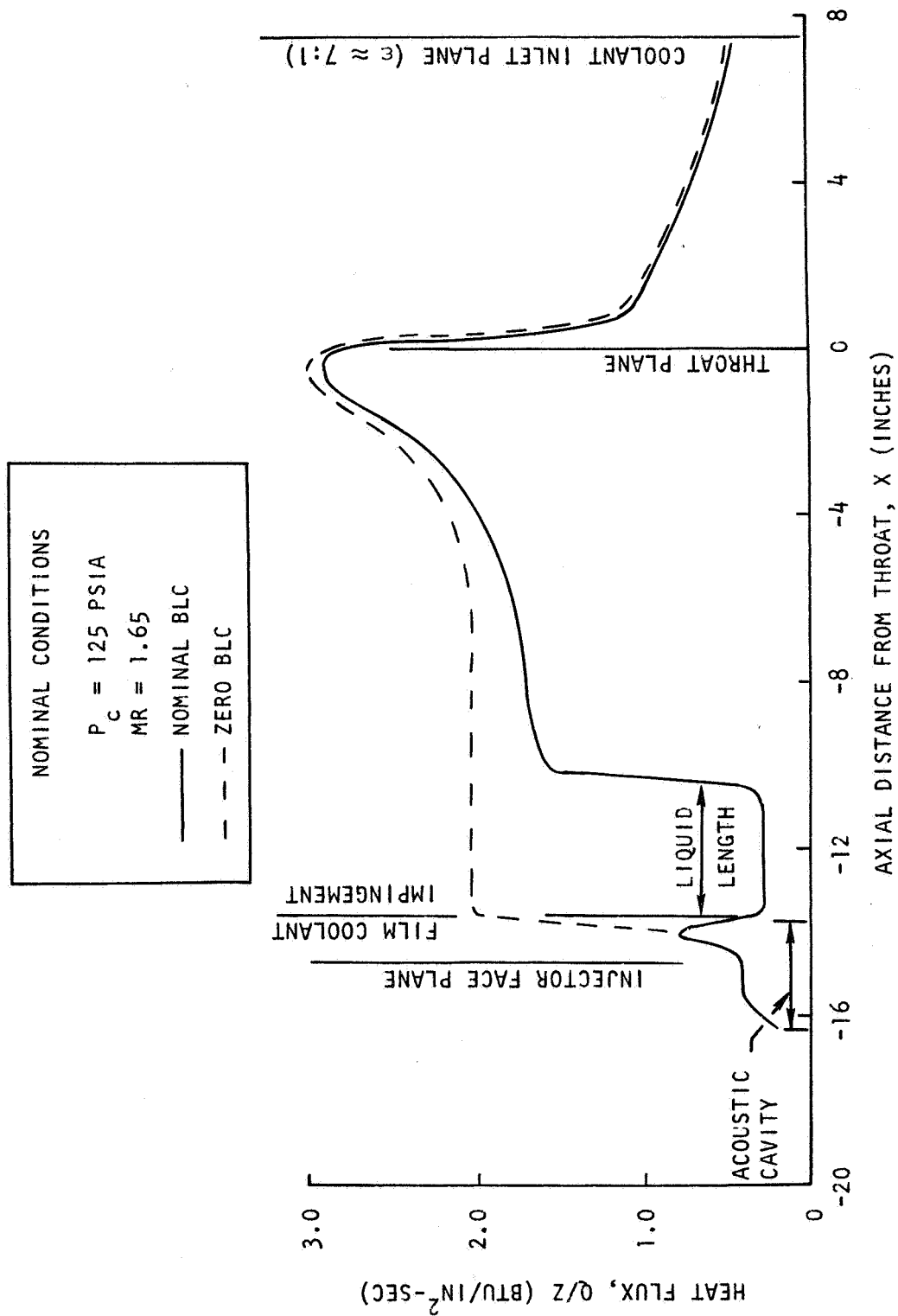
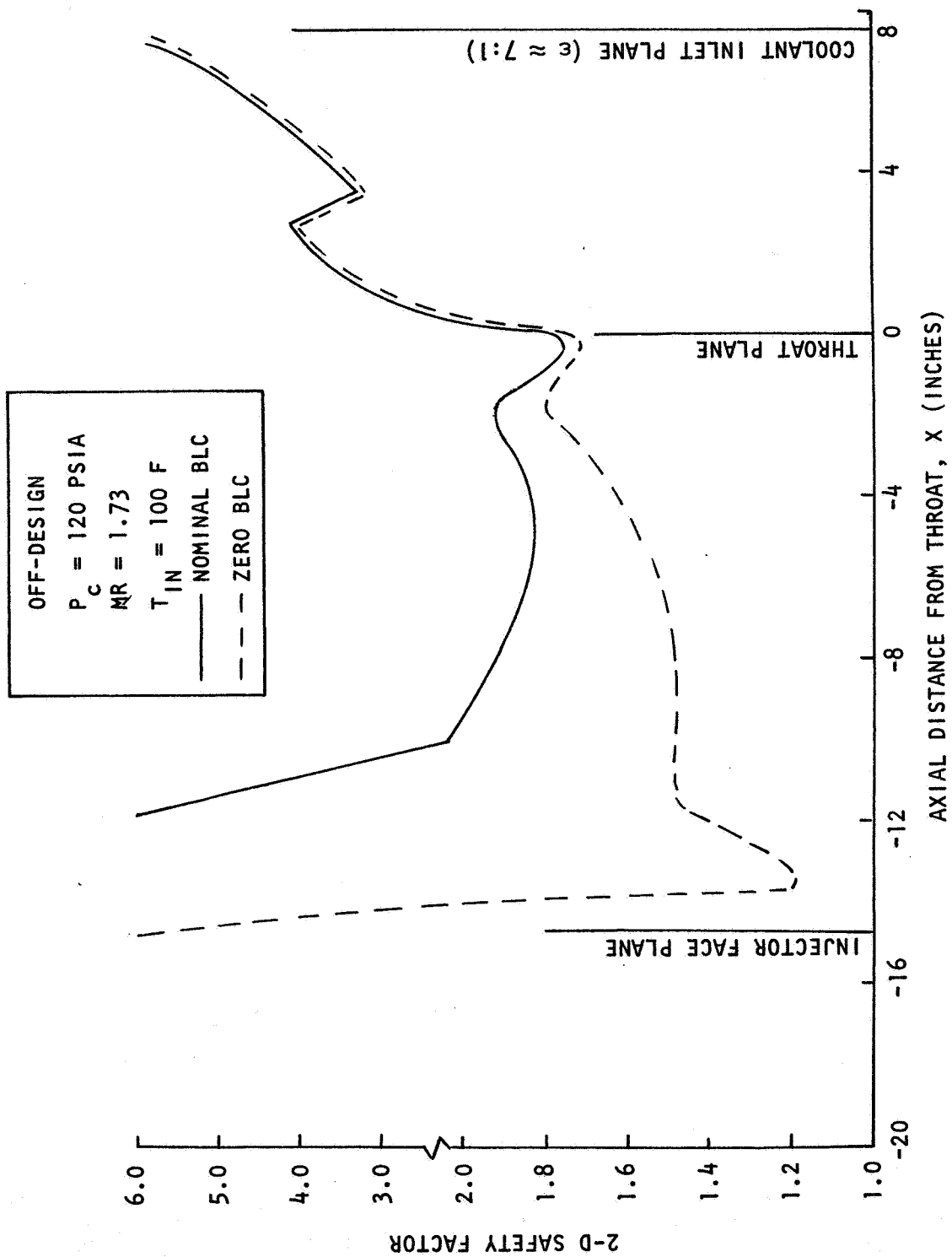Figure 133A. Integrated Thrust Chamber Heat Flux Profiles

R-9686
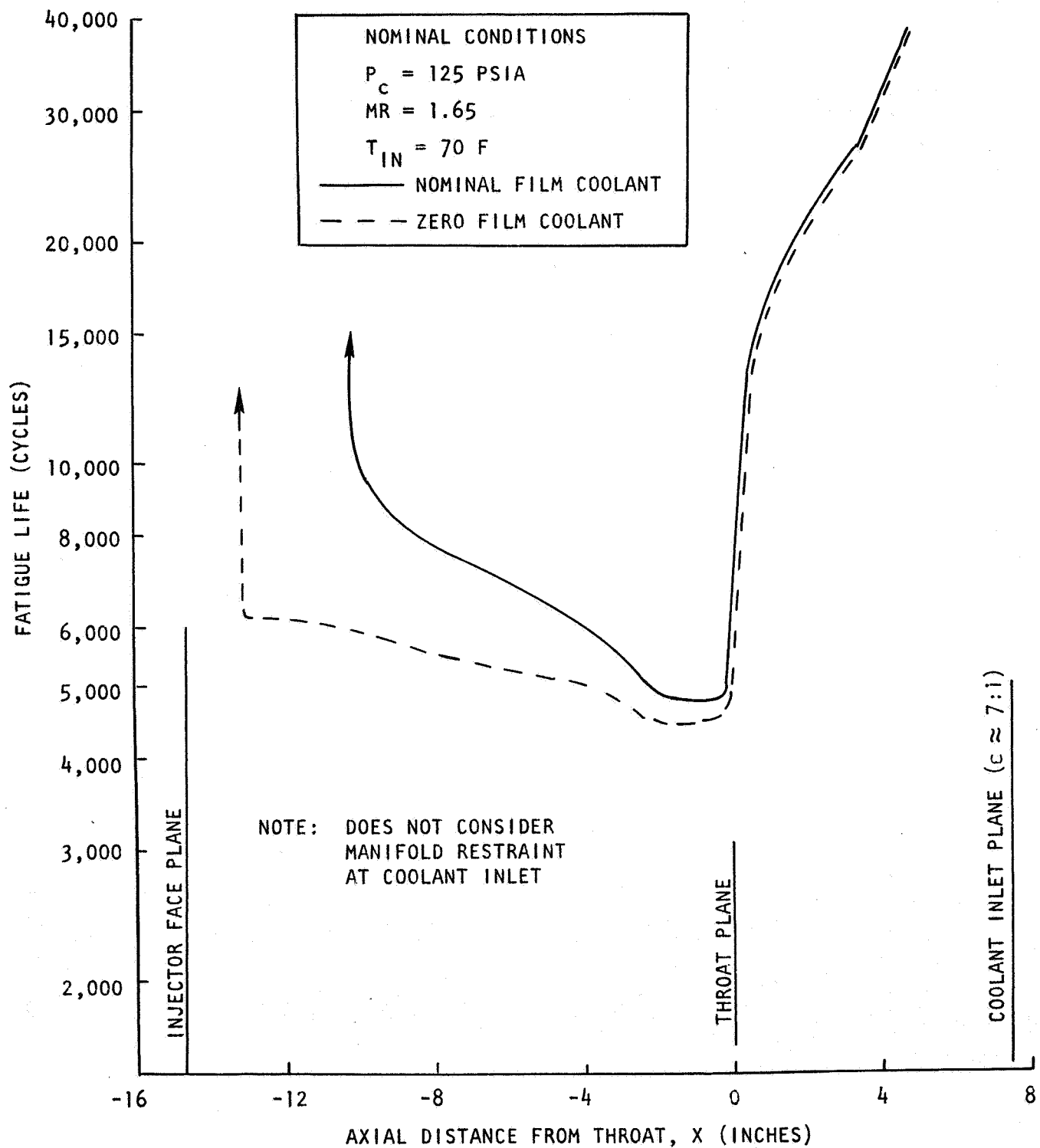
Figure 134. Regenerative Coolant Safety Factor Profile

Figure   135 Predicted Fatigue Life Capability Profile

R-9686

divided more equally between the CRES liner and nickel closeout. Life can also be increased by reducing the thickness of the nickel closeout and/or CRES liner.

7.0 COMPARISON OF 8- AND 10-INCH DIAMETER THRUST CHAMBERS

7.1 BASIC ENGINE DESIGN AND GROUND RULES

The point design SS/OME Regeneratively Cooled Orbit Maneuvering Engine described by Rocketdyne in the Task I, II Data Dump includes a regeneratively cooled thrust chamber having a contraction ratio of 2 and an injector-to-throat distance of 14.7 inches. The chamber has a diameter of 8.2 inches at the injector end and was designed with constant width channels from the injector through the throat region into the diverging section where a step change in the channel width was made to reduce the weight of the chamber. Since that Data Dump was prepared, potential advantages in performance, stability, and heat transfer characteristics have been indicated for a chamber having a contraction ratio 3 instead of 2. Also, significant weight advantages have been shown for fabrication of a chamber using constant land thicknesses instead of constant channel widths. Finally, experimental heat flux profiles became available for both chambers. The purpose of this analytical and design study was to compare the high and low contraction ratio thrust chambers and the two channel design concepts on the basis of weight, pressure drop, and performance. Only the basic thrust chamber assembly was considered in this analysis. The assembly consists of the injector, the regeneratively cooled thrust chamber, and the radiation cooled nozzle. Engine design factors from the Rocketdyne Data Dump, NASA CR-128675, and vehicle trade factors furnished by NASA were used in the study which is reported in more detail in NASA CR-141675.

Three chamber configurations were analyzed: 1) an 8-inch diameter (ϵ_c = 2) chamber having constant width channels; 2) an 8-inch diameter chamber having constant width lands; and 3) a 10-inch diameter chamber (ϵ_c = 3) having constant width lands. Component weights, pressure drops, and nozzle performance were calculated for each configuration using experimental heat transfer data. OMS trade factors were used to convert the weights and pressure drops to equivalent specific impulse values for: 1) constant OMS inert weight, and 2) constant OMS wet (tanked) weight.

Ground rules for the study are summarized in Table 44. The heat flux profiles are based on experimental data taken with Rocketdyne (ϵ_c = 2) and Bell Aerosystems (ϵ_c = 3) chambers. Two-dimensional analyses were used to calculate the temperature distribution for the chamber with constant-width channels. The simpler, one-dimensional analyses were used for the chambers having constant-width lands. The narrow (0.040 inch) width chosen for the land results in lower wall temperature because the heat flux is uniformly distributed. To verify this, one- and two-dimensional analyses were made of chamber with ϵ_c = 2. The one-dimensional analysis indicated a wall temperature of 389.5F in contact with the coolant. The results of the two-dimensional analysis, shown

TABLE 44 .   GROUND RULES

Components: Injector, Chamber, Nozzle

Regeneratively Cooled Nozzle Area Ratio: 7

Nozzle Area Ratio: 72

  Chamber Length for ϵ_c = 2: 14.7 Inches

  Nozzle % Length for ϵ_c = 2: 70

Injector ΔP not dependent on ϵ_c

Experimental Heat Flux Profiles

Hot and Cold Wall Thicknesses: 0.030 Inches

Regen Safety Factor: 1.5 at Off Design

in the schematic computer printout of Fig.136 indicate essentially the same temperatures implying that no two-dimensional conduction penalty results from the narrow land.

If a land width much greater than 0.040 inches must be used (generally because of fabrication constraints), the two-dimensional penalty can be significant. For example, the two-dimensional analysis of a configuration with a 0.103-inch wide land (Fig.137) resulted in a maximum coolant side wall temperature of 402F compared to the one-dimensional value of 389F. The increased corner temperature implies a higher local heat flux and resultant reduced local safety factor.

All chambers were designed to have a safety factor of 1.5 at the following off-design conditions: 100F fuel inlet temperature, 120 psia chamber pressure and 1.73 propellant mixture ratio.

Guided by previous designs and the data shown in Fig.138 and 139, 120 channels were selected for all chambers. Land widths of 0.04 inches at the throat and inner and outer wall thicknesses of 0.03 inches were used for consistency on both chambers. The low contraction ratio chamber could use a 0.05-inch constant land if required by fabrication constraints. Use of the 0.05-inch land on the high contraction ratio chamber would result in branching. In practice, a very slight reduction in the contraction ratio from the value of 3:1 would be required to eliminate the branching constraint. Alternatively, the extraneous lands could be machined out. This would result in a maximum channel width of 0.26 inches which would be marginal from the stress consideration and require further analysis. A more detailed discussion of branching of lands follows.

7.2 CHANNEL GEOMETRY

Figures 138 and 139 are useful in making the initial estimates of design parameters for chambers having constant width lands. The geometric relationships between channel width, land width, and number of channels are shown in Fig.138. If the number of channels is small or the land width is large, as the straddle mill cutter moves from the throat region towards the injector-end the increasing chamber circumference results in the initiation and formation of a gradually widening land extraneous to the desired constant-width land. This extraneous land would probably have to be at least partially machined away to avoid the feather-edge pointing toward the throat region and may, in the extreme, present an unacceptably thick land near the injector-end. The curves shown in Fig.139 indicate the combinations of channel and land widths and number of channels which can be used to avoid branching and extraneous lands. The branching constraint does not unduly restrict

CHANNEL DIMENSIONS (IN.)

WALL THICKNESS = 0.0300
CHANNEL HEIGHT = 0.0911
CHANNEL WIDTH = 0.1771
LAND WIDTH = 0.0400
CLOSEOUT THICK = 0.0300

TWG(1-D) = 599.89 F
TWC(1-D) = 389.45 F
HC (1-D) = 0.8018E-02

TAW = 3049.69 F
HG = 0.6730E-03
(BTU/IN2-S-F)

TBULK = 183.81 F

TEMPERATURES (F)

582.98	582.82	582.43	582.23	590.46	595.27	596.65
512.82	512.47	511.54	510.71	520.23	525.20	526.57
444.40	443.35	440.41	436.70	450.52	455.52	456.77
380.79	378.39	370.83	357.00	381.80	386.26	387.25
253.75	251.81	245.97	236.15			
207.08	206.38	204.32	200.97			
189.70	189.55	189.08	188.25	186.63	185.94	185.74
188.94	188.85	188.59	188.21	186.80	186.09	185.87
188.58	188.52	188.36	188.13	186.88	186.17	185.94
188.46	188.42	188.30	188.10	186.91	186.20	185.96

Figure 136. Two-Dimensional Thermal Analysis of Channel
Section - Constant Land Width Design

CHANNEL DIMENSIONS (IN.)

WALL THICKNESS = 0.0300
CHANNEL HEIGHT = 0.0850
CHANNEL WIDTH = 0.1140
LAND WIDTH = 0.1031
CLOSEOUT THICK = 0.0300

$TWG(1-D) = 599.41$ F
$TWC(1-D) = 388.89$ F
$HC(1-D) = 0.8040E-02$

$TAW = 3049.69F$
$HG = 0.6730E-03$
$(BTU/IN2-S-F)$

$TBULK = 183.77$ F

TEMPERATURES (F)

677.31	670.92	653.37	631.21	617.74	611.52	609.72
611.53	604.69	585.52	560.34	547.09	541.09	539.33
550.41	542.68	519.74	485.24	474.47	469.47	467.97
494.58	485.85	457.89	402.17	400.23	396.88	395.76
368.66	360.18	333.73	286.23			
288.86	283.40	266.92	239.30			
238.79	236.66	230.36	219.55	212.35	208.83	207.72
235.83	233.96	228.60	220.67	214.13	210.50	209.34
234.13	232.43	227.70	221.15	215.11	211.51	210.33
233.57	231.94	227.42	221.28	215.42	211.84	210.66

Figure 137. Two-Dimensional Thermal Analysis of Channel
Section - Constant Land Width Design
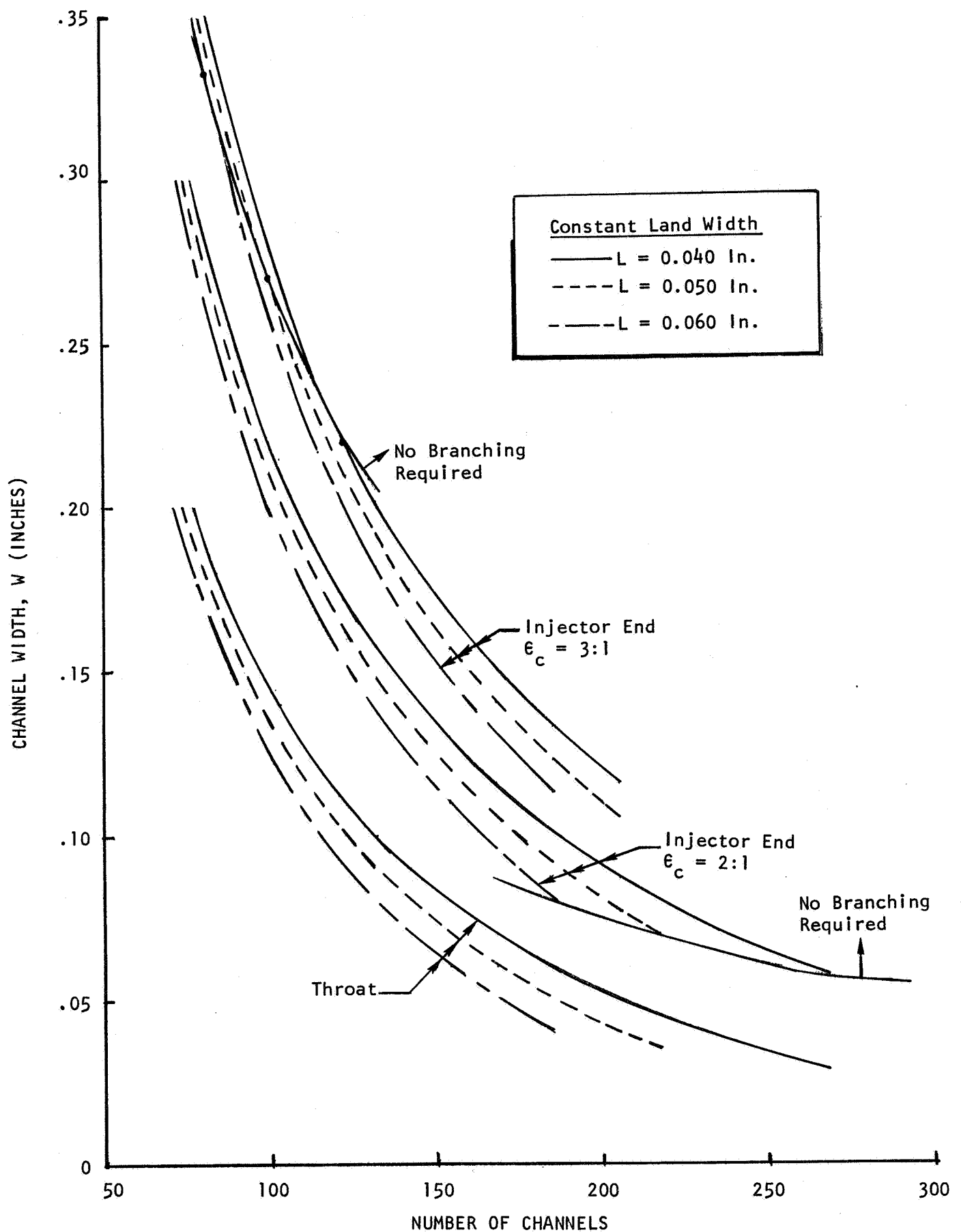
Figure 138. Channel Geometry Relationships For Constant Land
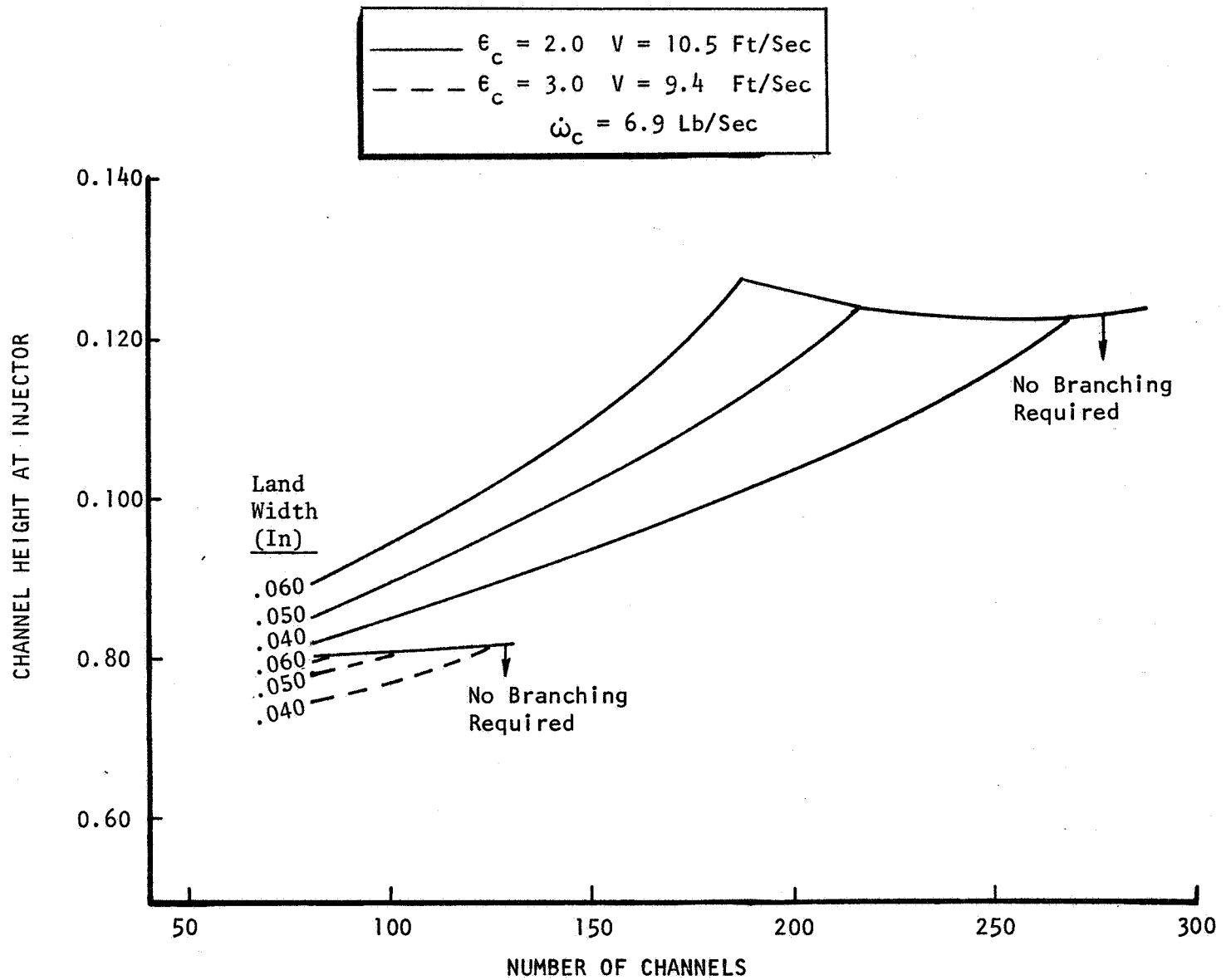Width Chamber Design

R-9686

Figure 139. Channel Height Requirements For Constant Land Width Chamber Designs

the combination of design parameters available for a constant land chamber with a contraction ratio of 2:1 using a straddle mill cutter. For the chamber with a contraction area ratio of 3:1 and a land width restricted to 0.040 inches or larger for fabrication and structural reasons, the number of channels must be restricted to 120 or less to avoid channel branching. This results in a channel width of approximately 0.225 inches near the injector-end. Reducing the number of channels below 120 results in wider channels which are not structurally acceptable. The sensitivity of the branching constraint to the chamber contraction ratio is obvious in Fig.138 where it is shown that for a land width of 0.040 inches the maximum allowable number of channels is approximately doubled in the 2:1 contraction ratio chamber compared to that of the 3:1 chamber. The constraint on minimum channel width is reduced by almost a factor of 4 for the lower contraction area chamber.

The constant land design is not unduly constrained by channel height limits as shown in Fig.139 . For typical land widths and number of channels, the minimum channel height is greater than 0.08 inches for the small diameter chamber and greater than .075 inches for the larger diameter chamber. Selecting a large number of channels could result in a large ratio of the land (channel) height to width ratio which would be somewhat difficult to machine. However, this only occurs when the number of channels exceeds about 200 for the smaller diameter chamber.

7.3 ANALYSES AND RESULTS

The three chambers described above were designed and analyzed to determine pressure drops and channel height profiles. Weights were calculated for the chambers, injectors, and radiation nozzles. The chamber with the higher contraction area ratio is 2½ inches shorter than the other chambers so that a longer, higher performing nozzle can be used. Space Shuttle trade factors were used to convert differences in weight and pressure drop between the chambers to effective specific impulse differences. Combining these with the nozzle performance difference resulted in comparisons in performance between the three chambers for injectors with performance assumed to be equal. Alternatively, the injector performance requirements for equal effective specific impulse were determined.

Thermal Analyses

The height profiles required to maintain the required safety factor at off design conditions in the various chamber design concepts are shown in Fig.140 The channel width and land width profiles are shown in Fig.141 A typical pressure profile for the 8" diameter constant channel width chamber is shown in Fig.142. The jacket pressure drops and life
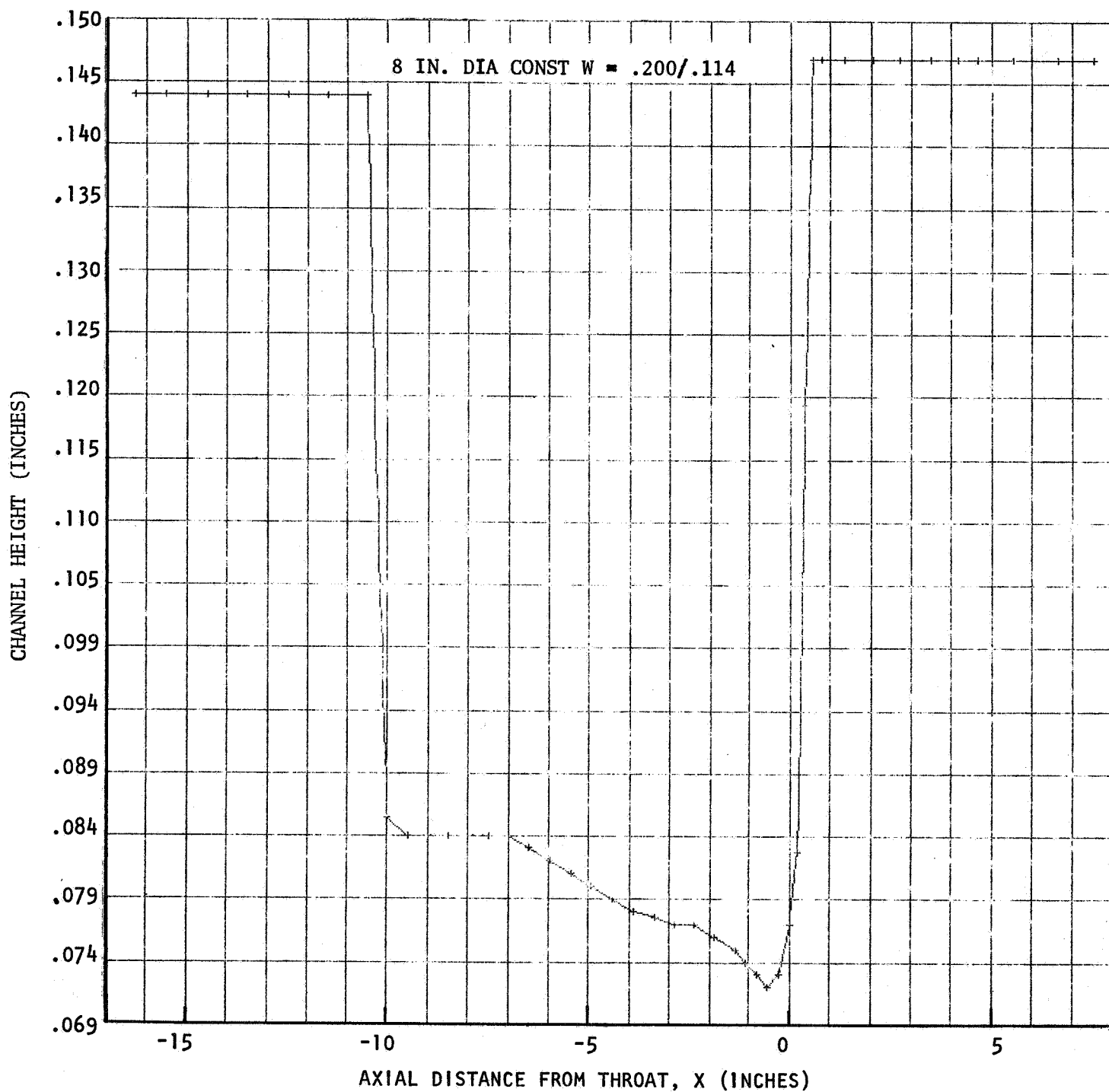
Figure 140a.   Channel Height Profile For 8-Inch Diameter Chamber -
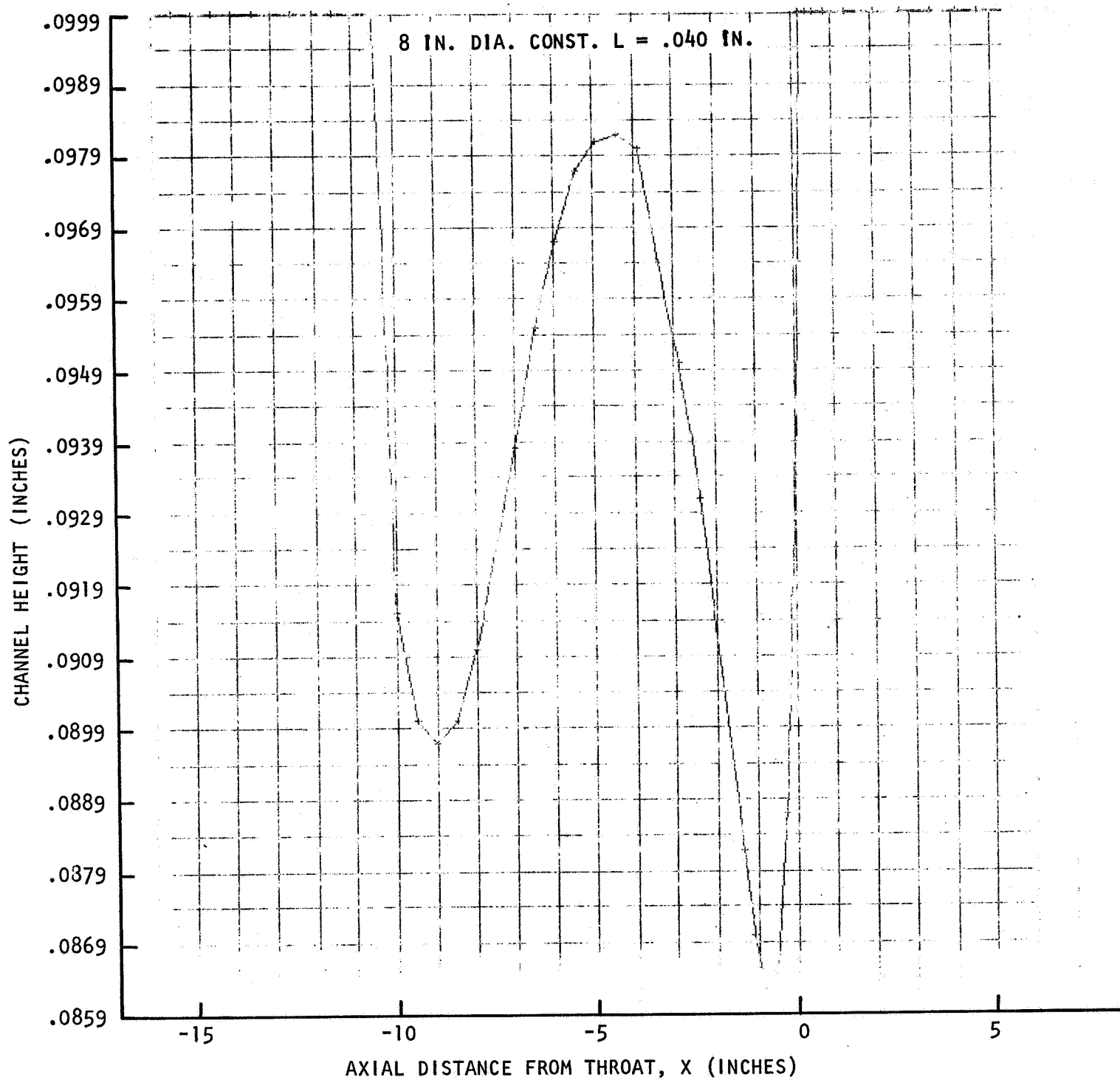Constant Channel Width Design

Figure 140b. Channel Height Profile For 8-Inch Diameter Chamber -
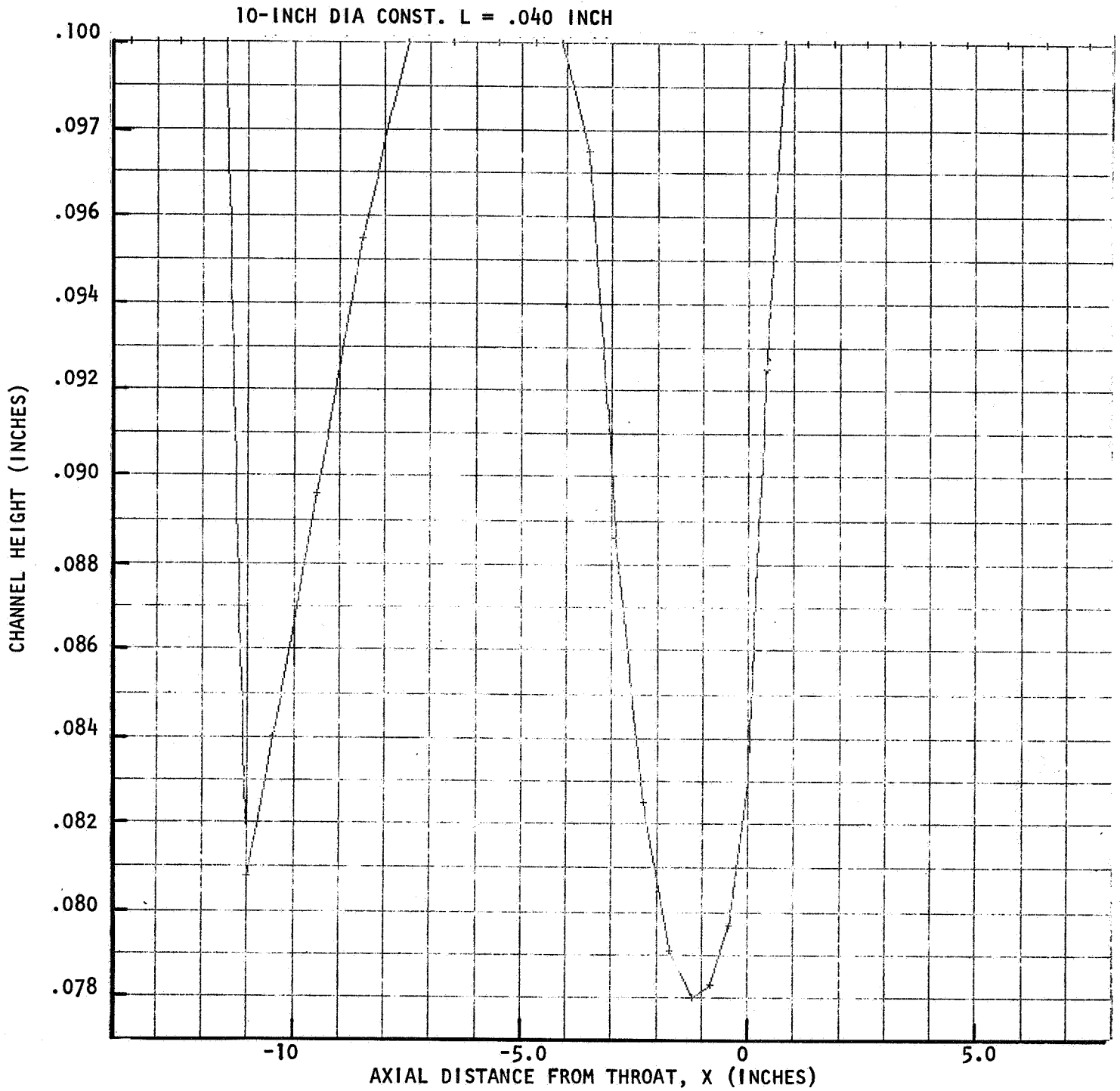Constant Land Width Design

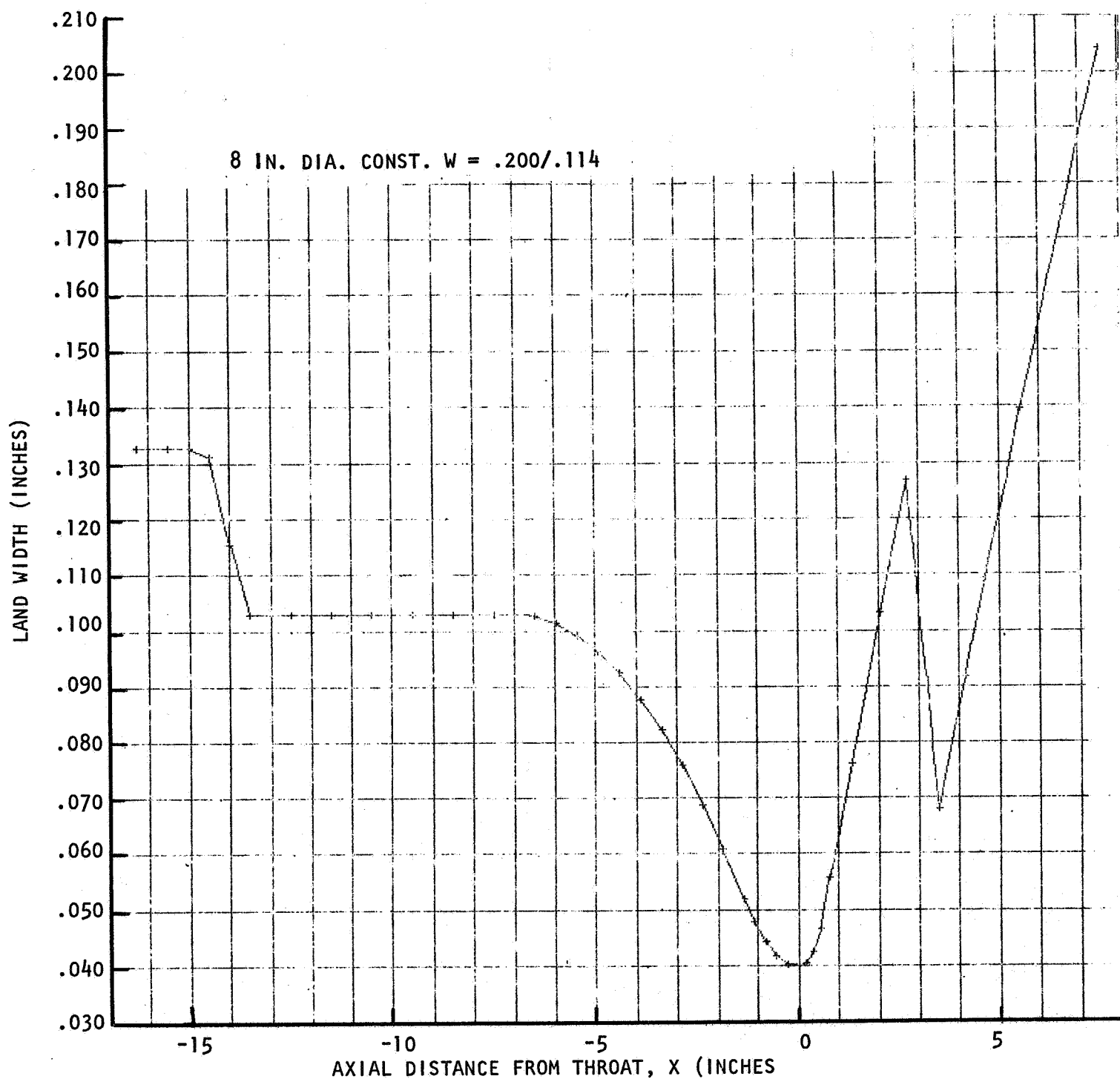Figure 140c. Channel Height Profile For 10-Inch Diameter Chamber
Constant Land Width Design

Figure 141a. Land Width Profile For 8-Inch Diameter Chamber
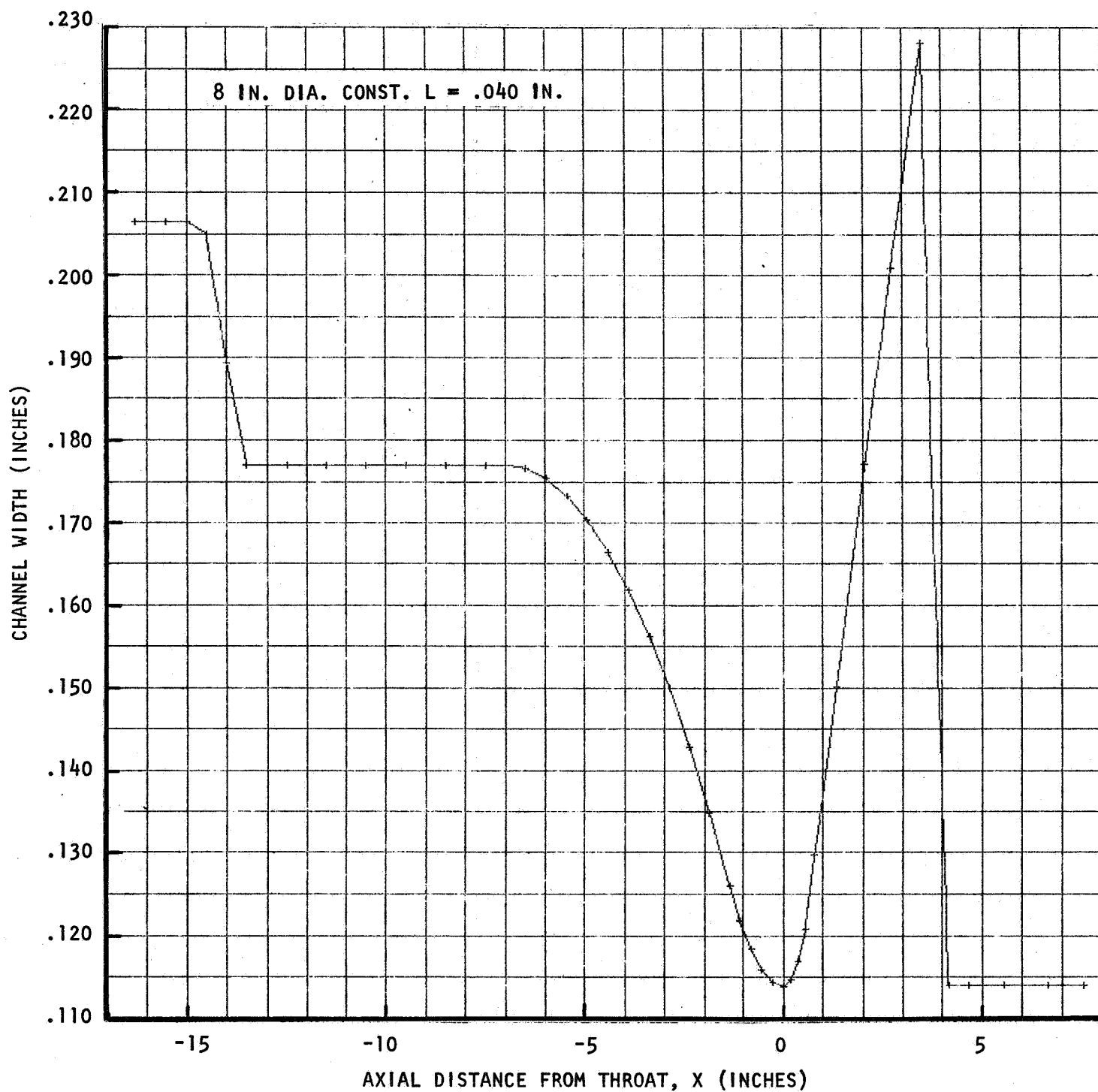Constant Channel Width Design

R-9686

Figure 141b. Channel Width Profile For 8-Inch Diameter Chamber
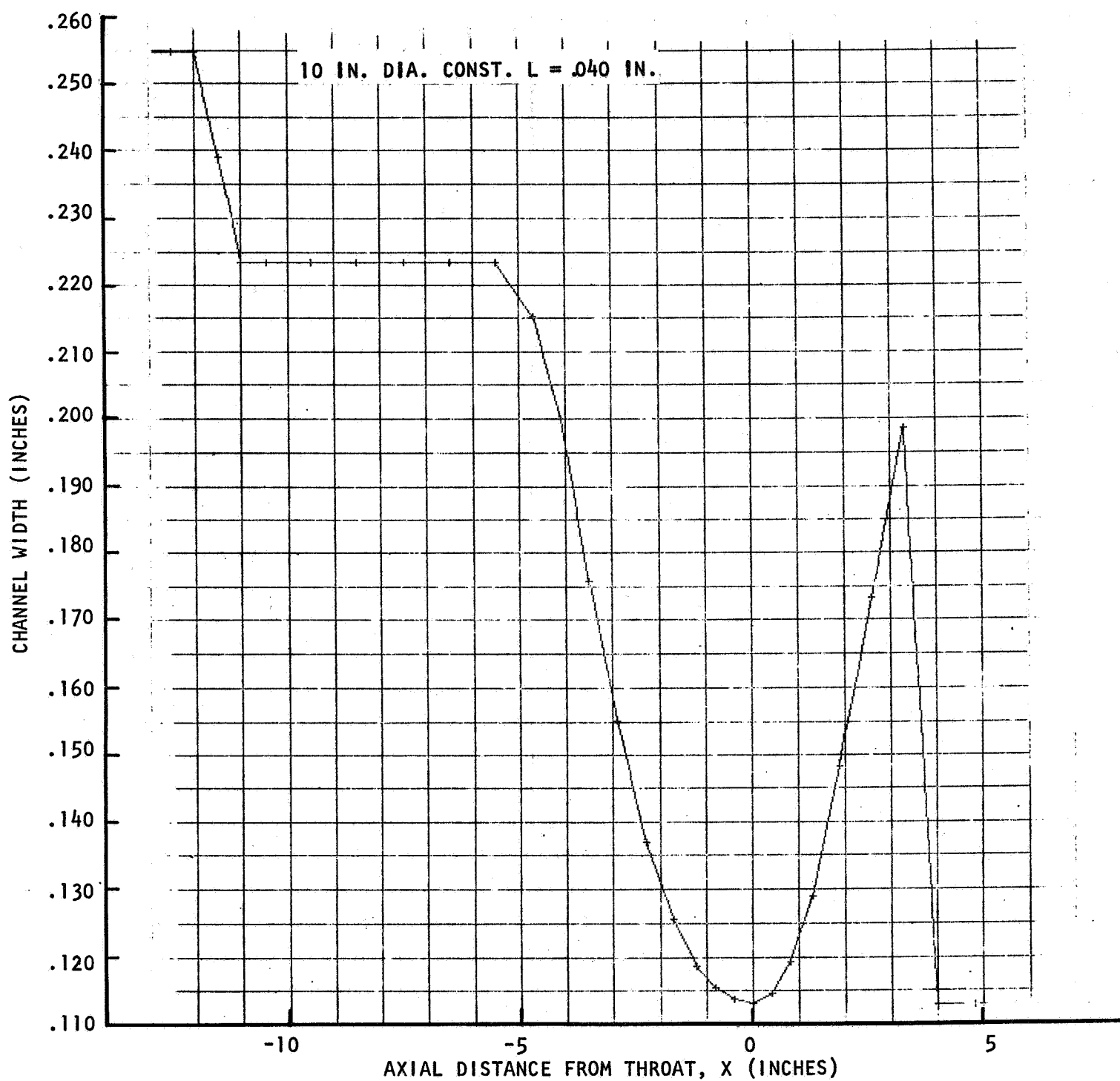Constant Land Width Design

R-9686

Figure 141c. Channel Width Profile For 10-Inch Diameter Chamber
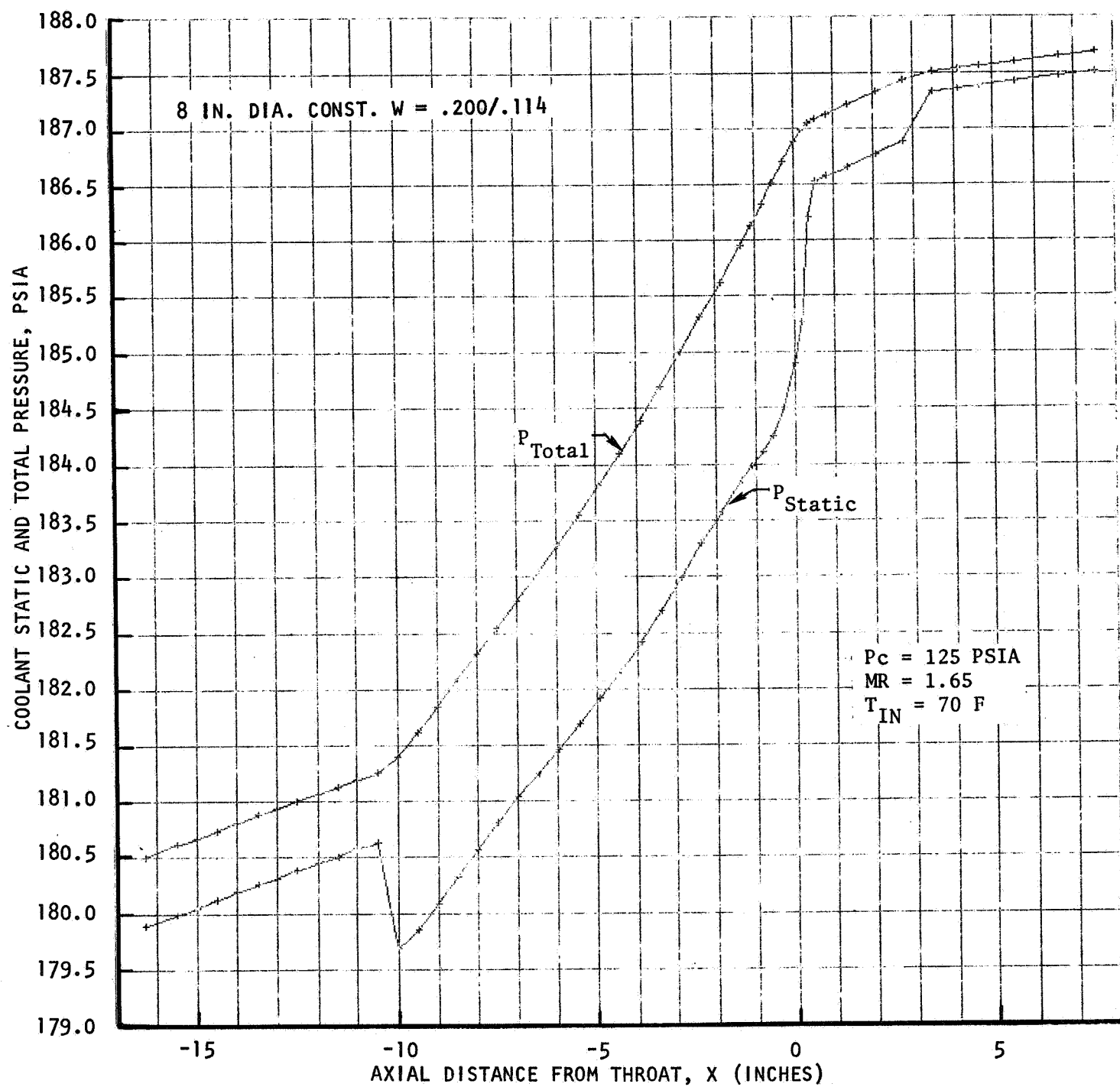Constant Land Width Design

Figure 142. Coolant Pressure Profile For 8-Inch Diameter Chamber
Constant Channel Width Design

expectancies are summarized below.

Construction	ε_c	Jacket ΔP, psi	Life, cycles
Constant Channel	2	7.7	5100
Constant Land	2	4.1	5100
Constant Land	3	3.9	4500

The drop for the chamber with low contraction ratio and constant width channels is less than that measured on Rocketdyne's Demonstrator and Integrated thrust chambers because the latter were designed to accommodate a theoretical heat flux which was considerably higher than the experimental profile near the injector. Experimental heat flux profiles are shown in Fig. 143.

Weight and Performance Analyses

Jacket weights were calculated from the channel dimension profiles. Injector, coolant outlet manifold, and radiation nozzle weights for the high contraction chamber were scaled from the low contraction chamber weights. The resulting values (pounds) are tabulated below:

Construction	ε_c	Jacket	Injector	Manifold	Nozzle	Total
Constant Channel	2	24.0	23.6	11.4	41.2	100.2
Constant Land	2	17.5	23.6	11.4	41.2	93.7
Constant Land	3	17.0	35.4	12.1	42.5	106.8

The results presented in NASA Memorandum EP22/M11-74 were used to estimate the performance advantage of the longer nozzle used with the high contraction ratio chamber. The increment was 0.9 seconds specific impulse.

7.4 COMPARISONS

Differences in weights and interface pressures were converted to effective specific impulse using the following OMS sensitivity data furnished by the NASA Program Manager

-4 lb system inert wt/psi interface pressure (oxidizer and fuel)

3 lb system inert wt/sec engine specific impulse

75 lb system wet wt/sec engine specific impulse

The results are summarized in Table 45 with comparisons made both on the basis of OMS wet weight and OMS inert weight. The chambers having
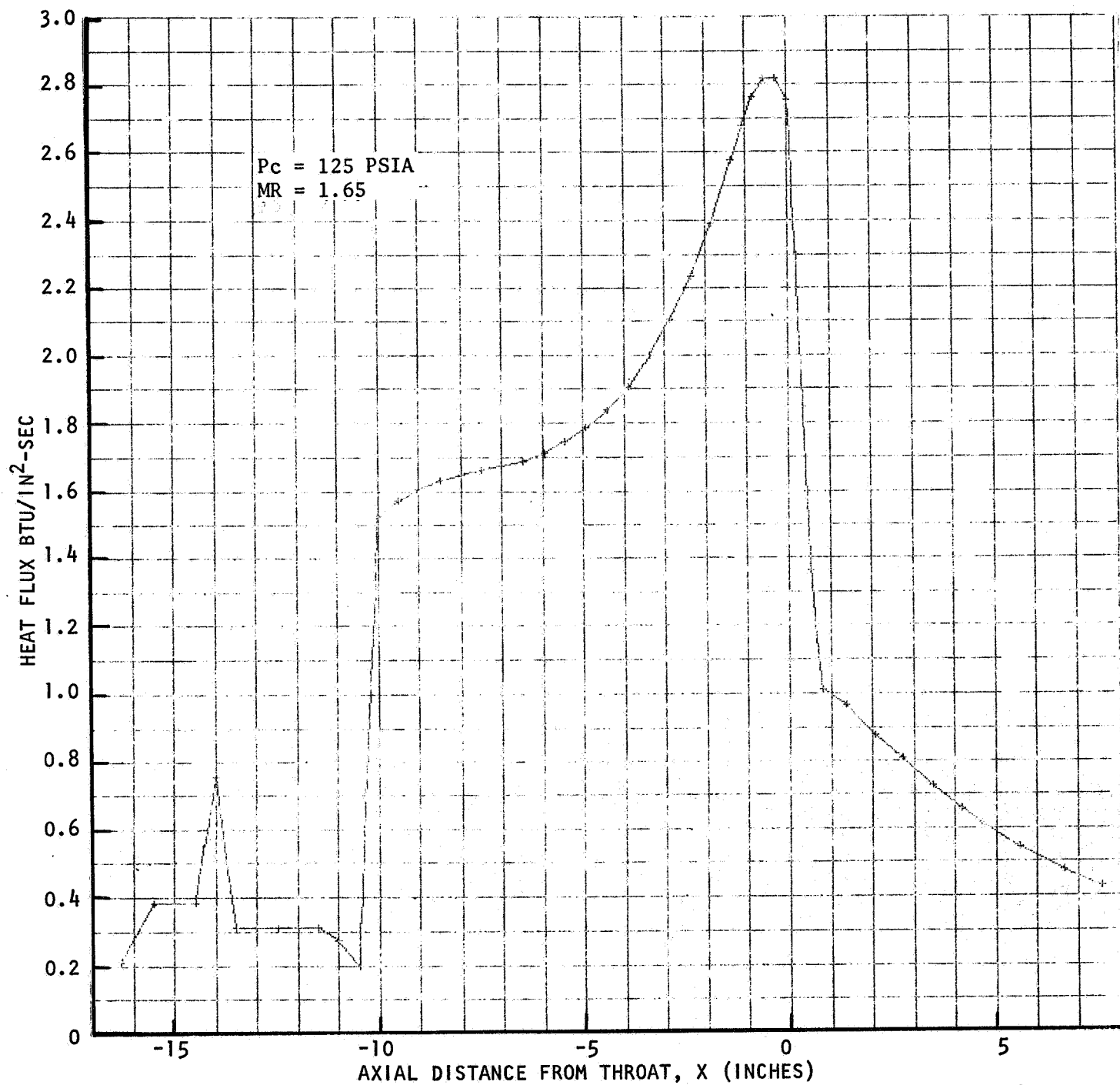
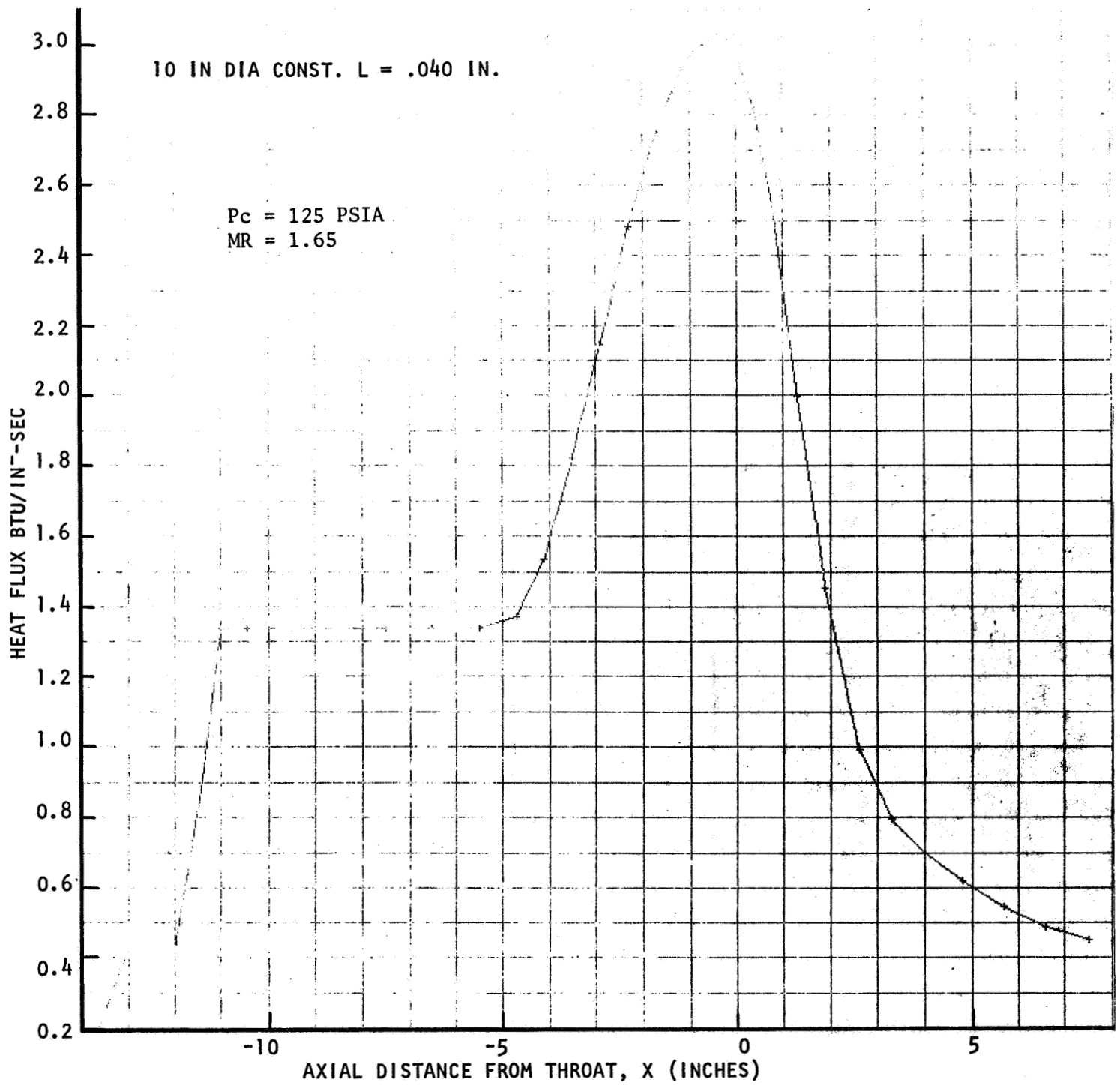Figure 143a. Heat Flux Profile For 8-Inch Diameter Chamber

R-9686

Figure 143b.   Heat Flux Profile For 10-Inch Diameter Chamber

TABLE 45. SUMMARY OF THRUST CHAMBER ASSEMBLY CHARACTERISTICS

Configuration	ϵ_c	Wt. Difference Lb	Equivalent ΔI_s, Sec		Δ Inlet Press., PSI	Equivalent ΔI_s, Sec		Nozzle I_s Δ Sec	Net Equiv. ΔI_s, Sec		Allowable Loss in $*_c$, %	
		Nominal	Nominal		Nominal	Nominal		Nominal	Nominal		Nominal	
			Inert	Wet		Inert	Wet		Inert	Wet	Inert	Wet
Constant Channel Width	2											
Constant Land Width	2	-6.5	2.2	0.1	-3.6	4.8	0.2	0	7.0	0.3	2.2	0.1
Constant Land Width	3	6.6	-2.2	-0.1	-3.8	5.1	0.2	0.9	3.8	1.0	1.2	0.3

constant width lands are superior to the chamber having constant width channels on either basis. The low contraction ratio chamber is significantly superior (3.2 sec) on the basis of inert weight. Comparison based on OMS wet weight put more emphasis on performance so the longer nozzle of the high contraction chamber gives it a slight advantage (0.7 sec).

APPENDIX A

THRUST CHAMBER TEST FACILITIES

Uncooled and regeneratively cooled thrust chambers were tested during the course of the program at Rocketdyne and NASA White Sands test facilities. The Propulsion Research Area and Component Test Laboratory facilities were used at Rocketdyne. Altitude Cell 401 was used for the tests at NASA/WSTF.

UNCOOLED CHAMBER TEST FACILITY

Victor Test Stand in the Propulsion Research Area was used to test the 8- and 10-inch diameter thrust chambers. The facility configurations were similar for testing both chambers. The facility is shown in Fig. 144. A schematic of the feed system is shown in Fig. 145. NTO and MMH were supplied from pressurized tanks having maximum pressure capabilities of 2500 and 1500 psig, respectively. The propellants passed through 40 filters before entering the engine valves. No attempt was made to simulate OME valve operation or duct volumes other than to assure that an oxidizer lead of approximately 100ms occurred. GN_2 purges were supplied downstream of the engine valves and were sequenced to purge the engine immediately at cutoff.

The oxidizer flowed to the engine at ambient temperature while the MMH was batch heated in quantities required for a single firing through the use of a 4.5 gallon heat exchanger located upstream of the main fuel valve. In this heater the water flowed in stainless steel tubing and provided a limited temperature heat source for the fuel. The water was heated by an 18 kilowatt Chromalox heater. An alternate supply of cold water was used to cool the tank between tests for personnel safety.

Instrumentation

Facility instrumentation is shown in the schematic. Engine instrumentation was provided to measure pressures and temperatures.

Three type 614A Kistler high frequency response pressure pickups were used to monitor chamber pressure. The steady-state value of chamber pressure was measured using two Taber type transducers with sensing ports located in the acoustic cavities. These same type transducers were used to measure the fuel and oxidizer injection pressures and the feed system pressures. The temperature of the gas in the acoustic cavities was measured using tungsten/rhenium thermocouples. Thrust chamber wall temperatures were measured with chromel/alumel thermo-
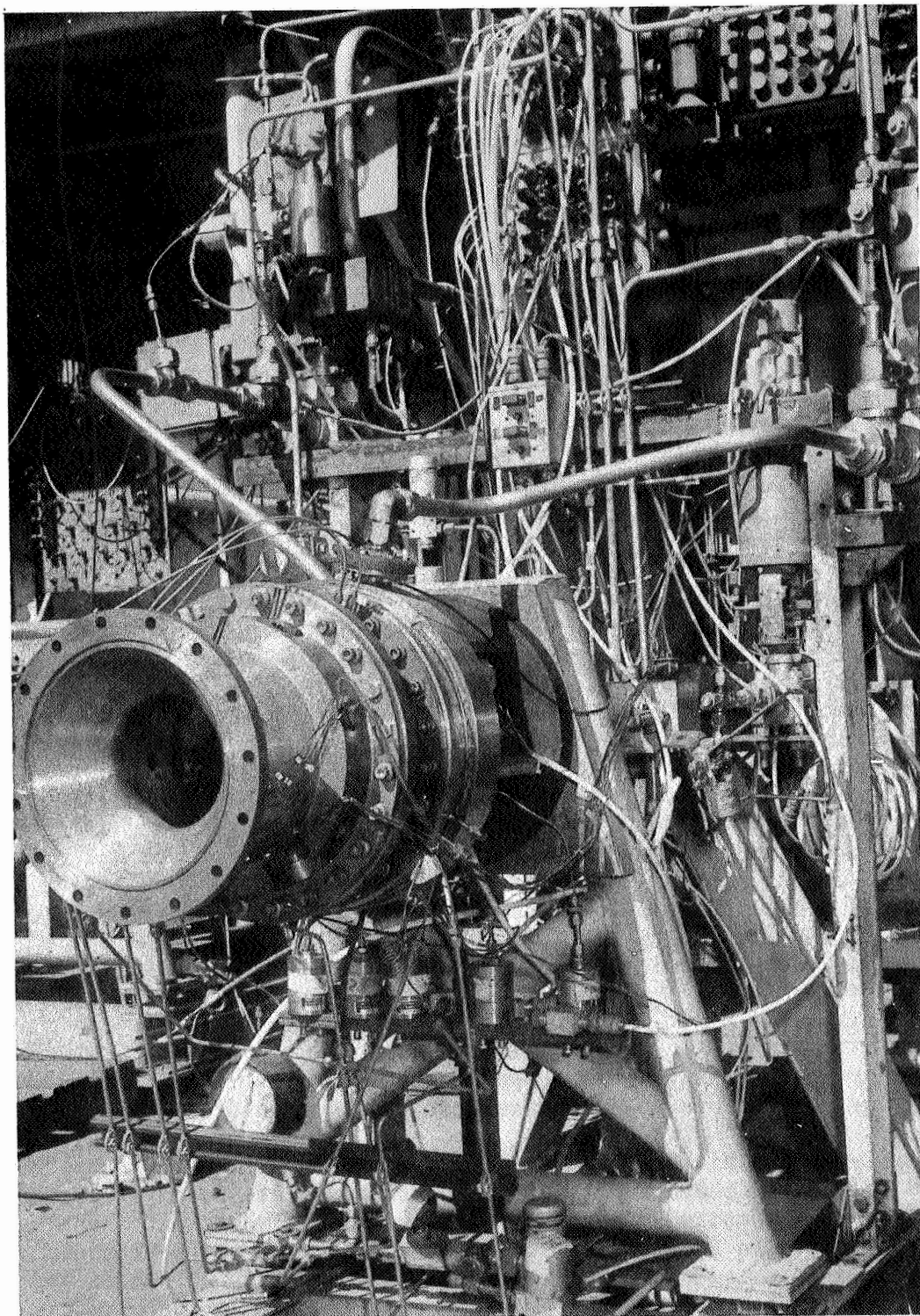
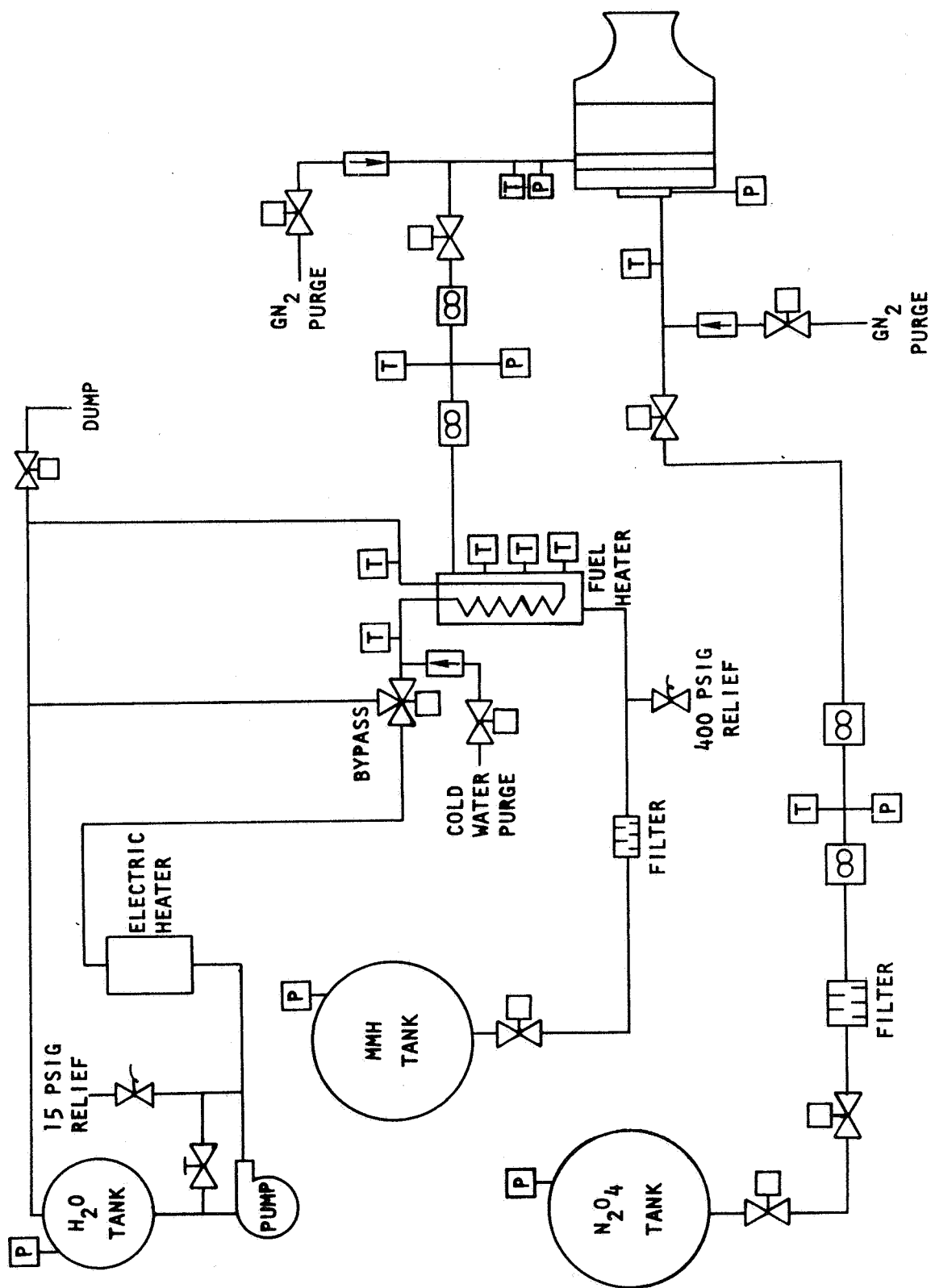Figure 144. Uncooled Engine in Victor Test Stand at PRA

Figure 145. Propellant Feed Systems and Instrumentation Schematic

R-9686

A-3

couples. Propellant feed system temperatures were measured with iron/
constantan thermocouples. Two turbine flow meters were used to measure
each propellant flow rate. Thrust was also measured for computation of
c*. The estimated precision of each of the critical measurements
(thrust, chamber pressure, and flow rate) is 0.25 percent.

High response data were recorded on tape and oscillograph. The oscillo-
graph was also used to record the slower responding chamber pressure
measurements, the flowrates, and the injection pressures. Most data
except the high speed data were also recorded on a digital tape. Direct
inking charts were used to provide quick-look data.

REGENERATIVELY COOLED CHAMBER TEST FACILITIES

The OME demonstrator thrust chamber and the integrated thrust chamber
were tested at Rocketdyne and NASA/WSTF. These tests were part of
Tasks V, VIII, and XII.

Rocketdyne Test Facility for Demonstrator Chamber

Cell 29-B of Rocketdyne's Component Test Laboratory IV was the test site
for initial tests on the demonstrator thrust chamber.

Figure 146 is a photograph of Rocketdyne's Component Test Laboratory IV.
The engine is shown installed in this facility in Fig.147. Two feed
system arrangements were used for the engine in this facility. One of
the configurations shown in Fig.148 was used to provide a bypass cooling
system in which coolant flowed through the regenerative jacket and was
dumped into a catch tank. A separate feed system (from the same propel-
lant tank) provided fuel for the injector. The fuel in this system was
heated in a hot water heat exchanger to simulate the temperature of the
propellant leaving the regeneratively cooled jacket. Oxidizer flow to
the engine was controlled by regulating the oxidizer tank pressure to a
predetermined value dependent upon the system and engine hydraulic
resistance. The coolant flowrate and pressure levels were adjusted by
the use of appropriately sized fixed orifices at the inlet and exit to
the thrust chamber cooling jacket. Fuel flow for the injector was
obtained from a branch (tee) in this line and the flowrate was adjusted
by a variable area throttling servo-controlled valve. The injector
fuel feed system and the oxidizer feed system contained dual flowmeters
for measurement of propellant flowrates while a single flowmeter was
used in the thrust chamber bypass cooling system. Boundary layer coolant
flow was taken from the injector feed system and controlled and measured
by means of a calibrated orifice. Gaseous nitrogen purges were supplied
at the engine for all feed systems and a water flush was provided at the
injector interface. Purges were operated manually at the end of each
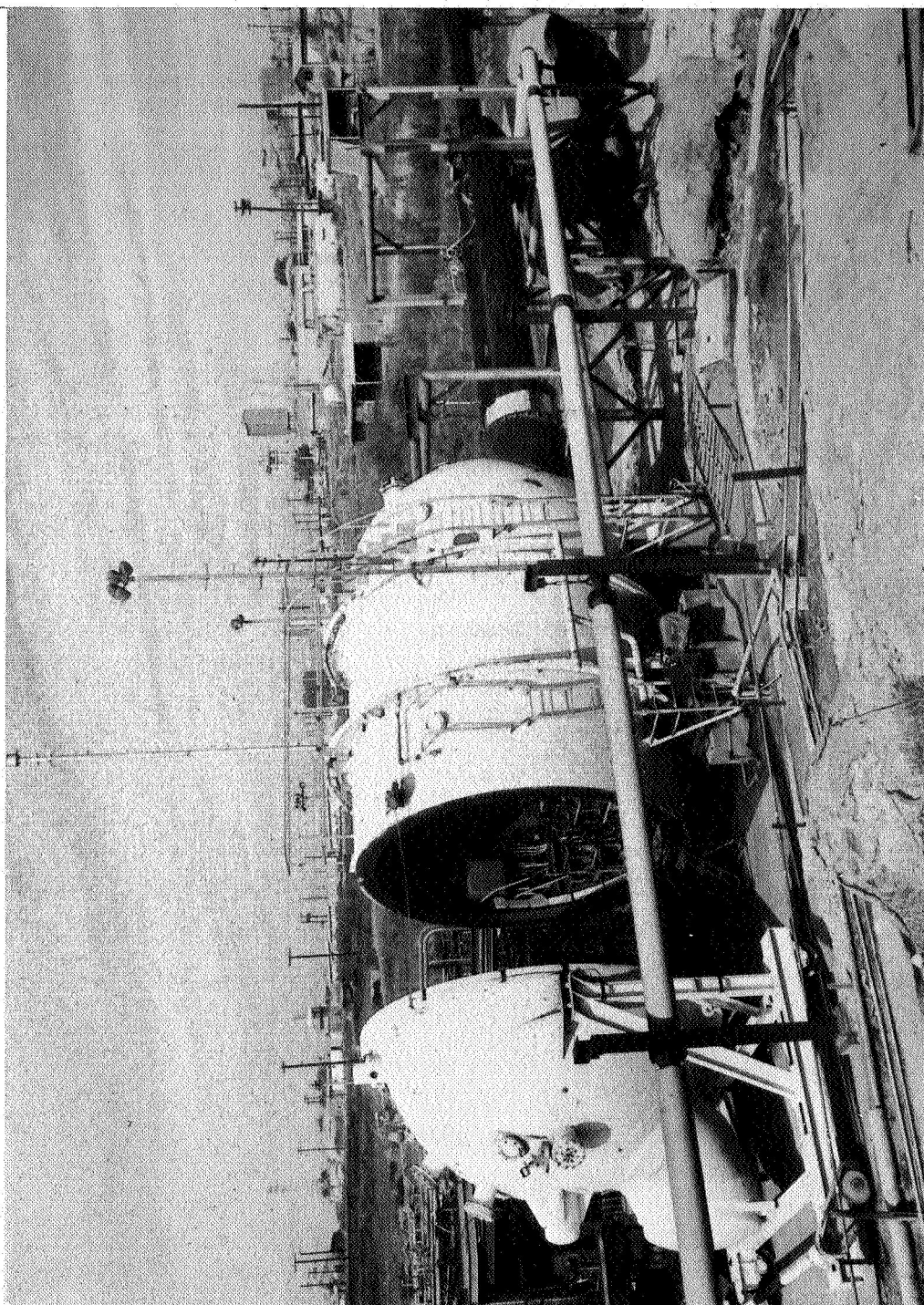test series to permit safe inspection of the thrust chamber and injector.
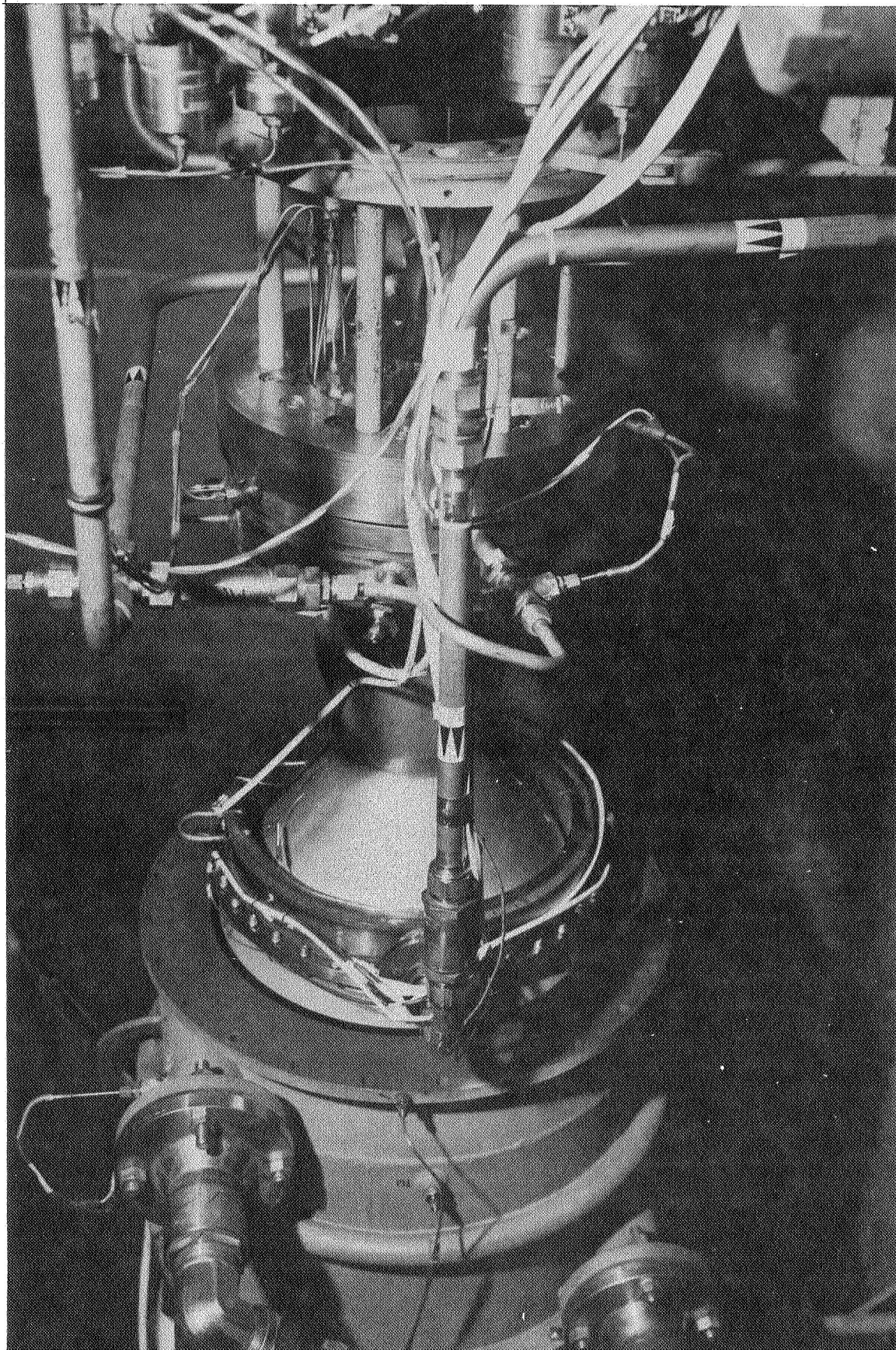
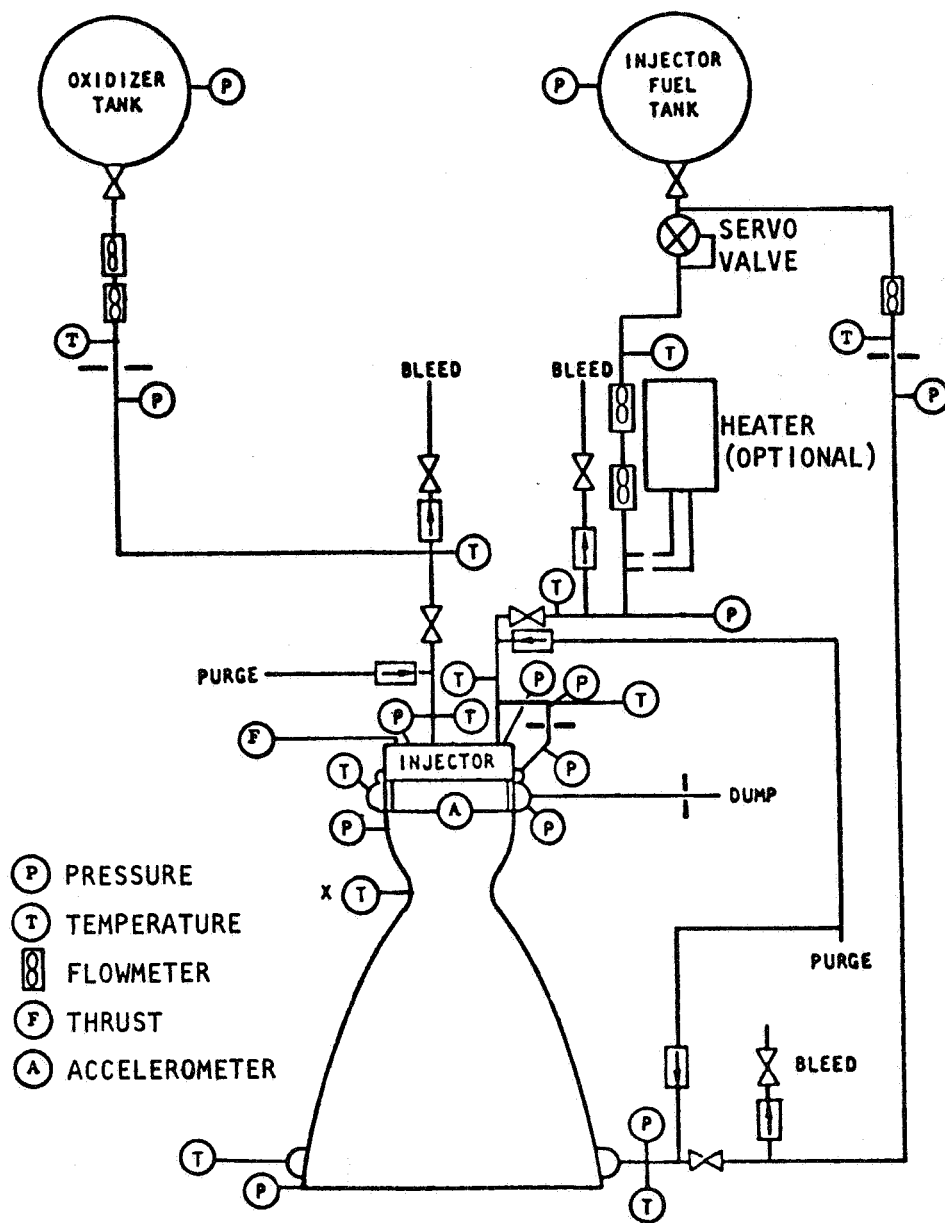Figure 146. CTL-IV Altitude Cell

Figure 147. OME Demonstrator Chamber In CTL-IV

Figure 148   Facility And Instrumentation Schematic
For Bypass Cooling

After the first checkout tests, the feed system was replumbed to the configuration shown in Fig.149, in which coolant exiting the regenerative jacket was ducted directly into the injector manifold. The servo valve was used to control the fuel flowrate. The oxidizer and fuel tanks were each rated at 665 psig and had capacities of 1600 and 1200 gallons, respectively. Several hundred seconds of operation at OME conditions were, therefore, possible with these propellant tanks.

The CTL-IV altitude facility in which the engine was tested is shown schematically in Fig.150. The engine was mounted horizontally in the 16-foot diameter altitude capsule and fired into a water cooled diffuser duct. The capsule is 31 feet long with hemispherical ends, one of which is roller mounted to provide access to the engine. A gas generator driven ejector was initially fired to reduce the pressure in the altitude capsule with the 42-inch flapper valve closed. When the engine ignited, the valve was opened by a pneumatic actuator and the engine exhaust maintained the capsule at the low pressure. A simulated altitude of 75,000 feet (0.5 psia) is attainable with this configuration. At engine shut-down, the 42-inch vlave was closed to minimize blowback into the altitude capsule.

The ejector was run continuously during the test and was shut down after engine shutoff. When the ejector was shut down, the isolation valve was closed and the capsule slowly brought up to pressure by bleeding in external air through the 6-inch vent valve. The gas generator system for the ejector has sufficient propellants to provide for 45 minutes of operation.

Thrust was measured by a single axis dual bridge load cell so that two thrust readings were obtained. Two independent flow measurements were made for each propellant entering the injector and a single flow measurement was made of the fuel coolant when the configuration was plumbed for bypass operation.

The testing at CTL-IV was initiated by preparing the engine test stand for operation by bringing the propellant tanks up to the required run pressure and assuring that the engine stand and the engine data acquisition systems were in readiness for the test. The hyperflow gas generator system was started and brought up to full operation. At this time the altitude capsule isolation valve was opened to permit the hyperflow action to pump down the altitude cell to the run pressure (0.5 psia).

Throughout the entire program, the engine valves were individually activated from a sequence timer so that signals to the valves could be controlled independently.

Figure 149   Facility and Instrumentation Schematic
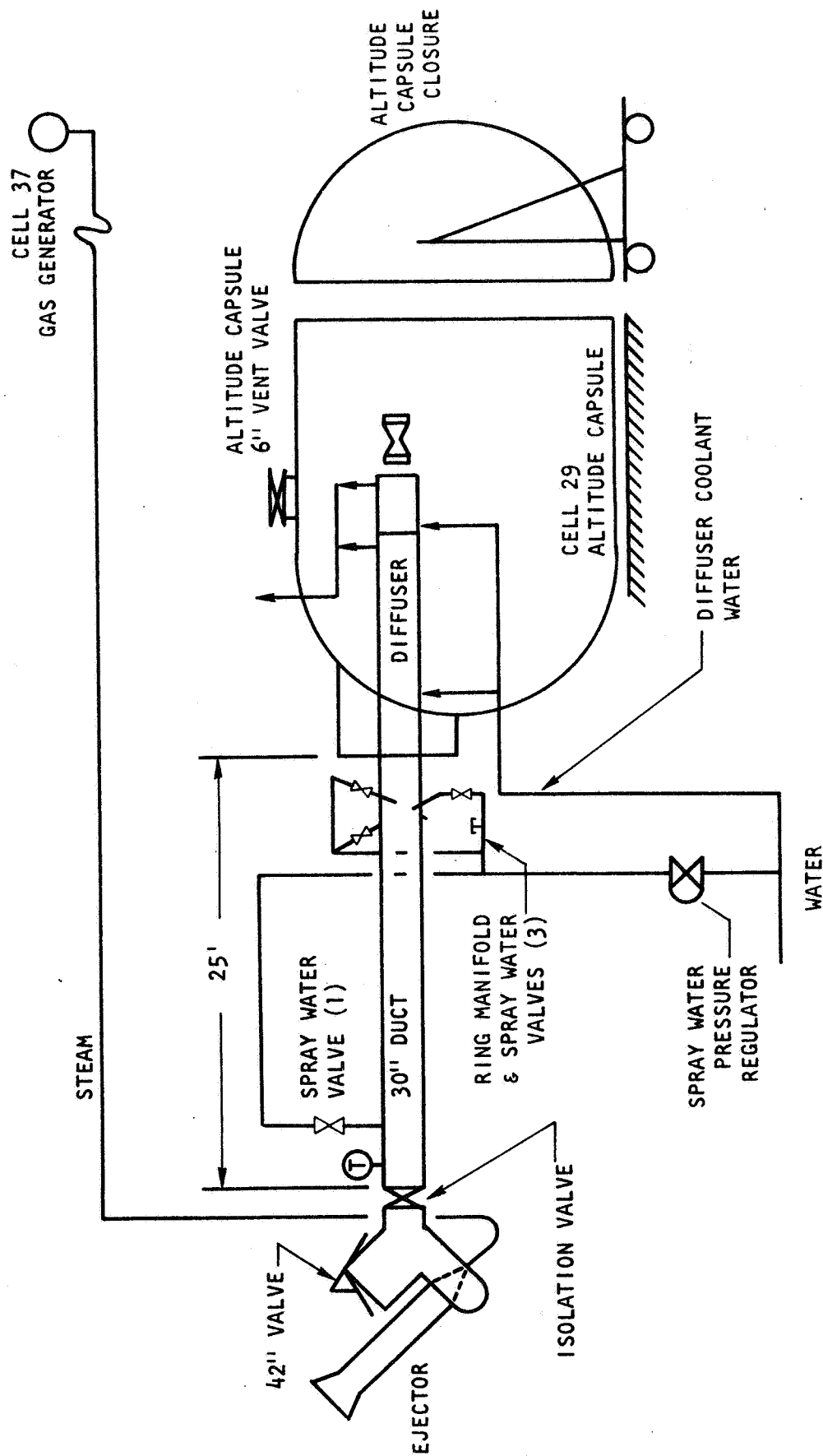Regeneratively Cooled Engine With BLC
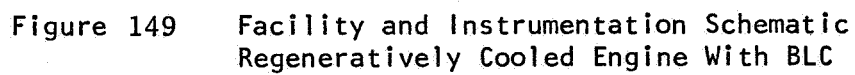
Figure 150 Cell 29 Facility Schematic

R-9686

A-10

During the bypass cooled phase of the program, three main propellant valves were used:

1. An oxidizer propellant valve.

2. A fuel propellant valve for controlling fuel flow to the injector.

3. A fuel valve for controlling fuel flow to the thrust chamber coolant jacket.

Test firing was initiated by opening the fuel coolant valve approximately 2 seconds prior to hot fire. The coolant outlet pressure was monitored by an automatic shutdown system so that if no coolant flow was observed, the propellant valves would not receive a signal to open. The 2 second time period allowed ample time for the coolant flow to establish and for manual observation of the flow on the "quick look" data recording system. The main oxidizer valve was then signaled to open and the fuel valve was signaled to open from 100 to 300 milliseconds later. This fuel valve delay assured that oxidizer would reach the injector prior to the fuel to assure an oxidizer-rich start and, thus, more nearly simulate an actual engine start sequence. The tests were automatically terminated after the predetermined duration by removing electrical power from the propellant valves. The oxidizer valve closed first and the fuel valve then closed within 100 milliseconds and the fuel coolant valve closed about 1 second later. This shutdown sequence assured that the thrust chamber coolant passages would be full of fuel during the shutdown transient to eliminate a possible hazard to the chamber. There was no posttest purge. The time required for each test was about 3 to 4 minutes, the variation dependent upon the tank pressure changes required and whether any difficulties were encountered making these changes.

The opening and closing sequence of the propellant valves was varied somewhat during the program to determine the effect of different oxidizer leads into the engine. The shortest oxidizer lead, as determined from review of the oxidizer injection pressure trace on the oscillogram, was less than 50 milliseconds, while the longest oxidizer lead was several hundred milliseconds. No significant difference in the engine ignition characteristics was observed with these different start transients.

Upon completion of the test series, the engine propellant manifolds were purged with GN_2 in order to clear the propellants from the engine for the posttest engine inspection. When the engine was sufficiently purged, the duct isolation valve was closed and the hyperflow gas generator was shut down. The altitude cell was returned to ambient pressure by opening a valve which allowed external air to bleed into the cell. After the cell was at ambient pressure and the cell door opened, additional engine purges were used to clear residual propellants from the engine.

The test sequence for regeneratively cooled operation was essentially the same except that there were only two propellant valves. The fuel was opened about 200 milliseconds prior to the oxidizer valve. With the additional distance traveled by the fuel in going through the engine regenerative cooling jacket, this resulted in a nominal oxidizer lead of about 200 milliseconds. There were no variations in the start sequence.

White Sands Test Facility Configuration for Demonstrator Chamber

The demonstrator thrust chamber assembly was also tested at Cell 401 of the NASA White Sands Test Facility at Las Cruces, New Mexico. The installation is shown schematically in Fig.151, and is similar to the setup used at CTL-IV. Figure 152 is a photograph of the installation in the Shite Sands Test Facility. Facility pressure drops under rated flow conditions were 40 psi for the oxidizer side, and 35 psi for the fuel side. Propellant tank capacities were 2000 gallons for both the fuel and oxidizer. Propellant tank pressures were limited to 372 psia on the oxidizer fuel sides. The altitude system was initially pumped down to a pressure of approximately 0.1 psia, and then a gas generator-driven ejector system pumped the capsule down to a pressure of 0.06 to 0.07 psia, equivalent to an altitude in excess of 100,000 feet.

Thrust measurements were made using a multi-axis measuring system with three axial dual bridge load cells for recording the main thrust. Instrumentation was similar to that used at Rocketdyne's CTL-IV, except that accelerometers were used to monitor the stability of the engine.

The test operation at WSTF was initiated with a vacuum pump evacuation of test stand 401. This operation was performed about 2-3 hours prior to the actual test operation. The engine test stand was then readied for operation by bringing the propellant tanks up to the required run pressure and assuring that the engine stand and the engine instrumentation were in readiness for the test. With this assurance that the engine was ready for testing, the hyperflow gas generator system was started and brought up to full operation. At this time the altitude capsule isolation valve was opened to permit the hyperflow action to pump down the altitude cell to the final run pressure.

The cell pressure was continuously monitored and when it reached 0.1 psia, engine test activity commenced. The first event, at sequence time equals zero, was activation of the "fire switch". At this time the electrical signal was simultaneously applied to both fuel and oxidizer main propellant valves.

Figure 151   Facility And Instrumentation Schematic
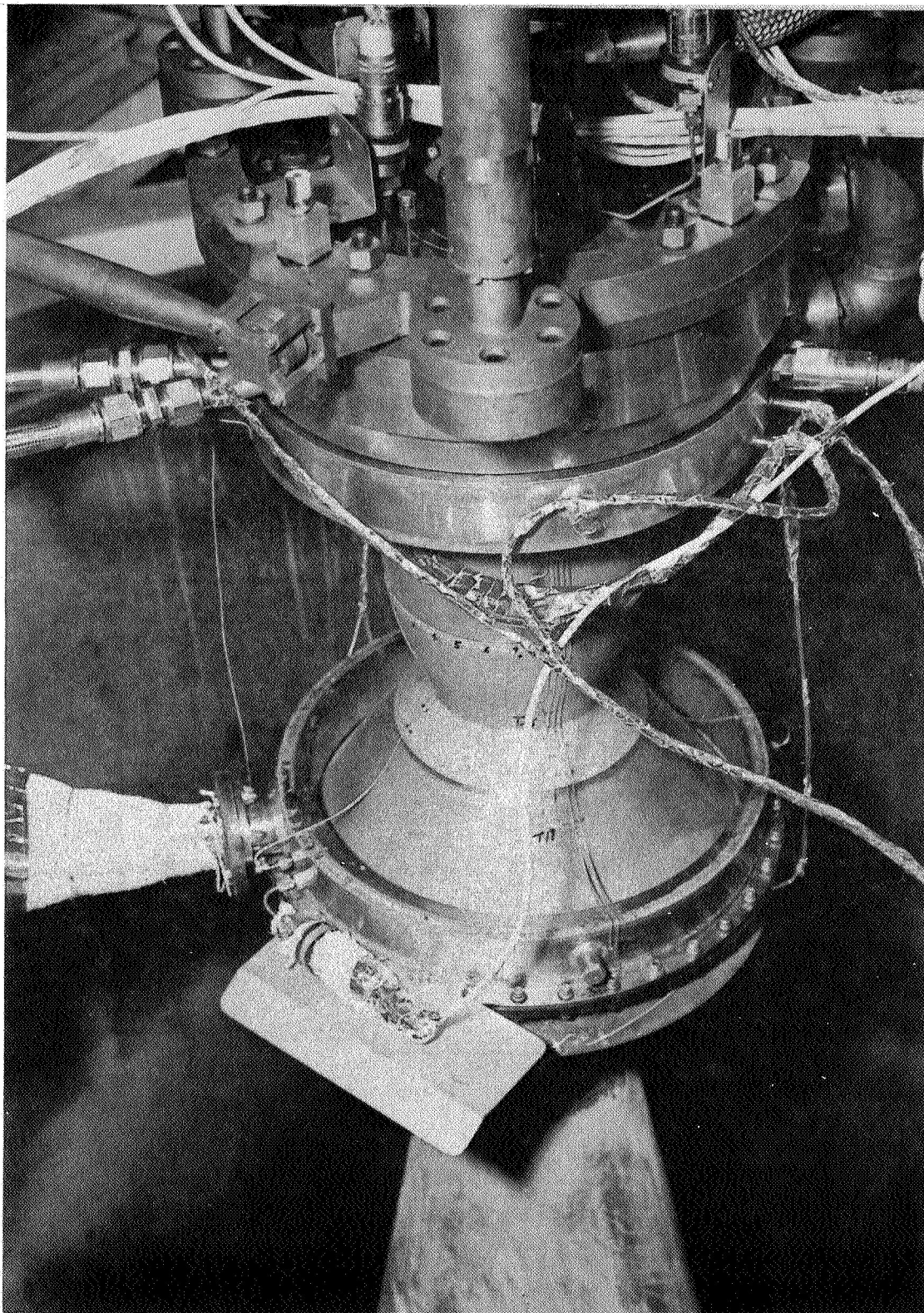For Regenerative Cooling

R-9686

A-13

Figure 152.   OME Demonstrator Chamber In WSTF

R-9686

A-14

The tests were automatically terminated after the predetermined duration by simultaneously removing power from the main propellant valves. The oxidizer valve closed first and the fuel valve then closed within 40 milliseconds as shown in Fig. 153. This shutdown sequence assured that the thrust chamber coolant passages would be full of fuel during the shutdown transient to eliminate a possible hazard to the chamber.

Following each test, the engine was purged with gaseous nitrogen. At 5 seconds after shutdown, the oxidizer side purge was turned on to empty the oxidizer side of the injector. Then 5 seconds later, the fuel side purge was activated to clear residual fuel from the thrust chamber coolant passages and from the injector manifold. Then the two purges were alternately cycled on and off at 5-second intervals until no propellant vapors could be seen, usually about 20 to 25 seconds after test shutdown. During this purge cycle, the propellant tank pressures were reset to the predetermined levels for the next test. The time required for each test was between 30 and 120 seconds, the variation generally dependent upon the magnitude of the tank pressure change. Following the last test of a sequence, the engine was purged as before. On completion of the purge, the altitude cell isolation valve was closed and the hyperflow steam generator system shut down. The altitude cell pressure was then returned to ambient by bleeding in gaseous nitrogen.

White Sands Facility Configuration for Phase I Tests on Integrated Chamber

The same test cell used for the demonstration chamber was used to test the integrated chamber. Instrumentation and feed system configurations were also similar. However, since boundary layer coolant was supplied by the injector and the transfer of fuel from the coolant jacket to the injector was internal to the thrust chamber, only one fuel feed line and associated instrumentation was required.

The installation of the integrated chamber in Cell 401 of WSTF is shown in Fig. 154 Testing with the steel high area ratio (72:1) nozzle required bleeding external air onto the nozzle between tests to prevent overheating. Additional nozzle temperature data was also recorded and used to terminate tests if the temperature exceeded 1500F.

White Sands Facility Configuration for Phase II Tests on Integrated Chamber

The primary purpose of the Phase II tests was to investigate OME start, shutdown, and restart transients. The propellant feed system was, therefore, reconfigured to simulate the Space Shuttle Orbiter feed system. Details of the plumbing are shown in Fig.155 and 156 . Figure 157 is a
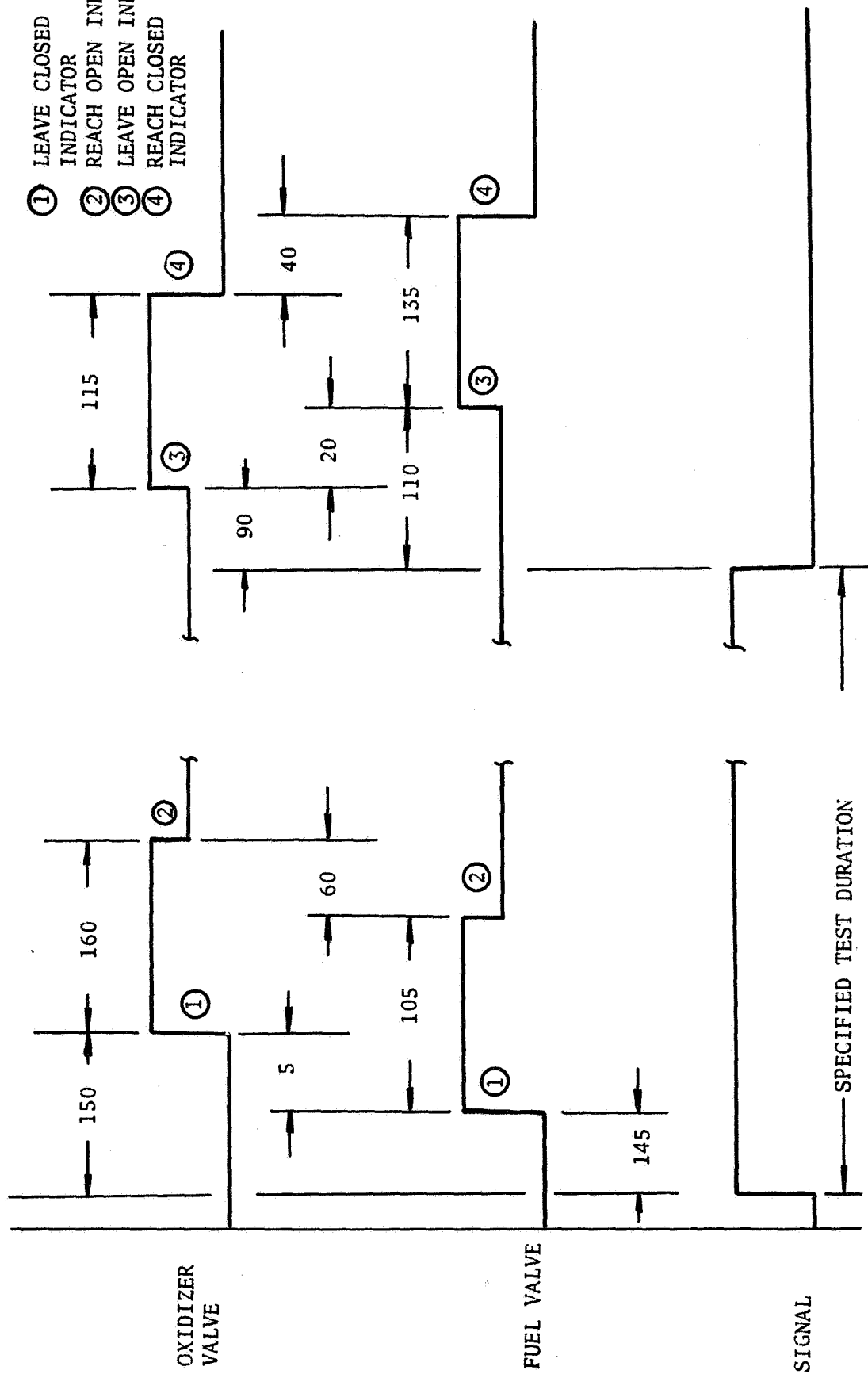
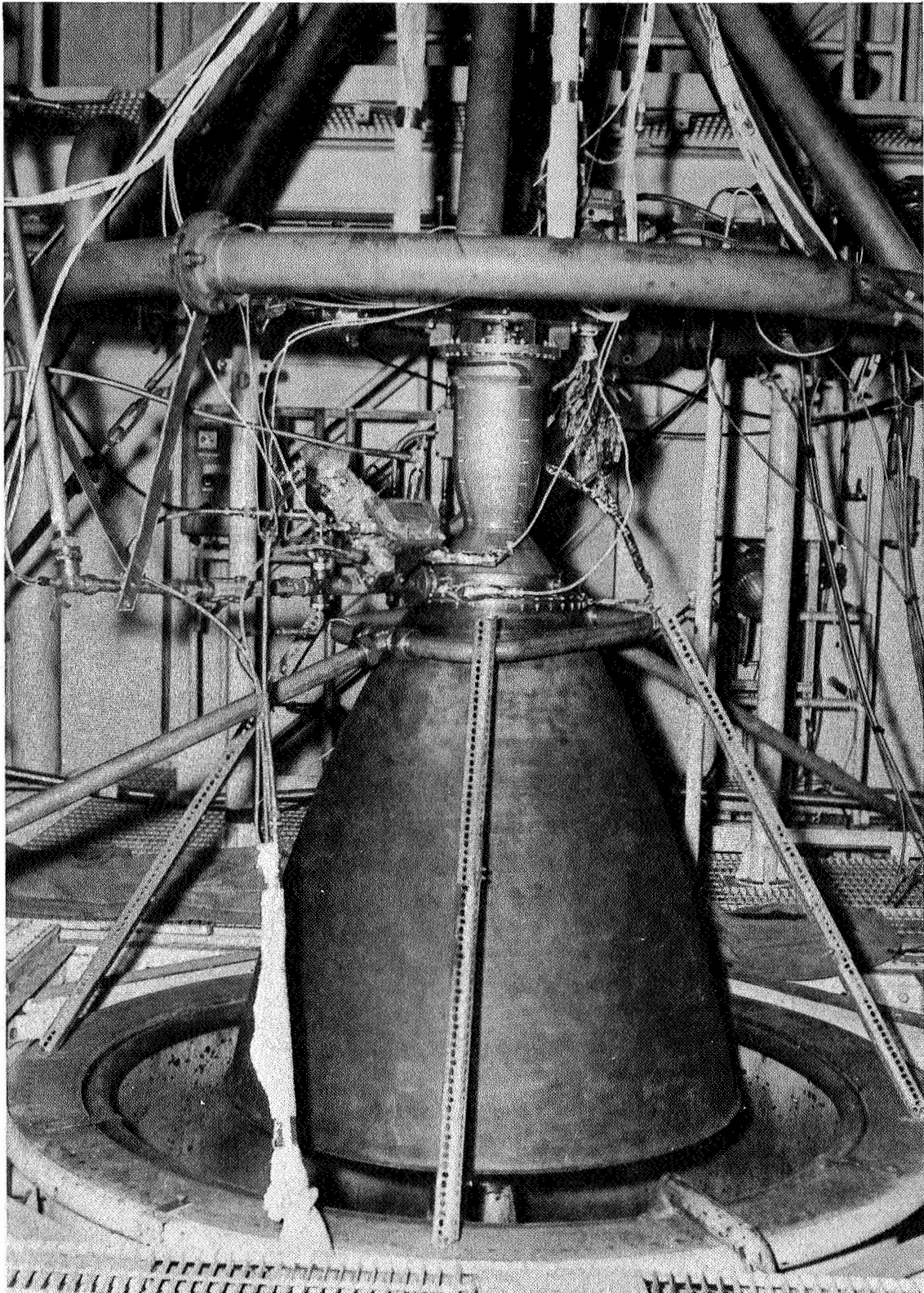Figure 153 OME Test Valve Sequencing (All Times in Milliseconds)

R-9686

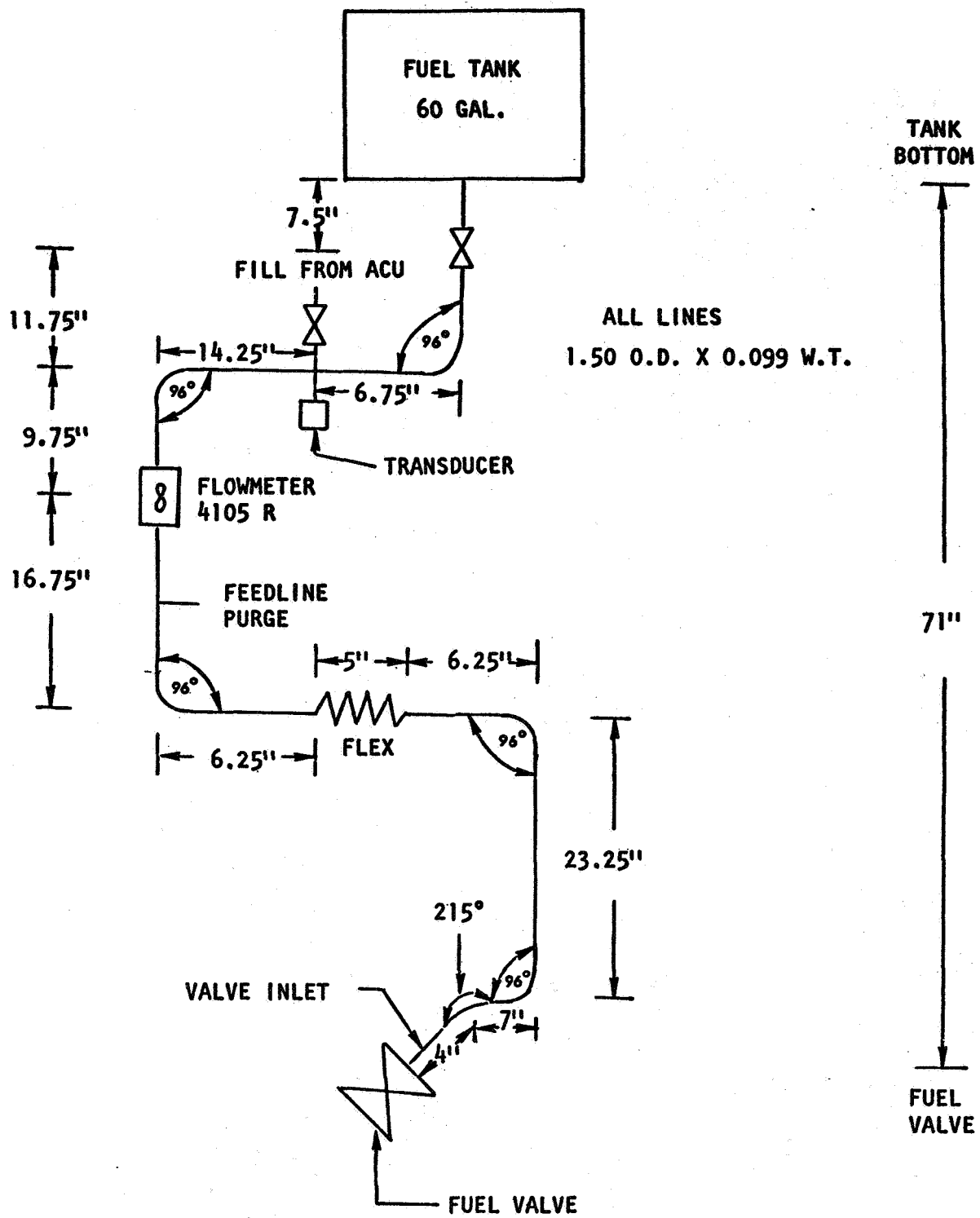Figure 154. Integrated Thrust Chamber Installed At WSTF

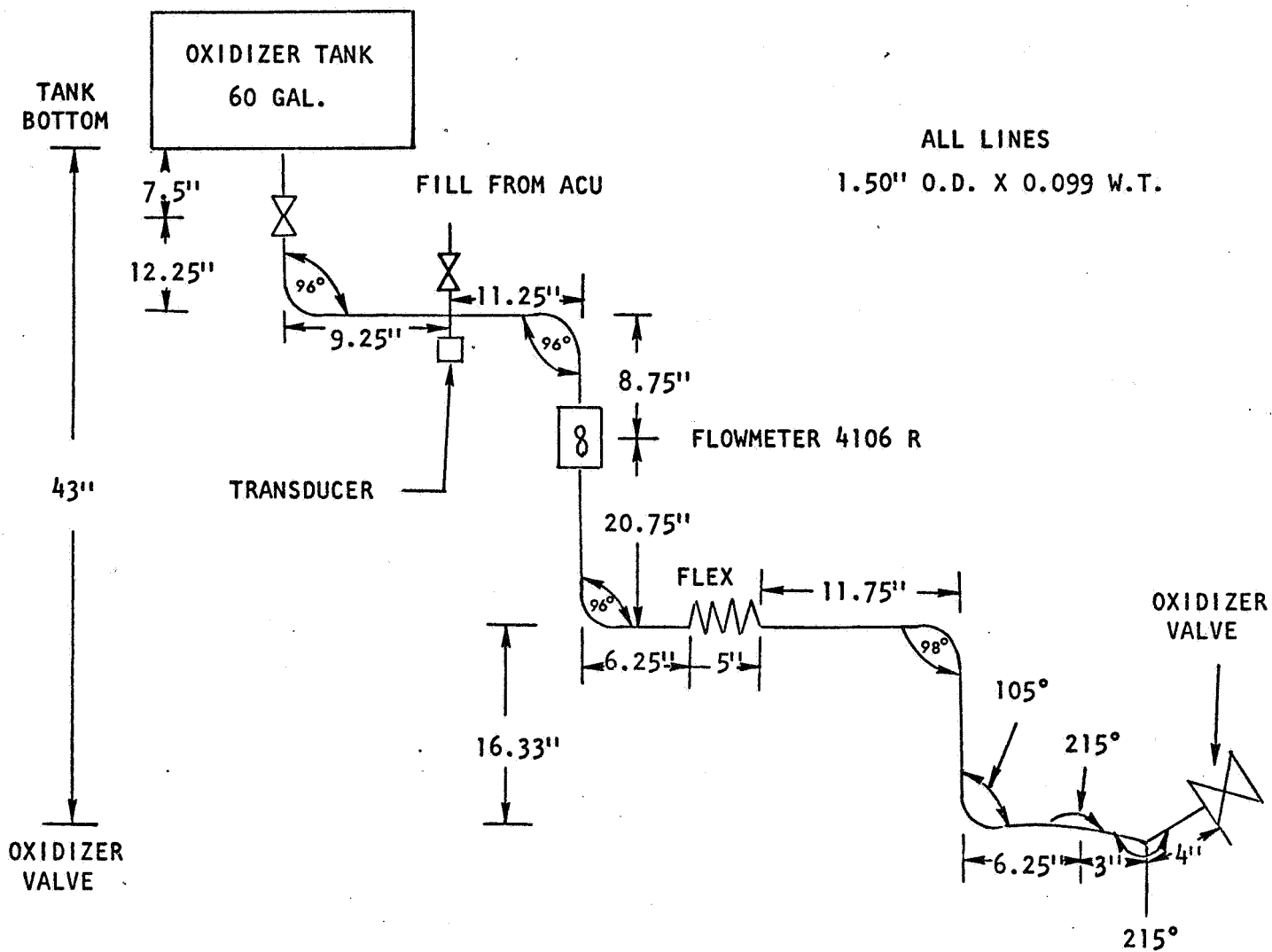Figure 155   Simulated OMS Fuel Feed System

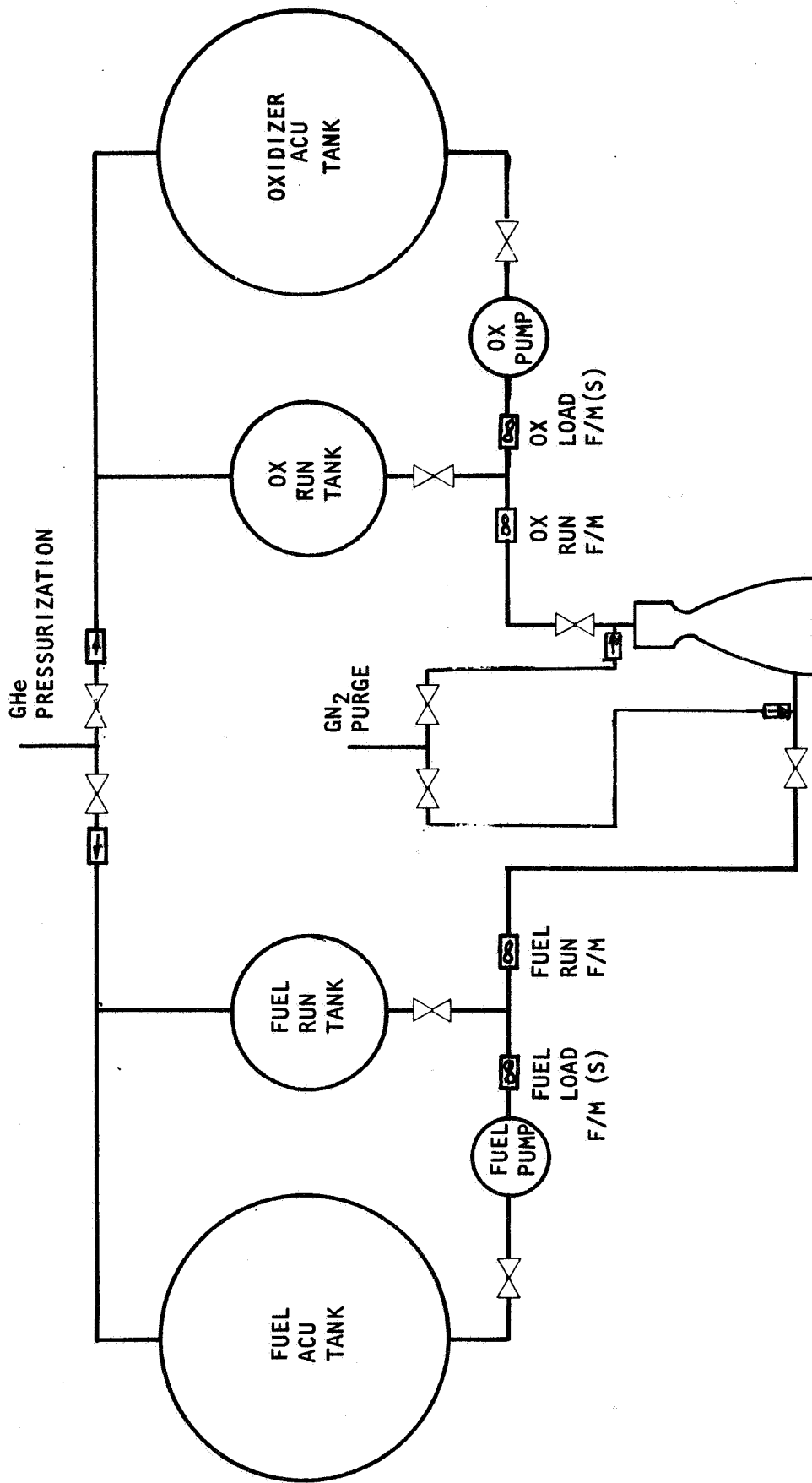Figure 156   Simulated OMS Oxidizer Feed System

Figure 157 Simplified NASA/WSTF Propellant Feed System Schematic

simplified schematic of the system. Fuel (MMH) and oxidizer (NTO) was stored and conditioned in 2000 gallon propellant tanks external to the vacuum cell. The propellant was pumped from the external tanks to the two 60 gallon tanks inside the vacuum cell simulating the OMS tankage exits. Line sizes and lengths from the propellant tanks to the OME interface were configured so as to simulate OMS ducting. A flow meter was located in each propellant feedline between the tanks and the engine interface. A common pressure source was used to pressurize both the internal and external fuel tanks.

The fuel sides of two LM descent engine valves were used as the engine propellant control valves. Fuel valves were used for both fuel and oxidizer sides because these valves contained the actuators and the position indicator. Each valve was series and parallel redundant including upstream isolation valves and downstream shutoff valves. Positions were measured on one of the isolation valves and one of the shutoff valves for each propellant. The valves were located so as to provide a slight positive drain into the engine inlets in an attempt to simulate the depletion which would occur after shutdown under zero 'g' conditions. The ducting between the valves and the engines was configured to simulate typical line volumes and sizes for the flight OME.

Provisions for GN_2 purges were made downstream of the valves. Provision for an isopropyl alcohol flush was also made downstream of the fuel valve. A water spray ring was provided at the radiation side of the regen/radiation nozzle interface. Finally, a high volume air cooling purge of the radiation nozzle was provided to cool the nozzle after testing.

APPENDIX B
OME PERFORMANCE DATA REDUCTION

Measurement	Symbol	Units
1. Thrust	F	lb
2. Injector end chamber pressure	P_c	psia
3. Oxidizer flowrate	$\dot{W}_o$	lb/sec
4. Total fuel flowrate	$\dot{W}_F$	lb/sec
5. Fuel injection manifold temperature	T_F	F
6. Ambient pressure (exit)	P_a	psia
7. Throat area	A_t	in^2
8. Expansion area ratio	ϵ	
9. Oxidizer injection pressure	P_{OI}	psia
10. Fuel injection pressure	P_{FI}	psia
11. BLC orifice downstream pressure	P_{BLC}	psia
12. BLC orifice diameter	D	in.
13. Fuel specific gravity	ρ_F	

PROCEDURE

1. Compute boundary layer flowrate ($\dot{W}_{BLC}$)

$$\dot{W}_{BLC} = 2.9 \times D^2 \times \sqrt{\rho_F \times (P_{FI} - P_{BLC})}$$

2. Compute total propellant flowrate ($\dot{W}_T$)

$$\dot{W}_T = \dot{W}_o + \dot{W}_F$$

3. Compute boundary layer coolant fraction (BLC)

$$BLC = \frac{\dot{W}_{BLC}}{\dot{W}_T}$$

4. Compute mixture ratio (MR)

$$MR = \frac{\dot{W}_o}{\dot{W}_F}$$

5. Compute nozzle stagnation pressure (P_{NS})

$$P_{NS} = 0.95 \times P_c$$

6. Compute characteristic velocity (C*)

$$C^* = \frac{32.174 \times P_{NS} \times A_t}{\dot{W}_T}$$

7. Compute site thrust coefficient ($C_{F\ SITE}$)

$$C_{F\ SITE} = \frac{F}{P_{NS}\ A_t}$$

8. Compute vacuum thrust coefficient ($C_{F\ VAC}$)

$$C_{F\ VAC} = C_{F\ SITE} + \frac{\epsilon\ P_a}{P_{NS}}$$

9. Compute expected vacuum thrust coefficient (C_{FVE})

$$C_{FVE} = 1.360 \times [1 + 0.06 \times BLC] + [(MR - 1.65) \times 0.021] \text{ for } \epsilon = 3$$

$$C_{FVE} = 1.519 \times [1 + 0.14 \times BLC] + [(MR - 1.65) \times 0.057] \text{ for } \epsilon = 9$$

$$C_{FVE} = 1.783 \times [1 + 0.23 \times BLC] + [(MR - 1.65) \times 0.12] \text{ for } \epsilon = 72$$

10. Compute C_F correlation (K)

$$K = \frac{C_{F\ VAC}}{C_{FVE}}$$

11. Adjust thrust coefficient to nominal ϵ

$$C_{F\ VAC} = 1.311 \times C_{F\ VAC} [1 - 0.06 \times BLC] \text{ for } \epsilon = 3$$
$$\epsilon = 72$$

$$C_{F\ VAC} = 1.1738 \times C_{F\ VAC} [1 - 0.14 \times BLC] \text{ for } \epsilon = 9$$
$$\epsilon = 72$$

$$C_{F\ VAC} = C_{F\ VAC} [1 - 0.23 \times BLC] \text{ for } \epsilon = 72$$
$$\epsilon = 72$$

12. Compute vacuum thrust (F_{VAC})

$$F_{VAC} = F + \epsilon \times A_t \times P_a$$

13. Find stratification C* loss (ΔC^*_{BLC}) from table of ΔC^*_{BLC} vs blc,

$$mr \text{ at } blc = BLC$$
$$mr = MR$$

14. Compute C* adjusted for BLC (C^*_{UMR})

$$C^*_{UMR} = C^* - \Delta C^*_{BLC}$$

15. Find stratification specific impulse loss ($\Delta I_{s \, BLC}$) from table of $\Delta I_{s \, BLC}$

$$vs \text{ blc, } mr \text{ at } blc = BLC$$
$$mr = MR$$

16. Compute vacuum specific impulse (I_{s1}) at test MR, BLC

$$I_{s1} = \frac{C_{F \, VAC} \times C^*_{UMR}}{32.174} \Big|_{\epsilon = 72} + \Delta I_{s \, BLC}$$

17. Find theoretical I_s ($I_{s \, TH}$) from table of $I_{s \, TH}$ vs

$$mr, P \text{ at } mr = MR$$
$$P = P_{NS}$$

18. Compute specific impulse efficiency (ηI_s) for test

$$\eta_{I_s} = \frac{I_{s1}}{I_{s \, TH}}$$

19. Compute test vacuum specific impulse $(I_{s\,VT})$

$$I_{s\,VT} = \frac{C^* \times C_{F\,VAC}}{32.174}$$

20. Find TDK specific impulse $(I_{s\,TDK})$

$$\text{from table of } I_{s\,TDK} \text{ vs mr, P at mr} = MR$$
$$P = P_{NS}$$

21. Compute energy release efficiency (η_{ER})

$$\eta_{ER} = \frac{I_{s\,VT} + 40/\dot{W}_T}{I_{s\,TDK}} \times 100 \text{ for } \epsilon = 3$$

$$\eta_{ER} = \frac{I_{s\,VT} + 58/\dot{W}_T}{I_{s\,TDK}} \times 100 \text{ for } \epsilon = 9$$

$$\eta_{ER} = \frac{I_{s\,VT} + 127/\dot{W}_T}{I_{s\,TDK}} \times 100 \text{ for } \epsilon = 72$$

APPENDIX C

THERMAL FATIGUE ANALYSIS

The model used to calculate stress and strain is shown in Fig. 158.
A plain strain state of stress was assumed. A three-element finite
element model was used (Elements B, L, W). Only thermal loading was
analyzed because, for this case, pressure loading combined with thermal
loading is predicted to give smaller strains than thermal load alone.
Since thermal load can exist alone for a short period after cut off,
this is a realistic case.

The fundamental equation used was:

$$\varepsilon_m + \varepsilon_\alpha = \varepsilon_a$$

where

ε_m = mechanical strain for an element

ε_α = $\alpha \Delta T$ for an element

ε_a = apparent strain for the model

Because the strain is in the inelastic range, the procedure was iterative
in that trial values of ε_a were selected. $\varepsilon_m = \varepsilon_a - \alpha \Delta T$ was used to determine
stress in the elements. Element total forces were then summed. If the
element force summation equaled zero, the correct value of ε_a had been used.
If stress was elastic, the value was found by using E. If stress was
plastic, a stress versus strain diagram was used to determine stress.

Table 46 is a sample of the calculations for one station in the thrust
chamber. The following definitions will be helpful in following the

calculations:

ϵ_A = axial mechanical strain

ϵ_{aA} = axial apparent strain

$\epsilon_{aA} - \alpha \Delta Twg$ = peak mechanical axial strain at the hot gas face

ϵ_T = tagential mechanical strain

ϵ_{aT} = tangential apparent strain

$\epsilon_{aT} - \alpha \Delta Twg$ = peak tangential s rain at the hot gas face

ϵ_e = effective strain at the hot gas face

N_f = cycles read from fatigue data plot using ϵ_e

The fatigue data that was used to convert ϵ_e to cycles was calculated using the universal slopes equation. Figure 159 is a plot of this data at 70 F and 1000 F. N_f was read from the plot approximately half-way between the 70 F and 1000 F lines. This fatigue data plot represents what would be expected as typical fatigue test results. Design life was calculated as $N_f \div 4$. This means that strain rate and hold time effects were assumed negligible.

Several references have been used to study the validity of the fatigue data used and the assumption that strain rate and hold time effects are negligible. The data from two of the references are plotted on Fig.159 . The 800 F data is the most applicable data for this case since the OME maximum hot gas wall temperature is approximately 750 F.

This data shows the univeral slopes plot of Fig. 159 to be slightly conservative. The 1 percent strain data in NASA TND-1574 indicates that at 750 F there would be negligible hold time effect.
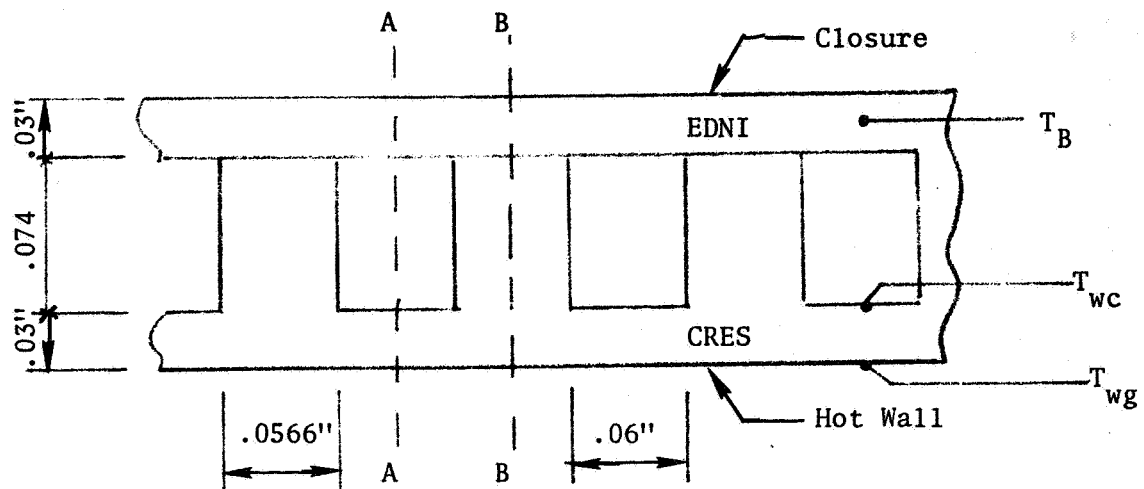
$$T_{wg} = 685^{\circ} \text{ F}$$

$$T_{wc} = 379^{\circ} \text{ F}$$

$$T_{B} = 154^{\circ} \text{ F}$$

$$T_{L} = \frac{T_{wc} + T_{B}}{2}$$

$$T_{L} = 267^{\circ} \text{ F}$$

$$T_{W} = \frac{T_{wg} + T_{wc}}{2}$$

$$T_{W} = 532^{\circ} \text{ F}$$
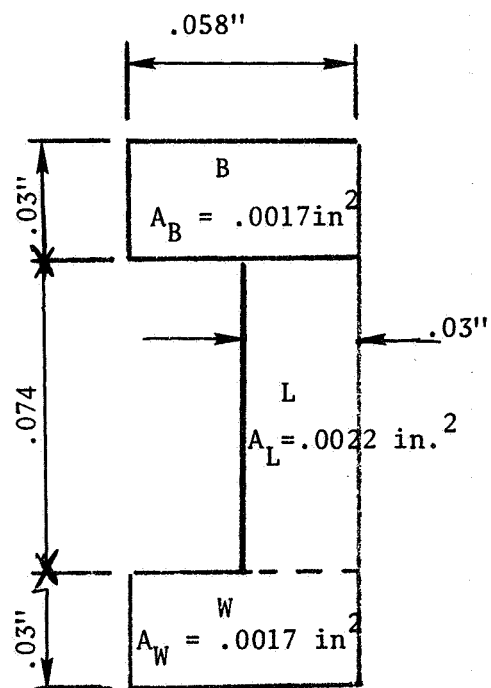
Section AA to BB

Fig. 158 Model For Thermal Fatigue Analysis

R-9686

C-3

TABLE 46
LIFE ESTIMATES
CRES HOTWALL - E.D. NICKEL CLOSURE

STA. 19 X = -1.8577		

T_{wg} = 685 F $\alpha\Delta T$ = .0059 ΔT = 615 F

T_W = 532 F $\alpha\Delta T$ = .00585   E = 24.05 X 10^6 ΔT = 462 F

T_L = 267 F $\alpha\Delta T$ = .00170   E = 25.9 X 10^6 ΔT = 197 F

T_B = 154 F $\alpha\Delta T$ = .00055   E = 25.86 X 10^6 ΔT = 84 F

CALCULATE ϵ_A : ϵ_{aA} = .00165

AREA	AREA IN.^{2}	ΔT ^{o}F	$\alpha\Delta T$ IN/IN	ϵ_A $\epsilon_{aA} - \alpha\Delta T$	σ PSI	F
A_W	.0017	462	.00585	-.0042	-26,000	-44.1
A_L	.0022	197	.00170	-.00005	- 1,300	- 2.9
A_B	.0017	84	.00055	+.0011	+28,500	-48.4

$\epsilon_A = \epsilon_{aA} - \alpha\Delta T_{wg}$ = .00165 - .0059 = .00425

CALCULATE ϵ_T : ϵ_{aT} = .0016

AREA	AREA IN.^{2}	ΔT ^{o}F	$\alpha\Delta T$ IN./IN.	ϵ_T $\epsilon_{aT} - \alpha\Delta T$	σ PSI
A_W	.0017	462	.00585	-.00425	-26,000
A_B	.0017	84	.00055	+.00105	-27,200

$\epsilon_T = \epsilon_{aT} - \alpha\Delta T_{wg}$ = .0016 - .0059 = .0043

CALCULATE C_e :

$\epsilon_e = 1.155 \sqrt{\epsilon_A \epsilon_T + \epsilon_A^2 + \epsilon_T^2}$
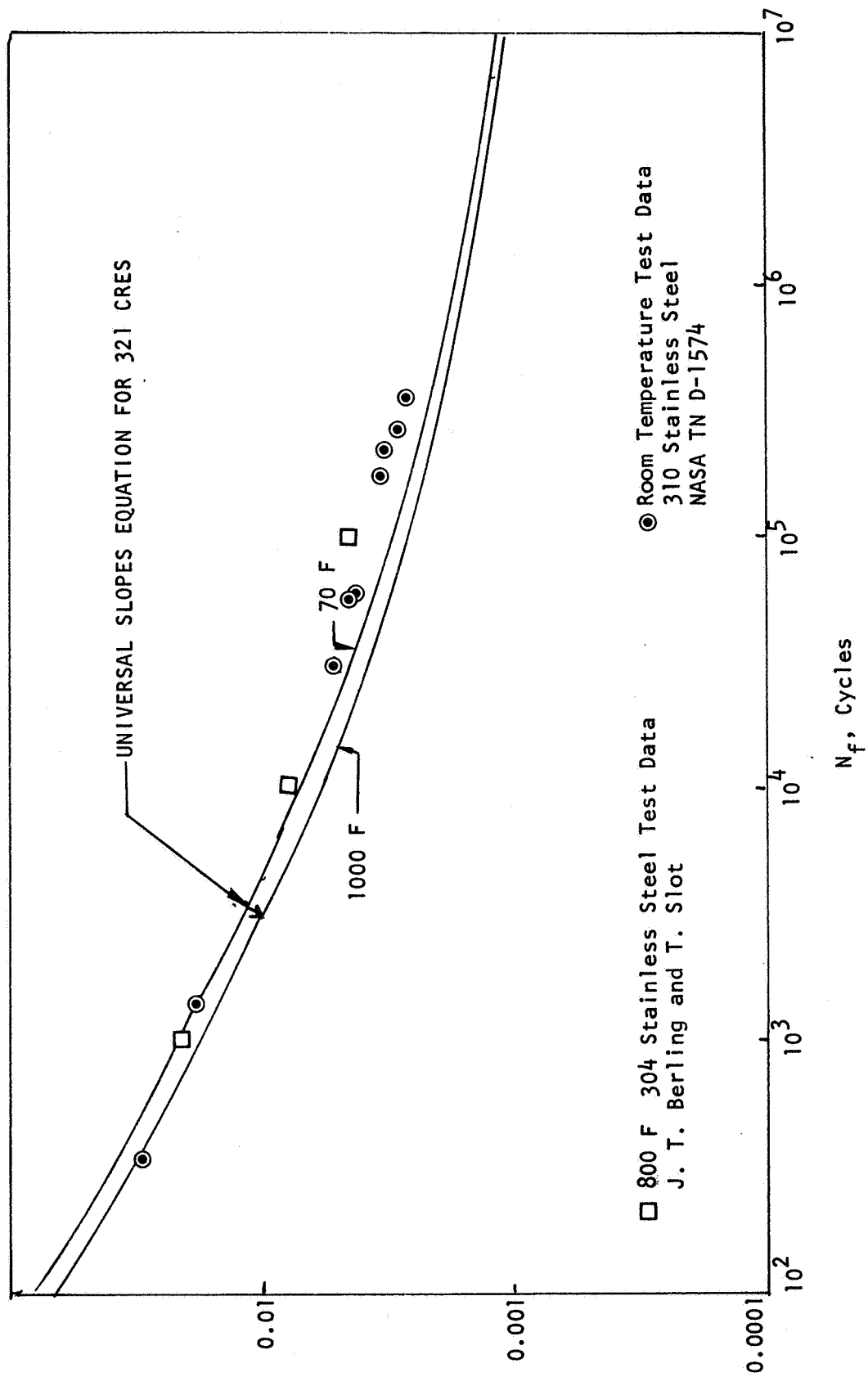
ϵ_e = .0086

N_f = 5200

R-9686

C-4

Fig. 159 Analytic and Experimental Fatigue Data